Amine Borane Dehydrocoupling with d(0) Complexes

Bellham, Peter

Award date:
2014

Awarding institution:
University of Bath

Amine Borane Dehydrocoupling with d^0 Complexes

Peter Bellham

A thesis submitted for the degree of Doctor of Philosophy

University of Bath

Department of Chemistry

June 2014

Publications Resulting from this Thesis

Alkylstrontium diamidoboranes: beta-hydride elimination and Sr-C insertion. Bellham, P., Hill, M. S., Liptrot, D. J., MacDougall, D. J. and Mahon, M. F., *Chem. Commun.*, **2011**, *47 (32)*, 9060-9062.

Alkaline earth alkyl insertion chemistry of in situ generated aminoboranes. Bellham, P., Hill, M.S., Kociok-Köhn, G. and Liptrot, D.J., *Dalton Trans.*, **2013**, *42 (3)*, 737-745.

Bespoke synthesis of unsymmetrical diaminoboranes by alkaline earth catalysis. Bellham, P., Hill, M.S., Kociok-Köhn, G. and Liptrot, D.J., *Chem. Commun.*, **2013**, *49 (19)*, 1960-1962.

Contents

Acknowledgements

Undertaking a PhD is a very personal project and journey, testing your resolve in so many ways and, as those around me will testify, I have usually gone about overcoming those things in a typically unique way. This journey would not have been possible without Mike, whose faith in giving me the opportunity to undertake this PhD, combined with enthusiasm about chemistry and style of supervision have all been greatly appreciated.

I am grateful for the support of my parents, family and friends who continually ask me how everything is going. Whilst they may not understand what it is that I'm doing I know that I have all of their support. The non-chemist who knows most about my thesis is my wife Michelle, whose support, belief in me and listening ear for me to grumble about kinetics and general amine borane based woes has been constant and unwavering. It has been reassuring to have someone by my side who knows what it's like to undertake a PhD and know without me saying.

Within the chemistry department I wish to thank Gabriele Kociok-Köhn for all of the crystallography, John Lowe for all of his NMR help and allowing me to run so many NMRs on the 300 MHz spectrometer, Carlo Di Iulio and Rhodri Owen for their help with GC MS and Stephen Boyer at London Metropolitan University for CHN microanalysis. I also extend my gratitude to my colleagues in the Hill, Johnson and Molloy groups and the University of Bath for funding.

My PhD moved me away from friends and family, but brought me to the lovely city of Bath, a place which has changed my life in so many ways and somewhere I will greatly miss.

Abstract

As the developed world seeks to reduce the dependence upon fossil fuels, amine boranes have received increased interest as a clean, stable hydrogen source. This thesis sought to scrutinise the mechanism of amine borane dehydrocoupling proposed by Hill and provide quantitative evidence for the dependence of dehydrocoupling activity upon identity of the metal centre. This work led to a refined mechanism, shown in Figure A1, incorporating proton-assisted β-hydride elimination steps, occurring via potentially concerted processes. A pathway to account for the previously unreported reactivity of $[R_2N\text{-}BH_2]_2$ to ultimately afford $[HB(NR_2)_2]$ is also included.

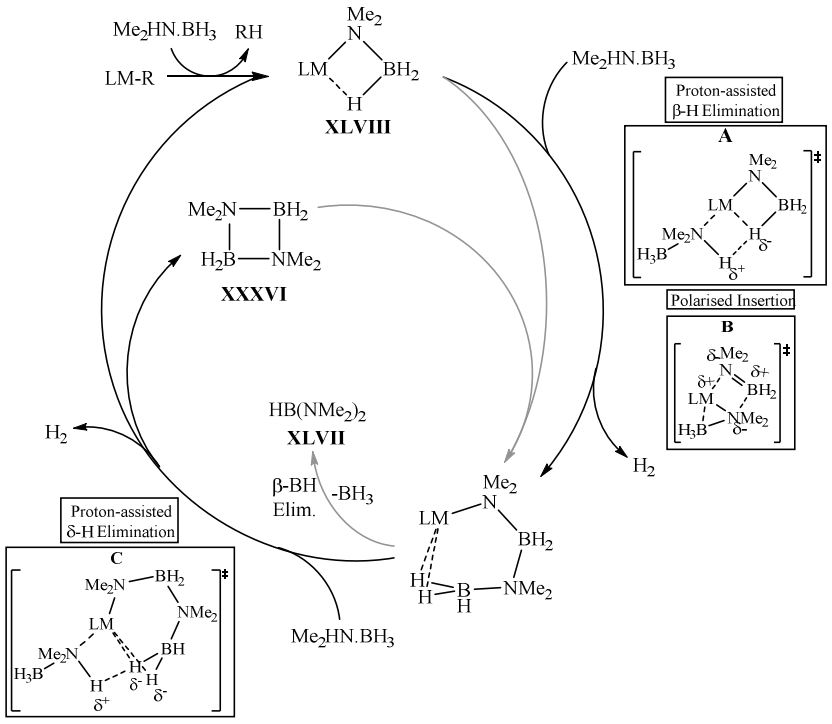

Figure A1: Proposed mechanism of amine borane dehydrocoupling by alkaline earth elements (M = Mg, Ca, Sr, Ba).

A dependence upon the identity of the metal centre on the dehydrocoupling activity was found, identifying a decrease in reactivity with increasing ionic radius and decreasing cation charge density as each group is descended. This thesis showed that the mechanism of secondary amine borane dehydrocoupling by d^0 reagents is complex, suggesting that a generic mechanism which fully describes dehydrocoupling of all amine boranes would be too much of an oversimplification.

Abbreviations Used in This Thesis

β-diketiminate	Dipp-nacnac ligand
AB	Ammonia borane
br.	Broad NMR resonance
Dipp	2,6-di-*iso*-propylphenyl
DMAB	Dimethylamine borane
DMAP	4-Dimethylaminopyridine
FLP	Frustrated Lewis Pair
GC MS	Gas Chromatography Mass Spectrometry
HMBC	Heteronuclear Multiple Bond Correlation
HMQC	Heteronuclear Multiple Quantum Correlation
HSQC	Heteronuclear Single Quantum Correlation
^{i}Pr	*Iso*-propyl
L	Supporting ligand
KIE	Kinetic Isotope Effect
Me	Methyl
^{n}Bu	Normal butyl
NMR	Nuclear Magnetic Resonance
OTf	Triflate
PB	Pyrrolidine borane
Ph	Phenyl
TBAB	*Tert*-butylamine borane
THF	Tetrahydrofuran
^{t}Bu	*Tert*-butyl
TOCSY	Total Correlation Spectroscopy

Table 1: Literature Compounds Referred to in This Thesis

I	$[M\{P(SiMe_3)_2\}_2(THF)_4]$
II	$[M\{N(SiMe_3)_2\}_2(THF)_2]$
III	$[Ba\{C(Ph)_2(CH_2CH_2Ph)\}_2(THF)_2]$
IV	$[M(DMAT)_2(THF)_2]$
V	$[M[N(SiMe_3)_2]_2]_2$ **V-Mg**, M = Mg **V-Ca**, M = Ca **V-Sr**, M = Sr
VI	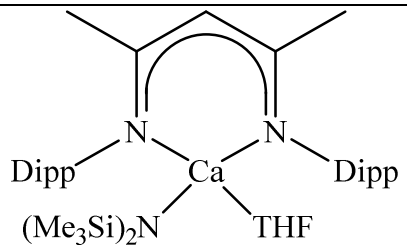
VII	$[M\{CH(SiMe_3)_2\}_2(THF)_2]$ **VIIMg**, M = Mg **VIICa**, M = Ca **VIISr**, M = Sr
VIII	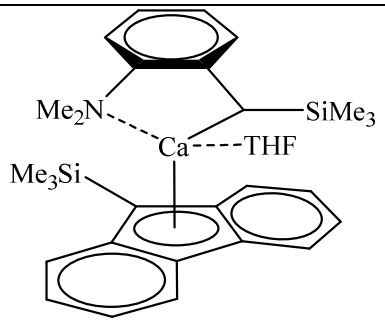

IX	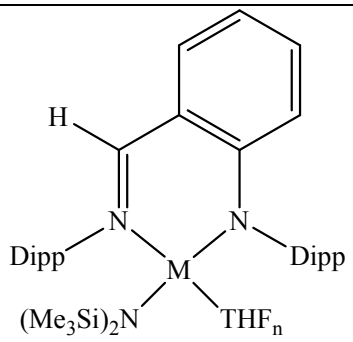 M = Ca, n = 1 M = Sr, n = 2 M = Ba, n = 2
X	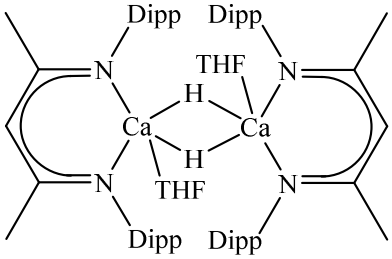
XI	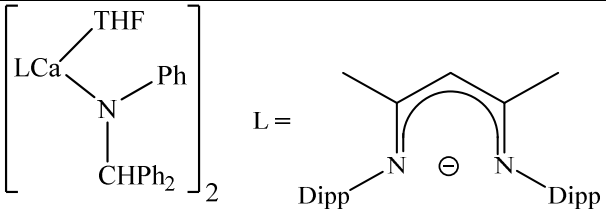
XII	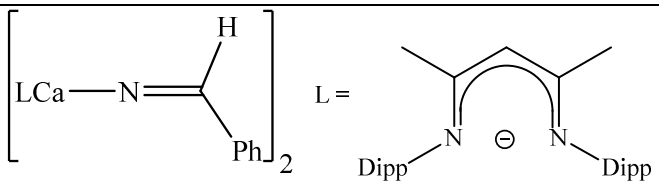
XIII	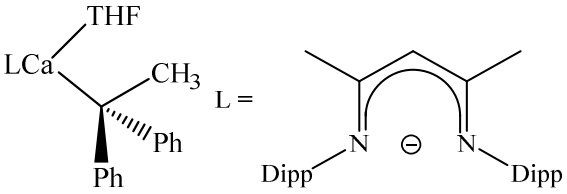
XIV	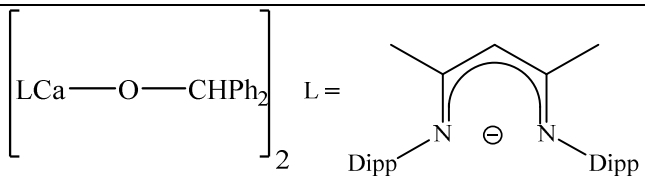
XV	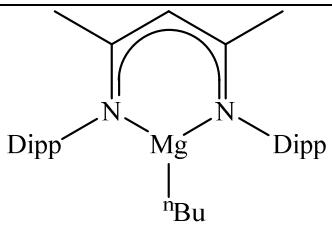

XVI	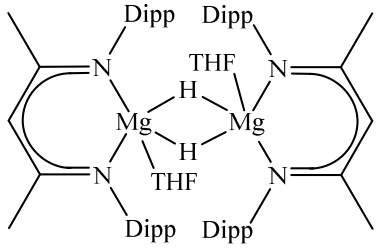
XVII	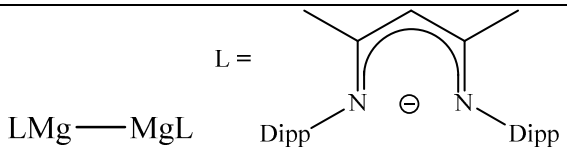
XVIII	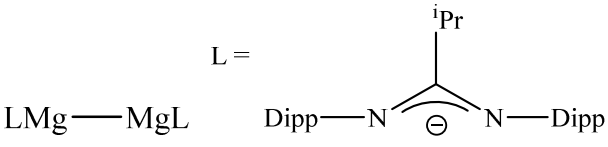
XIX	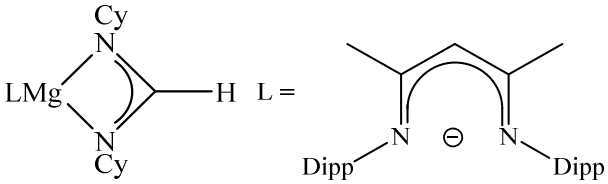
XX	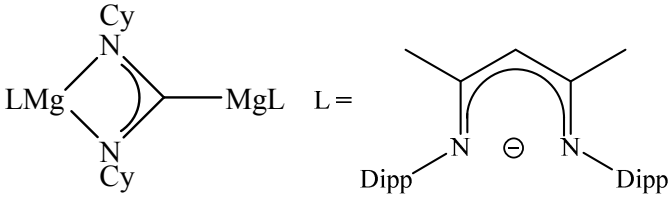
XXI	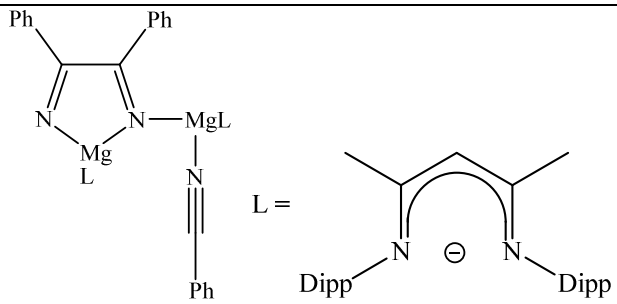
XXII	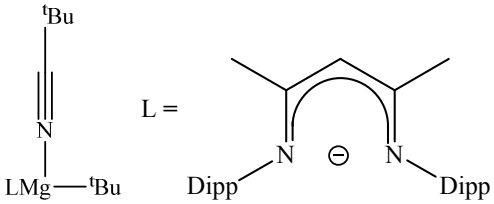

XXIII	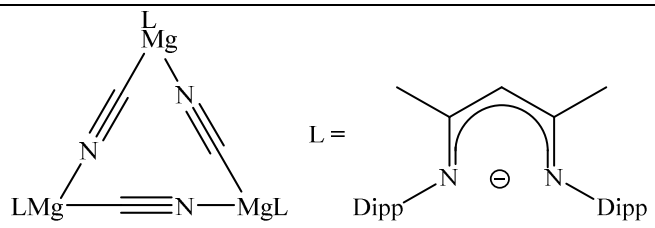
XXIV	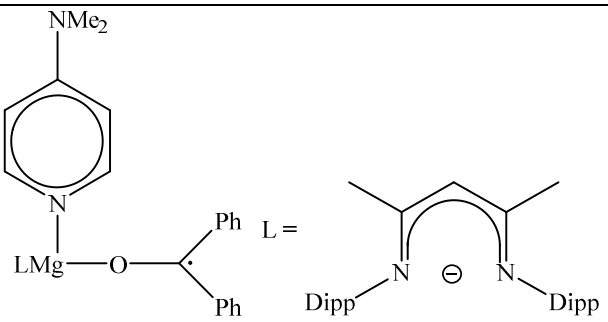
XXV	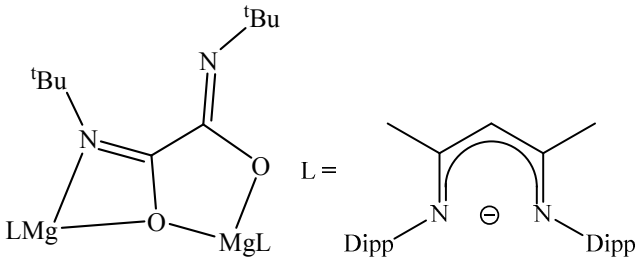
XXVI	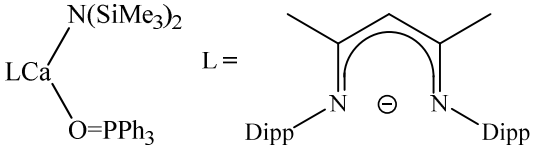
XXVII	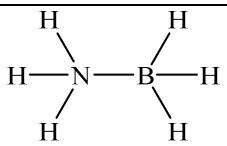
XXVIII	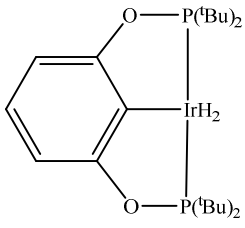
XXIX	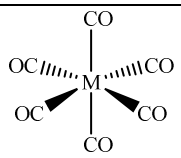 M = Cr, Mo, W

XXX	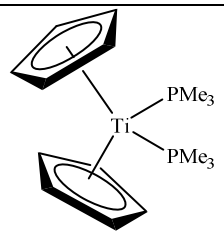
XXXI	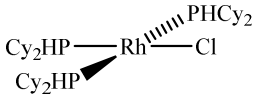
XXXII	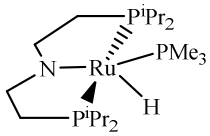
XXXIII	$Cp_2TiCl_2/2^nBuLi$
XXXIV	Dimethylamine borane
XXXV	$HMe_2N\text{-}BH_2\text{-}NMe_2\text{-}BH_3$
XXXVI	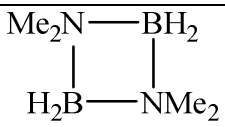
XXXVII	$Me_2N{=}BH_2$
XXXVIII	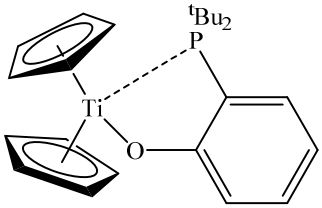
XXXIX	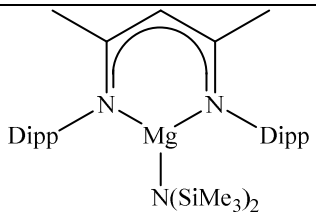
XL	$Sc(N(SiHMe_2)_2)_3(THF)_2$
XLI	$Y(N(SiMe_3)_2)_3$

XLII	(a) $Al(N^iPr_2)_3$ (b) $E(NMe_2)_3$ E = Al, Ga
XLIII	$(Dipp)NH_2.BH_3$
XLIV	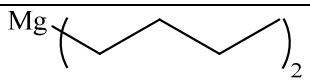
XLV	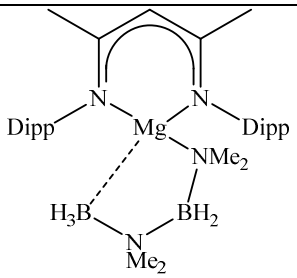
XLVI	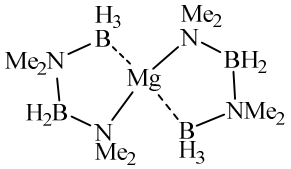
XLVII	$HB(NMe_2)_2$
XLVIII	$LM[NMe_2BH_3]$
XLIX	$LM[NMe_2BH_2NMe_2BH_3]$
L	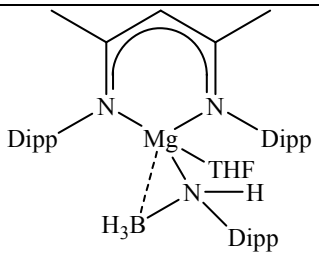
LI	$[HB\{NH(Dipp)\}_2]$
LII	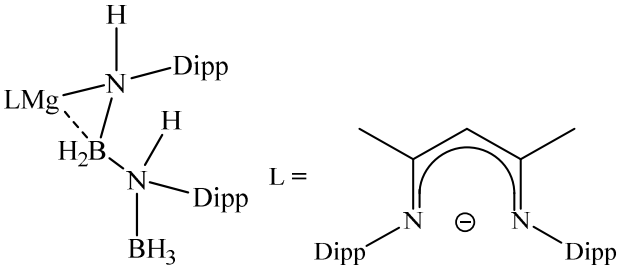

LIII	Pyrrolidine borane
LIV	$[H_2BNC_4H_8]_2$
LV	di-*iso*-propylamine borane
LVI	$^{i}Pr_2N{=}BH_2$
LVII	Trimethylamine borane
LVIII	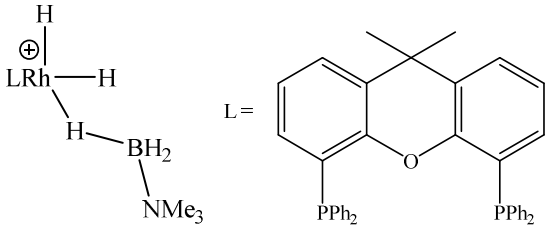
LIX	$MN(SiMe_3)_2$ **LIX-Li**, M = Li **LIX-Na**, M = Na **LIX-K**, M = K
LX	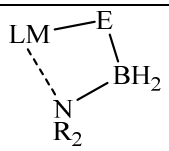
LXI	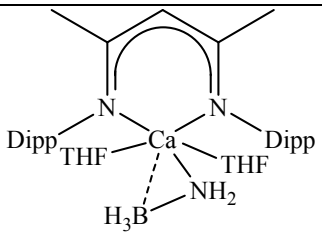
LXII	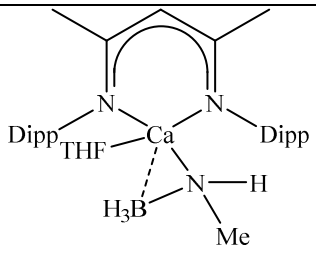

LXIII	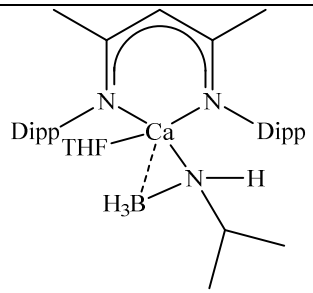
LXIV	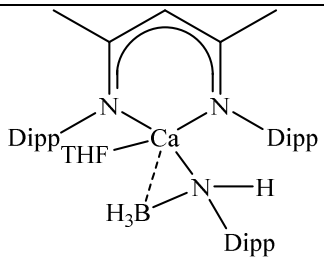
LXV	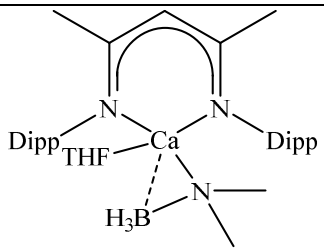
LXVI	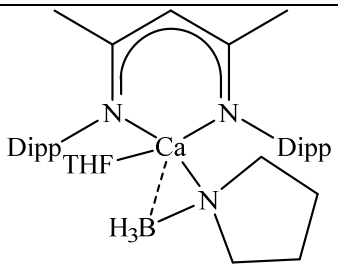
LXVII	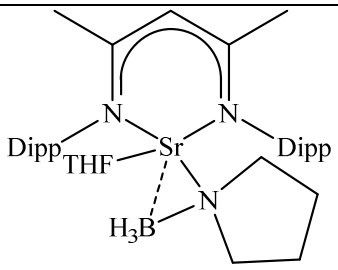

LXVIII	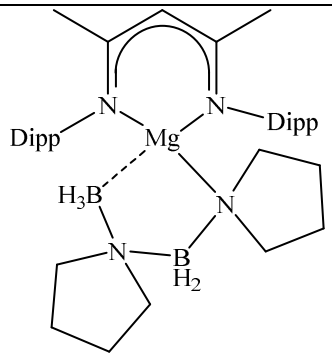
LXIX	$HB(NC_4H_8)_2$
LXX	$B(NMe_2)_3$
LXXI	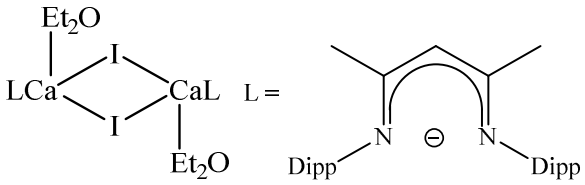
LXXII	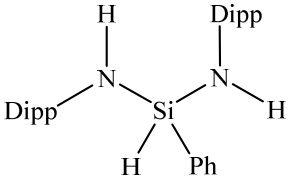
LXXIII	$Li[NMe_2BH_3]$
LXXIV	$K[NMe_2BH_3]$
LXXV	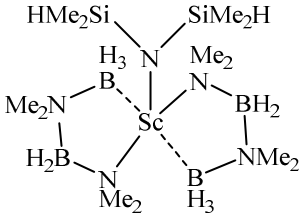
LXXVI	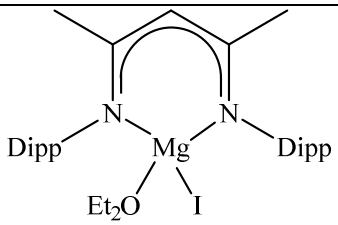

LXXVII	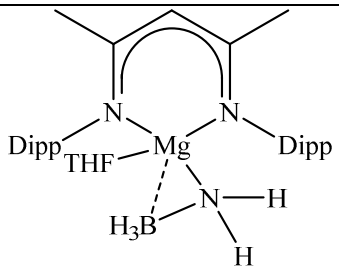
LXXVIII	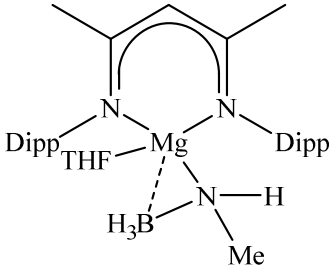
LXXIX	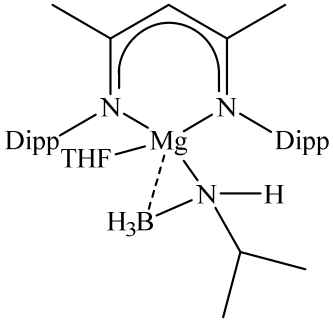
LXXX	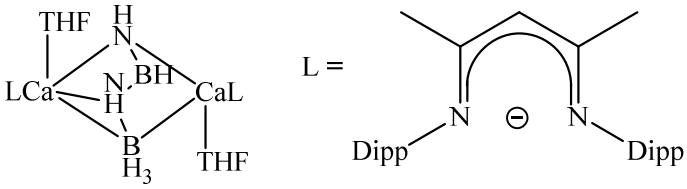
LXXXI	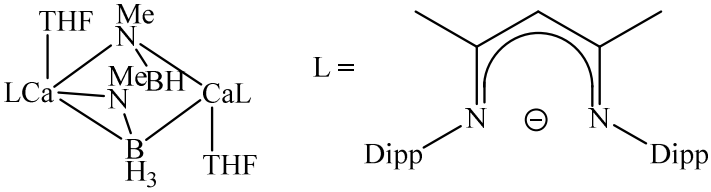
LXXXII	$Me_2NH.BD_3$
LXXXIII	$[H_2B(\mu\text{-}H)(\mu\text{-}NMe_2)BH_2]$
LXXXIV	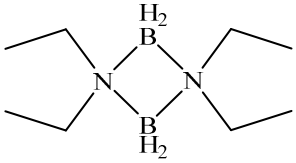

LXXXV	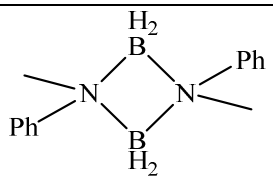
LXXXVI	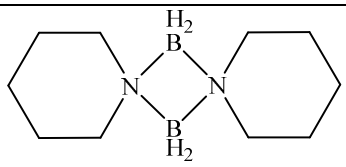
LXXXVII	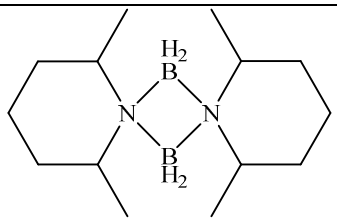
LXXXVIII	$Ca(BH_4)_2.NH_3$
LXXXIX	$Ca(BH_4)_2.(NH_3)_2$
XC	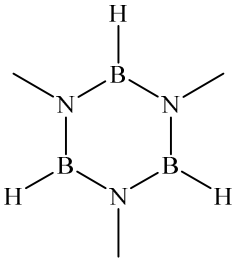
XCI	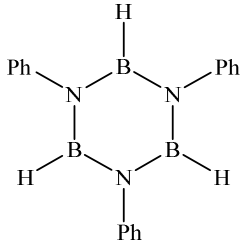

XCII	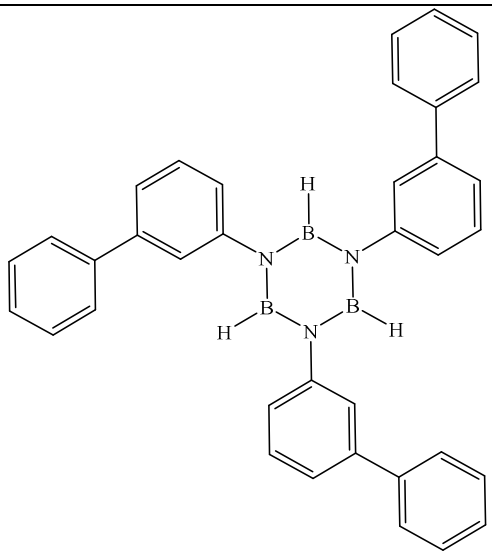
XCIII	$Me_2ND.BH_3$
XCIV	$HN(SiMe_3)_2$
XCV	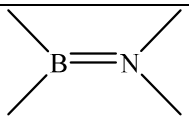
XCVI	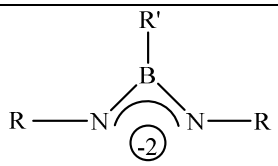
XCVII	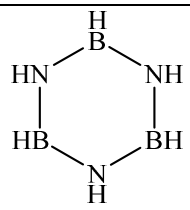

Table 2: Compounds Produced in this Thesis

1	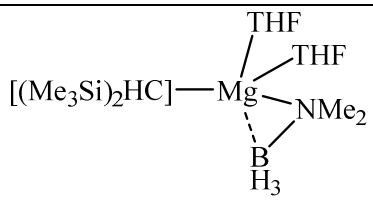
2	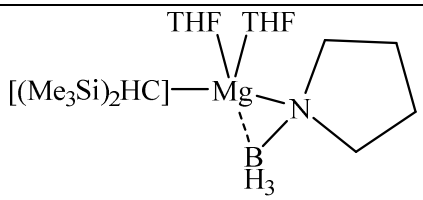
3	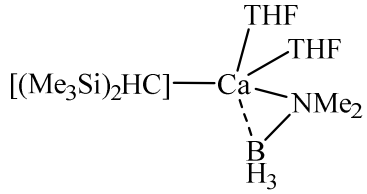
4	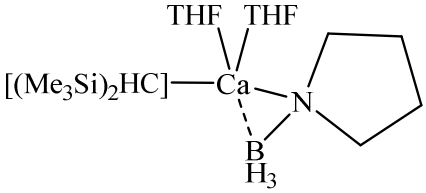
5	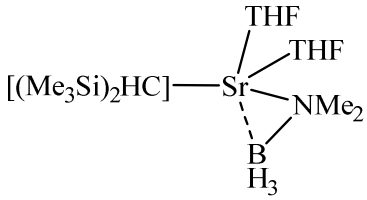
6	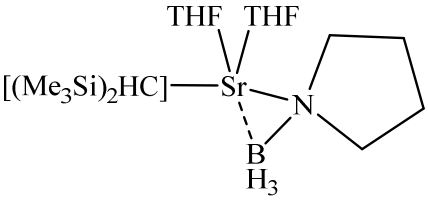
7	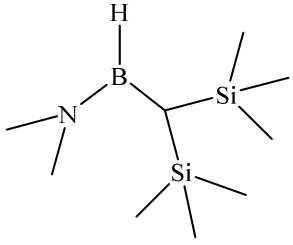

8	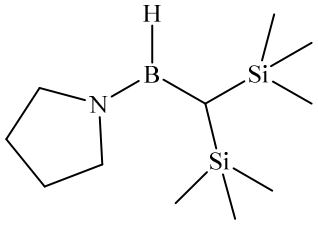
9	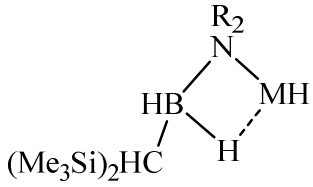 **9Mg**, M = Mg **9Ca**, M = Ca **9Sr**, M = Sr
10	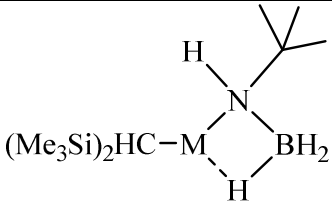
11	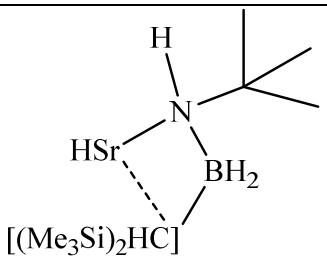
12	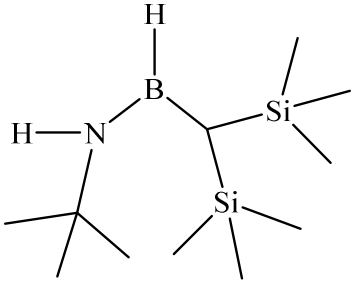

13	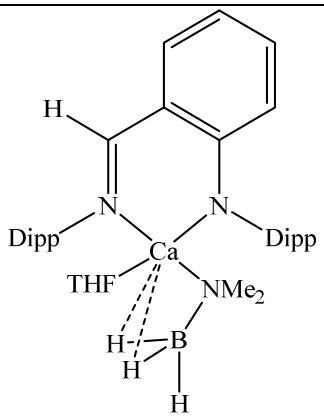
14	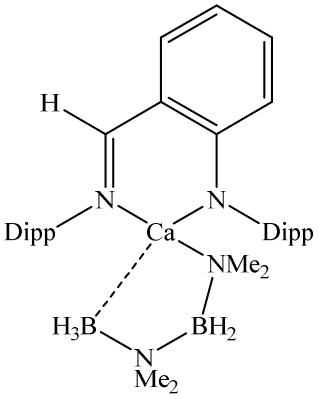
15	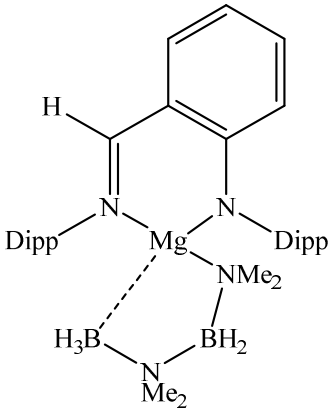
16	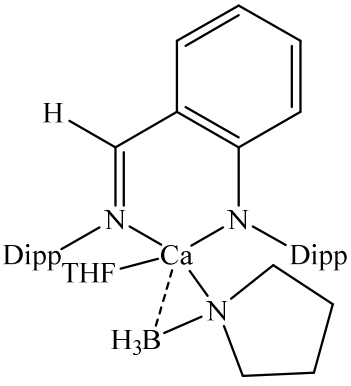

17	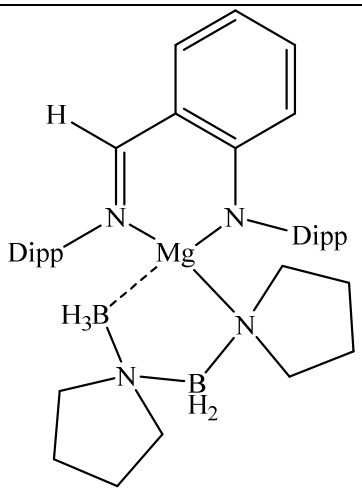
18	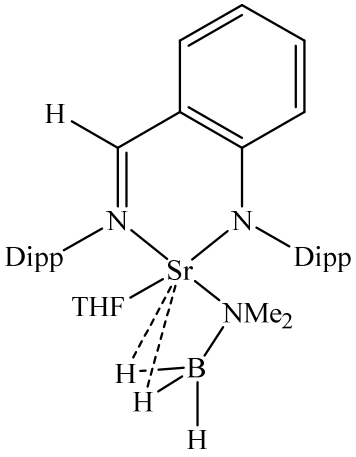
19	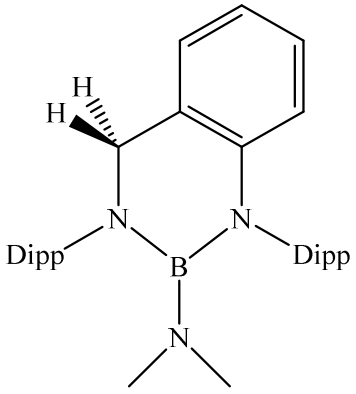

20	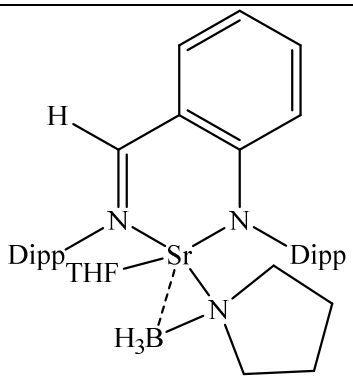 H N N Dipp THF Sr Dipp N H_3B
21	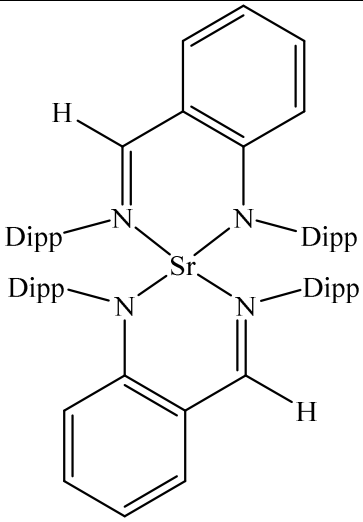 H N N Dipp Dipp Sr Dipp N N Dipp H
22	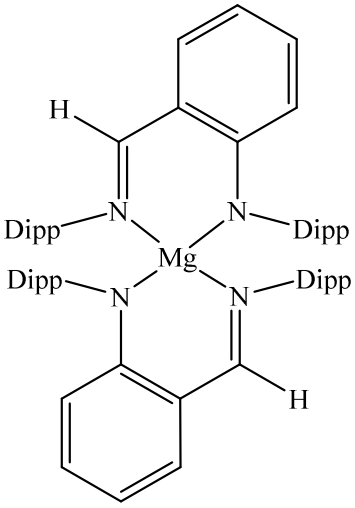 H N N Dipp Dipp Mg Dipp N N Dipp H

23	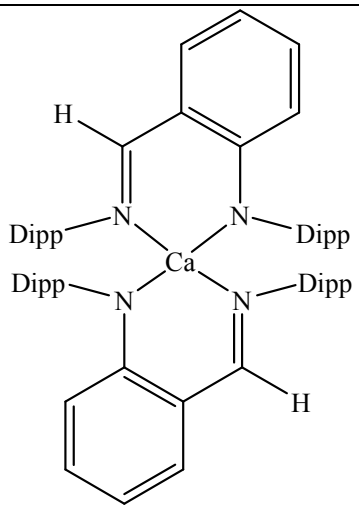 H N N Dipp Dipp Ca Dipp N N Dipp H
24	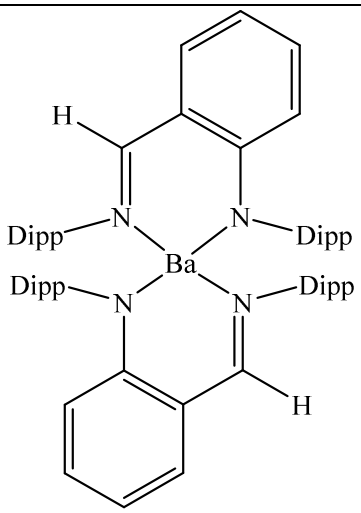 H N N Dipp Dipp Ba Dipp N N Dipp H
25	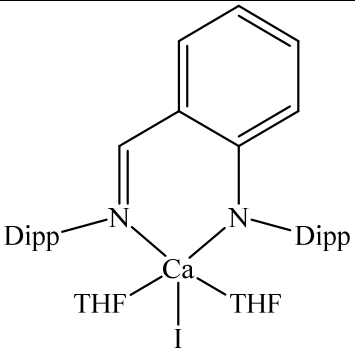 N N Dipp Dipp Ca THF THF I

26	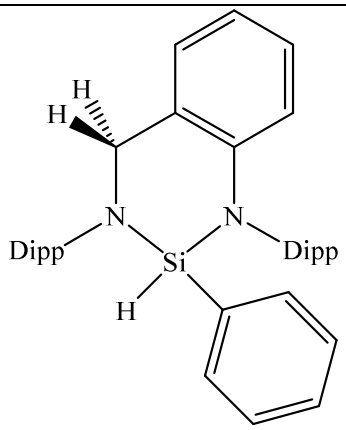
27	$[HB\{NMe_2\}\{N(SiMe_3)_2\}]$
28	$[H_3B.NH(SiMe_3)_2]$
29	$K[NMe_2BH_2NMe_2BH_3]THF_2$
30	$Li[NMe_2BH_2NMe_2BH_3]$
31	$Na[NMe_2BH_2NMe_2BH_3]$
32	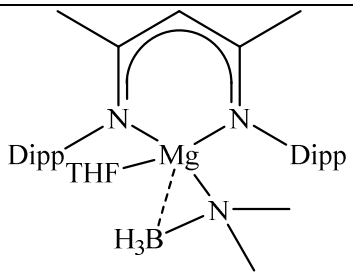
33	$Ca[NMe_2BH_2NMe_2BH_3]_2$
34	$Sr[NMe_2BH_2NMe_2BH_3]_2$
35	$Ba[NMe_2BH_2NMe_2BH_3]_2$
36	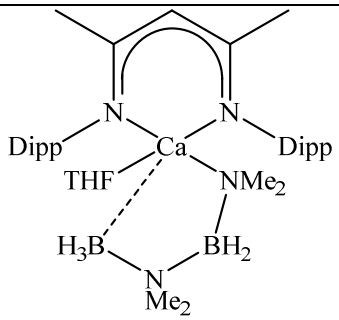

37	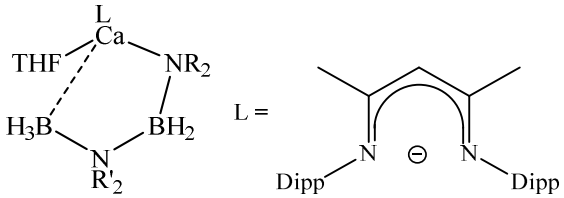
38	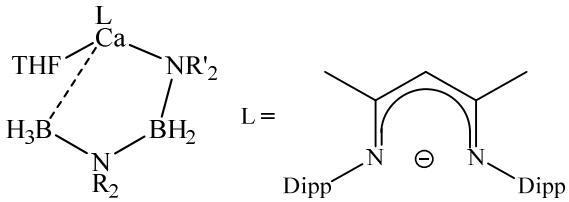
39	Unidentified product quartet resonance at δ = –8.7 ppm, $^{1}J_{BH}$ = 91 Hz in the ^{11}B NMR spectrum of the reaction between **XXXVI** and **LXV** at 60 °C
40	Unidentified product doublet resonance at δ = 33.7 ppm, $^{1}J_{BH}$ = 132 Hz in the ^{11}B NMR spectrum of the reaction between **XXXVI** and **LXV** at 60 °C
41	$HB(NC_4H_8)_2$
42	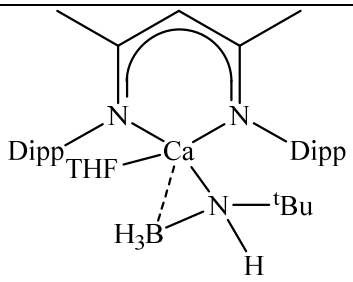
43	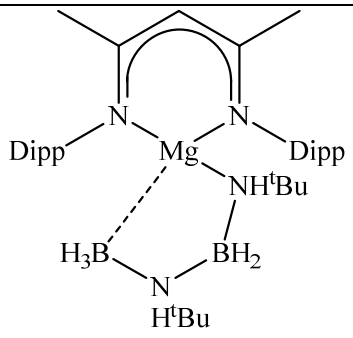
44	$LMg\text{-}NH^tBuBH_3$
45	$H^tBuN{=}BH_2$

46	$HB(NH^tBu)_2$
47	$[H^tBuN\text{-}BH_2]_2$
48	$[H_2B(\mu\text{-}H)(\mu\text{-}NH^tBu)BH_2]$
49	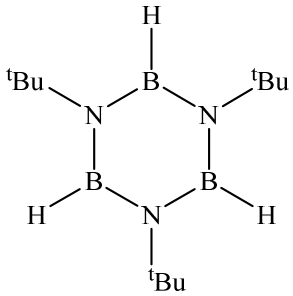
50	$Ca(BH_4)_2$THF polymer
51	$RR'Y[NMe_2BH_2NMe_2BH_3]$
52	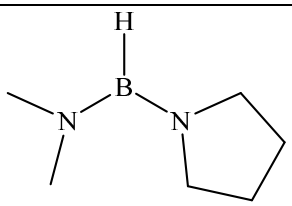
53	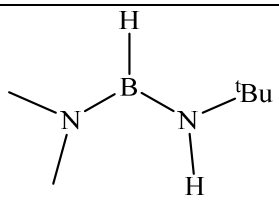
54	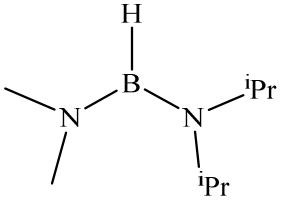
55	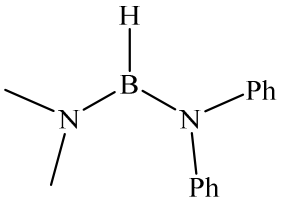

56	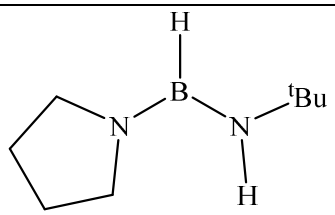
57	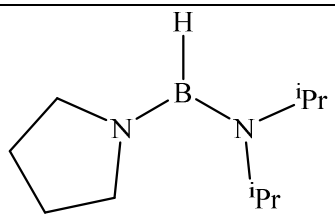
58	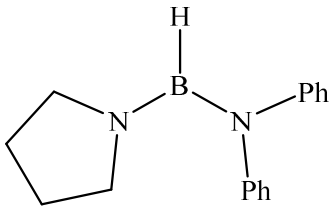
59	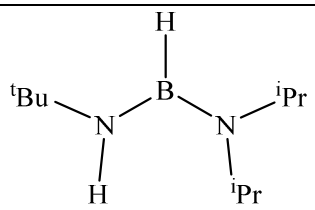
60	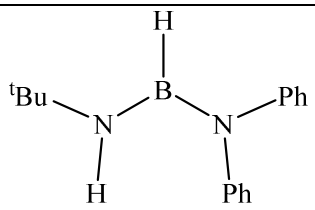
61	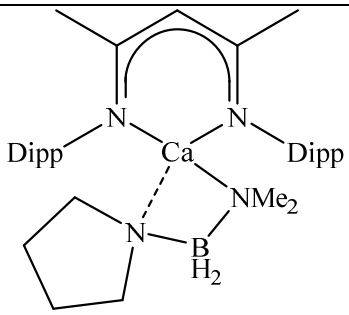

62	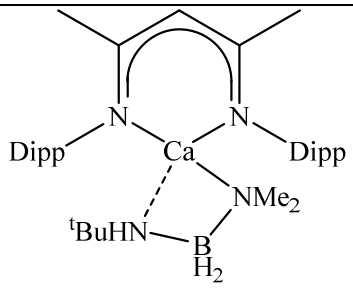

1 Introduction

1.1 Alkaline Earth Chemistry

Transition-metals are synonymous with catalysis, encompassing a plethora of chemical transformations that have created the world we live in, incorporating a wealth of metallic species with well-defined coordination chemistry and mechanistic diversity. Since the early 20th Century magnesium-based compounds such as Grignard reagents have been commonly utilised as stoichiometric reagents in organic synthesis.[1-3] A disparity exists, however, between the widespread application of transition-metal complexes and the catalytic and coordination behaviour of the s- and p-block elements and, with particular regard to the contents of this thesis, the utilisation of magnesium-based compounds and the heavier Group 2 metals (Ca, Sr and Ba). The use of heavy transition metal (e.g. Pd, Ru, Ir) catalysts requires assessment of the uneconomic and environmental impact, especially for such widespread intended use. These, in some cases toxic, metals are less abundant, often expensive, and both difficult and environmentally damaging to extract whereas advocation of the alkaline earth elements, magnesium, calcium, strontium and barium, highlights their low cost, abundance and environmentally benign nature.

The Group 2 elements form divalent compounds which are redox inactive, apart from a few notable exceptions.[4-6] Their M^{2+} ions possess a d^0 electronic configuration and increase in ionic radii as the group is descended,[7] Figure 1.1.

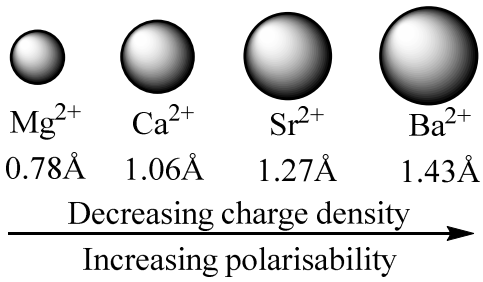

Figure 1.1: Ionic radii of the heavier Group 2 M^{2+} ions.[7]

The consequent increase in polarisability and electropositive character on descending Group 2 causes the metal-ligand interactions in organometallic magnesium species to

exhibit some covalent character, whilst the interactions in organometallic complexes of the heavier Group 2 elements are predominantly ionic. In this respect the coordination behaviour of heavier alkaline earth metals is somewhat mimetic of the lanthanides. Groundbreaking work by Marks et al with similarly d^0 trivalent organolanthanide complexes of the form L_2LnX (in which L is a monoanionic ligand and X is a substituent), demonstrated the catalytic activity of these species via mechanistic schemes based upon σ-bond metathesis and insertion of unsaturated C=C or C=E bonds into Ln-X σ-bonds via four-membered transition states.[8] These fundamental reactions are shown in Figure 1.2.

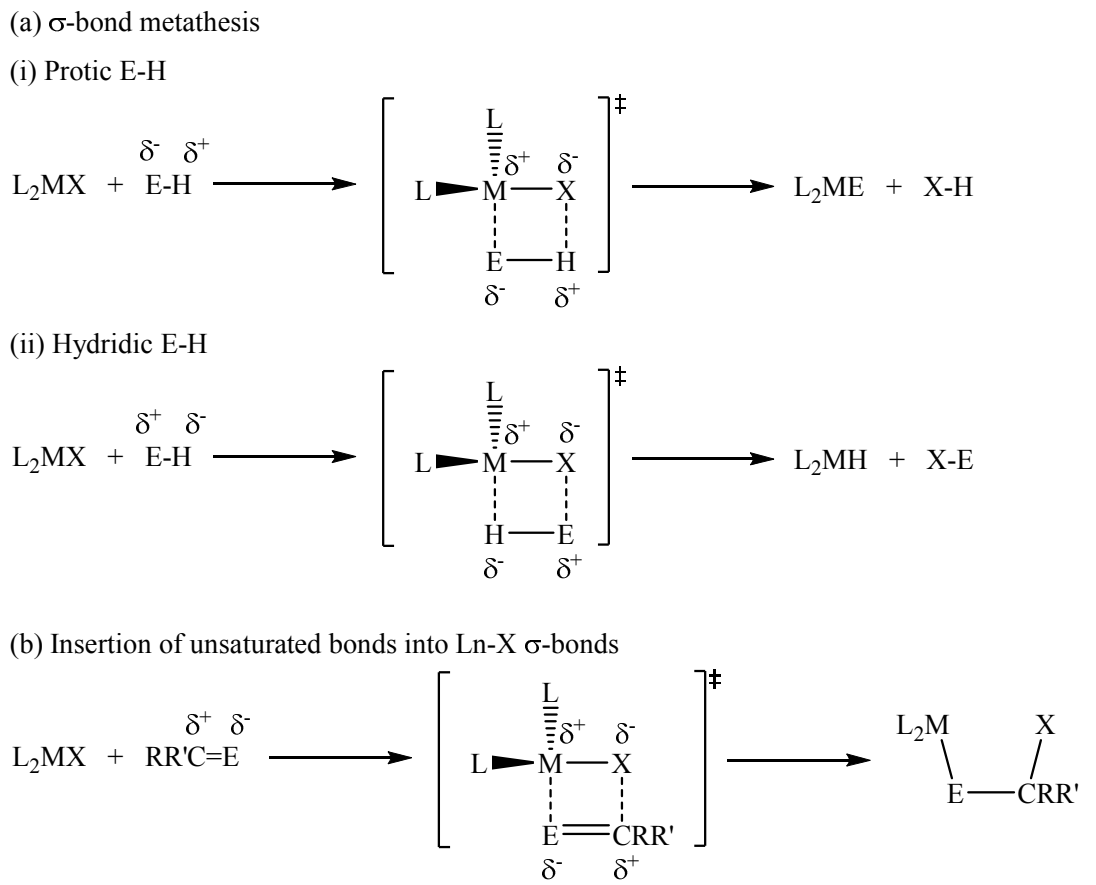

Figure 1.2: **(a)(i)** σ-bond metathesis for a substrate with a protic E-H; **(ii)** σ-bond metathesis for a substrate with a hydridic E-H; **(b)** insertion of unsaturated bonds into the M-X bond, where M is a trivalent d^0 organolanthanide complex.

Figure 1.2(a) demonstrates divergent σ-bond metathesis reactivity, dependent upon the polarity of the E-H bond. In the case of a protic substrate, when element E is

more electronegative than H [Figure 1.2(a)(i)] protonolysis occurs, resulting in the formation of a new M-E bond and protonation of the substituent group X. An example for the reactivity towards a protic reagent is the reaction between a lanthanide species, L_2LnX, and an amine, R_2NH, forming a lanthanide amide, L_2LnNR_2.[9] A different four-membered transition state arises between the lanthanide complex when E-H describes a hydridic substrate, such as a silane R_3SiH. In this case H is more electronegative than element E [Figure 1.2(a)(ii)], wherein metathesis results in formation of a metal hydride, L_2MH and a new X-E bond. With particular relevance to this thesis is the insertion of an unsaturated species into the polarised M-X bond, shown in Figure 1.2(b). When the unsaturated substrate is an alkene or alkyne, i.e. E = C, the unsaturated bond is not polarised, requiring polarisation by the M-X bond to enable insertion to occur. This scenario possesses a higher energy barrier to reaction, resulting in limited examples of such reactions and rates are often slow and regioselectivity is often poor. An example of this reactivity is the hydroamination of alkenes and alkynes by lanthanide amide species, L_2LnNR_2.[10-15] In contrast when $E \neq C$, for example an aldehyde, ketone (E = O), or an imine (E = NR), the reagent is already polarised across the unsaturated bond, assisting in coordination to the polarised M-X bond, lowering the energy barrier to reaction and leading to a wide variety of synthetic reactions.

These fundamental reactions can be used to construct catalytic cycles, examples of which are shown in Figure 1.3.

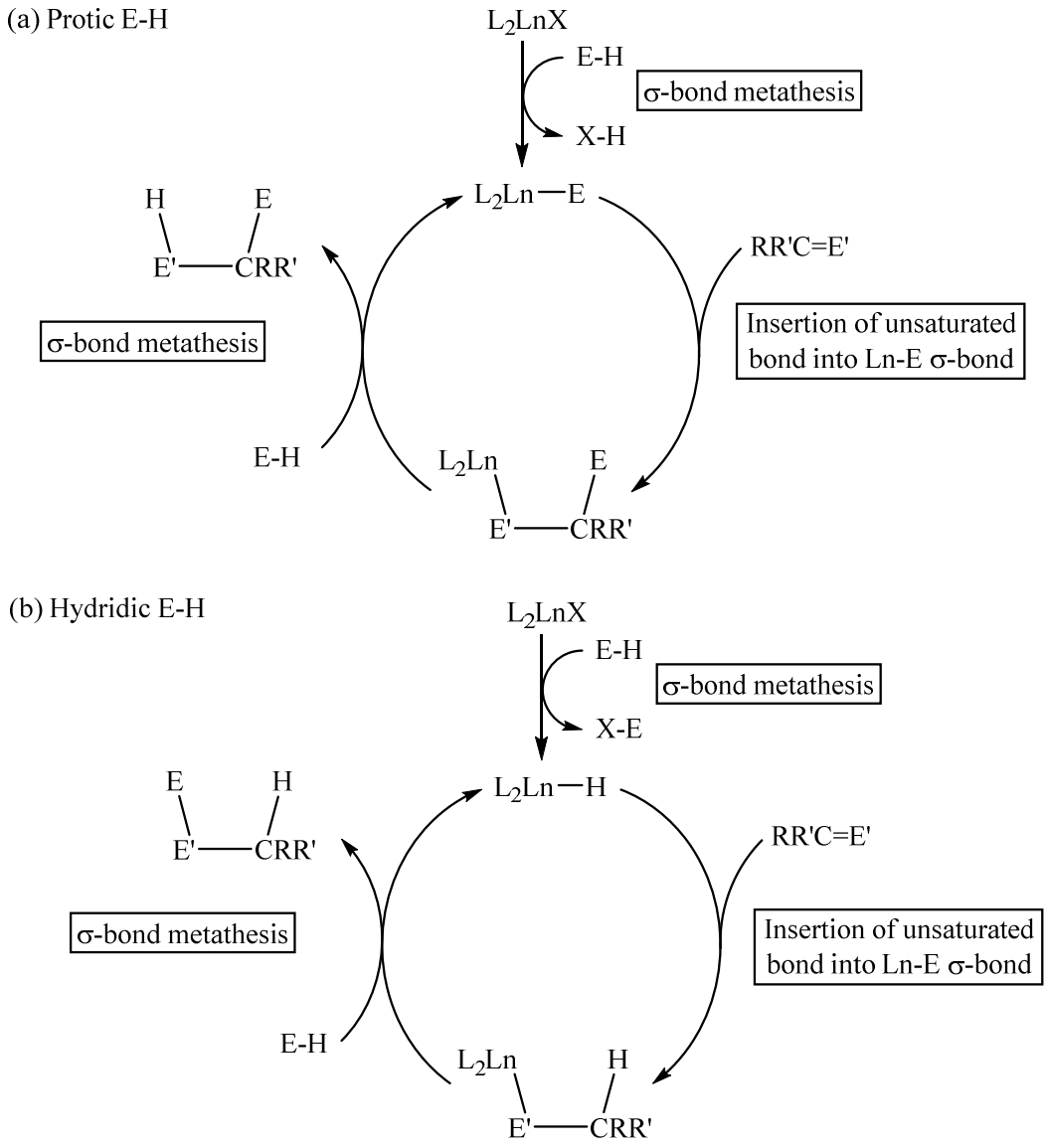

Figure 1.3: Generalised catalytic cycles for the reaction between the trivalent lanthanide precatalyst, L_2LnX, and reagents E-H and RR'C=E', mediated by steps involving σ-bond metathesis and insertion of an unsaturated bond into a M-E bond, in which E-H is protic **(a)**, and hydridic **(b)**.

Figure 1.3(a) demonstrates a system in which the lanthanide precatalyst, L_2LnX, reacts with a protic reagent, E-H, undergoing an initial protonolysis step via σ-bond metathesis. The catalytic cycle is composed of insertion of an unsaturated bond into the Ln-X bond, followed by a σ-bond metathesis, forming the product, HE'-CERR', and regenerating the L_2LnE species. When E-H is hydridic, however, the initial σ-bond metathesis results in the formation of a metal hydride, the active catalytic

species, producing a different product, EE'-CHRR', following sequential insertion and σ-bond metathesis steps.

L_2LnX compounds have since been demonstrated to mediate a wide array of synthetic reactions via schemes similar to those shown in Figure 1.3, including hydroamination, hydroboration, hydrophosphination and hydroalkoxylation of unsaturated C=C bonds as well as the polymerisation of low molecular weight olefins.[15-44]

This work raised the possibility of chemical change mediated by the redox inactive Group 2 metals via analogous σ-bond metathesis reactivity and insertion of unsaturated bonds into M-E σ-bonds via regimes similar to those shown in Figure 1.3. This supposition was subsequently proven to be correct, leading to a wealth of new Group 2 chemistry, characterising these species and their reactivity.[45-71]

In initial work which illustrated the potential of this reactivity, Westerhausen et al observed the insertion of 1,4-diphenylbutadiyne into the M-P bond of the homoleptic Group 2 phosphides, $[M\{P(SiMe_3)_2\}_2(THF)_4]$, **I**, where M = Ca, Sr and Ba, and benzonitrile into the M-P bond of the Group 2 phosphides and analogous amides $[M\{N(SiMe_3)_2\}_2(THF)_2]$, **II**.[50, 72-76] Styrene polymerisation reactions, mediated by multiple insertions of the alkene into the M-C bond of an intermediate organometallic species, were also shown to be accessible using Group 2 catalysts by virtue of Harder's highly reactive Group 2 benzyl complexes $[Ba\{C(Ph)_2(CH_2CH_2Ph)\}_2(THF)_2]$ **III** and $[M(DMAT)_2(THF)_2]$ **IV** (where M = Ca and Sr, and DMAT = 2-dimethylamino-α-trimethylsilylbenzyl).[77-80]

By analogy to the reaction of lanthanide species with protic reagents in Figure 1.2(a)(i), a common synthetic route to Group 2 organometallic species is via σ-bond metathesis/protonolysis in stoichiometric reactions between species such as the metal amides $[M[N(SiMe_3)_2]_2]_2$ **V** (where M = Mg, Ca, Sr and Ba) and reagents including alcohols, pyrroles, terminal alkynes and phosphines, yielding the corresponding metal alkoxides,[81-83] pyrrolide,[84] acetylides,[85-88] and phosphides,[74, 89-91] in addition to $HN(SiMe_3)_2$. This is shown in Figure 1.4.

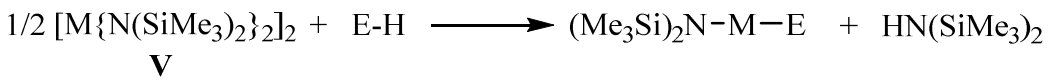

Figure 1.4: Synthesis of organometallic species via σ-bond metathesis using heavier Group 2 metal amides $[M[N(SiMe_3)_2]_2(THF)_x]$ **V** (where M = Mg, Ca, Sr and Ba).

In the case of stoichiometric reactions with hydridic substrates, for example silanes (R_3Si-H) or boranes (R_2B-H), mimetic of the lanthanide reactivity shown in Figure 1.2(a)(ii), a metal hydride is formed in addition to a new E-X bond.

Insertion reactions of unsaturated substrates into alkaline earth M-X bonds proceed in an analogous manner to that shown in Figure 1.2(b), displaying facile reactivity for substrates in which the substrate is polarised (i.e. E = O, N, X; E ≠ C). The following sections evidence heterofunctionalisation chemistry displayed by alkaline earth precatalysts involving polarised unsaturated substrates.

1.1.1 Group 2-Centred Hydroamination

Following the report of the calcium β-diketiminate complex, **VI** Figure 1.5, as a catalyst for polmerisation of *rac*-lactide by Chisholm et al,[92, 93] the Hill group demonstrated its effectiveness as a precatalyst for intramolecular hydroamination of aminoalkenes and aminoalkynes.[94-96] A series of Group 2 β-diketiminate, amide and alkyl complexes have subsequently been developed which are effective catalysts for intramolecular hydroamination of a range of aminoalkenes.[95-102] Examples of these complexes are shown in Figure 1.5.

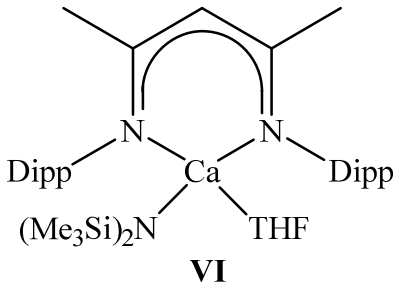

VI

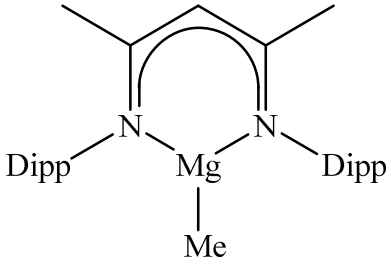

$[M\{N(SiMe_3)_2\}_2(THF)_2]$ $[M\{N(SiMe_3)_2\}_2]_2$ $[M\{CH(SiMe_3)_2\}_2(THF)_2]$

II **V** **VII**

(Where M = Mg, Ca, Sr, Ba)

Figure 1.5: Chisholm's calcium β-diketiminate complex, **VI**;[92, 93] and other Group 2 catalysts used for intramolecular hydroamination of aminoalkenes.[94, 95]

Following initial work on intramolecular hydroamination, the catalytic intermolecular hydroamination of alkenes, dienes and alkynes,[97, 103] was demonstrated using the metal amides **V**, and alkyls **VII** (where M = Ca, Sr). By analogy to the lanthanide chemistry of Marks, Figures 1.2 and 1.3,[8] a catalytic cycle with this protic substrate was proposed to occur by σ-bond metathesis and C=C bond insertion via a four-membered transition state,[96] shown in Figure 1.6, yielding exclusively the *anti*-Markovnikov product.

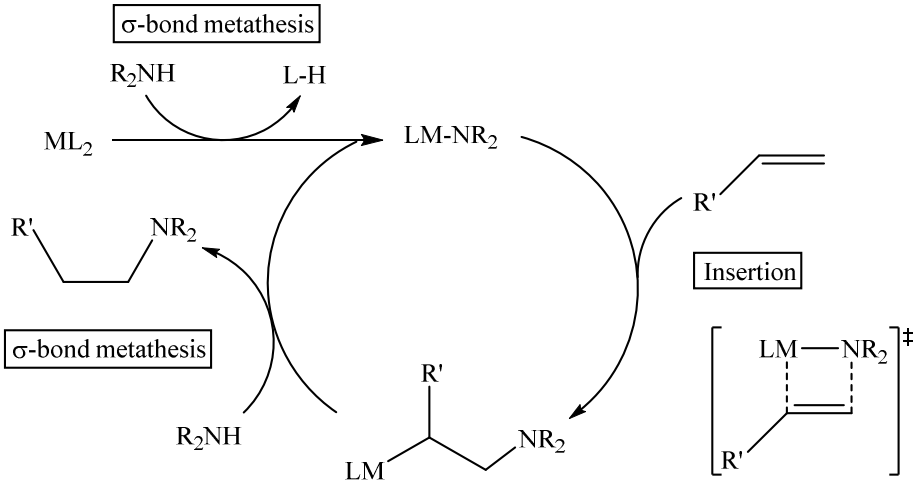

Figure 1.6: Proposed catalytic cycle for the catalytic hydroamination of alkenes by Group 2 amides **V** and alkyls **VII**.

The rate determining step was identified as the insertion of the alkene into the M-N bond, via the four-membered transition state shown in Figure 1.6. Kinetic investigations showed that the rates of these reactions displayed a much more marked dependence upon the identity of the Group 2 metal centre than comparable reactions catalysed by trivalent lanthanide species. This was attributed to the greater variation in ionic radius for the M^{2+} ions of Group 2 as the group is descended from Mg to Ba, causing a more pronounced change in charge density for the alkaline earth elements. The dependence upon the identity and charge density of the Group 2 metal centre results in a much more complicated trend in reaction chemistry than for the trivalent lanthanides Ln^{3+}. For these reactions it was found that for each system of catalysts the strontium congener yielded the most rapid reaction, followed by calcium. Reactions of the magnesium and barium congeners were found to be much slower, rationalised by the suggestion that a weaker polarising effect of these elements was a key factor in the rate determining insertion step.

The metal amides **II**, **V** and **VI** were also shown to be suitable catalysts for the intermolecular hydroamination of carbodiimides and isocyanates,[104, 105] whilst **VI** was shown to be a suitable catalyst for the intermolecular hydrophosphination of alkenes, alkynes and carbodiimides,[106, 107] proceeding via a mechanism analogous to that shown in Figure 1.6.

1.1.2 Group 2-Centred Hydrosilylation

Harder demonstrated hydrosilylation of alkenes using the heteroleptic calcium-DMAT **VIII** and homoleptic calcium- and strontium- DMAT complexes **IV**.[69, 100] Analogous to the cycle shown in Figure 1.3(b), a proposed catalytic cycle for this reaction is shown in Figure 1.7, featuring initial σ-bond metathesis steps with the hydridic Si-H, forming a metal silyl as the active catalytic species.

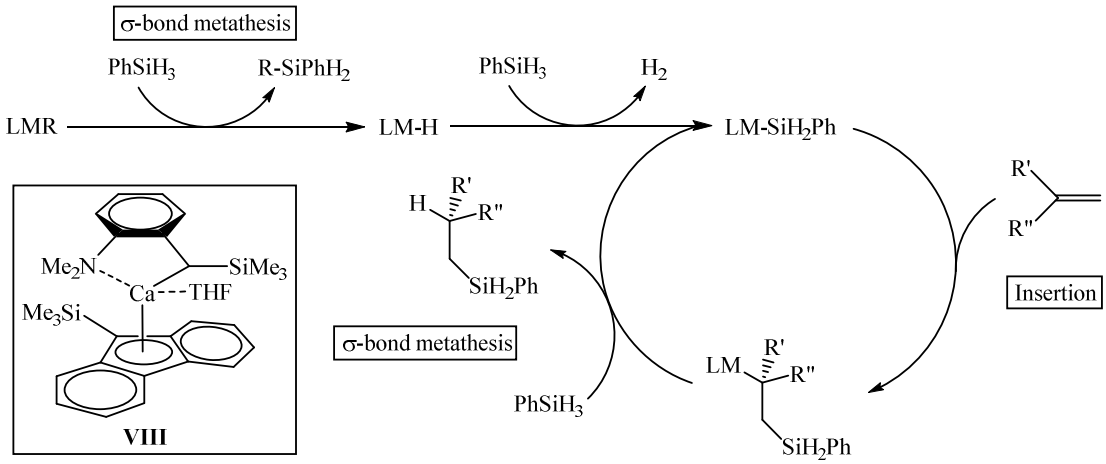

Figure 1.7: Harder's mechanism for hydrosilylation of alkenes,[69, 100] utilising heteroleptic, **VIII** shown by inset, and homoleptic, **IV**, 2-dimethylamino-*R*-trimethylsilylbenzyl (DMAT) complexes.

Insertion of the unsaturated alkene into the M-Si bond via a four-membered transition state, followed by σ-bond metathesis, produces the hydrosilylated product, in addition to reforming the metal silyl.

1.1.3 Group 2-Centred Dehydrogenative Silicon-Nitrogen Coupling

Sections 1.1.1 and 1.1.2 described catalytic reactions with protic N-H, and hydridic Si-H, bonds, in which the key bond-forming steps require the polarised insertion of an unsaturated bond to form the hydroaminated and hydrosilylated products respectively. Of greater potential generality is the cross-coupling of two sigma bonded substrates (E-H, E'-H) to form a new E-E' bond, with the elimination of a small molecule, H_2. The combination of a protic amine and hydridic silane with a suitable catalyst has thus provided a suitable prototype for such a dehydrocoupling reaction with formation of Si-N bonds and concomitant release of dihydrogen.

Using the homoleptic Group 2 amides **V**, Hill has reported the dehydrogenative silicon-nitrogen coupling of silanes and amines.[108] A catalytic regime can be constructed in which the Si-N bond formation and hydrogen release is mediated by σ-bond metathesis in which metal hydride and metal amide species are key intermediates. This is shown in Figure 1.8.

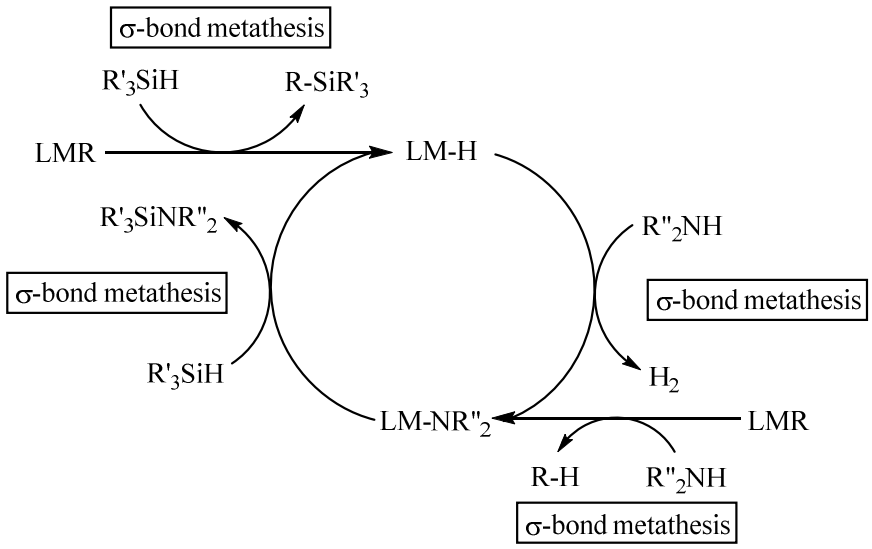

Figure 1.8: Catalytic dehydrogenative silicon-nitrogen coupling of amines and silanes via a cycle involving σ-bond metathesis.[108]

The kinetics of these silicon-nitrogen coupling reactions again evidenced a dependence upon the identity of the Group 2 metal centre, reminiscent of that observed in the catalysed hydroamination of alkenes described in Section 1.1.1. In this case, however, the calcium analogue displayed the highest catalytic activity, followed by strontium and magnesium. In addition, the rate law derived for the strontium-based reaction deviated from that found for the magnesium and calcium analogues, suggesting that divergent mechanistic pathways may operate which are dependent upon the system in question. The difference in efficacy of the various Group 2 catalysts towards hydroamination of alkenes was rationalised in terms of the change in charge density and polarisability of the M^{2+} metal centre. Although a different scenario, these factors can also be invoked to rationalise the observed differences in activity towards dehydrogenative silicon-nitrogen coupling.

The reactions described in this and Section 1.1.1 clearly display contrasting reactivity within a homologous series of Group 2 catalysts, with reaction paths which are sensitive to changes in the charge density and polarisability of the M^{2+} metal centre, in combination with steric and electronic effects imposed by both the supporting ligand and substrates. The combined characteristics of the metal centre and ligand also influence the tendency of the alkaline-earth metals to undergo

Schlenk redistribution, reducing the activity of the catalytic species. This redistribution equilibrium is shown in Figure 1.9.

$$2\ LMX \rightleftharpoons L_2M + MX_2$$

(Where M = Mg, Ca, Sr, Ba)

Figure 1.9: Schlenk equilibrium of heavier Group 2 complexes.

Although heteroleptic β-diketiminate complexes of magnesium are relatively stable to Schlenk equilibration, as the group is descended there is an increasing tendency towards the formation of homoleptic species. Indeed, the series of homoleptic β-diketiminate alkaline earth complexes have been reported by Harder.[60] Work by Piers to synthesise an "anilido-imine" ligand with properties similar to that of the β-diketiminate ligand,[109] and that of Sarazin in utilising the heavier Group 2 homologues of this ligand, **IX** shown in Figure 1.10, for hydroamination and hydrophosphonylation reactions have recently highlighted a system which could be utilised to investigate the reactivity of these heavier elements.[110, 111]

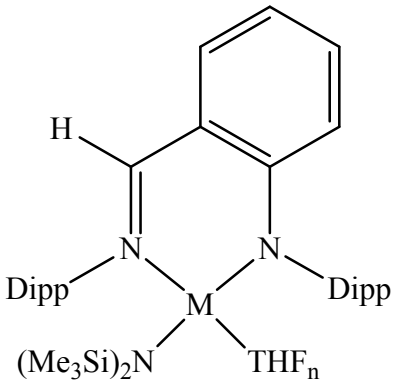

M = Ca, n = 1
M = Sr, n = 2
M = Ba, n = 2

Figure 1.10: Group 2 anilido-imine complexes utilised by Sarazin for heterofunctionalisation reactions.[110, 111]

Sarazin also observed kinetics which were metal-dependent, but in this case it was the barium complex which provided the fastest reaction in benchmark hydroamination catalysis.[110] This highlights once again not only the difference in character of the alkaline earth elements, but also that the ligand and reaction in question have a great bearing on reactivity trends.

1.1.4 Hydrocarbon-Soluble Alkaline Earth Metal Hydrides

Many catalytic cycles based on transition metal or main group elements require the formation of hydride species as key intermediates. The hydrides of alkaline earth elements, often hydrocarbon-insoluble solids, had previously only been inferred, so the β-diketiminato-calcium hydride species reported by Harder,[112] **X** shown in Figure 1.11(a), was of fundamental importance in corroborating proposed reaction schemes. The reactivity of this hydride with a range of unsaturated substrates was explored,[45, 61, 62, 113, 114] selected examples of which are shown in Figure 1.11(b).

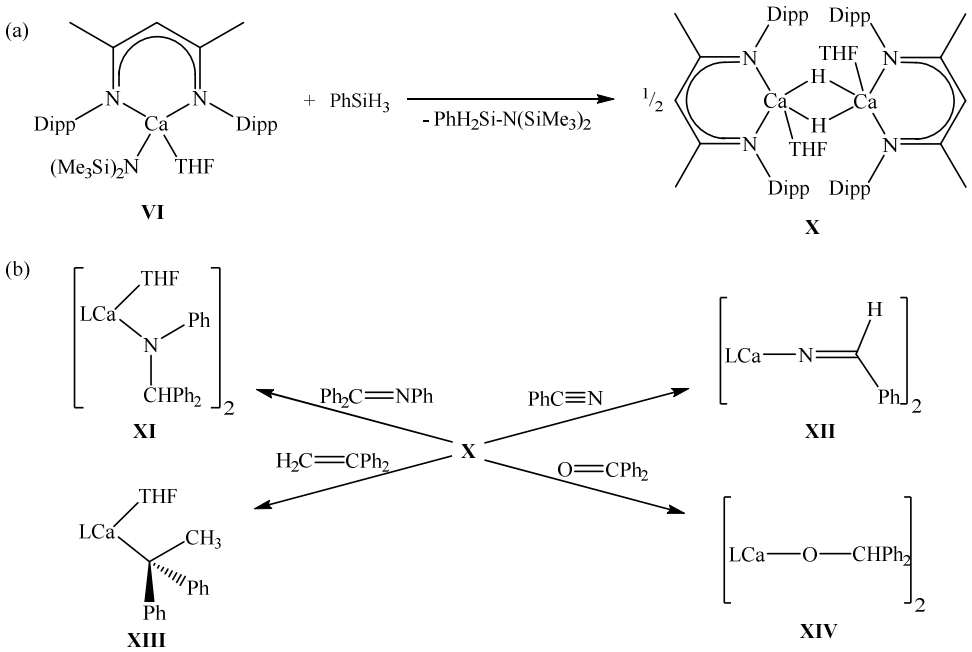

Figure 1.11: (a) β-diketiminato-calcium hydride, **X**, reported by Harder;[112] (b) Reaction of **X** with unsaturated substrates.[61] (L = β-diketiminate ligand)

By an analogous method, Gibson's *n*-butyl-β-diketiminato-magnesium species, **XV**,[115] was used by Jones to synthesise the dimeric β-diketiminato-magnesium hydride, **XVI**.[116] In a landmark study alkaline earth chemistry was taken beyond the confines of the +2 oxidation state when Jones also isolated the first Mg(I) species by reduction of Mg^{2+} complexes with potassium metal, **XV** and **XVI** Figure 1.10.[4, 116, 117]

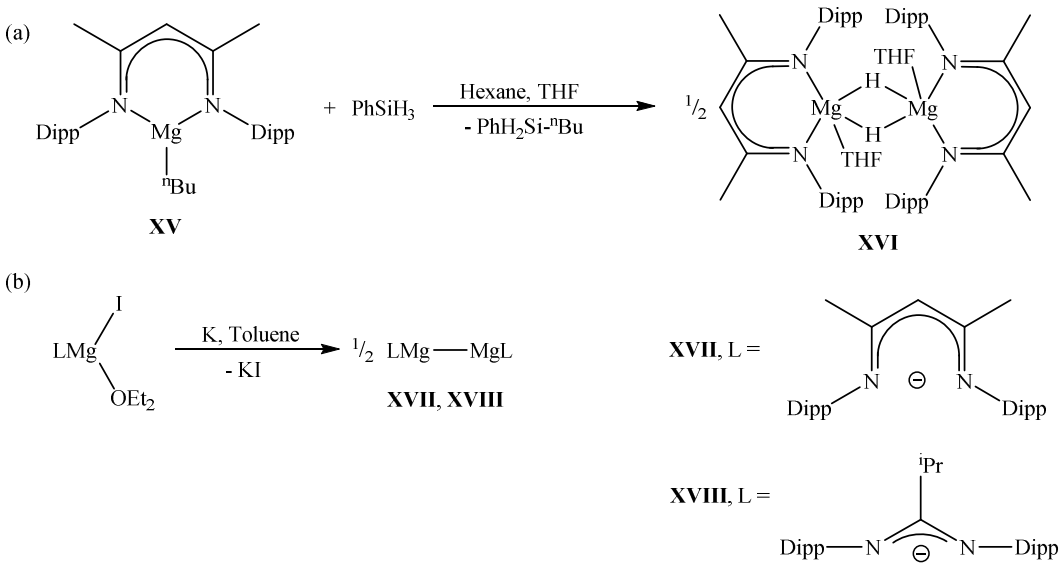

Figure 1.12: (a) β-diketiminato-magnesium hydride, **XVI**, reported by Jones;[116] (b) Jones' magnesium(I) species.[4, 116]

The dimeric β-diketiminato-magnesium(II) hydride, **XVI**, and -magnesium(I) complex, **XVII**, have been utilised as effective reducing agents for a range of reagents including carbodiimide, isocyanate, azobenzene, azide, nitrile and benzophenone.[118-120] Selected examples are shown in Figure 1.13.

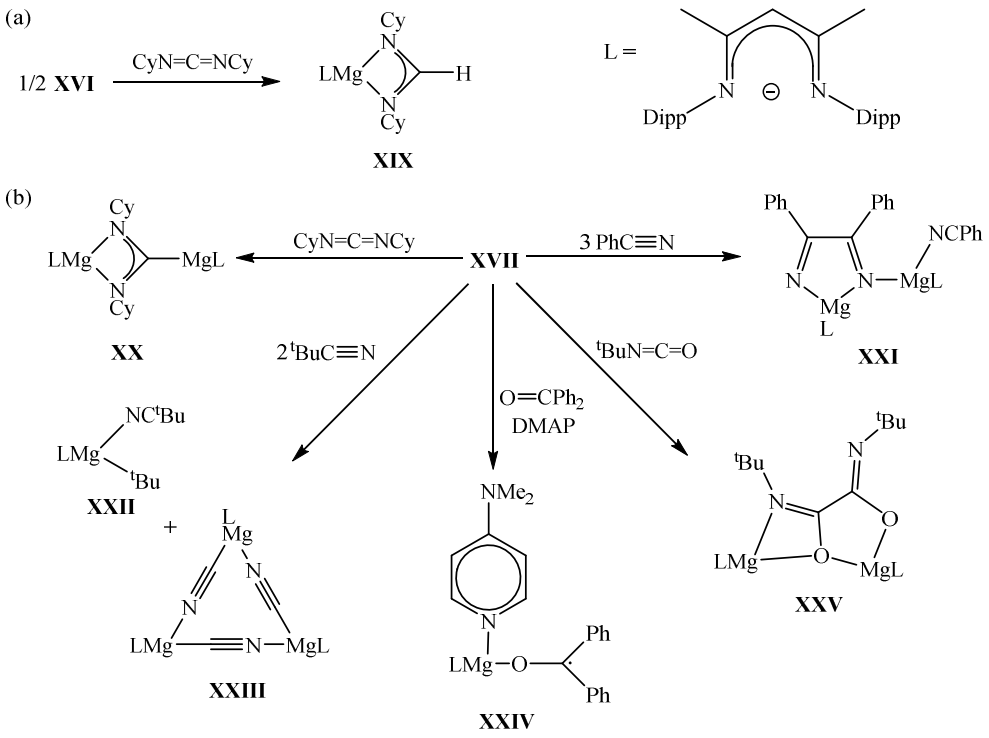

Figure 1.13: Reductive chemistry of the β-diketiminato-magnesium(II) hydride **XVI**, (a), and -magnesium(I) complex **XVII**, (b).[118-120]

Figure 1.13 demonstrates some of the novel chemistry exhibited by these highly reactive species, including the facile C-C bond formation in reactions of **XVII** with nitrile (**XXI**), and isocyanate (**XXV**) substrates.

Alkaline earth complexes can be utilised to facilitate an array of novel syntheses, such as the unprecedented calcium-mediated reduction and P-P coupling of triphenylphosphine oxide or diphenylphosphine oxide by **V**, **VI** and **VII** in the presence of phenylsilane, reported by Hill.[121] Although no mechanism was postulated for this reaction, initial formation of a phosphine oxide adduct **XXVI** (Figure 1.14) is followed by what is believed to be discrete P-C bond cleavage to liberate benzene in the case of triphenylphosphine oxide, or hydrogen in the case of diphenylphosphine oxide, reduction of the P(V) centre and ultimate formation of the P-P coupled product $Ph_2P\text{-}PPh_2$.

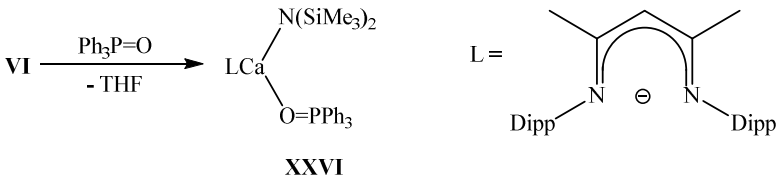

XXVI

Figure 1.14: Adduct formation between **VI** and triphenylphosphine oxide.[121]

Although not yet as wide-ranging as transition-metal catalysis, the preceding discussion demonstrates some of the depth and diversity of chemistry displayed by alkaline earth complexes.

1.2.1 Hydrogen Storage and Amine Boranes

As the modern world seeks to utilise more sustainable and environmentally friendly sources of energy and achieve a reduced dependence on fossil fuels, hydrogen fuel sources and associated technologies have received a great deal of interest and investment. An area which has received particular attention is that of transportation, aiming to reduce the use of petrol and diesel for vehicular use.[122-124] For any new fuel source to replace petrol it must match or surpass this energy-dense, easily stored fuel which is quickly dispensed into vehicles, imposing tough performance criteria that any new fuel must satisfy. The direct utilisation of gaseous hydrogen as a fuel encounters problems associated with storage, stability, its low density and consequent low energy density. To replace one litre of petrol, approximately 762 L of hydrogen (at 1 bar) is required, which is unfeasible for vehicular use.[125] At 150 bar the volume of hydrogen required to replace 1L petrol is a more reasonable 6 L (approx.), but the weight penalty due to the use of steel storage containers, energy required for compression and hydrogen losses due to escape and expansion present possibly insurmountable issues. There are also safety concerns associated with the use of pressurised cylinders of a flammable gas in vehicles. Therefore systems have been explored in which the hydrogen is bound to a carrier medium, creating a more stable and safer source of hydrogen, which may be evolved in a controlled manner as hydrogen gas for use as a fuel. This approach encompasses both physical adsorption technologies including carbon nanotubes and metal organic frameworks (MOFs),[126-136] and chemical storage via metal hydrides,[137-139] ammonia,[140-142] formic acid and amine boranes.[143-145] Each of these potential hydrogen storage methods has

associated issues, commonly energy density and associated weight, which need to be overcome to be considered a viable system.

Over the last 10 years amine boranes, in particular ammonia borane, have received great attention as potential hydrogen fuel sources.[146-154] Most notably the US Department of Energy has invested a great deal of attention to amine boranes over the last 30 years for application as a civil and military fuel source, commissioning research related to all areas concerned with its use.[155-167] Ammonia borane (AB, **XXVII**) is structurally the simplest amine borane molecule and, at 19.6 % hydrogen by weight, is the most hydrogen-rich amine borane, releasing potentially three equivalents of hydrogen if fully dehydrogenated, shown by Figure 1.15.

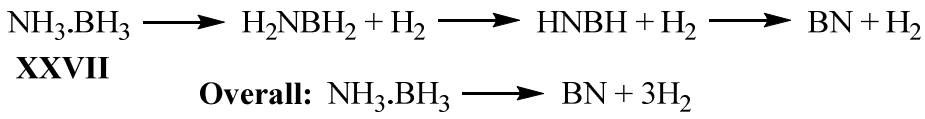

Figure 1.15: Equation for the dehydrogenation of ammonia borane (AB) to liberate three equivalents of hydrogen.

Although isoelectronic to ethane, the B-N bond in ammonia borane is polarised and the molecule bears hydrogen atoms at nitrogen with protic character while at boron they are best characterised as hydridic due to the differing effective nuclear charges (electronegativities) of the Group 13 and Group 15 elements. This is shown in Figure 1.16.

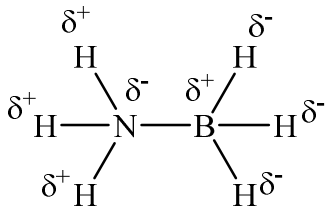

Figure 1.16: Ammonia borane, (AB), isoelectronic to ethane but possessing hydridic and protic hydrogens.

1.2.2 Hydrogen Evolution Via Thermolysis

Hydrogen evolution occurs via thermolysis of AB, requiring temperatures of 120 - 300 °C to release two equivalents of hydrogen and in excess of 1200 °C to release the final equivalent of hydrogen with formation of boron nitride.[168, 169] These temperatures required for thermolysis of pure AB are impractical for hydrogen evolution in vehicular applications and have prompted investigation of the thermolysis of metal amidoboranes of Groups 1 and 2.[170] Although the first metal amidoborane, sodium amidoborane,[171] was reported in 1938 it was not until around 70 years later that an alkali-metal amidoborane, [$LiNH_2BH_3$], was suggested and investigated as a hydrogen storage material. Amidoboranes are synthesised via either ball milling,[172] or reaction in THF of a mixture of ammonia borane and the metal hydride or amide, producing the amidoborane as a powder directly or by removal of THF under vacuum,[173] Figure 1.17.

(a) $Na + NH_3 + Et_2O.BH_3 \longrightarrow NaNH_2.BH_3 + Et_2O + {}^1/_2\, H_2$

(b) $NaH + NH_3.BH_3 \xrightarrow{THF/mill} NaNH_2.BH_3 + H_2$

(c) $NaNH_2 + NH_3.BH_3 \xrightarrow{THF} NaNH_2.BH_3 + NH_3$

Figure 1.17: (a) Reaction for the first reported metal-amidoborane;[171] (b) and (c): Alternative reactions to produce sodium amidoborane via the hydride (b), or amide (c).[173]

The hydrogen storage potential and thermolysis behaviour of amidoboranes of lithium and the alkaline earth metals magnesium, calcium and strontium, as well as mixed metal amidoboranes have also been investigated.[114, 174-206] Although the presence of impurities can affect the hydrogen release temperature, these systems consistently show onset temperatures for hydrogen evolution which are lower than that of pure AB.[173, 207, 208] For utilisation in fuel cells, however, a clean supply of hydrogen is required, which is free of volatile products that would poison the fuel cell. The process of thermolysis of these compounds does not lend itself to control over volatile products and the requirement of temperatures above 100 °C are, thus, impractical.

1.2.3 Metal-Assisted Hydrogen Release

Attempted methods to provide greater control over the formation of volatile products and further reduce the reaction temperature include mechanical stirring of AB with $CoCl_2$, $NiCl_2$ or $CuCl_2$, which has been reported to release hydrogen free of borazine and ammonia impurities.[209] The thermolysis behaviour of AB has also been investigated in the presence of the range of cobalt halides.[210] Addition of lithium imide or nitride to AB has also been reported to effect hydrogen release, reacting spontaneously in the solid state but requiring heating when in solution (THF).[211, 212] This process is less desirable, however, due to the release of ammonia.

Metal-catalysed hydrolysis of AB in protic solvents at ambient or near-ambient temperatures has been extensively investigated using Fe,[213-216] Ru,[217-225] Co,[218, 223, 226-241] Rh,[222, 228, 242-248] Ir,[228] Ni,[223, 227, 231, 232, 249-257] Pd,[222, 223, 225, 226, 251, 258-263] Pt,[222, 251, 264] and Cu,[227, 265, 266] as either the pure metals, as the oxides or chlorides, supported on carbon, silica, titania, alumina or zeolite, or present as nanoparticles or nanoclusters. Mixed metallic systems incorporating Pd, Ni, Pt, Au, Ag, Sn, Co, Cu, Ir, Ru have also been described.[219, 226, 267-270]

The homogeneous catalytic dehydrocoupling activity of a wealth of transition metal complexes, including those of V,[271] Cr,[271-274] Mo,[275] W,[274-276] Mn,[271, 274] Re,[277, 278] Fe,[213, 279-281] Ru,[218, 281-300] Rh,[291, 299, 301-316] Ir,[291, 296, 299, 304, 310, 317-326] Ni,[327-331], or Pd,[299, 332-334] has been explored in hydrocarbon solvents, utilising a wide variety of organo-amineboranes (ammonia borane in addition to primary, secondary and tertiary amineboranes). Examples of such complexes are shown in Figure 1.18.

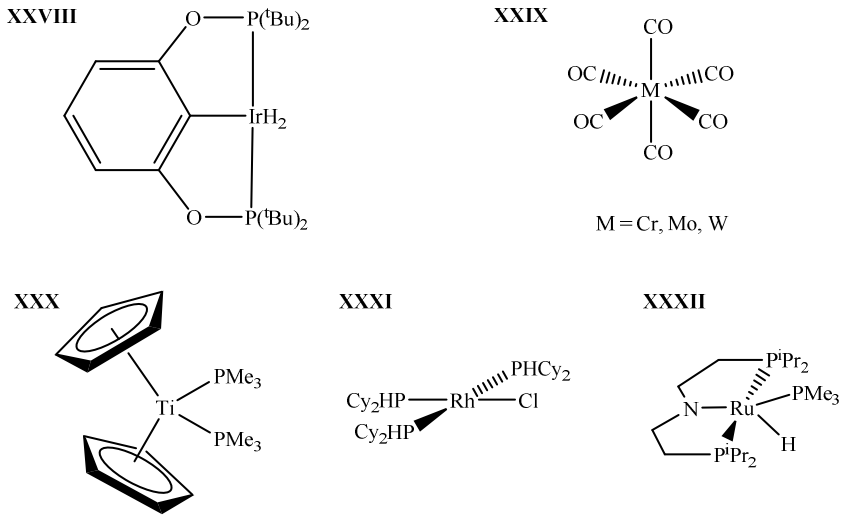

Figure 1.18: Brookhart's IrH_2POCOP pincer complex, **XXVIII**; Shimoi's Group 6 photoactivated metal carbonyl complex, **XXIX**; Manners' titanocene complex, **XXX**; Analogue of Wilkinson's complex, **XXXI**; Ruthenium pincer complex, **XXXII**.[273, 290, 294, 296, 313, 335]

Dehydrocoupling using catalysts incorporating these metals is proposed to occur via processes involving redox changes. Manners' work on reactions between the titanocene derivatives **XXX** and $Cp_2TiCl_2/2^nBuLi$ **XXXIII** and the secondary amine borane dimethylamine borane (DMAB, **XXXIV**) provided the first comprehensive mechanistic study of transition-metal dehydrocoupling of amine boranes.[335, 336] Although the active catalytic species in these reactions is not known, experimental observations and kinetic experiments led to the proposed mechanism shown in Figure 1.19.

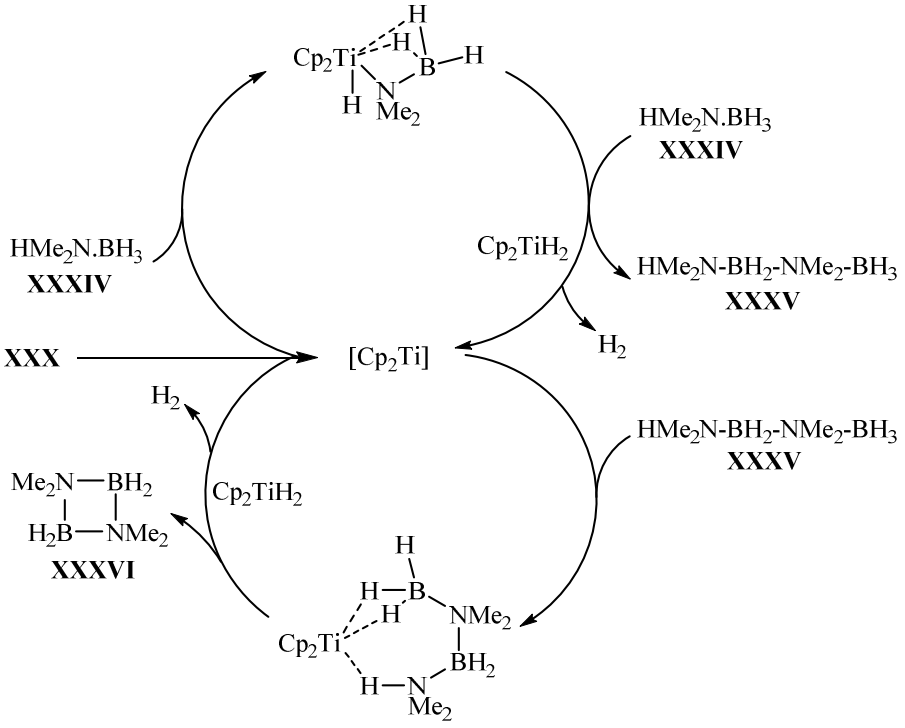

Figure 1.19: Manners' proposed mechanism for the dehydrocoupling of DMAB (**XXXIV**) by the titanocene complex **XXX**.

In this proposed scheme, HMe_2N-BH_2-NMe_2-BH_3 **XXXV** is a key intermediate, formed via interaction of DMAB and $Cp_2Ti(H)(NMe_2BH_3)$ with the formation of a new B-N bond by an undescribed process at the metal centre. **XXXV** dissociates from the metal centre and the resultant titanocene dihydride complex loses dihydrogen to regenerate the active catalyst. The cyclic dimer $[Me_2N\text{-}BH_2]_2$ **XXXVI**, or cycloborazane to use Wiberg's nomenclature,[337] is formed from **XXXV** in a metal-mediated process. This mechanism, derived from experimental observations, is in contrast to the mechanism suggested by Ohno based upon computational studies,[338] who suggested that **XXXV** is not formed in the reaction and is therefore not an intermediate in the formation of **XXXVI**. Rather, **XXXVI** results from an off-metal cyclo-dimerisation of $Me_2N{=}BH_2$ **XXXVII**, formed in the reaction between the active catalyst and DMAB. Manners' experimental observations suggest that **XXXVII** is stable to cyclo-dimerisation when a catalytic species is not present. Schneider's mechanistic investigation of the dehydrocoupling activity of the ruthenium pincer complex **XXXII** also identifies **XXXV** as an

intermediate in the formation of **XXXVI**, but suggests that **XXXV** and **XXXVII** are formed via competitive reactions, shown in Figure 1.20.[294]

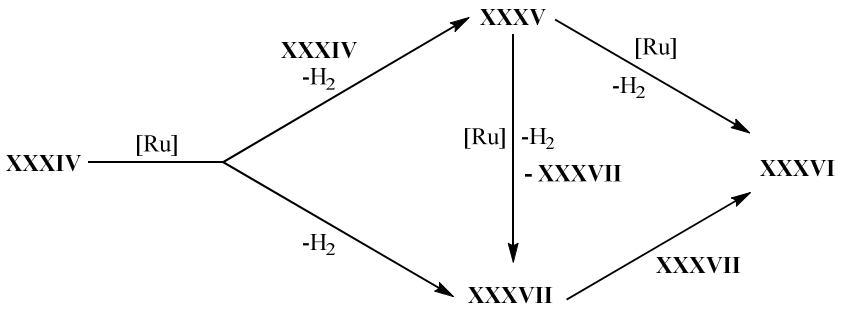

Figure 1.20: Schneider's proposed mechanism for dehydrocoupling DMAB/**XXXIV** using a ruthenium pincer complex **XXXII**, suggesting competitive reaction pathways.[294]

In this regime it is proposed that **XXXVII** undergoes an off-metal cyclo-dimerisation to form **XXXVI**, in addition to the metal-mediated dehydrocyclisation of **XXXV** in another competitive pathway. Once again, the mechanism of B-N bond formation in generating **XXXV** is not accounted for.

Despite the differences in transition metal-mediated dehydrocoupling activity, dependent upon ligand characteristics, metal centre and amine borane, Weller, Lloyd-Jones and co-workers attempted to derive a unified dehydrocoupling scheme,[316] building upon previous mechanistic studies.[290, 325, 336, 339, 340] Although the investigation was simplified by a focus on reactions between precatalysts based upon $[Rh(PCy_3)_2]^+$ and DMAB, complicated time-dependent concentration profiles resulted, as observed by Manners' with titanocene complexes.[336] Kinetic modelling highlighted the presence of a previously unexpected catalytic species, $Rh(PCy_3)_2H_2Cl$, which was subsequently investigated after rational synthesis of the complex.[315] A general mechanism was formulated for the transition metal catalysed dehydrocoupling of DMAB, shown in Figure 1.21. It is noteworthy that it does not present mechanistic detail regarding the key B-N bond formation step, which is of fundamental importance to the formation of the dehydrocoupled products. In an equilibrium reaction **XXXVII** is implicated along with a metal dihydride species and DMAB in the formation of **XXXV**, involving a necessary B-N bond formation,

however, how this occurs is not considered. In this scheme an off-metal dimerisation of **XXXVII**, which is formed by several reactions in the proposed scheme, is proposed as a route to formation of **XXXVI** in addition to metal-mediated dehydrocyclisation of **XXXV**.

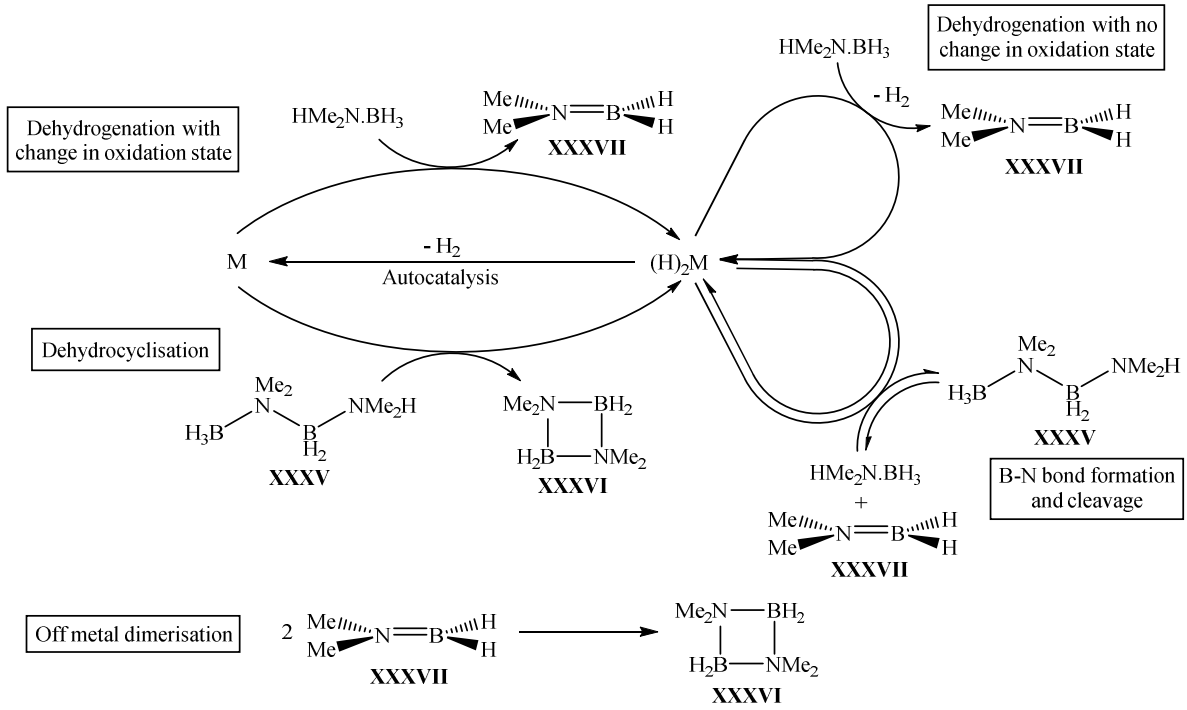

Figure 1.21: General scheme for dehydrocoupling of DMAB using transition metal catalysts, proposed by Weller et al.[316]

1.2.4 Dehydrocoupling of Amine Boranes with Frustrated Lewis Pairs

The research described in the previous section highlights the fundamental importance of metal species in mechanisms of hydrogen release from amine boranes which are thermally accessible for transportation. Metal-free processes of dehydrocoupling have also been explored, most notably with "frustrated" Lewis pairs (FLPs), reactive complexes incorporating a Lewis-acid/Lewis-base pair that is either too sterically encumbered to react directly, or which exist in a metastable form. The first example of an FLP-induced amine borane dehydrocoupling was provided by Bercaw at al,[341] who described the stoichiometric dehydrocoupling of DMAB and AB with $P^tBu_3/B(C_6F_5)_3$ at room temperature. This was followed

shortly after by Manners' stoichiometric dehydrocoupling of DMAB by a $^{n}Bu_3SnOTf$/2,2,6,6-tetramethylpiperidine FLP,[342] shown Figure 1.22.

(a) $P^{t}Bu_3 + B(C_6F_5)_3 + HR_2N.BH_3 \xrightarrow[25°C]{C_6D_5Cl} (R_2NBH_2)_x + [^{t}Bu_3PH][HB(C_6F_5)_3]$

R = Me, x = 2
R = H, x = n

(b)

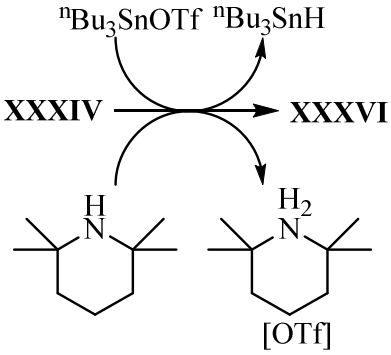

Figure 1.22: (a) First reported dehydrocoupling of amine borane by a $P^{t}Bu_3/B(C_6F_5)_3$ "frustrated" Lewis pair (FLP) by Bercaw;[341] (b) Manners' dehydrocoupling of DMAB with a $^{n}Bu_3SnOTf$/2,2,6,6-tetramethylpiperidine FLP.[342]

In subsequent "FLP-inspired" work, Wass showed that the titanocene complex, **XXXVIII** shown in Figure 1.23, could be employed for the dehydrocoupling of DMAB.[343]

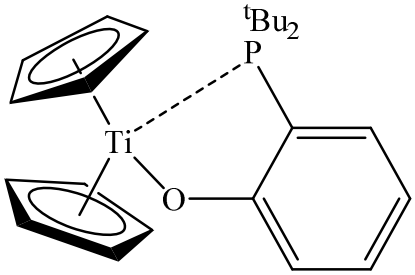

Figure 1.23: The first FLP-catalysed dehydrocoupling of amine borane, using a titanocene-phosphinoaryloxide **XXXVIII**.[344]

1.3 Dehydrocoupling of Amine Boranes by d^0 Complexes

Despite the advances in transition metal amine borane dehydrocoupling catalysis there are relatively few examples of the use of d^0 metal catalysts of Groups 1-2 and

the early transition metals in Groups 3-5. In addition to the use of **VI** and **V**, selected examples are shown in Figure 1.24.

XXXIX

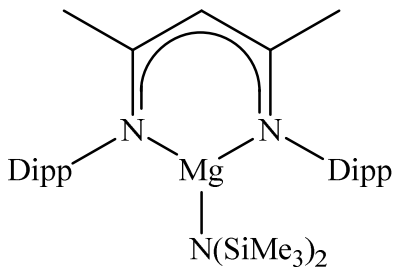

XL

$Sc(N(SiHMe_2)_2)_3(THF)_2$

XLI

$Y(N(SiMe_3)_2)_3$

XLII

(a) $Al(N^iPr_2)_3$

(b) $E(NMe_2)_3$

E = Al, Ga

Figure 1.24: Examples of d^0 metal pre-catalysts used for dehydrocoupling of amine boranes.[345-349]

Research by Harder and co-workers has focused on Group 2 β-diketiminate complexes of calcium and magnesium, **X** and **XXXIX**, forming dimeric β-diketiminato-Group 2 metal complexed amidoboranes,[114, 176, 202, 203, 205, 350] whilst Jones has used his magnesium(I) dimer **XVII** in reactions with AB to form a β-diketiminato-magnesium amidoborane.[204] The Hill group has also utilised Group 2 metals,[351, 352] in addition to Sc **XL** and Y **XLI** of Group 3.[346] Recent work by the groups of Chen (Y^{III} and Lu^{III} species) and Okuda (Y^{III} and La^{III} hydrides) further demonstrates the dehydrocoupling activity of such species whilst also highlighting the effect of supporting ligation on reactivity towards amine boranes.[353, 354] Wright's research using Group 13 Al^{III} and Ga^{III} **XLII** species, in addition to $LiAlH_4$, and Harder's use of a β-diketiminate supported Al^{III} hydride, has broadened the range of d^0 species investigated, with Wright reporting that these p-block complexes exhibit transition metal mimetic reactivity.[347-349, 355, 356] The research of Okuda and Wright also demonstrates that ligands are not always innocent in the reaction with amine boranes, especially when the ligands are nitrogen derivatives.[347-349, 354, 355] Baker's published work with a Ni carbene system documents the dehydrocoupling of DMAB by a Cu^I carbene complex but only in the supplementary information to the paper, demonstrating dehydrocoupling to **XXXVI** by this complex but giving no other information regarding its activity. As a closed shell d^{10} species, the mechanism of dehydrocoupling by a Cu^I complex would provide an interesting comparison to that of d^0 species.

Dehydrocoupling by d^0 metal catalysts is proposed to deviate from the generalised scheme for transition metals, shown in Figure 1.21. The limited range of accessible oxidation states for these d^0 species effectively discounts catalytic pathways involving oxidative addition and reductive elimination steps, which are commonplace for transition metals. Instead, catalysis may be expected to proceed via sigma bond metathesis steps and/or polarised insertion, as introduced in Section 1.1. Catalysts based upon the group 4 metals Ti,[335, 338, 357-360] Zr,[336, 360-362] and Hf,[336, 361, 363] have been explored, but whilst the presence of d^0 species is implicated in catalytic cycles for these species, oxidation state changes of the metal centre occur, necessitating the presence of species which are no-longer d^0, as evidenced by Manners' proposed mechanism in Figure 1.19. The relative lack of mechanistic characterisation of d^0-metal catalysed dehydrocoupling and the divergence from that of transition metal-mediated dehydrocoupling highlights the importance of such investigations.

Comparison of the dehydrocoupling reactivity of alkaline earth elements to transition metals reveals that alkaline earth catalysed dehydrocoupling proceeds far more slowly and requires higher temperatures. Despite positive comparisons of cost and availability, this decrease in reactivity ensures that it is unlikely that technology would ever be developed using Group 2 metals. The reduced reactivity of these metal complexes, however, presents an opportunity to more easily investigate and characterise the fundamental characteristics and mechanisms involved, thus enabling valuable insight into amine borane dehydrocoupling reactivity in general.

The report by the Hill group of stoichiometric reactions between **VI**, diphenylamine and 9-borabicyclo[3.3.1]nonane (9-BBN),[364] shown in Figure 1.25, with formation of a new boron-nitrogen bond, provided the first evidence that d^0 species could potentially dehydrocouple amine boranes, with concomitant B-N bond formation.

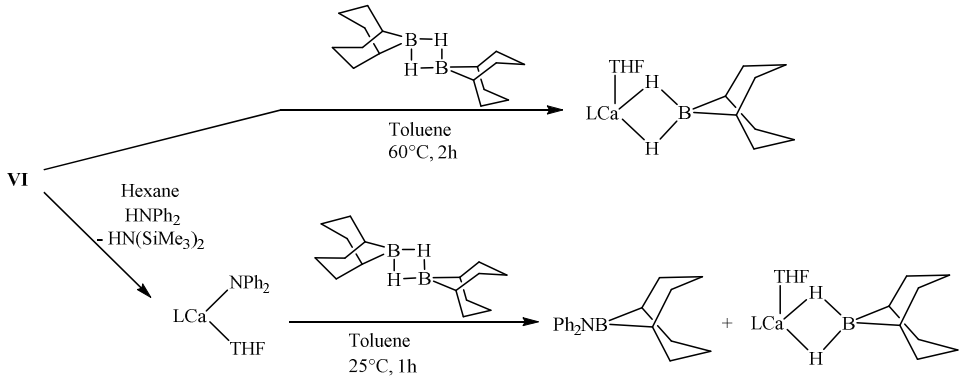

Figure 1.25: Stoichiometric reactions of β-diketiminato calcium amide, **VI**, diphenylamine and 9-borabicyclo[3.3.1]nonane (9-BBN).[364] (L = β-diketiminate).

The reaction was expected to proceed via a scheme mediated entirely by σ-bond metathesis, similar to that shown earlier in Figure 1.8 for dehydrogenative silicon-nitrogen coupling arising via σ-bond metathesis reactivity with the Si-H and N-H bonds. The report suggested that these boron-nitrogen coupling reactions could be extended to a catalytic regime and proposed a mechanism based upon σ-bond metathesis reactivity with the B-H and N-H bonds.

Harder et al subsequently reacted the calcium β-diketiminato hydride **X** with AB and primary amine boranes, proposing a step-wise loss of H_2, in which an initial protonation step is followed by thermally induced B-N bond formation, producing a dimeric β-diketiminato calcium complex of a $[RN\text{-}BH\text{-}NR\text{-}BH_3]^{2-}$ ion.[114] This is shown in Figure 1.26.

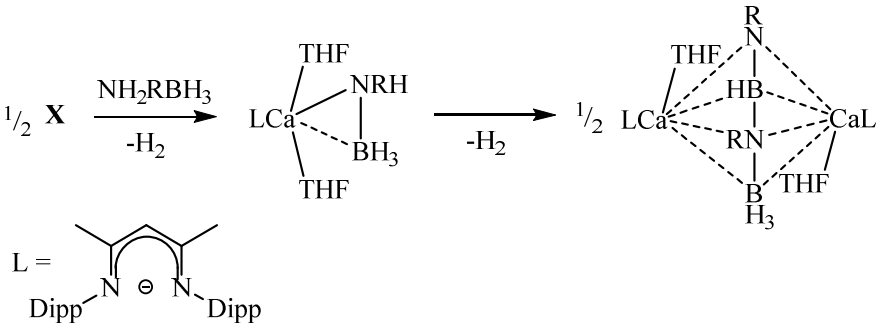

Figure 1.26: Harder's reported formation of a dimeric β-diketiminato calcium complexed $[RN\text{-}BH\text{-}NR\text{-}BH_3]^{2-}$ ion. (R = H, Me, ^{i}Pr).[114]

Following this initial report, the reactivity was extended to the primary amine borane (Dipp)$NH_2.BH_3$ **XLIII**.[203] With the greater steric bulk of the Dipp group in **XLIII** no dimerisation occurred, producing a β-diketiminate coordinated imidoborane. This is shown in Figure 1.27.

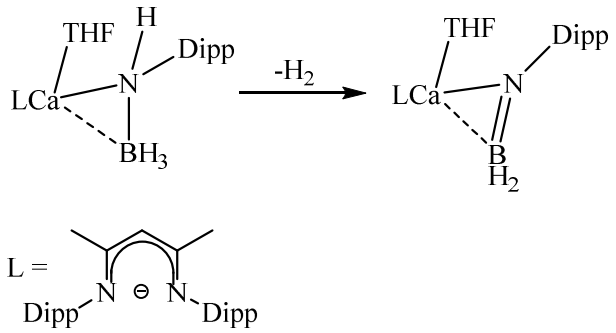

Figure 1.27: Formation of a β-diketiminato coordinated imidoborane with 2,6-di-*iso*-propylaniline borane, **XLIII**.[203]

The work of Harder in forming the β-diketiminato calcium-supported imidoborane species shown in Figure 1.27, featuring an unsaturated B=N bond, suggested that the mechanism may not be confined to σ-bond metathesis reactivity alone. In the light of the earlier work shown in Figure 1.25, in which a new B-N bond was proposed to form via a scheme consisting exclusively of σ-bond metathesis reactivity, this was an unexpected finding, prompting further investigation by the Hill group.

Following the lead of Harder's work with amine boranes, research in the Hill group was conducted using the less complex secondary amine boranes, enabling mechanistic insight and characterisation to be carried out more easily. Initial investigations into amine borane reactivity by the Hill group were conducted using the magnesium compound **XV** and dibutylmagnesium **XLIV**.[351]

Compounds **XV** and **XLIV** were reacted with two and four equivalents of DMAB respectively, resulting in compounds containing a magnesium coordinated $[H_3BNMe_2BH_2Me_2N]^-$ ion (compounds **XLV** and **XLVI** respectively in Figure 1.28). This ion coordinates via a Mg-N bond and interactions with hydrides of the terminal BH_3 unit.

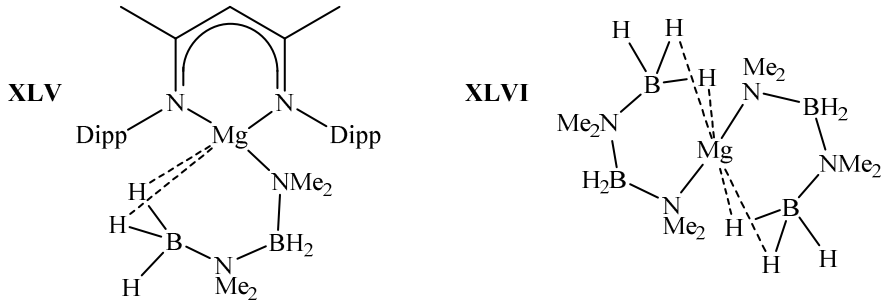

Figure 1.28: Compounds **XLV** and **XLVI**, magnesium-coordinated $[H_3BNMe_2BH_2Me_2N]^-$ ions formed by addition of four and two equivalents of DMAB to compounds **XIII** and **XIV** respectively.

On heating, the respective triplet and quartet ^{11}B NMR resonances of the magnesium-coordinated species were seen to disappear and be replaced by a triplet resonance attributable to **XXXVI**. This was proposed to occur via an intramolecular σ-bond metathesis and an effective δ-hydride elimination step, producing **XXXVI** and the magnesium hydride species **XVI**. This is shown in Figure 1.29.

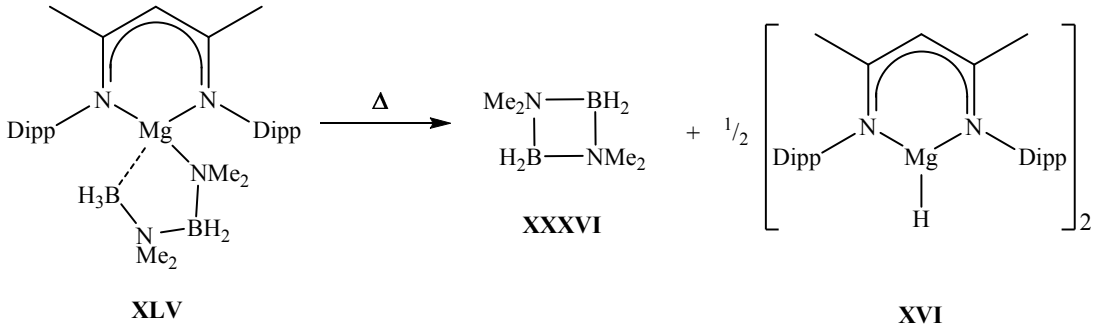

Figure 1.29: Formation of $[H_2BNMe_2]_2$, **XXXVI**, and magnesium hydride species, **XVI**, on heating **XLV**.

Further investigation highlighted the possibility that **XVI** could take part in a catalytic pathway featuring consecutive protonolysis and σ-bond metathesis. This was proven experimentally, by a 5 mol % catalytic reaction resulting in the formation of the cyclic dimer along with small quantities of the diamineborane $HB(NMe_2)_2$ **XLVII**, and a resonance attributed to the coordination of a single DMAB unit by the magnesium centre which was observed throughout the reaction. The formation of **XLVII** was attributed to a parallel reaction pathway in which the coordinated $[H_3BNMe_2BH_2Me_2N]^-$ ion undergoes β-hydride elimination followed by

loss of BH_3. It might be expected that this BH_3 unit would result in the appearance of a magnesium tetrahydridoborate resonance, but this was not observed in the ^{11}B NMR spectrum. The lack of this resonance was attributed to the as yet unproven formation of gaseous B_2H_6.

Analogous reactions with calcium species showed the formation of the unsaturated **XXXVII**, species as a triplet at around 36 ppm in the ^{11}B NMR spectrum. The observation of these species during catalytic reactions led to the construction of the proposed DMAB dehydrocoupling reaction scheme shown in Figure 1.30.

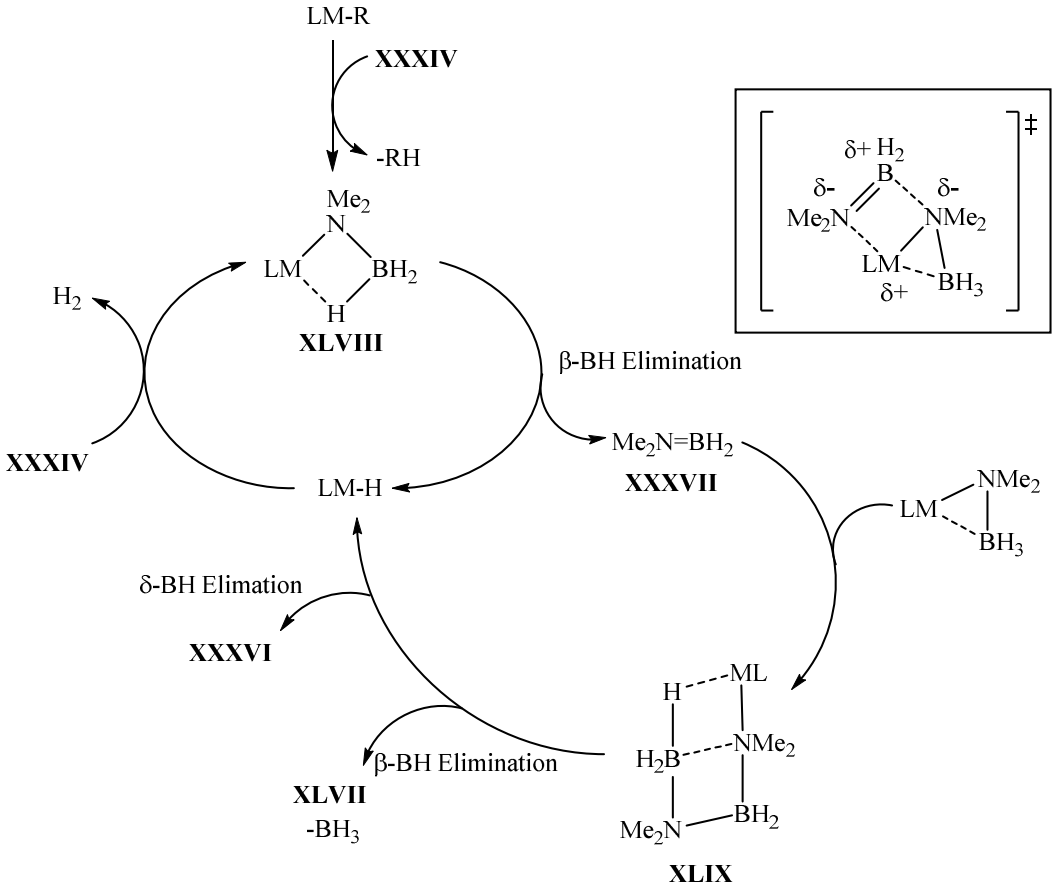

Figure 1.30: Proposed DMAB (**XXXIV**) dehydrocoupling reaction scheme by Mg and Ca amides **V**, **VI**, **XV**.[351]

In this proposed mechanism the new boron-nitrogen bond is formed by the insertion of **XXXVI** into the metal-nitrogen bond of the amidoborane. **XXXVI** is isoelectronic to an alkene C=C bond which, as mentioned in Section 1.1, has been shown to insert into a Group 2 metal-element bond. As alluded to in Section 1.2.1,

however, amine boranes and hence **XXXVI** differ from alkanes and alkenes repectively in their polarisation, facilitating insertion into a suitably polarised M-X bond. This insertion is depicted by the transition state shown in the inset in Figure 1.30. The key B-N bond forming step was proposed to be dependent upon production and insertion of the polarised and unsaturated **XXXVI** species, forming LM[$NMe_2BH_2NMe_2BH_3$], **XLIX**. This can undergo either β-hydride or δ-hydride elimination, forming **XLVII** or **XXXVI** respectively, the formation of which is dictated by whichever process has the greater kinetic favourability.

The proposed mechanism for dehydrocoupling of DMAB by magnesium and calcium in Figure 1.30 differs from a mechanism based upon σ-bond metathesis reactivity, depicted in Figure 1.31.

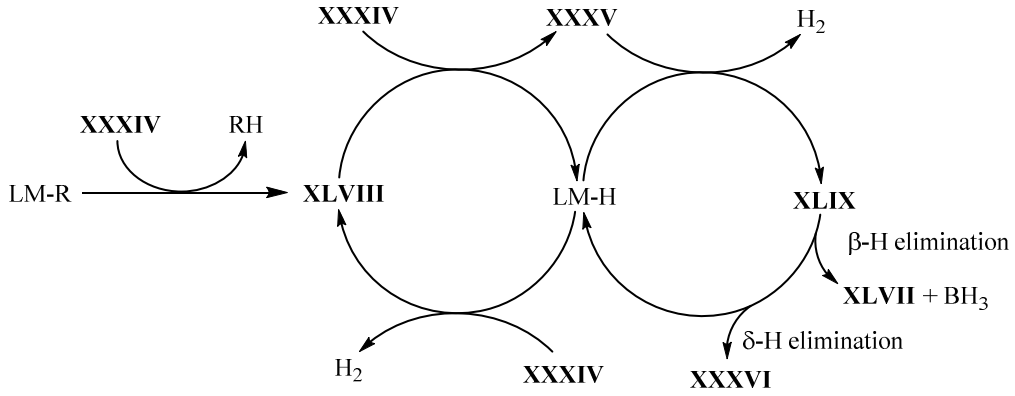

Figure 1.31: DMAB (**XXXIV**) dehydrocoupling scheme based upon σ-bond metathesis reactivity.

In the scheme shown in Figure 1.31, the new boron-nitrogen bond is formed via σ-bond metathesis between a metal-amidoborane **XLVIII** and the B-H bond of a molecule of amine borane, forming **XXXV**, in preference to the proposed insertion of the unsaturated **XXXVII** species into the M-N bond of **XLVIII** in Figure 1.30. In this scheme the unsaturated species **XXXVII** is not formed. **XLVII** and **XXXVI** are once again formed by δ– and β–hydride elimination respectively from **XLIX**, formed in this regime by σ-bond metathesis between **XXXV** and the metal hydride, LM-H.

Research by Wright, using Group 13 Al^{III} and Ga^{III} species, and Harder using a β-diketiminato-Al^{III} hydride, propose possible mechanisms which invoke an insertion

of **XXXVII**.[347-349, 356] **XXXVII** has been implicated in mechanisms for transition metal catalysis (see Section 1.2.3), but detail regarding formation of the new B-N bond is neglected, with no previous suggestion that it behaves in an analogous manner to that of a simple alkene insertion.

Harder et al have also reported catalytic dehydrocoupling of **XLIII** by **VI** and **XXXIX**, Figure 1.32, proceeding by the structurally characterised β-diketiminato magnesium anilidoborane intermediate **L**.[350]

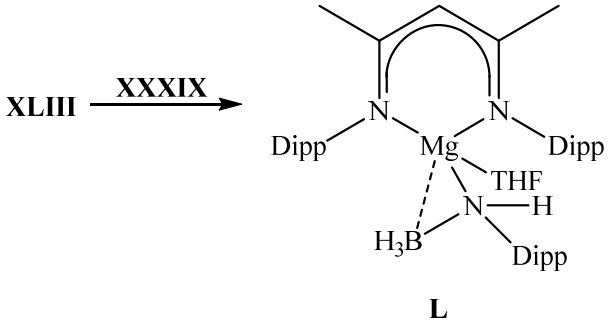

L

Figure 1.32: Reaction between **XXXIX** and **XLIII**, forming a β-diketiminato magnesium 2,6-di-*iso*-propylanilidoborane intermediate **L**.[350]

The only product of this dehydrocoupling reaction was identified as [HB{NH(Dipp)}$_2$] **LI**, characterised by NMR and X-ray crystallography, formed via the β-hydride elimination of a proposed but unidentified intermediate **LII**. This is shown in Figure 1.33.

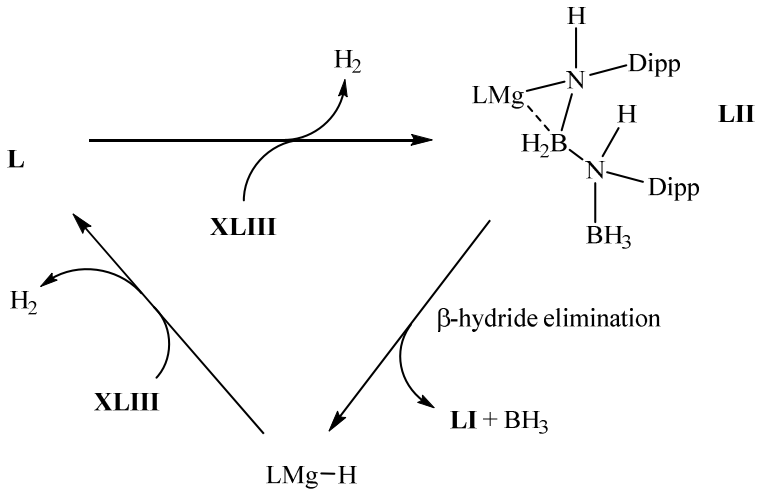

Figure 1.33: Proposed reaction scheme for the dehydrocoupling of **XLIII**, via an intermediate **LII**.[350] (L = β-diketiminate)

Supporting evidence for a scheme such as that in Figure 1.33 lies with the isolation of a magnesium tetrahydroborate species and a resonance in the ^{1}H NMR spectrum assigned to B_2H_6 (formed by the BH_3 byproduct). However, no mechanism is proposed to account for the formation of the additional B-N linkage of the as yet unidentified intermediate **LII**. The only explanation provided is the suggestion that **LII** results from reaction of the magnesium anilidoborane with the acidic aniline borane.

The Hill group continued to investigate the proposed reaction scheme in Figure 1.30, whilst expanding the range of amine boranes and Group 2 metal centres.[352] The mechanism of dehydrocoupling of pyrrolidine borane (PB, **LIII**) was found to be consistent with Figure 1.30, with stoichiometric reactions showing coordination to the metal species followed by proposed β-hydride elimination to produce the corresponding cycloborazane, $[H_2BNC_4H_8]_2$ **LIV**, on heating. The bis(trimethylsilyl)amides **VII**, of the Group 2 metals (Mg, Ca, Sr, Ba) were used to investigate the variation in reactivity of different metal centres along with testing the reaction scheme in Figure 1.30. Reaction of a single equivalent of DMAB with $[Mg\{N(SiMe_3)_2\}_2]$ was observed to produce an almost complete conversion to **XXXVII**. The lack of other boron species in the NMR spectra suggested that the initial β-hydride elimination to produce **XXXVII** is faster than any other process. The apparent stability of **XXXVII** in these catalytic reactions led the Hill group to

suggest that the formation of **XVI** is a metal-mediated process whereas, as mentioned previously in Section 1.2.3, many transition-metal-based catalyses invoke an off-metal process.[294, 316, 338]

Stoichiometric reactions were also conducted with di-*iso*-propylamine borane **LV**, in which there was no evidence for the formation of an analogous metal-coordinated anion. Rather, total conversion to the unsaturated $iPr_2N{=}BH_2$ **LVI** species occurred in conjunction with regeneration of the catalyst, shown in Figure 1.34.

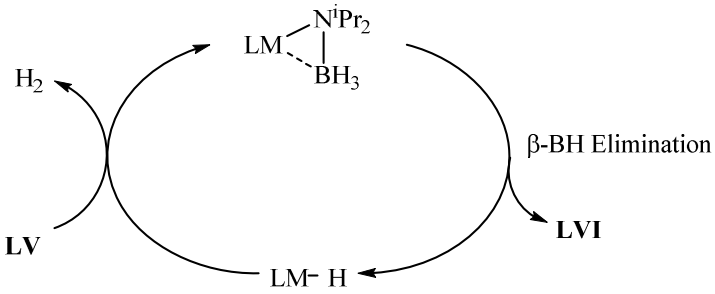

Figure 1.34: Proposed catalytic cycle for the dehydrocoupling of di-*iso*-propylamine borane **LV**.

It was suggested that the increased steric demands of the di-*iso*-propyl groups slowed or prevented the Mg-N / **LVI** insertion to produce the metal-coordinated complex anion. Similar activity was observed when the reaction was performed under catalytic conditions. Comparison of the formation of **LVI** using Mg, Ca, Sr and Ba bis(trimethylsilyl)amides showed results consistent with a β-hydride elimination of the metal-amidoborane species. During these reactions the cycloborazane, $(^iPr_2N\text{-}BH_2)_2$, was not observed, consistent with the stability of this species to self dimerisation.[310, 365]

Throughout these experiments it was observed that the rates of reaction apparently varied according to the ionic radius and resultant charge density of the M^{2+} centre, following the trend Mg > Ca > Sr > Ba. It was proposed that all of the Group 2 catalysts reacted in a manner similar to that shown in Figure 1.30, but that the rates of these reactions vary with the charge density of the metal centre, in addition to subtleties arising from the particular steric and electronic properties of the amine group. Initial investigations of the reactivity of the Group 3 amides, **XL** and **XLI**,

suggested that these species reacted in a similar manner to the Group 2 metals, with qualitative data suggesting that reaction rates followed the trend Sc > Y > Mg > Ca, further supporting the suggestion that reaction rate varies with charge density of the metal centre.[346]

1.4 Amine Boranes Beyond Hydrogen Storage

Whether or not a hydrogen economy comes to fruition and systems based around amine boranes become viable hydrogen storage materials, amine boranes represent useful molecules for chemical transformations. For example, simple pyrolysis of AB can be used to form boron nitride,[366-372] with uses in ceramics, abrasives and composite materials. Furthermore, transition-metal catalysed dehydrocoupling of AB has produced polyaminoboranes, $(NH_2BH_2)_n$,[296, 373, 374] with uses as a preceramic material for the formation of boron nitride and boron carbide on pyrolysis. Amine boranes also represent a useful synthetic tool for reactions such as controlled reduction, transfer hydrogenation and hydroboration, enabling novel routes to functionalised molecules.

Metal amidoboranes, in particular lithium amidoborane and latterly calcium amidoborane, have been widely investigated as a milder alternative to $LiAlH_4$ by Singaram,[375, 376] demonstrating reduction of aldehydes and ketones,[377-379] aromatic and aliphatic esters,[380-382] tertiary amides,[380, 383] azides and imines.[384-386] A proposed two-step reduction by the metal amidoborane, via hydroboration followed by hydrolysis/solvolysis, for ketones and imines is shown in Figure 1.35.

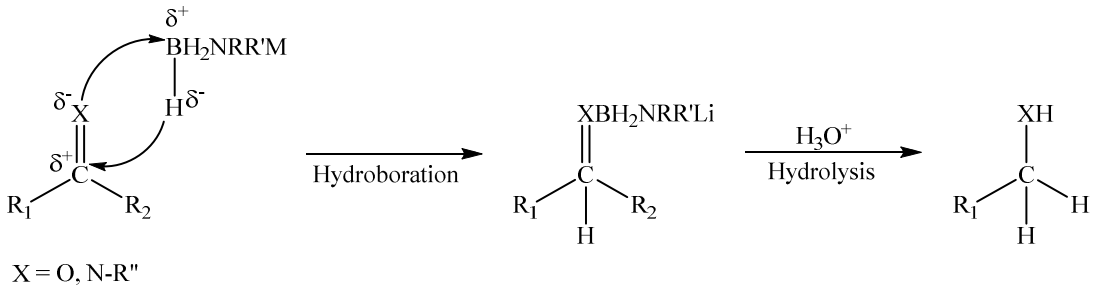

Figure 1.35: Reduction of ketones and imines using metal amidoborane, where M = Li, Na, Ca.[377, 380, 385, 386]

Borane-bound hydrides can react with functional groups such as ketones and aldehydes, with reduction to the corresponding alcohol.[387-393] Metal-free hydrogenation using AB can also occur with imines, mechanistically characterised as occurring via boron-bound hydrides attacking the more nucleophilic carbon, whilst a nitrogen-bound proton attacks the more electronegative imine nitrogen.[394]

A true transfer hydrogenation occurs when the hydride does not dissociate from the metal centre, i.e. there is not merely a dehydrogenation of amine borane followed by hydrogenation of a substrate. Early palladium-catalysed reactions include transfer hydrogenation via amine borane methanolysis of nitroaromatics, alkenes, alkynes and aromatics, displaying functional group tolerance.[251, 258, 395] In hydrocarbon solvents, the first transition metal complexes shown to dehydrocouple AB were utilised to hydrogenate substrates such as cyclohexene and octane,[396, 397] whilst ketones and imines have also been hydrogenated using PB,[293] all proceeding via initial dehydrocoupling followed by hydrogenation. The first true transfer hydrogenation was achieved using rhenium complexes to hydrogenate olefins using DMAB.[277, 278] Following these reports, transition-metal hydrogenations have been reported with a variety of substrates.[151, 292, 334, 366] Metal-free hydrogen transfer between amine boranes and aminoboranes has also been reported,[398, 399] in addition to aldehydes,[400, 401] ketones and imines.[400, 402-405]

In Section 1.2.4, FLPs were noted as being able to dehydrocouple amine boranes. Similarly, stoichiometric hydrogenation/reduction of CO_2 to methanol has been achieved using an aluminium-based FLP and AB, shown in Figure 1.36(a),[406] followed by subsequent work on reduction of CO_2 using DMAB with a bis-borane based FLP and aluminium-based FLP,[407-409] Figure 1.36(b). Catalytic reduction of CO_2 is a very desirable process for the generation of methanol on an industrial scale.

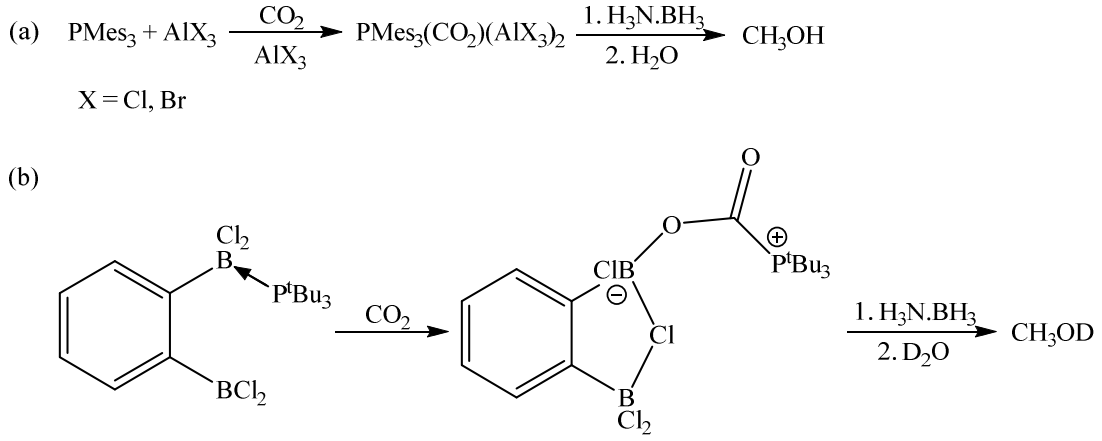

Figure 1.36: Stoichiometric reduction of CO_2 with ammonia borane and FLP complexes.[409, 410]

Amine boranes have been utilised for hydroborations due their advantageous stability and ease of use. Other hydroborating agents include diborane, a toxic and pyrophoric gas, whilst borane-THF is only available as a low concentration solution, and borane dimethylsulphide produces stoichiometric quantities of dimethylsulphide byproduct on reaction. The stability of amine boranes, however, often necessitates higher hydroboration reaction temperatures and harsher reaction conditions, though room temperature reactions have been achieved using more reactive amine boranes.[411-416]

In related work, Weller has recently reported the dehydrogenative B-B coupling of trimethylamine borane **LVII** by a rhodium complex, producing a rhodium-bound diborane, shown in Figure 1.37.[417] This represents the first example of B-B bond formation using amine boranes. The formation of the rhodium-bound diborane is mediated in the presence of *tert*-butyl-ethene, which undergoes hydroboration, and the yield is increased by the presence of cyclohexene, which undergoes hydrogenation by **LVIII**.

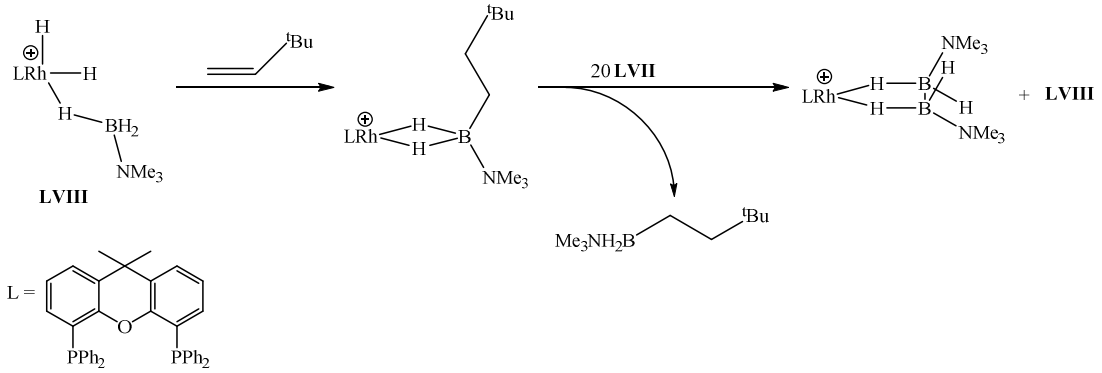

Figure 1.37: The dehydrogenative B-B coupling of trimethylamine borane (**LVII**) by a cationic rhodium complex **LVIII** ($[BAr^F_4]^-$ counter anions not shown).

This latter work demonstrates that amine boranes provide opportunities for elegant reduction and functionalisation chemistry, with reactivity tuned by both the amine substituent and the metal catalyst.

1.5 Aims of The Research Described In This Thesis

The research which is presented in subsequent chapters of this thesis aims to investigate as comprehensively as possible the mechanism of Group 2-promoted dehydrocoupling of secondary amine boranes. This is achieved through a combination of stoichiometric and catalytic reactivity studies, in addition to a kinetic investigation to provide a more quantitative comparison of the dependence of these reactions upon the identity of the metal centre. By addition of protic (*Chapter 5*) substrates to these reactions, Group 2 dehydrocoupling reactivity is further explored, in addition to the formation of novel molecules.

Chapter 2 investigates stoichiometric reactions of the Group 2 dialkyl catalysts **VII** with the secondary amine boranes DMAB and PB, in addition to the primary amine borane *tert*-butylamine borane (TBAB) for comparative purposes. This section assesses the viability of the proposed insertion of the unsaturated $R_2N{=}BH_2$ fragment into a M-C bond, with analysis of isolated intermediates, products and *in situ* NMR studies.

Chapter 3 presents an investigation of the proposed dehydrocoupling mechanism in Figure 1.30, highlighting corroborative data or suggesting amendments to the

proposed mechanism as required. This chapter begins with a consideration of precatalyst identity, before isolation of dimethylamine borane reaction intermediates, enabling the kinetics of the thermal decomposition and elementary reactions of the otherwise inaccessible isolated processes of the proposed mechanism to be investigated in as much detail as possible.

Chapter 4 presents a kinetic study of the dehydrocoupling activity of Group 2 complexes, in addition to those of Group 3, providing a quantitative profile of the dependence of the metal centre upon reactivity, validating or amending statements made regarding trends in reactivity from qualitative data. Comparison is made between the reactivity of the secondary amine borane DMAB and that of primary amine borane TBAB, as well as deuterated substrates. The previously unexplored catalytic dehydrocoupling activity of the Group 1 bis(trimethylsilyl)amides, $MN(SiMe_3)_2$ **LIX**, is also investigated.

Chapter 5 deviates from systems involving dehydrocoupling of pure amine boranes to regimes in which other protic substrates are present with the amine borane. Previous work on the dehydrocoupling of secondary amine boranes, Section 1.3, indicated that following the initial β-hydride elimination from a metallated amidoborane **XLVIII**, the polarised and unsaturated aminoborane intermediate **XXXVII** can undergo insertion reactions into other available M-E bonds. It is hypothesised that interception of this aminoborane could occur if a better nucleophile than the R_2HNBH_3 molecule itself is present in the reaction. The metal centre could coordinate and deprotonate the nucleophile, intercepting the aminoborane which inserts into the M-E bond, forming an intermediate **LX**. This process is represented in Figure 1.38.

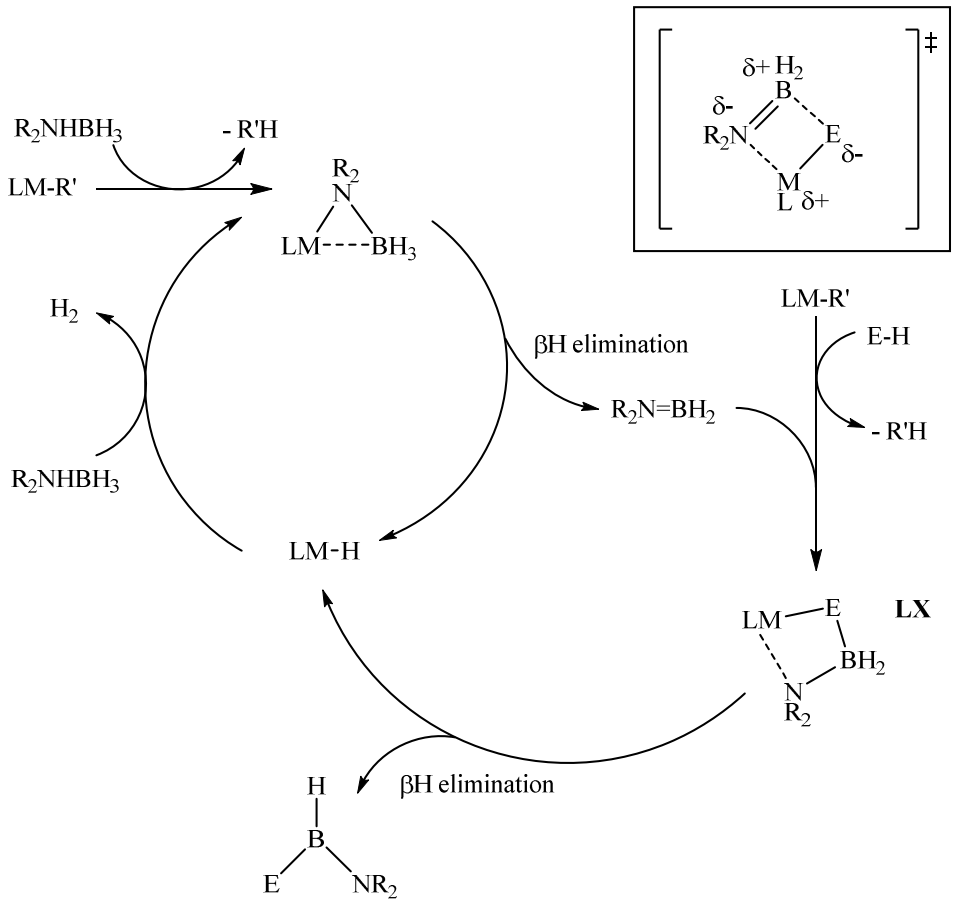

Figure 1.38: General reaction profile for the proposed insertion of $R_2N{=}BH_2$ into an M-E bond when another protic nucleophile is present in the reaction, where E-H = R_2N-H, RO-H, R_2P-H etc.

Chapter 5 explores reactions in which a protic amine is present during amine borane dehydrocoupling, providing further mechanistic evidence for the validity of the insertive scheme suggested in Figure 1.30. Utilisation of amine borane β-hydride elimination to produce **XXXVII**, isoelectronic to an olefin, followed by B=N insertion into the E-H bond of a more nucleophilic species than $R_2HN.BH_3$ thus provides sophisticated routes to new boron-containing molecules.

Chapter 6 discusses the findings of this thesis, highlighting the information discovered regarding the proposed dehydrocoupling mechanism in Figure 1.30, evaluating evidence in support of this reaction sequence, in addition to any which contradict it. This chapter also assesses the contribution made to current knowledge regarding both d^0-metal catalysed dehydrocoupling of amine boranes and amine

borane reactivity in general, in addition to the production of novel molecules and complexes.

1.6 Chapter 1 References

1. R. W. Hoffmann, *Chem. Soc. Rev.*, 2003, **32**, 225-230.
2. F. Bickelhaupt, *Chem. Soc. Rev.*, 1999, **28**, 17-23.
3. T. Satoh, *Chem. Soc. Rev.*, 2007, **36**, 1561-1572.
4. S. P. Green, C. Jones and A. Stasch, *Science*, 2007, **318**, 1754-1757.
5. S. Krieck, H. Gorls, L. Yu, M. Reiher and M. Westerhausen, *J. Am. Chem. Soc.*, 2009, **131**, 2977-2985.
6. M. Westerhausen, *Angew. Chem.-Int. Ed.*, 2008, **47**, 2185-2187.
7. R. D. Shannon, *Acta Crystallogr. Sect. A*, 1976, **32**, 751-767.
8. S. Hong and T. J. Marks, *Acc. Chem. Res.*, 2004, **37**, 673-686.
9. R. Anwander, *Lanthanide amides*, Springer Berlin Heidelberg, 1996.
10. J. Barluenga, F. Aznar, R. Liz and R. Rodes, *J. Chem. Soc.-Perkin Trans. 1*, 1980, 2732-2737.
11. P. J. Walsh, A. M. Baranger and R. G. Bergman, *J. Am. Chem. Soc.*, 1992, **114**, 1708-1719.
12. D. R. Coulson, *Tetrahedron Lett.*, 1971, 429-430.
13. A. L. Casalnuovo, J. C. Calabrese and D. Milstein, *J. Am. Chem. Soc.*, 1988, **110**, 6738-6744.
14. J. J. Brunet, D. Neibecker and K. Philippot, *Tetrahedron Lett.*, 1993, **34**, 3877-3880.
15. Y. W. Li and T. J. Marks, *Organometallics*, 1996, **15**, 3770-3772.
16. G. A. Molander and J. A. C. Romero, *Chem. Rev.*, 2002, **102**, 2161-2185.
17. S. W. Hong, S. Tian, M. V. Metz and T. J. Marks, *J. Am. Chem. Soc.*, 2003, **125**, 14768-14783.
18. S. D. Wobser, C. J. Stephenson, M. Delferro and T. J. Marks, *Organometallics*, 2013, **32**, 1317-1327.
19. B. D. Stubbert and T. J. Marks, *J. Am. Chem. Soc.*, 2007, **129**, 4253-4271.
20. X. H. Yu, S. Seo and T. J. Marks, *J. Am. Chem. Soc.*, 2007, **129**, 7244.
21. A. Dzudza and T. J. Marks, *Organic Lett.*, 2009, **11**, 1523-1526.
22. P. W. Roesky, U. Denninger, C. L. Stern and T. J. Marks, *Organometallics*, 1997, **16**, 4486-4492.

23. A. Motta, I. L. Fragala and T. J. Marks, *Organometallics*, 2005, **24**, 4995-5003.
24. A. M. Kawaoka, M. R. Douglass and T. J. Marks, *Organometallics*, 2003, **22**, 4630-4632.
25. S. Y. Seo, X. H. Yu and T. J. Marks, *J. Am. Chem. Soc.*, 2009, **131**, 263-276.
26. S. Hong, A. M. Kawaoka and T. J. Marks, *J. Am. Chem. Soc.*, 2003, **125**, 15878-15892.
27. M. R. Douglass, C. L. Stern and T. J. Marks, *J. Am. Chem. Soc.*, 2001, **123**, 10221-10238.
28. C. J. Weiss, S. D. Wobser and T. J. Marks, *Organometallics*, 2010, **29**, 6308-6320.
29. A. Dzudza and T. J. Marks, *J. Org. Chem.*, 2008, **73**, 4004-4016.
30. S. Seo and T. J. Marks, *Chem.- Eur. J.*, 2010, **16**, 5148-5162.
31. S. Seo and T. J. Marks, *Organic Lett.*, 2008, **10**, 317-319.
32. C. J. Weiss and T. J. Marks, *Dalton Trans.*, 2010, **39**, 6576-6588.
33. A. M. Seyam, B. D. Stubbert, T. R. Jensen, J. J. O'Donnell, C. L. Stern and T. J. Marks, *Inorg. Chim. Acta*, 2004, **357**, 4029-4035.
34. A. Motta, I. L. Fragala and T. J. Marks, *Organometallics*, 2006, **25**, 5533-5539.
35. V. M. Arredondo, S. Tian, F. E. McDonald and T. J. Marks, *J. Am. Chem. Soc.*, 1999, **121**, 3633-3639.
36. Y. W. Li and T. J. Marks, *J. Am. Chem. Soc.*, 1998, **120**, 1757-1771.
37. J. S. Ryu, T. J. Marks and F. E. McDonald, *J. Org. Chem.*, 2004, **69**, 1038-1052.
38. A. M. Kawaoka and T. J. Marks, *J. Am. Chem. Soc.*, 2005, **127**, 6311-6324.
39. J. S. Ryu, G. Y. Li and T. J. Marks, *J. Am. Chem. Soc.*, 2003, **125**, 12584-12605.
40. X. H. Yu and T. J. Marks, *Organometallics*, 2007, **26**, 365-376.
41. L. Jia, X. M. Yang, A. M. Seyam, I. D. L. Albert, P. F. Fu, S. T. Yang and T. J. Marks, *J. Am. Chem. Soc.*, 1996, **118**, 7900-7913.
42. S. Seo, X. H. Yu and T. J. Marks, *Tetrahedron Lett.*, 2013, **54**, 1828-1831.
43. G. Jeske, H. Lauke, H. Mauermann, H. Schumann and T. J. Marks, *J. Am. Chem. Soc.*, 1985, **107**, 8111-8118.

44. G. Jeske, H. Lauke, H. Mauermann, P. N. Swepston, H. Schumann and T. J. Marks, *J. Am. Chem. Soc.*, 1985, **107**, 8091-8103.
45. S. Harder, *Chem. Rev.*, 2010, **110**, 3852-3876.
46. T. P. Hanusa, *Polyhedron*, 1990, **9**, 1345-1362.
47. T. P. Hanusa, *Chem. Rev.*, 1993, **93**, 1023-1036.
48. M. J. Harvey and T. P. Hanusa, *Organometallics*, 2000, **19**, 1556-1566.
49. T. P. Hanusa, *Organometallics*, 2002, **21**, 2559-2571.
50. M. Westerhausen, M. H. Digeser and W. Schwarz, *Inorg. Chem.*, 1997, **36**, 521-527.
51. M. Westerhausen, J. Langer, S. Krieck and C. Glock, *Rev. Inorg. Chem.*, 2011, **31**, 143-184.
52. M. Westerhausen, M. Gartner, R. Fischer, J. Langer, L. Yu and M. Reiher, *Chem.- Eur. J.*, 2007, **13**, 6292-6306.
53. M. Westerhausen, *Z. Anorg. Allg. Chem.*, 2009, **635**, 13-32.
54. M. Gartner, R. Fischer, J. Langer, H. Gorls, D. Walther and M. Westerhausen, *Inorg. Chem.*, 2007, **46**, 5118-5124.
55. M. Westerhausen, *Coord. Chem. Rev.*, 1998, **176**, 157-210.
56. S. Harder, F. Feil and T. Repo, *Chem.- Eur. J.*, 2002, **8**, 1991-1999.
57. C. Ruspic and S. Harder, *Inorg. Chem.*, 2007, **46**, 10426-10433.
58. D. F. J. Piesik, S. Range and S. Harder, *Organometallics*, 2008, **27**, 6178-6187.
59. J. Spielmann, F. Buch and S. Harder, *Angew. Chem.-Int. Ed.*, 2008, **47**, 9434-9438.
60. S. Harder, *Organometallics*, 2002, **21**, 3782-3787.
61. J. Spielmann and S. Harder, *Chem.- Eur. J.*, 2007, **13**, 8928-8938.
62. S. Harder, *Chem. Commun.*, 2012, **48**, 11165-11177.
63. S. Harder, F. Feil and K. Knoll, *Angew. Chem.-Int. Ed.*, 2001, **40**, 4261-4264.
64. S. Harder, M. Lutz and A. W. G. Straub, *Organometallics*, 1997, **16**, 107-113.
65. S. Harder, S. Muller and E. Hubner, *Organometallics*, 2004, **23**, 178-183.
66. L. Orzechowski, G. Jansen and S. Harder, *J. Am. Chem. Soc.*, 2006, **128**, 14676-14684.

67. C. Ruspic, S. Nembenna, A. Hofmeister, J. Magull, S. Harder and H. W. Roesky, *J. Am. Chem. Soc.*, 2006, **128**, 15000-15004.
68. J. A. Kanters, S. Harder and N. S. Poonia, *Acta Crystallogr. Sect. C-Cryst. Struct. Commun.*, 1987, **43**, 1042-1045.
69. F. Buch, H. Brettar and S. Harder, *Angew. Chem.-Int. Ed.*, 2006, **45**, 2741-2745.
70. M. S. Hill, in *Annu. Rep. Prog. Chem., Vol 103, Sect. A: Inorg. Chem.*, eds. F. J. Berry and E. G. Hope, 2007, vol. 103, pp. 39-53.
71. M. S. Hill, in *Annu. Rep. Prog. Chem., Vol 105, Sect. A: Inorg. Chem.*, eds. F. J. Berry and E. G. Hope, 2009, vol. 105, pp. 55-74.
72. M. Westerhausen, M. H. Digeser, H. Noth, W. Ponikwar, T. Seifert and K. Polborn, *Inorg. Chem.*, 1999, **38**, 3207-3214.
73. M. Westerhausen, M. H. Digeser, C. Guckel, H. Noth, J. Knizek and W. Ponikwar, *Organometallics*, 1999, **18**, 2491-2496.
74. M. Westerhausen, M. H. Digeser, M. Krofta, N. Wiberg, H. Noth, J. Knizek, W. Ponikwar and T. Seifert, *Eur. J. Inorg. Chem.*, 1999, 743-750.
75. M. Westerhausen, H. D. Hausen and W. Schwarz, *Z. Anorg. Allg. Chem.*, 1992, **618**, 121-130.
76. M. Westerhausen and H. D. Hausen, *Z. Anorg. Allg. Chem.*, 1992, **615**, 27-34.
77. A. Weeber, S. Harder, H. H. Brintzinger and K. Knoll, *Organometallics*, 2000, **19**, 1325-1332.
78. F. Feil and S. Harder, *Organometallics*, 2000, **19**, 5010-5015.
79. F. Feil and S. Harder, *Organometallics*, 2001, **20**, 4616-4622.
80. S. Harder, F. Feil and A. Weeber, *Organometallics*, 2001, **20**, 1044-1046.
81. M. Westerhausen, S. Schneiderbauer, A. N. Kneifel, Y. Soltl, P. Mayer, H. Noth, Z. Y. Zhong, P. J. Dijkstra and J. Feijen, *Eur. J. Inorg. Chem.*, 2003, 3432-3439.
82. Y. Sarazin, R. H. Howard, D. L. Hughes, S. M. Humphrey and M. Bochmann, *Dalton Trans.*, 2006, 340-350.
83. M. G. Davidson, C. T. O'Hara, M. D. Jones, C. G. Keir, M. F. Mahon and G. Kociok-Kohn, *Inorg. Chem.*, 2007, **46**, 7686-7688.
84. W. Vargas and K. Ruhlandt-Senge, *Eur. J. Inorg. Chem.*, 2003, 3472-3479.

85. D. J. Burkey and T. P. Hanusa, *Organometallics*, 1996, **15**, 4971-4976.

86. D. C. Green, U. Englich and K. Ruhlandt-Senge, *Angew. Chem.-Int. Ed.*, 1999, **38**, 354-357.

87. A. G. M. Barrett, M. R. Crimmin, M. S. Hill, P. B. Hitchcock, S. L. Lomas, M. F. Mahon, P. A. Procopiou and K. Suntharalingam, *Organometallics*, 2008, **27**, 6300-6306.

88. A. G. Avent, M. R. Crimmin, M. S. Hill and P. B. Hitchcock, *Organometallics*, 2005, **24**, 1184-1188.

89. M. Westerhausen, M. H. Digeser, B. Wieneke, H. Noth and J. Knizek, *Eur. J. Inorg. Chem.*, 1998, 517-521.

90. M. Westerhausen, C. Birg, M. Krofta, P. Mayer, T. Seifert, H. Noth, A. Pfitzner, T. Nilges and H. J. Deiseroth, *Z. Anorg. Allg. Chem.*, 2000, **626**, 1073-1080.

91. M. Westerhausen, M. H. Digeser, H. Noth and J. Knizek, *Z. Anorg. Allg. Chem.*, 1998, **624**, 215-220.

92. M. H. Chisholm, J. Gallucci and K. Phomphrai, *Chem. Commun.*, 2003, 48-49.

93. M. H. Chisholm, J. C. Gallucci and K. Phomphrai, *Inorg. Chem.*, 2004, **43**, 6717-6725.

94. M. R. Crimmin, I. J. Casely and M. S. Hill, *J. Am. Chem. Soc.*, 2005, **127**, 2042-2043.

95. A. G. M. Barrett, M. R. Crimmin, M. S. Hill, P. B. Hitchcock, G. Kociok-Koehn and P. A. Procopiou, *Inorg. Chem.*, 2008, **47**, 7366-7376.

96. M. R. Crimmin, M. Arrowsmith, A. G. M. Barrett, I. J. Casely, M. S. Hill and P. A. Procopiou, *J. Am. Chem. Soc.*, 2009, **131**, 9670-9685.

97. A. G. M. Barrett, C. Brinkmann, M. R. Crimmin, M. S. Hill, P. Hunt and P. A. Procopiou, *J. Am. Chem. Soc.*, 2009, **131**, 12906-12907.

98. S. Datta, P. W. Roesky and S. Blechert, *Organometallics*, 2007, **26**, 4392-4394.

99. S. Datta, M. T. Gamer and P. W. Roesky, *Organometallics*, 2008, **27**, 1207-1213.

100. F. Buch and S. Harder, *Z. Naturforsch. Sect. B - J. Chem. Sci.,* 2008, **63**, 169-177.

101. B. Liu, T. Roisnel, J.-F. Carpentier and Y. Sarazin, *Chem.- Eur. J.*, 2013, **19**, 2784-2802.

102. M. Arrowsmith, M. R. Crimmin, A. G. M. Barrett, M. S. Hill, G. Kociok-Koehn and P. A. Procopiou, *Organometallics*, 2011, **30**, 1493-1506.

103. C. Brinkmann, A. G. M. Barrett, M. S. Hill and P. A. Procopiou, *J. Am. Chem. Soc.*, 2012, **134**, 2193-2207.

104. A. G. M. Barrett, T. C. Boorman, M. R. Crimmin, M. S. Hill, G. Kociok-Kohn and P. A. Procopiou, *Chem. Commun.*, 2008, 5206-5208.

105. J. R. Lachs, A. G. M. Barrett, M. R. Crimmin, G. Kociok-Koehn, M. S. Hill, M. F. Mahon and P. A. Procopiou, *Eur. J. Inorg. Chem.*, 2008, 4173-4179.

106. M. R. Crimmin, A. G. M. Barrett, M. S. Hill, P. B. Hitchcock and P. A. Procopiou, *Organometallics*, 2007, **26**, 2953-2956.

107. M. R. Crimmin, A. G. M. Barrett, M. S. Hill, P. B. Hitchcock and P. A. Procopiou, *Organometallics*, 2008, **27**, 497-499.

108. M. S. Hill, D. J. Liptrot, D. J. MacDougall, M. F. Mahon and T. P. Robinson, *Chem. Sci.*, 2013, **4**, 4212-4222.

109. P. G. Hayes, G. C. Welch, D. J. H. Emslie, C. L. Noack, W. E. Piers and M. Parvez, *Organometallics*, 2003, **22**, 1577-1579.

110. B. Liu, T. Roisnel, J.-F. Carpentier and Y. Sarazin, *Angew. Chem.-Int. Ed.*, 2012, **51**, 4943-4946.

111. B. Liu, J.-F. Carpentier and Y. Sarazin, *Chem.- Eur. J.*, 2012, **18**, 13259-13264.

112. S. Harder and J. Brettar, *Angew. Chem.-Int. Ed.*, 2006, **45**, 3474-3478.

113. J. Spielmann and S. Harder, *Eur. J. Inorg. Chem.*, 2008, 1480-1486.

114. J. Spielmann, G. Jansen, H. Bandmann and S. Harder, *Angew. Chem.-Int. Ed.*, 2008, **47**, 6290-6295.

115. A. P. Dove, V. C. Gibson, P. Hormnirun, E. L. Marshall, J. A. Segal, A. J. P. White and D. J. Williams, *Dalton Trans.*, 2003, 3088-3097.

116. S. P. Green, C. Jones and A. Stasch, *Angew. Chem.-Int. Ed.*, 2008, **47**, 9079-9083.

117. S. J. Bonyhady, C. Jones, S. Nembenna, A. Stasch, A. J. Edwards and G. J. McIntyre, *Chem.- Eur. J.*, 2010, **16**, 938-955.

118. S. J. Bonyhady, S. P. Green, C. Jones, S. Nembenna and A. Stasch, *Angew. Chem.-Int. Ed.*, 2009, **48**, 2973-2977.
119. M. T. Ma, A. Stasch and C. Jones, *Chem.- Eur. J.*, 2012, **18**, 10669-10676.
120. C. Jones, L. McDyre, D. M. Murphy and A. Stasch, *Chem. Commun.*, 2010, **46**, 1511-1513.
121. M. S. Hill, M. F. Mahon and T. P. Robinson, *Chem. Commun.*, 2010, **46**, 2498-2500.
122. H. T. Hwang, A. Al-Kukhun and A. Varma, *Ind. Eng. Chem. Res.*, 2010, **49**, 10994-11000.
123. M. Diwan, H. T. Hwang, A. Al-Kukhun and A. Varma, *Aiche J.*, 2011, **57**, 259-264.
124. D. Wechsler, Y. Cui, D. Dean, B. Davis and P. G. Jessop, *J. Am. Chem. Soc.*, 2008, **130**, 17195-17203.
125. J. Graetz, *Chem. Soc. Rev.*, 2009, **38**, 73-82.
126. C. W. Tan, K. H. Tan, Y. T. Ong, A. R. Mohamed, S. H. S. Zein and S. H. Tan, *Environ. Chem. Lett.*, 2012, **10**, 265-273.
127. H. M. Cheng, Q. H. Yang and C. Liu, *Carbon*, 2001, **39**, 1447-1454.
128. M. Hirscher and M. Becher, *J. Nanosci. Nanotechnol.*, 2003, **3**, 3-17.
129. R. G. Ding, G. Q. Lu, Z. F. Yan and M. A. Wilson, *J. Nanosci. Nanotechnol.*, 2001, **1**, 7-29.
130. R. Orinakova and A. Orinak, *Fuel*, 2011, **90**, 3123-3140.
131. F. L. Darkrim, P. Malbrunot and G. P. Tartaglia, *Int. J. Hydrogen Energy*, 2002, **27**, 193-202.
132. B. Xiao and Q. C. Yuan, *Particuology*, 2009, **7**, 129-140.
133. S. V. Kolotilov and V. V. Pavlishchuk, *Theor. Exp. Chem.* 2009, **45**, 277-301.
134. D. Zhao, D. Q. Yuan and H. C. Zhou, *Energy Environ. Sci.*, 2008, **1**, 222-235.
135. J. Sculley, D. Q. Yuan and H. C. Zhou, *Energy Environ. Sci.*, 2011, **4**, 2721-2735.
136. L. J. Murray, M. Dinca and J. R. Long, *Chem. Soc. Rev.*, 2009, **38**, 1294-1314.

137. J. M. Pasini, C. Corgnale, B. A. van Hassel, T. Motyka, S. Kumar and K. L. Simmons, *Int. J. Hydrogen Energy*, 2013, **38**, 9755-9765.
138. B. Sakintuna, F. Lamari-Darkrim and M. Hirscher, *Int. J. Hydrogen Energy*, 2007, **32**, 1121-1140.
139. J. Graetz, *ISRN Materials Sci.*, 2012, **2012**.
140. R. Lan, J. T. S. Irvine and S. Tao, *Int. J. Hydrogen Energy*, 2012, **37**, 1482-1494.
141. T. Hügle, M. Hartl and D. Lentz, *Chemistry*, 2011, **17**, 10184-10207.
142. A. Klerke, C. H. Christensen, J. K. Norskov and T. Vegge, *J. Mat. Chem.*, 2008, **18**, 2304-2310.
143. S. Enthaler, J. von Langermann and T. Schmidt, *Energy Environ. Sci.*, 2010, **3**, 1207-1217.
144. M. Grasemann and G. Laurenczy, *Energy Environ. Sci.*, 2012, **5**, 8171-8181.
145. T. C. Johnson, D. J. Morris and M. Wills, *Chem. Soc. Rev.*, 2010, **39**, 81-88.
146. K. Mueller, K. Stark, B. Mueller and W. Arlt, *Energy & Fuels*, 2012, **26**, 3691-3696.
147. F. H. Stephens, V. Pons and R. T. Baker, *Dalton Trans.*, 2007, 2613-2626.
148. N. C. Smythe and J. C. Gordon, *Eur. J. Inorg. Chem.*, 2010, 509-521.
149. B. Peng and J. Chen, *Energy Environ. Sci.*, 2008, **1**, 479-483.
150. C. W. Hamilton, R. T. Baker, A. Staubitz and I. Manners, *Chem. Soc. Rev.*, 2009, **38**, 279-293.
151. Z. Huang and T. Autrey, *Energy Environ. Sci.*, 2012, **5**, 9257-9268.
152. T. Autrey, M. Bowden and A. Karkamkar, *Faraday Discuss.,* 2011, **151**, 157-169.
153. V. M. Parvanov, G. K. Schenter, N. J. Hess, L. L. Daemen, M. Hartl, A. C. Stowe, D. M. Camaioni and T. Autrey, *Dalton Trans.*, 2008, 4514-4522.
154. A. Staubitz, A. P. M. Robertson and I. Manners, *Chem. Rev.*, 2010, **110**, 4079-4124.
155. http://hydrogen.energy.gov/pdfs/12017_historical_fuel_cell_h2_budgets.pdf.
156. S. Satyapal, J. Petrovic, C. Read, G. Thomas and G. Ordaz, *Catal. Today*, 2007, **120**, 246-256.
157. M. Dresselhaus, G. Crabtree and M. Buchanan, Basic Energy Sciences, Office of Science, U.S. Department of Energy, Washington, DC, 2003.

158. S. G. Shore and R. W. Parry, *J. Am. Chem. Soc.*, 1955, **77**, 6084-6085.
159. http://www1.eere.energy.gov/hydrogenandfuelcells/mypp/pdfs/exec_sum.pdf.
160. http://www1.eere.energy.gov/hydrogenandfuelcells/mypp/pdfs/storage.pdf, http://www1.eere.energy.gov/hydrogenandfuelcells/mypp/pdfs/storage.pdf.
161. http://www1.eere.energy.gov/hydrogenandfuelcells/pdfs/1_milliken_final.pdf.
162. http://www1.eere.energy.gov/hydrogenandfuelcells/pdfs/executive_summaries_h2_storage_coes.pdf.
163. http://www1.eere.energy.gov/hydrogenandfuelcells/pdfs/fct_h2_storage.pdf.
164. http://www1.eere.energy.gov/hydrogenandfuelcells/pdfs/h2_production_roadmap.pdf.
165. http://www1.eere.energy.gov/hydrogenandfuelcells/pdfs/h2_stor_mat_work_proceedings.pdf.
166. http://www1.eere.energy.gov/hydrogenandfuelcells/pdfs/storage.pdf.
167. http://www.sandia.gov/MHCoE/pdfs/Fuel-Cell%20Review%20Article.pdf.
168. K. A. Schwetz, *A.L. Ullmann's Encyclopedia of Industrial Chemistry*, VCH, Deerfield Beach, 1985.
169. M. G. Hu, R. A. Geanangel and W. W. Wendlandt, *Thermochim. Acta*, 1978, **23**, 249-255.
170. Y. S. Chua, P. Chen, G. T. Wu and Z. T. Xiong, *Chem. Commun.*, 2011, **47**, 5116-5129.
171. H. I. Schlesinger and A. B. Burg, *J. Am. Chem. Soc.*, 1938, vol. 60, p. 290.
172. S. De Benedetto, M. Carewska, C. Cento, P. Gislon, M. Pasquali, S. Scaccia and P. P. Prosini, *Thermochim. Acta*, 2006, **441**, 184-190.
173. Z. T. Xiong, C. K. Yong, G. T. Wu, P. Chen, W. Shaw, A. Karkamkar, T. Autrey, M. O. Jones, S. R. Johnson, P. P. Edwards and W. I. F. David, *Nat. Mater.*, 2008, **7**, 138-141.
174. G. Xia, X. Yu, Y. Guo, Z. Wu, C. Yang, H. Liu and S. Dou, *Chem.- Eur. J.*, 2010, **16**, 3763-3769.
175. Y. S. Chua, G. Wu, Z. Xiong, T. He and P. Chen, *Chem. Mat.*, 2009, **21**, 4899-4904.

176. S. Harder, J. Spielmann and B. Tobey, *Chem.- Eur. J.*, 2012, **18**, 1984-1991.
177. X. Kang, J. Luo, Q. Zhang and P. Wang, *Dalton Trans.*, 2011, **40**, 3799-3801.
178. S. M. Lee, X. D. Kang, P. Wang, H. M. Cheng and Y. H. Lee, *ChemPhysChem*, 2009, **10**, 1825-1833.
179. S. A. Shevlin, B. Kerkeni and Z. X. Guo, *Phys. Chem. Chem. Phys.*, 2011, **13**, 7649-7659.
180. K. Shimoda, A. Yamane, T. Ichikawa and Y. Kojima, *J. Phys. Chem. C*, 2012, **116**, 20666-20672.
181. F. Li, J. Gao, J. Zhang, F. Xu, J. Zhao and L. Sun, *J. Mater. Chem. A*, 2013, **1**, 8016-8022.
182. F. Leardini, J. R. Ares, J. Bodega, M. J. Valero-Pedraza, M. A. Banares, J. F. Fernandez and C. Sanchez, *J. Phys. Chem. C*, 2012, **116**, 24430-24435.
183. Z. Yang, Y. Wang, J. Liang and J. Chen, *Mater. Trans.*, 2011, **52**, 651-653.
184. K. J. Fijalkowski, R. Jurczakowski, W. Koźmiński and W. Grochala, *Phys. Chem. Chem. Phys.*, 2012, **14**, 5778-5784.
185. J. Luo, H. Wu, W. Zhou, X. Kang and P. Wang, *Int. J. Hydrogen Energy*, 2013, **38**, 197-204.
186. W. Li, L. Miao, R. H. Scheicher, Z. Xiong, G. Wu, C. M. Araujo, A. Blomqvist, R. Ahuja, Y. Feng and P. Chen, *Dalton Trans.*, 2012, **41**, 4754-4764.
187. Y. S. Chua, W. Li, W. J. Shaw, G. Wu, T. Autrey, Z. Xiong, M. W. Wong and P. Chen, *Chem. Sus. Chem.*, 2012, **5**, 927-931.
188. T. He, J. Wang, Z. Chen, A. Wu, G. Wu, J. Yin, H. Chu, Z. Xiong, T. Zhang and P. Chen, *J. Mater. Chem.*, 2012, **22**, 7478-7483.
189. G. Xia, Y. Tan, X. Chen, Z. Guo, H. Liu and X. Yu, *J. Mater. Chem. A*, 2013, **1**, 1810-1820.
190. Y. S. Chua, H. Wu, W. Zhou, T. J. Udovic, G. Wu, Z. Xiong, M. W. Wong and P. Chen, *Inorg. Chem.*, 2012, **51**, 1599-1603.
191. K. J. Fijalkowski, R. V. Genova, Y. Filinchuk, A. Budzianowski, M. Derzsi, T. Jaron, P. J. Leszczynski and W. Grochala, *Dalton Trans.*, 2011, **40**, 4407-4413.
192. Z. Tang, Y. Tan, X. Chen and X. Yu, *Chem. Commun.*, 2012, **48**, 9296-9298.

193. W. Li, G. Wu, Y. Chua, Y. P. Feng and P. Chen, *Inorg. Chem.*, 2012, **51**, 76-87.

194. X. Kang, H. Wu, J. Luo, W. Zhou and P. Wang, *J. Mater. Chem.*, 2012, **22**, 13174-13179.

195. F. P. R. Sandra, U. B. Demirci, R. Chiriac, R. Moury and P. Miele, *Int. J. Hydrogen Energy*, 2011, **36**, 7423-7430.

196. H. Wu, W. Zhou, F. E. Pinkerton, M. S. Meyer, Q. Yao, S. Gadipelli, T. J. Udovic, T. Yildirim and J. J. Rush, *Chem. Commun.*, 2011, **47**, 4102-4104.

197. K. Shimoda, Y. Zhang, T. Ichikawa, H. Miyaoka and Y. Kojima, *J. Mater. Chem.*, 2011, **21**, 2609-2615.

198. K. J. Fijakowski and W. Grochala, *J. Mater. Chem.*, 2009, **19**, 2043-2050.

199. Z. Xiong, G. Wu, Y. S. Chua, J. Hu, T. He, W. Xu and P. Chen, *Energy Environ. Sci.*, 2008, **1**, 360-363.

200. Q. Zhang, C. Tang, C. Fang, F. Fang, D. Sun, L. Ouyang and M. Zhu, *J. Phys. Chem. C*, 2010, **114**, 1709-1714.

201. H. V. K. Diyabalanage, R. P. Shrestha, T. A. Semelsberger, B. L. Scott, M. E. Bowden, B. L. Davis and A. K. Burrell, *Angew. Chem.-Int. Ed.*, 2007, **46**, 8995-8997.

202. J. Spielmann and S. Harder, *Dalton Trans.*, 2011, **40**, 8314-8319.

203. J. Spielmann and S. Harder, *J. Am. Chem. Soc.*, 2009, **131**, 5064-5065.

204. C. Jones, S. J. Bonyhady, S. Nembenna and A. Stasch, *Eur. J. Inorg. Chem.*, 2012, 2596-2601.

205. J. Spielmann, D. F. J. Piesik and S. Harder, *Chem.- Eur. J.*, 2010, **16**, 8307-8318.

206. D. J. Wolstenholme, J. Flogeras, F. N. Che, A. Decken and G. S. McGrady, *J. Am. Chem. Soc.*, 2013, **135**, 2439-2442.

207. X. D. Kang, Z. Z. Fang, L. Y. Kong, H. M. Cheng, X. D. Yao, G. Q. Lu and P. Wang, *Adv. Mater.*, 2008, **20**, 2756-2759.

208. Z. Xiong, Y. S. Chua, G. Wu, W. Xu, P. Chen, W. Shaw, A. Karkamkar, J. Linehan, T. Smurthwaite and T. Autrey, *Chem. Commun. (Camb)*, 2008, 5595-5597.

209. S. B. Kalidindi, J. Joseph and B. R. Jagirdar, *Energy Environ. Sci.*, 2009, **2**, 1274-1276.

210. R. Chiriac, F. Toche, U. B. Demirci, O. Krol and P. Miele, *Int. J. Hydrogen Energy*, 2011, **36**, 12955-12964.
211. K. R. Graham, T. Kemmitt and M. E. Bowden, *Energy Environ. Sci.*, 2009, **2**, 706-710.
212. Z. T. Xiong, Y. S. Chua, G. T. Wu, L. Wang, M. W. Wong, Z. M. Kam, T. Autrey, T. Kemmitt and P. Chen, *Dalton Trans.*, 2010, **39**, 720-722.
213. S. Duman, O. Metin and S. Ozkar, *J. Nanosci. Nanotech.*, 2013, **13**, 4954-4961.
214. J. F. Sonnenberg and R. H. Morris, *ACS Catal.*, 2013, **3**, 1092-1102.
215. J. M. Yan, X. B. Zhang, S. Han, H. Shioyama and Q. Xu, *Angew. Chem. Int. Ed. Engl.*, 2008, **47**, 2287-2289.
216. F. Pelletier, D. Ciuculescu, J. G. Mattei, P. Lecante, M. J. Casanove, N. Yaacoub, J. M. Greneche, C. Schmitz-Antoniak and C. Amiens, *Chemistry*, 2013, **19**, 6021-6026.
217. S. Basu, A. Brockman, P. Gagare, Y. Zheng, P. V. Ramachandran, W. N. Delgass and J. P. Gore, *J. Power Sources*, 2009, **188**, 238-243.
218. C.-H. Liu, Y.-C. Wu, C.-C. Chou, B.-H. Chen, C.-L. Hsueh, J.-R. Ku and F. Tsau, *Int. J. Hydrogen Energy*, 2012, **37**, 2950-2959.
219. G. Chen, S. Desinan, R. Rosei, F. Rosei and D. Ma, *Chemistry*, 2012, **18**, 7925-7930.
220. F. Durap, M. Zahmakiran and S. Ozkar, *Int. J. Hydrogen Energy*, 2009, **34**, 7223-7230.
221. Q. Xu and M. Chandra, *J. Alloys Compd.*, 2007, **446**, 729-732.
222. M. Chandra and Q. Xu, *J. Power Sources*, 2007, **168**, 135-142.
223. P. V. Ramachandran and P. D. Gagare, *Inorg. Chem.*, 2007, **46**, 7810-7817.
224. S. Basu, Y. Zheng, A. Varma, W. N. Delgass and J. P. Gore, *J. Power Sources*, 2010, **195**, 1957-1963.
225. O. Metin, S. Sahin and S. Ozkar, *Int. J. Hydrogen Energy*, 2009, **34**, 6304-6313.
226. D. Sun, V. Mazumder, Ö. Metin and S. Sun, *ACS Nano*, 2011, **5**, 6458-6464.
227. S. B. Kalidindi, M. Indirani and B. R. Jagirdar, *Inorg. Chem.*, 2008, **47**, 7424-7429.

228. T. J. Clark, G. R. Whittell and I. Manners, *Inorg. Chem.*, 2007, **46**, 7522-7527.
229. H.-B. Dai, L.-L. Gao, Y. Liang, X.-D. Kang and P. Wang, *J. Power Sources*, 2010, **195**, 307-312.
230. O. Metin, M. Dinc, Z. S. Eren and S. Ozkar, *Int. J. Hydrogen Energy*, 2011, **36**, 11528-11535.
231. O. Metin and S. Ozkar, *Int. J. Hydrogen Energy*, 2011, **36**, 1424-1432.
232. Q. Xu and M. Chandra, *J. Power Sources*, 2006, **163**, 364-370.
233. S. B. Kalidindi, A. A. Vernekar and B. R. Jagirdar, *Phys. Chem. Chem. Phys.*, 2009, **11**, 770-775.
234. O. Metin and S. Ozkar, *Energy Fuels*, 2009, **23**, 3517-3526.
235. K. Eom, K. Cho and H. Kwon, *Int. J. Hydrogen Energy*, 2010, **35**, 181-186.
236. M. Rakap and S. Ozkar, *Int. J. Hydrogen Energy*, 2010, **35**, 3341-3346.
237. R. Chamoun, U. B. Demirci, D. Cornu, Y. Zaatar, A. Khoury, R. Khoury and P. Miele, *Appl. Surf. Sci.*, 2010, **256**, 7684-7691.
238. R. Benzouaa, U. B. Demirci, R. Chiriac, F. Toche and P. Miele, *Thermochim. Acta*, 2010, **509**, 81-86.
239. D. G. Tong, X. L. Zeng, W. Chu, D. Wang and P. Wu, *J. Mater. Sci.*, 2010, **45**, 2862-2867.
240. N. Patel, R. Fernandes, G. Guella and A. Miotello, *Appl. Catal. B*, 2010, **95**, 137-143.
241. T. Umegaki, J. M. Yan, X. B. Zhang, H. Shioyama, N. Kuriyama and Q. A. Xu, *J. Power Sources*, 2010, **195**, 8209-8214.
242. M. Zahmakiran and S. Ozkar, *Inorg. Chem.*, 2009, **48**, 8955-8964.
243. S. Karahan, M. Zahmakıran and S. Özkar, *Chem. Commun. (Camb)*, 2012, **48**, 1180-1182.
244. M. Fetz, R. Gerber, O. Blacque and C. M. Frech, *Chemistry*, 2011, **17**, 4732-4736.
245. T. Ayvali, M. Zahmakiran and S. Ozkar, *Dalton Trans.*, 2011, **40**, 3584-3591.
246. M. Zahmakiran and S. Ozkar, *Appl. Catal. B*, 2009, **89**, 104-110.

247. V. I. Simagina, P. A. Storozhenko, O. V. Netskina, O. V. Komova, G. V. Odegova, Y. V. Larichev, A. V. Ishchenko and A. M. Ozerova, *Catal. Today*, 2008, **138**, 253-259.
248. F. Durap, M. Zahmakiran and S. Ozkar, *Appl. Catal. A*, 2009, **369**, 53-59.
249. A. P. Robertson, R. Suter, L. Chabanne, G. R. Whittell and I. Manners, *Inorg. Chem.*, 2011, **50**, 12680-12691.
250. C. Y. Cao, C. Q. Chen, W. Li, W. G. Song and W. Cai, *ChemSusChem*, 2010, **3**, 1241-1244.
251. M. Couturier, J. L. Tucker, B. M. Andresen, P. Dube and J. T. Negri, *Org. Lett.*, 2001, **3**, 465-467.
252. J. M. Yan, X. B. Zhang, S. Han, H. Shioyama and Q. Xu, *Inorg. Chem.*, 2009, **48**, 7389-7393.
253. P. Z. Li, K. Aranishi and Q. Xu, *Chem. Commun. (Camb)*, 2012, **48**, 3173-3175.
254. T. Umegaki, J. M. Yan, X. B. Zhang, H. Shioyama, N. Kuriyama and Q. Xu, *J. Power Sources*, 2009, **191**, 209-216.
255. T. Umegaki, J. M. Yan, X. B. Zhang, H. Shioyama, N. Kuriyama and Q. Xu, *Int. J. Hydrogen Energy*, 2009, **34**, 3816-3822.
256. O. Metin, S. Ozkar and S. H. Sun, *Nano Res.*, 2010, **3**, 676-684.
257. O. Metin, V. Mazumder, S. Ozkar and S. S. Sun, *J. Am. Chem. Soc.*, 2010, **132**, 1468-1469.
258. M. Couturier, J. L. Tucker, B. M. Andresen, E. Dube, S. J. Brenek and J. T. Negri, *Tetrahedron Lett.*, 2001, **42**, 2285-2288.
259. H. Erdogan, O. Metin and S. Oezkar, *Phys. Chem. Chem. Phys.*, 2009, **11**, 10519-10525.
260. O. Metin, S. Duman, M. Dinc and S. Ozkar, *J. Phys. Chem. C*, 2011, **115**, 10736-10743.
261. S. K. Kim, T. J. Kim, T. Y. Kim, G. Lee, J. T. Park, S. W. Nam and S. O. Kang, *Chem. Commun. (Camb)*, 2012, **48**, 2021-2023.
262. M. Rakap and S. Ozkar, *Int. J. Hydrogen Energy*, 2010, **35**, 1305-1312.
263. M. Chandra and Q. Xu, *J. Power Sources*, 2006, **156**, 190-194.
264. N. Mohajeri, A. T-Raissi and O. Adebiyi, *J. Power Sources*, 2007, **167**, 482-485.

265. S. B. Kalidindi, U. Sanyal and B. R. Jagirdar, *Phys. Chem. Chem. Phys.*, 2008, **10**, 5870-5874.

266. M. Zahmakiran, F. Durap and S. Ozkar, *Int. J. Hydrogen Energy*, 2010, **35**, 187-197.

267. C. F. Yao, L. Zhuang, Y. L. Cao, X. P. Ai and H. X. Yang, *Int. J. Hydrogen Energy*, 2008, **33**, 2462-2467.

268. J. H. Park, H. S. Kim, H. J. Kim, M. K. Han and Y. G. Shul, *Res. Chem. Intermed.*, 2008, **34**, 709-715.

269. F. Cheng, H. Ma, Y. Li and J. Chen, *Inorg. Chem.*, 2007, **46**, 788-794.

270. H. L. Jiang, T. Umegaki, T. Akita, X. B. Zhang, M. Haruta and Q. Xu, *Chem.- Eur. J.*, 2010, **16**, 3132-3137.

271. T. Kakizawa, Y. Kawano, K. Naganeyama and M. Shimoi, *Chem. Lett.*, 2011, **40**, 171-173.

272. B. Bera and B. R. Jagirdar, *Inorg. Chim. Acta*, 2011, **372**, 200-205.

273. Y. Kawano, M. Uruichi, M. Shimoi, S. Taki, T. Kawaguchi, T. Kakizawa and H. Ogino, *J. Am. Chem. Soc.*, 2009, **131**, 14946-14957.

274. Y. Kawano, K. Yamaguchi, S. Y. Miyake, T. Kakizawa and M. Shimoi, *Chem.- Eur. J.*, 2007, **13**, 6920-6931.

275. Y. Kawano, M. Uruichi, M. Shimoi, S. Taki, T. Kawaguchi, T. Kakizawa and H. Ogino, *J. Am. Chem. Soc.*, 2009, **131**, 14946-14957.

276. R. Tian and F. Mathey, *Chemistry*, 2012, **18**, 11210-11213.

277. Y. Jiang and H. Berke, *Chem. Commun.*, 2007, 3571-3573.

278. Y. Jiang, O. Blacque, T. Fox, C. M. Frech and H. Berke, *Organometallics*, 2009, **28**, 5493-5504.

279. R. T. Baker, J. C. Gordon, C. W. Hamilton, N. J. Henson, P. H. Lin, S. Maguire, M. Murugesu, B. L. Scott and N. C. Smythe, *J. Am. Chem. Soc.*, 2012, **134**, 5598-5609.

280. J. R. Vance, A. P. Robertson, K. Lee and I. Manners, *Chemistry*, 2011, **17**, 4099-4103.

281. T. Miyazaki, Y. Tanabe, M. Yuki, Y. Miyake and Y. Nishibayashi, *Organometallics*, 2011, **30**, 2394-2404.

282. S. Musa, S. Fronton, L. Vaccaro and D. Gelman, *Organometallics*, 2013, **32**, 3069-3073.

283. G. Alcaraz, M. Grellier and S. Sabo-Etienne, *Acc. Chem. Res.*, 2009, **42**, 1640-1649.
284. B. L. Conley and T. J. Williams, *Chem. Commun. (Camb)*, 2010, **46**, 4815-4817.
285. C. J. Wallis, H. Dyer, L. Vendier, G. Alcaraz and S. Sabo-Etienne, *Angew. Chem.-Int. Ed.*, 2012, **51**, 3646-3648.
286. S. Caliskan, M. Zahmakiran, F. Durap and S. Ozkar, *Dalton Trans.*, 2012, **41**, 4976-4984.
287. B. L. Conley, D. Guess and T. J. Williams, *J. Am. Chem. Soc.*, 2011, **133**, 14212-14215.
288. A. E. W. Ledger, C. E. Ellul, M. F. Mahon, J. M. J. Williams and M. K. Whittlesey, *Chem.- Eur. J.*, 2011, **17**, 8704-8713.
289. G. Alcaraz, L. Vendier, E. Clot and S. Sabo-Etienne, *Angew. Chem.-Int. Ed.*, 2010, **49**, 918-920.
290. M. Käss, A. Friedrich, M. Drees and S. Schneider, *Angew. Chem. Int. Ed. Engl.*, 2009, **48**, 905-907.
291. G. Alcaraz, A. B. Chaplin, C. J. Stevens, E. Clot, L. Vendier, A. S. Weller and S. Sabo-Etienne, *Organometallics*, 2010, **29**, 5591-5595.
292. T. D. Nixon, M. K. Whittlesey and J. M. J. Williams, *Tetrahedron Lett.*, 2011, **52**, 6652-6654.
293. N. Blaquiere, S. Diallo-Garcia, S. I. Gorelsky, D. A. Black and K. Fagnou, *J. Am. Chem. Soc.*, 2008, **130**, 14034-14035.
294. A. Friedrich, M. Drees and S. Schneider, *Chem.-Eur. J.*, 2009, **15**, 10339-10342.
295. D. F. Schreiber, C. O'Connor, C. Grave, Y. Ortin, H. Mueller-Bunz and A. D. Phillips, *ACS Catal.*, 2012, **2**, 2505-2511.
296. A. Staubitz, M. E. Sloan, A. P. Robertson, A. Friedrich, S. Schneider, P. J. Gates, J. Schmedt auf der Günne and I. Manners, *J. Am. Chem. Soc.*, 2010, **132**, 13332-13345.
297. C. Boulho and J. P. Djukic, *Dalton Trans.*, 2010, **39**, 8893-8905.
298. M. Zahmakiran, T. Ayvalı and K. Philippot, *Langmuir*, 2012, **28**, 4908-4914.
299. C. A. Jaska, K. Temple, A. J. Lough and I. Manners, *J. Am. Chem. Soc.*, 2003, **125**, 9424-9434.

300. A. N. Marziale, A. Friedrich, I. Klopsch, M. Drees, V. R. Celinski, J. Schmedt auf der Günne and S. Schneider, *J. Am. Chem. Soc.*, 2013.
301. A. B. Chaplin and A. S. Weller, *Inorg. Chem.*, 2010, **49**, 1111-1121.
302. T. M. Douglas, A. B. Chaplin and A. S. Weller, *J. Am. Chem. Soc.*, 2008, **130**, 14432-14433.
303. A. B. Chaplin and A. S. Weller, *Angew. Chem.-Int. Ed.*, 2010, **49**, 581-584.
304. C. Y. Tang, A. L. Thompson and S. Aldridge, *J. Am. Chem. Soc.*, 2010, **132**, 10578-10591.
305. V. Butera, N. Russo and E. Sicilia, *Chemistry*, 2011, **17**, 14586-14592.
306. C. A. Jaska and I. Manners, *J. Am. Chem. Soc.*, 2004, **126**, 9776-9785.
307. L. J. Sewell, A. B. Chaplin and A. S. Weller, *Dalton Trans.*, 2011, **40**, 7499-7501.
308. Y. S. Chen, J. L. Fulton, J. C. Linehan and T. Autrey, *J. Am. Chem. Soc.*, 2005, **127**, 3254-3255.
309. T. M. Douglas, A. B. Chaplin, A. S. Weller, X. Yang and M. B. Hall, *J. Am. Chem. Soc.*, 2009, **131**, 15440-15456.
310. C. Y. Tang, A. L. Thompson and S. Aldridge, *Angew. Chem.-Int. Ed.*, 2010, **49**, 921-925.
311. A. B. Chaplin and A. S. Weller, *Acta Crystallogr. Sect. C-Cryst. Struct. Commun.*, 2011, **67**, M355-M358.
312. C. A. Jaska, K. Temple, A. J. Lough and I. Manners, *Chem. Commun.*, 2001, 962-963.
313. M. E. Sloan, T. J. Clark and I. Manners, *Inorg. Chem.*, 2009, **48**, 2429-2435.
314. A. B. Chaplin and A. S. Weller, *Inorg. Chem.*, 2010, **49**, 1111-1121.
315. L. J. Sewell, M. A. Huertos, M. E. Dickinson, A. S. Weller and G. C. Lloyd-Jones, *Inorg. Chem.*, 2013, **52**, 4509-4516.
316. L. J. Sewell, G. C. Lloyd-Jones and A. S. Weller, *J. Am. Chem. Soc.*, 2012, **134**, 3598-3610.
317. A. Paul and C. B. Musgrave, *Angew. Chem. Int. Ed. Engl.*, 2007, **46**, 8153-8156.
318. H. C. Johnson, A. P. M. Robertson, A. B. Chaplin, L. J. Sewell, A. L. Thompson, M. F. Haddow, I. Manners and A. S. Weller, *J. Am. Chem. Soc.*, 2011, **133**, 11076-11079.

319. K. Ghatak and K. Vanka, *Comp. Theor. Chem.*, 2012, **992**, 18-29.

320. G. C. Fortman, A. M. Z. Slawin and S. P. Nolan, *Organometallics*, 2011, **30**, 5487-5492.

321. A. Staubitz, A. P. Soto and I. Manners, *Angew. Chem.-Int. Ed.*, 2008, **47**, 6212-6215.

322. B. L. Dietrich, K. I. Goldberg, D. M. Heinekey, T. Autrey and J. C. Linehan, *Inorg. Chem.*, 2008, **47**, 8583-8585.

323. H. C. Johnson and A. S. Weller, *J. Organomet. Chem.*, 2012, **721**, 17-22.

324. M. C. Denney, V. Pons, T. J. Hebden, D. M. Heinekey and K. I. Goldberg, *J. Am. Chem. Soc.*, 2006, **128**, 12048-12049.

325. C. J. Stevens, R. Dallanegra, A. B. Chaplin, A. S. Weller, S. A. Macgregor, B. Ward, D. McKay, G. Alcaraz and S. Sabo-Etienne, *Chemistry*, 2011, **17**, 3011-3020.

326. B. L. Dietrich, K. I. Goldberg, D. M. Heinekey, T. Autrey and J. C. Linehan, *Inorg. Chem.*, 2008, **47**, 8583-8585.

327. M. Vogt, B. de Bruin, H. Berke, M. Trincado and H. Gruetzmacher, *Chem. Sci.*, 2011, **2**, 723-727.

328. P. M. Zimmerman, A. Paul, Z. Zhang and C. B. Musgrave, *Angew. Chem. Int. Ed. Engl.*, 2009, **48**, 2201-2205.

329. S. Harder, C. Ruspic, N. N. Bhriain, F. Berkermann and M. Schuermann, *Z. Nat. B-J. Chem. Sci.*, 2008, **63**, 267-274.

330. X. Yang and M. B. Hall, *J. Organomet. Chem.*, 2009, **694**, 2831-2838.

331. R. J. Keaton, J. M. Blacquiere and R. T. Baker, *J. Am. Chem. Soc.*, 2007, **129**, 1844-1845.

332. A. Rossin, G. Bottari, A. M. Lozano-Vila, M. Paneque, M. Peruzzini, A. Rossi and F. Zanobini, *Dalton Trans.*, 2013, **42**, 3533-3541.

333. S. K. Kim, W. S. Han, T. J. Kim, T. Y. Kim, S. W. Nam, M. Mitoraj, Ł. Piekoś, A. Michalak, S. J. Hwang and S. O. Kang, *J. Am. Chem. Soc.*, 2010, **132**, 9954-9955.

334. C. E. Hartmann, V. Jurčík, O. Songis and C. S. Cazin, *Chem. Commun. (Camb)*, 2013, **49**, 1005-1007.

335. T. J. Clark, C. A. Russell and I. Manners, *J. Am. Chem. Soc.*, 2006, **128**, 9582-9583.

336. M. E. Sloan, A. Staubitz, T. J. Clark, C. A. Russell, G. C. Lloyd-Jones and I. Manners, *J. Am. Chem. Soc.*, 2010, **132**, 3831-3841.
337. K. W. Boddeker, S. G. Shore and R. K. Bunting, *J. Am. Chem. Soc.*, 1966, **88**, 4396-4401.
338. Y. Luo and K. Ohno, *Organometallics*, 2007, **26**, 3597-3600.
339. G. Alcaraz and S. Sabo-Etienne, *Angew. Chem.-Int. Ed.*, 2010, **49**, 7170-7179.
340. V. Pons, R. T. Baker, N. K. Szymczak, D. J. Heldebrant, J. C. Linehan, M. H. Matus, D. J. Grant and D. A. Dixon, *Chem Commun. (Camb)*, 2008, 6597-6599.
341. A. J. Miller and J. E. Bercaw, *Chem Commun. (Camb)*, 2010, **46**, 1709-1711.
342. G. R. Whittell, E. I. Balmond, A. P. M. Robertson, S. K. Patra, M. F. Haddow and I. Manners, *Eur. J. Inorg. Chem.*, 2010, 3967-3975.
343. A. M. Chapman, M. F. Haddow and D. F. Wass, *J. Am. Chem. Soc.*, 2011, **133**, 8826-8829.
344. A. M. Chapman and D. F. Wass, *Dalton Trans.*, 2012, **41**, 9067-9072.
345. J. Spielmann, M. Bolte and S. Harder, *Chem. Commun.,* 2009, 6934-6936.
346. M. S. Hill, G. Kociok-Köhn and T. P. Robinson, *Chem. Commun. (Camb)*, 2010, **46**, 7587-7589.
347. H. J. Cowley, M. S. Holt, R. L. Melen, J. M. Rawson and D. S. Wright, *Chem. Commun. (Camb)*, 2011, **47**, 2682-2684.
348. R. J. Less, R. L. Melen and D. S. Wright, *RSC Adv.*, 2012, **2**, 2191-2199.
349. M. M. Hansmann, R. L. Melen and D. S. Wright, *Chem. Sci.*, 2011, **2**, 1554-1559.
350. J. Spielmann, M. Bolte and S. Harder, *Chem. Commun. (Camb)*, 2009, 6934-6936.
351. D. J. Liptrot, M. S. Hill, M. F. Mahon and D. J. MacDougall, *Chem. Eur. J.*, 2010, **16**, 8508-8515.
352. M. S. Hill, M. Hodgson, D. J. Liptrot and M. F. Mahon, *Dalton Trans.*, 2011, **40**, 7783-7790.
353. E. Lu, Y. Yuan, Y. Chen and W. Xia, *ACS Catal.*, 2013, **3**, 521-524.
354. P. Cui, T. P. Spaniol, L. Maron and J. Okuda, *Chem. Eur. J.*, 2013, 19 (40), 13437-13444.

355. R. J. Less, H. R. Simmonds, S. B. J. Dane and D. S. Wright, *Dalton Trans.*, 2013, **42**, 6337-6343.
356. S. Harder and J. Spielmann, *Chem. Commun.*, 2011, **47**, 11945-11947.
357. A. J. Mountford, S. J. Lancaster, S. J. Coles, P. N. Horton, D. L. Hughes, M. B. Hursthouse and M. E. Light, *Inorg. Chem.*, 2005, **44**, 5921-5933.
358. T. Beweries, J. Thomas, M. Klahn, A. Schulz, D. Heller and U. Rosenthal, *Chemcatchem*, 2011, **3**, 1865-1868.
359. A. J. Mountford, W. Clegg, S. J. Coles, R. W. Harrington, P. N. Horton, S. M. Humphrey, M. B. Hursthouse, J. A. Wright and S. J. Lancaster, *Chem. Eur. J.*, 2007, **13**, 4535-4547.
360. H. Helten, B. Dutta, J. R. Vance, M. E. Sloan, M. F. Haddow, S. Sproules, D. Collison, G. R. Whittell, G. C. Lloyd-Jones and I. Manners, *Angew. Chem.-Int. Ed.*, 2013, **52**, 437-440.
361. D. Pun, E. Lobkovsky and P. J. Chirik, *Chem. Commun.*, 2007, 3297-3299.
362. T. D. Forster, H. M. Tuononen, M. Parvez and R. Roesler, *J. Am. Chem. Soc.*, 2009, **131**, 6689-6691.
363. E. A. Jacobs, A. Fuller, S. J. Coles, G. A. Jones, G. J. Tizzard, J. A. Wright and S. J. Lancaster, *Chemistry*, 2012, **18**, 8647-8658.
364. A. G. M. Barrett, M. R. Crimmin, M. S. Hill, P. B. Hitchcock and P. A. Procopiou, *Organometallics*, 2007, **26**, 4076-4079.
365. L. Euzenat, D. Horhant, Y. Ribourdouille, C. Duriez, G. Alcaraz and M. Vaultier, *Chem. Commun. (Camb)*, 2003, 2280-2281.
366. S. S. Barnes, C. M. Vogels, A. Decken and S. A. Westcott, *Dalton Trans.*, 2011, **40**, 4707-4714.
367. J. Bill, R. Riedel and G. Passing, *Z. Anorg. Allg. Chem.*, 1992, **610**, 83-90.
368. J. Bill, F. Aldinger, G. Petzow, M. Sloma, J. Maier and R. Riedel, *J. Mater. Sci. Lett.*, 1999, **18**, 1513-1516.
369. X. Wang, A. Pakdel, C. Zhi, K. Watanabe, T. Sekiguchi, D. Golberg and Y. Bando, *J. Phys. Condens. Matter*, 2012, **24**, 314205.
370. D. Neiner, A. Karkamkar, J. C. Linehan, B. Arey, T. Autrey and S. M. Kauzlarich, *J. Phys. Chem. C*, 2009, **113**, 1098-1103.
371. S. Frueh, R. Kellett, C. Mallery, T. Molter, W. S. Willis, C. King'ondu and S. L. Suib, *Inorg. Chem.*, 2011, **50**, 783-792.

372. D. P. Kim, K. T. Moon, J. G. Kho, J. Economy, C. Gervais and F. Babonneau, *Polym. Adv. Technol.*, 1999, **10**, 702-712.

373. T. He, J. Wang, G. Wu, H. Kim, T. Proffen, A. Wu, W. Li, T. Liu, Z. Xiong, C. Wu, H. Chu, J. Guo, T. Autrey, T. Zhang and P. Chen, *Chemistry*, 2010, **16**, 12814-12817.

374. A. Staubitz, A. Presa Soto and I. Manners, *Angew. Chem. Int. Ed. Engl.*, 2008, **47**, 6212-6215.

375. L. Pasumansky, D. Haddenham, J. W. Clary, G. B. Fisher, C. T. Goralski and B. Singaram, *J. Org. Chem.*, 2008, **73**, 1898-1905.

376. L. Pasumansky, C. T. Goralski and B. Singaram, *Org. Process Res. Dev.*, 2006, **10**, 959-970.

377. J. C. Fuller, E. L. Stangeland, C. T. Goralski and B. Singaram, *Tetrahedron Lett.*, 1993, **34**, 257-260.

378. W. Xu, R. Wang, G. Wu and P. Chen, *RSC Advances*, 2012, **2**, 6005-6010.

379. W. Xu, X. Zheng, G. Wu and P. Chen, *Chin. J. Chem.*, 2012, **30**, 1775-1780.

380. G. B. Fisher, J. C. Fuller, J. Harrison, S. G. Alvarez, E. R. Burkhardt, C. T. Goralski and B. Singaram, *J. Org. Chem.*, 1994, **59**, 6378-6385.

381. J. M. Flaniken, C. J. Collins, M. Lanz and B. Singaram, *Org. Lett.*, 1999, **1**, 799-801.

382. L. Dubois, J. C. Fiaud and H. B. Kagan, *Tetrahedron*, 1995, **51**, 3803-3812.

383. G. B. Fisher, J. C. Fuller, J. Harrison, C. T. Goralski and B. Singaram, *Tetrahedron Lett.*, 1993, **34**, 1091-1094.

384. S. G. Alvarez, G. B. Fisher and B. Singaram, *Tetrahedron Lett.*, 1995, **36**, 2567-2570.

385. J. C. Fuller, C. M. Belisle, C. T. Goralski and B. Singaram, *Tetrahedron Lett.*, 1994, **35**, 5389-5392.

386. W. Xu, G. Wu, W. Yao, H. Fan, J. Wu and P. Chen, *Chem.- Eur. J.,* 2012, **18**, 13885-13892.

387. M. Periasamy, J. V. B. Kanth and C. K. Reddy, *J. Chem. Soc.-Perkin Trans. 1*, 1995, 427-430.

388. Y. Kikugawa, *Chem. Lett.*, 1979, 415-418.

389. Y. Kikugawa and Y. Ogawa, *Chem. Pharm. Bull.*, 1979, **27**, 2405-2410.

390. G. C. Andrews, *Tetrahedron Lett.*, 1980, **21**, 697-700.

391. C. Uyeda, M. Biscoe, P. LePlae and R. Breslow, *Tetrahedron Lett.*, 2006, **47**, 127-130.
392. L. Shi, Y. Liu, Q. Liu, B. Wei and G. Zhang, *Green Chem.*, 2012, **14**, 1372-1375.
393. G. C. Andrews and T. C. Crawford, *Tetrahedron Lett.*, 1980, **21**, 693-696.
394. X. Yang, L. Zhao, T. Fox, Z. X. Wang and H. Berke, *Angew. Chem. Int. Ed. Engl.*, 2010, **49**, 2058-2062.
395. M. Couturier, B. M. Andresen, J. L. Tucker, P. Dube, S. J. Brenek and J. T. Negri, *Tetrahedron Lett.*, 2001, **42**, 2763-2766.
396. C. A. Jaska and I. Manners, *J. Am. Chem. Soc.*, 2004, **126**, 2698-2699.
397. T. J. Clark, C. A. Russell and I. Manners, *J. Am. Chem. Soc.*, 2006, **128**, 9582-9583.
398. N. E. Stubbs, A. P. M. Robertson, E. M. Leitao and I. Manners, *J. Organomet. Chem.*, 2013, **730**, 84-89.
399. A. P. M. Robertson, E. M. Leitao and I. Manners, *J. Am. Chem. Soc.*, 2011, **133**, 19322-19325.
400. H. C. Kelly and J. O. Edwards, *J. Am. Chem. Soc.*, 1960, **82**, 4842-4846.
401. C. K. Lau, S. Tardif, C. Dufresne and J. Scheigetz, *J. Org. Chem.*, 1989, **54**, 491-494.
402. R. E. Dolle, S. J. Schmidt, K. F. Erhard and L. I. Kruse, *J. Am. Chem. Soc.*, 1989, **111**, 278-284.
403. M. B. Eleveld and H. Hogeveen, *Tetrahedron Lett.*, 1986, **27**, 635-638.
404. F. Toda and K. Mori, *J. Chem. Soc.-Chem. Commun.*, 1989, 1245-1246.
405. J. H. Billman and J. W. McDowell, *J. Org. Chem.*, 1961, **26**, 1437-1440.
406. G. Ménard and D. W. Stephan, *J. Am. Chem. Soc.*, 2010, **132**, 1796-1797.
407. G. Ménard and D. W. Stephan, *Dalton Trans.*, 2013, **42**, 5447-5453.
408. M. J. Sgro, J. Domer and D. W. Stephan, *Chem. Commun.*, 2012, **48**, 7253-7255.
409. V. Sumerin, K. Chernichenko, F. Schulz, M. Leskelä, B. Rieger and T. Repo, *Top. Curr. Chem.*, 2013, **332**, 111-155.
410. G. Menard and D. W. Stephan, *J. Am. Chem. Soc.*, 2010, **132**, 1796-1797.
411. R. O. Hutchins, K. Learn, B. Nazer, D. Pytlewski and A. Pelter, *Org. Prep. Proced. Int.*, 1984, **16**, 337-372.

412. C. Camacho, G. Uribe and R. Contreras, *Synthesis-Stuttgart*, 1982, 1027-1030.

413. J. V. B. Kanth, *Aldrichim. Acta*, 2002, **35**, 57-66.

414. H. C. Brown, J. V. B. Kanth and M. Zaidlewicz, *J. Org. Chem.,* 1998, **63**, 5154-5163.

415. H. C. Brown, J. V. B. Kanth and M. Zaidlewicz, *Organometallics*, 1999, **18**, 1310-1317.

416. H. C. Brown, J. V. B. Kanth, P. V. Dalvi and M. Zaidlewicz, *J. Org. Chem.*, 1999, **64**, 6263-6274.

417. H. C. Johnson, C. L. McMullin, S. D. Pike, S. A. Macgregor and A. S. Weller, *Angew. Chem. Int. Ed.*, 2013, 52, 9776-9780.

2 Stoichiometric Reactions of Alkaline Earth Dialkyls with Amine Boranes

This chapter explores the stoichiometric reactivity of alkaline earth dialkyl species, **VII** $[M\{CH(SiMe_3)_2\}_2(THF)_2]$ where M = Mg, Ca, Sr, with secondary, dimethylamine borane (DMAB) and pyrrolidine borane (PB), and primary, *tert*-butylamine borane (TBAB), amine boranes. These reactions assess the viability of the proposed formation and subsequent insertion of an *in situ* generated unsaturated aminoborane species, $R_2N{=}BH_2$, in a stoichiometric regime.

2.1 Stoichiometric Reactions Between Alkaline Earth Dialkyls **VII** and Secondary Amine Boranes

The stoichiometric reaction between the alkaline earth dialkyl species **VIIMg, VIICa** and **VIISr**, with DMAB and PB, resulted in formation of the corresponding alkyl-metal amidoborane compounds **1** to **6.** An equation for these reactions is shown in Figure 2.1.

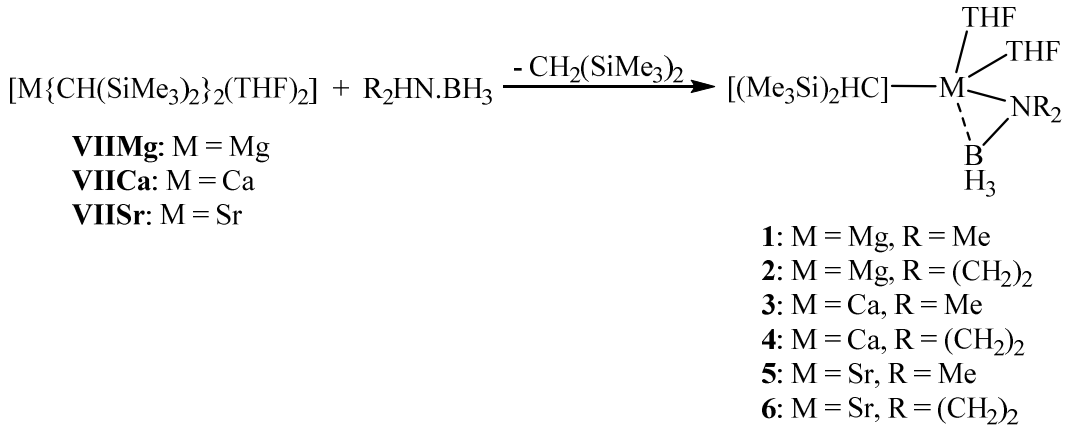

Figure 2.1: General equation for the stoichiometric reaction of alkaline earth dialkyl species $[M\{CH(SiMe_3)_2\}_2(THF)_2]$ **VIIMg**, **VIICa** and **VIISr**, with DMAB and PB, resulting in formation of compounds **1** to **6** respectively (**1**, **3**, **5**: R = Me; **2**, **4**, **6**: R = $(CH_2)_2$)), where M = Mg (**1** and **2**), Ca (**3** and **4**), Sr (**5** and **6**).

Stoichiometric reactions of **VIIMg** and **VIICa** with DMAB and PB, resulted in the formation of the corresponding alkylmagnesium-amidoborane species **1** and **2** and alkylcalcium-amidoborane species **3** and **4**, respectively. In all cases, however,

additional triplet resonances were observed in the ^{11}B NMR spectra for these reactions. In the case of reactions between **VIICa** and DMAB or PB triplet resonances were observed at ca. δ = –4.7 ppm integrating to ca. 19.6 % of the boron species and ca. δ = –7.9 ppm integrating to ca. 36.4 % respectively, indicating that compounds **3** and **4** were unstable at room temperature. In the case of reactions between **VIIMg** and DMAB or PB, however, triplet resonances were observed at ca. δ = 6.4 ppm integrating to ca. 37.3 % of the boron species and ca. δ = 5.0 ppm integrating to ca. 34.8 % respectively, which by comparison to magnesium amidoborane species reported by Hill could indicate the formation of species containing the $[NR_2BH_2NR_2BH_3]^-$ anion in addition to compounds **1** and **2**.[1, 2] The reactions of **VIISr** with DMAB and PB, however, proved to be the least complex, and resulted in clean conversion to compounds **5** and **6** respectively. Investigation of reactions with **VIISr** provided the clearest insight into the course of reaction.

The ^1H NMR spectra of compounds **5** and **6** indicated the presence of a single strontium-bound -$CH(SiMe_3)_2$ unit, evidenced by broadened singlet resonances integrating to 1H at δ = –1.7 ppm (**5** and **6**), in addition to the formation of one equivalent of $CH_2(SiMe_3)_2$, observed as singlet resonances integrating to 2H at δ = –0.36 ppm (**5**) and δ = –0.36 ppm (**6**) respectively, resulting from the protonation of the second -$CH(SiMe_3)_2$ group. The single quartet resonance in the ^{11}B NMR spectra for these compounds (**5**: δ = –9.3 ppm, $^1J_{BH}$ = 82 Hz, **6:** δ = –10.9 ppm, $^1J_{BH}$ = 82 Hz) was assigned to the BH_3 units of the respective strontium-bound amidoboranes, with shifts and coupling constants comparable to previously reported β-diketiminato calcium dimethylamidoborane **LXV** (δ = –11.5 ppm, $^1J_{BH}$ = 86 Hz), -pyrrolididoborane **LXVI** (δ = –11.5 ppm, $^1J_{BH}$ = 87 Hz) and β-diketiminato strontium dimethylamidoborane **LXVII** (δ = –10.7 ppm).[1,2] Isolation of **5** and **6** under vacuum yielded oily residues from which an accurate CHN microanalysis of **6** containing two molecules of coordinated THF was obtained. Although no accurate microanalytical data could be obtained for compound **5**, the solid-state structure, shown in Figure 2.2, was confirmed by X-ray diffraction analysis of a single crystal, obtained by crystallisation from a concentrated toluene solution at –30 °C.[3]

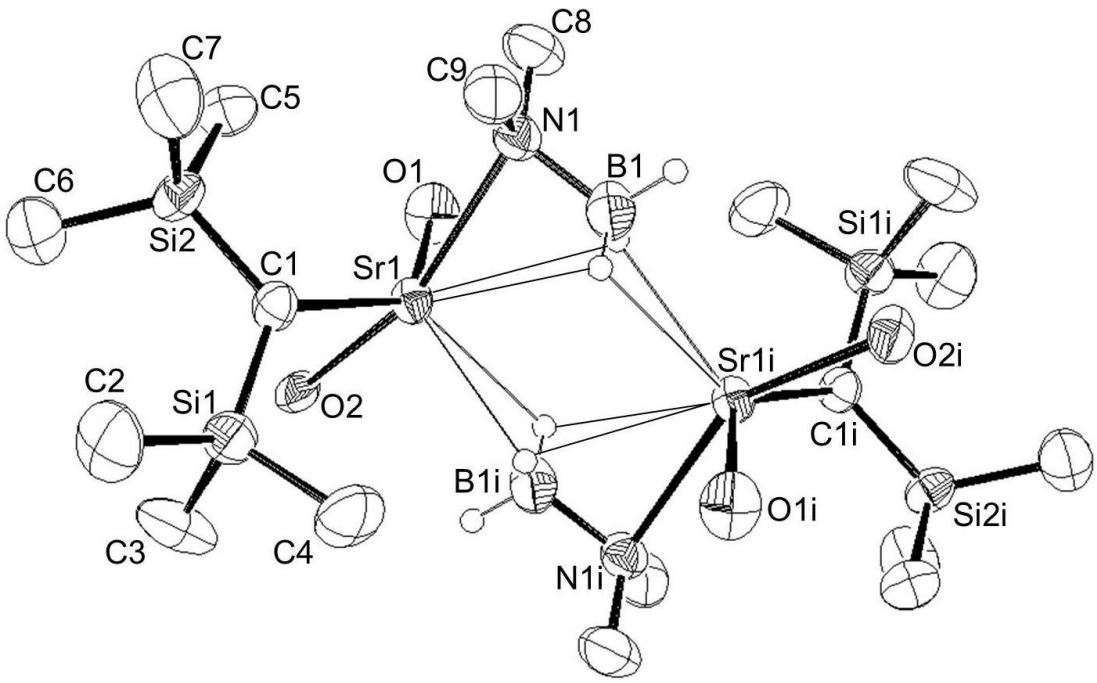

Figure 2.2: ORTEP representation of the solid-state structure of compound **5**, formed by the stoichiometric reaction between **VIISr** and DMAB. Thermal ellipsoids set at 50 % probability. Hydrogen atoms other than the boron-bound hydrides, and THF carbon atoms removed for clarity. Selected bond lengths (Å) and angles (°); B1-N1 1.519(4), B1-Sr1 2.960(4), N1-Sr1 2.673(19), B1-Sr1i 2.912(4), Sr1-C1 1.804(3), Sr1-N1-B1 85.2(2), Sr1-B1-Sr1i 96.8(1), N1-Sr1-C1 92.39(8).

Compound **5** is the first reported strontium amidoborane, a dimeric species formed of two $[Sr\{CH(SiMe_3)_2\}(NMe_2BH_3)(THF)_2]$ units, bound by the nitrogen of the amidoborane and bridged by Sr-H-Sr interactions between the strontium atom and boron bound hydrides of adjacent units. The Sr-N bond length [2.673(2) Å] in this structure is longer than the Ca-N bond lengths for Harder's β-diketiminato calcium-coordinated ammonia borane derivative **LXI** [2.399(2) Å], the methylamido borane **LXII** [2.382(4) Å], the *iso*-propylamido borane **LXIII** [2.406(4) Å] and the 2,6-di-*iso*-propylphenylanilido borane **LXIV** [2.460(2) Å],[4] which is attributed to the change in metal centre, ligand and amine group.

Although compounds **5** and **6** exhibited room temperature stability, heating at 80 °C for *ca.* 78 hours and 70 °C for *ca.* 102 hours respectively, resulted in reaction of these species, as evidenced by monitoring of the ^{1}H and ^{11}B NMR spectra. In both

cases the dialkylstrontium amidoborane species, **5** and **6**, underwent complete conversion to single boron containing species, **7** and **8** respectively, observed as doublet resonances in the ^{11}B NMR spectra (d_8-tol, **7**: δ = 44.8 ppm $^1J_{BH}$ = 102 Hz, C_6D_6, **8**: δ = 43.3 ppm $^1J_{BH}$ = 93 Hz). These are shown in Figures 2.3 and 2.4 respectively. A powdery precipitate was also observed in both of these reactions, thought to be SrH_2.

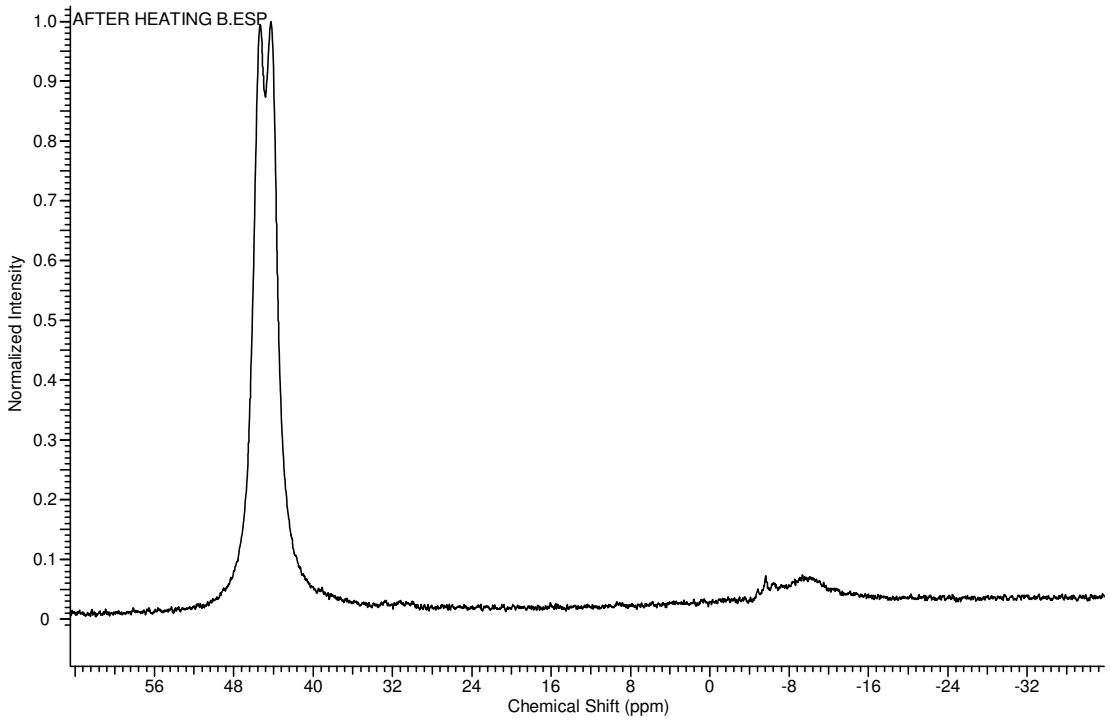

Figure 2.3: ^{11}B NMR spectrum of **7**, formed by thermolysis of compound **5**. (d_8-tol, 298 K, 96.3 MHz)

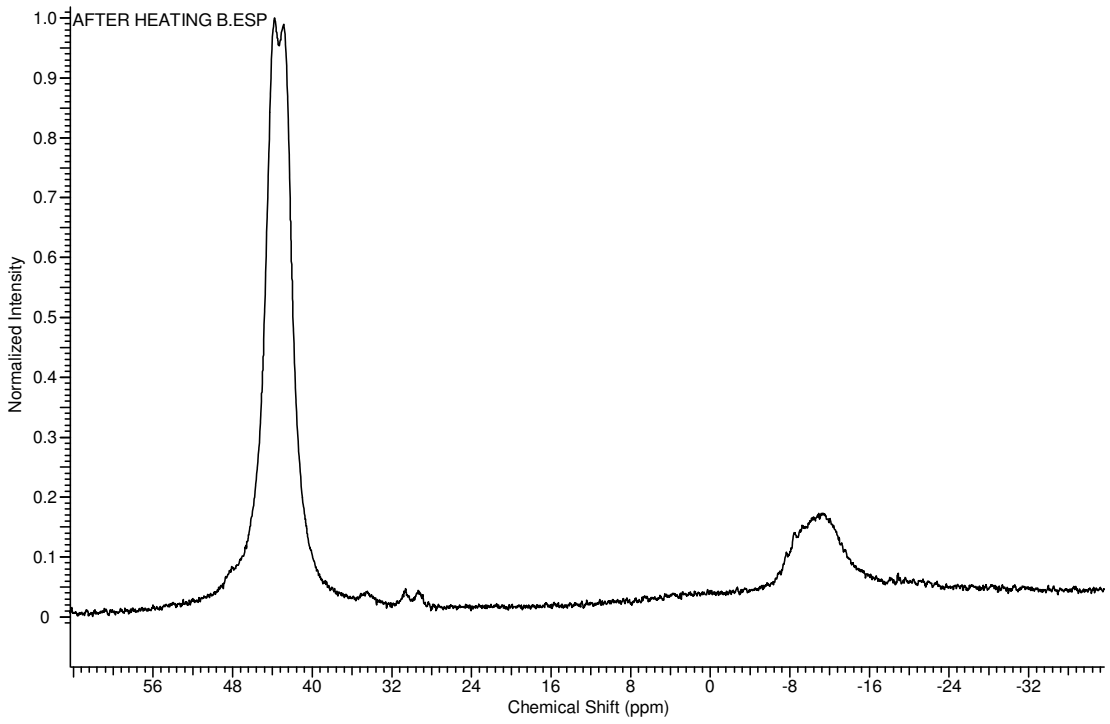

Figure 2.4: ^{11}B NMR spectrum of **8**, formed by thermolysis of compound **6**. (C_6D_6, 298 K, 96.3 MHz)

Although compounds **7** and **8** proved unstable to concentration under vacuum, ruling out structural confirmation by CHN microanalysis and X-ray crystallography, they were ultimately identified as the alkylaminoboranes shown in Figure 2.5 through a combination of NMR spectroscopic techniques.

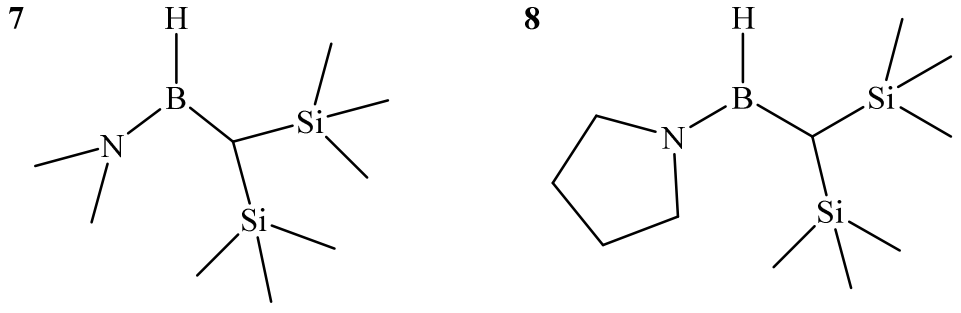

Figure 2.5: Structures of compounds **7** and **8**, formed by clean conversion of the corresponding alkylstrontium-amidoborane derivatives at elevated temperature.

The ^{1}H NMR spectra of both compounds displayed magnetic inequivalence for the nitrogen bound alkyl groups. Variable temperature ^{1}H NMR (d_8-tol) carried out on **7**

revealed a 96.5 Hz separation between the nitrogen bound methyl peaks at 298 K, decreasing to 84.4 Hz at 368 K in addition to a slight broadening of the resonances. This is shown in Figure 2.6.

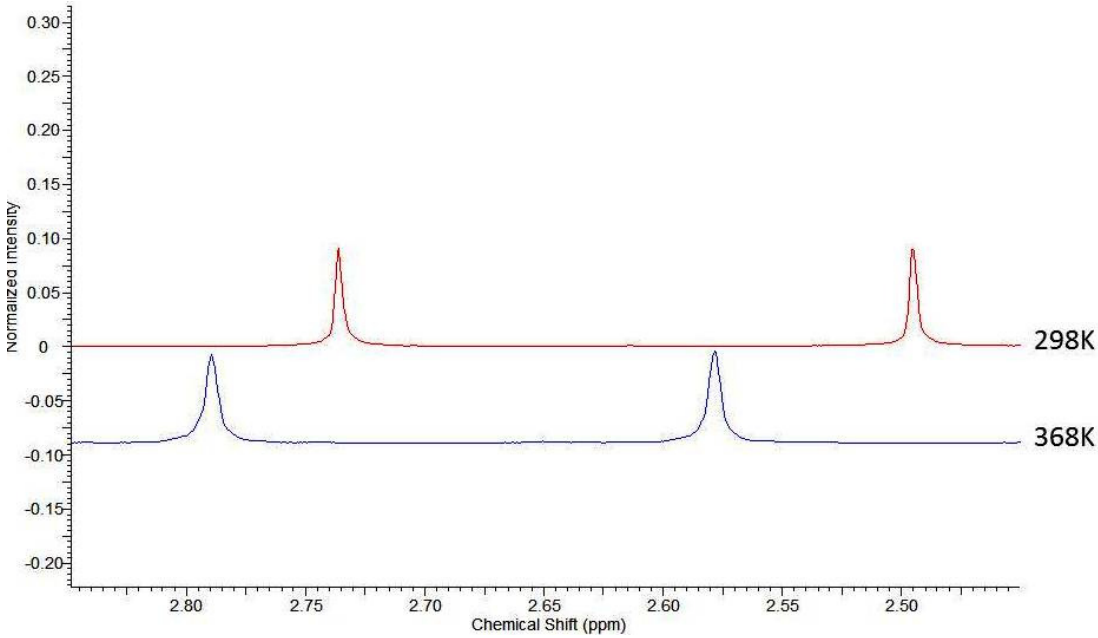

Figure 2.6: Variable temperature ^{1}H NMR spectra of compound **7** at 298 K and 368 K, showing the change in separation and shape of nitrogen methyl peaks. (d_8-tol, 400 MHz)

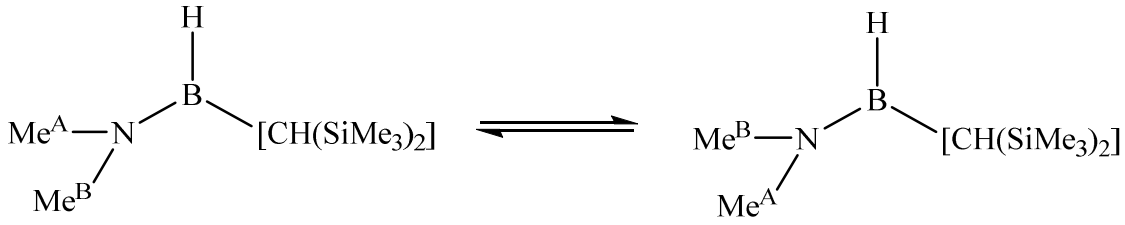

Figure 2.7: Exchange of the nitrogen-bound methyl groups of **7** by thermally induced rotation of the B-N bond.

The magnetic inequivalence of the nitrogen-bound methyl groups is consistent with hindered rotation about the B-N bond of **7**. Barriers to rotation in related aminoboranes have previously been estimated to be of the order 10 - 24 kcal mol^{-1}.[5-10] Although no numerical value could be calculated for the barrier to rotation in **7**, the separation of the N-Me resonances even at elevated temperatures indicated this energy was not insignificant.

Figure 2.8 is a ^{1}H NMR spectrum for compound **7**, showing the broad, low intensity BH resonance which is not observed until the scale is adjusted significantly.

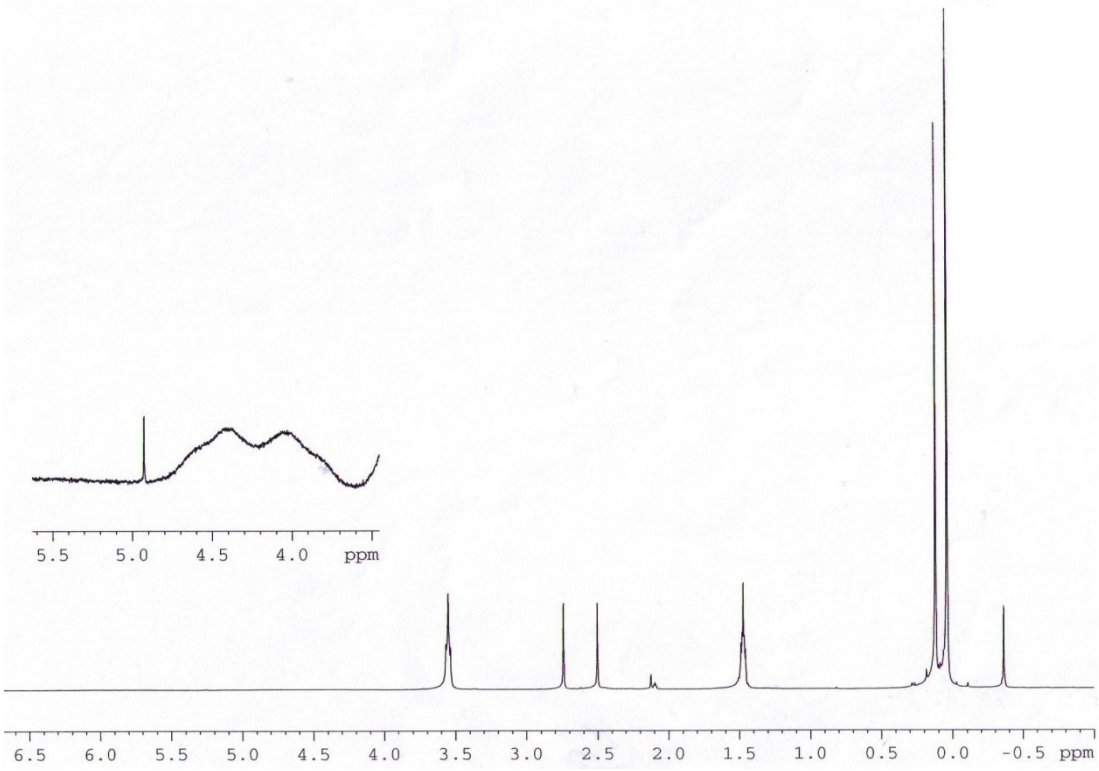

Figure 2.8: ^{1}H NMR spectrum of compound **7** showing the low intensity BH resonance (inset). (d_8-tol, 298 K, 400 MHz)

A ^{1}H-^{11}B HMQC NMR experiment for compound **7**, optimised for one bond 110 Hz couplings, identified the correlation between the doublet resonance in the ^{11}B NMR spectrum and the broad low intensity BH doublet in the ^{1}H NMR spectrum. This is shown in Figure 2.9.

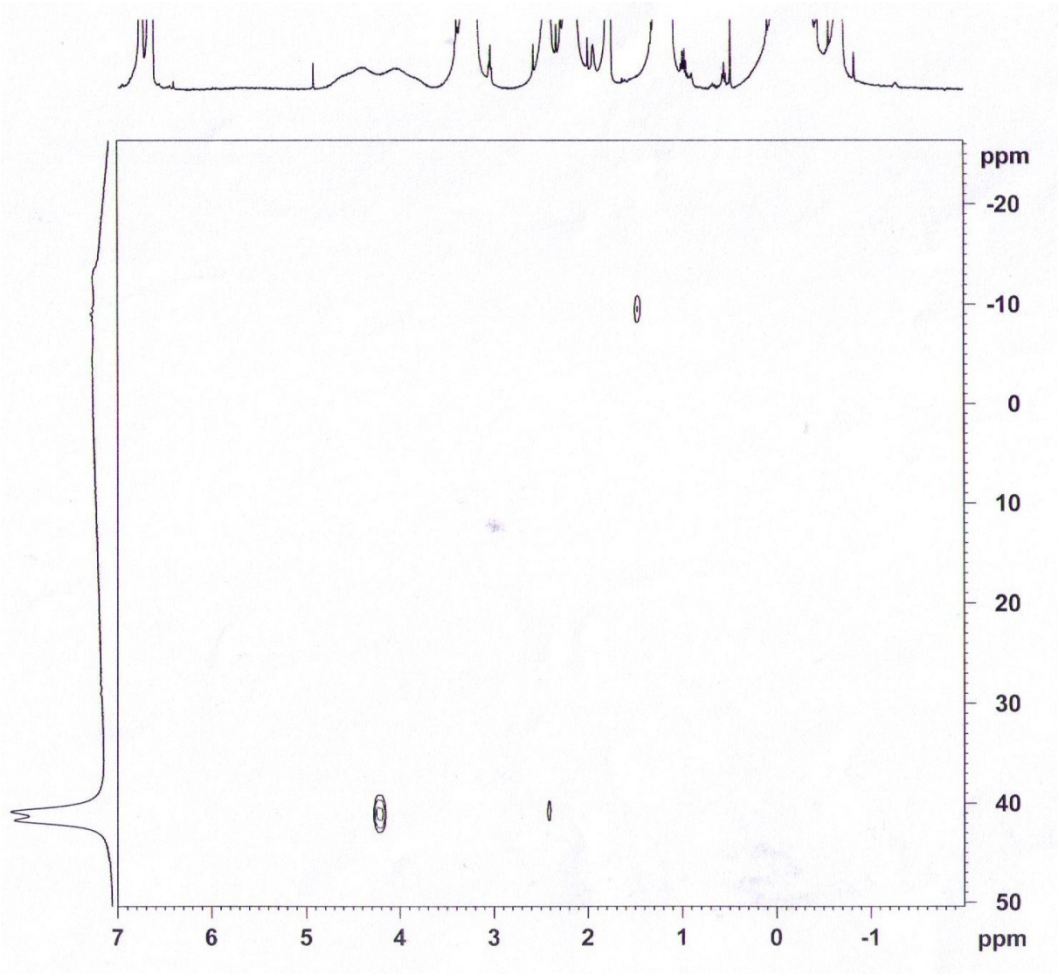

Figure 2.9: ^{1}H-^{11}B HMQC NMR spectrum of compound **7** showing the correlation of the BH resonance in the ^{1}H and ^{11}B NMR spectra. (d_8-tol, 298 K, 400 MHz)

A ^{1}H-^{11}B HMQC NMR experiment, in this instance optimised for long range 10 Hz couplings, identified a correlation of the doublet in the ^{11}B NMR to both methyl groups and the $CH(SiMe_3)_2$ methine peak in the ^{1}H NMR spectrum. This is shown in Figure 2.10.

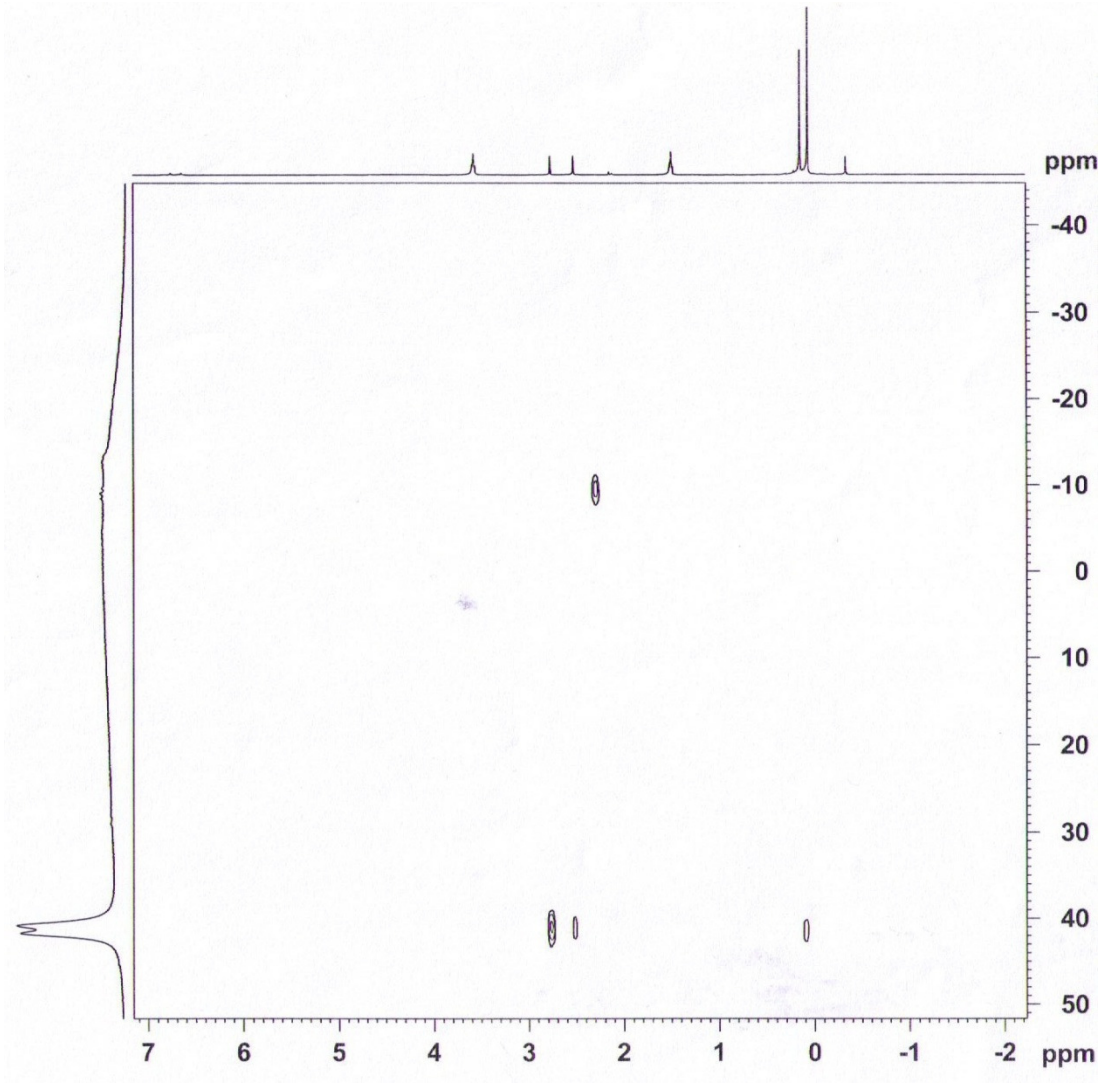

Figure 2.10: ^{1}H-^{11}B HMQC NMR spectrum of compound **7** showing the correlation between the BH resonance in the ^{11}B NMR spectrum with that of the nitrogen-bound methyl groups and methine of the $CH(SiMe_3)_2$ group in the ^{1}H NMR spectrum. (d_8-tol, 298 K, 400 MHz)

These NMR experiments confirmed that the doublet boron resonance arises from the same molecule as the dimethylamino and $CH(SiMe_3)_2$ groups, consistent with the connectivity of compound **7** shown in Figure 2.5. Analogous ^{1}H-^{11}B HMQC NMR experiments were, thus, carried out for compound **8**. The nitrogen-bound methyl groups of compound **7** were easily identified, however, in the case of **8** not all of the pyrrolidine protons could be identified by initial inspection of the ^{1}H NMR spectrum. A TOCSY NMR experiment was therefore carried out, irradiating the

sample at the frequency necessary to stimulate the 3.25 ppm pyrrolidine methylene resonance, resulting in a spectrum consisting solely of resonances for protons to which it directly couples within the molecule – i.e. the other pyrrolidine protons. The resulting spectrum showed the existence of a pyrrolidine resonance at ca. 1.43 ppm, which was otherwise obscured by a THF signal in the standard ^{1}H NMR spectrum.

These NMR studies successfully elucidated the structures of **7** and **8**, with further confirmation provided by GCMS data in which molecular ions were identified at 215.2 and 241.2 *m/z* respectively, corresponding to the complete structures of **7** and **8**.

Heating the magnesium- and calcium-dimethylamidoborane species, **1** and **3**, also resulted in formation of **7**, supported by identical ^{1}H NMR and ^{11}B NMR chemical shifts to those identified for the reaction of **5**, and GCMS data identified a molecular ion at 215.2 *m/z*, corresponding to the complete structure of **7**. Similarly, heating the analogous magnesium- and calcium-pyrrolididoboranes, compounds **2** and **4**, resulted in formation of **8**, supported by ^{1}H NMR and ^{11}B NMR chemical shifts which were identical to those identified for the reaction of **6**, and GCMS data identified a molecular ion at 241.2 *m/z*, corresponding to the complete structure of **8**. The formation of the additional triplet species in the room temperature reactions of **VIIMg** and **VIICa** with DMAB and PB, whilst forming **7** and **8** when heated, suggested that these species were in fact defined compounds formed *en route* to the final alkylaminoborane products, **7** and **8**.

A proposed reaction scheme, shown in Figure 2.11, has been constructed to account for the formation of the alkylated-amine boranes **7** and **8** by these Group 2 alkyl reagents. In this scheme an initial β-hydride elimination from the amidoborane is followed by insertion of the resulting unsaturated and polarised $H_2B{=}NR_2$ species. In contrast to catalytic conditions, in this stoichiometric scenario the only suitable polarised bond available for this insertion is the M-C bond, resulting in an intramolecular insertion reaction, represented by the four-membered transition state (**A**). The observed products, **7** and **8**, are produced by a further β-hydride elimination, in addition to metal dihydride, MH_2.

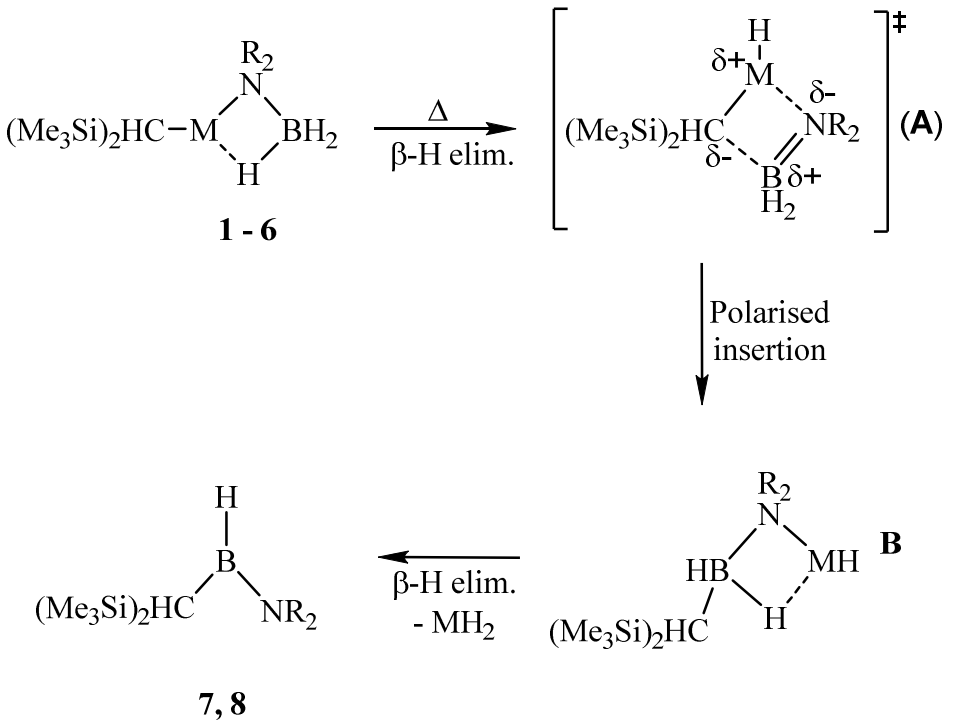

Figure 2.11: Proposed reaction scheme to account for the formation of **7** and **8** (**1**, **3**, **5**, **7**: R = Me; **2**, **4**, **6**, **8**: R = $(CH_2)_2$), where M = Mg (**1** and **2**), Ca (**3** and **4**), Sr (**5** and **6**).[4]

The reactions of these species at room temperature, in which a stable strontium amidoborane forms, whilst the calcium- and magnesium- amidoboranes are observed to have partially reacted to form an intermediate species **B**, suggested metal-dependent reactivity. Tentative evidence from NMR-scale reactions performed to obtain compounds **7** and **8** in high yields suggested that reactions with **VIIMg** proceeded at a much slower rate than those with either **VIISr** or **VIICa**. Although a marked dependence upon metal identity has been previously observed in Group 2 mediated reactions of DMAB the speed of reaction followed the trend Mg > Ca > Sr.[1] In the current case, however, the trend in reactivity was reversed.

2.2 Kinetic NMR Experiments on the Reaction of Strontium Dialkyl **VIISr** with DMAB

Initial kinetic experiments using ^{11}B NMR spectroscopy focused on the reaction between **VIISr** and DMAB, which exhibited more favourable behaviour during the preliminary studies detailed in Section 2.1. Examples of data from kinetic

experiments monitoring the change in ^{11}B NMR spectra with time at 70 °C are shown in Figures 2.12 and 2.13. Figure 2.12 shows that on heating at 70 °C, compound **5** is rapidly consumed, forming an intermediate species, compound **9Sr**. On further heating the concentration of compound **9Sr** decreases, with the formation of compound **7**.

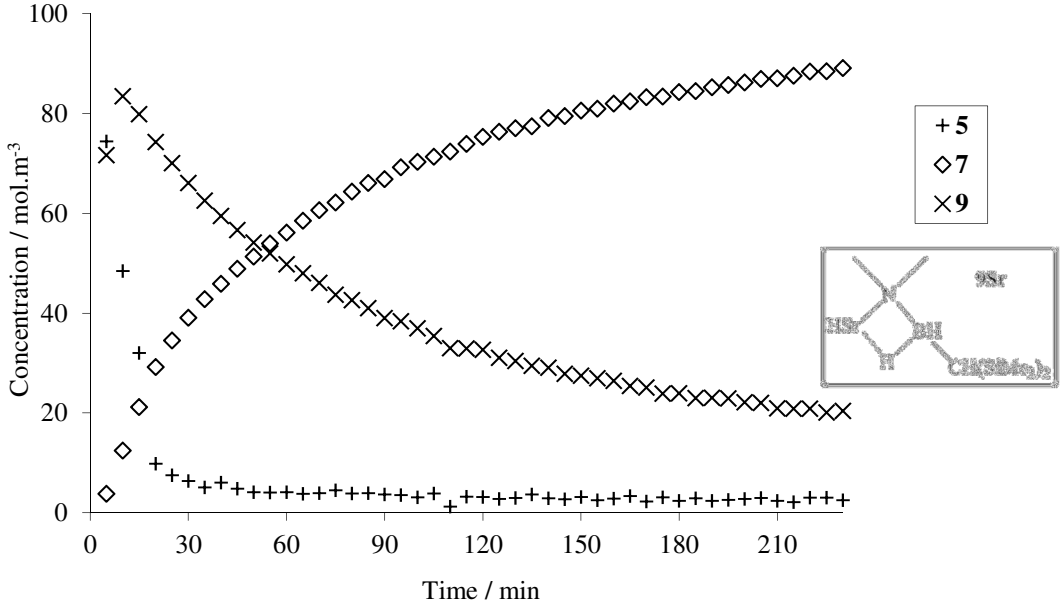

Figure 2.12: Zero order kinetic data plot for the conversion of compound **5** to **7** via an intermediate, compound **9Sr** shown by inset, at 70 °C. (d_8-tol, 343 K, 400 MHz)

This previously uncharacterised intermediate, **9Sr**, appeared as a triplet resonance at δ = 7.9 ppm ($^1J_{BH}$ = 83 Hz) in the ^{11}B NMR spectrum. Further investigation of **9Sr** by ^{1}H-^{11}B HMBC NMR experiments correlated the triplet resonance in the ^{11}B NMR with singlet signals at δ = –0.9 ppm and 2.2 ppm and a broad, low intensity quartet at *ca.* 1.7 ppm in the ^{1}H NMR spectrum. These peaks were assigned as C*H*(SiMe$_3$)$_2$, N-C*H*$_3$ and B*H*$_2$ of a strontium-dimethylamidoborane species, a structure which bears close resemblance to the intermediate depicted in Figure 2.11.

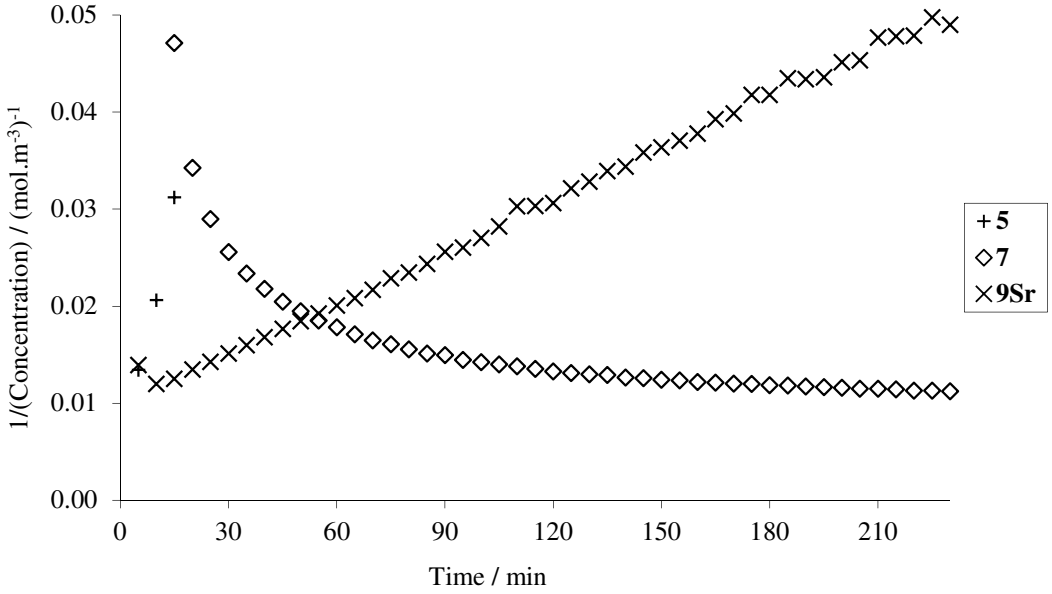

Figure 2.13: Second order kinetic data plot for the conversion of **5** to **7**, via the intermediate compound **9Sr**, at 70 °C. (d_8-tol, 343 K, 400 MHz)

Figure 2.13 shows that after building to a maximum concentration the decrease in concentration of **9Sr** appears to be described by second order kinetics. However, the increase in concentration of the final product, **7**, does not appear to follow either zero, first or second order kinetics.

At 70 °C the formation of **9Sr** was too fast to gain meaningful insight into the kinetics of this process. Therefore, experiments were conducted at 50 °C, shown in Figure 2.14, to better observe the consumption of **5** and formation of **9Sr**. Although this data shows that the consumption of **5** appears to follow second order kinetics, the increase in concentration of **9Sr** did not satisfy either zero, first or second order kinetics. This may be complicated by the competitive formation of **9Sr** and consumption to form compound **7** even at this reduced temperature. These kinetic investigations therefore highlighted additional complexities in this reaction.

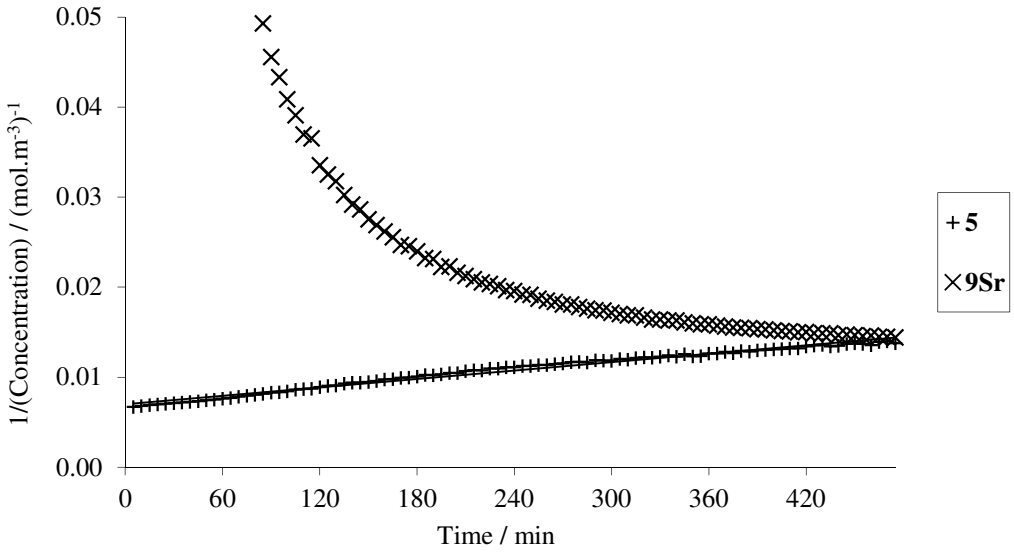

Figure 2.14: Second order kinetic data plot for the conversion of **5** to **9Sr** at 50 °C, with adjusted scale. (d_8-tol, 323 K, 400 MHz)

2.3 Kinetic NMR Experiments on the Reaction of Magnesium- and Calcium-Dialkyls (**VIIMg**, **VIICa**) with DMAB

In Section 2.1 it was stated that strontium-dimethylamidoborane **5** exhibits room temperature stability, whilst Section 2.2 presented kinetic data suggesting this species rapidly converts to an intermediate species **9Sr** at elevated temperature. The analogous magnesium- and calcum- species, **1** and **3**, were stated in Section 2.1 as being unstable at room temperature, evidenced by the presence of triplet resonances in the ^{11}B NMR, assigned to formation of intermediates. Kinetic experiments at 70 °C showed that the reaction of **VIICa** and DMAB displayed similarities to the reactivity of **VIISr**, with rapid formation of the intermediate triplet species **9Ca**, followed by conversion of this species to **7** at a slower rate. Once again the consumption of the intermediate species **9Ca** exhibited 2nd order kinetics, whilst the consumption of **3** and formation of **7** exhibited neither 0, 1st nor 2nd order kinetics. Figure 2.15 shows the second order kinetic data plot for the consumption of intermediate species in the reactions of **VIICa** and **VIISr** with DMAB at 70 °C.

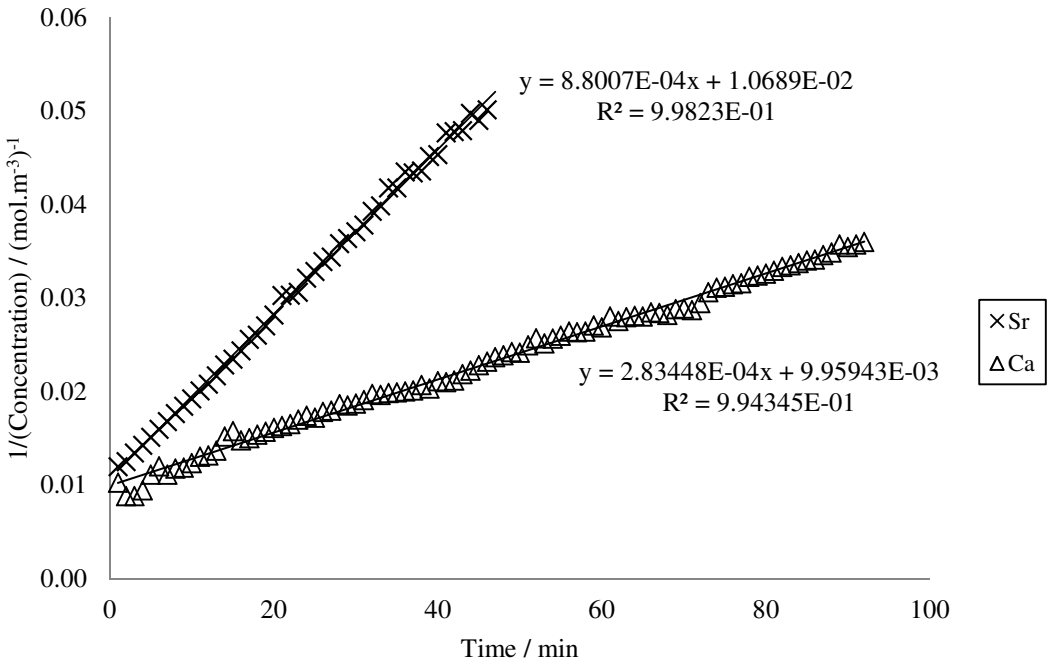

Figure 2.15: Second order kinetic data plot showing the consumption of intermediate species **9Ca** and **9Sr** in the reactions of **VIICa** (triangles) and **VIISr** (crosses) with DMAB at 70 °C.

Figure 2.15 shows that the consumption of the intermediate **9Sr** is more rapid in the case of the strontium reaction, with a second order rate constant which is approximately three times the magnitude of that observed for the calcium reaction.

At room temperature the reaction between **VIIMg** and DMAB underwent the highest conversion to the intermediate species **9Mg** out of the alkaline earth dialkyl species investigated. Investigation into the kinetics of the reaction between **VIIMg** and DMAB at 70 °C highlighted further divergent behaviour compared to the reactions of calcium and strontium. Kinetic data plots are shown in Figures 2.16 and 2.17. The consumption of **1** and formation of **7** once again could not be modelled by 0, 1st nor 2nd order kinetics. However, in this case **9Mg** underwent conversion to **7** with consumption modelled by 1st order kinetics, Figure 2.16, differing from the 2nd order kinetic behaviour exhibited by reactions with **VIICa** and **VIISr**. The divergence in rate order is reminiscent of the alkaline earth catalysed silicon-nitrogen dehydrocoupling kinetics described in Section 1.1.3 in which the magnesium

precatalyst displayed the lowest activity and a change in rate equation was observed for strontium.[11]

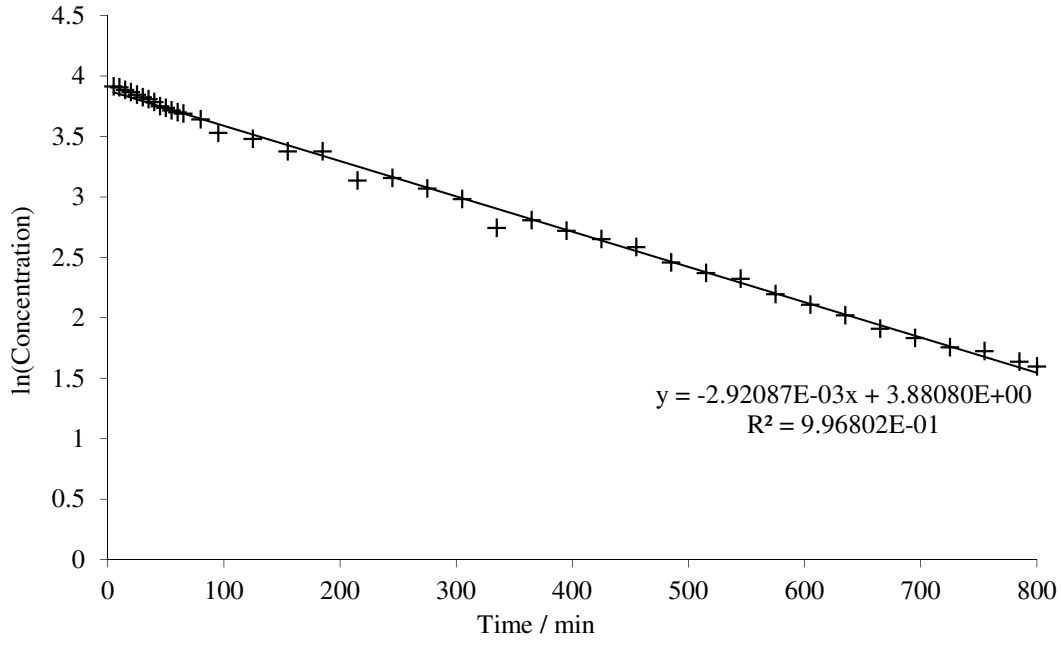

Figure 2.16: First order kinetic data plot for the consumption of **9Mg** at 70 °C.

Whilst the formation of **7** cannot be described by either 0, 1st nor 2nd order kinetics, the zero order kinetic data plot for the formation of **7** by all three dialkyl reagents, Figure 2.17, can be used to compare the relative rates of these reactions. This figure highlights that the rate of reaction for **VIIMg** is markedly slower than that of **VIICa** and **VIISr**.

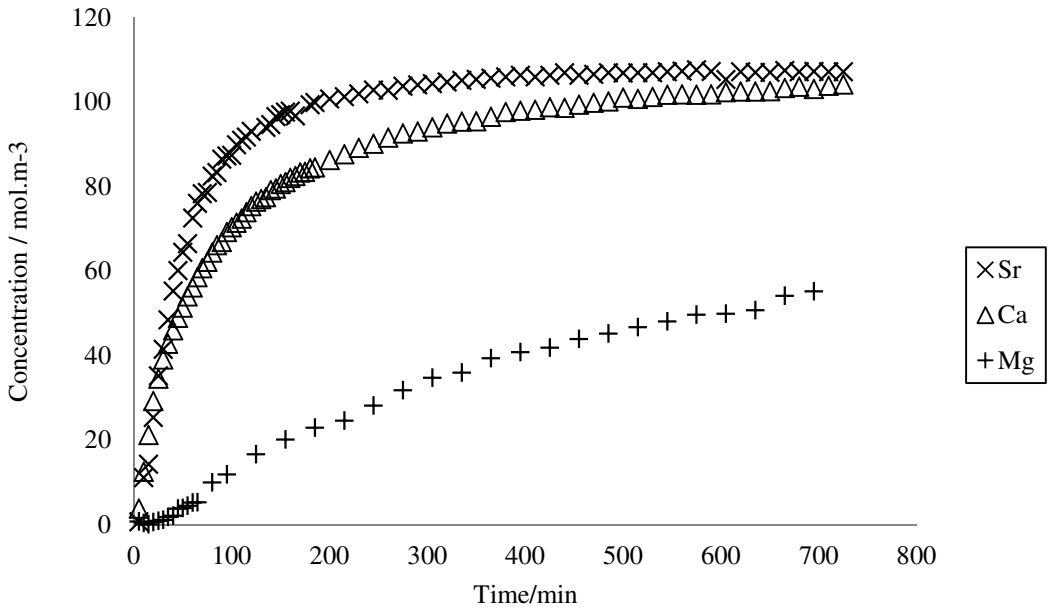

Figure 2.17: Zero order kinetic data plots for the formation of **7** by **VIISr** (crosses), **VIICa** (triangles) and **VIIMg** (pluses) at 70 °C.

The reactions described here present activity which is dependent upon the identity of the metal centre, the trend of which is dependent upon the reaction step in question. These observations are summarised in Figure 2.18. The rate of reaction of the initial β-hydride elimination and proposed polarised insertion of the *in-situ* generated $R_2N{=}BH_2$, labelled k_1 in Figure 2.18, follows the reactivity trend Mg > Ca > Sr. However, it is the rate-determining β-hydride elimination of **9** to form **7**, with rate constants k_2 characterised by a reactivity trend Sr > Ca >> Mg, which dictates the overall rate of reaction.

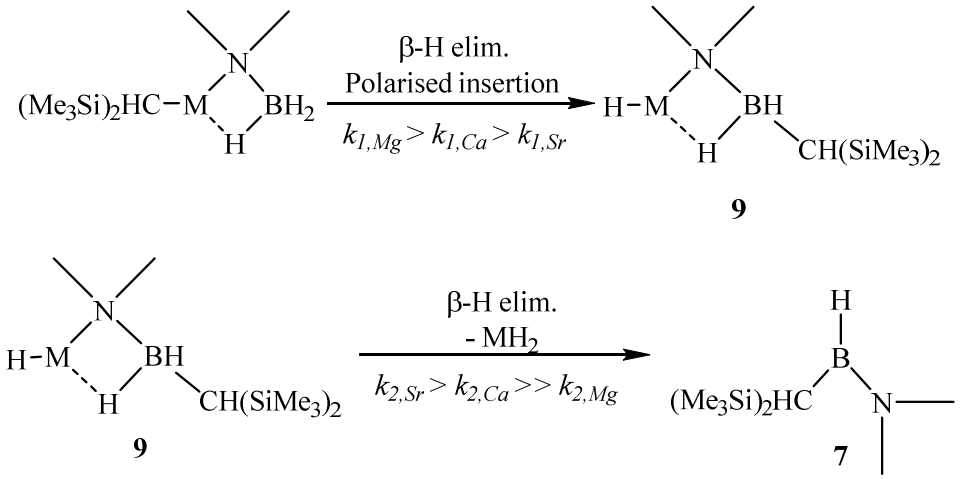

Where $k_{1,M} > k_{2,M}$ and M = Mg, Ca, Sr.

Figure 2.18: Scheme for reaction of alkaline earth amidoborane to form **7**, showing the dependence of reaction rate between species upon the identity of the metal centre, where M = Mg, Ca, Sr.

The rates of reaction can be rationalised in terms of the variation in M^{2+} ionic radius as Group 2 is descended, reminiscent of the alkaline earth catalysed hydroamination catalysis described in Section 1.1.1, the dehydrogenative silicon-nitrogen coupling described in Section 1.1.3 and the catalytic dehydrocoupling of amine boranes presented in Section 1.3. The facile β-hydride elimination from **1** and subsequent insertion chemistry can be rationalised by the highly polarised Mg^{2+} metal centre, with activity decreasing as the Group is descended. The β-hydride elimination from **9Mg**, however, is relatively slow, possibly as a consequence of the combined effect of the small ionic radius of the metal centre and the steric bulk of the $[NMe_2BH_2CH(SiMe_3)_2]^-$ group. This would account for the observed faster reaction for the larger Group 2 cations of calcium and strontium, which would facilitate any necessary rearrangement of intermediate **9Ca** and **9Sr** respectively and enhance reactivity. The change in rate order for reactions with **VIIMg** also indicates that a different process is operating in the rate-determining step for this reaction, which once again is possibly a reflection of the reduced cationic radius and steric bulk of **9Mg**.

2.4 Stoichiometric Reaction of a Strontium Dialkyl **VIISr** with a Primary Amine Borane

Following the investigation of the reactivity of secondary amine boranes with the dialkyl reagents **VIISr**, **VIICa** and **VIIMg** in Section 2.1 the reactivity of the primary amine borane *tert*-butylamine borane (TBAB) was investigated. The stoichiometric reaction between **VIISr** and TBAB at room temperature resulted in the formation of two resonances, a quartet and triplet, in the ^{11}B NMR spectrum, shown in Figure 2.19.

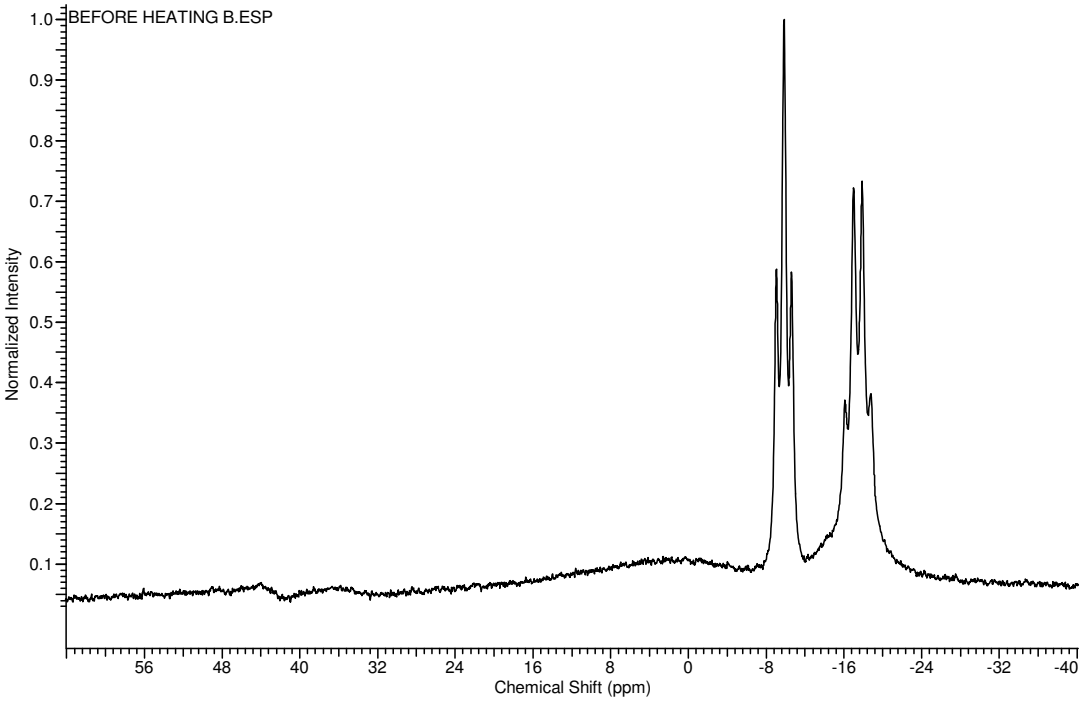

Figure 2.19: ^{11}B NMR spectrum for the stoichiometric reaction between **VIISr** and TBAB at room temperature. (d_8-tol, 298 K, 96.3 MHz)

By comparison with the ^{1}H and ^{11}B NMR spectra for compounds **7** and **8**, the presence of a singlet resonance at δ = –1.65 ppm in the ^{1}H NMR spectrum and a quartet at δ = –17.5 ppm ($^{1}J_{BH}$ = 87 Hz) in the ^{11}B NMR spectrum were consistent with the formation of an alkylstrontium-*tert*-butylamidoborane, [Sr{CH(SiMe$_3$)$_2$}{(NH^{t}Bu)(BH$_3$)}] compound **10**, in addition to the elimination of one equivalent of CH$_2$(SiMe$_3$)$_2$. The solid-state structure of **10**, shown in Figure

2.20, was deduced by X-ray diffraction analysis of a single crystal isolated by crystallisation from this toluene mixture at –30 °C.

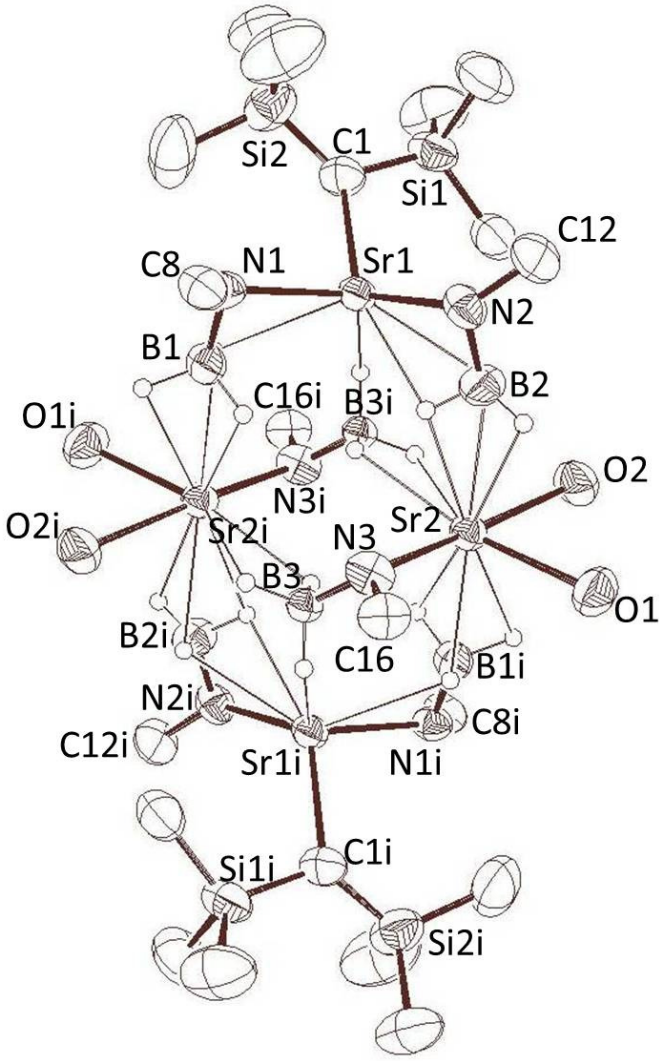

Figure 2.20: ORTEP representation of the solid-state structure of **10**, formed by the stoichiometric reaction between **VIISr** and TBAB. Thermal ellipsoids shown at 50 % probability. Hydrogen atoms other than boron bound hydrides have been removed for clarity, along with THF and nitrogen-bound *tert*-butyl methyl carbon atoms. Selected bond lengths (Å) and angles (°); C1-Sr1 2.685(6), B1-Sr1 2.877(7), N1-B1 1.521(8), N1-Sr1 2.606(4), B1-Sr2 2.852(6), Sr1-B2 2.835(8), Sr1-N2 2.636(7), N2-B2 1.567(10), Sr2-B2 3.146(6), Sr1-B3 3.183(6), Sr2-B3 3.230(6), Sr2-N3 2.659(5), B3-N3 1.529(7), Sr1-N1-B1 84.0(3), C1-Sr1-N1 103.7(18), Sr1-N2-B2 80.5(4), N1-Sr1-N2 99.8(3), Sr2-N3-B3 97.3(3).

The crystal structure of compound **10** reveals a tetrameric aggregate of two $[Sr\{CH(SiMe_3)_2\}(NH^tBu)BH_3]$ and two $[Sr\{(NH^tBu)(BH_3)\}_2]$ fragments. The B-N, Sr-N and Sr-B bond lengths in this structure are similar to those for **5**, Figure 2.2, the dimeric $[Sr\{CH(SiMe_3)_2\}(NMe_2BH_3)(THF)_2]_2$ species. However, the Sr-C bond length in **10** [2.685(6) Å] is longer than in **1** [1.804(3) Å]. This could be a result of the steric demands of the *tert*-butyl groups of the Sr1-bound nitrogen. Compound **10** exhibits a range of Sr-N-B bond angles [Sr1-N1-B1 84.0(3)°, Sr1-N2-B2 80.5(4)°, Sr2-N3-B3 97.3(3)°] suggesting that each of the *tert*-butylamido borane units in this structure is present in a unique environment. The structure of **10** was expected to be similar in form to **5**, the dimeric $[Sr\{CH(SiMe_3)_2\}(NMe_2BH_3)(THF)_2]_2$ species shown in Figure 2.2, but by inspection these crystal structures are quite different. At 298 K the ^{11}B NMR spectrum of **10** displays a single quartet resonance irrespective of the differing bonding modes of the $^tBuNHBH_3$ ligands within the solid state structure, most likely as a result of rapid exchange between the differing environments. Cooling of the NMR sample to 228 K did not result in the appearance of additional signals in the ^{11}B NMR spectrum, suggesting that in solution **10** exists in an analogous form to **5**, represented by the solid-state crystal structure in Figure 2.2. If **10** exists in an analogous form to **5** in solution, it is suggested that Schlenk-like redistribution occurs in solution, which upon crystallisation results in the more complex solid-state structure shown in Figure 2.20. A proposed scheme for this redistribution is shown in Figure 2.21.

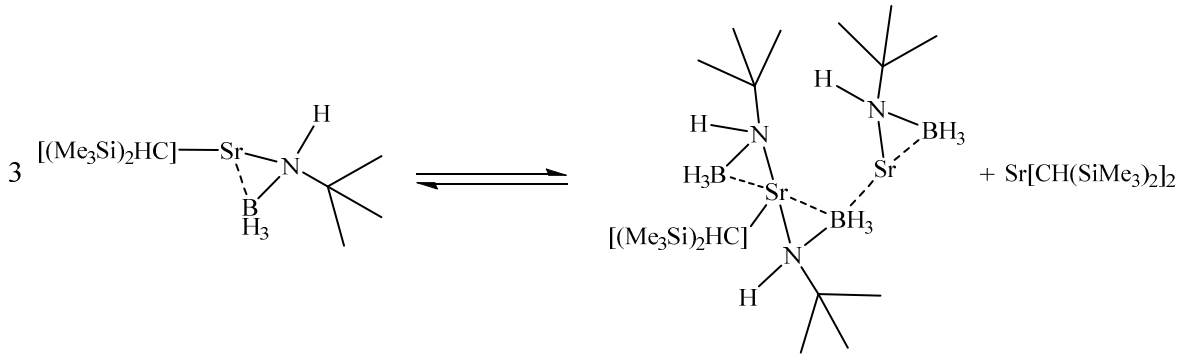

Figure 2.21: Proposed scheme for redistribution and formation of the solid-state structure of **10**.

The room temperature ^{11}B NMR spectrum of compound **10** was also observed to display a triplet resonance at δ = –9.9 ppm ($^{1}J_{BH}$ = 80 Hz), shown in Figure 2.19, reminiscent of the species, **9**, identified as an intermediate formed during the thermolysis of compound **5**. It was suggested, therefore, that this triplet species was an analogous intermediate, compound **11**, the structure of which was proposed to be similar to that of compound **9**. Compound **11** is shown in Figure 2.22.

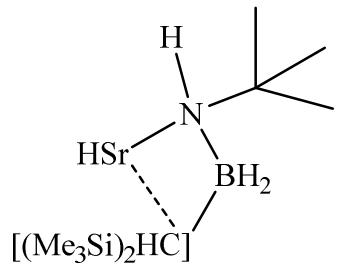

Figure 2.22: Proposed structure of compound **11**, an intermediate analogous to **9**.

The presence of this intermediate species at room temperature demonstrates a difference in thermal stability of this strontium-bound primary amidoborane compared to that of the strontium-bound secondary amidoboranes, compounds **5** and **6**.

Upon heating, compound **10** formed a single boron containing species, present as a doublet signal in the ^{11}B NMR spectrum, Figure 2.23. The formation of this species, compound **12,** shown in Figure 2.24, is consistent with the observations for compounds **7** and **8** and was identified as the primary aminoalkylborane, compound **12** Figure 2.24, by GCMS analysis.

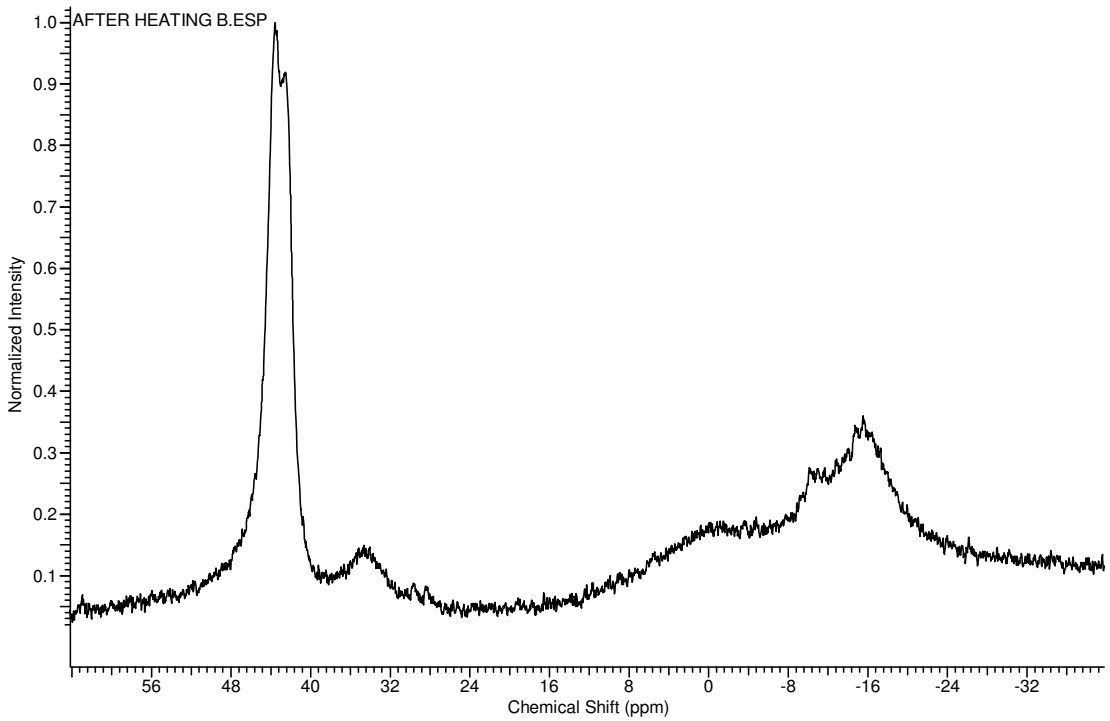

Figure 2.23: ^{11}B NMR spectrum of compound **12**, formed by heating alkylstrontium *tert*-butylamidoborane, **10**. (d_8-tol, 298 K, 96.3 MHz)

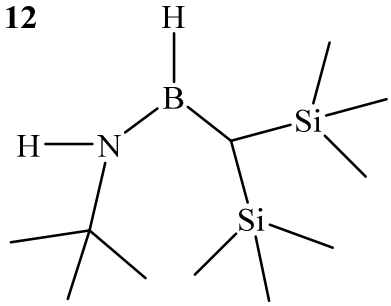

Figure 2.24: The structure of **12**, formed by heating **10**.

It is proposed that this reaction follows a similar mechanism to that of the secondary amine boranes in Sections 2.1-2.3, namely β-hydride elimination, insertion of $H_2B{=}NR_2$ into the M-C bond via a four-membered transition state (**C**), and a final β-hydride elimination. The proposed mechanism is shown in Figure 2.25.

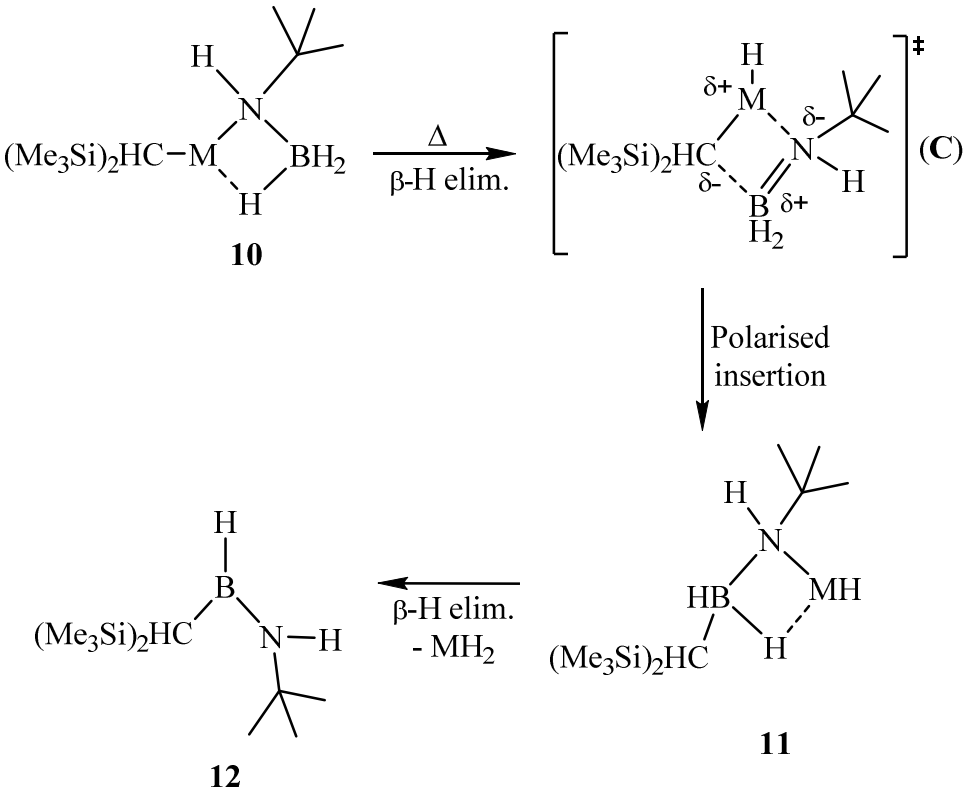

Figure 2.25: Proposed reaction scheme to account for the formation of **12** on heating of **10**, via an intermediate, **11**, where M = Sr.[4]

In Sections 2.2 and 2.3 results from kinetic experiments suggested that the conversion of **1**, **3** and **5** to **7** is a complicated process. The conversion of **10** to **12** is expected to be similarly, if not more, complicated due to the involvement of a less sterically hindered primary amine borane. This comparison in reactivity between secondary- and primary amine boranes has been investigated using the strontium precatalyst **VIISr**. Although reactions have not been carried out using the calcium- and magnesium-dialkyl species, **VIICa** and **VIIMg**, they are expected to exhibit analogous reactivity to that observed for the secondary amineboranes.

2.5 Conclusion for Chapter 2

The stoichiometric reactions described in this chapter have evidenced facile stoichiometric reactions between Group 2 dialkyl species (**VIISr**, **VIICa** and **VIIMg**) and secondary amine boranes. Interpretation of experimental data and observations led to a proposed reaction scheme to account for the identified reaction intermediates and products, Figure 2.26, in which an initial β-hydride elimination from the metal-amidoborane is followed by insertion of the unsaturated and polarised $H_2B{=}NR_2$ unit into the M-C bond, the only suitably polarised bond in this stoichiometric regime. This occurs via a four-membered transition state, to form an intermediate which has been characterised by NMR spectroscopy. A final β-hydride elimination results in formation of the alkyl-aminoborane product in addition to what is believed to be a MH_2 precipitate.

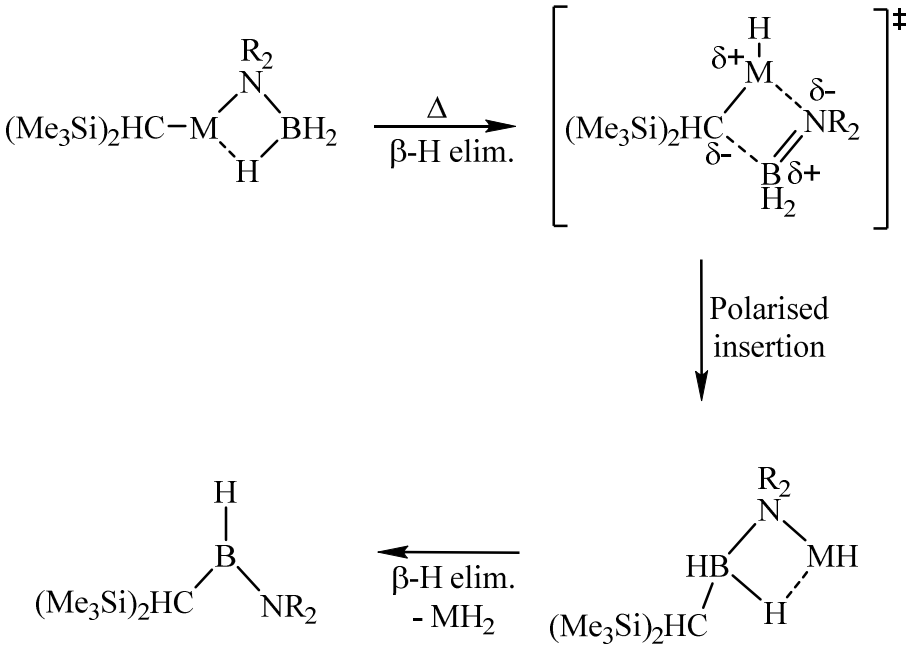

Figure 2.26: Proposed reaction scheme for the stoichiometric reaction of Group 2 dialkyl precatalysts (**VIIMg**, **VIICa** and **VIISr**) with secondary- and primary- amine boranes (where M = Mg, Ca, Sr).

These reactions support the validity of a polarised insertion of the unsaturated $H_2B{=}NR_2$ into a M-C bond, or more generally a M-E bond, as a viable pathway for B-E bond formation.

The kinetic investigation described in Sections 2.2 and 2.3 showed that complicated time-dependent concentration profiles result from these stoichiometric reactions which, in most cases, cannot be resolved to simple rate dependences.

Sections 2.1.3 and 2.1.4 demonstrated that this reaction is dependent upon the identity of the Group 2 metal centre, with the relative stability of the strontium dimethylamidoborane **5** enabling isolation, whilst the analogous calcium- and magnesium- species were unstable to β-hydride elimination at room temperature. The kinetic investigation in Section 2.3, in which the reactivity of **9Mg** was seen to exhibit 2nd order kinetics and an inferior reaction rate to that of the strontium and calcium species, both exhibiting 1st order kinetics, confirms that the reactivity between these species and DMAB is metal dependent. This dependence can be rationalised in terms of the change in ionic radius and polarisability as Group 2 is descended.

The reaction of **VIISr** with TBAB, a primary amine borane, displayed reactivity consistent with the proposed mechanism in Figure 2.26. The solid-state structure of **10**, Figure 2.20, and the instability of this species at room temperature compared to **5**, shows the increased reactivity of primary amine-boranes and suggests that the kinetics of this reaction would be no less complicated than that of secondary amine boranes.

2.6 General Experimental Procedures for Chapter 2

All reactions were carried out using standard Schlenk line and glovebox techniques under an inert argon atmosphere. NMR experiments were conducted in Youngs tap NMR tubes prepared and sealed in a glovebox. NMR spectra were collected on a Bruker AV300 spectrometer operating at 75.5 MHz (^{13}C), 96.3 MHz (^{11}B). Variable-temperature ^{1}H NMR data**,** ^{1}H-^{11}B HMQC, ^{1}H TOCSY and kinetic experiments were recorded on a Bruker AV400 spectrometer. Solvents (toluene, THF, hexane) were dried by a commercially available solvent purification system (Innovative Technologies) under nitrogen before storage in ampoules over molecular sieves. C_6D_6 and d_8-toluene were purchased from Goss Scientific Instruments Ltd., dried over molten potassium before distillation under nitrogen and storage over molecular sieves. $Me_2NH.BH_3$ and $^{t}BuNH_2.BH_3$ were purchased from Sigma-Aldrich Ltd. and used without further purification. $C_4H_8NH.BH_3$ and alkaline earth dialkyl reagents $[M\{CH(SiMe_3)_2\}_2(THF)_2]$ **VII** were synthesised by literature procedures.[12, 13] GCMS data was obtained on an Agilent Technologies 5975C GCMS using 0.5 mg/ml samples in toluene. CHN microanalysis was conducted by Mr. Stephen Boyer of London Metropolitan University.

2.6.1 Typical Procedure for Stoichiometric NMR-Scale Reactions

C_6D_6 or d_8-toluene (ca. 0.5 ml) was added to a solid mixture of Group II dialkyl $[M\{CH(SiMe_3)_2\}_2(THF)_2]$ and one molar equivalent of amine borane ($Me_2NH.BH_3$ or $C_4H_8NH.BH_3$) in a glovebox and the solution sealed in a Youngs tap NMR tube. The reactions were monitored by ^{1}H and ^{11}B NMR spectroscopy. Reactions requiring elevated temperatures were heated using an oil bath.

2.6.1.1 NMR-Scale Synthesis of $[Mg\{NMe_2BH_3\}\{CH(SiMe_3)_2\}(THF)_2]$, **1**

C_6D_6 (ca. 0.5 ml) was added to a solid mixture of $[Mg\{CH(SiMe_3)_2\}_2(THF)_2]$ (49 mg, 0.1 mmol) and one molar equivalent of $Me_2NH.BH_3$ (6 mg, 0.1 mmol) and the solution sealed in a Youngs tap NMR tube before standing at room temperature for ca. 2 hours. ^{1}H NMR (d_8-tol, 298 K) δ = –1.65 (s broad, 1H, C*H*), 0.37 (s, 18H, $Si(CH_3)_3)_2$), 1.36 (THF), 2.25 (s broad, 6H, $N(CH_3)_2$), 3.60 (THF). $^{13}C\{^{1}H\}$ NMR

(d_8-tol, 298 K) δ = 4.3 (*C*H), 5.9 (Si(*C*H_3)$_3$)$_2$), 25.3 (THF), 52.3 (N(*C*H_3)$_2$), 69.1 (THF). ^{11}B NMR (d_8-tol, 298 K) δ = ca. –9.7 (q, *B*H, $^1J_{BH}$ = 86 Hz).

2.6.1.2 NMR-Scale Synthesis of [Mg{N(C_4H_8)BH_3}{CH($SiMe_3$)$_2$}(THF)$_2$], **2**

C_6D_6 (ca. 0.5 ml) was added to a solid mixture of [Mg{CH($SiMe_3$)$_2$}$_2$(THF)$_2$] (49 mg, 0.1 mmol) and one molar equivalent of $C_4H_8NH.BH_3$ (8 mg, 0.1 mmol) and the solution sealed in a Youngs tap NMR tube before standing at room temperature for ca. 2 hours. ^{1}H NMR (C_6D_6, 298 K) δ = –1.64 (s broad, 1H, C*H*), 0.46 (s, 18H, Si(C*H*$_3$)$_3$)$_2$), 1.37 (THF), 1.76 (s broad, 4H, N(CH$_2$)$_2$(C*H*$_2$)$_2$), 2.81 (s broad, 4H, N(C*H*$_2$)$_2$(CH$_2$)$_2$), 3.61 (THF). ^{13}C{^{1}H} NMR (d_8-tol, 298 K) δ = 4.3 (*C*H), 5.9 (Si(*C*H_3)$_3$)$_2$), 25.3 (THF), 52.6 (N(*C*H$_2$)$_2$(CH$_2$)$_2$), 69.0 (THF). ^{11}B NMR (C_6D_6, 298 K) δ = –12.3 (q, *B*H, $^1J_{BH}$ = 100 Hz).

2.6.1.3 NMR-Scale Synthesis of [Ca{N$Me_2$$BH_3$}{CH($SiMe_3$)$_2$}(THF)$_2$], **3**

C_6D_6 (ca. 0.5 ml) was added to a solid mixture of [Ca{CH($SiMe_3$)$_2$}$_2$(THF)$_2$] (50 mg, 0.1 mmol) and one molar equivalent of $Me_2NH.BH_3$ (6 mg, 0.1 mmol) and the solution sealed in a Youngs tap NMR tube before standing at room temperature for ca. 2 hours. ^{1}H NMR (d_8-tol, 298 K) δ = –1.65 (s broad, 1H, C*H*), 0.38 (s, 18H, Si(C*H*$_3$)$_3$)$_2$), 1.32 (THF), 2.44 (s broad, 6H, N(C*H*$_3$)$_2$), 3.54 (THF). ^{13}C{^{1}H} NMR (d_8-tol, 298 K) δ = 4.3 (*C*H), 6.2 (Si(*C*H_3)$_3$)$_2$), 25.2 (THF), 47.4 (N(*C*H_3)$_2$), 69.2 (THF). ^{11}B NMR (d_8-tol, 298 K) δ = –10.1 (q, *B*H, $^1J_{BH}$ = 86 Hz).

2.6.1.4 NMR-Scale Synthesis of [Ca{N(C_4H_8)BH_3}{CH($SiMe_3$)$_2$}(THF)$_2$], **4**

C_6D_6 (ca. 0.5 ml) was added to a solid mixture of [Ca{CH($SiMe_3$)$_2$}$_2$(THF)$_2$] (50 mg, 0.1 mmol) and one molar equivalent of $C_4H_8NH.BH_3$ (8 mg, 0.1 mmol) and the solution sealed in a Youngs tap NMR tube before standing at room temperature for ca. 2 hours. ^{1}H NMR (C_6D_6, 298 K) δ = –1.66 (s broad, 1H, C*H*), 0.40 (s, 18H, Si(C*H*$_3$)$_3$)$_2$), 1.34 (THF), 1.80 (s broad, 4H, N(CH$_2$)$_2$(C*H*$_2$)$_2$), 2.84 (s broad, 4H, N(C*H*$_2$)$_2$(CH$_2$)$_2$), 3.58 (THF). ^{13}C{^{1}H} NMR (d_6-tol, 298 K) δ = 4.3 (*C*H), 6.2 (Si(*C*H_3)$_3$)$_2$), 25.2 (THF), 26.1 (N(CH$_2$)$_2$(*C*H$_2$)$_2$), 55.8 (N(*C*H$_2$)$_2$(CH$_2$)$_2$), 69.1 (THF). ^{11}B NMR (C_6D_6, 298 K) δ = –12.4 (q, *B*H, $^1J_{BH}$ = 86 Hz).

2.6.2 Experimental Procedures for Stoichiometric Reactions of Secondary Amine Boranes with **VIISr**

2.6.2.1 Synthesis of [Sr{NMe_2BH_3}{$CH(SiMe_3)_2$}$(THF)_2$], **5**

Toluene (ca. 10ml) was added to solid [Sr{$CH(SiMe_3)_2$}$_2(THF)_2$] (130 mg, 0.23 mmol) and $Me_2NH.BH_3$ (0.013 mg, 0.23 mmol) in a Schlenk tube and stirred at room temperature for ca. 18 hours before concentration under vacuum. Accurate CHN microanalysis was not obtainable due to instability of the species. ^{1}H NMR (d_8-tol, 298 K) δ = –1.68 (s broad, 1H, C*H*), 0.33 (s, 18H, Si(CH_3)$_3$)$_2$), 1.47 (THF), 2.38 (s broad, 6H, N(CH_3)$_2$), 3.66 (THF). ^{13}C{^{1}H} NMR (d_8-tol, 298 K) δ = 4.7 (*C*H), 6.8 (Si(*C*H_3)$_3$)$_2$), 25.9 (THF), 47.6 (N(*C*H_3)$_2$), 69.2 (THF). ^{11}B NMR (d_8-tol, 298 K) δ = –9.3 (q, *B*H, $^1J_{BH}$ = 82 Hz).

2.6.2.2 Synthesis of [Sr{$N(C_4H_8)BH_3$}{$CH(SiMe_3)_2$}$(THF)_2$], **6**

Toluene (ca. 10ml) was added to solid [Sr{$CH(SiMe_3)_2$}$_2(THF)_2$] (130 mg, 0.23 mmol) and $C_4H_8NH.BH_3$ (20 mg, 0.23 mmol) in a Schlenk tube and stirred at room temperature for ca. 18 hours before concentration under vacuum to provide an oily residue. Anal. Calc. for $C_{30}H_{76}B_2N_2O_2Si_4Sr_2$: C, 44.74; H, 9.39; N, 3.48 %. Found: C, 44.32; H, 9.11; N, 3.23 %. ^{1}H NMR (C_6D_6, 298 K) δ = –1.65 (s broad, 1H, C*H*), 0.38 (s, 18H, Si(CH_3)$_3$)$_2$), 1.40 (THF), 1.78 (s broad, 4H, N(CH_2)$_2$(CH_2)$_2$), 2.80 (s broad, 4H, N(CH_2)$_2$(CH_2)$_2$), 3.60 (THF). ^{13}C{^{1}H} NMR (C_6D_6, 298 K) δ = 4.6 (*C*H), 6.8 (Si(*C*H_3)$_3$)$_2$), 25.8 (THF), 26.4 (N(CH_2)$_2$(*C*H_2)$_2$), 56.0 (N(*C*H_2)$_2$(CH_2)$_2$), 69.1 (THF). ^{11}B NMR (C_6D_6, 298 K) δ = –10.8 (q, *B*H, $^1J_{BH}$ = 82 Hz).

2.6.3 Experimental Procedures for Thermolysis Reactions of Secondary Amine Boranes with **VIIMg**, **VIICa** and **VIISr**

2.6.3.1 NMR-Scale Synthesis of [{Me_2N}BH{$CH(SiMe_3)_2$}], **7**

(i) [Mg{$CH(SiMe_3)_2$}$_2$(THF)] **VIIMg**

C_6D_6 (ca. 0.5 ml) was added to a solid mixture of [Mg{$CH(SiMe_3)_2$}$_2$(THF)] (49 mg, 0.1 mmol) and one molar equivalent of $Me_2NH.BH_3$ (6 mg, 0.1 mmol) and the

solution sealed in a Youngs tap NMR tube before heating to 80 °C for ca. 437 hours. Approx. 60 % conversion using ^{11}B NMR.

(ii) [Ca{CH(SiMe$_3$)$_2$}$_2$(THF)$_2$] **VIICa**

C_6D_6 (ca. 0.5 ml) was added to a solid mixture of [Ca{CH(SiMe$_3$)$_2$}$_2$(THF)$_2$] (50 mg, 0.1 mmol) and one molar equivalent of $Me_2NH.BH_3$ (6 mg, 0.1 mmol) and the solution sealed in a Youngs tap NMR tube before heating to 70 °C for ca. 18 hours. Approx. 85 % conversion using ^{11}B NMR.

(iii) [Sr{CH(SiMe$_3$)$_2$}$_2$(THF)$_2$] **VIISr**

D_8-toluene (ca. 0.5 ml) was added to a solid mixture of [Sr{CH(SiMe$_3$)$_2$}$_2$(THF)$_2$] (55 mg, 0.1 mmol) and one molar equivalent of $Me_2NH.BH_3$ (6 mg, 0.1 mmol) and the solution sealed in a Youngs tap NMR tube before heating to 80 °C for ca. 78 hours. Approx. 86 % conversion using ^{11}B NMR.

(iv) Data

Compound **7** proved unstable to concentration under vacuum or by evaporation in a glovebox. GCMS results identified an ion with *m/z* of 215.2 corresponding to the complete molecule. ^{1}H NMR (d_8-tol, 298 K) δ = ca. 0.10 (s, 1H, C*H*), 0.12 (s, 18H, Si(C*H*$_3$)$_3$)$_2$), 2.50 (s, 3H, N-C*H*$_3$), 2.74 (s, 3H, N-C*H*$_3$), 4.52 (d broad, 1H, B*H*, $^1J_{BH}$ ca. 147 Hz). ^{13}C{^{1}H} NMR (d_8-tol, 298 K) δ = 2.2 (Si(*C*H$_3$)$_3$)$_2$), 4.8 (*C*H), 37.8 (N-*C*H$_3$), 45.7 (N-*C*H$_3$). ^{11}B NMR (d_8-tol, 298 K) δ = 44.8 (d, *B*H, $^1J_{BH}$ = 102 Hz).

2.6.3.2 NMR-Scale Synthesis of [{H$_8$C$_4$N}BH{CH(SiMe$_3$)$_2$}], **8**

(i) [Mg{CH(SiMe$_3$)$_2$}$_2$(THF)] **VIIMg**

C_6D_6 (ca. 0.5 ml) was added to a solid mixture of [Mg{CH(SiMe$_3$)$_2$}$_2$(THF)] (49 mg, 0.1 mmol) and one molar equivalent of $C_4H_8NH.BH_3$ (8 mg, 0.1 mmol) and the solution sealed in a Youngs tap NMR tube before heating to 70 °C for ca. 12 hours. Approx. 61 % conversion using ^{11}B NMR.

(ii) [Ca{CH(SiMe$_3$)$_2$}$_2$(THF)$_2$] **VIICa**

C_6D_6 (ca. 0.5 ml) was added to a solid mixture of [Ca{CH(SiMe$_3$)$_2$}$_2$(THF)$_2$] (50 mg, 0.1 mmol) and one molar equivalent of $C_4H_8NH.BH_3$ (8 mg, 0.1 mmol) and the solution sealed in a Youngs tap NMR tube before heating to 70 °C for ca. 102 hours. Approx. 64 % conversion using ^{11}B NMR.

(iii) Using [Sr{CH(SiMe$_3$)$_2$}$_2$(THF)$_2$] **VIISr**

C_6D_6 (ca. 0.5 ml) was added to a solid mixture of [Sr{CH(SiMe$_3$)$_2$}$_2$(THF)$_2$] (55 mg, 0.1 mmol) and one molar equivalent of $C_4H_8NH.BH_3$ (8 mg, 0.1 mmol) and the solution sealed in a Youngs tap NMR tube before heating to 70 °C for ca. 12 hours. Approx. 70 % conversion using ^{11}B NMR.

(iv) Data

Compound **8** proved unstable to concentration under vacuum or by evaporation in a glovebox. GCMS results identified an ion with *m/z* of 241.2 corresponding to the complete molecule. ^{1}H NMR (C_6D_6, 298 K) δ = ca. 0.10 (s, 1H, C*H*), 0.18 (s, 18H, Si(C*H*$_3$)$_3$)$_2$), ca. 1.43 (m, 4H, (N(CH$_2$)$_2$(C*H*$_2$)$_2$)), 3.01 (t, 2H, C*H*$_2$, J_{HH} = 13.2 Hz), 3.25 (t, 2H, C*H*$_2$, J_{HH} = 13.2 Hz), 4.84 (d broad, 1H, B*H*, $^1J_{BH}$ ca. 136 Hz). ^{13}C{^{1}H} NMR (C_6D_6, 298 K) δ = 2.3 (Si(*C*H$_3$)$_3$)$_2$), 4.6 (*C*H), 26.3 (N(CH$_2$)$_2$(CH$_2$)(*C*H$_2$)), 26.6 (N(CH$_2$)$_2$(*C*H$_2$)(CH$_2$)), 47.1 (N(CH$_2$)(*C*H$_2$)(CH$_2$)$_2$), 53.2 (N(*C*H$_2$)(CH$_2$)(CH$_2$)$_2$). ^{11}B NMR (C_6D_6, 298 K) δ = 43.3 (d, *B*H, $^1J_{BH}$ = 93 Hz).

2.6.4 Reaction of **VIISr** with Primary Amine Borane, TBAB

2.6.4.1 NMR-Scale Synthesis of [Sr{NH^{t}BuBH$_3$}{CH(SiMe$_3$)$_2$}(THF)$_2$], **10**, and intermediate **11**

D_8-toluene (ca. 0.5 ml) was added to a solid mixture of [Sr{CH(SiMe$_3$)$_2$}$_2$(THF)$_2$] (55 mg, 0.1 mmol) and one molar equivalent of ^{t}BuNH$_2$.BH$_3$ (4 mg, 0.1 mmol) and the solution sealed in a Youngs tap NMR tube before standing at room temperature for ca. 2 hours. ^{1}H NMR (d_8-tol, 298 K) δ = –1.65 (br. s, C*H*), 0.04 (s, Si(C*H*$_3$)$_3$)$_2$), ca. 0.32 (br. s, Si(C*H*$_3$)$_3$)$_2$), ca. 1.28 (s, C(C*H*$_3$)$_3$), 1.30 (br. s, C(C*H*$_3$)$_3$), 1.43 (THF), 3.63 (THF). ^{13}C{^{1}H} NMR (d_8-tol, 298 K) δ = 1.8 (Si(*C*H$_3$)$_3$)$_2$), 2.8 (C(*C*H$_3$)$_3$), 3.1

($C(CH_3)_3$), 4.7 (CH), 25.9 (THF), 32.0 ($C(CH_3)_3$), 33.7 ($C(CH_3)_3$), 33.8 ($C(CH_3)_3$), 69.1 (THF). ^{11}B NMR (d_8-tol, 298 K) δ = –17.5 (q, *B*H **11**, $^1J_{BH}$ = 86 7Hz), –9.9 (t, *B*H **10**, $^1J_{BH}$ = 80 Hz).

A single crystal of **10** suitable for X-ray diffraction analysis was isolated from concentrated toluene.

Molecular Formula	$C_{54}H_{148}B_6N_6O_4Si_4Sr_4$
Formula Weight / g.mol^{-1}	1473.48
Crystal System, Space Group	Monoclinic, P 1 2_1/c 1
a, b, c / Å	13.4450(3), 15.1050(4), 22.1862(6)
α, β, γ / °	90, 107.657(2), 90
V / Å^3	4293.45(19)
Z	2
μ / mm^{-1}	2.564
ρ / g.cm^{-1}	1.140
θ range / °	4.68 - 25.05
Collected / Unique Reflections / R_{int}	60465 / 7484 / 0.1073
R_1, wR_2 [I > 2σ(I)]	R_1 = 0.0525, wR_2 = 0.1041
R_1, wR_2 (All data)	R_1 = 0.0926, wR_2 = 0.1253

2.6.4.2 NMR-Scale Synthesis of [{$(CH_3)_3$CHN}BH{$CH(SiMe_3)_2$}], **12**, with [Sr{$CH(SiMe_3)_2$}$_2$$(THF)_2$] **VIISr**

D_8-toluene (ca. 0.5 ml) was added to a solid mixture of [Sr{$CH(SiMe_3)_2$}$_2$$(THF)_2$] (55 mg, 0.1 mmol) and one molar equivalent of ^{t}BuNH$_2$.BH$_3$ (4 mg, 0.1 mmol) and the solution sealed in a Youngs tap NMR tube before heating to 70 °C for ca. 6 hours. Approx. 75 % conversion using ^{11}B NMR. ^{1}H NMR (d_8-tol, 298 K) δ = ca. 0.10 (s, 1H, C*H*), 0.13 (s, 18H, (Si(CH_3)$_3$)$_2$), 1.09 (br. s., 9H, C(CH_3)$_3$). ^{13}C{^{1}H}

NMR (d_8-tol, 298 K) δ = 1.8 ($Si(CH_3)_3)_2$), 2.2 ($C(CH_3)_3$), 4.7 (*C*H), 33.1 ($C(CH_3)_3$). ^{11}B NMR (d_8-tol, 298 K) δ = 43.0 (d, *B*H, $^1J_{BH}$ = 89 Hz).

2.6.5 Typical Procedure for Kinetic Experiments

D_8-toluene (0.5 ml) was added to a solid mixture of Group II dialkyl reagent $[M\{CH(SiMe_3)_2\}_2(THF)_2]$ **VII** and one molar equivalent of amine borane ($Me_2NH.BH_3$) in a glovebox and the solution sealed in a Youngs tap NMR tube. Using a Bruker AV400 spectrometer, reactions were monitored by ^{11}B NMR spectroscopy with measurements taken every 5 minutes during the course of the reaction. Samples were heated inside the spectrometer to achieve elevated temperatures and allowed an equilibration time ca. 5 - 10 minutes before starting the experiment. Analysis was conducted using the integration of all peaks in the ^{11}B NMR spectra and assuming that the total integration corresponds to a fixed concentration.[14-16]

2.7 References for Chapter 2

1. M. S. Hill, M. Hodgson, D. J. Liptrot and M. F. Mahon, *Dalton Trans.*, 2011, **40**, 7783-7790.
2. D. J. Liptrot, M. S. Hill, M. F. Mahon and D. J. MacDougall, *Chem.- Eur. J.*, 2010, **16**, 8508-8515.
3. P. Bellham, M. S. Hill, D. J. Liptrot, D. J. MacDougall and M. F. Mahon, *Chem. Commun.*, 2011, **47**, 9060-9062.
4. J. Spielmann, G. Jansen, H. Bandmann and S. Harder, *Angew. Chem.-Int. Ed.*, 2008, **47**, 6290-6295.
5. A. J. Ashe, W. Klein and R. Rousseau, *J. Organomet. Chem.*, 1994, **468**, 21-23.
6. J. D. Dill, P. V. Schleyer and J. A. Pople, *J. Am. Chem. Soc.*, 1975, **97**, 3402-3409.
7. P. A. Barfield, M. F. Lappert and J. Lee, *J. Chem. Soc. A*, 1968, 554-559.
8. P. A. Barfield, J. Lee and M. F. Lappert, *Proc. Chem. Soc. London*, 1961, 421-422.
9. M. J. S. Dewar and P. Rona, *J. Am. Chem. Soc.* 1969, **91**, 2259-2264.
10. C. Brown, R. H. Cragg, T. J. Miller and D. O. Smith, *J. Organomet. Chem.*, 1983, **244**, 209-215.
11. M. S. Hill, D. J. Liptrot, D. J. MacDougall, M. F. Mahon and T. P. Robinson, *Chem. Sci.*, 2013, **4**, 4212-4222.
12. C. A. Jaska, K. Temple, A. J. Lough and I. Manners, *J. Am. Chem. Soc.*, 2003, **125**, 9424-9434.
13. M. R. Crimmin, A. G. M. Barrett, M. S. Hill, D. J. MacDougall, M. F. Mahon and P. A. Procopiou, *Chem. - Eur. J.*, 2008, **14**, 11292-11295.
14. M. M. Hansmann, R. L. Melen and D. S. Wright, *Chem. Sci.*, 2011, **2**, 1554-1559.
15. L. J. Sewell, G. C. Lloyd-Jones and A. S. Weller, *J. Am. Chem. Soc.*, 2012, **134**, 3598-3610.
16. K. Ishihara, A. Nagasawa, K. Umemoto, H. Ito and K. Saito, *Inorg. Chem.*, 1994, **33**, 3811-3816.

3 Mechanistic Investigation of d^0 Complex Dehydrocoupling of Amine Boranes

This chapter presents an investigation of the proposed mechanism for amine borane dehydrocoupling by alkaline earth precatalysts shown in Figure 3.1.

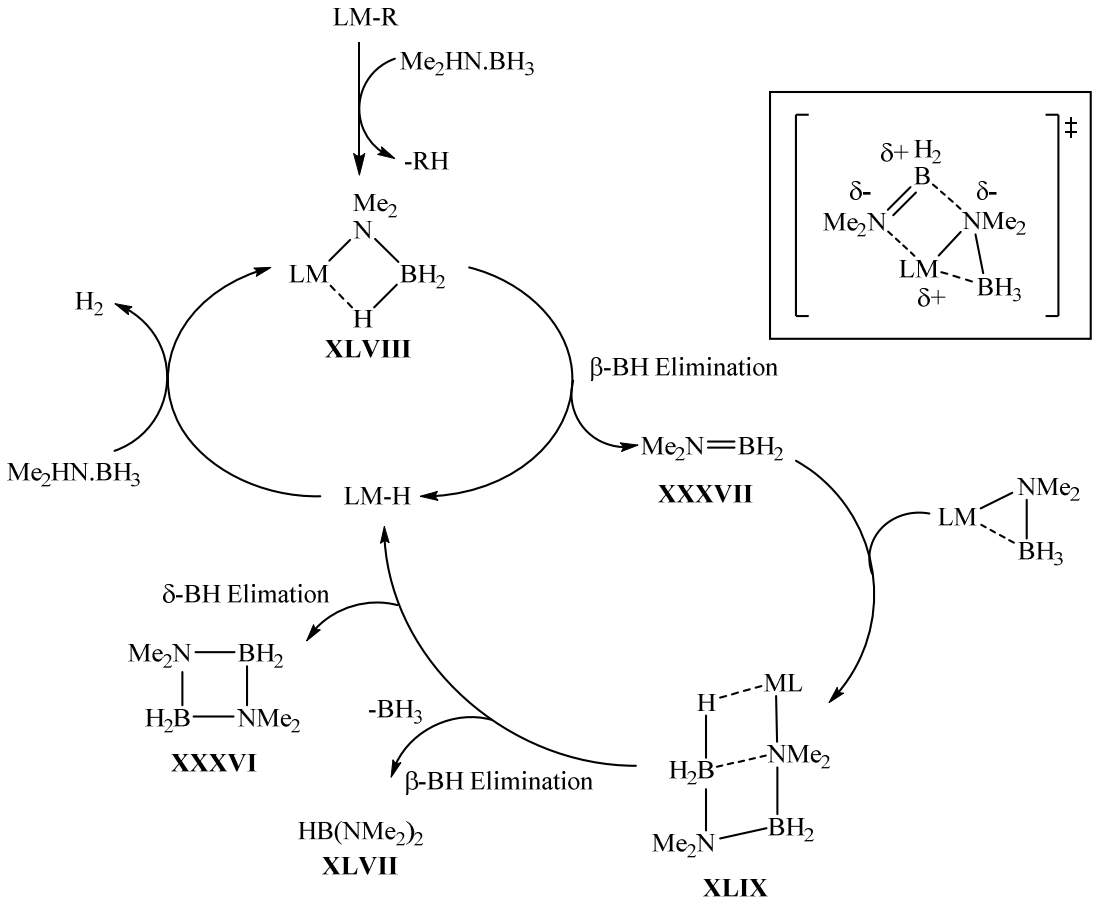

Figure 3.1: Proposed scheme for dehydrocoupling of amine boranes by alkaline earth precatalysts (where M = Mg, Ca, Sr, Ba).[1-3]

The chapter begins with a consideration of the alkaline earth precatalyst, before presenting an investigation of stoichiometric reactions between reagents from Groups 1 and 2 with dimethylamine borane (DMAB) to form amidoborane reaction intermediates. This study was performed with a view to enabling an investigation of the kinetics of the thermal decomposition and elementary reactions of the otherwise inaccessible isolated processes of the proposed mechanism.

3.1.1 Consideration of Alkaline Earth Pre-catalyst for Amine Borane Dehydrocoupling: Limitations of Previously Studied Pre-catalysts

To facilitate an investigation of the proposed mechanism in as much detail as possible, a suitable supporting ligand was required to enable the isolation of stable reaction intermediates for each of the heavier alkaline earth elements (M = Mg, Ca, Sr, Ba). Although the complete series of heavier alkaline earth analogues are accessible for both $[M(N(SiMe_3)_2)_2]_2$ **V** and $[M\{CH(SiMe_3)_2\}_2(THF)_2]$ **VII**, these species possess characteristics which are less desirable for mechanistic analysis. As reported in Chapter 2 amidoborane complexes of **VII** are generally isolated as oily residues, making them less desirable for isolation and handling. For characterisation of catalytic dehydrocoupling the supporting ligands of **V** and **VII** are inadequate in their provision of sufficient stability to constrain solution molecularity and ligand exchange at the metal centre, potentially resulting in a range of processes which cannot be made to fit simple kinetic models. Precatalysts of **V** possess bis(trimethylsilyl)amide groups, one of which is necessarily protonated during reaction with amine borane, liberating an amine which is potentially non-innocent in the subsequent dehydrocoupling reaction. Both (trimethylsilyl)amide groups can potentially undergo protonation, releasing two equivalents of amine per metal centre. In this scenario the metal centre, supported only by amidoborane substituents, could subsequently form hydrocarbon insoluble hydrides.

The β-diketiminate-supported precatalysts, **VI** and **XV**, provided routes to isolable amidoborane intermediates of calcium and magnesium respectively. Although the series of homoleptic β-diketiminate alkaline earth complexes has been reported,[4] as Group 2 is descended there is an increased tendency towards the formation of homoleptic species by Schlenk equilibration, rendering the heteroleptic β-diketiminate complexes of strontium and barium difficult to access.

The requirement for a complete series of heavier alkaline earth precatalysts which possess adequate stability against Schlenk redistribution has recently been realised by use of Piers' "anilido-imine" ligand.[5] The Group 2 homologues of this ligand **IX**, shown in Figure 3.2, were reported by Sarazin in 2012 and proved to be effective catalysts for a range of heterofunctionalisation reactions.[6, 7] This ligand was reported

to possess properties similar to that of the β-diketiminate ligand, but with increased stability towards Schlenk redistribution, enabling investigation of the reactivity of a complete congeneric series of heavier alkaline earth precatalysts.

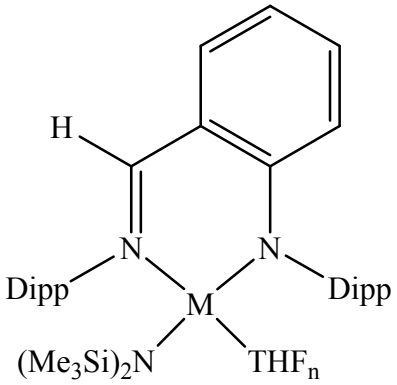

M = Ca, n = 1
M = Sr, n = 2
M = Ba, n = 2

IX

Figure 3.2: Group 2 anilido-imine complexes utilised by Sarazin for heterofunctionalisation reactions.[6, 7]

3.1.2 Stoichiometric Reactions Between Calcium and Magnesium Anilido-Imine Reagents, **IX-Ca** and **IX-Mg**, and Secondary Amine Boranes

The viability of the use of complexes **IX** as precatalysts towards the dehydrocoupling of secondary amine boranes was investigated. Preliminary experiments focussed on the calcium and magnesium derivatives, **IX-Ca** and **IX-Mg**, mimicking the work of the Hill Group in using the β-diketiminate reagents, **VI** and **XV**.[2, 8] Addition of **IX-Ca** to one equivalent of dimethylamine borane (DMAB) on an NMR scale at room temperature resulted in clean conversion to a new species characterised by a single quartet resonance in the ^{11}B NMR spectrum at δ = –12.4 ppm, $^{1}J_{BH}$ = 80.3 Hz, assigned to the BH_3 unit of an anilido-imine supported calcium dimethylamidoborane **13**, in addition to a singlet resonance in the ^{1}H NMR spectrum at δ = 0.08 ppm integrating to 18H resulting from the formation of $HN(SiMe_3)_2$. The quartet resonance in the ^{11}B NMR spectrum of **13** is comparable to that of **LXV** (δ = –12.5 ppm, $^{1}J_{BH}$ = 86 Hz), the β-diketiminato calcium dimethylamidoborane species reported by Hill.[2] The solid-state structure of **13**, shown in Figure 3.3, was confirmed by X-ray diffraction analysis of a single crystal obtained by crystallisation

from a concentrated toluene solution at –30 °C and the constitution of the bulk material was supported by accurate microanalytical data.

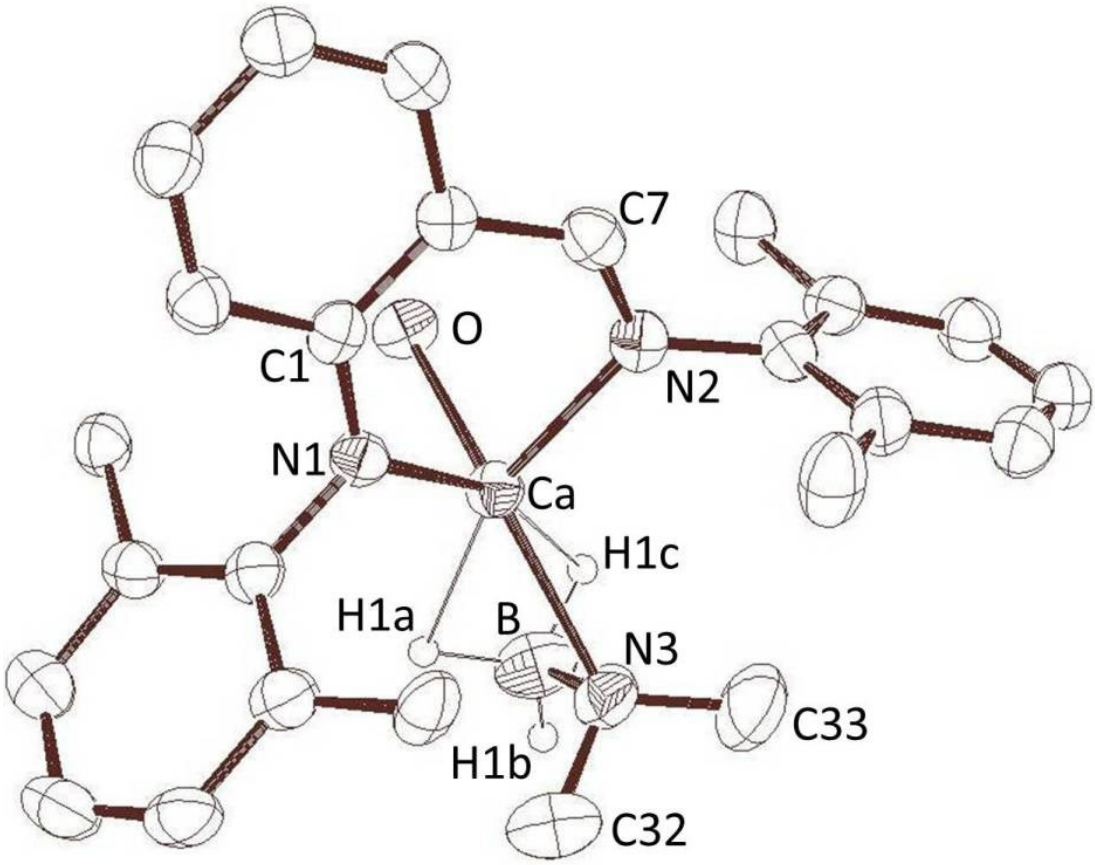

Figure 3.3: ORTEP representation of the solid-state structure of compound **13**. Thermal ellipsoids set at 50 % probability. Hydrogen atoms other than the boron bound hydrides, THF carbon atoms and 2,6-di-*iso*-propylphenyl *iso*-propyl methyl carbons removed for clarity. Selected bond lengths (Å) and angles (°); Ca-N1 2.317(2), Ca-N2 2.388(2), Ca-N3 2.382(2), N3-B 1.537(5), N1-C1 1.349(3), N2-C7 1.299(3), N1-Ca-N2 76.16(7) N1-Ca-N3 120.34(8), Ca-N3-B 79.03(19).

The solid-state structure of **13** is analogous to **LXV**, the β-diketiminato calcium dimethylamidoborane species reported by Hill,[2] with the anilido-imine supported calcium centre coordinated by the amidoborane nitrogen and anagostic interactions with the boron bound hydrides, in addition to a molecule of THF. The solid-state structure exhibits identical Ca-N1, Ca-N2 and Ca-N3 bond distances but a longer N2-B bond distance than **LXV** [1.497(6) Å]. The N1-Ca-N2 bond angle of **13**

[76.16(7)°] is more acute than that of **LXV** [81.71(8)°], whilst the N1-Ca-N3 bond angle of **13** [120.34(8)°] is more obtuse than that of **LXV** [113.99(7)°]. The different N1-C1 and N2-C7 bond distances of **13** clearly display the imino nature of the N2-C7 bond and anilido nature of the N1-C1 bond.

Attempts to prepare **13** in high yield on a preparative scale were frustrated by contamination by competitive protonation of the anilido-imine ligand (approx. 13 %), unidentified d_8-tol insoluble material and approx. 31 % of compound **14** (by integration of the ^{11}B NMR spectrum), comprising an anilido-imine calcium coordinated $[NMe_2BH_2NMe_2BH_3]^-$ anion, which could not be separated from **13**. The ^{11}B NMR spectrum showed a quartet resonance coincident with the quartet resonance for **13** and an unresolved resonance at $\delta = -1.8$ ppm, tentatively assigned to the BH_3 and BH_2 units of the $[NMe_2BH_2NMe_2BH_3]^-$ anion of **14**. The formation of compound **14** in this reaction is rationalised as a consequence of ligand protonation, resulting in an excess of DMAB which is available to react with **13**. The disparity between the results of NMR scale and larger scale synthesis was rationalised as resulting from instability of the reaction mixture in higher concentrations. Following these reactions, a rational synthesis of **14** was carried out by heating equimolar quantities of **13** and DMAB on an NMR scale at 30 °C for ca. 16 hours. The ^{11}B NMR spectrum of this reaction showed quartet and triplet resonances at $\delta = -11.2$ ppm, $^1J_{BH} = 89$ Hz and $\delta = -1.8$ ppm, $^1J_{BH} = 96$ Hz respectively. In this reaction approximately 25 % of protonated ligand was formed in addition to small quantities of **XXXVI** (ca. 7 %) and **XLVII** (ca. 4 %). The formation of **14** was confirmed by multinuclear NMR spectroscopy, however attempts to crystallise **14** were unsuccessful.

Stoichiometric addition of **IX-Mg** to two equivalents of DMAB on an NMR scale at room temperature resulted in the formation of a single compound, **15**, represented by a quartet and triplet resonance in the ^{11}B NMR spectrum at $\delta = -16.0$ ppm, $^1J_{BH} = 86$ Hz and $\delta = 3.3$ ppm, $^1J_{BH} = 99$ Hz respectively, assigned to the BH_3 and BH_2 units of an anilido-imine supported magnesium $[NMe_2BH_2NMe_2BH_3]^-$ complex. The triplet and quartet resonances in the ^{11}B NMR spectrum of **15** are marginally upfield compared to those of **XLV** ($\delta = 4.1$ ppm and $\delta = -14.9$ ppm respectively),

containing the β-diketiminato magnesium bound $[NMe_2BH_2NMe_2BH_3]^-$ anion reported by Hill.[2] The solid-state structure of **15**, shown in Figure 3.4, was confirmed by X-ray diffraction analysis of a single crystal, obtained by crystallisation from a concentrated toluene solution at –30 °C and was supported by accurate microanalytical data.

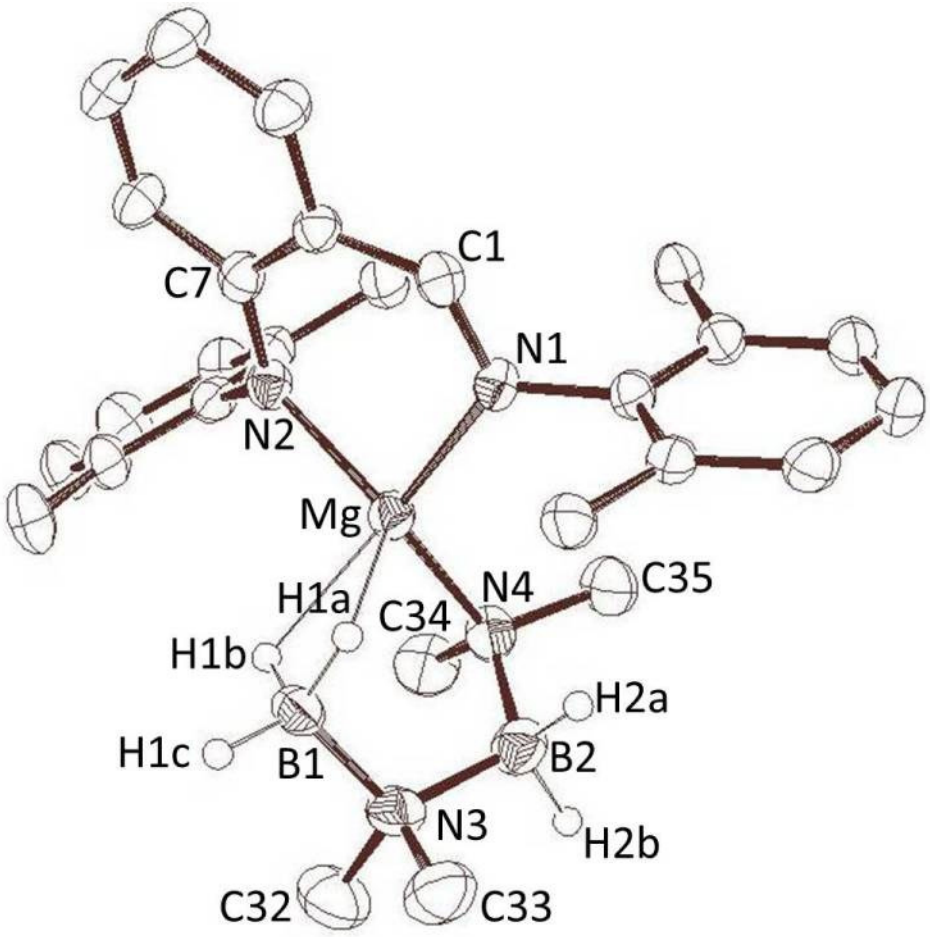

Figure 3.4: ORTEP representation of the solid-state structure of compound **15**. Thermal ellipsoids set at 50 % probability. Hydrogen atoms other than the boron-bound hydrides, and 2,6-di-*iso*-propylphenyl *iso*-propyl methyl carbons removed for clarity. Selected bond lengths (Å) and angles (°); Mg-N1 2.089(2), Mg-N2 2.029(2), Mg-N4 2.088(2), N4-B2 1.587(4), N3-B2 1.613(4), N3-B1 1.558(4), N1-C1 1.306(3), N2-C7 1.359(3), N1-Mg-N2 92.05(9), N1-Mg-N4 116.89(9), N2-Mg-N4 128.46(10), Mg-N4-B2 110.93(18), N4-B2-N3 114.2(2), B1-N3-B2 112.3(2).

The solid-state structure of **15** is analogous to **XLV**, comprising the β-diketiminato magnesium bound $[NMe_2BH_2NMe_2BH_3]^-$ anion reported by Hill,[2] with the anilido-imine supported magnesium centre coordinated by the nitrogen and anagostic interactions with the boron-bound hydrides of the $[NMe_2BH_2NMe_2BH_3]^-$ anion. The solid-state structure of **15** exhibits identical Mg-N4, N4-B2, N3-B2 and N3-B1 bond distances to those for **XLV**. The Mg-N1 and Mg-N2 bond distances are, however, different to one another and are longer and shorter respectively than those exhibited by **XLV** for which these bond distances are identical [2.0531(13) and 2.0529(13) Å]. The different N1-C1 and N2-C7 bond distances of **15** clearly display the imino nature of the N1-C1 bond and anilido nature of the N2-C7 bond. Compared to the bond angles for **XLV** the N1-Mg-N2, N1-Mg-N4 and Mg-N4-B2 bond angles are more acute, the N2-Mg-N4 and B1-N3-B2 bond angles are more obtuse and the N3-B2-N4 bond angle is identical to that of **15**.

Having displayed analogous stoichiometric reactivity with DMAB to that of **VI** and **XV**, compounds **IX-Ca** and **IX-Mg** were reacted with one and two equivalents respectively of pyrrolidine borane (PB), another secondary amine borane. These compounds, **16** and **17**, were once again characterised by multinuclear NMR spectroscopy. The ^{11}B NMR spectrum of **16**, an anilido-imine calcium pyrrolididoborane, showed a quartet at $\delta = -11.7$ ppm, $^1J_{BH} = 86$ Hz, whilst the ^{11}B NMR spectrum of **17**, containing an anilido-imine magnesium bound $[N(C_4H_8)BH_2N(C_4H_8)BH_3]^-$ anion, showed quartet and triplet resonances at $\delta = -15.9$ ppm, $^1J_{BH} = 89$ Hz and $\delta = 4.9$ ppm, $^1J_{BH} = 99$ Hz respectively. The ^{11}B NMR spectrum of **16** displayed a quartet resonance at a similar shift to that of **LXVI** ($\delta = -11.5$ ppm, $^1J_{BH} = 87$ Hz), however the ^{11}B NMR spectrum of **17** displayed quartet and triplet resonances shifted upfield and downfield respectively to those of the ^{11}B NMR spectrum of **LXVIII** ($\delta = -14.0$ ppm, $^1J_{BH} = 89$ Hz and $\delta = 4.1$ ppm, $^1J_{BH} = 100$ Hz respectively).

3.1.3 Catalytic Dehydrocoupling of Secondary Amine Boranes by Calcium and Magnesium Anilido-Imine Precatalysts **IX-Ca** and **IX-Mg**

Section 3.1.2 described stoichiometric reactions of **IX-Ca** and **IX-Mg** with the secondary amine boranes DMAB and PB, demonstrating that these reagents reacted

in an analogous way to the β-diketiminate compounds **VI** and **XV**, used by Hill et al.[2, 8] This section presents results of catalytic dehydrocoupling reactions of **IX-Ca** and **IX-Mg** conducted to establish whether these precatalysts were suitable for a mechanistic study.

Catalytic dehydrocoupling reactions of DMAB were carried out on an NMR scale at 70 °C using 5 mol % **IX-Ca** and **IX-Mg**. The catalyses proceeded via intermediate species analogous to those using β-diketiminate precatalysts and consistent with the proposed mechanism in Figure 3.1, resulting in the predominant formation of **XXXVI** in addition to a small proportion of **XLVII** (Table 3.1). Catalytic dehydrocoupling reactions of PB were also carried out using 5 mol % **IX-Ca** and **IX-Mg**, mirroring the results observed for DMAB. As shown by Table 3.1, judged by the relative percentages of $[R_2N\text{-}BH_2]_2$ and $HB(NR_2)_2$ determined by integration of the ^{11}B NMR spectra, **IX-Mg** was the more active precatalyst for these reactions, forming higher proportions of product species at identical or reduced heating times.

Amine Borane	Precatalyst	Reaction Conditions	$[R_2N\text{-}BH_2]_2$ / % (1d.p.)	$HB(NR_2)_2$ / % (1d.p.)
DMAB	**IX-Ca**	74 hrs 70 °C	8.3	3.0
	IX-Mg	19 hrs 70 °C	92.9	2.0
PB	**IX-Ca**	90 hrs 70 °C	17.2	5.3
	IX-Mg	90 hrs 70 °C	27.0	4.6

Table 3.1: Tabulated results from dehydrocoupling reactions of **IX-Ca** and **IX-Mg** with DMAB and PB, showing the percentage by ^{11}B NMR of $[R_2N\text{-}BH_2]_2$ and $HB(NR_2)_2$ formed.

Throughout the reactions with **IX-Mg** a small proportion (ca. 5 %) of protonated ligand could be observed in the ^1H NMR spectrum, however in reactions with **IX-Ca** complete protonation of the ligand was observed. Qualitative evidence suggested that magnesium-catalysed reactions proceeded at a faster rate than the analogous calcium reactions, consistent with the previously observed reactivity for amine borane dehydrocoupling using Group 2 β-diketiminate and bis(trimethylsilyl)amide complexes.[2, 8] A full kinetic study would be required to characterise and provide

quantitative data on the effect of metal centre and ligand on these reactions, which was beyond the scope of this initial study.

3.1.4 Stoichiometric Reactivity of Strontium Anilido-Imine **IX-Sr** with Secondary Amine Boranes and Anilido-Imine Ligand Stability

Addition of **IX-Sr** to one equivalent of DMAB on an NMR scale at room temperature resulted in clean conversion to a single product evidenced by a quartet resonance in the ^{11}B NMR spectrum at δ = –12.1 ppm, $^{1}J_{BH}$ = 78 Hz, assigned to the BH_3 unit of an anilido-imine strontium dimethylamidoborane **18**. A singlet resonance was observed in the ^{1}H NMR spectrum at δ = 0.09 ppm integrating to 18H resulting from the formation of $HN(SiMe_3)_2$. Heating an *in situ* prepared NMR sample of **18** for 19 hours at 80 °C resulted in formation of a single resonance in the ^{11}B NMR spectrum, a singlet at 30.6 ppm. This species was tentatively assigned as $B(NMe_2)_3$ **LXX** by comparison to the ^{11}B NMR spectrum of a commercial sample (singlet at 30.7 ppm).

Addition of **IX-Sr** to one equivalent of PB on an NMR scale at room temperature resulted in the observation of a single quartet resonance in the ^{11}B NMR spectrum at δ = –10.9 ppm, $^{1}J_{BH}$ = 82 Hz, assigned to the BH_3 unit of an anilido-imine supported strontium pyrrolididoborane **20**, a singlet resonance was again observed in the ^{1}H NMR spectrum at δ = 0.08 ppm integrating to 18H resulting from the formation of $HN(SiMe_3)_2$. The quartet resonance in the ^{11}B NMR spectrum of **20** is at a comparable shift to that of **LXVII** (δ = –10.7 ppm), the β-diketiminato strontium pyrrolididoborane species reported by Hill.[8] Multiple attempts to obtain the solid-state structure of **20** by crystallisation of a concentrated toluene solution at –30 °C resulted on each occasion, however, in the structure shown in Figure 3.5, the previously unreported homoleptic strontium bis(anilido-imine) species **21**.

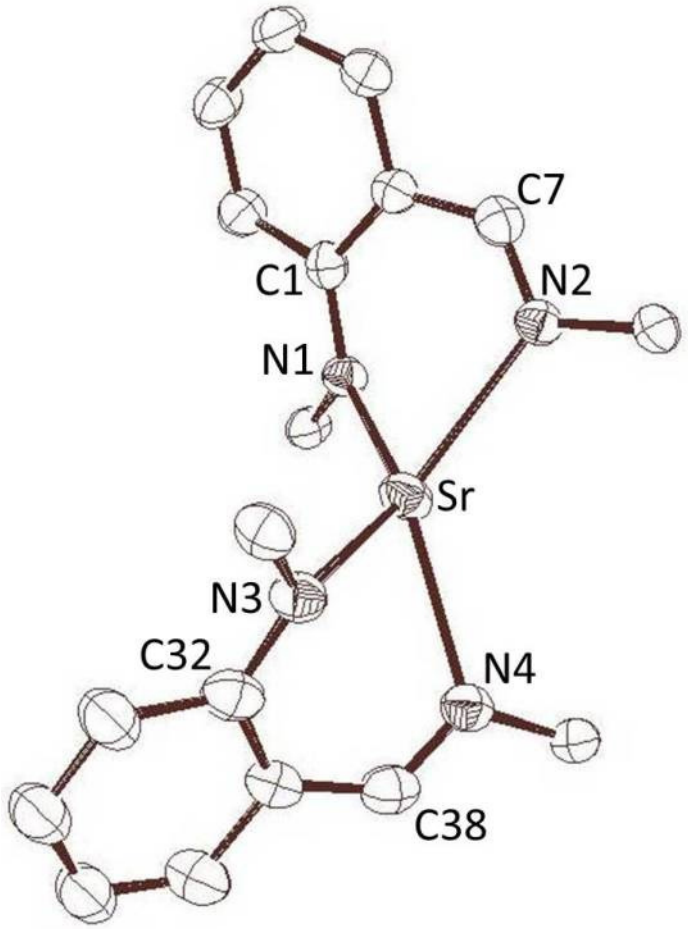

Figure 3.5: ORTEP representation of the solid-state structure of **21**, strontium bis(anilido-imine), formed by crystallisation from the stoichiometric reaction between **IX-Sr** and DMAB. Thermal ellipsoids set at 50 % probability. Apart from the *ipso*–carbons the 2,6-di-*iso*-propylphenyl carbons and all hydrogen atoms are removed for clarity. Selected bond lengths (Å) and angles (°); Sr-N1 2.527(2), Sr-N2 2.533(2), Sr-N3 2.534(3), Sr-N4 2.535(3), N1-C1 1.361(4), N2-C7 1.287(4), N3-C32 1.345(4), N4-C38 1.302(4), N1-Sr-N2 72.22(8), N3-Sr-N4 72.17(9), N1-Sr-N3 134.60(8), N2-Sr-N4 126.63(9).

The solid-state structure of **21** comprises a pseudo-tetrahedral strontium centre coordinated by two units of the bidentate anilido-imine ligand. Although compound **21** has identical Sr-N bond lengths it is still possible to discriminate the anilido N1-C1 and N3-C32 bond lengths which are longer than the imino N2-C7 and N4-C38 bonds. These anilido and imino N-C bonds are identical to those of the anilido-imine calcium- and magnesium- amidoborane complexes **13** and **15**. The formation

of this species demonstrates that even with literature reports of increased stability of this ligand, redistributive formation of homoleptic heavier alkaline earth species is possible with the appropriate substrates and conditions.

Assessment of the catalytic dehydrocoupling of DMAB was carried out on an NMR scale using 5 mol % **IX-Sr**. This proceeded via intermediate species analogous to those using β-diketiminate precatalysts and was consistent with the proposed mechanism in Figure 3.1. After ca. 67 hours at 70 °C, however, only ca. 9.2 % of **XXXVI** and ca. 1.5 % **XLVII** had formed. Catalytic dehydrocoupling of PB on an NMR scale using 5 mol % **IX-Sr** and heating for ca. 66 hours at 70 °C resulted in formation of ca. 12.5 % **LIV** and ca. 9.8 % **LXIX**. Continued heating of both reactions at 70 °C revealed only very slow conversion to the dehydrocoupled products. By comparison to the tabulated results in Table 3.1, the dehydrocoupling activity of **IX-Sr** is lower than that of **IX-Mg** and **IX-Ca**. The ^{1}H NMR spectra of these reactions revealed complete protonation of the anilido-imine ligand, in mitigation of the reduced activity.

Following the characterisation of **21** the analogous homoleptic alkaline earth anilido-imine species were rationally synthesised using potassium hydride and the Group 2 diiodide, as shown in Figure 3.6.

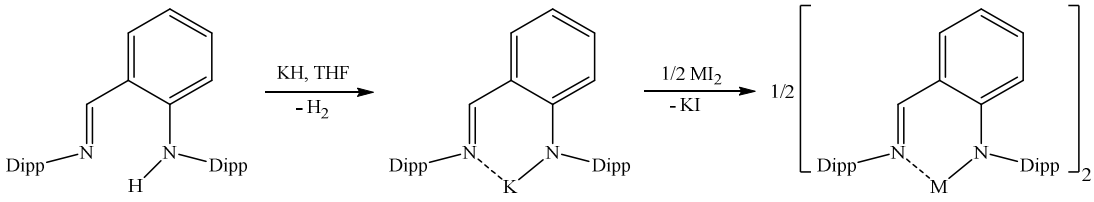

Figure 3.6: Reaction scheme for the rational synthesis of alkaline earth bis(anilido-imine) species, where M = Mg **22**, Ca **23**, Ba **24**.

Although attempts to crystallise the calcium- and barium bis(anilido-imine) (**23** and **24**) species proved unsuccessful the solid-state structure of magnesium bis(anilido-imine) **22** shown in Figure 3.7, was obtained by X-ray diffraction analysis of a single crystal isolated by crystallisation from a concentrated toluene solution at –30 °C.

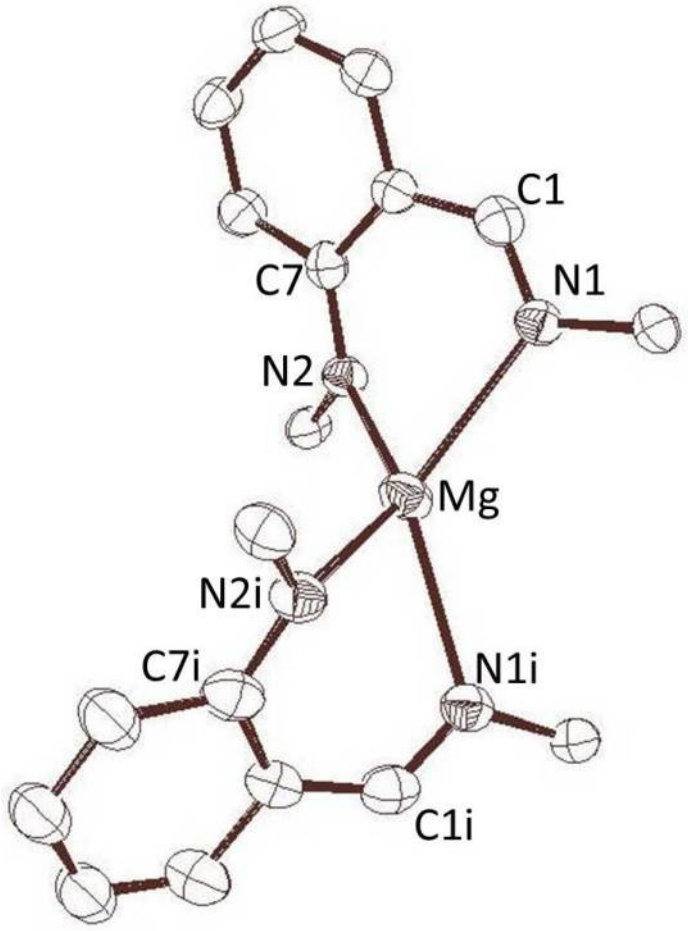

Figure 3.7: ORTEP representation of the solid-state structure of **22**, magnesium bis(anilido-imine). Thermal ellipsoids set at 50 % probability. Apart from the *ipso*–carbons the 2,6-di-*iso*-propylphenyl carbons and all hydrogen atoms are removed for clarity. Selected bond lengths (Å) and angles (°); Mg-N1 2.1300(12), Mg-N2 2.0590(12), N1-C1 1.3009(19), N2-C7 1.3640(18), N1-Mg-N2 90.71(4), N1-Mg-N1i 127.00(7), N1-Mg-N2i 114.57(4), N2-Mg-N2i 122.67(7). Symmetry transformations used to generate equivalent atoms: -*x*,*y*,-*z*+1/2 and -*x*+1,-*y*+1,-*z*+1.

The solid-state structure of **22** contains a magnesium centre in a similar pseudo-tetrahedral coordination geometry to that of the homoleptic strontium species, compound **21**. The shorter Mg-N1 and Mg-N2 bond lengths are reflected by the more obtuse N1-Mg-N2 bond angle and may be rationalised as a consequence of the smaller ionic radius of the magnesium atom. The imino N1-C1 and anilido N2-C7 bond lengths are identical to those of **21** in addition to the anilido-imine calcium- and magnesium- amidoborane complexes **13** and **15**.

An equimolar reaction of the anilido-imine ligand precursor, potassium hydride and calcium iodide, Figure 3.8, yielded the anilido-imine calcium iodide species **25**.

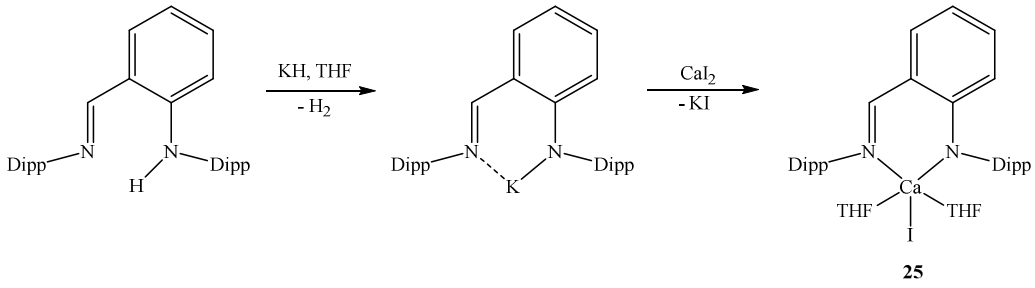

Figure 3.8: Reaction scheme for the preparation of **25**, through the stoichiometric reaction of the anilido-imine ligand precursor, potassium hydride and calcium iodide.

Single crystals of this sparingly soluble species suitable for X-ray diffraction analysis were isolated from a concentrated THF solution at –30 °C. The solid-state structure of **25** is shown in Figure 3.9.

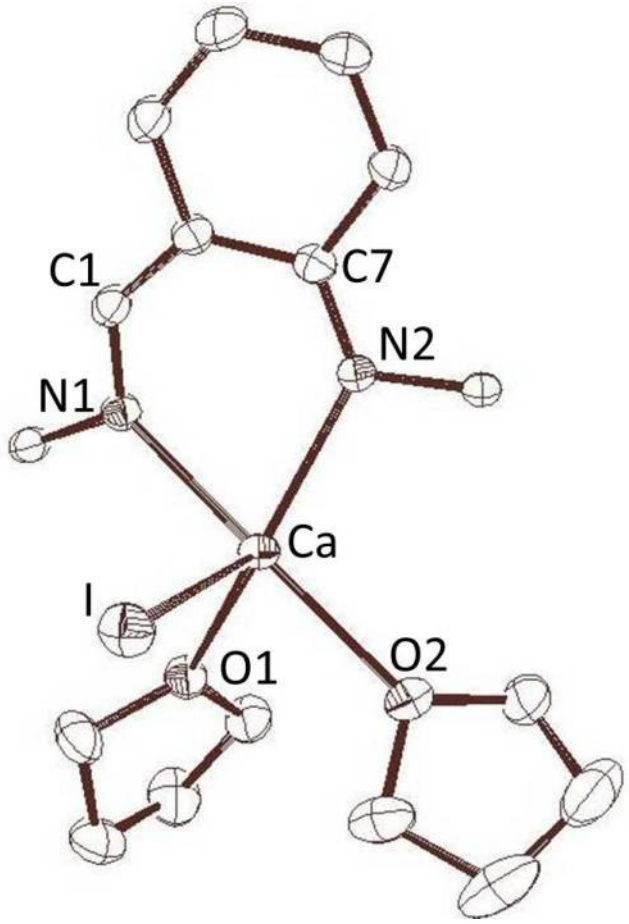

Figure 3.9: ORTEP representation of the solid-state structure of **25**. Thermal ellipsoids set at 50 % probability. Apart from the *ipso*–carbons the 2,6-di-*iso*-propylphenyl carbons and all hydrogen atoms are removed for clarity. Selected bond lengths (Å) and angles (°); Ca-N1 2.4372(16), Ca-N2 2.3267(16), Ca-I 3.0055(4), N1-C1 1.298(3), N2-C7 1.352(2), Ca-O1 2.3598(14), Ca-O2 2.4051(15), N1-Ca-N2 76.87(5), N1-Ca-O1 87.14(5), N2-Ca-O2 105.77(5), N1-Ca-I 99.07(4), N2-Ca-I 111.45(4).

The solid-state structure of compound **25** consists of a five-coordinate calcium centre in a pseudo-square-based pyramidal coordination geometry, coordinated by the nitrogen atoms of the bidentate anilido-imine ligand, an iodide anion and two molecules of THF. The Ca-N1 and Ca-N2 bond lengths are longer and shorter respectively than those of **13**, the anilido-imine calcium dimethylamidoborane shown in Figure 3.3, because of the change in coordinating anion and the higher calcium coordination number results in a slightly more obtuse N1-Ca-N2 bond angle than **13**.

The N1-C1 and N2-C7 bond lengths once again evidence the imino and anilido character of these bonds and are identical to those of **13**. The terminal Ca-I bond length of compound **25** is shorter than those of the dimeric [β-diketiminato.CaI(Et_2O)]$_2$ species **LXXI** [3.1224(8) and 3.090(1) Å] reported by Jones.[9]

As discussed in Chapter 1, Section 1.1.4, hydrocarbon soluble metal hydrides have been identified as key intermediates in catalysis and β-diketiminate supported alkaline earth metal hydrides have been reported for magnesium and calcium,[10, 11] but not for strontium. Attempted formation of the anilido-imine strontium hydride was thus attempted on an NMR scale by stoichiometric addition of **IX-Sr** to phenylsilane and heating at 70 °C for ca. 16 hours. This procedure, however, resulted in reduction of the ligand's imine functionality via a silicon-nitrogen coupling reaction, forming **26**. Single crystals of **26** suitable for X-ray diffraction analysis were obtained from a concentrated toluene solution at –30 °C. The solid-state structure of **26** is shown in Figure 3.10.

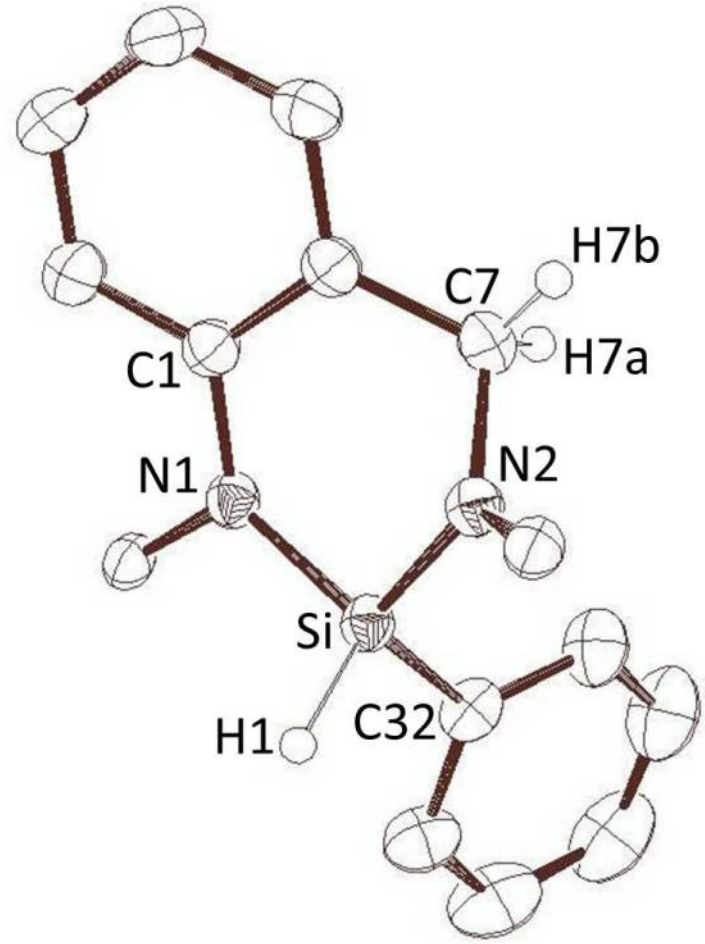

Figure 3.10: ORTEP representation of the solid-state structure of **26**, formed in the stoichiometric reaction of **IX-Sr** and phenylsilane and heating at 70 °C for ca. 16 hrs. Thermal ellipsoids set at 50 % probability. Hydrogen atoms other than those bonded to silicon and the reduced carbon atom of the ligand (C7) removed for clarity. Apart from the *ipso*–carbons the 2,6-di-*iso*-propylphenyl carbons are removed for clarity. Selected bond lengths (Å) and angles (°); Si-N1 1.7412(13), Si-N2 1.6992(13), Si-C32 1.8669(16), N1-C1 1.4153(19), N2-C7 1.478(2), N1-Si-N2 102.66(6), N1-Si-C32 110.34(7), N2-Si-C32 115.94(7), C1-N1-Si 123.64(10), C7-N2-Si 115.82(10).

The solid-state structure of **26** comprises a silicon(IV) centre coordinated by a hydride and phenyl group, supported by the chelating dianionic anilido-amido ligand, formed by reduction of the previously monoanionic ligand's imine functionality. The anilido C1-N1 bond length is longer than those previously observed for **13**, **15**, **21**, **22** and **25**, as a combined effect of the Si-N bond and the

reduced state of the ligand, which also causes a loss of planarity across the ligand. The N2-C7 bond is no longer an imine bond and the longer bond length reflects this. In comparison to the silicon-nitrogen dehydrocoupling product DippNH-SiPh(H)NHDipp **LXXII** reported by Hill,[12] shown in Figure 3.11, the Si-N bond lengths of **26** are longer and shorter respectively than those of **LXXII** [1.7119(16) and 1.7281(17)], possibly arising from the combined effects of the cyclic structure and more substituted nitrogen atoms of **26**.

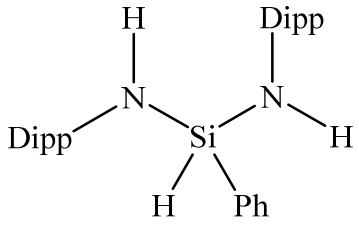

Figure 3.11: Silicon-nitrogen dehydrocoupling product **LXXII** reported by Hill.[12]

The formation of **26**, the mechanism of which is unknown and of limited interest to this study, provides evidence of the susceptibility of this ligand towards ligand reduction. The lack of hydrocarbon insoluble species suggests that the formation of **26** may involve the elimination of a [HSr{N(SiMe$_3$)$_2$}] species, Figure 3.12.

$$\textbf{IX-Sr} + PhSiH_3 \xrightarrow[16hrs\ 70°C]{Tol} \textbf{26} + [HSr\{N(SiMe_3)_2\}]$$

Figure 3.12: Proposed reaction scheme for the formation of **26**, formed by heating the stoichiometric reaction of **IX-Sr** and phenylsilane at 70 °C for ca. 16 hours.

3.1.5 Selection of Alkaline Earth Precatalyst for Amine Borane Dehydrocoupling

The results described in Section 3.1.4 indicate that although initial reactions of amine boranes with anilido-imine alkaline earth species **IX** mimicked those of β-diketiminate species, subsequent reactivity revealed less favourable properties. The formation of the previously unreported strontium bis(anilido-imine) species **21** and the rational synthesis of the magnesium, calcium and barium analogues **22**-**24**, along with the reduction product **26**, demonstrates that this ligand does not provide sufficiently enhanced stability towards Schlenk equilibration in comparison to the β-

diketiminate ligand to enable an in-depth investigation of the dehydrocoupling of amine boranes with the full series of heavier Group 2 elements or the isolation of intermediate species.

Although the dehydrocoupling reactivity of **IX** exhibited an identical trend in dependence upon identity of metal centre to that observed for β-diketiminate and bis(trimethylsilyl)amide species, the ease of protonation and reduction of the anilido-imine ligand displayed in Section 3.1.4 indicated this ligand provides limited advantage over these species essentially discounting it as a viable alternative.

For this reason further mechanistic investigation of the dehydrocoupling of amine boranes by d^0 species described in this chapter and Chapter 4 utilised the magnesium- and calcium β-diketiminate species **XV** and **VI** for investigation of reaction intermediates, whilst the bis(trimethylsilyl)amides $[M(N(SiMe_3)_2)_2]$ **V** were employed in kinetic experiments to investigate the dependence upon the identity of the metal centre. Comparison of the dehydrocoupling activity of Group 2 to scandium and yttrium of Group 3 was made using the respective Group 3 tris(amides) **XL** and **XLI**, the stoichiometric reactivity of which was reported by Hill and will not be investigated further.[1] Extension to Group 1 species was made using the bis(trimethylsilyl)amides, $MN(SiMe_3)_2$ **LIX**, to enable the first comparisons of the amine borane dehydrocoupling activity of this congeneric series of elements.

3.2.1 Stoichiometric Reactivity of Group 1 bis(trimethylsilyl)amides $MN(SiMe_3)_2$ **LIX** with DMAB

As described in Chapter 1, Section 1.4, the solid-state thermolysis of alkali metal amidoboranes and their hydrogen release has been described in the literature.[13-27] Predating recent interest in hydrogen storage, by over 30 years, is the research by Keller of the reactivity of Group 1 reagents with boranes, including dimethylamine borane.[28-34] This section investigates stoichiometric reactions between Group 1 bis(trimethylsilyl)amides, $MN(SiMe_3)_2$ **LIX**, and DMAB.

Literature syntheses of $[Li(NMe_2BH_3)]$ **LXXIII** and $[K(NMe_2BH_3)]$ **LXXIV** has been achieved by the stoichiometric reactions of DMAB with *n*-butyl-lithium, or potassium hydride respectively, evolving butane and hydrogen respectively.[35, 36]

Although the solid-state structures of **LXXIII** and **LXXIV** have recently been reported and other groups have utilised **LXXIII** as an intermediate in the synthesis of amine borane derivatives,[35, 36] the synthesis of these compounds was frustrated by their apparent instability in ethereal solvents. This resulted in isolated samples which included ca. 45 – 50 % impurity, observed as triplet and multiple quartet resonances in the ^{11}B NMR spectra. These syntheses of **LXXIII** and **LXXIV** employed an excess of Group 1 reagent used to counteract the effect of the unknown concentration of the starting materials, which are prone to impurities and variation in concentration. An excess of either Group 1 reagent or DMAB could, however, have unforeseen consequences on the course of the reaction. Thus, the use of Group 1 bis(trimethylsilyl)amides, $MN(SiMe_3)_2$ **LIX**, reagents of a higher and known purity was investigated. Stoichiometric addition of $[K\{N(SiMe_3)_2\}]$ **LIX-K** to DMAB in THF on an NMR scale at room temperature resulted in clean conversion to **LXXIV**, with concomitant formation of $HN(SiMe_3)_2$ observed as a singlet at δ = 0.13 ppm integrating to 18H in the ^{1}H NMR spectrum. Heating of this sample at 60 °C for ca. 24 hours induced reaction of ca. 73.3 % **LXXIV** by integration of the ^{11}B NMR spectrum to form several boron-containing species. A doublet resonance assigned to **XLVII** (ca. 32.5 %) was observed in addition to a second doublet resonance at δ = 33.8 ppm, $^1J_{BH}$ = 135 Hz tentatively attributed to $[HB\{NMe_2\}\{N(SiMe_3)_2\}]$ **27** integrating to 10.4 % of the total $^{`11}$B NMR signal intensity. A new quartet resonance at δ = –20.8 ppm, $^1J_{BH}$ = 85 Hz, integrating to 34.5 % of the boron species, was tentatively assigned as a $[H_3B.NH(SiMe_3)_2]$ **28** species formed by reaction of BH_3, generated by β-hydride elimination to form **XLVII**, with $[H\{N(SiMe_3)_2\}]$, formed in the initial protonolysis to form **LXXIII**.

As previously described, **LXXIV** appeared unstable in ethereal solvent whilst attempting the literature syntheses.[35, 36] Keller's work with dimethylamine borane, however, reported that $[K(NMe_2BH_3)]$ **LXXIV** forms via an intermediate, metallated, $[NMe_2BH_2NMe_2BH_3]^-$ anion which is unstable to formation of **LXXIV** in the presence of excess metal hydride.[29, 31] An equation for this decomposition is shown in Figure 3.13.

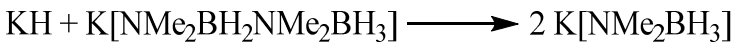

Figure 3.13: Decomposition reaction of metallated $[NMe_2BH_2NMe_2BH_3]^-$ anion in the presence of metal hydride to form an alkali metal amidoborane, reported by Keller.[29, 31]

The production of a $[NMe_2BH_2NMe_2BH_3]^-$ anion necessitates the formation of a new B-N bond. This report, backed by ^{11}B NMR spectra of unsuccessful syntheses of pure **LXXIV**, which also suggested formation of a $[NMe_2BH_2NMe_2BH_3]^-$ species, prompted further analysis of the reactivity of Group 1 reagents towards amine boranes. Stoichiometric reaction of potassium hydride and two equivalents of DMAB at room temperature resulted in the formation of $K[NMe_2BH_2NMe_2BH_3]$ **29**. This reaction was repeated with $[K\{N(SiMe_3)_2\}]$ replacing potassium hydride, which provided smooth access to **29** owing to its superior purity. An equation for the formation of **29** is shown in Figure 3.14.

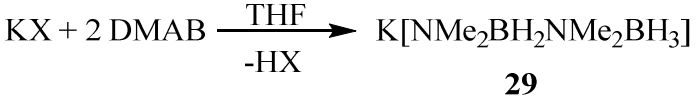

Figure 3.14: Stoichiometric reaction between potassium reagent and two equivalents of DMAB to form **29**, where X = H, $[N(SiMe_3)_2]$.

The ^{11}B NMR spectrum of **29** showed broad, unresolved resonances at δ = –12.3 ppm and δ = 2.6 ppm, assigned to the BH_3 and BH_2 units of a potassium-coordinated $[NMe_2BH_2NMe_2BH_3]^-$ anion. These ^{11}B NMR chemical shifts of **29** differ to those of homoleptic $Mg[NMe_2BH_2NMe_2BH_3]_2$ **XLVI** (quartet: δ = –15.3 ppm, $^1J_{BH}$ = 89 Hz and triplet: δ = 4.0 ppm, $^1J_{BH}$ = 102Hz) and the scandium species $[Sc(NMe_2BH_2NMe_2BH_3)_2\{N(SiMe_2H)_2\}]$ **LXXV** (quartet: δ = –12.9 ppm, $^1J_{BH}$ = 89 Hz and triplet: δ = 4.0 ppm, $^1J_{BH}$ = 102Hz),[1, 2] rationalised as a consequence of the greater lability of the Group 1 element.

Single crystals of **29** suitable for X-ray diffraction analysis were isolated from a concentrated THF solution at –30 °C. The solid-state structure of **29** is shown in Figure 3.15.

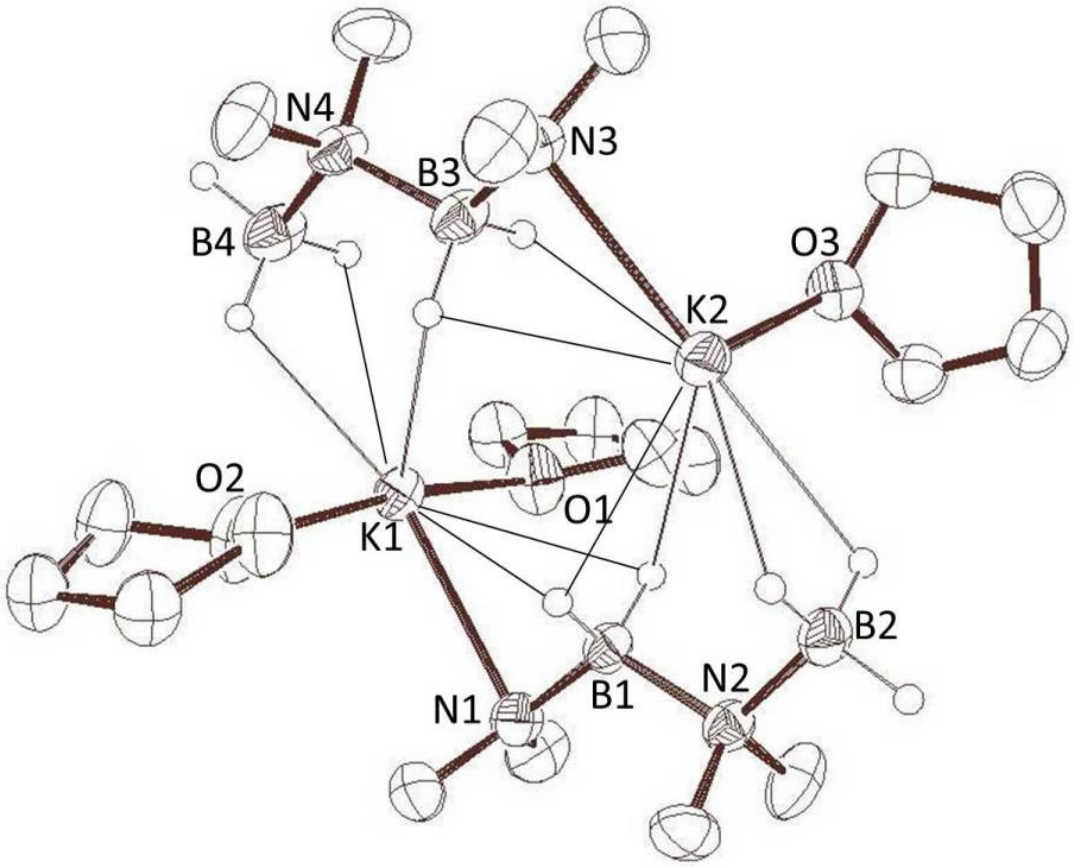

Figure 3.15: ORTEP representation of the asymmetric unit of **29**, formed by the stoichiometric reaction of potassium hydride and two equivalents of DMAB. Thermal ellipsoids set at 50 % probability. Hydrogen atoms other than the boron-bound hydrides removed for clarity. Selected bond lengths (Å) and angles (°); K1-N1 2.8726(16), K2-N3 2.8679(17), K1-O1 2.7781(15), K1-O2 2.7448(15), K2-O3 2.7328(16), N1-B1 1.496(3), B1-N2 1.635(2), N2-B2 1.588(3), N3-B3 1.509(3), B3-N4 1.643(3), N4-B4 1.592(3), O2-K1-O2 172.76(5), K1-N1-B1 86.39(10), N1-B1-N2 116.87(16), B1-N2-B2 111.73(14), O3-K2-N3 98.79(5), K2-N3-B3 86.58(11), N3-B3-N4 116.85(17), B3-N4-B4 112.16(15).

The solid-state structure of **29** may be considered as a dimeric molecule which propagates as a linear coordination polymer, formed of a $K[NMe_2BH_2NMe_2BH_3].THF_2$ unit linked to a $K[NMe_2BH_2NMe_2BH_3].THF$ unit by BH_2 and BH_3 anagostic interactions. The potassium centres are coordinated by the nitrogen atom and further anagostic interactions with two boron-bound hydrides of the same $[NMe_2BH_2NMe_2BH_3]^-$ anion and anagostic interactions with boron-bound

hydrides of a secondary $[NMe_2BH_2NMe_2BH_3]^-$ unit, augmented by molecules of THF. The linear coordination polymer which propagates through intermolecular interactions of the BH_3 units with the K atoms of adjacent dimeric units is shown in Figure 3.16.

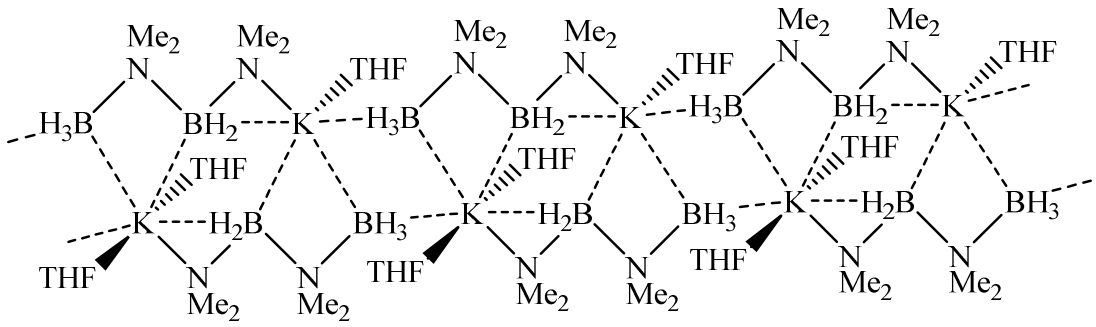

Figure 3.16: Linear coordination polymer formed by compound **29**.

The solid-state structure of compound **29** exhibits different K-O bond lengths, but K1-N1 and K2-N3 bond lengths which are identical to one another. As shown by the table in Figure 3.19 the N(i)-B(i) bond length of **29** is shorter than any previously reported metallated $[NMe_2BH_2NMe_2BH_3]^-$ anion, whilst the B(i)-N(ii) and N(ii)-B(ii) bond lengths are both longer than any previously reported.[1, 2] Although this can be rationalised by the change from a Group 2 to a Group 1 metal centre and the absence of a supporting ligand, a potentially crucial difference in the solid-state structure of **29** is the formation of a coordination polymer with anagostic interactions between the potassium centres and hydrides of both the B(i) and B(ii) atoms. This is not observed in any of the other metallated $[NMe_2BH_2NMe_2BH_3]^-$ species shown in Table 3.2. The $[NMe_2BH_2NMe_2BH_3]^-$ unit is represented as $[N(i)Me_2B(i)H_2N(i)Me_2B(ii)H_3]$ shown in Figure 3.17 to enable comparisons of bond lengths shown in Table 3.2.

	XLV	XLVI	LXXV	15	29
N(i)-B(i)	1.586(3)	1.5647(17) 1.5646(17)	1.572(3)	1.587(4)	1.496(3) 1.509(3)
B(i)-N(ii)	1.620(3)	1.6145(17) 1.6131(17)	1.608(3)	1.613(4)	1.635(2) 1.643(3)
N(ii)-B(ii)	1.570(3)	1.5762(17) 1.5731(18)	1.567(3)	1.558(4)	1.588(3) 1.592(3)

Table 3.2: Table of bond lengths for species containing $[NMe_2BH_2NMe_2BH_3]^-$ anions; β-diketiminato-Mg$[NMe_2BH_2NMe_2BH_3]$ **XLV**,[2] Mg$[NMe_2BH_2NMe_2BH_3]$ **XLVI**,[2] $[Sc(NMe_2BH_2NMe_2BH_3)_2\{N(SiMe_2H)_2\}]$ **LXXV**,[1] **15** and **29**, simplified as $[N(i)Me_2B(i)H_2N(i)Me_2B(ii)H_3]$ to enable comparisons of bond lengths.

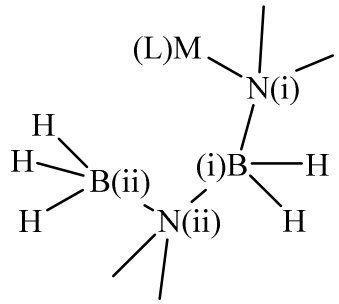

Figure 3.17: A metallated $[NMe_2BH_2NMe_2BH_3]^-$ unit represented as $[N(i)Me_2B(i)H_2N(i)Me_2B(ii)H_3]$ to enable comparisons of bond lengths utilised in Table 3.2, where M is the Group 1, 2 or 3 metal centre and L is a supporting ligand.

The K-N(i)-B(i), N(i)-B(i)-N(ii) and B(i)-N(ii)-B(ii) bond angles for the two K$[NMe_2BH_2NMe_2BH_3]$ units of **29** are identical, deviating from those of **XLV**, **XLVI**, **LXXV** and **15** and rationalised as a consequence of the formation of the linear coordination polymer shown in Figure 3.16.

The reaction of $[Li\{N(SiMe_3)_2\}]$ **LIX-Li** with two equivalents of DMAB on an NMR scale at room temperature formed Li$[NMe_2BH_2NMe_2BH_3]$ **30**, observed as quartet and triplet resonances at δ = –14.7 ppm, $^1J_{BH}$ = 89 Hz and δ = 3.5 ppm, $^1J_{BH}$ = 98 Hz respectively in the ^{11}B NMR spectrum, but proceeded markedly more slowly than the analogous potassium reaction. The reaction of $[Na\{N(SiMe_3)_2\}]$

LIX-Na with two equivalents of DMAB on an NMR scale at room temperature similarly formed $Na[NMe_2BH_2NMe_2BH_3]$ **31**, observed as quartet and triplet resonances at δ = –14.7 ppm, $^1J_{BH}$ = 87 Hz and δ = 1.9 ppm, $^1J_{BH}$ = 98 Hz respectively in the ^{11}B NMR spectrum. This reaction was contaminated by $Na[NMe_2BH_3]$, appearing as a coincidental quartet resonance with the BH_3 unit of **31** in the ^{11}B NMR spectrum.

3.2.2 Catalytic Dehydrocoupling of DMAB By Group 1 Bis(trimethylsilyl)amides **LIX**

Section 3.2.1 described stoichiometric reactions between alkali metal bis(trimethylsilyl)amides **LIX** (M = Li, Na, K) and amine boranes to form alkali metal amidoboranes, demonstrating their potential for catalytic dehydrocoupling of amine boranes.

Catalytic dehydrocoupling reactions of DMAB were thus carried out on an NMR scale using 5 mol % **LIX-Li**, **LIX-Na** and **LIX-K** and heated at 80 °C. In all cases dehydrocoupling was observed to occur, proceeding via intermediate species analogous to those using alkaline earth precatalysts and consistent with the proposed mechanism in Figure 3.1, with formation of **XXXVI** and **XLVII** as a minor product. Qualitative assessment of these reactions, however, suggested that dehydrocoupling proceeded relatively quickly at first before a marked reduction in rate. The conversions in Table 3.3 show that **LIX-Li**, the reaction of which was also heated for a shorter time, was the most active catalyst.

	LIX-Li	**LIX-Na**	**LIX-K**
XXXVI	72.0	43.0	43.0
XLVII	5.0	2.8	6.0

Table 3.3: Tabulated conversions (%) for the dehydrocoupling of DMAB by 5 mol % **LIX-Li** after heating at 80 °C for ca. 124 hours, and **LIX-K** and **LIX-Na** after heating at 80 °C for 172 hours, with percentage of each species by integration of ^{11}B NMR spectra.

The observed reduction in activity of these Group 1 reagents after an initial period may have occurred via formation of hydrocarbon-insoluble hydrides. This may be expected to retard the reaction even though these species react with amine boranes, as evidenced by the synthesis of $Li(NMe_2BH_3)$ **LXXII** and $K(NMe_2BH_3)$ **LXXIII**. In addition to this, resonances attributed to BH_4^- were observed in the ^{11}B NMR spectra of these reactions with formation of alkali metal borohydrides causing a reduction in activity. A full kinetic investigation of the dehydrocoupling activity of these species would be required to validate these qualitative statements and compare the relative activity of these Group 1 species.

3.2.3 Stoichiometric Reactivity of β-diketiminato-Magnesium Amidoborane

Chapter 1, Section 1.3, described work by the Hill Group in which the stoichiometric reaction of *n*-butyl-β-diketiminato-magnesium species **XV** with two equivalents of DMAB resulted in the formation of **XLV**, containing a β-diketiminato-magnesium coordinated $[NMe_2BH_2NMe_2BH_3]^-$ anion. The reported reactions of secondary amine boranes (other than di-*iso*-propylamine borane) with magnesium species, whether bis(trimethylsilyl)amide **V**, *n*-butyl-β-diketiminato **XV** or di-*n*-butyl **XLIV**, also resulted in isolation of coordinated magnesium species incorporating $[NR_2BH_2NR_2BH_3]^-$ anions, in which a new B-N bond had already formed. This was rationalised as resulting from the rapidity of the proposed β-hydride elimination and insertion of the unsaturated and polarised $[R_2N{=}BH_2]$ **XXXVII** fragment.

A mechanistic investigation of this initial process required synthesis of the corresponding β-diketiminato-magnesium-dimethylamidoborane **32**, which, unlike the calcium analogue **LXV**, cannot be formed by simple reaction between one equivalent of DMAB and **XV**. The synthesis of **32**, shown in Figure 3.18, comprised a salt metathesis reaction between β-diketiminato-magnesium-iodide **LXXVI** and either $[Li(NMe_2BH_3)]$ **LXXIII** or $[K(NMe_2BH_3)]$ **LXXIV**, prepared by literature procedures.[35-37]

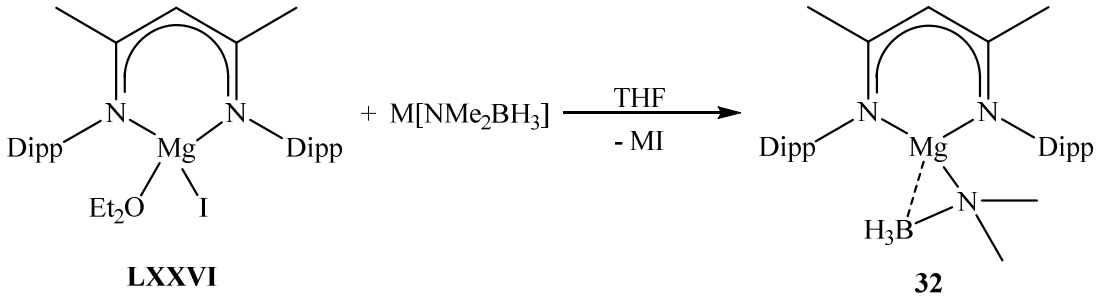

LXXVI **32**

Figure 3.18: Reaction scheme for the preparation of **32**, by a salt metathesis reaction between **LXXVI** and **LXXIII** (M = Li) or **LXXIV** (M = K).

The ^{11}B NMR spectrum of **32** comprised a single quartet resonance at δ = –11.8 ppm, $^{1}J_{BH}$ = 91 Hz. The range of β-diketiminato-magnesium amidoboranes reported by Harder provide the closest comparable magnesium species, although the ^{11}B NMR shift of **32** is upfield of the β-diketiminato-magnesium amido borane **LXXVII** (δ = –2.4 ppm, $^{1}J_{BH}$ = 87 Hz), it is downfield of -methylamidoborane **LXXVIII** (δ = – 19.0 ppm, $^{1}J_{BH}$ = 86 Hz), -*iso*-propylamidoborane **LXXIX** (δ = –22.0 ppm, $^{1}J_{BH}$ = 88 Hz) and -2,6-di-*iso*-propylanilidoborane **L** (δ = –17.7 ppm).[38, 39] These latter species are ammonia or primary amido boranes, however, so, whilst they may provide comparison to β-diketiminato-magnesium amidoboranes, it is Hill's analogous β-diketiminato-calcium dimethylamidoborane **LXV** which bears the closest resemblance, with a comparable ^{11}B NMR shift (δ = –11.5 ppm, $^{1}J_{BH}$ = 86 Hz).[2]

Storage of solutions of **32** resulted in the formation of intractable and insoluble material, possibly magnesium hydride or amidoborane, in addition to free ligand, preventing confirmation of this species by crystallographic and microanalytical data analysis.

Stoichiometric reactions of **32** could, however, be carried out with amine boranes prior to decomposition, to investigate the reactivity of this species and the proposed β-hydride elimination-insertion mechanism to form species such as β-diketiminato-Mg[$NMe_2BH_2NMe_2BH_3$] **XLV**. Addition of **32** to one equivalent of DMAB on an NMR scale resulted in the formation of ca. 13.4 % **XLV** after 15 minutes at room temperature. Reaction for ca. 16 hours at room temperature, however, resulted in

conversion to ca. 48.9 % $[H_2N\text{-}BH_2]_2$ **XXXVI** and ca. 9.5 % $[HB(NMe_2)_2]$ **XLVII** with no **XLV** evident in the ^{11}B NMR spectrum. The reaction of **XV** with two equivalents of DMAB,[2, 3] therefore, results in a different outcome to that of **32** with one equivalent of DMAB.

In an attempt to slow this reaction the cyclic secondary amine borane pyrrolidine borane (PB) was added to **32** in a stoichiometric NMR scale reaction at room temperature. This reaction once again, however, resulted in ca. 52 % conversion to cyclo diborazane products after ca. 16 hours at room temperature, observed as overlapping resonances at ca. 5.5 ppm in the ^{11}B NMR spectrum. The multiple boron-containing species are believed to be a combination of **XXXVI** and $[C_4H_8N\text{-}BH_2]_2$ **LIV**, unreacted PB and **32**, and possibly a magnesium $[NR_2BH_2NR_2BH_3]$ species, the identity of which could not be confirmed. In a further attempt to elucidate the nature of the proposed insertion step, DMAB deuterated at the borane, $Me_2NH.BD_3$ **XXVIII**, was added to **32** in a stoichiometric NMR scale reaction at room temperature. This reaction, however, once again resulted in formation of a mixture of δ-hydride elimination products after ca. 16 hours at room temperature, observed as coincidental resonances at ca. 5 ppm in the ^{11}B NMR spectrum, broadened through deuteration of the borane.

The stoichiometric addition of **32** to di-*iso*-propylamine borane (DiPAB) **LV** on an NMR scale at room temperature resulted in rapid formation of ca. 50 % $[^iPr_2N{=}BH_2]$ **LVI** by integration of the ^{11}B NMR spectrum in the time it took to obtain the NMR spectrum. The remaining 50 % of boron-containing species consisted of **XLVII**, **XXXVI**, **XLV**, unresolved low intensity resonances at ca. –16 to –22 ppm and a BH_4^- species.

These results suggest that the presence of an additional equivalent of amine borane promotes β-hydride elimination of **32** at room temperature. This is unlike the reaction of **XV** with two equivalents of either DMAB or PB,[2, 3] in which case reactions of compound **32** proceed through to products such as **XXXVI** and **LIV**. This situation is, thus, indicative of a Curtin-Hammett scenario, in which a lower activation barrier is provided by addition of a second equivalent of the borane reagent.

3.2.4 Heavier Alkaline Earth $M[NMe_2BH_2NMe_2BH_3]_2$ Complexes

As discussed in Chapter 1, Section 1.3, the homoleptic $Mg[NMe_2BH_2NMe_2BH_3]_2$.THF species **XLVI**, synthesised by reaction between **XLIV** and two equivalents of DMAB, was reported by Hill and represents the only homoleptic alkaline earth coordinated $[NMe_2BH_2NMe_2BH_3]^-$ complex.[2] Although analogous calcium, strontium and barium species are not accessible by such a reaction, the synthesis and isolation of **29** enabled a potential synthetic route to these compounds via the salt metathesis reaction shown in Figure 3.19.

$$\underset{\mathbf{29}}{2\ K[NMe_2BH_2NMe_2BH_3]} + MI_2 \xrightarrow[-\ KI]{THF} \underset{\mathbf{33\text{ - }35}}{M[NMe_2BH_2NMe_2BH_3]_2}$$

Figure 3.19: Reaction scheme for the formation of homoleptic $[NMe_2BH_2NMe_2BH_3]^-$ complexes of calcium, strontium and barium, via a salt metathesis reaction of **29** with the alkaline earth diiodides. Where M = Ca **33**, Sr **34**, Ba **35**.

Synthesis of **33**, **34** and **35** was successful, but resulted in contamination by $XM[NMe_2BH_3]$ species (where X could be H, NMe_2BH_3 or potentially $[NMe_2BH_2NMe_2BH_3]$), appearing as overlapping quartet resonances with the BH_3 unit of the $[NMe_2BH_2NMe_2BH_3]^-$ anion in the ^{11}B NMR spectrum. The ^{11}B NMR data for these compounds are shown in Table 3.4, exhibiting downfield shifts compared to **XLVI**.

	33	**34**	**35**
BH_2	δ = 1.8ppm, $^1J_{BH}$ = 97 Hz	δ = 2.4 ppm, $^1J_{BH}$ = 90 Hz	δ = 2.5 ppm, $^1J_{BH}$ = 87 Hz
BH_3	δ = –11.8 ppm, $^1J_{BH}$ = 88 Hz	δ = –12.6 ppm, $^1J_{BH}$ = 75 Hz	δ = –11.5 ppm, $^1J_{BH}$ = 87 Hz

Table 3.4: Tabulated ^{11}B NMR chemical shifts and coupling constants for the homoleptic alkaline earth coordinated $[NMe_2BH_2NMe_2BH_3]^-$ species **33**, **34** and **35**.

Attempts to crystallise these compounds were frustrated by the presence of contaminants and the formation of intractable material on storage in solution, which precluded confirmation of these species by crystallographic and microanalytical analysis.

To assess the stability of **XLVI**, an NMR sample was heated to 100 °C and monitored by ^{11}B NMR with negligible decomposition over the course of ca. 4 hours. Only on the addition of additional equivalents of DMAB and heating at 60 °C was any reaction observed, with formation of the cyclic diborazane **XXXVI**. Unfortunately comparative studies between **XXXVI**, **33**, **34** and **35** could not be conducted as the impurities in these species would result in minimal insight from any such investigation. The formation of additional boron-containing species whilst synthesising these compounds could indicate a lower stability of these heavier alkaline earth amidoboranes relative to **XLVI**.

3.2.5 Stoichiometric Reactivity of β-diketiminato-Calcium Amidoboranes

The stability of β-diketiminato-calcium-dimethylamidoborane **LXV** was studied by heating an NMR sample overnight at 80 °C and monitoring by ^{11}B NMR spectroscopy. This species failed to react under these conditions. The NMR sample was thus heated at 100 °C and 120 °C for ca. 3 hours at each temperature, but again proved stable. On addition of one equivalent of DMAB, however, **LXV** was observed to react at 30 °C with formation of a β-diketiminato-Ca[$NMe_2BH_2NMe_2BH_3$] species **36**, observed as quartet and triplet resonances at δ = –11.2 ppm, $^1J_{BH}$ = 99 Hz and δ = 2.1 ppm, $^1J_{BH}$ = 96 Hz respectively in the ^{11}B NMR spectrum. These ^{11}B NMR shifts are upfield for the BH_2 unit whilst downfield for the BH_3 unit of the analogous β-diketiminato magnesium species **XLV** (δ = 4.1 ppm and δ = –14.9 ppm respectively). Compound **36** exhibits similar ^{11}B NMR shifts to that of anilido-imine calcium [$NMe_2BH_2NMe_2BH_3$] **14** (δ = –11.2 ppm, $^1J_{BH}$ = 89 Hz and δ = 1.8 ppm, $^1J_{BH}$ = 96 Hz). Compound **36** also provides a similar ^{11}B NMR spectrum to that of homoleptic Ca[$NMe_2BH_2NMe_2BH_3$]$_2$ **33** (δ = –11.8 ppm, $^1J_{BH}$ = 88 Hz and δ = 1.8 ppm, $^1J_{BH}$ = 97 Hz). Full conversion was observed to occur within ca. 72 hours at 30 °C and was also successful at 35 °C. The reaction temperature was not increased further to minimise the risk of thermal decomposition of **36**. The

formation of **36** is thus proposed to occur via the scheme shown in Figure 3.20. The necessity for an additional equivalent of DMAB to induce β-hydride elimination of **LXV** suggests that this could be a proton-assisted process, shown by transition state **A** in Figure 3.20 (*vide infra*). In this regime a concerted loss of dihydrogen could occur, with insertion of the polarised and unsaturated [$Me_2N{=}BH_2$] **XXXVII** species into the metal-nitrogen bond of the amidoborane **LXV**, shown by transition state **B**, to form compound **36**.

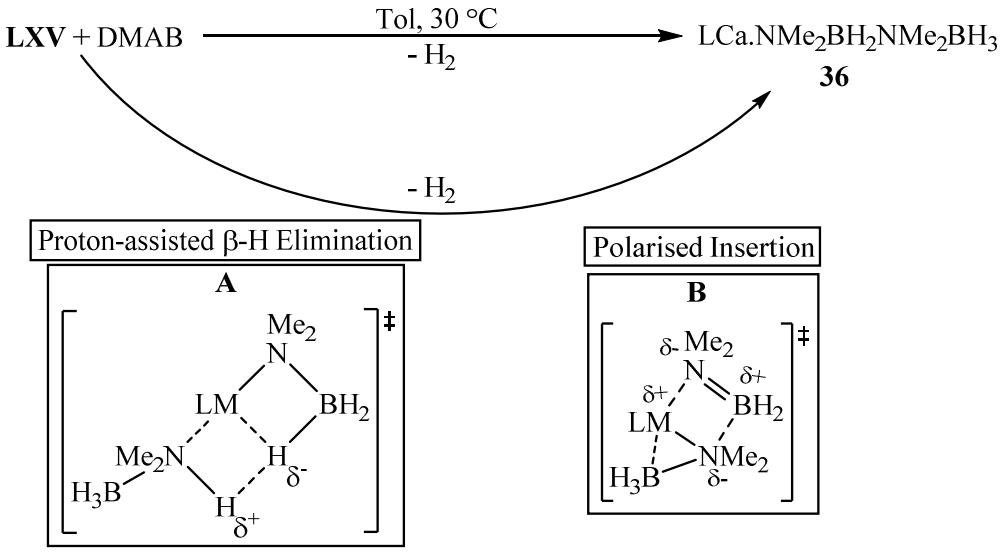

Figure 3.20: Proposed mechanism for the formation of **36** by stoichiometric addition of **LXV** to DMAB and heating at 30 °C for ca. 72 hours, via a proton-assisted β-hydride elimination and polarised insertion.

The mechanism in Figure 3.20 depicts transition states **A** and **B** as two distinct steps, however, the process could also occur via a concerted dihydrogen elimination and insertion/B-N bond formation process. Monitoring the ^{11}B NMR spectra of alkaline earth mediated amine borane dehydrocoupling reactions reveals that [$R_2N{=}BH_2$] is only ever observed in very minor concentrations in the reaction mixture, if detected at all, suggesting rapid consumption of this species and the occurrence of both processes in a single concerted elimination/insertion step.

Single crystals of **36** suitable for X-ray diffraction analysis were isolated from a concentrated toluene solution at –30 °C. The solid-state structure of **36** is shown in Figure 3.21.

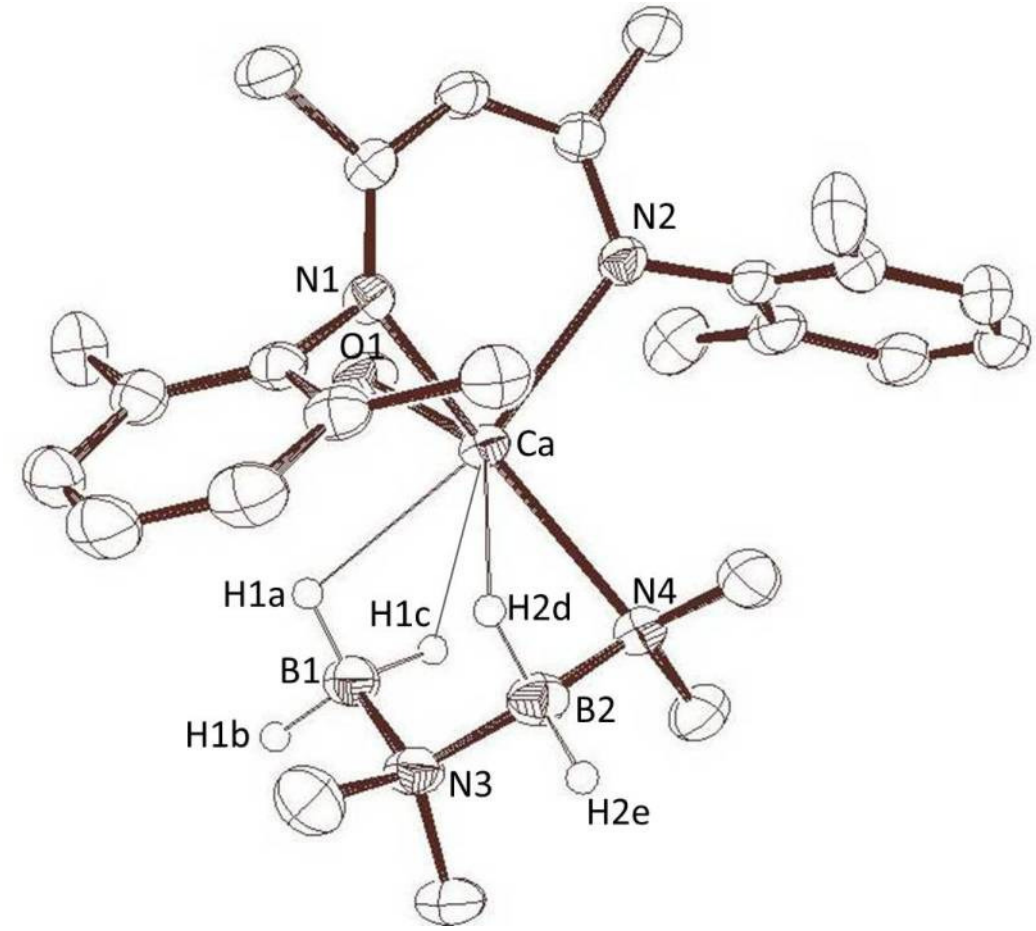

Figure 3.21: ORTEP representation of the solid-state structure of compound **36**, formed by the stoichiometric reaction between **LXV** and DMAB. Thermal ellipsoids set at 50 % probability. Hydrogen atoms other than the boron bound hydrides, 2,6-di-*iso*-propylphenyl *iso*-propyl methyl and THF carbon atoms removed for clarity. Selected bond lengths (Å) and angles (°); Ca-N1 2.4008(11), Ca-N2 2.3694(11), Ca-N4 2.4758(11), N4-B2 1.550(2), N3-B2 1.598(2), N3-B1 1.587(2), N1-Ca-N2 78.42(4), N1-Ca-N4 130.76(4), N2-Ca-N4 103.06(4), Ca-N4-B2 88.53(8), N4-B2-N3 117.14(12), B1-N3-B2 112.91(10).

The solid-state structure of **36** is analogous to compound **XLV**, the β-diketiminato magnesium bound $[NMe_2BH_2NMe_2BH_3]^-$ anion reported by Hill,[2] with the β-diketiminate supported calcium centre coordinated by the nitrogen and anagostic interactions with the boron-bound hydrides of the $[NMe_2BH_2NMe_2BH_3]^-$ anion, and the calcium coordination sphere augmented by a molecule of THF. Unlike **XLV**, however, in the solid-state structure of **36** the calcium centre interacts anagostically

with a hydride of BH_2 unit, depicted as B2 in Figure 3.22, in addition to two hydrides of the terminal BH_3 unit, depicted as B1 in Figure 3.22. The Ca-N4 bond length of **36** is longer than the Ca-N bonds of **LXV** [2.375(3) Å] and **13** [2.382(2) Å], the β-diketiminato- and anilido-imine supported calcium dimethylamidoborane species respectively, and the bond angles along the $[NMe_2BH_2NMe_2BH_3]^-$ unit of **36** are distorted compared to the magnesium compounds **LXV** and **13**. The differences observed in the solid-state structure of **36** may be rationalised by the change in metal centre in addition to the presence of an anagostic interaction with a hydride bound to B(i) (Figure 3.17) in the solid-state structure of **36** which is not observed in the solid-state structures of **XLV** and **15**. The table of bond lengths shown in Table 3.5 shows that the N(i)-B(i) bond length is shorter than for the β-diketiminato- and anilido-imine magnesium analogues, whilst the B(i)-N(ii) bond length is identical and the N(ii)-B(ii) bond length is longer.

	XLV	**15**	**36**
N(i)-B(i)	1.586(3)	1.587(4)	1.550(2)
B(i)-N(ii)	1.620(3)	1.613(4)	1.598(2)
N(ii)-B(ii)	1.570(3)	1.558(4)	1.587(2)

Table 3.5: Table of bond lengths for ligand-supported species containing $[NMe_2BH_2NMe_2BH_3]^-$ anions; β-diketiminato $Mg[NMe_2BH_2NMe_2BH_3]$ **XLV**,[2] anilido-imine $Mg[NMe_2BH_2NMe_2BH_3]$ **15** and **36**, simplified as $[N(i)Me_2B(i)H_2N(i)Me_2B(ii)H_3]$ to enable comparisons of bond lengths.

The N(i)-B(i) and B(i)-N(ii) bond lengths in the solid-state structure of **36** are longer than those of $[(\beta\text{-diketiminato-calcium})_2\{N(H)B(H)N(H)BH_3\}]$ **LXXX** and $[(\beta\text{-diketiminato-calcium})_2\{N(Me)B(H)N(Me)BH_3\}]$ **LXXXI** reported by Harder and shown in Figure 3.22, formed by heating the corresponding amidoborane complexes **LXI** and **LXII** with loss of dihydrogen.[40, 41] The N(ii)-B(ii) bond length of **36** is identical to that of **LXXX** [1.593(6) Å], whilst it is longer than that of **LXXXI** [1.538(3) Å]. This difference in B-N bond lengths can be rationalised as resulting from combined effects of amine borane steric demands and the dianionic nature of

the $[NRBHNRBH_3]^{2-}$ ligand which is coordinated to two calcium centres compared to **36**.

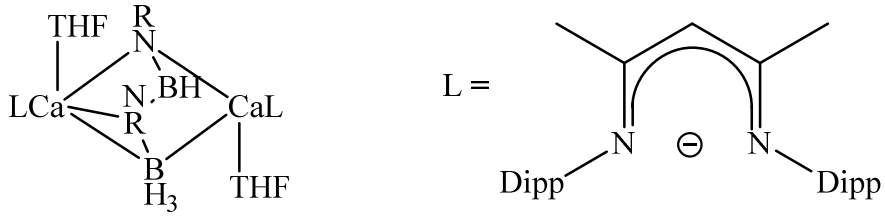

Figure 3.22: [(β-diketiminato-calcium)$_2${NH-BH-NH-BH_3}] **LXXX**, where R = H, and [(β-diketiminato-calcium)$_2${NMe-BH-NMe-BH_3}] **LXXXI**, where R = Me, reported by Harder.[40]

Although the stability of **LXV** was unexpected given the previously reported reactivity of this species at 80 °C,[3] in the earlier report **LXV** was formed via an *in situ* stoichiometric NMR reaction between **VI** and DMAB. These apparently incongruent observations were rationalised as resulting from the presence of an excess of DMAB in the stoichiometric NMR scale reaction inducing further reaction with **LXV** and giving the appearance that **LXV** is undergoing decomposition.

The stoichiometric addition of isolated **LXV** to trimethylamine borane (TMAB) on an NMR scale and heating at 80 °C for ca. 65 hours resulted in formation of ca. 12.0 % of a BH_4^- species, 8.7 % of a $[NR_2BH_2NR_2BH_3]^-$ species, 5.0 % **XXXVI** and 3.3 % **XLVII**. Although the presence of TMAB resulted in reaction of **LXV**, the high reaction temperature suggested that the boron-containing species reacted via a different mechanism to that proposed in Figure 3.1, namely a less kinetically accessible pathway than the proposed β-hydride elimination/polarised insertion mechanism. These reactions suggested that the addition of a suitable protic reagent was required to induce facile reaction of **LXV**. The results described here are the first time that the stability of isolated **LXV** has been investigated and demonstrate the necessity to produce samples of utmost purity to gain meaningful insight into their reactivity.

The controlled formation and isolation of **36**, the calcium analogue of **XLV**, represents the synthesis of a species which had only previously been observed in low

concentrations in ^{11}B NMR spectra of *in situ* reactions. Of fundamental importance to the proposed mechanism of amine borane dehydrocoupling depicted in Figure 3.1, however, is whether the B1-N3 or B2-N4 units in the solid-state structure of **36** shown in Figure 3.21 arise from the calcium amidoborane **LXV** or the added DMAB. Identification of the provenance of the two B-N units and their location in the $[NMe_2BH_2NMe_2BH_3]^-$ anion of compound **36** is key to establishing evidence regarding the proposed β-hydride elimination/polarised insertion mechanism. Figure 3.23 depicts the possible scenarios. Formation of product **37** is consistent with the proposed β-hydride elimination/polarised insertion mechanism, Path A, but may also be formed via an alternative mechanism, Path B. Formation of the alternative product **38**, Path C, would indicate that the proposed mechanism in Figure 3.1 is incorrect. A mixture of products **37** and **38** would indicate that the proposed mechanism does not adequately describe the process of amine borane dehydrocoupling, requiring further detailed investigation.

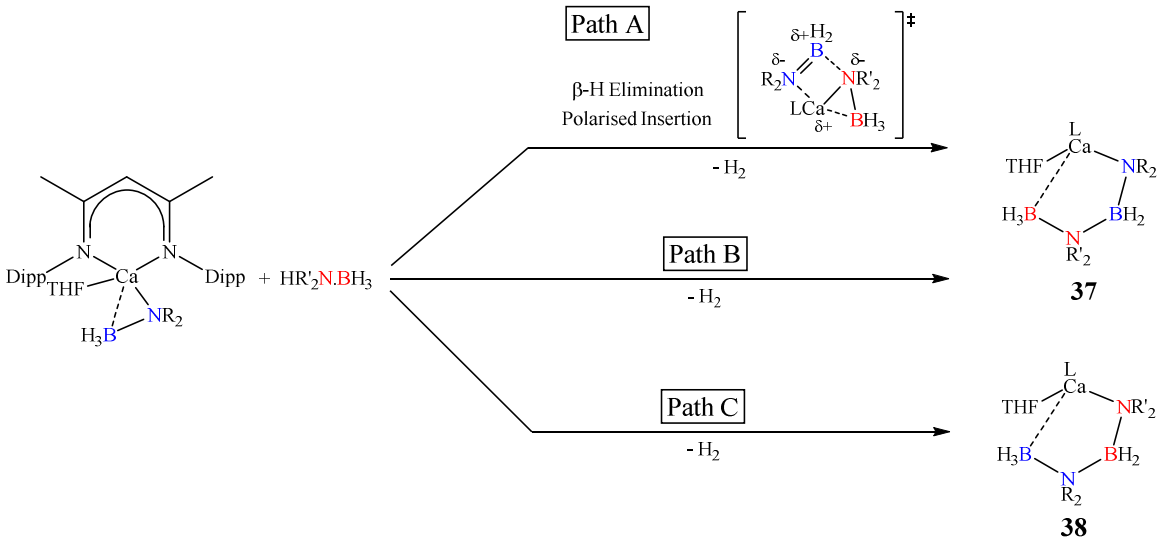

Figure 3.23: Reaction schemes to show the potential $[NR_2BH_2NR_2BH_3]$ species resulting from the stoichiometric reaction of **LXV** and an amine borane, producing either compound **37** or **38** (where L = β-diketiminate).

The stoichiometric addition of **LXV** to PB on an NMR scale and heating the reaction at 30 °C for ca. 72 hours resulted in formation of ca. 24.4 % of a β-diketiminato-calcium.$[NR_2BH_2NR'_2BH_3]$ species by integration of ^{11}B NMR spectrum, along with 10.2 % $[HB(NR_2)(NR'_2)]$ species. Overlapping resonances corresponding to

unreacted **LXV**, PB and potentially **LXVI** formed *in situ* by the reaction of a calcium hydride species and PB were also observed. The identity of the β-diketiminato-calcium.[$NR_2BH_2NR'_2BH_3$] species could not be confirmed from the reaction mixture and did not provide unambiguous diagnostic evidence. The formation of $HB(NR_2)$ species showed that the metallated [$NR_2BH_2NR'_2BH_3$]$^-$ anion was not stable under these conditions and may have contributed to formation of alternative products via the presence of calcium hydride species.

The corresponding stoichiometric reaction between **LXVI** and DMAB on an NMR scale and heating the reaction at 30 °C for ca. 72 hours resulted in formation of ca. 24.3 % of a β-diketiminato calcium [$NR_2BH_2NR'_2BH_3$] species by integration of the ^{11}B NMR spectrum, along with 13.1 % [$HB(NR_2)(NR'_2)$] species. The identity of the β-diketiminato calcium [$NR_2BH_2NR'_2BH_3$] species could not be confirmed from the reaction mixture. Overlapping resonances of unreacted **LXVI**, DMAB and potentially **LXV** formed *in situ* by the reaction of a calcium hydride species and DMAB were again apparent. Once again, an unambiguous [$NR_2BH_2NR'_2BH_3$]$^-$ product could not be obtained from this reaction. This could be due to the formation of a combination of products **37** and **38** via more than one of the mechanistic pathways in Figure 3.23. The situation is complicated, however, by the formation of calcium hydride species which is able to react with free amine borane and enable additional reaction pathways.

In an attempt to identify the β-diketiminato calcium [$NR_2BH_2NR'_2BH_3$] species by NMR spectroscopy the stoichiometric reaction of $Me_2HN.BD_3$ **LXXXII** with **LXV** was investigated. Once again heating at 30 °C for ca. 72 hours resulted in formation of β-diketiminato calcium [$NMe_2B(H/D)_2NMe_2B(H/D)_3$] species (ca. 26.3 %), the identity of which could not be established from the reaction mixture, in addition to [$(H/D)B(NMe_2)_2$] species (ca. 10.5 %) and unreacted reagents. The broadness of the resonances in the ^{11}B NMR spectrum suggested at least partial deuteration of each species.

All of the experiments which attempted to ascertain the structure of the [$NR_2BH_2NR'_2BH_3$] species were thus frustrated by the reactivity of the anion itself

and the production of a calcium hydride species, which is able to react with all species in the reaction mixture causing scrambling.

Kinetic experiments investigating the formation and reaction of **36** are described in section 3.3.1, however, initial investigation of the reactivity of compound **36** involved heating an NMR scale sample at 80 °C monitored by ^{11}B NMR spectroscopy. Analogous to the reactivity of **XLV** reported by Hill,[2] **36** was observed to undergo δ-hydride elimination, favouring the formation of the cyclic borazane **XXXVI** in addition to a proposed calcium hydride species. On continued heating, however, the integration of **XXXVI** in subsequent ^{11}B NMR spectra was observed to decrease, with concomitant formation of **LXV** and **36**, suggesting reaction of **XXXVI** to regenerate the calcium amidoborane species. Once again previous work by Keller was instructive, reporting that **XXXVI** reacted in solution with LiH at room temperature over the course of two months to form $Li[NMe_2BH_3]$ **LXXII**¸ proceeding via an intermediate containing a $[NMe_2BH_2NMe_2BH_3]^-$ anion.[30] Also reported was the reaction between **XXXVI** and $Li(NMe_2)$ which required two weeks at room temperature to form $B(NMe_2)_3$ and LiH.[29] Thus, reaction between **XXXVI** and a calcium hydride species, or indeed a calcium amidoborane species, at 80 °C to form **LXV** and **36** was considered not implausible. On continued heating the reaction was observed to form solely **XLVII**, with no regeneration of **XXXVI**. This was unexpected as, although **XXXVI** becomes depleted, the reaction would once again be expected to favour β-hydride elimination from **36**, formed either directly or through formation of **LXV**, with reformation of **XXXVI**. This behaviour is summarised in Figure 3.24 and indicates a possible divergence in mechanism once the concentration of **XXXVI** reaches a certain threshold level.

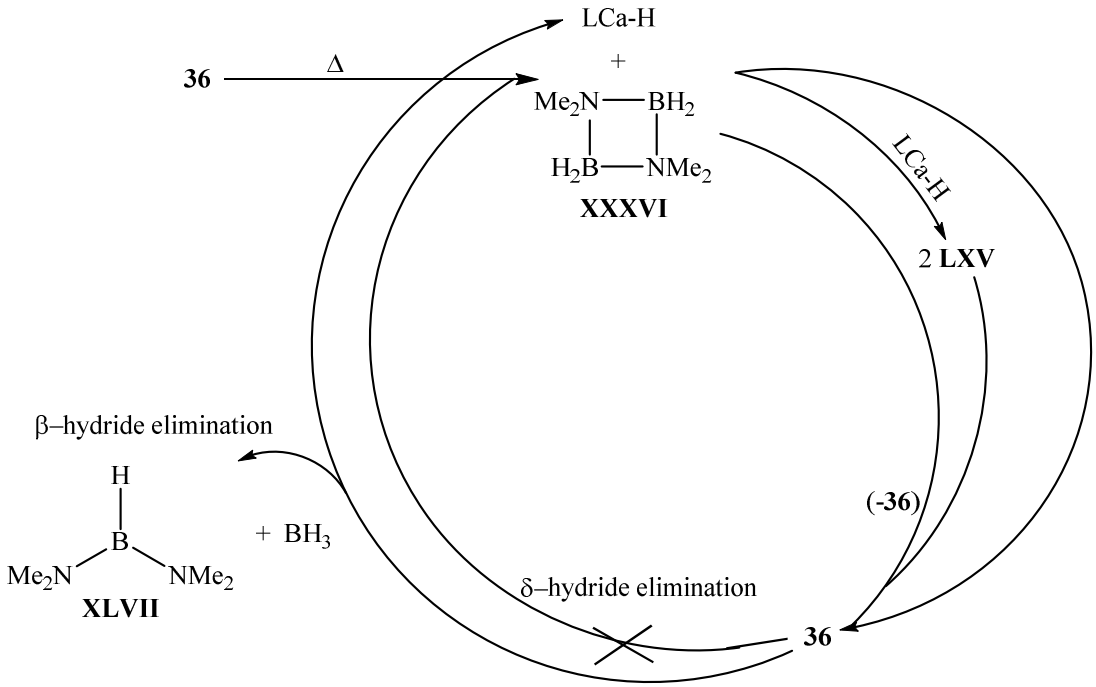

Figure 3.24: Scheme depicting the thermolysis reaction of **36**, with formation and subsequent depletion of the cyclic borazane **XXXVI** to ultimately form $HB(NMe_2)_2$ **XLVII**.

To further investigate the reactivity of **XXXVI** a stock solution was prepared by catalytic dehydrocoupling of DMAB by 5 mol % **VI** at 90 °C for 47 hours in 0.5 ml d_8-toluene. Stoichiometric NMR-scale reactions monitored by ^{11}B NMR spectroscopy between aliquots of this stock solution and β-diketiminato calcium dimethylamidoborane **LXV**, DMAB and pyrrolidine were carried out, with heating to 60 °C.

A graph showing the relative integration of ^{11}B NMR resonances for the stoichiometric reaction between **XXXVI** and **LXV** is shown in Figure 3.25.

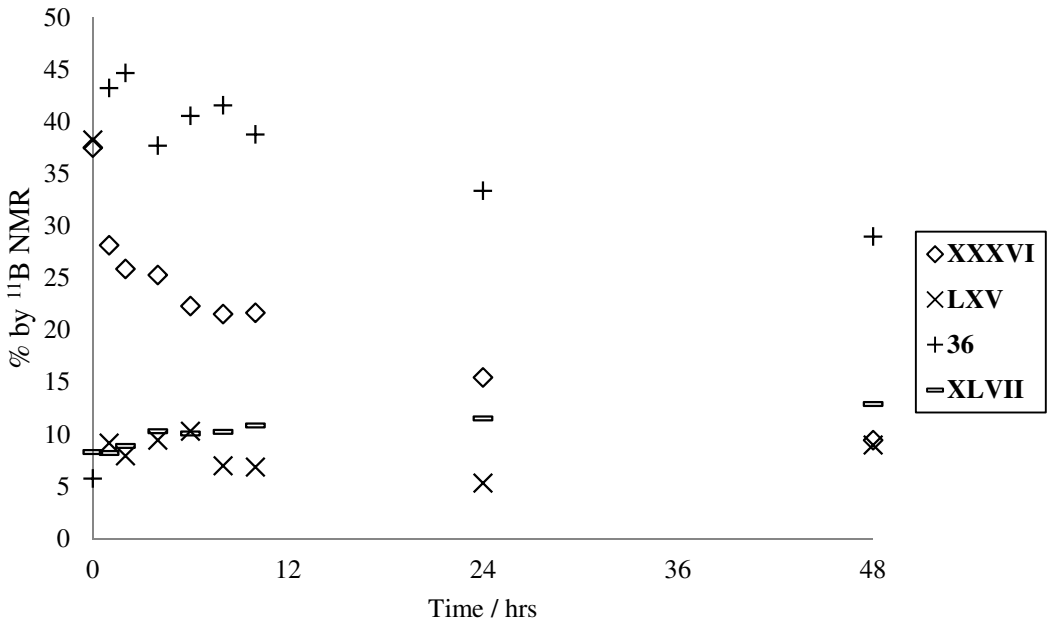

Figure 3.25: Graph showing the change in reaction composition during the stoichiometric reaction between a stock solution of $[H_2N\text{-}BH_2]_2$ **XXXVI** and β-diketiminato calcium dimethylamidoborane **LXV** at 60 °C, with % of **XXXVI**, **LXV**, β-diketiminato calcium $[NMe_2BH_2NMe_2BH_3]$ **36** and $[HB(NMe_2)_2]$ **XLVII** by integration of ^{11}B NMR spectra.

Figure 3.25 clearly shows that **LXV** reacted with **XXXVI**, with the percentage of **XXXVI** decreasing with time to under 10 % of the total boron-containing species after ca. 48 hours at 60 °C. The percentage of β-diketiminato calcium dimethylamidoborane **LXV** also decreased with time as this species reacted with the cyclic borazane **XXXVI**, whilst the concentration of β-diketiminato calcium $[NMe_2BH_2NMe_2BH_3]$ **36** showed an initial rapid increase as this species formed, before decreasing as it was consumed to form product species. The triplet resonance of the BH_2 unit of **36** was observed in the reaction mixture as an unresolved resonance, which appeared to be overlaying triplet resonances. This was tentatively attributed as resulting from solvated and unsolvated β-diketiminato calcium $[NMe_2BH_2NMe_2BH_3]$ **36**, causing a slight difference in the chemical shift of the BH_2 resonance. The proportion of $[HB(NMe_2)_2]$ **XLVII** slowly increased with heating time. These were not the only boron-containing species in the reaction, however, with Figure 3.26 showing the same reaction, but included two unidentified species, **39** and **40**.

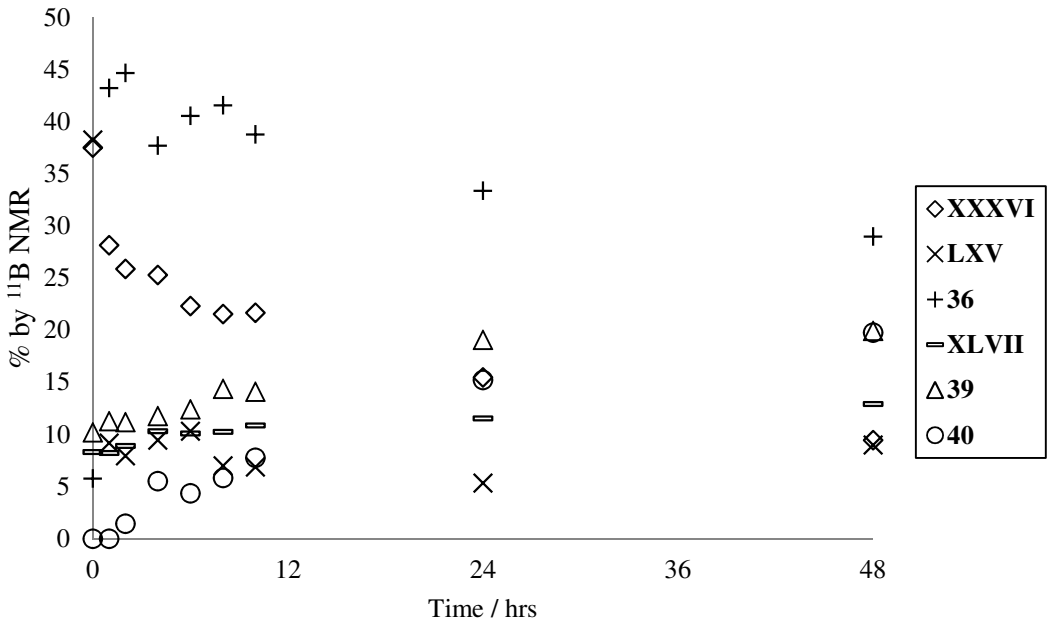

Figure 3.26: Graph showing the change in reaction composition during the stoichiometric reaction between a stock solution of $[H_2N\text{-}BH_2]_2$ **XXXVI** and β-diketiminato calcium dimethylamidoborane **LXV** at 60 °C, with % of **XXXVI**, **LXV**, β-diketiminato calcium $[NMe_2BH_2NMe_2BH_3]$ **36**, $[HB(NMe_2)_2]$ **XLVII**, **39** and **40** by integration of the ^{11}B NMR spectra.

Compounds **39** and **40**, observed as a quartet resonance at δ = –8.7 ppm, $^1J_{BH}$ = 91 Hz and a doublet resonance at δ = 33.7 ppm, $^1J_{BH}$ = 132 Hz in the ^{11}B NMR spectrum respectively, increased in concentration with heating time to not insignificant proportions of the reaction mixture (ca. 20 % of both **39** and **40**). The constitution of these species could not be confirmed from the reaction mixture. This reaction demonstrates that for this stoichiometric regime, in which a metal coordinated amidoborane is reacted with $[H_2N\text{-}BH_2]_2$ **XXXVI**, access is provided to high concentrations of species which are not observed in typical stoichiometric and catalytic dehydrocoupling of amine boranes by alkaline earth reagents. The intermediacy and rapid consumption of species such as **39** and **40** under catalytic conditions cannot, however, be discounted.

The addition of $[H_2N\text{-}BH_2]_2$ **XXXVI** to an equimolar quantity of DMAB and heating for ca. 48 hours at 60 °C resulted in no reaction. Catalytic quantities of a calcium hydride species would have been present in the reaction resulting from preparation of

the **XXXVI** stock solution. The failure of this mixture to react could indicate that the calcium hydride species was inactive, or in very low concentration resulting in a very slow reaction at 60 °C. If this is the case it would indicate that an active metal species of sufficiently high concentration is required in order for **XXXVI** to react. This criterion would be fulfilled in a stoichiometric scenario such as heating an isolated sample of **XXXVI** and would be exacerbated by heating equimolar quantities of $[H_2N\text{-}BH_2]_2$ **XXXVI** and β-diketiminato calcium dimethylamidoborane **LXV** in which stoichiometric amounts of metal species and cyclic borazane are present.

A graph showing the integration of ^{11}B NMR spectra for the stoichiometric NMR reaction between **XXXVI** and pyrrolidine is shown in Figure 3.27.

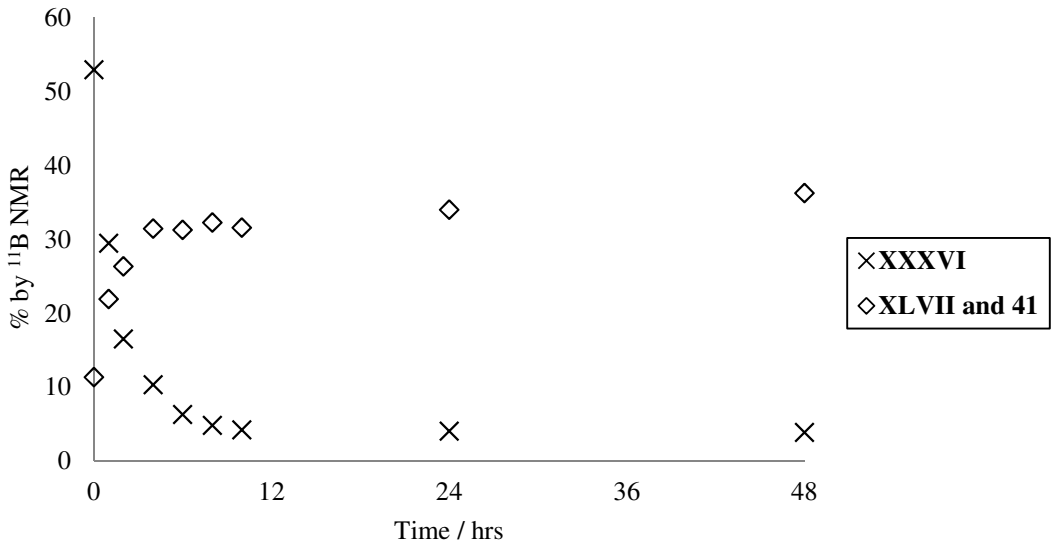

Figure 3.27: Graph showing the change in reaction composition during the stoichiometric reaction between a stock solution of $[H_2N\text{-}BH_2]_2$ **XXXVI** and pyrrolidine at 60 °C, with % of each species by integration of ^{11}B NMR spectra.

Figure 3.27 shows that $[H_2N\text{-}BH_2]_2$ **XXXVI** reacted with pyrrolidine faster than the reaction between **XXXVI** and **LXV** depicted in Figure 3.26. The percentage of **XXXVI** decreased to approximately 10 % after ca. 4 hours at 60 °C. The products of this reaction, which increased in concentration with heating time, were observed as overlapping doublet resonances in the ^{11}B NMR spectrum at ca. δ = 28 ppm, attributed to $[HB(NMe_2)_2]$ **XLVII** and the formation of a $HB(NC_4H_8)_2$, species **41**.

The ^{11}B NMR spectrum for this reaction also comprised several resonances which could not be identified, rationalised as boron-containing compounds resulting from the interaction of pyrrolidine with the reactive cyclic diborazane species **XXXVI**. This reaction suggests that protic reagents, such as amines, react in a facile manner with **XXXVI**. An in-depth study of alkaline-earth mediated dehydrocoupling reactions of amine boranes with amines is described in Chapter 5. Once again catalytic quantities of a calcium hydride species would be carried over in the stock solution from preparation of **XXXVI**, however it is not known whether this reaction is metal-mediated and reaction between the protic N-H and hydridic B-H could be envisaged. Although further analysis of this reaction, including isolation of metal-free **XXXVI**, would be required to evaluate the reaction mechanism and role of any metal species in this reaction this was not explored here.

These results demonstrate that $[H_2N\text{-}BH_2]_2$ **XXXVI** cannot be considered an innocent species in dehydrocoupling reactions of amine boranes and becomes a particularly important mechanistic consideration in regimes consisting of near stoichiometric proportions of **XXXVI** and metal species or protic reagent. In a catalytic regime, however, in which the concentration of metal species is relatively low, the impact of such a decomposition pathway on the overall mechanism is unknown or may only only become significant if **XXXVI** reaches a certain relative threshold concentration. Whilst this thesis has described reactions of **XXXVI** with calcium species, Hill reported that on heating equimolar quantities of the δ-diketiminato magnesium hydride species **X** and **XXXVI** at 50 °C formation of a magnesium $[NMe_2BH_2NMe_2BH_3]^-$ species was not observed, although other boron-containing species were formed.[8] The reactivity of **XXXVI** thus appears to display a dependence upon the identity of the Group 2 metal centre.

3.2.6 Reactivity of Alkaline Earth Reagents with a Primary Amine Borane

The dehydrocoupling of ammonia- and primary amine boranes by alkaline earth reagents has been investigated by Harder,[38-41] whilst research by the Hill Group has concentrated on the reactivity of secondary amine boranes,[1, 2, 8] which contain a single protic residue, with a view to reducing the potential complexity of the reaction and assisting with mechanistic characterisation. It is worthwhile, however, to

consider whether a primary amine borane exhibits behaviour consistent with the proposed dehydrocoupling scheme shown in Figure 3.1, to enable comparison and evaluation of generality. This section describes an investigation of the reactivity of *tert*-butylamine borane (TBAB), a commercially available primary amine borane whose reactivity with alkaline earth species has yet to be reported, with calcium reagents **VI** and **V-Ca** and the magnesium reagent **XV**.

The stoichiometric addition of **VI** to one equivalent of TBAB on an NMR scale at room temperature resulted in clean conversion to a single quartet resonance in the ^{11}B NMR spectrum at δ = –17.3 ppm, $^{1}J_{BH}$ = 80 Hz, assigned to the BH_3 unit of the β-diketiminato calcium *tert*-butylamidoborane **42**. This was observed in addition to a singlet resonance in the ^{1}H NMR spectrum at δ = 0.07 ppm integrating to 18H resulting from the formation of $HN(SiMe_3)_2$. The quartet resonance in the ^{11}B NMR spectrum of **42** is upfield compared to that of the secondary amidoborane species β-diketiminato calcium dimethylamidoborane **LXV** (δ = –11.5 ppm, $^{1}J_{BH}$ = 86 Hz) reported by Hill,[2] and downfield of that of Harder's β-diketiminato parent calcium amidoborane **LXI** (δ = –19.6 ppm, $^{1}J_{BH}$ = 84 Hz).[40] Compared to β-diketiminato calcium complexes of primary amidoboranes, however, **40** exhibits a similar ^{11}B NMR quartet resonance displayed by Harder's methylamido borane **LXII** (δ = –15.8 ppm, $^{1}J_{BH}$ = 87 Hz), the *iso*-propylamido borane **LXIII** (δ = –18.1 ppm, $^{1}J_{BH}$ = 88 Hz) and the 2,6-di-*iso*-propylanilido borane **LXIV** (δ = –14.7 ppm, $^{1}J_{BH}$ = 74 Hz) species.[40, 41]

Single crystals of **42** suitable for X-ray diffraction analysis were isolated from a concentrated toluene solution at –30 °C. The solid-state structure of **42** is shown in Figure 3.28.

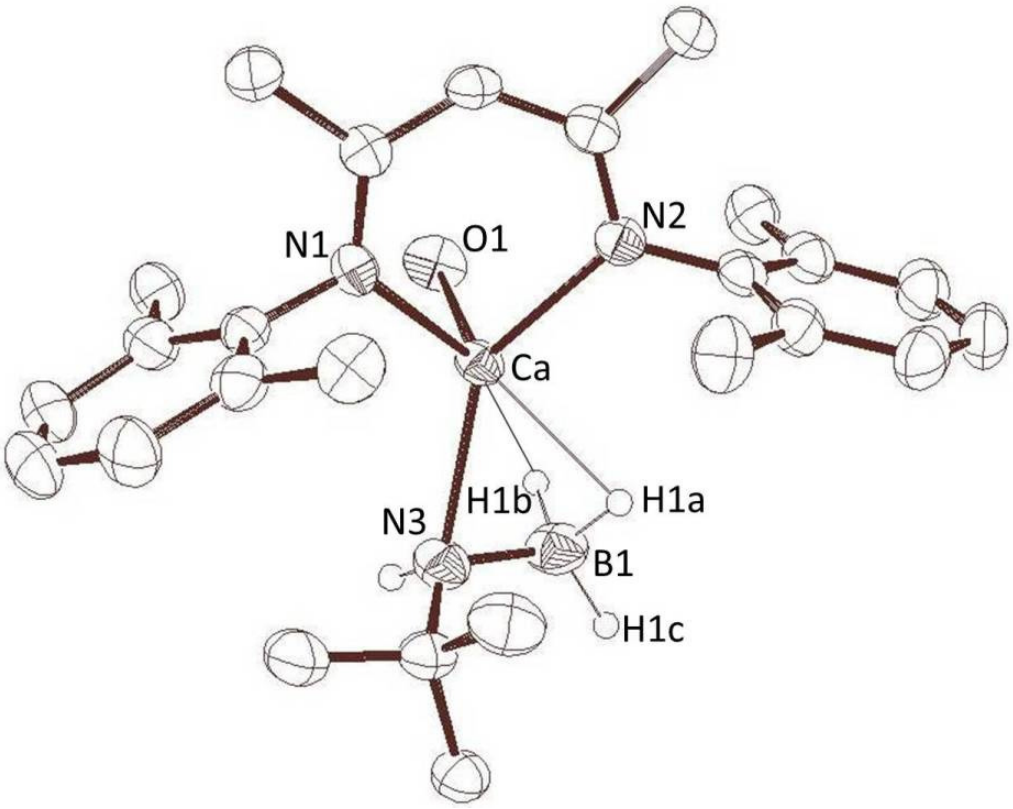

Figure 3.28: ORTEP representation of the solid-state structure of compound **42**, formed by the stoichiometric reaction between **VI** and TBAB. Thermal ellipsoids set at 50 % probability. Hydrogen atoms other than the boron bound hydrides, THF carbon atoms and 2,6-di-*iso*-propylphenyl *iso*-propyl methyl carbons removed for clarity. Selected bond lengths (Å) and angles (°); Ca-N1 2.372(3), Ca-N2 2.370(3), Ca-N3 2.414(3), N3-B1 1.554(6), N1-Ca-N2 79.76(9) N1-Ca-N3 113.61(10), Ca-N3-B 79.1(2).

The solid-state structure of **42** comprises a calcium centre supported by the bidentate β-diketiminate ligand, the nitrogen atom and anagostic interactions with boron-bound hydrides of the *tert*-butylamidoborane ligand, and a molecule of THF. The structure of compound **42** is, thus, somewhat analogous to the β-diketiminato-calcium secondary amidoborane complexes **LXV** and **LXVI**. The solid-state structure of **42** shows a close similarity, with an identical Ca-N3 bond length, to Harder's β-diketiminato calcium-coordinated *iso*-propylamido borane **LXIII** [2.406(4) Å] and the amido borane derivative **LXI** [2.399(2) Å]. This distance is longer, however, than the methylamido borane derivative **LXII** [2.382(4) Å], and

significantly shorter than the 2,6-di-*iso*-propylphenylanilido borane derivative **LXIV** [2.460(2) Å].[40, 41] This variation can be rationalised by the combined electronic effects and steric requirements of the nitrogen-bound substituent. The B1-N3 bond lengths of all of these primary amidoborane derivatives, however, are effectively identical [ranging from 1.581(4) to 1.587(4) Å].[40, 41]

The room temperature reaction between equimolar quantities of TBAB and **VI** therefore exhibited analogous behaviour to that of the secondary amine boranes DMAB and PB. The addition of **XV** to two equivalents of TBAB on an NMR scale at room temperature did not, however, result in clean formation of a β-diketiminato magnesium $[NH^tBuBH_2NH^tBuBH_3]^-$ species **43** analogous to **XLV** and **LXVIII**. An unresolved resonance at δ = –8.8 ppm in the ^{11}B NMR spectrum was tentatively assigned to the BH_2 unit of **43**, however, integrating to ca. 7 % of the total boron species. The ^{11}B NMR spectrum of this reaction showed multiple boron-containing species, including unreacted TBAB overlaying another resonance at a similar chemical shift, which could be a β-diketiminato-Mg$[NH^tBuBH_3]$ species **44** analogous to Harder's primary anilidoborane derivative β-diketiminato-Mg$[NHDippBH_3]$ **L**. A range of overlapping and unresolved resonances at δ = 28 – 43 ppm in the ^{11}B NMR spectrum, integrating to 32.6 % of the total boron species, suggested reaction to form species such as $[H^tBuN{=}BH_2]$ **45** and $[HB(NH^tBuBH_3)_2]$ **46**. The reactivity of the primary amine borane TBAB therefore justifies the initial selection of the secondary amine boranes DMAB and PB on the grounds of relative mechanistic simplicity.

Catalytic dehydrocoupling of TBAB using 5 mol % **VI** on an NMR scale and heating at 60 °C for ca. 24 hours resulted in reaction of ca. 34 % TBAB. The ^{11}B NMR spectrum showed formation of ca. 0.8 % of a triplet species at δ = 38.2 ppm, $^1J_{BH}$ = 128 Hz attributed to $[H^tBuN{=}BH_2]$ **45**, 12.7 % of a doublet species at δ = 29.1 ppm, $^1J_{BH}$ = 126 Hz attributed to formation of $[HB(NH^tBu)_2]$ **46** and 5.0 % of a triplet species at δ = –6.1 ppm, $^1J_{BH}$ = 109 Hz identified as the BH_2 unit of a $[H^tBuN{-}BH_2]_2$ species **47** (*vide infra*). The ^{11}B NMR spectrum also showed formation of ca. 6.5 % BH_4^- as a quintet at δ = –30.6 ppm, $^1J_{BH}$ = 82 Hz and a partially obscured resonance integrating to ca. 6.9 % of the total boron species at δ = –22.8 ppm, **48**,

appearing as a triplet of doublets in an apparent 1:1:2:2:1:1 ratio with $^{1}J_{BH}$ = 99 Hz and $^{2}J_{BH}$ = 31 Hz. Although the identitity of **48** could not be confirmed, Manners has reported the formation of small quantities of $[H_2B(\mu\text{-}H)(\mu\text{-}NMe_2)BH_2]$ **LXXXIII** which also appears as a triplet of doublets resonance in the ^{11}B NMR spectrum at δ = –19 ppm (J_{BH} = 129 Hz, J_{BH} =31 Hz) in reactions between DMAB and frustrated Lewis pairs.[42] This may suggest that the identity of compound **48** is similar in form to $[H_2B(\mu\text{-}H)(\mu\text{-}NH^tBu)BH_2]$, the mechanism of formation of which is not known. After heating at 60 °C for ca. 138 hours, approximately 86.4 % TBAB had reacted, with conversion to ca. 45.2 % $[H^tBuN\text{-}BH_2]_2$ **47**, 13.4 % $[HB(NH^tBu)_2]$ **46** and 20.1 % to a species characterised by a broad singlet resonance at δ = 34.4 ppm subsequently identified as the cyclic borazine $[^tBuN\text{-}BH]_3$ **49** (*vide infra*). The resonance attributed to BH_4^- in the ^{11}B NMR spectrum taken after ca. 24 hours heating had completely disappeared and the integration of the unidentified species **48** had decreased to 3.2 %. The NMR spectrum of the sample was not completely representative of the reaction outcome, however, due to formation of crystalline material inside the NMR tube. The solution phase from the NMR tube was stored at –30 °C, enabling isolation of single crystals of **47** suitable for X-ray diffraction analysis. The solid-state structure of **47** is shown in Figure 3.29.

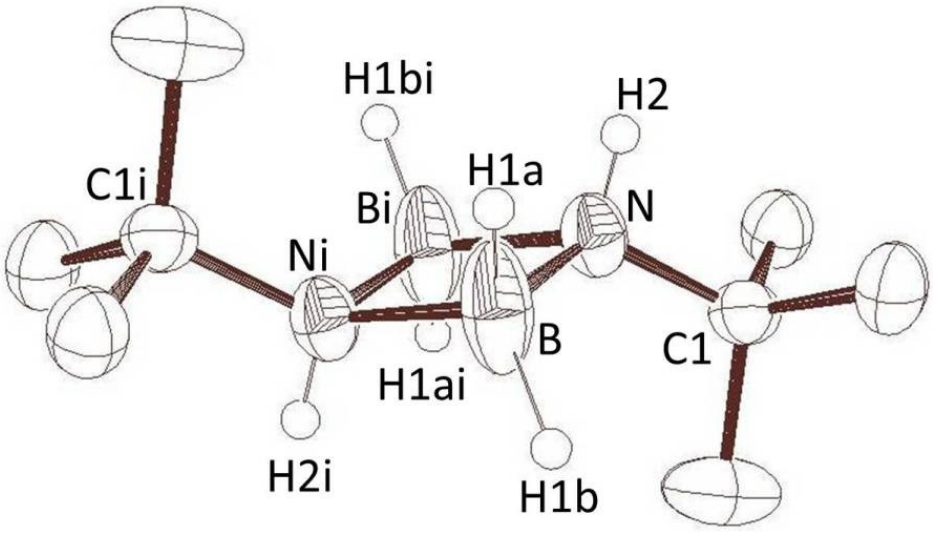

Figure 3.29: ORTEP representation of the solid-state structure of compound **47**, formed by catalytic dehydrocoupling of TBAB by **VI** on an NMR scale and heating at 60 °C for ca. 138 hrs. Thermal ellipsoids set at 50 % probability. Hydrogen atoms other than the boron-bound hydrides and nitrogen-bound protons removed for clarity. Selected bond lengths (Å) and angles (°); B-N 1.599(3), B-N(i) 1.600(3), N-C1 1.498(2), N-B-N(i) 92.13(15), B-N-C1 122.09(17). Symmetry transformations used to generate equivalent atoms: -*x*+1,-*y*+1,-*z*+1.

Compound **47** is a cyclo-dimeric $[H^tBuN\text{-}BH_2]_2$ species and is the first crystallographically characterised cyclo-dimeric product of a dehydrogenated primary amine borane, previously described products for transition-metal catalysed dehydrocoupling of primary amine boranes having been observed to be higher oligomers.[36, 43-45] Published crystallographic data on similar species to **47** but comprising secondary amine units include **XXXVI**,[45] **LIV**,[36, 45] and compounds **LXXXIV** to **LXXXVII** shown in Figure 3.30.[46-48]

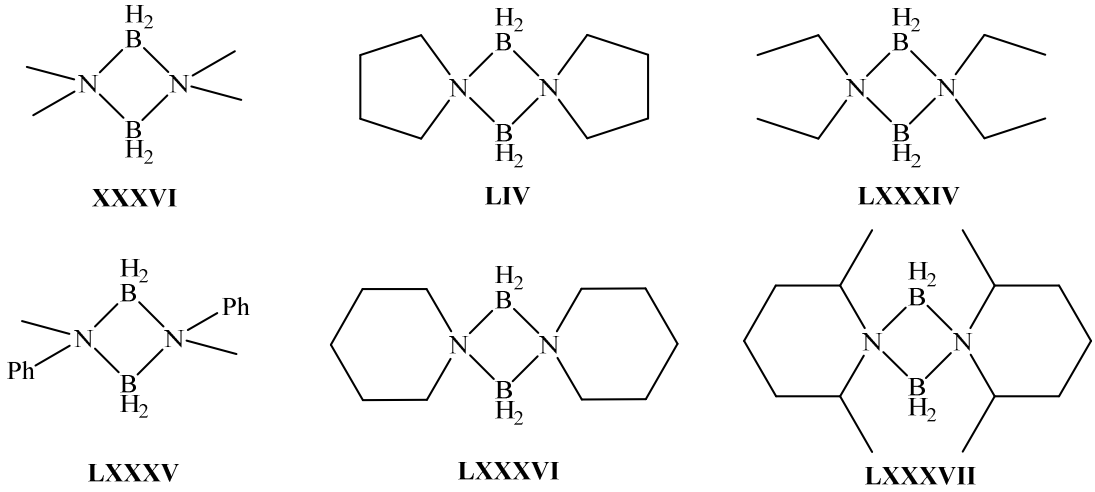

Figure 3.30: Reported crystallographically defined cyclo-dimeric species of the form [RR'N-BH_2].[36, 45-48]

The B-N bond distance of the solid-state structure of **47** is identical to that of **XXXVI** [1.594(4) Å],[42] **LIV** [four in unit cell in range 1.584(5) – 1.609(5) Å],[36, 45] **LXXXIV** [1.600 Å],[46] **LXXXV** [1.616 Å],[48] and **LXXXVI** [1.594(4) Å],[46, 47] but different to that of **LXXXVII** [1.621 Å] possessing the more sterically demanding 2,6-dimethylpiperidinyl nitrogen substituents.[46, 47] The N-B-N(i) bond angle is similar to that of **LIV** [92.9(3)°], **XXXVI** [93.7(3)°],[42] **LXXXIV** [93.5°],[46] **LXXXV** [93.4°],[48] **LXXXVI** [93.3°] and **LXXXVII** [94.1°].[46, 47]

As previously mentioned the NMR-scale reaction between TBAB and 5 mol % **VI** resulted in the formation of crystalline material inside the NMR tube after heating at 60 °C for ca. 138 hours. X-ray diffraction analysis of this crystalline material provided the solid-state structure of **50**, an inorganic calcium tetrahydroborate, shown in Figure 3.31.

(**a**)

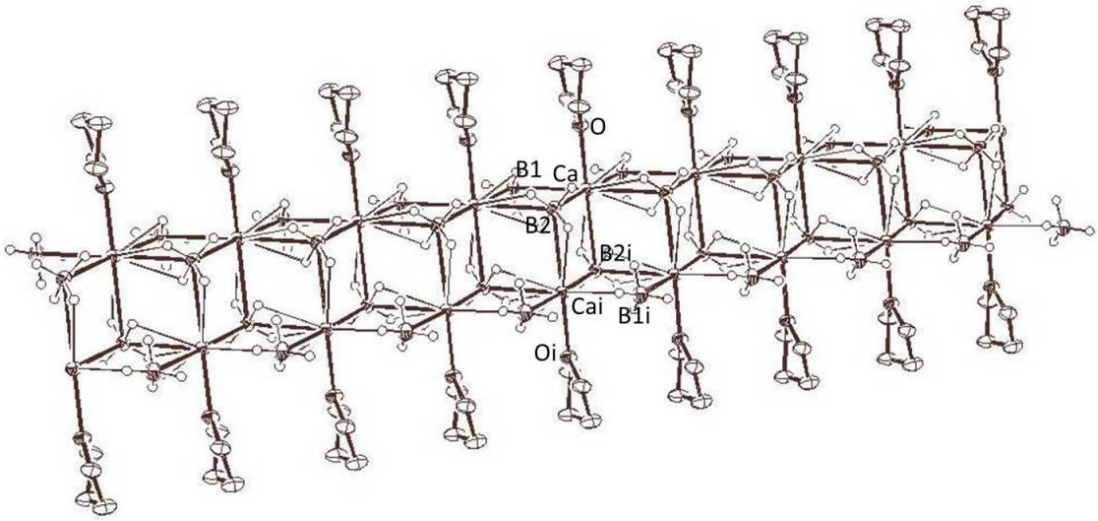

(**b**)

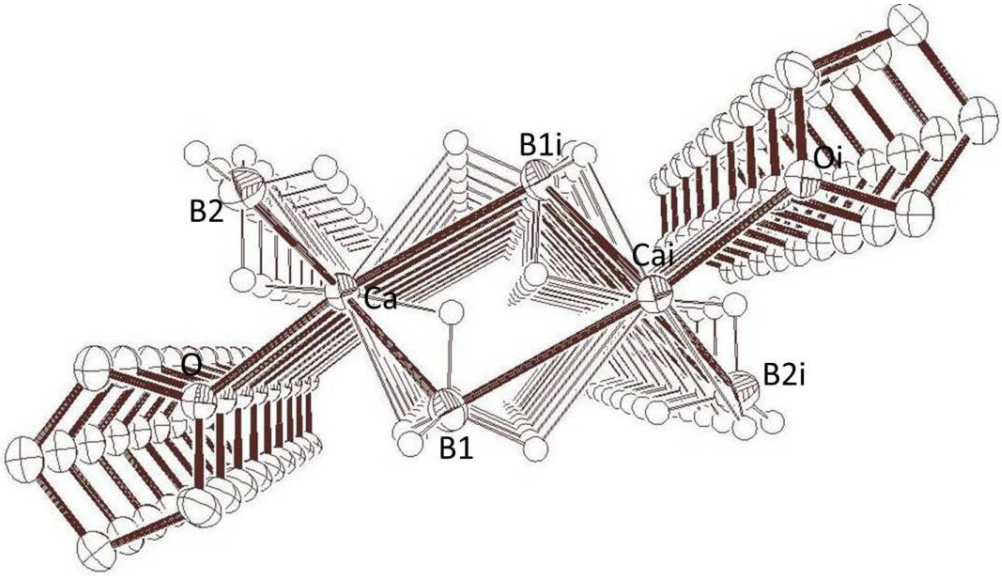

Figure 3.31: ORTEP representation of the solid-state structure of compound **50**, formed by catalytic dehydrocoupling of TBAB by **VI** and heating at 60 °C for ca. 138 hours, displayed (**a**) at an oblique angle and; (**b**) end-on. Thermal ellipsoids set at 50 % probability. Hydrogen atoms other than the boron bound hydrides removed for clarity.

The solid state structure of **50** propagates as a polymeric calcium bis(tetrahydroborate), with the coordination sphere of each calcium centre filled by bonding to five BH_4^- units with anagostic interaction with the boron-bound hydrides,

augmented by a molecule of THF. The crystallographic data collected for **50** produced an R-factor of 12.4 %, too high for discussion of bond length and bond angle. The solid-state structure of **50** is, however, similar to the structure of $Ca(BH_4)_2.NH_3$ **LXXXVIII** reported by Yu et al,[49] in which each calcium centre is supported by five BH_4^- units and one molecule of NH_3, and $Ca(BH_4)_2.(NH_3)_2$ **LXXXIX** reported by Chen et al,[50] in which each calcium centre is supported by four BH_4^- units and two molecules of NH_3. The effect of replacing the molecule of NH_3 for a molecule of THF, however, changes the structure of the calcium borohydride from a 3-D network for **LXXXVIII** to a linear polymer for **47**.

The formation of compound **50**, observed as toluene-insoluble crystalline material inside the NMR tube after heating at 60 °C for ca. 138 hours, indicates deactivation of the catalyst and ligand protonation by this more reactive primary amine borane.

Catalytic dehydrocoupling of TBAB using 5 mol % **V-Ca** on an NMR scale and heating at 70 °C for ca. 66 hours resulted in formation of, by integration of the ^{11}B NMR spectrum, ca. 31.0 % $[H^tBuN\text{-}BH_2]_2$ **47**, 13.5 % $[HB(NH^tBuBH_3)_2]$ **46**, 2.5 % of compound **48** and 44.4 % of compound **49** (broad resonance at δ = 34.4 ppm), as observed in the dehydrocoupling of TBAB by **VI**. On further heating of this sample the proportion of **47** decreased, falling to ca. 12.6 % after ca. 232 hours at 70 °C, whilst the proportion of **46** and **49** increased to 14.7 % and 67.3 % respectively. Similar to the reactivity of $[Me_2N\text{-}BH_2]_2$ **XXXVI** described in Section 3.2.4, this reaction demonstrates that the analogous species **47** undergoes decomposition in a catalytic reaction whereas a stoichiometric regime was required in order to observe the reaction of **XXXVI**. The conversion of **47** to **49** may be envisaged as occuring via a mechanism involving metal-mediated deprotonation of a second nitrogen-bound protic residue, with formation of an amidoborane, insertion into the metal-nitrogen bond by an aminoborane unit, followed by closure of the six-membered ring via a hydride elimination step. Study of this mechanism was beyond the scope of this thesis, but may provide meaningful insight into the dehydrocoupling reactivity of primary amine boranes.

Comparison of the ^{11}B NMR chemical shift for species **49** in these dehydrocoupling reactions reveals similarities to literature values for the borazine products [MeN-

$BH]_3$ **XC** (δ = 33.2 ppm, $^1J_{BH}$ = 132 Hz) and $[PhN\text{-}BH]_3$ **XCI** (δ = 32.8 ppm, br).[36] Storage of this reaction mixture at –30 °C yielded single crystals of **49** suitable for X-ray diffraction analysis. The solid-state structure of **49** is shown in Figure 3.32.

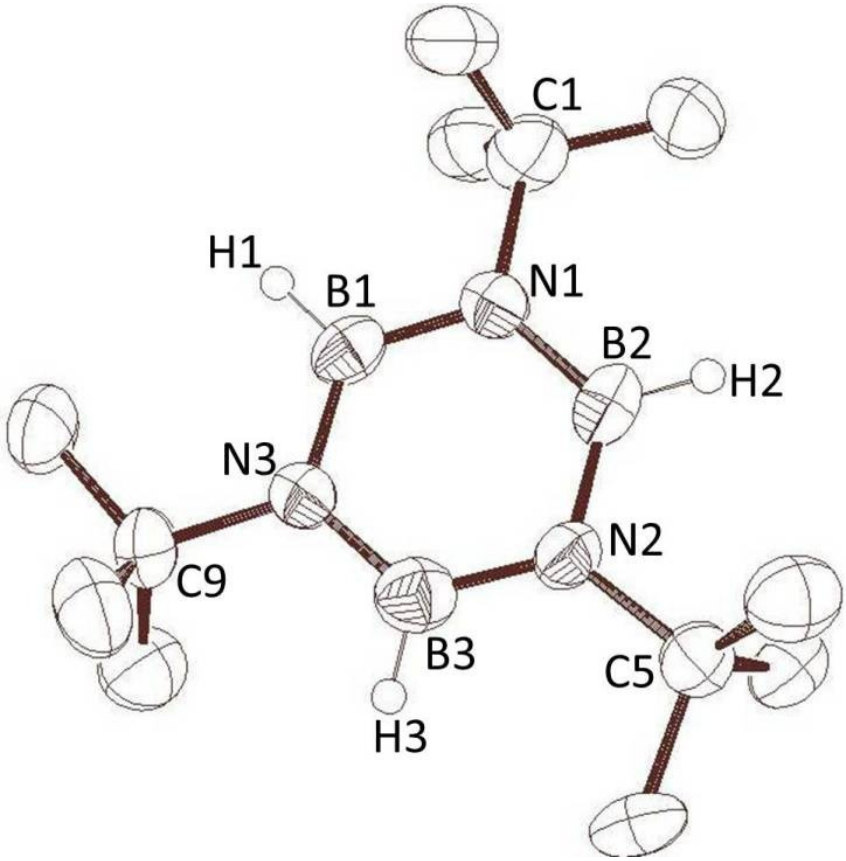

Figure 3.32: ORTEP representation of the solid-state structure of compound **49**, formed by catalytic dehydrocoupling of TBAB by **V-Ca** on an NMR scale and heating at 70 °C for 232 hours. Thermal ellipsoids set at 50 % probability. Hydrogen atoms other than the boron bound hydrides removed for clarity.

Compound **49**, 1,3,5-tri(*tert*-butyl)borazine, consisting of a planar six-membered ring, is analogous to the crystallographically defined compounds shown in Figure 3.33, both of which possess nitrogen-bound aryl groups aiding crystallisation of these compounds.[36, 51, 52]

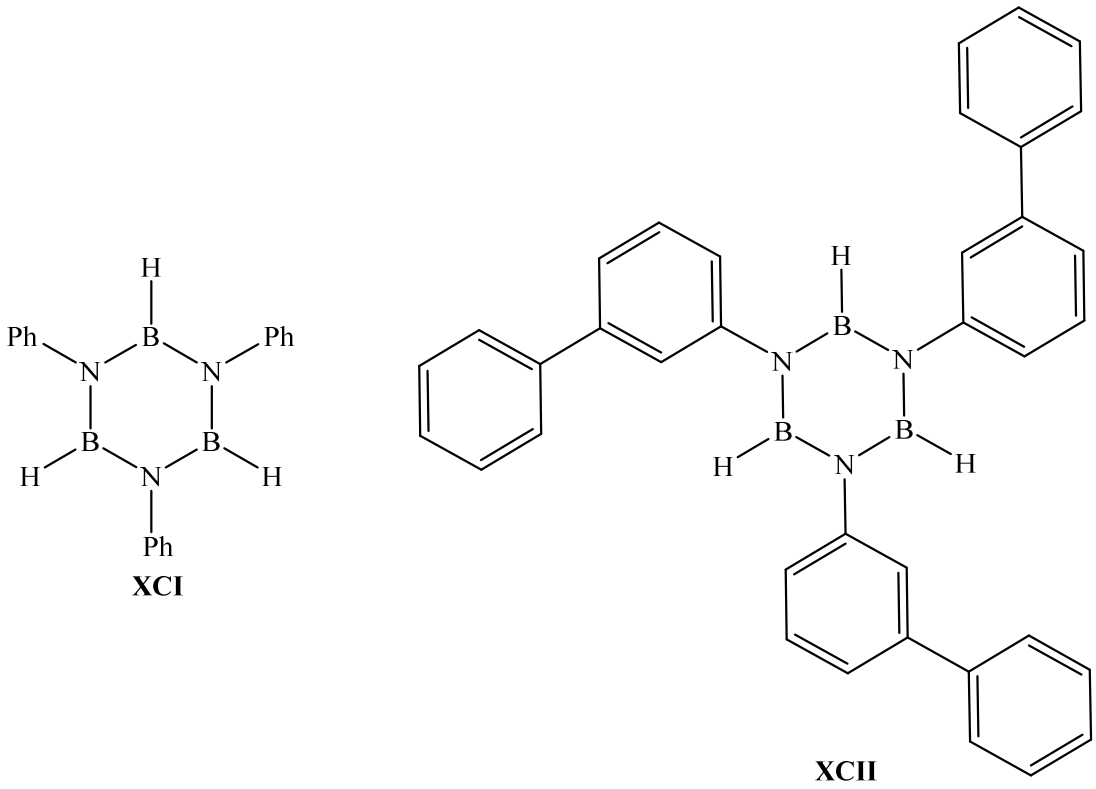

Figure 3.33: Reported crystallographically defined borazine species $[RN\text{-}BH]_3$; **XCI**,[36, 52] **XCII**.[51]

The crystallographic data for compound **49** produced an R-factor of 18.9 %, too high for discussion of bond lengths and bond angles. Isolation of this species does, however, provide evidence of the formation of species which are not observed during dehydrocoupling of secondary amine boranes by alkaline earth species.

The scheme in Figure 3.34 summaries the results of catalytic dehydrocoupling of TBAB reactions by calcium reagents **V-Ca** and **VI**.

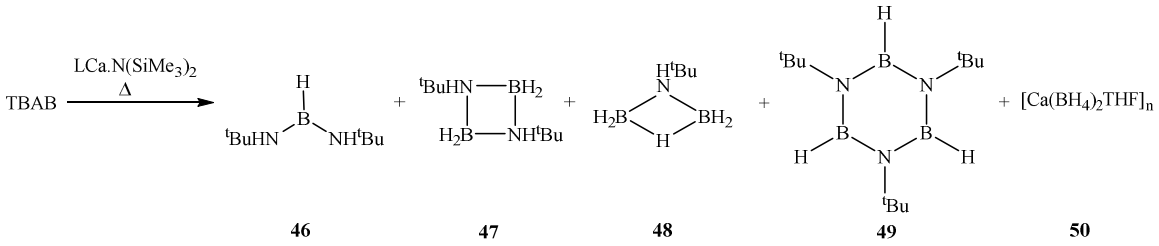

Figure 3.34: Scheme summarising the products formed by catalytic dehydrocoupling of TBAB by calcium reagents, **V-Ca** where L = $[N(SiMe_3)_2]^-$, and **VI** where L = β-diketiminate.

These results demonstrate that whilst the dehydrocoupling of the primary amine borane TBAB by alkaline earth reagents **VI** and **V-Ca** with formation of analogous species such as **46** and **47** appears to be consistent with the proposed mechanism in Figure 3.1, there are appreciable differences as evidenced by the formation of species such as **49** and **50**. The mechanism of dehydrocoupling TBAB by alkaline earth precatalysts is therefore expected to incorporate features of the mechanism shown in Figure 3.1, but include additional reaction pathways which deviate from those observed for secondary amine boranes. The increased reactivity of this primary amine borane and dehydrocoupled product species, and increased ambiguity in reaction pathway resulting from possession of two nitrogen-bound protons, compared to the secondary amine boranes DMAB and PB, highlights the difficulties associated with the development of a general mechanism for dehydrocoupling of amine boranes.

3.3 Kinetic Analysis of the Stoichiometric Reactivity of Alkaline Earth Amidoboranes

Section 3.2 described the synthesis and reactivity of alkaline earth amidoborane species under stoichiometric conditions, before investigating whether the primary amine borane *tert*-butylamine borane (TBAB) mimicked the reactivity observed with secondary amine boranes. The stoichiometric and catalytic reactivity of Group 1 species with amine boranes was also investigated. This section describes kinetic analysis of stoichiometric reactions of Group 2 amidoboranes in an attempt to provide quantitative data regarding reaction steps in the proposed mechanism.

The reaction between **VI** and DMAB to form the β-diketiminato calcium dimethylamidoborane **LXV** occurred rapidly at room temperature, with complete conversion within the time taken to record an NMR spectrum of the sample.[2] The rapidity of this reaction precluded a kinetic investigation of this process even if the NMR sample was frozen in liquid nitrogen prior to insertion into the spectrometer. Similarly, the reaction between β-diketiminato magnesium *n*-butyl species **XV** and two equivalents of DMAB to form the corresponding [$NMe_2BH_2NMe_2BH_3$] species **XLV** occurred rapidly at room temperature, with complete conversion within the time taken to record an NMR spectrum of the sample.[2] As described in Section 3.2.4, however, the stoichiometric reaction between **LXV** and DMAB to form β-diketiminato calcium [$NMe_2BH_2NMe_2BH_3$] **36** at 30 – 35 °C could be monitored by NMR spectroscopy. Kinetic NMR-scale studies of the reaction between **LXV** and DMAB, $Me_2NH.BD_3$ **LXXXII** and $Me_2ND.BH_3$ **XCIII** were, thus, conducted at 35 °C and monitored by ^{11}B NMR spectroscopy. The kinetic isotope effect (KIE) could not be found by experiments involving a mixture of deuterated and protio dimethylamine borane as the dehydrocoupled products cannot be discriminated from each other by ^{11}B NMR spectroscopy. Therefore, the method adopted by Manners was employed, in which experiments were conducted with each amine borane in isolation in order to compare the rate of reaction and establish an estimate of the KIE.[53]

The increase in concentration of **36** could not be modelled by 0, 1st nor 2nd order kinetic data plots, reminiscent of the kinetic investigation of the reaction between

VII and DMAB described in Chapter 2 Section 2.2. The consumption of DMAB, **LXXXII** or **XCIII**, however, could be modelled by the 2nd order kinetic plots, shown in Figure 3.35.

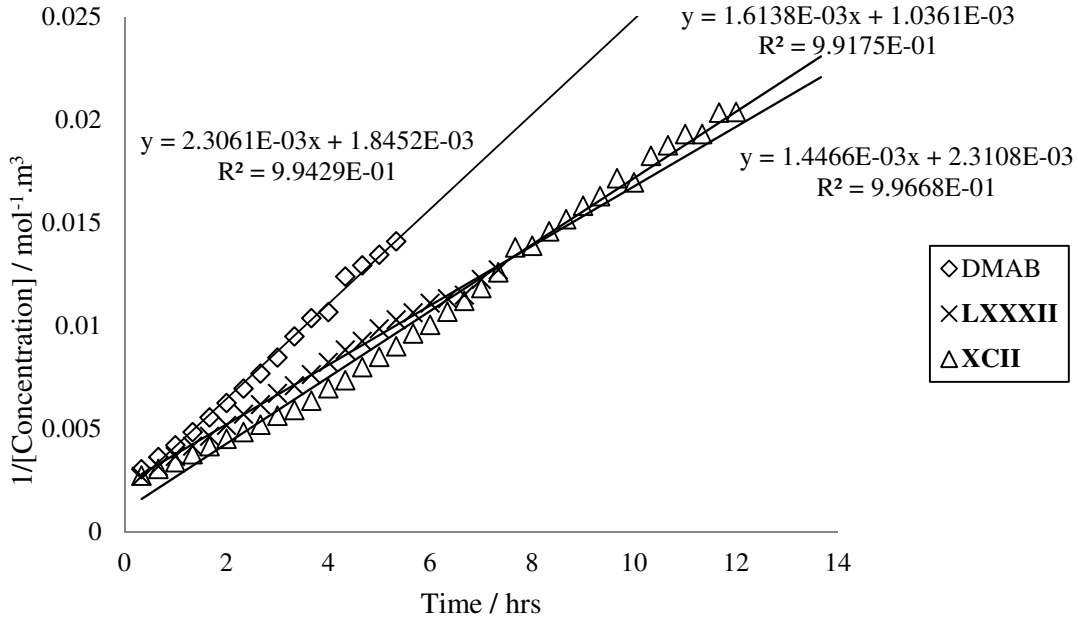

Figure 3.35: Second order kinetic data plots for the consumption of DMAB (diamonds), **LXXXII** (crosses) or **XCII** (triangles) in the stoichiometric reaction with **LXV** at 35 °C to form **36**.

The graph in Figure 3.35 shows that reaction of **LXV** with DMAB resulted in the fastest reaction, whilst the reaction of the *N*-deuterated and *B*-deuterated amine boranes, **LXXXII** and **XCIII** respectively, proceeded at a slower rate. The rates of reaction for **LXXXII** and **XCIII**, however, were very similar, resulting in k_H/k_D values of 1.4 (1d.p.) for N-H/D and 1.6 (1d.p.) for B-H/D variations. These data indicate that both N-H/B-H bond breaking/forming is relatively unimportant in the rate determining step (RDS) of the reaction.

The reaction temperature could not be raised above 35 °C or decomposition would become significant, releasing a calcium hydride species which would impact upon the concentration of DMAB, whilst at temperatures below 35 °C the reaction rate was found to decrease considerably, preventing the construction of Eyring and Arrhenius plots.

To further investigate the reactivity of β-diketiminato calcium dimethylamidoborane with increasing stroichiometric equivalents of DMAB reactions were monitored by ^{11}B NMR spectroscopy at 60 °C with the concentration of **LXV** held constant in an attempt to ascertain the partial rate order with respect to [DMAB]. The results of these reactions are illustrated by the zero order kinetic data plot for the consumption of DMAB in Figure 3.36. The decrease in concentration of **LXV** and increase in concentration of **XXXVI** did not fit 0, 1st nor 2nd order kinetic data plots. The decrease in concentration of DMAB, however, fitted straight-line 0, 1st and 2nd order kinetic data plots to a similar and varying degree for these experiments with no conclusive indication as to the order of reaction. A reliable dependence upon concentration of DMAB in these reactions, however, could not be ascertained even when plotting the 0, 1st and 2nd order rate constants for consumption of DMAB against the number of equivalents of DMAB.

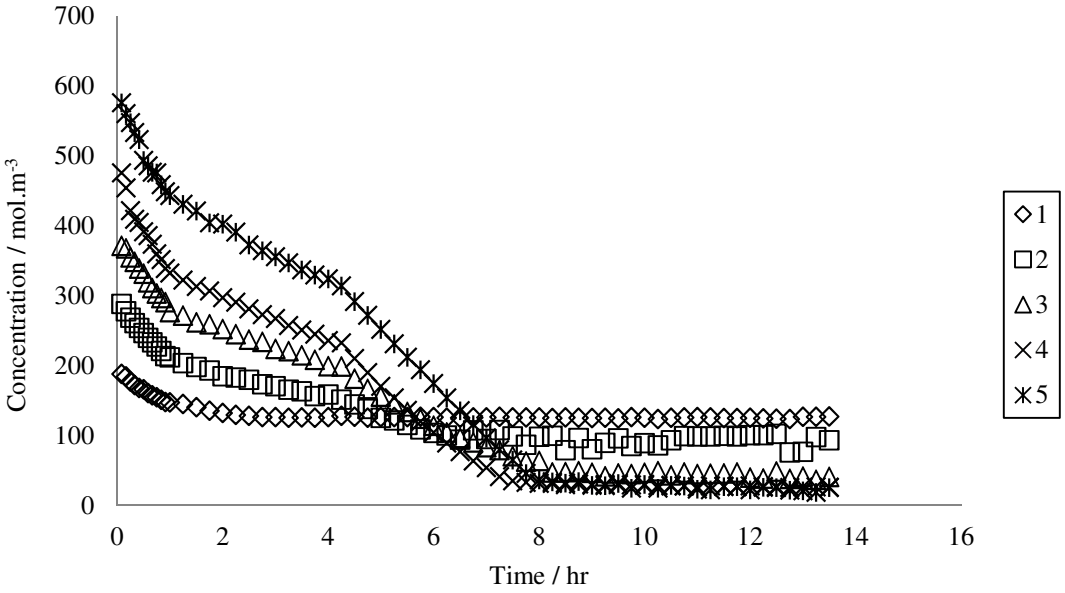

Figure 3.36: Zero order kinetic data plots for the consumption of DMAB, in the reaction with β-diketiminato calcium dimethylamidoborane **LXV** at 60 °C in the presence of; 1 (diamonds), 2 (squares), 3 (triangles), 4 (crosses) and 5 (stars) equivalents of DMAB.

As shown by Figure 3.36 the plotted data exhibited four clearly defined periods in the reaction, each with a different rate of reaction, which was observed to increase with increased number of equivalents of DMAB. The times and conversions of

DMAB at which these transitions occurred were, however, effectively invariant across each reaction;

(k_1) An initial period in which the rate of reaction is fast, ca. t = 0 to t = 0.75 hours, 0 to ca. 30 % consumption of DMAB;

(k_2) Rate of reaction decreases, ca. t = 0.75 hours to t = 4.25 hours, ca. 30 % to 50 % consumption of DMAB;

(k_3) Rate of reaction increases, $k_1 > k_3 > k_2$, ca. t = 4.25 hours to t = 8.0 hours, ca. 50 % to 80 % consumption of DMAB;

(k_4) Final stage of the reaction, rate of reaction decreases, $k_1 > k_3 > k_2 > k_4$, ca. t = 8.0 hours, ca. 80 % consumption of DMAB onwards.

The increase in reaction rate for each step of the reaction suggests a dependence upon [DMAB], whilst the transition point at which these reactions undergo a marked change in reaction rate suggests a cause which is independent of [DMAB]. Attempts to rationalise this behaviour and the dependence upon [DMAB] were tentatively based around the availability of the metal centre to react with DMAB, although a correlation between reaction rate and proportion of **LXV**, **36**, and inferred proportion of calcium hydride species at each stage of the reaction could not be established. Although monitoring of these reactions was hindered by the overlapping resonances of DMAB, **LXV** and BH_3 unit of **36** in the ^{11}B NMR spectra, approximate integrations of these species could be ascertained.

Reactions were carried out at 70 °C in which the concentration of β-diketiminato calcium dimethylamidoborane **LXV** was varied in the presence of excess DMAB, in an attempt to ascertain the rate order with respect to [**LXV**]. Once again these reactions were monitored by ^{11}B NMR spectroscopy, the results of which are shown by the zero order kinetic data plots for the consumption of DMAB in Figure 3.37.

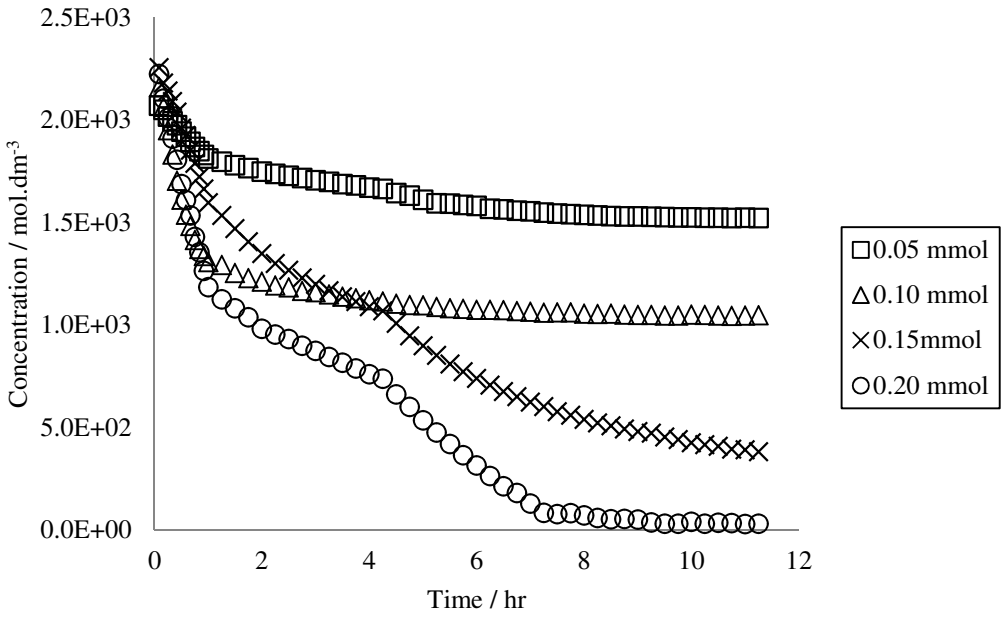

Figure 3.37: Zero order kinetic data plot for the consumption of DMAB, with varying concentrations of β-diketiminato calcium dimethylamidoborane **LXV** at 70 °C in the presence of an excess of DMAB. 0.05 mmol **LXV** (squares), 0.10 mmol **LXV** (triangles), 0.15 mmol **LXV** (crosses) and 0.20 mmol **LXV** (circles).

Similar to the results for reactions between **LXV** and DMAB in Figure 3.36 neither did the consumption of **LXV** and formation of **XXXVI** provide linear 0, 1st or 2nd order kinetic data plots, nor did the consumption of DMAB definitively fit any simple integer rate dependence. The results in Figure 3.37 clearly exhibited the marked changes in rate of reaction that had been previously observed. It must be noted, however, that the concentration of DMAB was held constant so that whilst DMAB was in 10-fold excess at low concentrations of **LXV**, at increased concentrations of **LXV** the 10-fold excess of DMAB was not maintained. To obtain accurate data for evaluation of the rate order with respect to [**LXV**] a large excess of DMAB should have been used, however, when dehydrocoupling to evolve dihydrogen in a closed system, an excess of DMAB must be limited to a level at which the sealed Youngs tap NMR tube is not over-pressurised, whilst at low concentrations of **LXV** the reaction rate may inhibit monitoring of the reaction. Although a rate dependence could not be obtained for [**LXV**], Figure 3.37 suggests similar complexity as Figure 3.36. A further peculiarity of the results in Figure 3.37

is the end point of the reactions which corresponds to a DMAB consumption which appears dependent upon [**LXV**]. This relationship is shown in Figure 3.38.

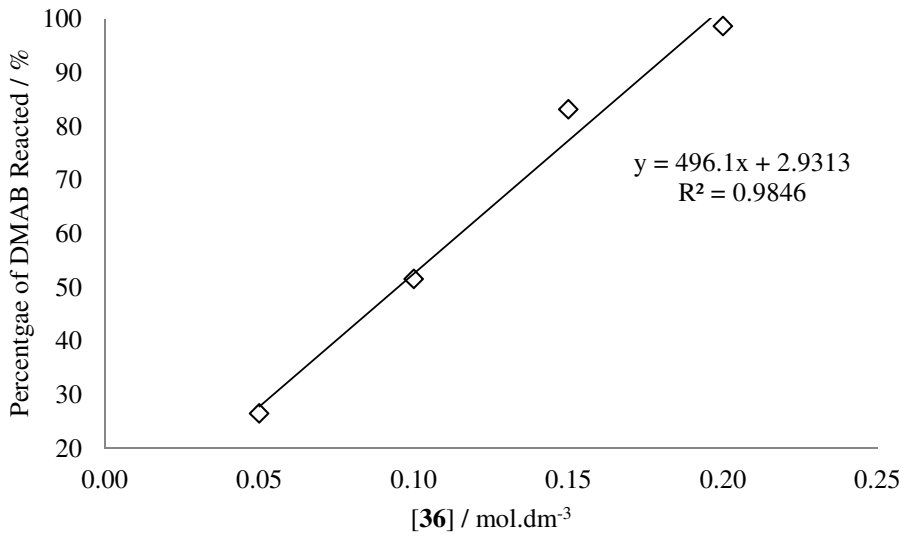

Figure 3.38: A graph of percentage of DMAB consumed against concentration of β-diketiminato calcium dimethylamidoborane **XLV**, in reactions between **XLV** and 0.5 mmol DMAB at 70 °C.

As described in Section 3.2.5 the decomposition of **36** resulted in a proposed δ-hydride elimination to form **XXXVI**, which was itself observed to react. To further investigate the reactivity of **36** NMR-scale reactions were carried out at 70 °C with additional equivalents of DMAB, whilst the concentration of **36** was held constant in an attempt to ascertain the partial rate order with respect [DMAB]. These reactions were monitored by ^{11}B NMR spectroscopy, the results of which are illustrated by the zero order kinetic data plots for the consumption of DMAB in Figure 3.39. The decrease in concentration of DMAB and **36** and increase in concentration of **XXXVI** did not fit straight line 0, 1st nor 2nd order kinetic data plots.

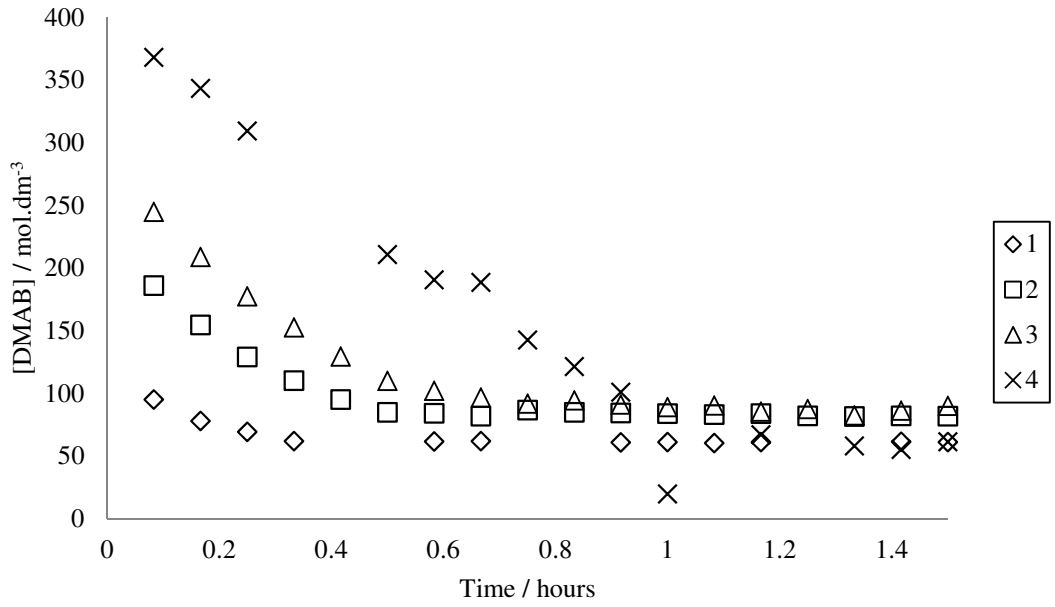

Figure 3.39: Zero order kinetic data plots for the consumption of DMAB, in the reaction of **36** at 70 °C in the presence of; 1 (diamonds), 2 (squares), 3 (triangles) and 4 (crosses) equivalents of DMAB.

These results demonstrate a high degree of complexity in both the formation and reaction of **36**, not only in the lack of a definitive fit to simple kinetic data plots, but also the unexplained changes in reaction rate and behaviour with varying reactant concentration. Based upon these results reactions in which the concentration of **36** was varied were not carried out.

For comparison the analogous β-diketiminato magnesium [$NMe_2BH_2NMe_2BH_3$] species **XLV** and homoleptic [$Mg\{NMe_2BH_2NMe_2BH_3\}_2(THF)$] species **XLVI**, reported by Hill,[2] were similarly heated with one equivalent of DMAB in NMR-scale reactions at 70 °C. Due to the complexity of reactions between **36** and DMAB, the method of initial rates was employed for reactions of these magnesium species, in which the reaction was monitored over the course of time during which 10 % of the initial concentration of DMAB was consumed. The results of the investigation are shown in Figures 3.40 (**XLV**) and 3.41 (**XLVI**).

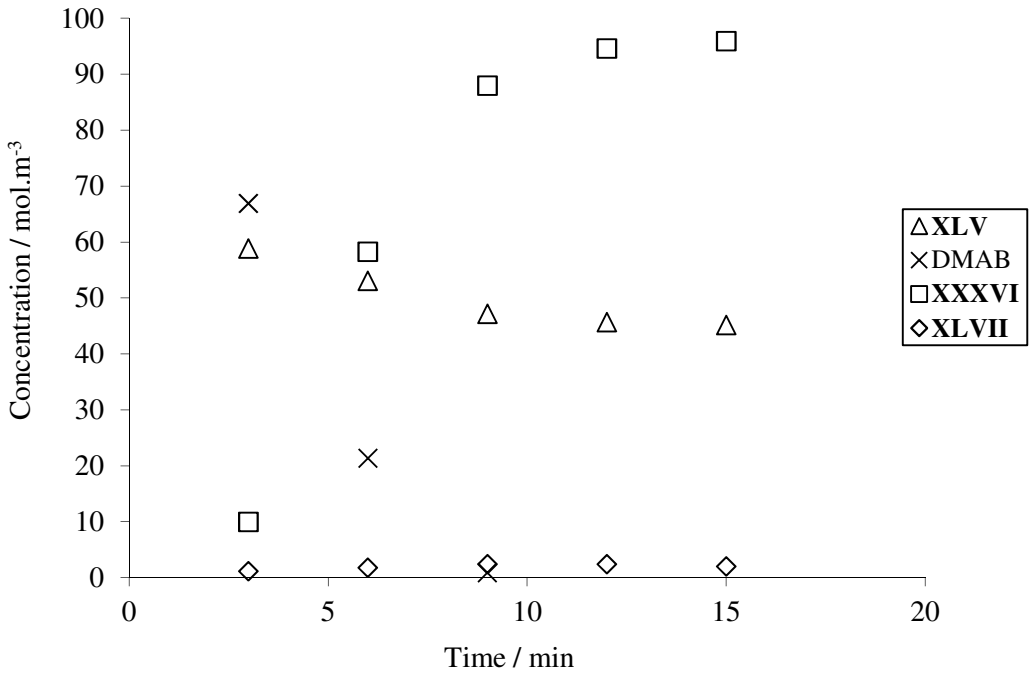

Figure 3.40: A zero-order kinetic data plot for the stoichiometric reaction between **XLV** and DMAB at 70 °C.

The results shown in Figure 3.40 indicate that at 70 °C the additional equivalent of DMAB reacts rapidly with formation of **XXXVI** and a minor quantity of **XLVII**. The concentration of **XLV** decreases slightly during this reaction while the DMAB is consumed. The consumption of DMAB and formation of **XXXVI** and **XLVII** could not, however, be fitted to either 0, 1st nor 2nd order kinetic data plots.

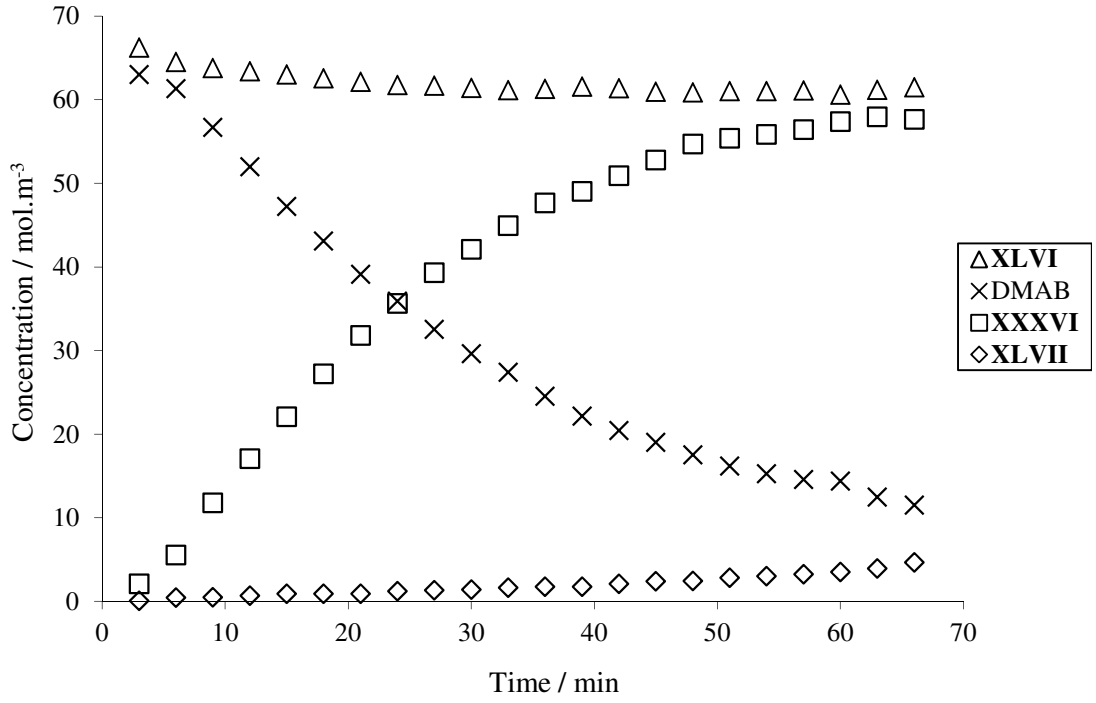

Figure 3.41: A zero-order kinetic data plot for the stoichiometric reaction between **XLVI** and DMAB at 70 °C.

The results shown in Figure 3.41 indicate that the additional equivalent of DMAB reacts to form **XXXVI** and a minor quantity of **XLVII**, mirroring the results of the reaction between **XLV** and DMAB shown in Figure 3.40, but occurring much more slowly. Although the concentration of **XLVI** decreases by approximately 50 % during this reaction it is the DMAB which is consumed. Similar to previous reactions, the increase in concentration of **XXXVI** could not be modelled by 0, 1st nor 2nd order kinetic data plots, however, the consumption of DMAB and formation of **XLVII** followed 1st order kinetics (Figure 3.42).

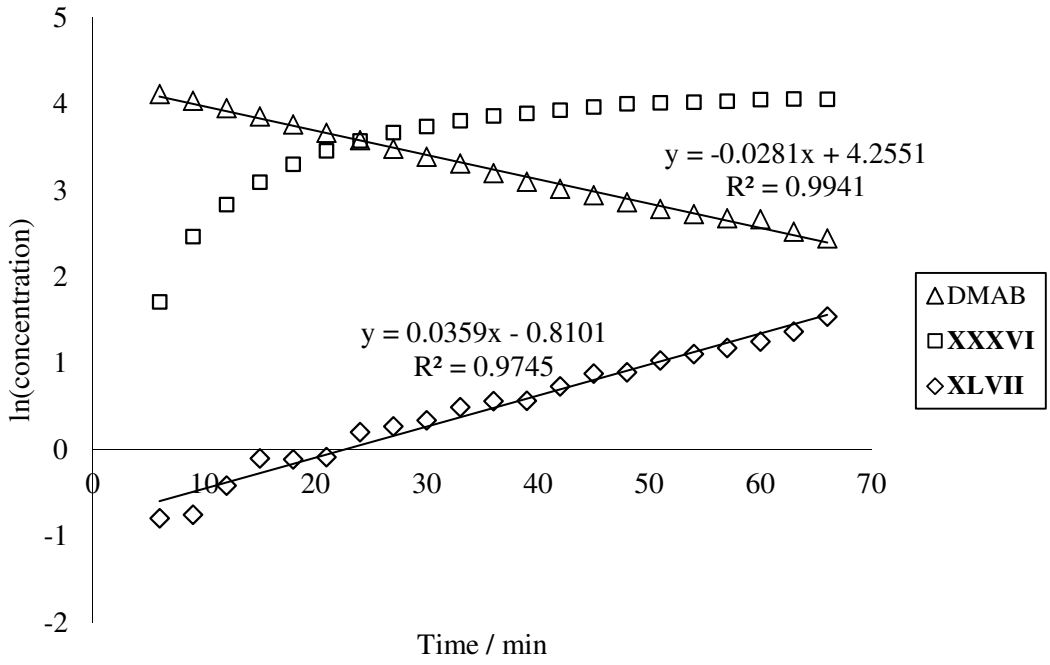

Figure 3.42: A first-order kinetic data plot for the stoichiometric reaction between **XLVI** and DMAB at 70 °C.

Although Figure 3.42 shows that the formation of **XLVII** appears to conform to 1st order kinetics the concentration of this species is small, accounting for ca. 1.5 % of the total boron-containing species after ca. 69 minutes heating time, indicating that any conclusions should be drawn with caution.

These reactions suggest that under these conditions the [$NMe_2BH_2NMe_2BH_3$]-containing species, **XLV** or **XLVI**, undergo partial reaction whilst DMAB is consumed, which may result from a mechanism involving the intermediacy and regeneration of these species. This behaviour is reminiscent of the previously described reactivity between DMAB and β-diketiminato calcium(NMe_2BH_3) **LXV**, in which this species reacted via a proposed proton-assisted β-hydride elimination. A system can, thus, be envisaged in which a DMAB-induced δ-hydride elimination from **XLV** or **XLVI** is followed by a rapid deprotonation of DMAB, β-hydride elimination and insertion of the as-generated, polarised, unsaturated **XXXVII** fragment possibly via a concerted reaction step. A tentatively proposed scheme to account for these observations is shown in Figure 3.42 with proposed transition states for these processes depicted as **A**, **B** and **C**. Similar to the proposed mechanism for the reaction between **LXV** and DMAB in Figure 3.20, the transition

states depicted **B** and **C** in Figure 3.43 are shown separately, but could be viewed as a continuum comprising a single concerted step. The ^{11}B NMR spectra for reactions between magnesium reagents **XLV** and **XLVI** and DMAB show only very low concentrations of [$Me_2N{=}BH_2$] **XXXVII**, consistent with a rapid reaction of this species or a possible concerted mechanism.

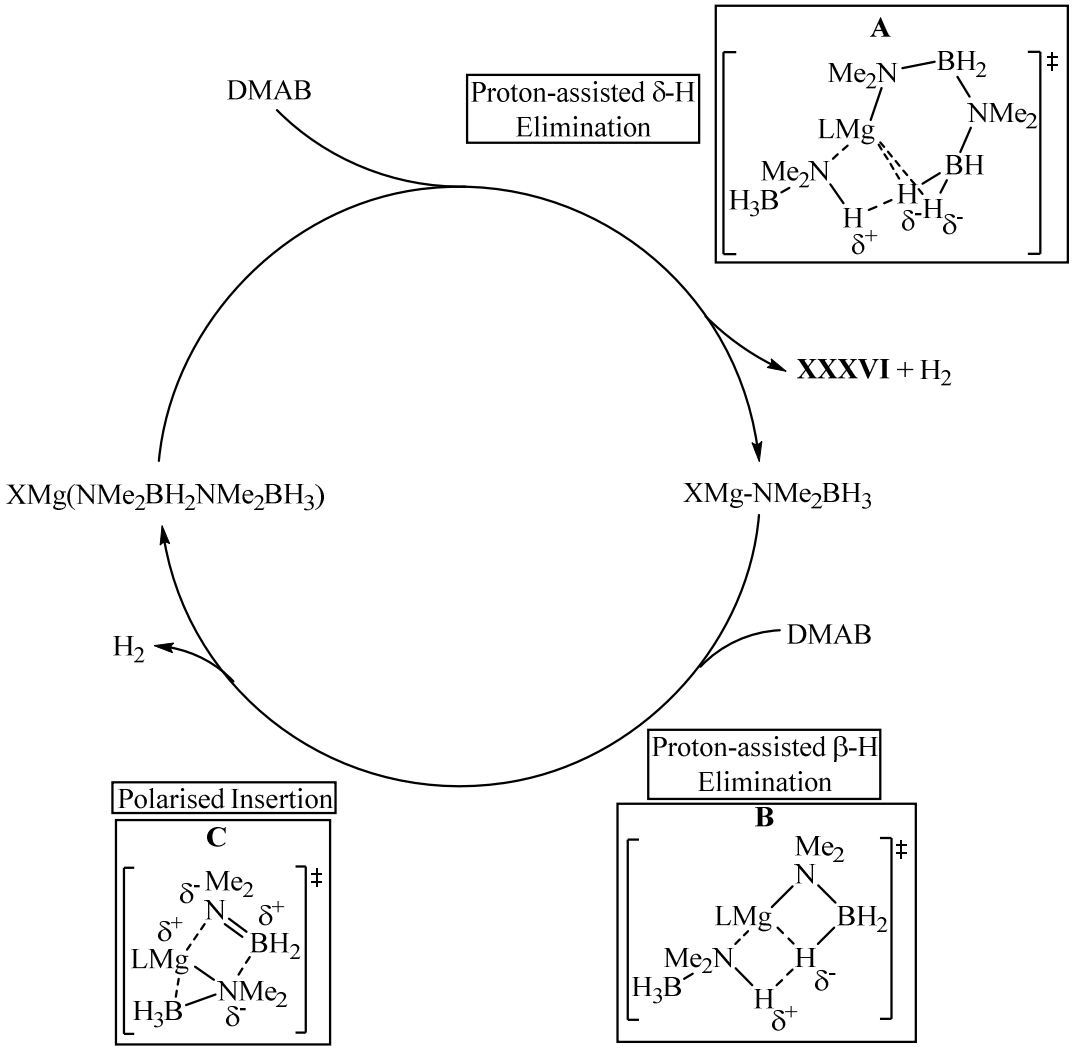

Figure 3.43: Proposed scheme to account for the reactivity of **XLV** and **XLVI** in the presence of an additional equivalent of DMAB, where X = β-diketiminate **XLV**, and X = [$NMe_2BH_2NMe_2BH_3$] **XLVI**.

To further investigate this behaviour four equivalents of DMAB were added to **XLVI** and the sample was heated at 80 °C for ca. 24 hours. The ^{11}B NMR spectrum for this reaction showed that ca. 85.7 % DMAB had reacted, with conversion to 5.0

% **XLVII**, 43.5 % **XXXVI** and 19.8 % **XLVI**. If **XLVI** was completely regenerated during the reaction a 2:1 ratio of **XXXVI**:**XLVI** would be expected. This did not occur, however, with formation of ca. 5.0 % **XLVII** occurring by a pathway which was not considered in the scheme proposed in Figure 3.42. Figure 3.42 is based upon a small number of observations and must be considered a working hypothesis, as clearly additional factors and mechanistic pathways are operational, demonstrated by the formation of **XLVII**.

3.4 Chapter 3 Conclusion

This chapter has described experiments that were conducted to investigate the reactivity of amine boranes with reagents from Groups 1, 2 and 3 in relation to the proposed mechanism in Figure 3.1 (reshown here as Figure 3.44).

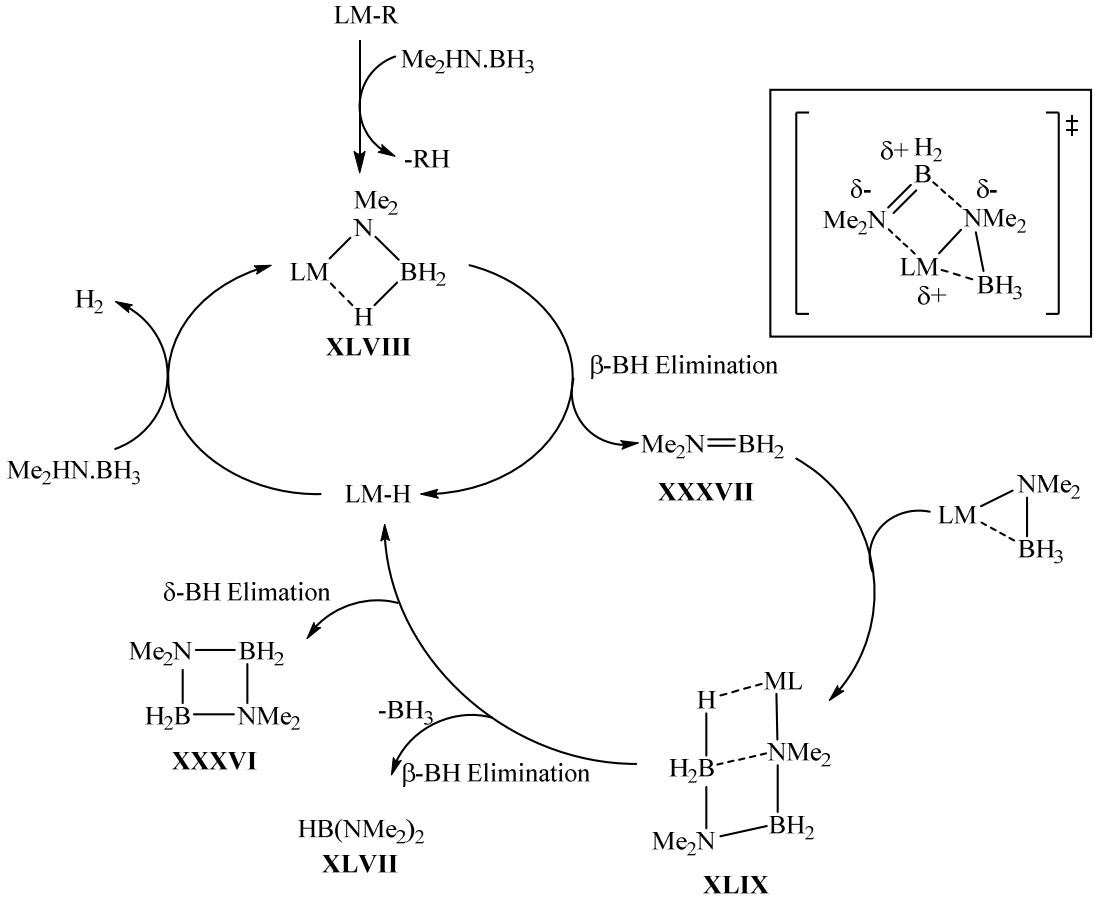

Figure 3.44: Proposed scheme for dehydrocoupling amine boranes by alkaline earth precatalysts (where M = Mg, Ca, Sr, Ba).[1-3]

The reactions with anilido-imine species (**IX**, M = Mg, Ca, Sr), described in Section 3.1, whilst ultimately failing to be of use for a study of the effect of the identity of the metal centre upon amine borane dehydrcocoupling reactivity, have extended the range of alkaline earth complexes investigated beyond β-diketiminato- (**VI** and **XV**) and $[M\{N(SiMe_3)_2\}_2]_2$ species (**V**, M = Mg, Ca, Sr). The formation and isolation of homoleptic anilido-imine species and reactions which resulted in ligand reduction represented the first findings of this kind for this ligand system, which has been

reported to provide greater stability than the isoteric β-diketiminate ligand. Thus, the kinetic investigations described in this chapter focused on reactions with metal species with either β-diketiminate or simple amide ligands of the form [$N(SiMe_3)_2$], which as evidenced by issues with ligand protonation for the calcium species **VI** and **V-Ca** also proved not to be ideal species for this investigation. In common with many studies of the catalytic competence of Group 2 complexes a kinetic investigation would, thus, have been greatly assisted by a ligand system which provides adequate stabilisation towards Schlenk-like equilibration and ligand protonation for the heavier alkaline earth metals (Mg to Ba).

The reactivity of alkaline earth amidoborane species revealed the high thermal stability of the β-diketiminato calcium dimethylamidoborane **LXV** and $Mg[NMe_2BH_2NMe_2BH_3]_2$ **XLVI**. Indeed, the stoichiometric reaction between **LXV** and DMAB at 30 – 35 °C provided access to the β-diketiminato calcium [$NMe_2BH_2NMe_2BH_3$] species **36**, evidence for the existence of which had only previously been inferred by the observation of low concentrations of this species from ^{11}B NMR spectra of reaction mixtures. In the presence of an additional equivalent of DMAB, however, these species are highly reactive, highlighting the requirement for an additional equivalent of amine borane to undergo a proton-assisted hydride elimination reaction via a potentially concerted process. This suggestion necessitates a modification to the proposed mechanism in Figure 3.44, resulting in the proposed mechanism shown in Figure 3.45 highlighting the requirement for a unit of DMAB in a proton-assisted β/δ-hydride elimination, occurring via the postulated concerted mechanism shown by transition states **A** and **B** in Figure 3.45.

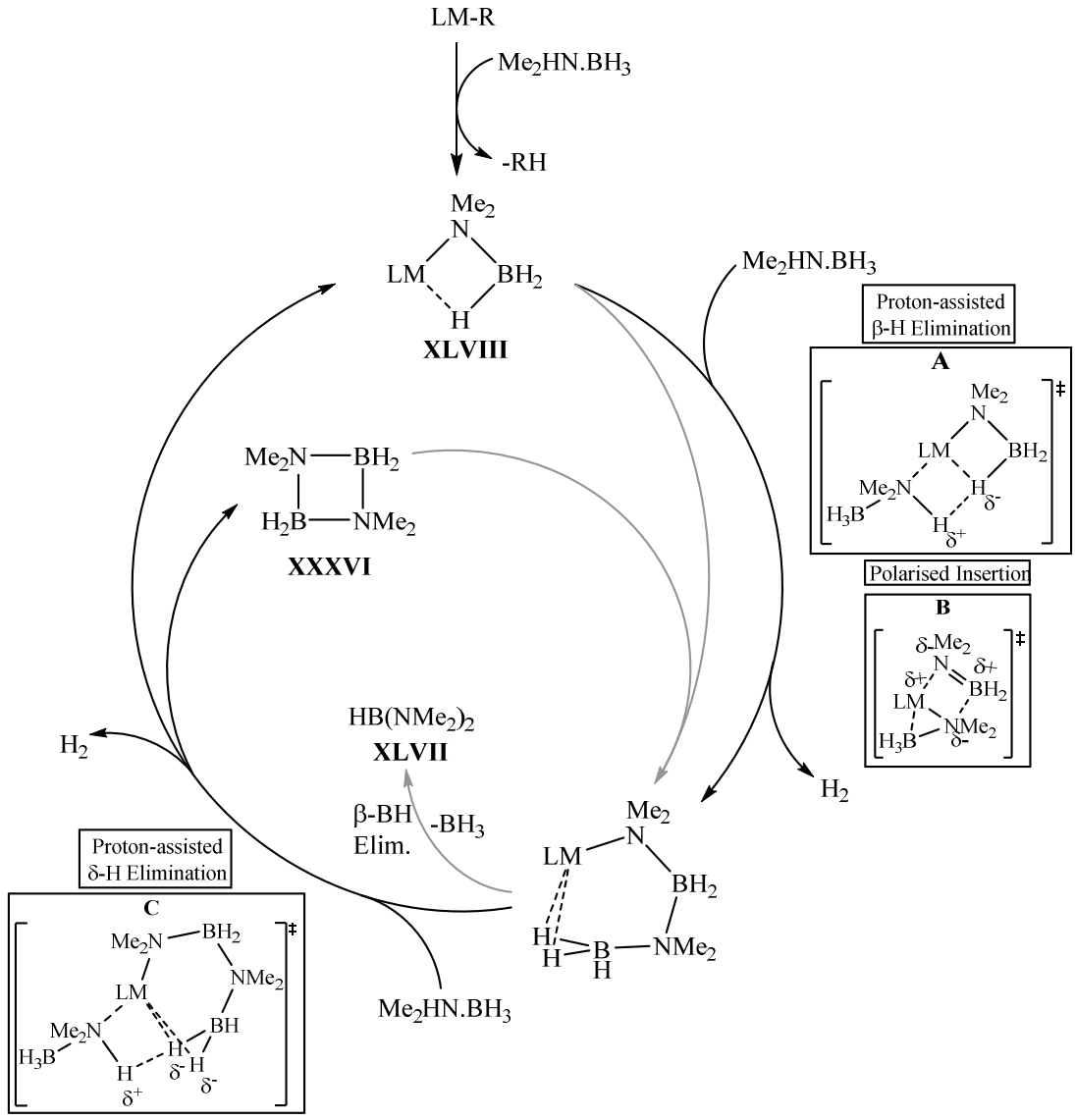

Figure 3.45: Proposed mechanism of amine borane dehydrocoupling by alkaline earth elements (M = Mg, Ca, Sr, Ba), with modifications based upon observations from the work described in Chapter 3.

The instantaneous formation of **LXV** at room temperature, combined with the relative ease of formation of **36**, suggested that the rate-determining step in these reactions is the δ/β-hydride elimination from the metallated [$NMe_2BH_2NMe_2BH_3$] species of the proposed mechanism in Figure 3.44. Indeed, reactions of these species required heating to temperatures of 60 °C and above and were assisted by the presence of free amine borane. Stoichiometric reactions of β-diketiminato calcium dimethylamidoborane **LXV** with additional equivalents of amine borane revealed

complicated profiles for consumption of DMAB which comprised different reaction phases, characterised by marked changes in reaction rate, the cause of which could not be rationalised. These reactions also highlighted that **XXXVI** is not a stable product under the conditions of reaction, undergoing decomposition with metal hydride, metal amidoborane species or amines to produce $[HB(NR_2)(NR'_2)]$ species. Although **XXXVI** was shown to be reactive in near stoichiometric proportions, it is not known whether such decomposition reactions operate or are significant in catalytic regimes. This observation also requires modification to be made to the proposed dehydrocoupling scheme, however, and is depicted by the grey arrows in Figure 3.45.

The mechanism of dehydrocoupling of amine boranes by d^0 species has throughout this chapter been revealed as a complex process giving rise to kinetic data that could not be modelled by simple kinetic data plots.

In Section 3.2.6 reactions of the primary amine borane *tert*-butylamine borane (TBAB) with calcium species **VI** and **V-Ca** were described. The reactivity of this primary amine borane revealed similarities to dehydrocoupling of secondary amine boranes with the isolation of β-diketiminato calcium *tert*-butylamidoborane **40** while catalytic dehydrocoupling by **VI** and **V-Ca** afforded the cyclic borazane $[H^tBuN\text{-}BH_2]_2$ **44**, the first crystallographically defined primary amine borane species of this type. Whilst exhibiting similarities, the stoichiometric reaction with the magnesium compound **XV**, which did not produce a stable magnesium coordinated $[N^tBuHBH_2N^tBuHBH_3]^-$ species, and catalytic reactions with **VI** and **V-Ca** which produced a calcium borohydride **47** and *tert*-butyl borazine **46**, revealed divergent behaviour. It was concluded that, although dehydrocoupling of TBAB by alkaline earth species appeared to be consistent with the proposed mechanism in Figure 3.45, additional reaction pathways must operate to account for the formation of species such as **46** - **48**. Exemplified by the reactivity of **44**, which was consumed to form **46**, these reactions highlighted the increased ambiguity introduced from possession of two nitrogen-bound protons for a primary amine borane, compared to the secondary amine boranes DMAB and PB. An interesting study would be to

investigate the role of metal species and mechanism of B-N bond formation for the conversion of the borazane **44** to borazine **46**, another dehydrogenative process.

Although Group 1 amidoborane species and their hydrogen evolution via thermolysis have been widely investigated, curiously the catalytic dehydrocoupling of amine boranes by Group 1 reagents has not been reported. Section 3.2.1 described stoichiometric reactions between Group 1 species and amine boranes to form Group 1 amidoboranes, whilst catalytic reactions described in Section 3.2.2 demonstrated dehydrocoupling activity, albeit at not particularly impressive rates compared to transition metal catalysts.

It is worth noting that all of the reactions described in this chapter have been undertaken under conditions of a closed system retaining volatile products including dihydrogen. Activation of dihydrogen by alkaline earth species has been reported,[54] while mechanisms of amine borane dehydrocoupling by transition metal species possess reversible hydrogen evolution reaction steps. In these systems high consumption of amine borane is only obtained when the reaction vessel is vented or degassed periodically, thereby removing excess dihydrogen.[53, 55] Further modifications to the proposed mechanism in Figure 3.45 could therefore be required to account for interaction of dihydrogen with amidoborane species and the presence of reversible reactions. In addition, the formation of [$HB(NMe_2)$] **XLVII** requires the formation of one equivalent of BH_3. Whilst reports by Hill suggested the unconfirmed formation of diborane (B_2H_6),[2, 3] in conducting the reactions described in this thesis the fate of this unaccounted BH_3 has not been resolved, highlighting that despite the work described herein there is still much that is not known regarding these reactions.

Whilst the reactions described in this chapter have not refuted the proposed mechanism in Figure 3.44, intricacies have been revealed which have led to the refined model proposed in Figure 3.45. This chapter has highlighted in particular that even when considering a simplified system the mechanism of dehydrocoupling of secondary amine boranes is far from simple and that the complexities of the process escalate when considering primary amine boranes or ammonia borane. Although generalisations can be made, therefore, a generic mechanism which fully

describes amine borane dehydrocoupling by d^0 species will likely be too much of an oversimplification.

3.5 Experimental Procedures for Chapter 3

All reactions were carried out using standard Schlenk line and glovebox techniques under an inert argon atmosphere. NMR experiments were conducted in Youngs tap NMR tubes prepared and sealed in a glovebox. NMR spectra were collected on a Bruker AV300 spectrometer operating at 75.5 MHz (^{13}C), 96.3 MHz (^{11}B). Variable-temperature ^{1}H NMR data**,** ^{1}H-^{11}B HMQC and ^{1}H TOCSY experiments were recorded on a Bruker AV400 spectrometer. Solvents (toluene, THF, hexane) were dried by a commercially available solvent purification system (Innovative Technologies) under nitrogen before storage in ampoules over molecular sieves. C_6D_6, d_8-toluene and d_8-THF were purchased from Goss Scientific Instruments Ltd., dried over molten potassium before distillation under nitrogen and storage over molecular sieves. $Me_2NH.BH_3$, $^{t}BuNH_2.BH_3$, BD_3.THF, $B(NMe_2)_3$, KH, Group 1 [M{N(SiMe$_3$)$_2$}] **LIX** (where M = Li, Na, K) reagents, and phenylsilane were purchased from Sigma-Aldrich Ltd. and used without further purification. Alkaline earth anilido-imine **IX**,[6] β-diketiminate **VI** and **XV**,[56-58] bis(trimethylsilyl)amide [M{N(SiMe$_3$)$_2$}$_2$]$_2$ **V**,[59] and Group 3 tris(amide) **XL** and **XLI** reagents were all synthesised by literature procedures.[60, 61] CHN microanalysis was conducted by Mr. Stephen Boyer of London Metropolitan University.

Typical Procedure for Stoichiometric NMR-Scale Reactions

C_6D_6, d_8-toluene or d_8-THF (ca. 0.5 ml) was added to a solid mixture of reactants in a glovebox and the solution sealed in a Youngs tap NMR tube. The reactions were monitored by ^{1}H and ^{11}B NMR spectroscopy. Reactions requiring elevated temperatures were heated using thermostatically controlled oil baths.

3.5.1 Reactions of Anilido-imine Species **IX** with Amine Boranes

3.5.1.1 NMR-Scale Synthesis of [Anilido-imine.Ca(NMe$_2$BH$_3$)(THF)] **13**

D_8-toluene (ca. 0.5 ml) was added to a solid mixture of **IX-Ca** (71 mg, 0.1 mmol) and one molar equivalent of $Me_2NH.BH_3$ (6 mg, 0.1 mmol) and the solution sealed in a Youngs tap NMR tube before standing at RT for ca. 2 hours. ^{1}H NMR (d_8-tol, 298 K) δ = 1.12 (d, $^{3}J_{HH}$ = 6.8 Hz, 6H, CH(C*H*$_3$)$_2$), 1.16 (d, $^{3}J_{HH}$ = 6.8 Hz, 6H,

$CH(CH_3)_2$), coincident with THF ca. 1.26 (d, $^3J_{HH}$ = 6.8 Hz, 6H, $CH(CH_3)_2$), coincident with THF ca. 1.29 (d, $^3J_{HH}$ = 6.8 Hz, 6H, $CH(CH_3)_2$), 1.88 (br. s, 6H, $N(CH_3)_2$), 3.55 (THF), 3.09 (spt, $^3J_{HH}$ = 6.8 Hz, 2H, $CH(CH_3)_2$), 3.27 (spt, $^3J_{HH}$ = 6.8 Hz, 2H, $CH(CH_3)_2$), 6.22 (m, 2H, arom-*H*), 6.82 (m, 1H, arom-*H*), 6.98 (m, 1H, arom-*H*), 7.14 (m, 3H, arom-*H*), 7.22 (t, $^3J_{HH}$ = 8.7 Hz, 1H, arom-*H*), 7.24 (m, 2H, arom-*H*), 7.95 (s, 1H, C*H*=N). $^{13}C\{^1H\}$ NMR (d_8-tol, 298 K) δ = 23.7 ($CH(CH_3)_2$), 25.3 ($CH(CH_3)_2$), 25.7 (THF), 26.1 ($CH(CH_3)_2$), 26.2 ($CH(CH_3)_2$), 28.8 ($CH(CH_3)_2$), 29.2 ($CH(CH_3)_2$), 46.7 ($N(CH_3)_2$), 70.3 (THF), 111.9 (C_6H_4), 117.1 (*i*-NC_6H_4), 118.7 (C_6H_4), 124.3 (*m*-NC_6H_4), 125.0 (*p*-NC_6H_4), 125.8 (*m*-NC_6H_4), 126.5 (*p*-NC_6H_4), 133.9 (C_6H_4), 139.3 (C_6H_4), 141.1 (*o*-NC_6H_4), 144.3 (*o*-NC_6H_4), 148.2 (*i*-NC_6H_4), 149.3 (*i*-NC_6H_4), 159.6 (*i*-N=CHC_6H_4), 171.0 (*C*H=N). ^{11}B NMR (d_8-tol, 298 K) δ = –12.4 (q, BH_3, $^1J_{BH}$ = 80 Hz). A single crystal of **13** suitable for X-ray diffraction analysis was isolated from a concentrated toluene solution at –30 °C. Accurate CHN microanalysis was obtained for **13**. Anal. Calc. for $C_{37}H_{56}BCaN_3O$: C: 72.88; H: 9.26; N: 6.89 %. Found: C: 72.69, 72.73; H, 9.15, 9.13; N: 6.75, 6.82 %.

Molecular Formula	$C_{37}H_{56}BCaN_3O$
Formula Weight / g.mol^{-1}	609.74
Crystal System, Space Group	Monoclinic, P 1 2_1/n 1
a, b, c / Å	10.3026(5), 31.9329(16), 11.9820(5)
α, β, γ / °	90, 110.693(3), 90
V / Å^3	3687.7(3)
Z	4
μ / mm^{-1}	0.200
ρ / g.cm^{-3}	1.098
θ range / °	3.83 – 25.36
Collected / Unique Reflections / R_{int}	24515 / 5846 / 0.0552
R_1, wR_2 [I > 2σ(I)]	R_1 = 0.0529, wR_2 = 0.1020
R_1, wR_2 (All data)	R_1 = 0.0994, wR_2 = 0.1170

Notes on refinement: A low completeness of data (87 %) was rationalised as resulting from movement of the crystal during data collection.

3.5.1.2 Synthesis of [Anilido-imine.Ca(NMe_2BH_3)(THF)] **13** and [Anilido-imine.Ca($NMe_2BH_2NMe_2BH_3$)] **14**

Toluene (ca. 10ml) was added to solid **IX-Ca** (0.503 g, 0.82 mmol) and one molar equivalent of $Me_2NH.BH_3$ (48.2 mg, 0.82 mmol) in a Schlenk tube and stirred at room temperature for ca. 18 hours. Removal of solvent under vacuum provided a yellow solid. Compounds **13** and **14** were identified by inspection of the ^{1}H NMR and ^{11}B NMR spectra and comparison to data from Sections 3.5.1.1 and 3.5.1.3. Conversion by integration of ^{11}B NMR spectrum: 50.7 % **13**, 49.3 % **14**.

3.5.1.3 Rational NMR-Scale Synthesis of [Anilido-imine.Ca($NMe_2BH_2NMe_2BH_3$)] **14**

D_8-toluene (ca. 0.5 ml) was added to solid **13** (0.122 g, 0.2 mmol) and one molar equivalent of $Me_2NH.BH_3$ (11.8 mg, 0.2 mmol) and the solution sealed in a Youngs tap NMR tube before heating at 30 °C for ca. 16 hours. Removal of solvent under vacuum provided a yellow solid. ^{1}H NMR (d_8-tol, 298 K) δ = 1.10 (d, J_{HH} = 6.8 Hz, 6H, CH(CH_3)$_2$), 1.13 (d, J_{HH} = 6.8 Hz, 6H, CH(CH_3)$_2$), 1.18 (d, J_{HH} = 6.8 Hz, 12H, CH(CH_3)$_2$), 1.75 (s, 3H, N(CH_3)$_2$), 1.84 (s, 3H, N(CH_3)$_2$), 2.30 (s, 3H, N(CH_3)$_2$), 2.37 (s, 3H, N(CH_3)$_2$), 3.22 (spt, J_{HH} = 6.8 Hz, 2H, CH(CH$_3$)$_2$), 3.35 (spt, J_{HH} = 6.8 Hz, 2H, CH(CH$_3$)$_2$), 6.19 - 6.35 (m, 2H, arom-*H*), 6.53 (m, 1H, arom-*H*), 6.93 (m, 1H, arom-*H*), 7.07 (m, 3H, arom-*H*), 7.16 (m, 1H, arom-*H*), 7.21 – 7.26 (m, 2H, arom-*H*), 8.20 (s, 1H, C*H*=N). ^{13}C{^{1}H} NMR (d_8-tol, 298 K) δ = 23.7 (CH(*C*H$_3$)$_2$), 24.1 (CH(*C*H$_3$)$_2$), 25.2 (CH(*C*H$_3$)$_2$), 26.6 (CH(*C*H$_3$)$_2$), 28.9 (*C*H(CH$_3$)$_2$), 29.3 (*C*H(CH$_3$)$_2$), 43.7 (N(*C*H$_3$)$_2$), 44.2 (N(*C*H$_3$)$_2$), 51.6 (N(*C*H$_3$)$_2$), 52.6 (N(*C*H$_3$)$_2$), 112.7 (*C*$_6$H$_4$), 117.2 (*i*-N*C*$_6$H$_4$), 118.2 (*C*$_6$H$_4$), 123.8 (*m*-N*C*$_6$H$_4$), 124.6 (*p*-N*C*$_6$H$_4$), 125.3 (*m*-N*C*$_6$H$_4$), 128.5 (*p*-N*C*$_6$H$_4$), 133.0 (*C*$_6$H$_4$), 138.8 (*C*$_6$H$_4$), 141.3 (*o*-N*C*$_6$H$_4$), 144.2 (*o*-N*C*$_6$H$_4$), 148.2 (*i*-N*C*$_6$H$_4$), 149.8 (*i*-N*C*$_6$H$_4$), 160.2 (*i*-N=CH*C*$_6$H$_4$), 170.3 (*C*H=N). ^{11}B NMR (C_6D_6, 298 K) δ = –11.2 (q, *B*H$_3$, $^1J_{BH}$ = 89 Hz) **14**, 1.8 (t, *B*H$_2$, $^1J_{BH}$ = 96 Hz) **14**. Conversion by integration of ^{11}B NMR spectrum: 78.2 % **14**, 13.6 % **XXXVI**, 8.2 % **XLVII**.

3.5.1.4 NMR-Scale Synthesis of [Anilido-imine.Mg($NMe_2BH_2NMe_2BH_3$)] **15**

D_8-toluene (ca. 0.5 ml) was added to a solid mixture of **IX-Mg** (40 mg, 0.0575 mmol) and one molar equivalent of $Me_2NH.BH_3$ (6 mg, 0.115 mmol) and the solution sealed in a Youngs tap NMR tube before standing at RT for ca. 2 hours. ^{1}H NMR (d_8-tol, 298 K) δ = 1.07 - 1.12 (m, 12H, 2 x CH(C*H*$_3$)$_2$), 1.26 – 1.30 (m, 12H, 2 x CH(C*H*$_3$)$_2$), 1.81 (s, 3H, N(C*H*$_3$)), 2.17 (s, 3H, N(C*H*$_3$)), 2.23 (s, 3H, N(C*H*$_3$)), 2.31 (s, 3H, N(C*H*$_3$)), 3.13 (spt, m, 2H, C*H*(CH$_3$)$_2$), 3.33 (m, 2H, C*H*(CH$_3$)$_2$), 6.25 (m, 2H, arom-*H*), 6.75 (m, 1H, arom-*H*), 6.89 (m, 1H, arom-*H*), 7.13 (m, 3H, arom-*H*), 7.17 (m, 1H, arom-*H*), 7.19 – 7.23 (m, 2H, arom-*H*), 7.99 (s, 1H, C*H*=N). ^{13}C{^{1}H} NMR (d_8-tol, 298 K) δ = 23.4 (CH(*C*H$_3$)), 24.8 (CH(*C*H$_3$)), 26.3 (CH(*C*H$_3$)), 26.4 (CH(*C*H$_3$)), 28.8 (*C*H(CH$_3$)$_2$), 28.9 (*C*H(CH$_3$)$_2$), 29.0 (*C*H(CH$_3$)$_2$), 29.1 (*C*H(CH$_3$)$_2$), 32.4 (N(*C*H$_3$)), 46.1 (N(*C*H$_3$)), 48.3 (N(*C*H$_3$)), 52.8 (N(*C*H$_3$)), 112.8 (*C*$_6$H$_4$), 116.8 (*i*-N*C*$_6$H$_4$), 120.4 (*C*$_6$H$_4$), 124.3 (*m*-N*C*$_6$H$_4$), 124.8 (*p*-N*C*$_6$H$_4$), 127.0 (*m*-N*C*$_6$H$_4$), 127.4 (*p*-N*C*$_6$H$_4$), 133.8 (*C*$_6$H$_4$), 138.4 (*C*$_6$H$_4$), 141.9 (*o*-N*C*$_6$H$_4$), 144.7 (*o*-N*C*$_6$H$_4$), 147.9 (*i*-N*C*$_6$H$_4$), 149.5 (*i*-N*C*$_6$H$_4$), 161.8 (*i*-N=CH*C*$_6$H$_4$), 172.6 (*C*H=N). ^{11}B NMR (d_8-tol, 298 K) δ = –16.0 (q, *B*H$_3$, $^1J_{BH}$ = 86 Hz), 3.3 (t, *B*H$_2$, $^1J_{BH}$ = 99 Hz). A single crystal of **15** suitable for X-ray diffraction analysis was isolated from a concentrated toluene solution at –30 °C. Accurate CHN microanalysis was obtained for **15**. Anal. Calc. for $C_{35}H_{56}B_2MgN_4$: C: 72.63; H: 9.75; N: 9.68 %. Found: C: 72.62, 72.71; H: 9.82, 9.90; N: 9.71, 9.73 %.

Molecular Formula	$C_{35}H_{56}B_2MgN_4$
Formula Weight / g.mol^{-1}	578.77
Crystal System, Space Group	Orthorhombic P b c a
a, b, c / Å	11.8779(2), 15.2518(3), 38.9205(8)
α, β, γ / °	90, 90, 90
V / Å^3	7050.8(2)
Z	8
μ / mm^{-1}	0.079
ρ / g.cm^{-3}	1.090
θ range / °	3.02 – 25.01
Collected / Unique Reflections / R_{int}	47170 / 6150 / 0.1699
R_1, wR_2 [I > 2σ(I)]	R_1 = 0.0662, wR_2 = 0.1315
R_1, wR_2 (All data)	R_1 = 0.1310, wR_2 = 0.1570

3.5.1.5 NMR-Scale Synthesis of [Anilido-imine.Ca{$N(CH_2)_4BH_3$}] **16**

D_8-toluene (ca. 0.5 ml) was added to a solid mixture of **IX-Ca** (71 mg, 0.1 mmol) and one molar equivalent of $(CH_2)_4HN.BH_3$ (8.5 mg, 0.1 mmol) and the solution sealed in a Youngs tap NMR tube before standing at RT for ca. 2 hours. ^{1}H NMR (d_8-tol, 298 K) δ = 1.13 (d, J_{HH} = 6.8 Hz, 6H, $CH(CH_3)_2$), 1.16 (d, J_{HH} = 6.8 Hz, 6H, $CH(CH_3)_2$), ca. 1.25 (unresolved s, $CH(CH_3)_2$), ca. 1.24 (m, 4H, $N(CH_2CH_2)_2$), ca. 1.29 (d, J_{HH} = 6.8 Hz, $CH(CH_3)_2$), ca. 1.34 (m, 2H, $N(CH_2CH_2)_2$), 2.34 (br. s, 2H, $N(CH_2CH_2)_2$), 3.10 (m, 2H, $CH(CH_3)_2$), 3.27 (m, 2H, $CH(CH_3)_2$), 6.22 (m, 2H, arom-*H*), 6.82 (m, 1H, arom-*H*), 6.98 (m, 1H, arom-*H*), 7.14 (m, 3H, arom-*H*), 7.22 (t, $^3J_{HH}$ = 8.7 Hz, 1H, arom-*H*), 7.24 (m, 2H, arom-*H*), 7.95 (s, 1H, C*H*=N). $^{13}C\{^1H\}$ NMR (d_8-tol, 298 K) δ = 23.6 ($CH(CH_3)_2$), 25.3 ($CH(CH_3)_2$), 26.2 ($CH(CH_3)_2$), 26.4 ($CH(CH_3)_2$), 28.9 ($CH(CH_3)_2$), 29.3 ($CH(CH_3)_2$), 32.4 ($N(CH_2CH_2)_2$), 55.8 ($N(CH_2CH_2)_2$),, 112.0 (C_6H_4), 117.2 (*i*-NC_6H_4), 118.7 (C_6H_4), 124.3 (*m*-NC_6H_4), 125.3 (*p*-NC_6H_4), 125.8 (*m*-NC_6H_4), 126.5 (*p*-NC_6H_4), 133.8 (C_6H_4), 139.2 (C_6H_4), 141.0 (*o*-NC_6H_4), 144.2 (*o*-NC_6H_4), 146.3 (*i*-NC_6H_4), 149.7 (*i*-NC_6H_4), 159.6 (*i*-N=CHC_6H_4), 171.1 (*C*H=N). ^{11}B NMR (d_8-tol, 298 K) δ = –11.7 (q, BH_3, $^1J_{BH}$ = 86 Hz).

3.5.1.6 NMR-Scale Synthesis of [Anilido-imine.Mg{$N(CH_2)_4BH_2N(CH_2)_4BH_3$}] **17**

D_8-toluene (ca. 0.5 ml) was added to a solid mixture of **IX-Mg** (69.5 mg, 0.1 mmol) and two molar equivalents of $(CH_2)_4HN.BH_3$ (17 mg, 0.2 mmol) and the solution sealed in a Youngs tap NMR tube before standing at RT for ca. 2 hours. ^{1}H NMR (d_8-tol, 298 K) δ = 1.09 (d, J_{HH} = 7.2 Hz, 6H, $CH(CH_3)_2$), 1.11 (d, J_{HH} = 7.2 Hz, 6H, $CH(CH_3)_2$), coincidental ca. 1.28 (m, $CH(CH_3)_2$), coincidental ca. 1.30 (m, $CH(CH_3)_2$), ca. 1.38 (m, $N(CH_2)_4$), ca. 1.45 (m, 8H, $N(CH_2)_4$), 2.29 (br. s, 4H, $N(CH_2)_4$), ca. 3.13 (m, 2H, $CH(CH_3)_2$), ca. 3.34 (m, 2H, $CH(CH_3)_2$), 6.24 (m, 2H, arom-*H*), 6.75 (m, 1H, arom-*H*), 6.98 (m, 1H, arom-*H*), 7.13 (m, 3H, arom-*H*), 7.21 (t, J_{HH} = 8.7 Hz, 1H, arom-*H*), 7.23 (m, 2H, arom-*H*), 7.95 (s, 1H, C*H*=N). ^{13}C{^{1}H} NMR (d_8-tol, 298 K) δ = 24.5 ($CH(CH_3)_2$), 24.8 ($CH(CH_3)_2$), 26.2 ($CH(CH_3)_2$), 26.3 ($CH(CH_3)_2$), 28.9 ($CH(CH_3)_2$), 29.0 ($CH(CH_3)_2$), 32.5 ($N(CH_2)_4$), 56.1 ($N(CH_2)_4$), 112.7 (C_6H_4), 116.7 (*i*-NC_6H_4), 120.4 (C_6H_4), 124.2 (*m*-NC_6H_4), 124.8 (*p*-NC_6H_4), 125.4 (*m*-NC_6H_4), 126.9 (*p*-NC_6H_4), 133.7 (C_6H_4), 138.3 (C_6H_4), 141.8 (*o*-NC_6H_4), 144.7 (*o*-NC_6H_4), 148.1 (*i*-NC_6H_4), 149.8 (*i*-NC_6H_4), 161.7 (*i*-N=CHC_6H_4), 172.6 (*C*H=N). ^{11}B NMR (d_8-tol, 298 K) δ = –15.9 (q, BH_3, $^1J_{BH}$ = 89 Hz), 4.9 (t, BH_2, $^1J_{BH}$ = 99 Hz).

3.5.1.7 Catalytic NMR-Scale Reaction Between **IX-Ca** and $Me_2NH.BH_3$

D_8-toluene (ca. 0.5 ml) was added to a solid mixture of $Me_2NH.BH_3$ (59 mg, 1 mmol) and 5 mol % **IX-Ca** (35.5 mg, 0.05 mmol) and the solution sealed in a Youngs tap NMR tube before heating at 70 °C for ca. 74 hours. Conversion by integration of ^{11}B NMR spectrum: 8.3 % **XXXVI**, 3.0 % **XLVII**.

3.5.1.8 Catalytic NMR-Scale Reaction Between **IX-Mg** and $Me_2NH.BH_3$

D_8-toluene (ca. 0.5 ml) was added to a solid mixture of $Me_2NH.BH_3$ (59 mg, 1 mmol) and 5 mol % **IX-Mg** (34.8 mg, 0.05 mmol) and the solution sealed in a Youngs tap NMR tube before heating at 70 °C for ca. 19 hours. Conversion by integration of ^{11}B NMR spectrum: 92.9 % **XXXVI**, 2.0 % **XLVII**.

3.5.1.9 Catalytic NMR-Scale Reaction Between **IX-Ca** and $(CH_2)_4HN.BH_3$

D_8-toluene (ca. 0.5 ml) was added to a solid mixture of $(CH_2)_4HN.BH_3$ (85 mg, 1 mmol) and 5 mol % **IX-Ca** (35.5 mg, 0.05 mmol) and the solution sealed in a Youngs tap NMR tube before heating at 70 °C for ca. 90 hours. Conversion by integration of ^{11}B NMR spectrum: 17.2 % **XXXVI**, 5.3 % **XLVII**.

3.5.1.10 Catalytic NMR-Scale Reaction Between **IX-Mg** and $(CH_2)_4HN.BH_3$

D_8-toluene (ca. 0.5 ml) was added to a solid mixture of $(CH_2)_4HN.BH_3$ (85 mg, 1 mmol) and 5 mol % **IX-Mg** (34.8 mg, 0.05 mmol) and the solution sealed in a Youngs tap NMR tube before heating at 70 °C for ca. 90 hours. Conversion by integration of ^{11}B NMR spectrum: 27.0 % **XXXVI**, 4.6 % **XLVII**.

3.5.1.11 NMR-Scale Synthesis of [Anilido-imine.Sr(NMe_2BH_3)] **18**

D_8-toluene (ca. 0.5 ml) was added to a solid mixture of **IX-Sr** (83 mg, 0.1 mmol) and one molar equivalent of $Me_2NH.BH_3$ (5.9 mg, 0.1 mmol) and the solution sealed in a Youngs tap NMR tube before standing at RT for ca. 2 hours. ^1H NMR (d_8-tol, 298 K) δ = 1.14 (d, $^3J_{HH}$ = 7.2 Hz, 6H, $CH(CH_3)_2$), 1.18 (d, $^3J_{HH}$ = 7.2 Hz, 6H, $CH(CH_3)_2$), coincident with THF ca. 1.28 (m, $CH(CH_3)_2$), coincident with THF ca. 1.30 (m, $CH(CH_3)_2$), ca. 1.33 (s, 3H, $N(CH_3)$), 1.95 (br. s, 3H, $N(CH_3)$), 3.15 (m, 2H, $CH(CH_3)_2$), 3.29 (m, 2H, $CH(CH_3)_2$), 6.21 (m, 2H, arom-*H*), 6.83 (m, 1H, arom-*H*), 6.98 (m, 1H, arom-*H*), 7.14 (m, 3H, arom-*H*), 7.22 (t, $^3J_{HH}$ = 8.7 Hz, 1H, arom-*H*), 7.24 (m, 2H, arom-*H*), 8.01 (s, 1H, C*H*=N). $^{13}C\{^1H\}$ NMR (d_8-tol, 298 K) δ = 23.7 ($CH(CH_3)_2$), 25.4 ($CH(CH_3)_2$), 26.3 ($CH(CH_3)_2$), 26.5 ($CH(CH_3)_2$), 28.8 ($CH(CH_3)_2$), 29.3 ($CH(CH_3)_2$), 47.0 ($N(CH_3)_2$), 112.7 (C_6H_4), 117.5 (*i*-NC_6H_4), 118.9 (C_6H_4), 123.8 (*m*-NC_6H_4), 124.6 (*p*-NC_6H_4), 125.4 (*m*-NC_6H_4), 128.5 (*p*-NC_6H_4), 135.4 (C_6H_4), 139.6 (C_6H_4), 141.1 (*o*-NC_6H_4), 144.3 (*o*-NC_6H_4), 148.2 (*i*-NC_6H_4), 149.8 (*i*-NC_6H_4), 166.9 (*i*-N=CHC_6H_4), 171.0 (*C*H=N). ^{11}B NMR (d_8-tol, 298 K) δ = –12.1 (q, BH_3, $^1J_{BH}$ = 78 Hz).

3.5.1.12 Thermolysis of [Anilido-imine.Sr(NMe_2BH_3)] **18**

D_8-toluene (ca. 0.5 ml) was added to a solid mixture of **IX-Sr** (83 mg, 0.1 mmol) and one molar equivalent of $Me_2NH.BH_3$ (5.9 mg, 0.1 mmol) and the solution sealed in a Youngs tap NMR tube before standing at RT for ca. 2 hours. The formation of **18** was confirmed by ^{11}B NMR spectroscopy. The NMR tube was heated at 80 °C for ca. 19 hours. Comparison of ^{1}H and ^{11}B NMR spectra suggested formation of $B(NMe_2)_3$. Conversion by integration of ^{11}B NMR spectrum: 27.0 % $B(NMe_2)_3$.

3.5.1.13 NMR-Scale Synthesis of [Anilido-imine.Sr{$N(CH_2)_4BH_3$}] **20**

D_8-toluene (ca. 0.5 ml) was added to a solid mixture of **IX-Sr** (41.5 mg, 0.05 mmol) and one molar equivalent of $(CH_2)_4HN.BH_3$ (4 mg, 0.05 mmol) and the solution sealed in a Youngs tap NMR tube before standing at RT for ca. 2 hours. ^{1}H NMR (d_8-tol, 298 K) δ = 1.13 (d, J_{HH} = 6.8 Hz, 6H, $CH(CH_3)_2$), 1.17 (d, J_{HH} = 6.8 Hz, 6H, $CH(CH_3)_2$), ca. 1.25 (unresolved s, $CH(CH_3)_2$), ca. 1.27 (m, 4H, $N(CH_2CH_2)_2$), ca. 1.30 (d, J_{HH} = 6.8 Hz, $CH(CH_3)_2$), ca. 1.32 (m, 2H, $N(CH_2CH_2)_2$), 2.31 (br. s, 2H, $N(CH_2CH_2)_2$), 3.15 (m, 2H, $CH(CH_3)_2$), 3.31 (m, 2H, $CH(CH_3)_2$), 6.19 (m, 2H, arom-*H*), 6.81 (m, 1H, arom-*H*), 6.96 (m, 1H, arom-*H*), 7.13 (m, 3H, arom-*H*), 7.22 (t, $^{3}J_{HH}$ = 8.7 Hz, 1H, arom-*H*), 7.22 (m, 2H, arom-*H*), 7.99 (s, 1H, C*H*=N). $^{13}C\{^{1}H\}$ NMR (d_8-tol, 298 K) δ = 23.7 ($CH(CH_3)_2$), 25.2 ($CH(CH_3)_2$), 26.3 ($CH(CH_3)_2$), 26.6 ($CH(CH_3)_2$), 28.9 ($CH(CH_3)_2$), 29.4 ($CH(CH_3)_2$), 32.4 ($N(CH_2CH_2)_2$), 59.7 ($N(CH_2CH_2)_2$), 112.7 (C_6H_4), 117.2 (*i*-NC_6H_4), 118.9 (C_6H_4), 123.8 (*m*-NC_6H_4), 124.6 (*p*-NC_6H_4), 125.4 (*m*-NC_6H_4), 128.5 (*p*-NC_6H_4), 133.0 (C_6H_4), 138.8 (C_6H_4), 141.0 (*o*-NC_6H_4), 144.0 (*o*-NC_6H_4), 148.2 (*i*-NC_6H_4), 151.0 (*i*-NC_6H_4), 159.5 (*i*-$N{=}CHC_6H_4$), 167.0 (*C*H=N). ^{11}B NMR (d_8-tol, 298 K) δ = –10.9 (q, BH_3, $^{1}J_{BH}$ = 82 Hz).

3.5.1.14 Catalytic NMR-Scale Reaction Between **IX-Sr** and $Me_2NH.BH_3$

D_8-toluene (ca. 0.5 ml) was added to a solid mixture of $Me_2NH.BH_3$ (59 mg, 1 mmol) and 5 mol % **IX-Sr** (41.5 mg, 0.05 mmol) and the solution sealed in a Youngs tap NMR tube before heating at 70 °C for ca. 140 hours. Conversion by integration of ^{11}B NMR spectrum: After ca. 67 hours at 70 °C: 9.2 % **XXXVI**, 1.5 % **XLVII**; After ca. 140 hours at 70 °C: 9.8 % **XXXVI**, 4.5 % **XLVII**.

3.5.1.15 Catalytic NMR-Scale Reaction Between **IX-Sr** and $(CH_2)_4HN.BH_3$

D_8-toluene (ca. 0.5 ml) was added to a solid mixture of $(CH_2)_4HN.BH_3$ (85 mg, 1 mmol) and 5 mol % **IX-Sr** (41.5 mg, 0.05 mmol) and the solution sealed in a Youngs tap NMR tube before heating at 70 °C for ca. 66 hours. Conversion by integration of ^{11}B NMR spectrum: After ca. 66 hours at 70 °C: 9.2 % **XXXVI**, 1.5 % **XLVII**; After ca. 140 hours at 70 °C: 17.6 % **XXXVI**, 11.4 % **XLVII**.

3.5.1.16 Isolation of Sr(Anilido-Imine)$_2$ **21**

A single crystal of **21** suitable for X-ray diffraction analysis was isolated from a concentrated toluene solution of **20** at –30 °C, having undergone a proposed Schlenk-like redistribution in solution. ^1H NMR featured many coincidental resonances, hampering accurate integrations. ^1H NMR (d_8-tol, 298 K) δ = 1.12 (d, J_{HH} = 6.8 Hz, CH(CH_3)$_2$), 1.15 (d, J_{HH} = 6.8 Hz, CH(CH_3)$_2$), 1.20 (d, J_{HH} = 6.8 Hz, CH(CH_3)$_2$), coincidental resonance ca. 1.25 (unresolved s, CH(CH_3)$_2$), coincidental resonance ca. 1.28 (unresolved s, CH(CH_3)$_2$), ca. 2.80 (m, CH(CH$_3$)$_2$), 3.20 (m, CH(CH$_3$)$_2$), 3.38 (m, CH(CH$_3$)$_2$), 6.24 (m, 2H, arom-*H*), 6.76 (m, 1H, arom-*H*), 6.91 (m, 1H, arom-*H*), 7.12 (m, 3H, arom-*H*), 7.20 (m, 1H, arom-*H*), 7.22 (m, 2H, arom-*H*), 7.84 (br. s, 1H, C*H*=N). $^{13}C\{^1H\}$ NMR (d_8-tol, 298 K) δ = 23.8 (CH(*C*H$_3$)$_2$), 25.1 (CH(*C*H$_3$)$_2$), 26.3 (CH(*C*H$_3$)$_2$), 27.8 (CH(*C*H$_3$)$_2$), 28.9 (*C*H(CH$_3$)$_2$), 29.4 (*C*H(CH$_3$)$_2$), 110.9 (*C*$_6$H$_4$), 116.5 (*i*-N*C*$_6$H$_4$), 118.9 (*C*$_6$H$_4$), 123.8 (*m*-N*C*$_6$H$_4$), 124.6 (*p*-N*C*$_6$H$_4$), 125.4 (*m*-N*C*$_6$H$_4$), 128.4 (*p*-N*C*$_6$H$_4$), 133.6 (*C*$_6$H$_4$), 138.8 (*C*$_6$H$_4$), 141.3 (*o*-N*C*$_6$H$_4$), 143.3 (*o*-N*C*$_6$H$_4$), 148.0 (*i*-N*C*$_6$H$_4$), 151.7 (*i*-N*C*$_6$H$_4$), 159.4 (*i*-N=CH*C*$_6$H$_4$), 168.2 (*C*H=N). Accurate CHN microanalysis could not be obtained for **21**.

Molecular Formula	$C_{68}H_{92}SrN_4$
Formula Weight / g.mol^{-1}	1053.08
Crystal System, Space Group	Monoclinic P 1 2_1/n 1
a, b, c / Å	12.0828(3), 28.9778(9), 17.4632(4)
α, β, γ / °	90, 91.1544(18), 90
V / Å^3	6113.2(3)
Z	4
μ / mm^{-1}	0.924
ρ / g.cm^{-3}	1.144
θ range / °	3.57 – 27.44
Collected / Unique Reflections / R_{int}	70844 / 13268 / 0.1426
R_1, wR_2 [$I > 2\sigma(I)$]	$R_1 = 0.0650$, $wR_2 = 0.1169$
R_1, wR_2 (All data)	$R_1 = 0.1400$, $wR_2 = 0.1400$

3.5.1.17 Synthesis of Mg(Anilido-Imine)$_2$ **22**

THF (ca. 10ml) was added to solid anilido-imine ligand precursor (0.4877 g, 1.107 mmol) and 1.5 molar equivalents of KH (66.6 mg, 1.66 mmol) in a Schlenk tube and stirred at room temperature for ca. 18 hours, allowing dihydrogen gas to vent under an inert atmosphere. The deep orange solution was filtered to remove excess KH before being added to a ca. 10 ml THF slurry of half an equivalent of MgI_2 (0.154 g, 0.553 mmol) and stirred at room temperature for ca. 16 hrs. Filtration to remove KI and removal of solvent under vacuum provided an orange solid **22**. Yield: 0.652 g, 65.2 %. ^{1}H NMR featured many coincidental resonances, hampering accurate integrations. ^{1}H NMR (C_6D_6, 298 K) δ = 1.10 (d, J_{HH} = 7.2 Hz, CH(CH_3)$_2$), 1.13 (d, J_{HH} = 6.8 Hz, CH(CH_3)$_2$), 1.17 (d, J_{HH} = 7.2 Hz,, CH(CH_3)$_2$), ca. 1.20 (m, CH(CH_3)$_2$), ca. 1.25 (m, CH(CH_3)$_2$), 3.25 (m, 4H, CH(CH$_3$)$_2$), 3.38 (spt, 4H, CH(CH$_3$)$_2$), 6.24 (m, arom-*H*), 6.39 (m, arom-*H*), 6.54 (m, arom-*H*), 6.82 (m, arom-*H*), 6.93 (m, arom-*H*), 7.08 (m, arom-*H*), 7.15 (m, arom-*H*), 7.20 (m, arom-*H*), 7.23 (m, arom-*H*), 7.26 (m, arom-*H*), 7.99 (s, C*H*=N). ^{13}C{^{1}H} NMR (C_6D_6, 298 K) δ = 24.1 (CH(*C*H$_3$)$_2$), 25.2 (CH(*C*H$_3$)$_2$), 28.9 (*C*H(CH$_3$)$_2$), 29.3 (*C*H(CH$_3$)$_2$), 112.8 (*C*$_6$H$_4$), 116.3 (*i*-N*C*$_6$H$_4$), 117.1 (*i*-N*C*$_6$H$_4$), 121.5 (*C*$_6$H$_4$), 123.8 (*m*-N*C*$_6$H$_4$), 124.7 (*p*-N*C*$_6$H$_4$), 125.4 (*m*-N*C*$_6$H$_4$), 133.0 (*p*-N*C*$_6$H$_4$), 135.4 (*C*$_6$H$_4$), 138.8 (*o*-N*C*$_6$H$_4$),

148.2 (*i*-N*C*$_6$H$_4$), 149.7 (*i*-N*C*$_6$H$_4$), 150.9 (*i*-N=CH*C*$_6$H$_4$), 166.9 (*C*H=N). A single crystal of **22** suitable for X-ray diffraction analysis was isolated from a concentrated toluene solution at –30 °C. Accurate CHN microanalysis was obtained for **22** after removal of toluene from the crystal structure *in vacuo*. Anal. Calc. for $C_{62}H_{77}MgN_4$: C: 82.41; H: 8.70; N: 6.20 %. Found: C: 82.35, 82.40; H: 8.82, 8.79; N: 6.36, 6.28 %.

Molecular Formula	$C_{69}H_{85}MgN_4$
Formula Weight / g.mol^{-1}	994.72
Crystal System, Space Group	Monoclinic C 1 2/c
a, b, c / Å	18.5428(5), 15.9850(5), 21.6253(4)
α, β, γ / °	90, 114.103(2), 90
V / Å^3	5851.0(3)
Z	4
μ / mm^{-1}	0.075
ρ / g.cm^{-3}	1.129
θ range / °	5.64 – 27.51
Collected / Unique Reflections / R_{int}	32507 / 6606 / 0.0595
R_1, wR_2 [I > 2σ(I)]	R_1 = 0.0477, wR_2 = 0.1083
R_1, wR_2 (All data)	R_1 = 0.0748, wR_2 = 0.1222

3.5.1.18 Synthesis of Ca(Anilido-Imine)$_2$ **23**

THF (ca. 10ml) was added to solid anilido-imine ligand precursor (0.433 g, 0.983 mmol) and 1.5 molar equivalents of KH (59 mg, 1.47 mmol) in a Schlenk tube and stirred at room temperature for ca. 18 hours, allowing dihydrogen gas to vent under an inert atmosphere. The deep orange solution was filtered to remove excess KH before being added to a ca. 10 ml THF slurry of half an equivalent of CaI_2 (0.144 g, 0.492 mmol) and stirred at room temperature for ca. 18 hrs. Filtration to remove KI and removal of solvent under vacuum provided a red solid **23**. Yield: 0.619 g, 61.9 %. ^{1}H NMR featured many coincidental resonances, hampering accurate integrations. ^{1}H NMR (C_6D_6, 298 K) δ = 1.13 (d, J_{HH} = 6.8 Hz, CH(C*H*$_3$)$_2$), ca. 1.22 (m, CH(C*H*$_3$)$_2$), ca. 1.27 (m, CH(C*H*$_3$)$_2$), ca. 1.30 (m, CH(C*H*$_3$)$_2$), ca. 3.12 (m,

C*H*(CH_3)$_2$), 3.20 (m, C*H*(CH_3)$_2$), 3.36 (m, C*H*(CH_3)$_2$), 6.18 (m, arom-*H*), 6.21 (m, arom-*H*), 6.49 (m, arom-*H*), 6.62 (m, arom-*H*), 6.88 (m, arom-*H*), 6.91 (m, arom-*H*), 7.12 (m, arom-*H*), 7.13 (m, arom-*H*), 7.19 (m, arom-*H*), 7.20 (m, arom-*H*), 7.22 (m, arom-*H*), 7.76 (s, C*H*=N), 8.03 (s, C*H*=N). $^{13}C\{^1H\}$ NMR (C_6D_6, 298 K) δ = 24.1 (CH(*C*H_3)$_2$), 25.2 (CH(*C*H_3)$_2$), 28.1 (CH(*C*H_3)$_2$), 28.4 (CH(*C*H_3)$_2$), 28.9 (*C*H(CH_3)$_2$), 29.3 (*C*H(CH_3)$_2$), 112.7 (*C*$_6H_4$), 116.3 (*i*-N*C*$_6H_4$), 117.1 (*i*-N*C*$_6H_4$), 121.5 (*C*$_6H_4$), 123.8 (*m*-N*C*$_6H_4$), 124.2 (*p*-N*C*$_6H_4$), 124.7 (*p*-N*C*$_6H_4$), 125.4 (*m*-N*C*$_6H_4$), 132.6 (*p*-N*C*$_6H_4$), 133.0 (*p*-N*C*$_6H_4$), 135.4 (*C*$_6H_4$), 138.8 (*C*$_6H_4$), 139.7 (*o*-N*C*$_6H_4$), 142.2 (*o*-N*C*$_6H_4$), 148.2 (*i*-N*C*$_6H_4$), 149.7 (*i*-N*C*$_6H_4$), 158.3 (*i*-N=CH*C*$_6H_4$), 166.9 (*C*H=N), 167.5 (*C*H=N).

3.5.1.19 Synthesis of Ba(Anilido-Imine)$_2$ **24**

THF (ca. 10ml) was added to solid anilido-imine ligand precursor (0.433 g, 0.984 mmol) and 1.5 molar equivalents of KH (59.2 mg, 1.476 mmol) in a Schlenk tube and stirred at room temperature for ca. 18 hours, allowing dihydrogen gas to vent under an inert atmosphere. The deep orange solution was filtered to remove excess KH before being added to a ca. 10 ml THF slurry of half an equivalent of BaI_2 (0.192 g, 0.492 mmol) and stirred at room temperature for ca. 18 hrs. Filtration to remove KI and removal of solvent under vacuum provided a red solid **24**. Yield: 0.720 g, 72.0 %. ^1H NMR (d_8-tol, 298 K) δ = 1.12 (d, J_{HH} = 6.8 Hz, CH(C*H*$_3$)$_2$), 1.13 (d, J_{HH} = 6.8 Hz, CH(C*H*$_3$)$_2$), 1.20 (d, J_{HH} = 6.8 Hz, CH(C*H*$_3$)$_2$), 1.25 (d, J_{HH} = 6.8 Hz, CH(C*H*$_3$)$_2$), 3.22 (m, C*H*(CH_3)$_2$), 3.43 (m, C*H*(CH_3)$_2$), 6.28 (m, arom-*H*), 6.56 (m, arom-*H*), 6.81 (m, arom-*H*), 6.95 (m, arom-*H*), 7.00 (m, arom-*H*), 7.19 (m, arom-*H*), 7.28 (m, arom-*H*), 7.87 (s, C*H*=N). $^{13}C\{^1H\}$ NMR (d_8-tol, 298 K) δ = 24.1 (CH(*C*H_3)$_2$), 24.7 (CH(*C*H_3)$_2$), 25.3 (CH(*C*H_3)$_2$), 28.1 (CH(*C*H_3)$_2$), 28.4 (*C*H(CH_3)$_2$), 29.3 (*C*H(CH_3)$_2$), 107.2 (*C*$_6H_4$), 116.9 (*i*-N*C*$_6H_4$), 117.6 (*C*$_6H_4$), 121.4 (*C*$_6H_4$), 124.1 (*m*-N*C*$_6H_4$), 124.5 (*p*-N*C*$_6H_4$), 125.3 (*m*-N*C*$_6H_4$), 132.3 (*C*$_6H_4$), 139.8 (*C*$_6H_4$), 142.2 (*o*-N*C*$_6H_4$), 148.1 (*o*-N*C*$_6H_4$), 152.2 (*i*-N*C*$_6H_4$), 152.7 (*i*-N*C*$_6H_4$), 158.4 (*i*-N=CH*C*$_6H_4$), 168.5 (*C*H=N). Although single crystals of **24** suitable for X-ray diffraction analysis could not be isolated, an accurate CHN microanalysis was obtained. Anal. Calc. for $C_{62}H_{78}BaN_4$: C: 73.25; H: 7.73; N: 5.51 %. Found: C:73.30, 73.38; H: 7.86, 7.92; N: 5.54, 5.56 %.

3.5.1.20 Synthesis of [Anilido-Imine.CaI(THF)$_2$] **25**

THF (ca. 10ml) was added to solid anilido-imine ligand precursor (0.217 g, 0.492 mmol) and 1.5 molar equivalents of KH (29.6 mg, 0.738 mmol) in a Schlenk tube and stirred at room temperature for ca. 18 hours, allowing dihydrogen gas to vent under an inert atmosphere. The deep orange solution was filtered to remove excess KH before being added to a ca. 10 ml THF slurry of one molar equivalent of CaI_2 (0.192 g, 0.492 mmol) and stirred at room temperature for ca. 18 hrs. Filtration to remove KI and removal of solvent under vacuum provided a sparingly soluble yellow solid **25**. Yield: 0.305 g, 82.5 %. ^{1}H NMR (C_6D_6, 298 K) δ = 1.13 (d, J_{HH} = 6.8 Hz, CH(CH_3)$_2$), 1.19 (d, J_{HH} = 6.8 Hz, CH(CH_3)$_2$), 1.26 (m, THF), 1.33 (d, J_{HH} = 6.8 Hz, CH(CH_3)$_2$), 1.40 (d, J_{HH} = 6.8 Hz, CH(CH_3)$_2$), 3.27 (m, C*H*(CH$_3$)$_2$), coincident with THF ca. 3.42 (m, C*H*(CH$_3$)$_2$), 3.47 (m, THF), 6.26 (m, arom-*H*), 6.58 (m, arom-*H*), 6.84 (m, arom-*H*), 7.00 (m, arom-*H*), 7.18 (m, arom-*H*), 7.23 (m, arom-*H*), 8.05 (s, C*H*=N). ^{13}C{^{1}H} NMR (C_6D_6, 298 K) δ = 23.9 (CH(*C*H$_3$)$_2$), 24.1 (CH(*C*H$_3$)$_2$), 25.2 (CH(*C*H$_3$)$_2$), 25.7 (THF), 26.3 (CH(*C*H$_3$)$_2$), 28.7 (*C*H(CH$_3$)$_2$), 29.4 (*C*H(CH$_3$)$_2$), 69.5 (THF), 112.0 (*C*$_6$H$_4$), 117.3 (*i*-N*C*$_6$H$_4$), 119.1 (*C*$_6$H$_4$), 124.3 (*m*-N*C*$_6$H$_4$), 125.0 (*p*-N*C*$_6$H$_4$), 125.3 (*m*-N*C*$_6$H$_4$), 126.2 (*p*-N*C*$_6$H$_4$), 133.7 (*C*$_6$H$_4$), 139.4 (*C*$_6$H$_4$), 141.2 (*o*-N*C*$_6$H$_4$), 144.9 (*o*-N*C*$_6$H$_4$), 147.7 (*o*-N*C*$_6$H$_4$), 148.2 (*i*-N*C*$_6$H$_4$), 151.0 (*i*-N*C*$_6$H$_4$), 159.7 (*i*-N=CH*C*$_6$H$_4$), 171.8 (*C*H=N). A single crystal of **25** suitable for X-ray diffraction analysis was isolated from a concentrated toluene solution at –30 °C. Accurate CHN microanalysis was obtained for **25** after removal of benzene from the crystal structure *in vacuo*. Anal. Calc. for $C_{39}H_{55}CaIN_2O_2$: C: 62.39; H: 7.38; N: 3.73 %. Found: C: 62.13, 62.09; H: 7.38, 7.24; N: 3.53, 3.57 %.

Molecular Formula	$C_{51}H_{67}CaIN_2O_2$
Formula Weight / g.mol^{-1}	907.05
Crystal System, Space Group	Monoclinic P 1 2_1/a 1
a, b, c / Å	16.0904(2), 14.6758(2), 23016(2)
α, β, γ / °	90, 105.4036(7), 90
V / Å^3	4849.46(10)
Z	4
μ / mm^{-1}	0.804
ρ / g.cm^{-3}	1.242
θ range / °	2.95 – 27.48
Collected / Unique Reflections / R_{int}	81285 / 11087 / 0.0790
R_1, wR_2 [I > 2σ(I)]	R_1 = 0.0351, wR_2 = 0.0716
R_1, wR_2 (All data)	R_1 = 0.0565, wR_2 = 0.0828

3.5.1.21 Synthesis of [Anilido-Amido.SiHPh] **26**

D_8-toluene (ca. 0.5 ml) was added to a solid mixture of **IX-Sr** (41.5 mg, 0.05 mmol) and one molar equivalent of phenylsilane (5.4 mg, 0.05 mmol) and the solution sealed in a Youngs tap NMR tube before heating at 70 °C for ca. 16 hours. Yield: 17 mg, 62.3 %. ^{1}H NMR (d_8-tol, 298 K) δ = 0.52 (d, 3H, J_{HH} = 6.8 Hz, CH(CH_3)$_2$), 0.63 (d, 3H, J_{HH} = 6.8 Hz, CH(CH_3)$_2$), 0.86 (d, 3H, J_{HH} = 6.8 Hz, CH(CH_3)$_2$), 0.90 (d, 3H, J_{HH} = 6.8 Hz, CH(CH_3)$_2$), 0.97 (d, 3H, J_{HH} = 6.8 Hz, CH(CH_3)$_2$), 1.23 (d, J_{HH} = 6.8 Hz, CH(CH_3)$_2$), 1.28 (d, J_{HH} = 6.8 Hz, CH(CH_3)$_2$), 3.26 (m, CH(CH$_3$)$_2$), ca. 3.64 (m, CH(CH$_3$)$_2$), 3.97 (d, 1H, J_{HH} = 15.4 Hz, CH), 4.99 (d, 1H, J_{HH} = 15.4 Hz, CH), 5.39 (s, 1H, Si-H), 6.41 (m, arom-*H*), 6.67 (m, arom-*H*), 6.87 (m, arom-*H*), 6.94 (m, arom-*H*), 7.06 (m, arom-*H*), 7.13 (m, arom-*H*), 7.16 (m, arom-*H*), 7.41 (m, arom-*H*), 7.58 (m, arom-*H*). ^{13}C{^{1}H} NMR (d_8-tol, 298 K) δ = 23.5 (CH(*C*H$_3$)$_2$), 23.7 (CH(*C*H$_3$)$_2$), 24.5 (CH(*C*H$_3$)$_2$), 24.9 (CH(*C*H$_3$)$_2$), 25.5 (CH(*C*H$_3$)$_2$), 26.0 (CH(*C*H$_3$)$_2$), 26.1 (CH(*C*H$_3$)$_2$), 26.3 (CH(*C*H$_3$)$_2$), 28.8 (*C*H(CH$_3$)$_2$), 28.9 (*C*H(CH$_3$)$_2$), 29.0 (*C*H(CH$_3$)$_2$), 29.3 (*C*H(CH$_3$)$_2$), 56.6 (N*C*H$_2$C$_6$H$_4$), 118.9 (Ar), 119.9 (Ar), 124.8 (Ar), 125.3 (Ar), 127.4 (Ar), 128.2 (Ar), 130.3 (Ar), 130.6 (Ar), 135.2 (Ar), 136.0 (Ar), 136.4 (Ar), 137.1 (Ar), 143.1 (Ar), 148.1 (Ar), 148.7 (Ar), 149.1 (Ar), 149.4 (Ar), 149.5 (Ar). A single crystal of **26** suitable for X-ray diffraction analysis was

isolated from a concentrated toluene solution at –30 °C. Accurate CHN microanalysis was obtained for **26**. Anal. Calc. for $C_{37}H_{46}N_2Si$: C: 81.26; H: 8.48; N: 5.12 %. Found: C: 81.13, 81.17; H: 8.40, 8.47; N: 4.97, 5.01 %.

Molecular Formula	$C_{37}H_{46}N_2Si$
Formula Weight / g.mol^{-1}	546.85
Crystal System, Space Group	Monoclinic P 1 2_1/n 1
a, b, c / Å	10.6650(3), 19.1606(6), 16.3982(4)
α, β, γ / °	90, 105.9064(15), 90
V / Å^3	3222.63(16)
Z	4
μ / mm^{-1}	0.100
ρ / g.cm^{-3}	1.127
θ range / °	3.82 – 27.51
Collected / Unique Reflections / R_{int}	34809 / 7367 / 0.0800
R_1, wR_2 [$I > 2\sigma(I)$]	R_1 = 0.0478, wR_2 = 0.1128
R_1, wR_2 (All data)	R_1 = 0.0826, wR_2 = 0.1274

3.5.2 Stoichiometric Reactions of Group 1 Reagents with Amine Boranes

3.5.2.1 Synthesis of $K(NMe_2BH_3)$ **LXXIII** by Literature Methods[35, 36]

$K(NMe_2BH_3)$ **LXXIII** was synthesised by literature methods,[35, 36] producing an impure white solid on isolation from THF. Comparison of literature NMR chemical shifts for dimethylamine borane, **LXXIII** and compound **29** (Section 3.5.2.4) revealed ca. 40 - 50 % purity of **LXXIII** by integration of ^{11}B NMR spectroscopy.

3.5.2.2 Synthesis of $K(NMe_2BH_3)$ **LXXIII** Using $[K\{N(SiMe_3)_2\}]$[35, 36]

D_8-THF (ca. 0.5 ml) was added to a solid mixture of $[K\{N(SiMe_3)_2\}]$ (49.9 mg, 0.25 mmol) and one molar equivalent of $Me_2NH.BH_3$ (14.7 mg, 0.25 mmol) and the solution sealed in a Youngs tap NMR before standing at room temperature for ca. 2 hours. The formation of **LXXIII** was confirmed by multinuclear NMR spectroscopy and comparison to literature values of NMR chemical shifts.[35, 36]

3.5.2.3 Thermolysis of $K(NMe_2BH_3)$ **LXXIII**

D_8-THF (ca. 0.5 ml) was added to a solid mixture of $[K\{N(SiMe_3)_2\}]$ (49.9 mg, 0.25 mmol) and one molar equivalent of $Me_2NH.BH_3$ (14.7 mg, 0.25 mmol) and the solution sealed in a Youngs tap NMR before heating at 60 °C for ca. 24 hours. Comparison of literature NMR chemical shifts revealed conversion to ca. 32.5 % **XLVII**, in addition to ca. 10.4 % **27** and ca. 34.5 % **28**. ^{1}H NMR (d_8-THF, 298 K) δ = 0.09 (s, $Si(CH_3)_3)_2$ **27**), 0.17 (s, $Si(CH_3)_3)_2$ **28**), 1.47 (s, NH **28**), 2.12 (s, $N(CH_3)_2$ **28**), 2.30 (s, $N(CH_3)_2$ **27**). $^{13}C\{^1H\}$ NMR (d_8-THF, 298 K) δ = 3.31 ($(Si(CH_3)_3)_2$ **27**), 3.74 ($(Si(CH_3)_3)_2$ **28**), 41.2 ($N(CH_3)_2$). ^{11}B NMR (d_8-THF, 298 K) δ = –20.8 (q, BH_3 **28**), 33.8 (d, BH **27**).

3.5.2.4 Synthesis of $[K(NMe_2BH_2NMe_2BH_3)]$ **29**

Toluene (ca. 10ml) was added to solid $[K\{N(SiMe_3)_2\}]$ (1.296 g, 6.5 mmol) and two molar equivalents of $Me_2NH.BH_3$ (0.764 g, 13 mmol) in a Schlenk tube and stirred at room temperature for ca. 3 hours, allowing dihydrogen gas to vent under an inert atmosphere. Solvent and volatile $[HN\{Si(CH_3)_2\}_2]$ byproduct were removed under vacuum to provide a white solid **29**. ^{1}H NMR (d_8-tol, 298 K) δ = 2.31 (s, 6H, $N(CH_3)_2$), 2.76 (s, 6H, $N(CH_3)_2$). $^{13}C\{^1H\}$ NMR (d_8-tol, 298 K) δ = 47.2 ($N(CH_3)_2$), 49.4 ($N(CH_3)_2$). ^{11}B NMR (d_8-tol, 298 K) δ = –12.3 (br. s, BH_3), 2.6 (br. s, BH_2). A single crystal of **29** suitable for X-ray diffraction analysis was isolated from a concentrated toluene solution at –30 °C. Accurate CHN microanalysis could not be obtained for this reactive species.

Molecular Formula	$C_{20}H_{58}B_4K_2N_4O_3$
Formula Weight / g.mol^{-1}	524.14
Crystal System, Space Group	Monoclinic P $2_1/c$
a, b, c / Å	12.5404(3), 17.0035(4), 15.9352(4)
α, β, γ / °	90, 106.6308(12), 90
V / Å^3	3255.74(14)
Z	4
μ / mm^{-1}	0.316
ρ / g.cm^{-3}	1.069
θ range / °	3.626 – 26.051
Collected / Unique Reflections / R_{int}	61939 / 6385 / 0.0977
R_1, wR_2 [$I > 2\sigma(I)$]	$R_1 = 0.0424$, $wR_2 = 0.0962$
R_1, wR_2 (All data)	$R_1 = 0.0699$, $wR_2 = 0.1096$

3.5.2.5 NMR-Scale Synthesis of [Li(NMe$_2$BH$_2$NMe$_2$BH$_3$)] **30**

D_8-toluene (ca. 0.5 ml) was added to a solid mixture of [Li{N(SiMe$_3$)$_2$}] (88 mg, 0.5 mmol) and two molar equivalents of $Me_2NH.BH_3$ (58.8 mg, 1.0 mmol) and the solution sealed in a Youngs tap NMR before standing at room temperature for ca. 16 hours. ^{1}H NMR (d_8-tol, 298 K) δ = 2.25 (s, 6H, N(C*H*$_3$)$_2$), 2.41 (s, 6H, N(C*H*$_3$)$_2$). ^{13}C{^{1}H} NMR (d_8-tol, 298 K) δ = 45.9 (N(*C*H$_3$)$_2$), 53.0 (N(*C*H$_3$)$_2$). ^{11}B NMR (d_8-tol, 298 K) δ = –14.7 (q, *B*H$_3$, $^1J_{BH}$ = 89 Hz), 3.5 (t, *B*H$_2$, $^1J_{BH}$ = 98 Hz).

3.5.2.6 NMR-Scale Synthesis of [Na(NMe$_2$BH$_2$NMe$_2$BH$_3$)] **31**

D_8-toluene (ca. 0.5 ml) was added to a solid mixture of [Na{N(SiMe$_3$)$_2$}] (49.9 mg, 0.25 mmol) and two molar equivalents of $Me_2NH.BH_3$ (14.7 mg, 0.25 mmol) and the solution sealed in a Youngs tap NMR before standing at room temperature for ca. 2 hours. ^{1}H NMR (d_8-tol, 298 K) δ = 2.20 (s, 6H, N(C*H*$_3$)$_2$), 2.33 (s, 6H, N(C*H*$_3$)$_2$). ^{13}C{^{1}H} NMR (d_8-tol, 298 K) δ = 47.4 (N(*C*H$_3$)$_2$), 50.1 (N(*C*H$_3$)$_2$). ^{11}B NMR (d_8-tol, 298 K) δ = –14.7 (q, *B*H$_3$, $^1J_{BH}$ = 87 Hz, coincidental with BH_3 of Na[NMe_2BH_3]), 1.9 (t, *B*H$_2$, $^1J_{BH}$ = 98 Hz).

3.5.3 Stoichiometric Reactions of β-diketiminato-Magnesium Species with Amine Boranes

3.5.3.1 Synthesis of [β-diketiminato-Mg(NMe_2BH_3)] **32**

A THF (ca. 10 ml) solution of β-diketiminato $MgIEt_2O$ **LXXVI** (0.4 g, 0.61 mmol) was added to a THF solution of (ca. 5 ml) $K(NMe_2BH_3)$ **LXXIII** (59.1 mg, 0.61 mmol) in a Schlenk tube cooled to –76 °C and stirred at room temperature for ca. 18 hours. Filtration to remove KI and removal of solvent under vacuum provided a white solid **32**. ^{1}H NMR (d_8-tol, 298 K) δ = 1.10 (d, *J* = 6.8 Hz, 12H, $CH(CH_3)_2$), 1.21 (d, *J* = 7.2 Hz, 12H, $CH(CH_3)_2$), 1.56 (s, 6H, $NC(CH_3)$), 1.60 (s, 6H, $N(CH_3)_2$), 3.16 (m, 4H, $CH(CH_3)_2$), 4.78 (s, 1H, C-*H*), 6.95 – 7.16 (m, 6H, arom-*H*). $^{13}C\{^1H\}$ NMR (d_8-tol, 298 K) δ = 24.9 ($CH(CH_3)$), 25.1 ($CH(CH_3)$), 25.6 ($CH(CH_3)$), 28.5 ($NC(CH_3)$), 48.5 ($N(CH_3)$), 95.8 (*C*H), 124.1 (*m*-C_6H_3), 125.5 (*p*-C_6H_3), 142.8 (*o*-C_6H_3), 147.4 (i-C_6H_3), 168.9 (*C*N). ^{11}B NMR (d_8-tol, 298 K) δ = –11.8 (q, BH_3, $^1J_{BH}$ = 91 Hz). Decomposition of **32** upon storage prevented characterisation by X-ray diffraction analysis or CHN microanalysis.

3.5.3.2 NMR-Scale Reaction Between **32** and $Me_2NH.BH_3$

D_8-toluene (ca. 0.5 ml) was added to a solid mixture of [β-diketiminato-Mg(NMe_2BH_3)] **32** (43 mg, 0.075 mmol) and one molar equivalent of $Me_2NH.BH_3$ (4.4 mg, 0.075 mmol) and the solution sealed in a Youngs tap NMR before standing at room temperature for ca. 16 hours. Comparison of chemical shifts in the NMR spectra to literature values revealed conversion to: ca. 48.9 % **XXXVI** and ca. 9.5 % **XLVII**.

3.5.3.3 NMR-Scale Reaction Between **32** and $C_4H_8HN.BH_3$

D_8-toluene (ca. 0.5 ml) was added to a solid mixture of [β-diketiminato-Mg(NMe_2BH_3)] **32** (28.5 mg, 0.05 mmol) and one molar equivalent of $C_4H_8HN.BH_3$ (4.2 mg, 0.005 mmol) and the solution sealed in a Youngs tap NMR before standing at room temperature for ca. 16 hours. Comparison of chemical shifts in the NMR spectra to literature values revealed conversion to ca. 48 % of a combination of

XXXVI, **LIV** and unidentified species, appearing as coincidental triplet resonances in the ^{11}B NMR spectrum.

3.5.3.4 NMR-Scale Reaction Between **32** and $Me_2NH.BD_3$

D_8-toluene (ca. 0.5 ml) was added to a solid mixture of [β-diketiminato-$Mg(NMe_2BH_3)$] **32** (28.5 mg, 0.075 mmol) and one molar equivalent of $Me_2HN.BD_3$ (4.6 mg, 0.075 mmol) and the solution sealed in a Youngs tap NMR before standing at room temperature for ca. 16 hours. Comparison of chemical shifts in the NMR spectra to literature values revealed conversion to ca. 48 % of a combination of protio and deuterated **XXXVI** and ca. 8.5 % protio and deuterated **XLVII**.

3.5.3.5 NMR-Scale Reaction Between **32** and $^{i}Pr_2HN.BH_3$

D_8-toluene (ca. 0.5 ml) was added to a solid mixture of [β-diketiminato-$Mg(NMe_2BH_3)$] **32** (46 mg, 0.15 mmol) and one molar equivalent of $^{i}Pr_2HN.BH_3$ (17 mg, 0.15 mmol) and the solution sealed in a Youngs tap NMR before standing at room temperature for ca. 30 minutes. Comparison of chemical shifts in the NMR spectra to literature values revealed conversion to ca. 50 % **LVI**, ca. 13.3 % **XXXVI** and ca. 6.0 % **XLV** in addition to an uncharacterised BH_4^- species evident as an unresolved resonance at ca. –32 ppm in the ^{11}B NMR spectrum (ca. 2.1 %).

3.5.4 Synthesis of Heavier Alkaline Earth $[M(NMe_2BH_2NMe_2BH_3)_2]$Complexes

3.5.4.1 Synthesis of $[Ca(NMe_2BH_2NMe_2BH_3)_2]$ **33**

THF (ca. 10 ml) was added to a solid mixture of CaI_2 (0.191 g, 0.65 mmol) and two molar equivalents of $[K(NMe_2BH_2NMe_2BH_3)]$ **29** (0.2 g, 1.3 mmol), prepared via the method in Section 3.5.2.4, in a Schlenk and stirred at room temperature for ca. 6 hours. Filtration to remove KI and removal of solvent under vacuum provided a white solid. ^1H NMR (d_8-tol, 298 K) δ = 2.32 (s, 6H, N(CH_3)), 2.37 (s, 6H, N(CH_3)$_2$). $^{13}C\{^1H\}$ NMR (d_8-tol, 298 K) δ = 44.1 (N(*C*H_3)), 52.5 (N(*C*H_3)). ^{11}B NMR (d_8-tol, 298 K) δ = –11.8 (q, *B*H_3, $^1J_{BH}$ = 88 Hz), 1.8 (t, *B*H_2, $^1J_{BH}$ = 97 Hz). Integration of ^{11}B NMR spectrum suggested conversion to ca. 85 % **33**, with

formation of an unidentified species with a resonance coincidental with the BH_3 unit of **33**.

3.5.4.2 Synthesis of [Sr($NMe_2BH_2NMe_2BH_3$)$_2$] **34**

THF (ca. 10 ml) was added to a solid mixture of SrI_2 (0.161 g, 0.65 mmol) and two molar equivalents of [K($NMe_2BH_2NMe_2BH_3$)] **29** (0.2 g, 1.3 mmol), prepared via the method in Section 3.5.2.4, in a Schlenk and stirred at room temperature for ca. 6 hours. Filtration to remove KI and removal of solvent under vacuum provided a white solid. ^{1}H NMR (d_8-tol, 298 K) δ = 2.33 (s, 6H, N(CH_3)), 2.60 (s, 6H, N(CH_3)$_2$). ^{13}C{^{1}H} NMR (d_8-tol, 298 K) δ = 46.6 (N(*C*H$_3$)), 50.4 (N(*C*H$_3$)). ^{11}B NMR (d_8-tol, 298 K) δ = –12.6 (q, *B*H$_3$, $^1J_{BH}$ = 75 Hz), 2.4 (t, *B*H$_2$, $^1J_{BH}$ = 90 Hz). Integration of ^{11}B NMR spectrum suggested conversion to ca. 80 % **34**, with formation of an unidentified species with a resonance coincidental with the BH_3 unit of **34** and ca. 4.8 % **XLVII**.

3.5.4.3 Synthesis of [Ba($NMe_2BH_2NMe_2BH_3$)$_2$] **35**

THF (ca. 10 ml) was added to a solid mixture of BaI_2 (0.923 g, 2.36 mmol) and two molar equivalents of [K($NMe_2BH_2NMe_2BH_3$)] **29** (0.728 g, 4.72 mmol), prepared via the method in Section 3.5.2.4, in a Schlenk and stirred at room temperature for ca. 16 hours. Filtration to remove KI and removal of solvent under vacuum provided a white solid. ^{1}H NMR (d_8-tol, 298 K) δ = 2.42 (s, 6H, N(CH_3)), 2.59 (s, 6H, N(CH_3)$_2$). ^{13}C{^{1}H} NMR (d_8-tol, 298 K) δ = 45.1 (N(*C*H$_3$)), 51.8 (N(*C*H$_3$)). ^{11}B NMR (d_8-tol, 298 K) δ = –11.5 (q, *B*H$_3$, $^1J_{BH}$ = 87 Hz), 2.5 (t, *B*H$_2$, $^1J_{BH}$ = 87 Hz). Integration of ^{11}B NMR spectrum suggested conversion to ca. 51 % **35**, with formation of several unidentified species with resonances coincidental with the BH_3 unit of **35** and ca. 7.7 % **XLVII**.

3.5.4.4 Thermolysis of [Mg($NMe_2BH_2NMe_2BH_3$)$_2$] **XLVI**

D_8-toluene (ca. 0.5 ml) was added to a solid mixture of [Mg($NMe_2BH_2NMe_2BH_3$)$_2$] **XLVI** (12.7 mg, 0.05 mmol) and the solution sealed in a Youngs tap NMR before heating at 100 °C for ca. 4 hours. Comparison of chemical shifts in the NMR spectra to literature values revealed conversion to ca. 2.4 % **XXXVI**.

Addition of four equivalents of $Me_2NH.BH_3$ (11.8 mg, 0.2 mmol) to the solution, the Youngs tap NMR tube resealed and heated at 60 °C for ca. 4 hours, revealed conversion to ca. 7.3 % **XXXVI**.

3.5.5 Stoichiometric Reactions of β-diketiminato-Calcium Amidoboranes

3.5.5.1 Thermolysis of [β-diketiminato-Ca.(NMe_2BH_3)THF] **LXV**

D_8-toluene (ca. 0.5 ml) was added to a solid mixture of [β-diketiminato-Ca.(NMe_2BH_3)THF] **LXV** (29.4 mg, 0.05 mmol) and the solution sealed in a Youngs tap NMR before heating at 80 °C for ca. 12 hours. Inspection of the ^{11}B NMR spectrum revealed no reaction. The sample was heated at 100 °C for ca. 3 hours and 120 °C for ca. 3 hours with no sign of reaction.

3.5.5.2 NMR-Scale Synthesis of [β-diketiminato-Ca.($NMe_2BH_2NMe_2BH_3$)THF] **36**

D_8-toluene (ca. 0.5 ml) was added to a solid mixture of [β-diketiminato-Ca.(NMe_2BH_3)THF] **LXV** (29.4 mg, 0.05 mmol) and one molar equivalent of $Me_2NH.BH_3$ (2.9 mg, 0.05 mmol) and the solution sealed in a Youngs tap NMR before heating at 30 °C for ca. 72 hours. ^1H NMR (d_8-tol, 298 K) δ = 1.13 (d, J = 7.2 Hz, 12H, CH(CH_3)$_2$), 1.20 (d, J = 7.2 Hz, 12H, CH(CH_3)$_2$), 1.64 (s, 6H, N(CH_3)$_2$), 1.70 (s, 6H, NC(CH_3)), 1.80 (s, 3H, N(CH_3)), 1.92 (s, 3H, N(CH_3)), 3.26 (m, 4H, CH(CH$_3$)$_2$), 4.80 (s, 1H, C-H), 6.95 – 7.16 (m, 6H, arom-H). $^{13}C\{^1H\}$ NMR (d_8-tol, 298 K) δ = 23.8 (CH(*C*H$_3$)), 24.9 (CH(*C*H$_3$)), 25.8 (*C*H(CH$_3$)), 29.0 (NC(*C*H$_3$)), 44.2 (N(*C*H$_3$)), 51.5 (N(*C*H$_3$)), 94.7 (*C*H), 123.9 (*m*-*C*$_6$H$_3$), 126.2 (*p*-*C*$_6$H$_3$), 141.7 (*o*-*C*$_6$H$_3$), 143.1 (*i*-*C*$_6$H$_3$), 161.8 (*C*N). ^{11}B NMR (d_8-tol, 298 K) δ = –11.2 (q, *B*H$_3$, $^1J_{BH}$ = 99 Hz), 2.1 (t, *B*H$_2$, $^1J_{BH}$ = 96 Hz). A single crystal of **36** suitable for X-ray diffraction analysis was isolated from a concentrated toluene solution at –30 °C. Accurate CHN microanalysis was obtained for **36**. Anal. Calc. for $C_{37}H_{66}B_2CaN_4O$: C: 68.94; H: 10.32; N: 8.64 %. Found: C: 68.85, 68.87; H: 10.19, 10.26; N: 8.69, 8.69 %.

Molecular Formula	$C_{37}H_{66}B_2CaN_4O$
Formula Weight / g.mol^{-1}	644.64
Crystal System, Space Group	Monoclinic P 1 2_1/n 1
a, b, c / Å	12.3115(2), 18.1303(3), 18.4090(3)
α, β, γ / °	90, 100.9010(10), 90
V / Å^3	4034.95(11)
Z	4
μ / mm^{-1}	0.186
ρ / g.cm^{-3}	1.061
θ range / °	3.68 – 27.51
Collected / Unique Reflections / R_{int}	57988 / 9193 / 0.0549
R_1, wR_2 [I > 2σ(I)]	R_1 = 0.0396, wR_2 = 0.1030
R_1, wR_2 (All data)	R_1 = 0.0562, wR_2 = 0.1145

3.5.5.3 NMR-Scale Reaction Between [β-diketiminato-Ca.(NMe_2BH_3)THF] **LXV** and [$Me_3N.BH_3$]

D_8-toluene (ca. 0.5 ml) was added to a solid mixture of [β-diketiminato-Ca.(NMe_2BH_3)THF] **LXV** (29.4 mg, 0.05 mmol) and an equimolar quantity of $Me_3N.BH_3$ (3.6 mg, 0.05 mmol) and the solution sealed in a Youngs tap NMR before heating at 80 °C for ca. 65 hours. Comparison of chemical shifts in the NMR spectra to literature values revealed conversion to ca. 5.0 % **XXXVI** and ca. 3.3 % **XLVII**, in addition to uncharacterised BH_4^- (ca. 12.0 %) and [$NR_2BH_2NR_2BH_3$] (ca. 8.7 %) species.

3.5.5.4 NMR-Scale Reaction Between [β-diketiminato-Ca.(NMe_2BH_3)THF] **LXV** and $C_4H_8HN.BH_3$

D_8-toluene (ca. 0.5 ml) was added to a solid mixture of [β-diketiminato-Ca.(NMe_2BH_3)THF] **LXV** (58.8 mg, 0.1 mmol) and an equimolar quantity of $C_4H_8HN.BH_3$ (8.5 mg, 0.1 mmol) and the solution sealed in a Youngs tap NMR before heating at 30 °C for ca. 72 hours. Comparison of chemical shifts in the NMR spectra to literature values and those in this thesis revealed conversion to ca. 10.2 %

$[HB(NR_2)(NR'_2)]$ species observed as overlapping resonances and $[NR_2BH_2NR_2BH_3]$ species (ca. 24.4 %).

3.5.5.5 NMR-Scale Reaction Between [β-diketiminato-Ca.{$N(C_4H_8)BH_3$}THF] **LXVI** and $Me_2NH.BH_3$

D_8-toluene (ca. 0.5 ml) was added to a solid mixture of [β-diketiminato-Ca.{$N(C_4H_8)BH_3$}THF] **LXVI** (61.4 mg, 0.1 mmol) and an equimolar quantity of $Me_2HN.BH_3$ (5.9 mg, 0.1 mmol) and the solution sealed in a Youngs tap NMR before heating at 30 °C for ca. 72 hours. Comparison of chemical shifts in the NMR spectra to literature values and those in this thesis revealed conversion to ca. 13.1 % $[HB(NR_2)(NR'_2)]$ species observed as overlapping resonances and $[NR_2BH_2NR_2BH_3]$ species (ca. 24.3 %).

3.5.5.6 NMR-Scale Reaction Between [β-diketiminato-Ca.(NMe_2BH_3)THF] **LXV** and $Me_2NH.BD_3$

D_8-toluene (ca. 0.5 ml) was added to a solid mixture of [β-diketiminato-Ca.(NMe_2BH_3)THF] **LXV** (58.8 mg, 0.1 mmol) and an equimolar quantity of $Me_2HN.BD_3$ (6.2 mg, 0.1 mmol) and the solution sealed in a Youngs tap NMR before heating at 30 °C for ca. 72 hours. Comparison of chemical shifts in the NMR spectra to literature values and those in this thesis revealed conversion to ca. 10.5 % $[(H/D)B(NMe_2)_2]$ species and $[NR_2B(H/D)_2NR_2B(H/D)_3]$ species (ca. 26.3 %), observed as overlapping resonances.

3.5.5.7 Thermolysis of [β-diketiminato-Ca.($NMe_2BH_2NMe_2BH_3$)THF] **36**

D_8-toluene (ca. 0.5 ml) was added to [β-diketiminato-Ca.(NMe_2BH_3)THF] **LXV** (32.2 mg, 0.1 mmol) and the solution sealed in a Youngs tap NMR before heating at 80 °C for ca. 12 hours, monitored *in situ* by ^{11}B NMR spectroscopy. Comparison of chemical shifts in the NMR spectra to literature values identified boron-containing species, with reaction composition given by integration of ^{11}B NMR spectra.

3.5.5.8 Synthesis of a $[Me_2N\text{-}BH_2]_2$ **XXXVI** Stock Solution For Use in Experiments 3.5.5.9 – 3.5.5.11

D_8-toluene (0.5 ml) was added to a solid mixture of $Me_2HN.BH_3$ (29.4 mg, 0.5 mmol) and [β-diketiminato-Ca{$N(SiMe_3)_2$}THF] **VI** (17 mg, 0.025 mmol) and the solution sealed in a Youngs tap NMR before heating at 90 °C for ca. 47 hours. Comparison of chemical shifts in the NMR spectra to literature values identified conversion to ca. 73 % **XXXVI**.

3.5.5.9 NMR-Scale Reaction Between an Aliquot of $[Me_2N\text{-}BH_2]_2$ **XXXVI** Stock Solution and [β-diketiminato-Ca.(NMe_2BH_3)THF] **LXV**

D_8-toluene (ca. 0.5 ml) was added to a mixture of [β-diketiminato-Ca.(NMe_2BH_3)THF] **LXV** (29.4 mg, 0.05 mmol) and an aliquot of the $[Me_2N\text{-}BH_2]_2$ **XXXVI** stock solution prepared in 3.5.5.8 (68.5 μl, 0.05 mmol) and the solution sealed in a Youngs tap NMR before heating at 60 °C for ca. 48 hours, monitored periodically by ^{11}B NMR spectroscopy. Comparison of chemical shifts in the NMR spectra to literature values and those listed in this thesis identified the boron-containing species, with reaction composition given by integration of ^{11}B NMR spectra, the results of which are shown in Figures 3.25 and 3.26. The ^{11}B NMR spectra revealed two unidentified boron-containing compounds, **39** [(d_8-tol, 298 K) δ = –8.7 (q, BH_3, $^1J_{BH}$ = 91 Hz)] and **40** [(d_8-tol, 298 K) δ = 33.7 (d, *B*H, $^1J_{BH}$ = 132 Hz)].

3.5.5.10 NMR-Scale Reaction Between an Aliquot of $[Me_2N\text{-}BH_2]_2$ **XXXVI** Stock Solution and $Me_2NH.BH_3$

D_8-toluene (ca. 0.5 ml) was added to a mixture of $Me_2NH.BH_3$ (0.29 mg, 0.05 mmol) and an aliquot of the $[Me_2N\text{-}BH_2]_2$ **XXXVI** stock solution prepared in 3.5.5.8 (68.5 μl, 0.05 mmol) and the solution sealed in a Youngs tap NMR before heating at 60 °C for ca. 48 hours, monitored periodically by ^{11}B NMR spectroscopy. Comparison of chemical shifts in the NMR spectra to literature values identified the boron-containing species, with reaction composition given by integration of ^{11}B NMR spectra. No reaction was observed.

3.5.5.11 NMR-Scale Reaction Between an Aliquot of $[Me_2N\text{-}BH_2]_2$ **XXXVI** Stock Solution and Pyrrolidine

D_8-toluene (ca. 0.5 ml) was added to a mixture of pyrrolidine (4.1 µl, 0.05 mmol) and an aliquot of the $[Me_2N\text{-}BH_2]_2$ **XXXVI** stock solution prepared in 3.5.5.8 (68.5 µl, 0.05 mmol) and the solution sealed in a Youngs tap NMR before heating at 60 °C for ca. 48 hours, monitored periodically by ^{11}B NMR spectroscopy. Comparison of chemical shifts in the NMR spectra to literature values and those listed in this thesis identified the boron-containing species, with reaction composition given by integration of ^{11}B NMR spectra, the results of which are shown in Figure 3.27. Coincident resonances attributed to $[HB(NR)_2(NR'_2)]$ species were observed, in addition to unrevolved resonances in the baseline in the region ca. $\delta = -3$ to 6 ppm.

3.5.6 Catalytic NMR-Scale Reactions Between Group 1 Bis(trimethylsilyl)amides $[MN(SiMe_3)_2]$ (M = Li, Na, K) **LIX** and $Me_2NH.BH_3$

3.5.6.1 Catalytic NMR-Scale Reaction Between $[LiN(SiMe_3)_2]$ **LIX-Li** and $Me_2NH.BH_3$

D_8-toluene (ca. 0.5 ml) was added to a mixture of $Me_2NH.BH_3$ (58.8 mg, 1.0 mmol) and $[LiN(SiMe_3)_2]$ **LIX-Li** (8 mg, 0.05 mmol) and the solution sealed in a Youngs tap NMR before heating at 80 °C for ca. 124 hours, monitored periodically by ^{11}B NMR spectroscopy. Comparison of chemical shifts in the NMR spectra to literature values identified conversion to ca. 72.0 % **XXXVI**, ca. 5.0 % **XLVII** and ca 2.8 % **30**.

3.5.6.2 Catalytic NMR-Scale Reaction Between $[NaN(SiMe_3)_2]$ **LIX-Na** and $Me_2NH.BH_3$

D_8-toluene (ca. 0.5 ml) was added to a mixture of $Me_2NH.BH_3$ (58.8 mg, 1.0 mmol) and $[NaN(SiMe_3)_2]$ **LIX-Na** (9 mg, 0.05 mmol) and the solution sealed in a Youngs tap NMR before heating at 80 °C for ca. 172 hours, monitored periodically by ^{11}B NMR spectroscopy. Comparison of chemical shifts in the NMR spectra to literature values identified conversion to ca. 43.0 % **XXXVI**, ca. 2.8 % **XLVII** and ca 6.0 % **31**.

3.5.6.3 Catalytic NMR-Scale Reaction Between [$KN(SiMe_3)_2$] **LIX-K** and $Me_2NH.BH_3$

D_8-toluene (ca. 0.5 ml) was added to a mixture of $Me_2NH.BH_3$ (58.8 mg, 1.0 mmol) and [$KN(SiMe_3)_2$] **LIX-K** (10 mg, 0.05 mmol) and the solution sealed in a Youngs tap NMR before heating at 80 °C for ca. 172 hours, monitored periodically by ^{11}B NMR spectroscopy. Comparison of chemical shifts in the NMR spectra to literature values identified conversion to ca. 43.0 % **XXXVI**, ca. 6.0 % **XLVII** and ca 4.4 % **29**.

3.5.7 NMR-Scale Reactions Between Calcium Reagents and $^tBuH_2N.BH_3$

3.5.7.1 Stoichiometric NMR-Scale Reaction Between [β-diketiminato-Ca{$N(SiMe_3)_2$}THF] **VI** and $^tBuH_2N.BH_3$ to Synthesise **42**

D_8-toluene (ca. 0.5 ml) was added to a solid mixture of [β-diketiminato-Ca.{$N(SiMe_3)_2$}THF] **VI** (103.4 mg, 0.15 mmol) and one molar equivalent of $^tBuH_2N.BH_3$ (13.0 mg, 0.15 mmol) and the solution sealed in a Youngs tap NMR before standing at room temperature for ca. 30 minutes. ^1H NMR (d_8-tol, 298 K) δ = 0.80 (s, 9H, $N(CH_3)_3$), 1.21 (d, J = 6.8 Hz, 12H, $CH(CH_3)_2$), 1.30 (d, J = 6.8 Hz, 12H, $CH(CH_3)_2$), 1.55 (s, 1H, N*H*), 1.65 (s, 6H, $NC(CH_3)$), 3.19 (m, 4H, $CH(CH_3)_2$), 4.75 (s, 1H, C-*H*), 6.95 – 7.16 (m, 6H, arom-*H*). $^{13}C\{^1H\}$ NMR (d_8-tol, 298 K) δ = 25.1 ($CH(CH_3)$), 25.2 ($CH(CH_3)$), 25.4 ($CH(CH_3)$), 25.9 ($CH(CH_3)$), 28.8 ($NC(CH_3)_3$), 28.9 ($NC(CH_3)$), 31.4 ($NC(CH_3)_3$), 94.1 (*C*H), 124.3 (*m*-C_6H_3), 125.1 (*p*-C_6H_3), 141.9 (*o*-C_6H_3), 147.4 (*i*-C_6H_3), 166.3 (*C*N). ^{11}B NMR (d_8-tol, 298 K) δ = –17.3 (q, BH_3, $^1J_{BH}$ = 80 Hz). A single crystal of **42** suitable for X-ray diffraction analysis was isolated from a concentrated toluene solution at –30 °C. Accurate CHN microanalysis was obtained for **42**. Anal. Calc. for $C_{37}H_{62}BCaN_3O$: C: 72.17; H: 10.15; N: 6.82 %. Found: C: 72.30, 72.32; H: 10.00, 10.06; N: 6.77, 6.75 %.

Molecular Formula	$C_{37}H_{62}BCaN_3O$
Formula Weight / g.mol^{-1}	615.79
Crystal System, Space Group	Orthorhombic P b c 2_1
a, b, c / Å	13.0933(5), 16.2620(5), 17.8153(5)
α, β, γ / °	90, 90, 90
V / Å^3	3793.3(2)
Z	4
μ / mm^{-1}	0.195
ρ / g.cm^{-3}	1.078
θ range / °	4.97 – 25.09
Collected / Unique Reflections / R_{int}	38706 / 6651 / 0.1174
R_1, wR_2 [$I > 2\sigma(I)$]	$R_1 = 0.0535$, $wR_2 = 0.1306$
R_1, wR_2 (All data)	$R_1 = 0.0739$, $wR_2 = 0.1461$

3.5.7.2 Stoichiometric NMR-Scale Reaction Between [β-diketiminato-Mg.^{n}Bu] **XV** and ^{t}BuH_2N.BH_3

D_8-toluene (ca. 0.5 ml) was added to a solid mixture of [β-diketiminato-Mg.^{n}Bu] **XV** (49.9 mg, 0.1 mmol) and two molar equivalents of ^{t}BuH_2N.BH_3 (17.4 mg, 0.2 mmol) and the solution sealed in a Youngs tap NMR before standing at room temperature for ca. 30 minutes. Inspection of the ^{11}B NMR spectrum revealed conversion to ca. 7.0 % **43**, an uncharacterised compound evidenced by an unresolved resonance at δ = –8.8 ppm, coincidental BH_3 resonances with the BH_3 resonance of ^{t}BuH_2N.BH_3, and unresolved resonances at δ = 28 – 43 ppm (ca. 32.6 %).

3.5.7.3 Catalytic NMR-Scale Reaction Between [β-diketiminato-Ca{N(SiMe_3)$_2$}THF] **VI** and ^{t}BuH_2N.BH_3

D_8-toluene (0.5 ml) was added to a solid mixture of ^{t}BuH_2N.BH_3 (87.0 mg, 1 mmol) and [β-diketiminato-Ca{N(SiMe_3)$_2$}THF] **VI** (29.4 mg, 0.05 mmol) and the solution sealed in a Youngs tap NMR before heating at 60 °C for ca. 138 hours. ^{1}H NMR (C_6D_6, 298 K) δ = 0.98 (s, C(C*H*$_3$)$_3$ **47**), 1.00 (s, C(C*H*$_3$)$_3$ **47**), 1.02 (s, N*H*), 1.03 (s, N*H*), 1.14 (s, C(C*H*$_3$)$_3$ **46**), 1.20 (s, N*H*), 1.38 (s, C(C*H*$_3$)$_3$ **49**). ^{13}C{^{1}H} NMR (C_6D_6,

298 K) δ = 27.3 (C(*C*H$_3$)$_3$ **47**), 27.6 (C(*C*H$_3$)$_3$ **47**), 33.7 (C(*C*H$_3$)$_3$ **46**), 34.4 (C(*C*H$_3$)$_3$ **49**). ^{11}B NMR (d$_8$-tol, 298 K) δ = –22.8 (td, $^1J_{BH}$ = 99Hz, $^2J_{BH}$ = 31 Hz, B*H*$_2$(μ-*H*)B*H*$_2$ **48**), –6.1 (t, J_{BH} = 109 Hz, B*H*$_2$ **47**), 29.1 (d, J_{BH} = 126 Hz, B*H* **46**), 38.2 (t, J_{BH} = 128 Hz, B*H*$_2$ **45**). Approximate conversion by integration of ^{11}B NMR spectrum: 4.3 % **45**, 13.4 % **46**, 45.2 % **47**, 3.2 % **48**, 20.1 % **49**.

A single crystal of **47** suitable for X-ray diffraction analysis was isolated from a concentrated toluene solution at –30 °C. Accurate CHN microanalysis was obtained for **47**. Anal. Calc. for $C_8H_{24}B_2N_2$: C: 56.55; H: 14.24; N: 16.49 %. Found: C: 56.67, 56.69; H: 14.34, 14.38; N: 16.58, 16.55 %.

Molecular Formula	$C_8H_{24}B_2N_2$
Formula Weight / g.mol^{-1}	169.91
Crystal System, Space Group	Orthorhombic P b c a
a, b, c / Å	9.3985(4), 7.3499(4), 17.0003(8)
α, β, γ / °	90, 90, 90
V / Å^3	1174.35(10)
Z	4
μ / mm^{-1}	0.054
ρ / g.cm^{-3}	0.961
θ range / °	5.03 – 27.44
Collected / Unique Reflections / R_{int}	21086 / 1330 / 0.1405
R_1, wR_2 [I > 2σ(I)]	R_1 = 0.0688, wR_2 = 0.1667
R_1, wR_2 (All data)	R_1 = 0.0936, wR_2 = 0.1833

X-ray diffraction analysis of crystalline precipitate isolated from inside the NMR tube yielded the solid-state structure of **50**. Accurate CHN microanalysis could not be obtained for this compound. Compound **50** could not be solubilised, however, the ^{11}B NMR spectrum showed a quintet at δ = –30.6 ppm, J_{BH} = 82 Hz, which could be the BH_4^- unit of **50**.

Molecular Formula	$C_4H_{16}B_2CaO$
Formula Weight / g.mol^{-1}	141.87
Crystal System, Space Group	Monoclinic P 2_1 n
a, b, c / Å	4.3659(3), 12.3208(8), 15.5787(10)
α, β, γ / °	90, 92.090(4), 90
V / Å^3	837.44(10)
Z	4
μ / mm^{-1}	0.665
ρ / g.cm^{-3}	1.125
θ range / °	3.56 – 25.04
Collected / Unique Reflections / R_{int}	11878 / 11878 / 0.0000
R_1, wR_2 [$I > 2\sigma(I)$]	R_1 = 0.1241, wR_2 = 0.3206
R_1, wR_2 (All data)	R_1 = 0.1557, wR_2 = 0.3430

3.5.7.4 Catalytic NMR-Scale Reaction Between $[Ca\{N(SiMe_3)_2\}_2]$ **V-Ca** and $^tBuH_2N.BH_3$

D_8-toluene (0.5 ml) was added to a solid mixture of $^tBuH_2N.BH_3$ (87.0 mg, 1 mmol) and $[Ca\{N(SiMe_3)_2]_2$ **V-Ca** (18 mg, 0.05 mmol) and the solution sealed in a Youngs tap NMR before heating at 70 °C for ca. 66 hours. ^{1}H NMR (C_6D_6, 298 K) δ = 1.28 (s, 1H, N*H*), 1.38 (s, 9H, C(C*H*$_3$)$_3$), ca. 5.1 (v. br. d, 1H, B*H*). ^{13}C{^{1}H} NMR (C_6D_6, 298 K) δ = 34.4 (C(*C*H$_3$)$_3$). ^{11}B NMR (d_8-tol, 298 K) δ = 34.4 (br. s, *B*H). A single crystal of **49** suitable for X-ray diffraction analysis was isolated from a concentrated toluene solution at –30 °C. Accurate CHN microanalysis was obtained for **49**. Anal. Calc. for $C_{12}H_{30}B_3N_3$: C: 57.92; H: 12.15; N: 16.89 %. Found: C: 57.90, 57.98; H: 11.98, 11.97; N: 16.78, 16.82 %.

Molecular Formula	$C_{12}H_{30}B_3N_3$
Formula Weight / g.mol^{-1}	248.82
Crystal System, Space Group	Triclinic P 1^-
a, b, c / Å	9.863(2), 9.9106(18), 10.587(2)
α, β, γ / °	96.748(12), 103.522(10), 119.493(8)
V / Å^3	842.1(3)
Z	2
μ / mm^{-1}	0.056
ρ / g.cm^{-3}	0.981
θ range / °	3.04 – 25.03
Collected / Unique Reflections / R_{int}	13134 / 2925 / 0.1850
R_1, wR_2 [$I > 2\sigma(I)$]	$R_1 = 0.1893$, $wR_2 = 0.4876$
R_1, wR_2 (All data)	$R_1 = 0.2711$, $wR_2 = 0.5174$

3.5.8 Kinetic Characterisation of Dehydrocoupling of $Me_2HN.BH$ with d^0 Reagents

General Experimental Procedure

All kinetic experiments were carried out on an NMR-scale in Youngs tap NMR tubes. Compounds were weighed out and added to 0.5 ml d_8-toluene inside a glovebox under an inert argon atmosphere, before being sealed inside a Youngs tap NMR tube. On removal from the glovebox the sample was frozen in liquid nitrogen and thawed before insertion into the NMR spectrometer. Reactions were monitored by ^{11}B NMR spectroscopy on a Bruker AV500 spectrometer, with concentration of boron-containing reaction species determined using integration across all boron-containing species. Boron-containing species were identified using values of chemical shift obtained from literature reports of known compounds and species described in this thesis. Reactions requiring elevated temperatures were heated inside the NMR spectrometer and equilibrated for ca. 10 minutes prior to use. The internal temperature of the NMR spectrometer deviated from the temperature at which it was set by a relationship characterised using methanol chemical shifts.[62] The resulting calibration curve was utilised to set the NMR spectrometer to a temperature at which the desired internal temperature for heating of the NMR tube

was achieved. Reactions requiring prolonged heating times (> ca. 13 hours) were heated in thermostatically controlled oil baths, monitored periodically by ^{11}B NMR spectroscopy, with spectra taken on a Bruker AV300 spectrometer. Kinetic experiments were conducted until 3 half-lives had passed, unless the reaction prohibited this (e.g. in the case of deactivation of catalyst). The method of initial rates was utilised to characterise reactions exhibiting more complex behaviour and the initial 10 % of the reaction was monitored.

Equations Used for Calculations:

$r = k\,[\text{Amine borane}]^{\alpha}\,[\text{Catalyst}]^{\beta}$

(a) Zero-order kinetics:

$r = k = -d[\text{Amine borane}]/dt$

(**Eqn 1**) $[\text{Amine borane}]_t = -kt + [\text{Amine borane}]_0$

(b) First-order kinetics:

$r = k[\text{Amine borane}] = -d[\text{Amine borane}]/dt$

(**Eqn 2**) $\ln[\text{Amine borane}]_t = -kt + \ln[\text{Amine borane}]_0$

(c) Pseudo first-order kinetics:

(**Eqn 3**) When [Y] is in excess, $r = k\,[X]^{\alpha}\,[Y]^{\beta} = k'[X]^{\alpha}$

(c) Second-order kinetics:

$r = -d[\text{Amine borane}]/dt = 2k[\text{Amine borane}]^2$

(**Eqn 4**) $(1/[\text{Amine borane}]_t) = (1/[\text{Amine borane}]_0) + kt$

Kinetic Isotope Effect (KIE):

(**Eqn 5**) KIE = k_H/k_D

Where:

k_H = Reaction rate constant for protio substrate

k_D = Reaction rate constant for deuterated substrate

3.5.9 Kinetic Characterisation of Stoichiometric Reactions of d^0 Amidoboranes

3.5.9.1 Stoichiometric Reactions Between [β-diketiminato-Ca.(NMe_2BH_3)THF] **LXV** and (i) [$Me_2HN.BH_3$], (ii) [$Me_2HN.BD_3$] and (iii) [$Me_2DN.BH_3$] to Determine Values of Kinetic Isotope Effect at 308 K

In an attempt to determine values of kinetic isototpe effect (KIE) isolated experiments were conducted similar to the method adopted by Manners. D_8-toluene (0.5 ml) was added to a solid mixture of [β-diketiminato-Ca.(NMe_2BH_3)THF] (58.8 mg, 0.1 mmol) and one molar equivalent of (i) $Me_2NH.BH_3$ (5.9 mg, 0.1 mmol), (ii) $Me_2NH.BD_3$ **LXXXII** (6.1 mg, 0.1 mmol), or (iii) $Me_2ND.BH_3$ **XCII** (6.0 mg, 0.1 mmol), and each solution sealed in a Youngs tap NMR tube before the reactions at 308 K were monitored using a Bruker AV400 spectrometer. The results of these reactions are shown in Figure 3.35, a second-order kinetic data plot for the consumption of amine borane. Equation **Eqn 9** was used to calculate KIE values.

3.5.9.2 Pseudo First-Order Stoichiometric Reactions Between [β-diketiminato-Ca.(NMe_2BH_3)THF] **LXV** and Additional Equivalents of [$Me_2HN.BH_3$] at 333 K for Determination of Partial Rate Order of [DMAB]

A mixture of [β-diketiminato-Ca.(NMe_2BH_3)THF] **LXV** (29.4 mg, 0.05 mmol) and (i) one (0.05 mmol, 50 μl of a $1x10^{-3}$ $mol.ml^{-1}$ stock solution), (ii) two (0.10 mmol, 100 μl of a $1x10^{-3}$ $mol.ml^{-1}$ stock solution), (iii) three (0.15 mmol, 150 μl of a $1x10^{-3}$ $mol.ml^{-1}$ stock solution), (iv) four (0.20 mmol, 200 μl of a $1x10^{-3}$ $mol.ml^{-1}$ stock solution) and (v) five (0.25 mmol, 250 μl of a $1x10^{-3}$ $mol.ml^{-1}$ stock solution) molar equivalents of $Me_2NH.BH_3$ was made up to 0.5 ml with d_8-toluene, and the solution

sealed in a Youngs tap NMR tube before the reaction at 333 K was monitored using a Bruker AV400 spectrometer. The results of these reactions are shown in Figure 3.36, a zero-order kinetic data plot for the consumption of amine borane.

3.5.9.3 Pseudo First-Order Stoichiometric Reactions Between [β-diketiminato-Ca.(NMe_2BH_3)THF] **LXV** and An Excess of [$Me_2HN.BH_3$] at 343 K for Determination of Partial Rate Order of [**LXV**]

D_8-toluene (0.5 ml) was added to a solid mixture of [β-diketiminato-Ca.(NMe_2BH_3)THF] **LXV** and an excess of $Me_2HN.BH_3$ according to Table 3.6.

	[β-diketiminato-Ca.(NMe_2BH_3)THF] **LXV**	[$Me_2HN.BH_3$]
(i)	29.4 mg, 0.05 mmol	20 equivalents; 59 mg, 1 mmol
(ii)	58.8 mg, 0.10 mmol	10 equivalents; 59 mg, 1 mmol
(iii)	88.2 mg, 0.15 mmol	6.67 equivalents; 59 mg, 1 mmol
(iv)	117.5 mg, 0.20 mmol	5 equivalents; 59 mg, 1 mmol

Table 3.6: Experiments at 343 K between various concentrations of [β-diketiminato-Ca.(NMe_2BH_3)THF] **LXV** and [$Me_2NH.BH_3$] to determine a partial orders of reaction for [β-diketiminato-Ca.(NMe_2BH_3)THF].

Each solution was sealed in a Youngs tap NMR tube before the reaction at 343 K was monitored using a Bruker AV400 spectrometer. The results of these reactions are shown in Figure 3.37, a zero-order kinetic data plot for the consumption of amine borane.

3.5.9.4 Pseudo First-Order Stoichiometric Reactions Between [β-diketiminato-Ca.($NMe_2BH_2NMe_2BH_3$)THF] **36** and Additional Equivalents of [$Me_2HN.BH_3$] at 343 K for Determination of Partial Rate Order of [DMAB]

A mixture of [β-diketiminato-Ca.($NMe_2BH_2NMe_2BH_3$)THF] **36** (31.5 mg, 0.05 mmol) and (i) one (2.9 mg, 0.05 mmol), (ii) two (5.9 mg, 0.10 mmol), (iii) three (8.8 mg, 0.15 mmol) and (iv) four (11.8 mg, 0.20 mmol) molar equivalents of $Me_2NH.BH_3$ was made up to 0.5 ml with d_8-toluene, and the solution sealed in a

Youngs tap NMR tube before the reaction at 343 K was monitored using a Bruker AV400 spectrometer. The results of these reactions are shown in Figure 3.38, a zero-order kinetic data plot for the consumption of amine borane.

3.5.9.5 Stoichiometric Reaction Between [β-diketiminato-Mg.($NMe_2BH_2NMe_2BH_3$)] **XLV** and [$Me_2HN.BH_3$] at 343 K

D_8-toluene (0.5 ml) was added to a solid mixture of [β-diketiminato-Mg.($NMe_2BH_2NMe_2BH_3$)] **XLV** (27.8 mg, 0.05 mmol) and one molar equivalent of $Me_2NH.BH_3$ (2.9 mg, 0.05 mmol), and the solution sealed in a Youngs tap NMR tube before the reaction at 343 K was monitored using a Bruker AV500 spectrometer by the method of initial rates. The results of this reaction are shown in Figure 3.39, a zero-order kinetic data plot for boron-containing species during the reaction.

3.5.9.6 Stoichiometric Reaction Between [Mg.($NMe_2BH_2NMe_2BH_3$)$_2$] **XLVI** and [$Me_2HN.BH_3$] at 343 K Using the Method of Initial Rates

D_8-toluene (0.5 ml) was added to a solid mixture of [Mg.($NMe_2BH_2NMe_2BH_3$)$_2$] **XLVI** (12.7 mg, 0.05 mmol) and one molar equivalent of $Me_2NH.BH_3$ (2.9 mg, 0.05 mmol), and the solution sealed in a Youngs tap NMR tube before the reaction at 343 K was monitored using a Bruker AV500 spectrometer by the method of initial rates. The results of this reaction are shown in Figure 3.40, a zero-order kinetic data plot for boron-containing species during the reaction and Figure 3.41, a first-order kinetic data plot for the consumption of $Me_2NH.BH_3$ and formation of $HB(NMe_2)_2$.

3.5.9.7 Stoichiometric Reaction Between [Mg.($NMe_2BH_2NMe_2BH_3$)$_2$] **XLVI** and [$Me_2HN.BH_3$] at 80 °C Using the Method of Initial Rates

D_8-toluene (0.5 ml) was added to a solid mixture of [Mg.($NMe_2BH_2NMe_2BH_3$)$_2$] **XLVI** (12.7 mg, 0.05 mmol) and four molar equivalents of $Me_2NH.BH_3$ (11.8 mg, 0.2 mmol), and the solution sealed in a Youngs tap NMR before the NMR tube was heated in a thermostatically controlled oil bath at 353 K for ca. 24 hours. The reaction was monitored periodically by ^{11}B NMR spectroscopy on a Bruker AV300 spectrometer. Integration of ^{11}B NMR spectra revealed conversion to ca. 5.0% **XLVII**, 43.5% **XXXVI** and 19.8% **XLVI**.

3.6 References for Chapter 3

1. M. S. Hill, G. Kociok-Köhn and T. P. Robinson, *Chem. Commun. (Camb)*, 2010, **46**, 7587-7589.
2. D. J. Liptrot, M. S. Hill, M. F. Mahon and D. J. MacDougall, *Chem.- Eur. J.* 2010, **16**, 8508-8515.
3. M. S. Hill, M. Hodgson, D. J. Liptrot and M. F. Mahon, *Dalton Trans.*, 2011, **40**, 7783-7790.
4. S. Harder, *Organometallics*, 2002, **21**, 3782-3787.
5. P. G. Hayes, G. C. Welch, D. J. H. Emslie, C. L. Noack, W. E. Piers and M. Parvez, *Organometallics*, 2003, **22**, 1577-1579.
6. B. Liu, T. Roisnel, J.-F. Carpentier and Y. Sarazin, *Angew. Chem.-Int. Ed.*, 2012, **51**, 4943-4946.
7. B. Liu, J.-F. Carpentier and Y. Sarazin, *Chem.-.Eur. J.*, 2012, **18**, 13259-13264.
8. M. S. Hill, M. Hodgson, D. J. Liptrot and M. F. Mahon, *Dalton Trans.*, 2011, **40**, 7783-7790.
9. S. J. Bonyhady, C. Jones, S. Nembenna, A. Stasch, A. J. Edwards and G. J. McIntyre, *Chem.- Eur. J.*, 2010, **16**, 938-955.
10. S. Harder and J. Brettar, *Angew. Chem.-Int. Ed.*, 2006, **45**, 3474-3478.
11. S. P. Green, C. Jones and A. Stasch, *Angew. Chem.-Int. Ed.*, 2008, **47**, 9079-9083.
12. M. S. Hill, D. J. Liptrot, D. J. MacDougall, M. F. Mahon and T. P. Robinson, *Chem. Sci.*, 2013, **4**, 4212-4222.
13. J. Luo, H. Wu, W. Zhou, X. Kang and P. Wang, *Int. J. Hydrogen Energy*, 2013, **38**, 197-204.
14. G. Xia, Y. Tan, X. Chen, Z. Guo, H. Liu and X. Yu, *J. Mater. Chem. A*, 2013, **1**, 1810-1820.
15. K. J. Fijalkowski, R. Jurczakowski, W. Koźmiński and W. Grochala, *Phys. Chem. Chem. Phys.*, 2012, **14**, 5778-5784.
16. W. Li, L. Miao, R. H. Scheicher, Z. Xiong, G. Wu, C. M. Araujo, A. Blomqvist, R. Ahuja, Y. Feng and P. Chen, *Dalton Trans.*, 2012, **41**, 4754-4764.

17. K. Shimoda, A. Yamane, T. Ichikawa and Y. Kojima, *J. Phys. Chem. C*, 2012, **116**, 20666-20672.
18. Z. Tang, Y. Tan, X. Chen and X. Yu, *Chem. Commun.*, 2012, **48**, 9296-9298.
19. W. Xu, G. Wu, W. Yao, H. Fan, J. Wu and P. Chen, *Chemistry*, 2012, **18**, 13885-13892.
20. W. Xu, X. Zheng, G. Wu and P. Chen, *Chin. J. Chem.*, 2012, **30**, 1775-1780.
21. K. J. Fijalkowski, R. V. Genova, Y. Filinchuk, A. Budzianowski, M. Derzsi, T. Jaron, P. J. Leszczynski and W. Grochala, *Dalton Trans.*, 2011, **40**, 4407-4413.
22. S. A. Shevlin, B. Kerkeni and Z. X. Guo, *Phys. Chem. Chem. Phys.*, 2011, **13**, 7649-7659.
23. K. Shimoda, Y. Zhang, T. Ichikawa, H. Miyaoka and Y. Kojima, *J. Mater. Chem.*, 2011, **21**, 2609-2615.
24. H. Wu, W. Zhou, F. E. Pinkerton, M. S. Meyer, Q. Yao, S. Gadipelli, T. J. Udovic, T. Yildirim and J. J. Rush, *Chem. Commun. (Camb)*, 2011, **47**, 4102-4104.
25. Z. Yang, Y. Wang, J. Liang and J. Chen, *Mater. Trans.*, 2011, **52**, 651-653.
26. G. Xia, X. Yu, Y. Guo, Z. Wu, C. Yang, H. Liu and S. Dou, *Chem.- Eur. J.*, 2010, **16**, 3763-3769.
27. Z. Xiong, G. Wu, Y. S. Chua, J. Hu, T. He, W. Xu and P. Chen, *Energy & Environ. Sci.*, 2008, **1**, 360-363.
28. C. R. Balulescu and P. C. Keller, *Inorg. Chem.*, 1978, **17**, 3707-3708.
29. P. C. Keller, *Inorg. Chem.*, 1975, **14**, 438-440.
30. P. C. Keller, *Inorg. Chem.*, 1975, **14**, 440-440.
31. P. C. Keller, *J. Am. Chem. Soc.*, 1974, **96**, 3078-3085.
32. L. D. Schwartz and P. C. Keller, *Inorg. Chem.*, 1973, **12**, 947-949.
33. P. C. Keller, *Inorg. Chem.*, 1971, **10**, 2256-2259.
34. L. D. Schwartz and P. C. Keller, *Inorg. Chem.*, 1971, **10**, 645-649.
35. D. J. Wolstenholme, J. Flogeras, F. N. Che, A. Decken and G. S. McGrady, *J. Am. Chem. Soc.*, 2013, **135**, 2439-2442.
36. C. A. Jaska, K. Temple, A. J. Lough and I. Manners, *J. Am. Chem. Soc.*, 2003, **125**, 9424-9434.

37. J. Prust, K. Most, I. Muller, E. Alexopoulos, A. Stasch, I. Uson and H. W. Roesky, *Z. Anorg. Allg. Chem.*, 2001, **627**, 2032-2037.

38. J. Spielmann, D. F. J. Piesik and S. Harder, *Chem.- Eur. J.*, 2010, **16**, 8307-8318.

39. J. Spielmann, M. Bolte and S. Harder, *Chem. Commun.*, 2009, 6934-6936.

40. J. Spielmann, G. Jansen, H. Bandmann and S. Harder, *Angew. Chem.-Int. Ed.*, 2008, **47**, 6290-6295.

41. J. Spielmann and S. Harder, *J. Am. Chem. Soc.*, 2009, **131**, 5064-5065.

42. G. R. Whittell, E. I. Balmond, A. P. M. Robertson, S. K. Patra, M. F. Haddow and I. Manners, *Eur. J. Inorg. Chem.*, 2010, 3967-3975.

43. J. R. Vance, A. P. M. Robertson, K. Lee and I. Manners, *Chem.- Eur. J.*, 2011, **17**, 4099-4103.

44. A. Staubitz, A. Presa Soto and I. Manners, *Angew. Chem. Int. Ed. Engl.*, 2008, **47**, 6212-6215.

45. C. A. Jaska, K. Temple, A. J. Lough and I. Manners, *Chem. Commun.*, 2001, 962-963.

46. W. Maringgele, M. Noltemeyer, J. Teichgraber and A. Meller, *Main Group Met.Chem.*, 2000, **23**, 735-760.

47. W. Maringgele, M. Noltemeyer, H. G. Schmidt and A. Meller, *Main Group Met. Chem.*, 1999, **22**, 715-732.

48. B. Wrackmeyer, E. Molla, P. Thoma, E. V. Klimkina, O. L. Tok, T. Bauer and R. Kempe, *Z. Anorg. Allg. Chem.*, 2011, **637**, 401-405.

49. Z. W. Tang, Y. B. Tan, Q. F. Gu and X. B. Yu, *J. Mater. Chem.,* 2012, **22**, 5312-5318.

50. H. L. Chu, G. T. Wu, Z. T. Xiong, J. P. Guo, T. He and P. Chen, *Chem. Mater.*, 2010, **22**, 6021-6028.

51. S. Biswas, M. Muller, C. Tonshoff, K. Eichele, C. Maichle-Mossmer, A. Ruff, B. Speiser and H. F. Bettinger, *Eur. J. Org. Chem.*, 2012, 4634-4639.

52. I. H. T. Sham, C. C. Kwok, C. M. Che and N. Y. Zhu, *Chem. Commun.*, 2005, 3547-3549.

53. M. E. Sloan, A. Staubitz, T. J. Clark, C. A. Russell, G. C. Lloyd-Jones and I. Manners, *J. Am. Chem. Soc.,* 2010, **132**, 3831-3841.

54. J. Spielmann, F. Buch and S. Harder, *Angew. Chem.-Int. Ed.*, 2008, **47**, 9434-9438.
55. L. J. Sewell, G. C. Lloyd-Jones and A. S. Weller, *J. Am. Chem. Soc.*, 2012, **134**, 3598-3610.
56. M. H. Chisholm, J. C. Gallucci and K. Phomphrai, *Inorg. Chem.*, 2004, **43**, 6717-6725.
57. M. H. Chisholm, J. Gallucci and K. Phomphrai, *Chem. Commun.*, 2003, 48-49.
58. A. P. Dove, V. C. Gibson, P. Hormnirun, E. L. Marshall, J. A. Segal, A. J. P. White and D. J. Williams, *Dalton Trans.*, 2003, 3088-3097.
59. M. Westerhausen, *Inorg. Chem.*, 1991, **30**, 96-101.
60. D. C. Bradley, J. S. Ghotra and F. A. Hart, *J. Chem. Soc.-Dalton Trans.*, 1973, 1021-1027.
61. R. Anwander, O. Runte, J. Eppinger, G. Gerstberger, E. Herdtweck and M. Spiegler, *J. Chem. Soc.-Dalton Trans.*, 1998, 847-858.
62. A. L. Vangeet, *Anal. Chem.,* 1968, **40**, 2227-2229.

4 Kinetic Analysis of Catalytic Dehydrocoupling of Amine Boranes by d^0 Precatalysts

This chapter describes kinetic experiments to characterise catalytic amine borane dehydrocoupling by reagents from Group 1 – Group 3, in an attempt to provide a quantitative comparison of the effect of the metal identity and establish a reactivity series. Chapter 3, Section 3.1, described the process of precatalyst selection for this study.

This chapter begins by investigating the dehydrocoupling activity of the Group 3 amides **XL** and **XLI**, which arguably exhibited the least complicated dehydrocoupling kinetics. Following this is a kinetic study of the dehydrocoupling activity of Group 2 precatalysts, in an attempt to provide a quantitative profile of the dependence of the metal centre upon reactivity. A comparison is also made between reactions of protio and deuterated versions of the secondary amine borane dimethylamine borane (DMAB) and the primary amine borane *tert*-butylamine borane (TBAB). The previously unexplored catalytic dehydrocoupling activity of the Group 1 bis(trimethylsilyl)amides, $MN(SiMe_3)_2$ (M = Li, Na, K) **LIX**, is also investigated. Finally, the dehydrocoupling activity of reagents from Group 1 – Group 3 is compared in an attempt to establish an overall reactivity trend.

Similar to other mechanistic amine borane dehydrocoupling studies,[1-3] simplification of the system was made by limiting the investigation to the dehydrocoupling of dimethylamine borane (DMAB), a commercially available amine borane with well-defined and precedented dehydrocoupling products. All of the reactions described in this chapter are performed on an NMR-scale, conducted in sealed Youngs tap NMR tubes, between amine borane and typically a 5 mol % catalytic loading. A brief discussion regarding dehydrocoupling reactions in a closed system was presented in Chapter 3, Section 3.5. Investigation of the Group 3 amides **XL** and **XLI** was carried out by monitoring reactions to over 80 % consumption of DMAB (i.e. three half-lives of the reaction). The more complicated dehydrocoupling behaviour of the calcium reagents **VI** and **V-Ca**, however, led to the adoption of the method of initial rates.[4] This method is employed when considering reactions incorporating

competing or complex pathways which cannot be modelled by simple kinetics. By limiting the investigation to the initial 10 % of reaction it is rationalised that complicated behaviour is avoided enabling data to be obtained and allowing the interrogation of straight line zero order kinetic data plots. This method, however, is less accurate than conventional kinetic analysis in which the reaction is monitored to 80 % consumption of reactants and monitors the behaviour of the reaction as a whole as a naïve assumption of linear zero order kinetics is not necessarily valid and data plots described in this chapter were often curved. In addition, reactions which rapidly form a coordinated [$NMe_2BH_2NMe_2BH_3$] anion, namely those with the scandium and magnesium reagents, **XL**, **XV** and **V-Mg**, instantaneously result in 10 % amine borane consumption, invalidating the method of initial rates when applied to dehydrocoupling catalysis. In these scenarios a *pseudo*-initial rates method was adopted in which the 10 % of reaction following the rapid formation of the coordinated [$NMe_2BH_2NMe_2BH_3$] anion was monitored. With due consideration of these limitations, however, valuable insight can still be obtained.

4.1 Kinetic Analysis of Catalytic Dehydrocoupling of Amine Boranes by Group 3 Precatalysts [$Sc\{N(SiHMe_2)_2\}_3(THF)_2$] **XL** and [$Y\{N(SiMe_3)_2\}_3$] **XLI**

The stoichiometric reactivity of [$Sc\{N(SiHMe_2)_2\}_3(THF)_2$] **XL** and [$Y\{N(SiMe_3)_2\}_3$] **XLI** with DMAB and initial observations of the catalytic reactivity of these species were reported by Hill, with qualitative data suggesting a reactivity trend wherein Sc > Y.[5]

An NMR scale reaction between 0.5 mmol DMAB and 5 mol % **XLI**, heated at 70 °C, was monitored by ^{11}B NMR spectroscopy. A zero-order kinetic data plot for this reaction is shown in Figure 4.1, showing the consumption of DMAB to form **XXXVI** as the major product, with other boron-containing species including an yttrium [$NMe_2BH_2NMe_2BH_3$]-species **48** in low concentration in the reaction mixture. After ca. 6 hours heating time the concentration of **XXXVI** was observed to begin to decrease in concentration, with concomitant increase in concentration of **XLVII**. The reactivity of **XXXVI** to form **XLVII** was described in Chapter 3, Section 3.2.4 when investigating the reactivity of β-diketiminato calcium [$NMe_2BH_2NMe_2BH_3$] **36**.

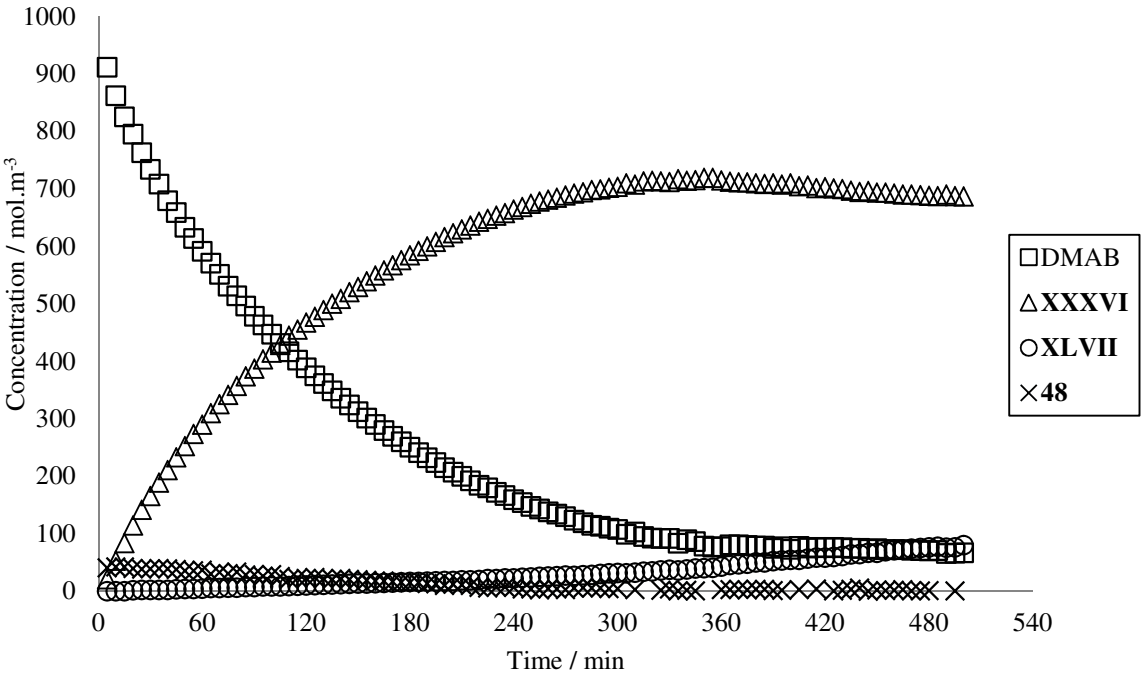

Figure 4.1: Zero order kinetic data plot for the reaction between 0.5 mmol DMAB and 5 mol % **XLI** at 70 °C.

Variable temperature experiments were conducted to ascertain the activation energy and the activation enthalpy and entropy changes for the reaction of 0.5 mmol DMAB with 5 mol % **XL** or **XLI**. Reactions with **XL** were heated at temperatures of 35 °C – 55 °C, whilst reactions with **XLI** were heated at temperatures of 55 °C – 75 °C due to the lower reactivity of this species. Reminiscent of the stoichiometric reactions described in Chapter 3, Section 3.3.1, the formation of **XXXVI** did not fit neither 0, 1st nor 2nd order kinetic data plots, however, the consumption of DMAB followed 1st order kinetics for both **XL** and **XLI**. The resultant Eyring and Arrhenius plots for these reactions are shown in Figures 4.2 and 4.3 respectively.

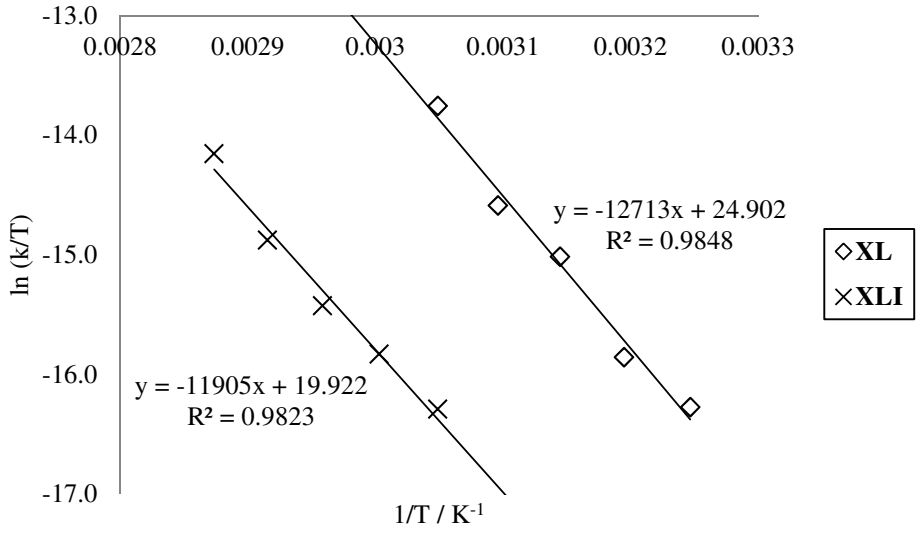

Figure 4.2: Eyring plot for variable temperature reactions between 0.5 mmol DMAB and 5 mol % **XL** (diamonds) or **XLI** (crosses).

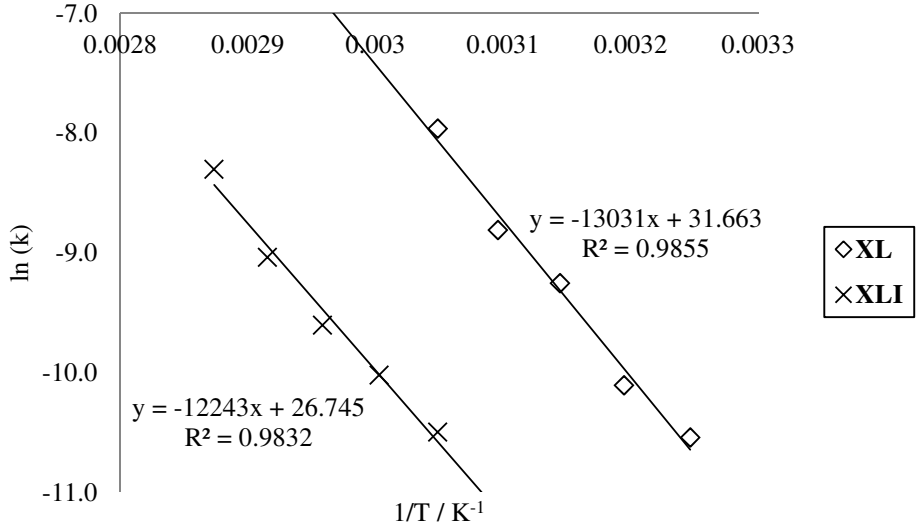

Figure 4.3: Arrhenius plot for variable temperature reactions between 0.5 mmol DMAB and 5 mol % **XL** (diamonds) or **XLI** (crosses).

The data plotted in Figures 4.2 and 4.3 were used to calculate the values displayed in Table 4.1. Although the dehydrocoupling reaction catalysed by **XL** required lower reaction temperatures than the reaction catalysed by **XLI** to achieve rapid reaction rates, the activation energy and enthalpy change for these reactions are effectively identical. These values appear counterintuitive set against the observed reactivity of

these species, with the values of $\Delta G_{298}^{\ddagger}$ indicating that the scandium and yttrium reagents possesses similar dehydrocoupling activity.

	E_a / kJmol^{-1}	$\Delta H^{\ddagger}$ / kJmol^{-1}	$\Delta S^{\ddagger}$ / JK^{-1}mol^{-1}	$\Delta G_{298}^{\ddagger}$ / kJmol^{-1}
XL (Sc)	108.3 $\pm$ 9.3	105.7 $\pm$ 9.3	9.5 $\pm$ 29.2	102.9 $\pm$ 18.0
XLI (Y)	101.8 $\pm$ 9.4	99.0 $\pm$ 9.4	-32.2 $\pm$ 27.8	108.5 $\pm$ 17.7

Table 4.1: Table of kinetic data from Eyring and Arrhenius plots for variable temperature reactions between DMAB and 5 mol % **XL** or **XLI**.

A cautious interpretation of the data in Table 4.1 suggests that these reactions are entropically controlled, with a less negative $\Delta S^{\ddagger}$ value for the scandium reagent **XL** resulting in a more favourable $\Delta G_{298}^{\ddagger}$, irrespective of the higher microscopic $\Delta H^{\ddagger}$ and macroscopic E_a values. Given the requirement for DMAB to observe reaction, this scenario seems reasonable. A more negative $\Delta S^{\ddagger}$ suggests a more ordered transition state or combination of molecules and is reminiscent of the entropically controlled alkaline earth-catalysed intermolecular hydroamination reactivity reported by Hill, in which strontium species were observed to possess superior activity, with a less negative $\Delta S^{\ddagger}$ and consequently lower $\Delta G_{298}^{\ddagger}$ values, than their calcium counterparts.[6] This was rationalised as resulting from a more loosely assembled transition state around the larger Sr^{2+} centre. In the case of amine borane dehydrocoupling described here it is the scandium species which qualitatively possesses higher activity. Although the smaller scandium species might therefore be expected to possess a more ordered transition state, the data do not reflect this.

To compare the effect of metal centre upon dehydrocoupling activity and illustrate the difference in reactivity of **XL** and **XLI**, reactions between 0.5 mmol DMAB and 5 mol % **XL** and **XLI** were carried out at 50 °C. The results of these reactions are shown in Figure 4.4.

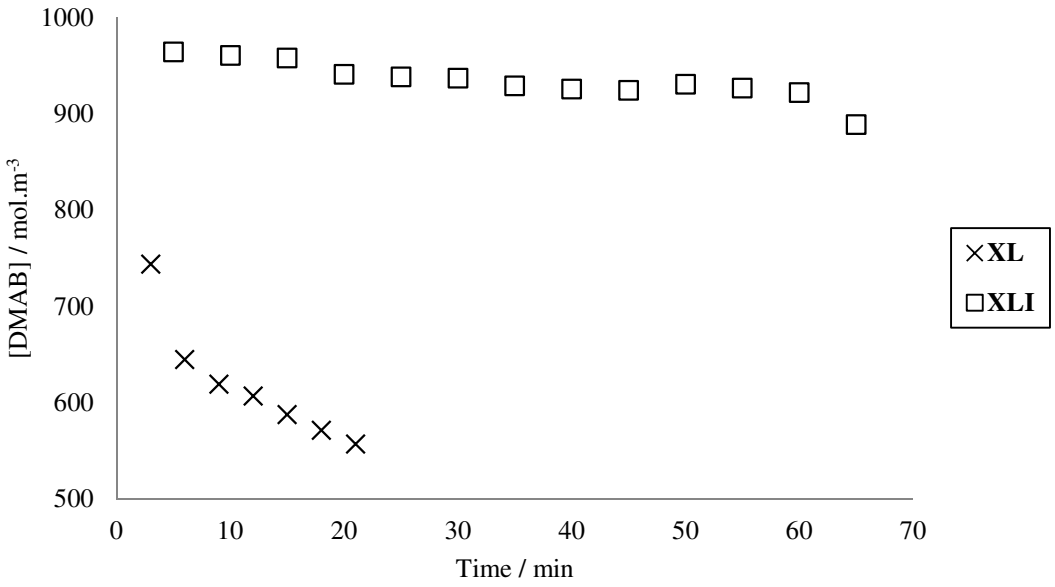

Figure 4.4: Initial rates zero-order kinetic data plot for reactions between 0.5 mmol DMAB and 5 mol % **XL** and **XLI** at 50 °C.

Consistent with the data presented in Table 4.1, the results in Figure 4.4 clearly demonstrate that **XL** is a much more active catalyst for dehydrocoupling DMAB than **XLI**, in agreement with the qualitative observations made by Hill et al.[5] Assuming a negligible effect upon the reactivity due to the change between the $[N(SiMe_2H)_2]^-$ ligand of **XL** and the $[N(SiMe_3)_2]^-$ ligand of **XLI**, the difference in rate can be rationalised as a consequence of the smaller, more highly polarised Sc^{3+} metal centre.

To investigate these reactions further, experiments were conducted for the dehydrocoupling of DMAB by $[Y\{N(SiMe_3)_2\}_3]$ **XLI** by the method of initial rates. Results from these experiments, conducted at 50 °C, are shown in Figures 4.5 and 4.6 in which the gradient of these natural logarithmic plots produces the partial orders of reaction with respect to that species.

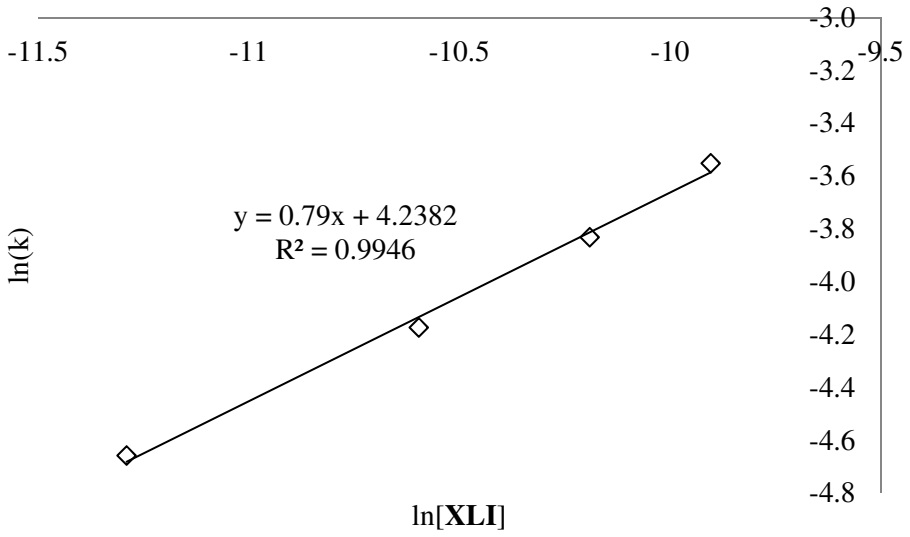

Figure 4.5: A plot of ln(k) against ln[**XLI**] from initial rates data for reactions between 0.5 mmol DMAB and 2.5, 5, 7.5 and 10 mol % **XLI** at 50 °C to establish the partial order of [**XLI**].

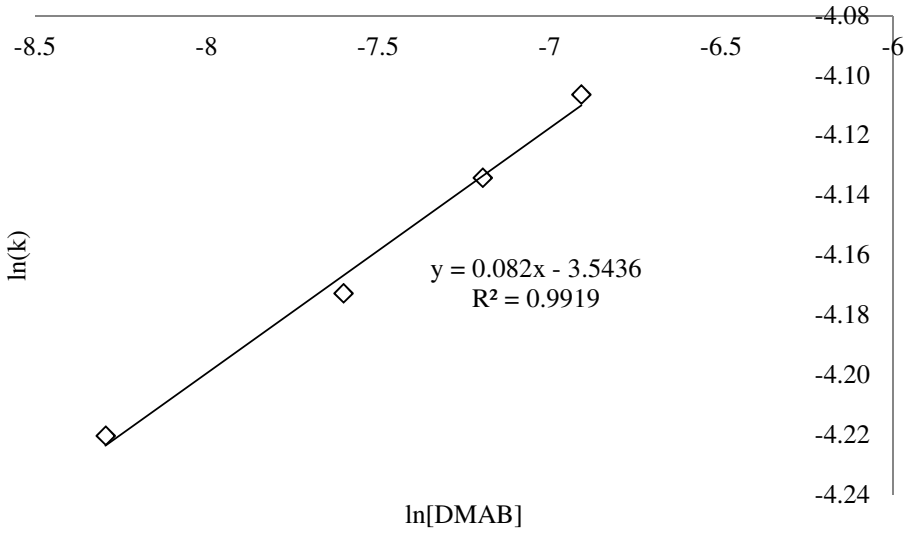

Figure 4.6: A plot of ln(k) against ln[DMAB] from initial rates data for reactions between 2.5 x10^{-5} mol **XLI** and 0.25, 0.5, 0.75 and 1.0 mmol DMAB at 50 °C to establish the partial order of [DMAB].

The method of initial rates requires the monitoring of the initial 10 % of the reaction which was not always possible at particular catalyst loadings and concentrations of DMAB, possibly leading to some error in calculated reaction rates. The data from

Figures 4.5 and 4.6, however, produced a partial order with respect to [**XLI**] of 1 and a partial order of 0 with respect to [DMAB]. This suggests an overall 1st order reaction, which is in agreement with variable temperature experiments of dehydrocoupling by **XLI** to above 80 % DMAB with consumption of DMAB modelled by 1st order kinetics. Although the lack of a dependence upon [DMAB] in the rate equation appears counterintuitive, it suggests saturation of the larger and more accessible yttrium centre by DMAB.

4.2 Kinetic Analysis of Catalytic Dehydrocoupling of Amine Boranes by Calcium Precatalysts **VI** and **V-Ca**

This section describes kinetic experiments with the β-diketiminato calcium silylamide **VI** and $[Ca\{N(SiMe_3)_2\}_2]_2$ **V-Ca**, characterising dehydrocoupling reactions of these species with DMAB.

The reaction between 0.5 mmol DMAB and 5 mol % **VI** at 70 °C was monitored by ^{11}B NMR spectroscopy. The results of this reaction are shown in Figure 4.7. Similar to the kinetic studies described previously in Chapter 3, Sections 3.3.1 and 3.3.2, the change in concentration could not be modelled by either 0, 1st nor 2nd order kinetics for any of the reaction species.

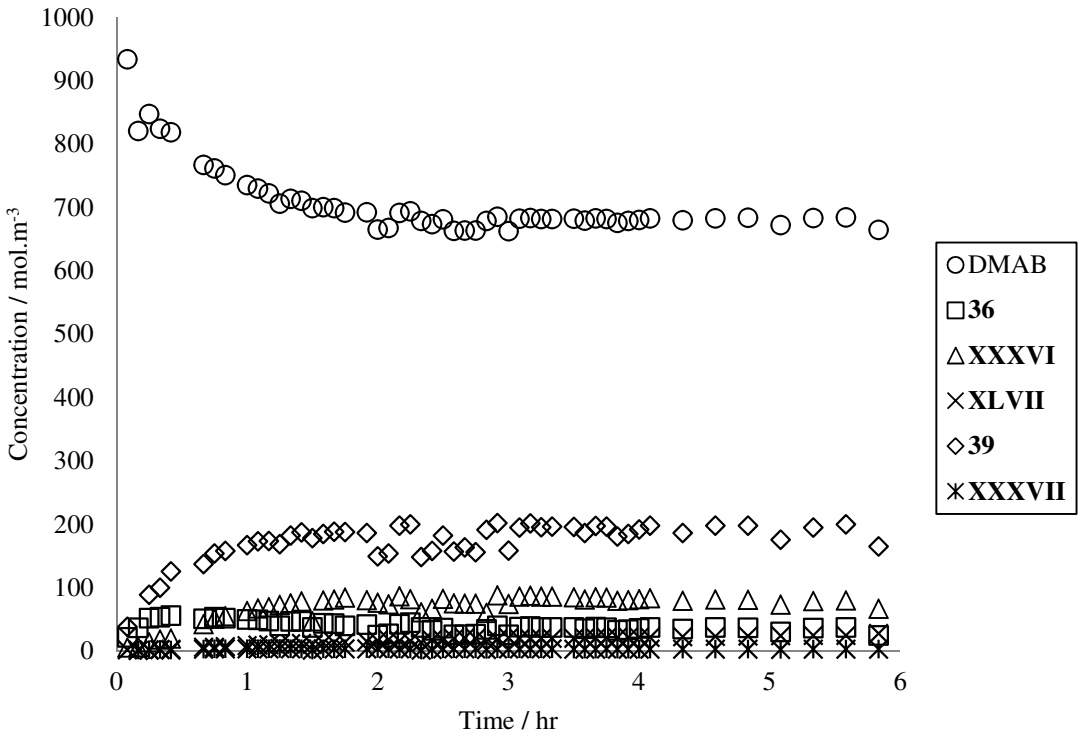

Figure 4.7: Zero order kinetic data plot for the reaction between 0.5 mmol DMAB and 5 mol % **VI** at 70 °C.

The results depicted in Figure 4.7 show that only ca. 28 % DMAB reacted, and that this occurred within the first 2 hours of heating to form a mixture of **36**, **XXXVI**, **XLVII** and **XXXVII**, before cessation of any observed reaction. Around 20 % of **39**, an unidentified species first observed in the reaction between **XXXVI** and **LXV** described in Chapter 3, Section 3.2.7, was formed during the reaction. A ^{1}H NMR spectrum of this reaction revealed that the β-diketiminate ligand had been completely protonated, through the observation of a singlet at δ = 12.32 ppm and integrating to 1H, corresponding to a N-H resonance. The presence of a small quantity of hydrocarbon-insoluble material in the bottom of the Youngs tap NMR tube suggested formation of insoluble CaH_2 or amidoborane derivative species. The metal centre, therefore, is no longer supported by the β-diketiminate ligand causing a reduction in solubility and availability of the metal centre to react with DMAB.

The reaction between 0.5 mmol DMAB and 5 mol % **VI** was repeated at 70 °C and monitored by ^{11}B NMR spectroscopy at regular intervals. The zero order kinetic data plot for this reaction, displayed in Figure 4.8, shows that the reaction continued

with conversion of DMAB to **XXXVI** at a much slower rate after an initial period before complete protonation of the β-diketiminate ligand had occurred. After the initial period of the reaction and reduction in reaction rate the decrease in concentration of DMAB and increase in concentration of **XXXVI** displayed zero order kinetics.

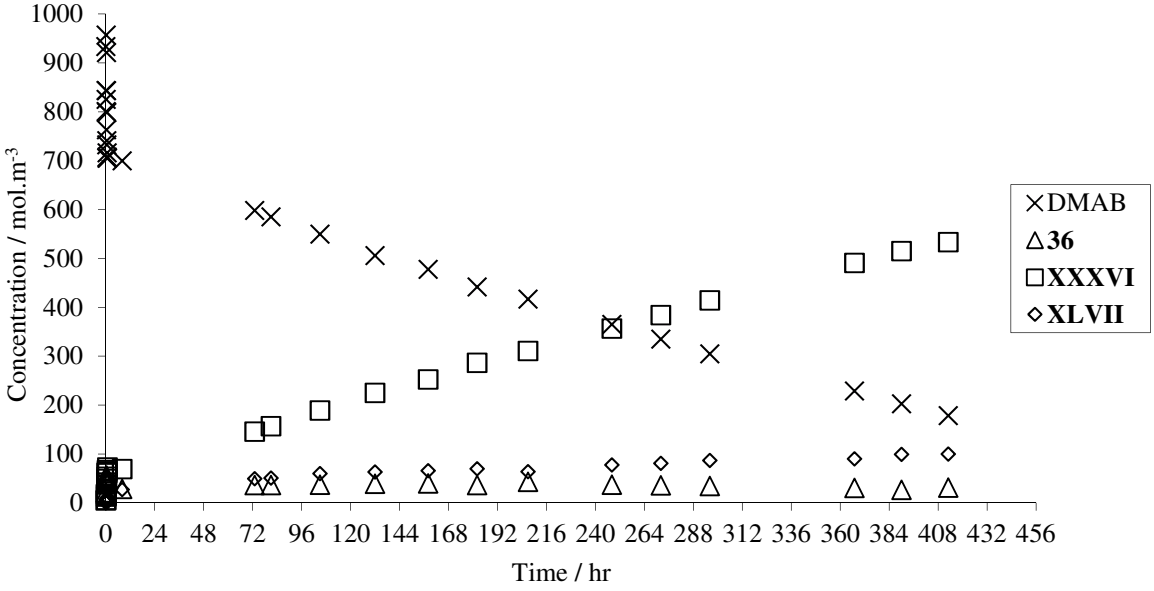

Figure 4.8: Zero order kinetic data plot for the reaction between 0.5 mmol DMAB and 5 mol % **VI**, heated for an extended period of time at 70 °C.

This reaction, repeated at 80 °C and 90 °C, once again required extended heating times. A zero order kinetic data plot for consumption of DMAB in the initial period of these experiments before the transition in reaction rate, including the experiment at 70 °C, is shown in Figure 4.9. The graph in Figure 4.9 shows that although the rate of consumption of DMAB increased with increasing temperature, consumption of DMAB could not be modelled by either 0, 1st nor 2nd order kinetics. The graph also shows that the decrease in reaction rate occurs at ca. 30 % consumption of DMAB in each case, suggesting that increasing temperature did not result in increased susceptibility to ligand protonation. The observations of the initial period of these reactions were rationalised by DMAB reacting with **VI** via the proposed mechanism discussed in Chapter 3 (Figure 3.45) in addition to reaction(s) resulting

in ligand protonation. This combination of processes may reasonably be expected to result in a complex kinetic profile.

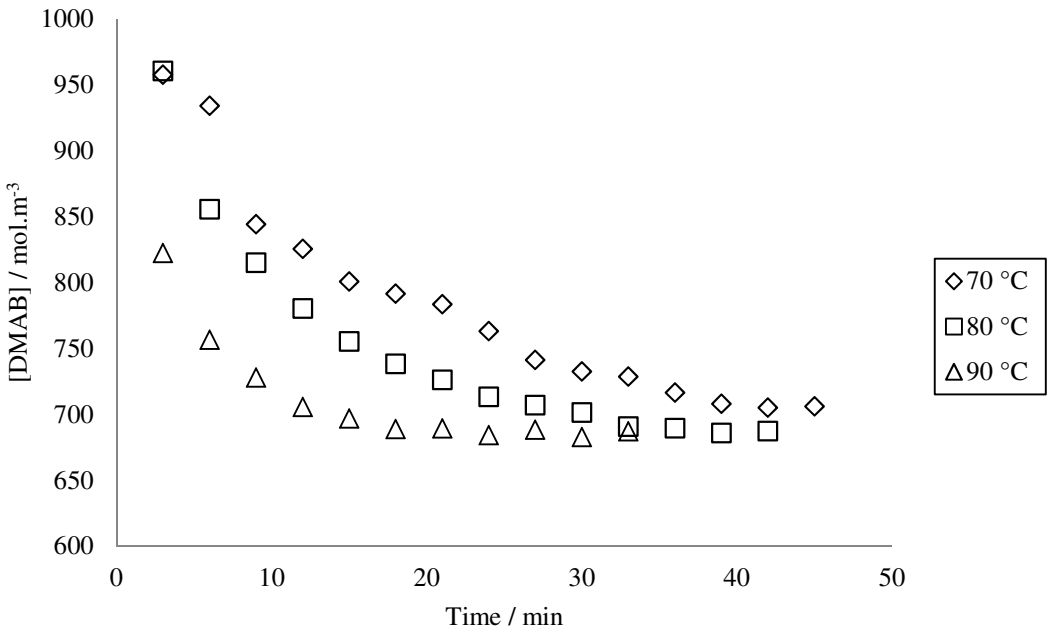

Figure 4.9: Zero order kinetic data plot for the initial period of reaction between 0.5 mmol DMAB and 5 mol % **VI**, heated at 70 °C (diamonds), 80 °C (squares) and 90 °C (triangles).

Zero order kinetic data plots for these reactions, after the initial period of ligand protonation, are shown in Figure 4.10 for the consumption of DMAB and a zero order kinetic data plot for the formation of **XXXVI** is shown in Figure 4.11.

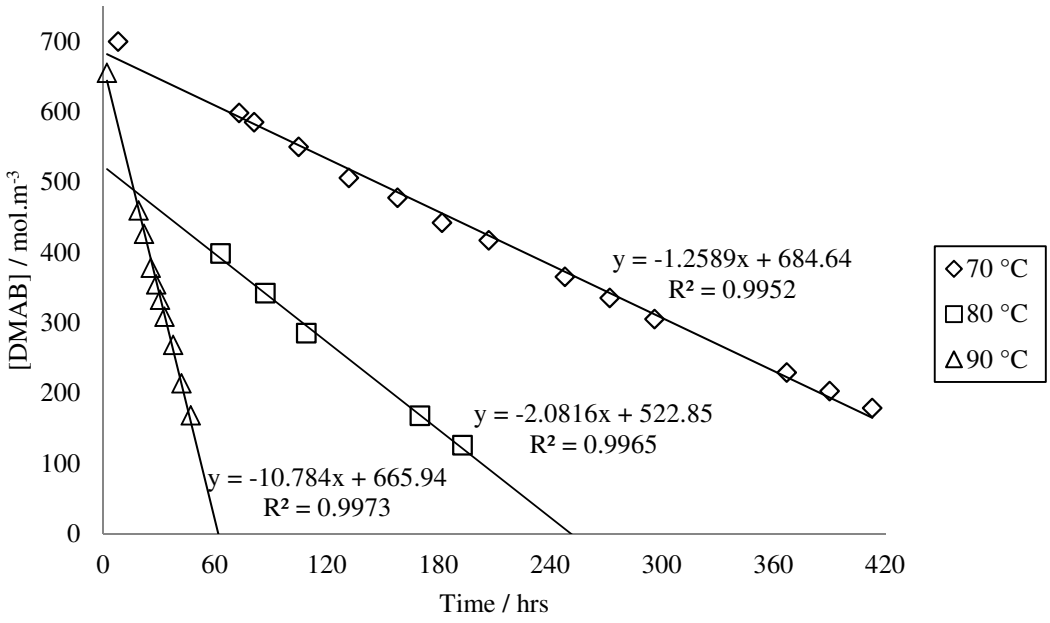

Figure 4.10: Zero order kinetic data plot for the consumption of DMAB in the reaction between 0.5 mmol DMAB and 5 mol % **VI**, heated at 70 °C (diamonds), 80 °C (squares) and 90 °C (triangles), after the initial period of reaction in which β-diketiminate ligand is protonated.

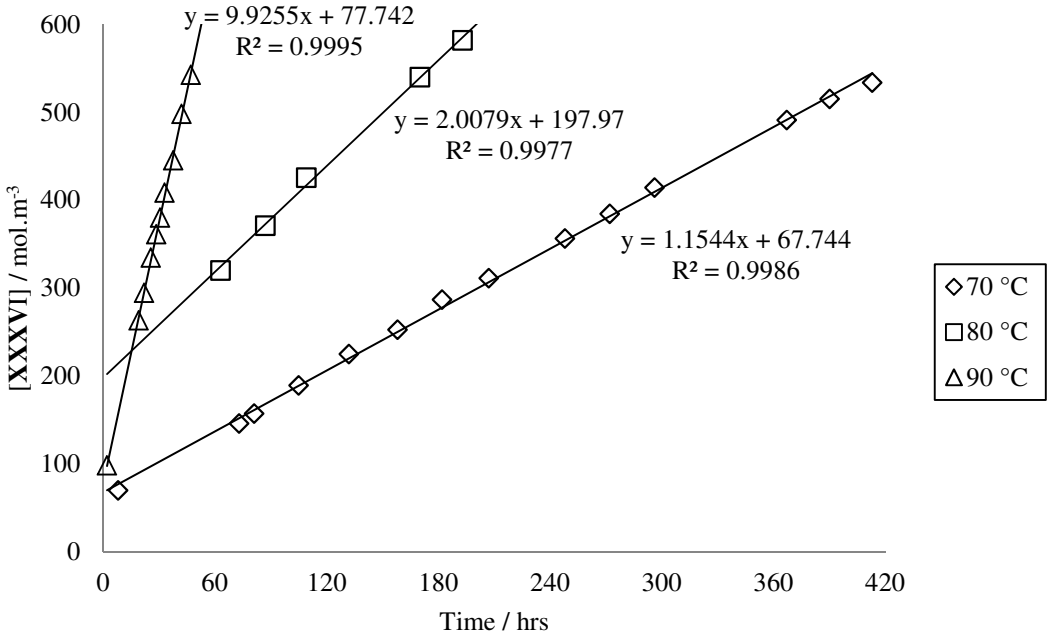

Figure 4.11: Zero order kinetic data plot for the formation of **XXXVI** in the reaction between 0.5 mmol DMAB and 5 mol % **VI**, heated at 70 °C (diamonds), 80 °C (squares) and 90 °C (triangles), after the initial period of reaction in which the β-diketiminate ligand is protonated.

An Arrhenius plot can be constructed using the data in Figure 4.10, however, Arrhenius plots should consist of at least four data points, whilst a plot using this data consists of only three (possessing an R^2 value of 0.9518). The activation energy of 110.8 $\pm$ 1.9 $kJmol^{-1}$ calculated using this plot should, thus, be treated with caution and consideration of its limitations due to these factors. This activation energy, however, is commensurate with that calculated for the dehydrocoupling of DMAB by **XL** and **XLI** described in Section 4.1. Once again the significance of this activation energy with regards to the potential rate-determining process is unclear, as the nature of the catalytic species is unknown.

The reaction between 0.5 mmol DMAB and 5 mol % **VI** at 80 °C was repeated in deuterated tetrahydrofuran (THF) rather than deuterated toluene as the NMR solvent to assess whether this solvent aided solubility of a catalytic species, proposed to be a calcium hydride/amidoborane species, produced after ligand protonation. The results of this reaction are shown in Figure 4.12.

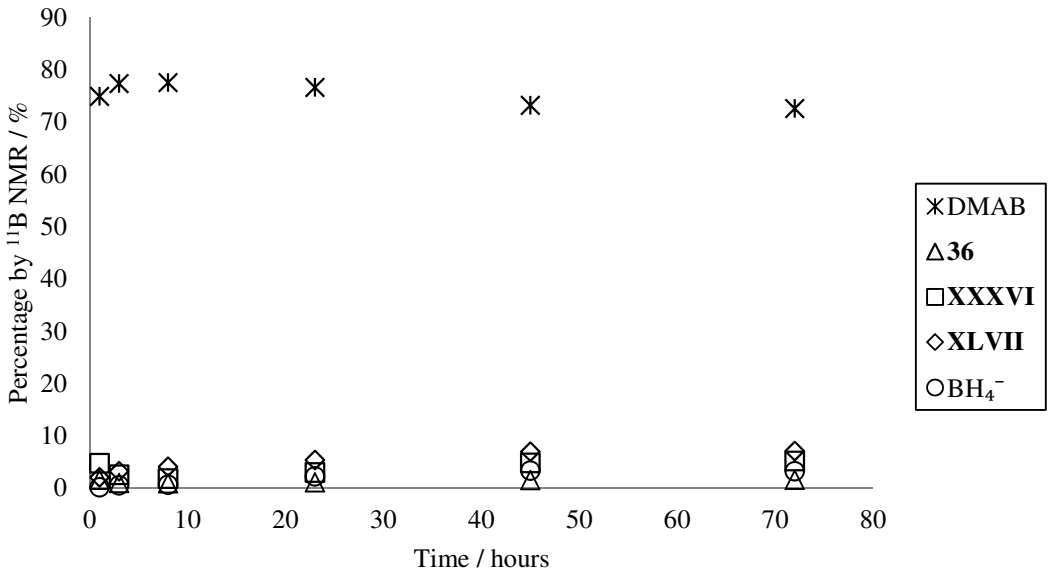

Figure 4.12: Zero order kinetic data plot for the reaction between 0.5 mmol DMAB and 5 mol % **VI** at 80 °C in tetrahydrofuran (THF) (percentage of each species calculated by integration of ^{11}B NMR spectra).

By comparison of Figures 4.10 and 4.12 it is clear that the use of THF as solvent for this reaction retarded the rate of the reaction rather than aiding solubility of the metal centre and increasing the rate of reaction. Figure 4.12 shows that only small quantities of **XXXVI**, **XLVII** and a BH_4^- species were produced which were observed in the ^{11}B NMR spectra for this reaction.

To investigate this apparent catalyst deactivation 0.5 mmol DMAB was reacted with 5 mol % **VI** at 70 °C for ca. 1 hour, after which the rate of reaction had reached a plateau relative to the initial more rapid kinetics. At this point the Youngs tap NMR tube was cooled to room temperature, opened inside an inert atmosphere glove box and a second 5 mol % aliquot of **VI** was added to the reaction mixture. The sample was then reheated at 70 °C and monitored by ^{11}B NMR spectroscopy. In a second experiment 0.5 mmol DMAB was reacted with 10 mol % **VI** at 70 °C to observe whether at this catalyst loading the metal centre would undergo similar deactivation via ligand protonation. The results of these experiments are shown in Figure 4.13 with the arrow indicating the break in the experiment for the reaction of DMAB and 5 mol % **VI** and the addition of a further 5 mol % **VI**.

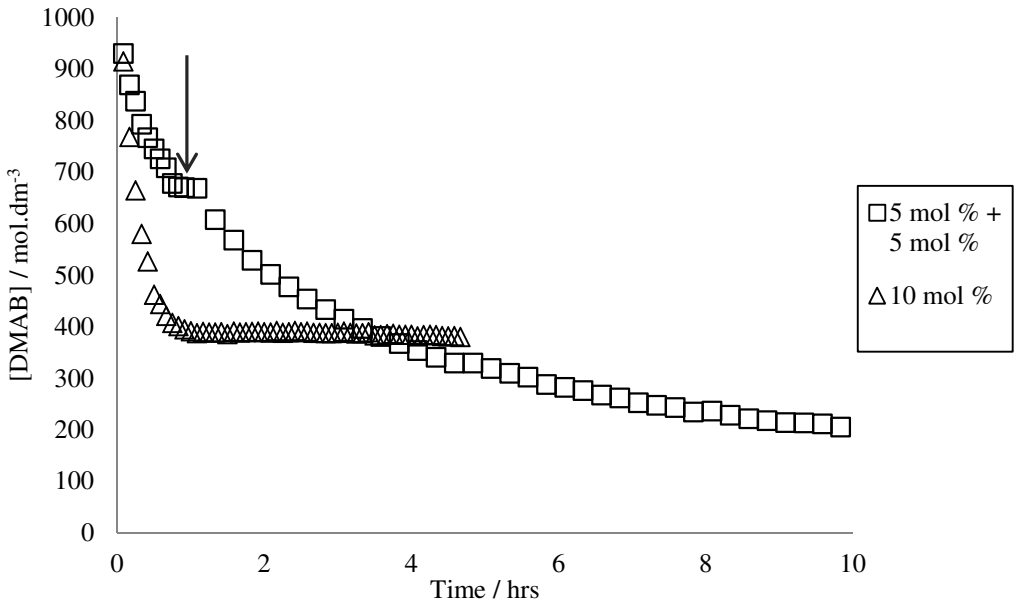

Figure 4.13: Zero order kinetic data plot for the reaction between 0.5 mmol DMAB and 5 mol % **VI** at 70 °C for ca. 1 hour, indicated by the arrow, followed by an additional 5 mol % **VI** and further heating (squares), and the reaction between DMAB and 10 mol % **VI** (triangles).

The results displayed in Figure 4.13 show that the reaction between 0.5 mmol DMAB and 5 mol % **VI** result in the consumption of ca. 32 % DMAB before the reaction stalls on protonation of the β-diketiminate ligand. On the other hand the reaction with 10 mol % **VI** proceeded to ca. 62 % consumption of DMAB before the rate of reaction decreased dramatically. These results demonstrate that approximately twice the amount of DMAB was consumed for double the catalyst loading, and indicated a correlation between the proportion of DMAB consumed before the rate of reaction underwent a marked change and the initial level of catalyst loading. While it is reasonable to expect a relationship between consumption of DMAB and catalyst loading given the proposed process of ligand protonation by reaction with DMAB, further details regarding the precise nature of this process are unknown. For the reaction in which a second 5 mol % aliquot of **VI** was added to the reaction mixture Figure 4.13 shows that the reaction proceeds to ca. 80 % consumption of DMAB after heating for ca. 9 hours. The reaction was expected to consume a second 32 % proportion of DMAB, proceeding to ca. 64 % consumption of DMAB. This observation could be rationalised by concentration effects and an

apparent Curtin-Hammett scenario, in which the addition of **VI** to a mixture of dehydrocoupled amine borane fragments and deactivated catalyst is not the same as the addition of the whole quantity of **VI** at the onset of the reaction.

To further investigate the initial period of reaction, the method of initial rates was used to analyse reactions between 0.5 mmol DMAB and 5 mol % **VI** at temperatures between 45 °C and 65 °C. Eyring and Arrhenius plots for these reactions are shown in Figures 4.14 and 4.15 respectively.

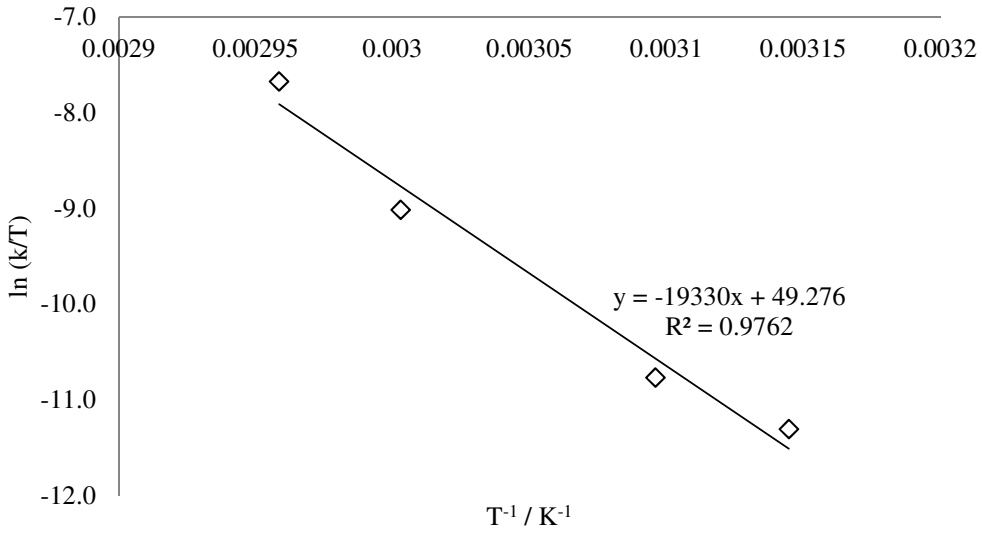

Figure 4.14: Eyring plot for variable temperature reactions between 0.5 mmol DMAB and 5 mol % **VI**.

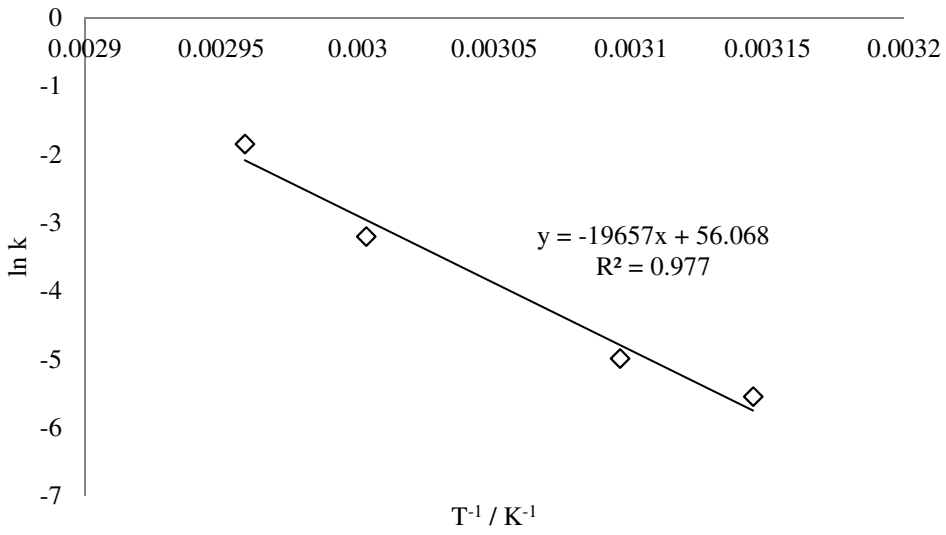

Figure 4.15: Arrhenius plot for variable temperature reactions between 0.5 mmol DMAB and 5 mol % **VI**.

The data plotted in Figures 4.14 and 4.15 was used to calculate E_a, $\Delta H^{\ddagger}$ and $\Delta S^{\ddagger}$ values of 163.4 $\pm$ 5.3 kJmol^{-1}, 160.7 $\pm$ 2.5 kJmol^{-1} and 212.2 $\pm$ 8.6 JK^{-1}mol^{-1} respectively and a $\Delta G^{\ddagger}_{298}$ value of 97.5 $\pm$ 5.1 kJmol^{-1}. Care should be taken in comparing these data to those in Table 4.1, as the two data sets characterise very different aspects of the reaction. The values in Table 4.1 were calculated from reactions monitored to above 80 % completion, evaluating the kinetics for all processes operating within the reaction, whereas these data are based upon the initial rates method which, by definition, seeks to neglect side reactions which may take place at higher product concentrations. Although these differing methods, therefore, produce data which cannot be directly compared, it is notable that the value for $\Delta S^{\ddagger}$ is approximately 20 times the magnitude of the value deduced for **XL** indicating that these data are probably a reflection of the process of β-diketiminate protonation of **VI** rather than any intrinsic ability of the calcium centre to effect dehydrocoupling catalysis.

Having investigated dehydrocoupling reactions between 0.5 mmol DMAB and **VI** and catalyst deactivation via a process involving ligand protonation, the dehydrocoupling activity of **V-Ca** was investigated by reacting 5 mol % of this

precatalyst with 0.5 mmol DMAB at 70 °C. The results of this experiment are shown in Figure 4.16.

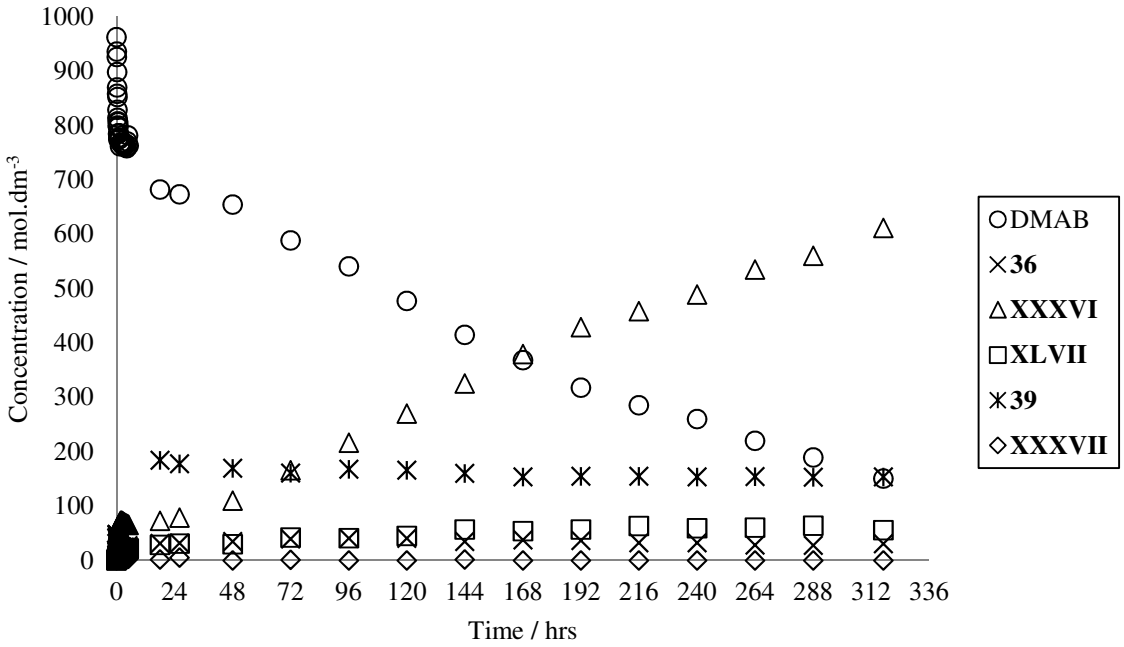

Figure 4.16: Zero order kinetic data plot for the reaction between 0.5 mmol DMAB and 5 mol % **V-Ca** at 70 °C.

As with the reaction between DMAB and **VI** the graph in Figure 4.16 demonstrates an initial period of rapid consumption of amine borane before a marked decrease in reaction rate after reaction of ca. 25 % DMAB. Once again **36**, **XXXVII** and **XLVII** remained at relatively low concentration during the reaction, however, the concentration of the unidentified species **39** again increased to ca. 18 % before decreasing gradually over the course of the reaction. After the initial high reaction rate, which may be rationalised as resulting from facile protonation of the $[N(SiMe_3)_2]$ ligand(s), the subsequent reduction in [DMAB] and increase in concentration of **XXXVI** appeared to be modelled by zero order kinetics.

Figure 4.17 shows a comparison between reactions of 5 mol % **VI** and **V-Ca** with 0.5 mmol DMAB at 70 °C after this initial period of protolytic reactivity. The reaction with **V-Ca** proceeds faster than the reaction with **VI** indicating that the presence of the protonated β-diketiminate ligand precursor has a retardant effect on dehydrocoupling reaction rate. Chapter 5 discusses reactions between amines and

amine boranes, suggesting that both ligands formed in these reactions are not innocent species and likely to be components in competitive transamination equilibria after protonation.

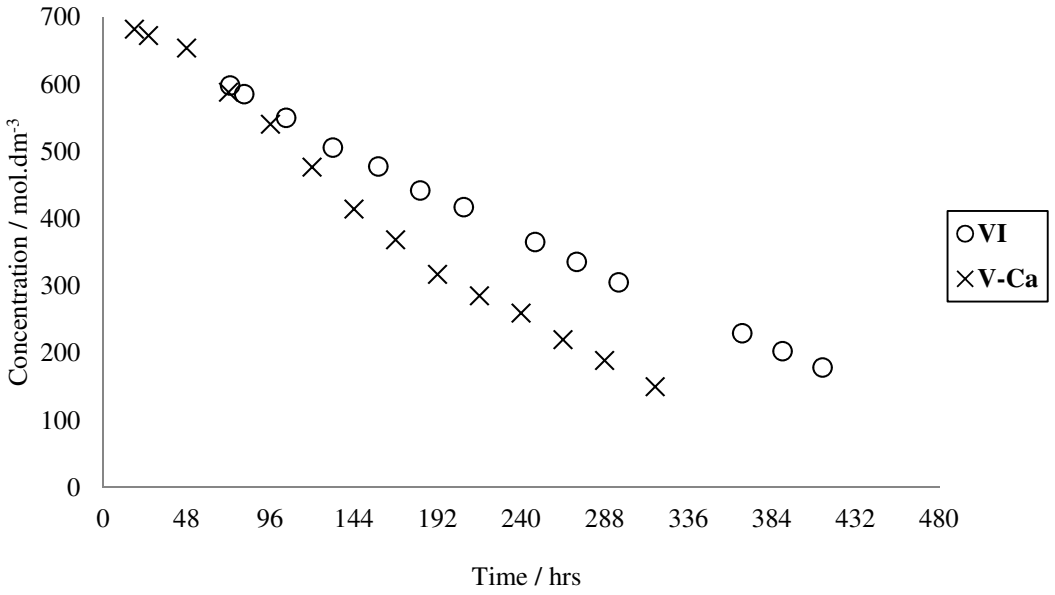

Figure 4.17: Zero order kinetic data plot for the reaction between 0.5 mmol DMAB and 5 mol % **VI** (circles) and **V-Ca** (crosses) at 70 °C after the initial period of reaction.

Variable temperature initial rate experiments between 0.5 mmol DMAB and 5 mol % **V-Ca** at temperatures between 45 °C – 65 °C, monitored by ^{11}B NMR spectroscopy, were employed to construct the Eyring and Arrhenius plots shown in Figures 4.18 and 4.19 respectively.

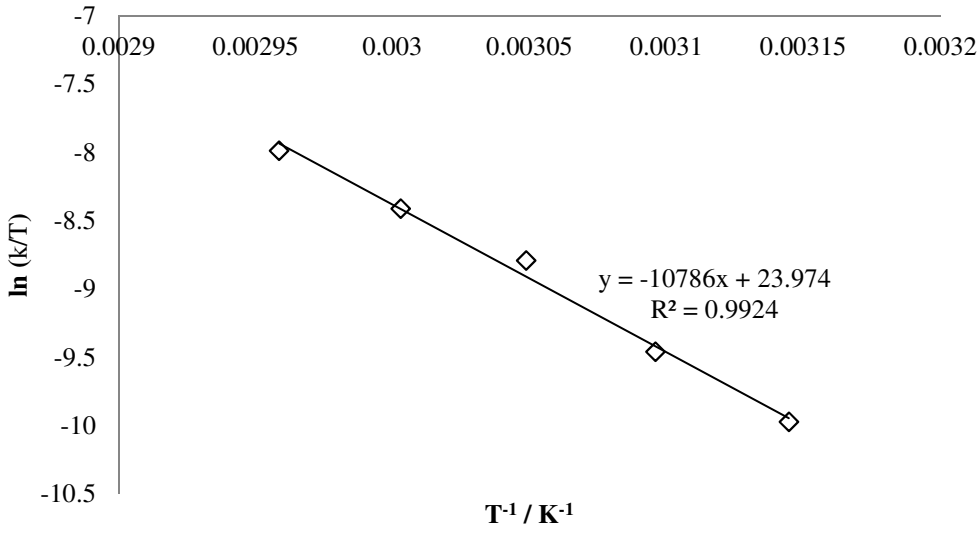

Figure 4.18: Eyring plot for variable temperature reactions between 0.5 mmol DMAB and 5 mol % **V-Ca**.

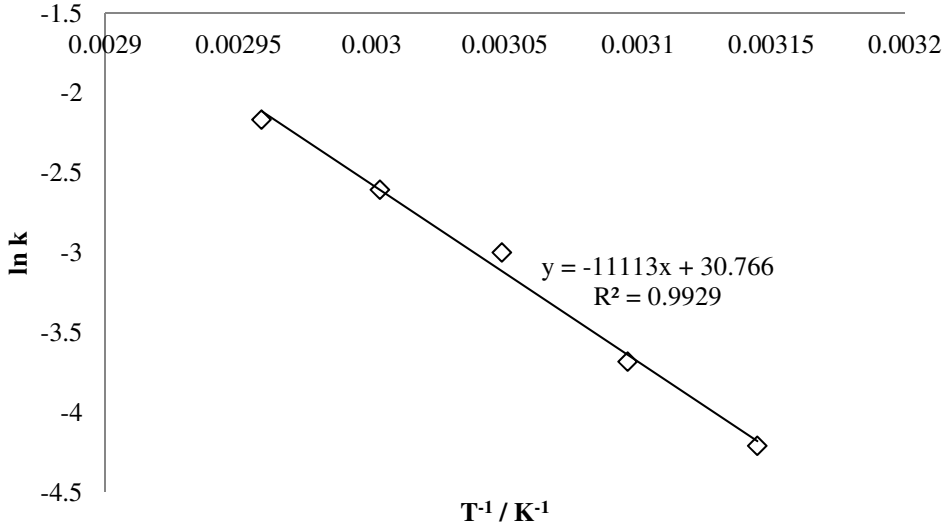

Figure 4.19: Arrhenius plot for variable temperature reactions between 0.5 mmol DMAB and 5 mol % **V-Ca**.

The data plotted in Figures 4.18 and 4.19 produced values for E_a, $\Delta H^{\ddagger}$, $\Delta S^{\ddagger}$ and $\Delta G^{\ddagger}_{298}$ of 92.4 $\pm$ 5.5 kJmol^{-1}, 89.7 $\pm$ 5.5 kJmol^{-1}, 1.8 $\pm$ 16.9 JK^{-1}mol^{-1} and 89.1 kJmol^{-1} respectively. As previously discussed, comparison of these data to the values in Table 4.1 may be ill-advised, but do reveal the more facile nature of the initiation of reaction with respect to the directly comparable system derived from the β-diketiminato species **VI** (Figure 4.14 and 4.15). In this case the data reflect more

facile [$N(SiMe_3)_2$] protonolysis rather than production of the more acidic β-diketiminato conjugate acid.

The method of initial rates was also utilised for reactions between DMAB and **V-Ca** at 50 °C, to ascertain partial rate orders with respect to [**V-Ca**] and [DMAB]. Results from these experiments are shown in Figures 4.20 and 4.21.

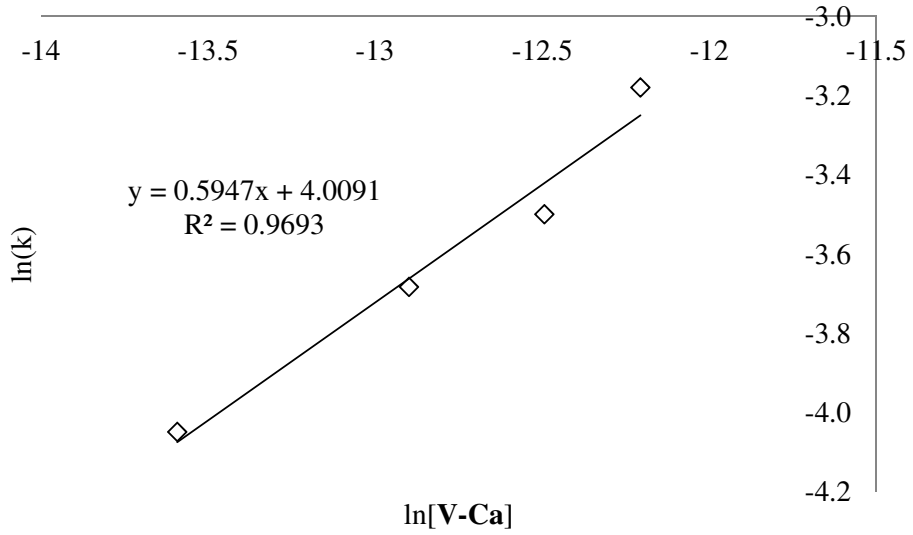

Figure 4.20: A plot of ln(k) against ln[**V-Ca**] from initial rates data for reactions between 0.5 mmol DMAB and 2.5, 5, 7.5 and 10 mol % **V-Ca** at 50 °C to establish the partial order with respect to [**V-Ca**].

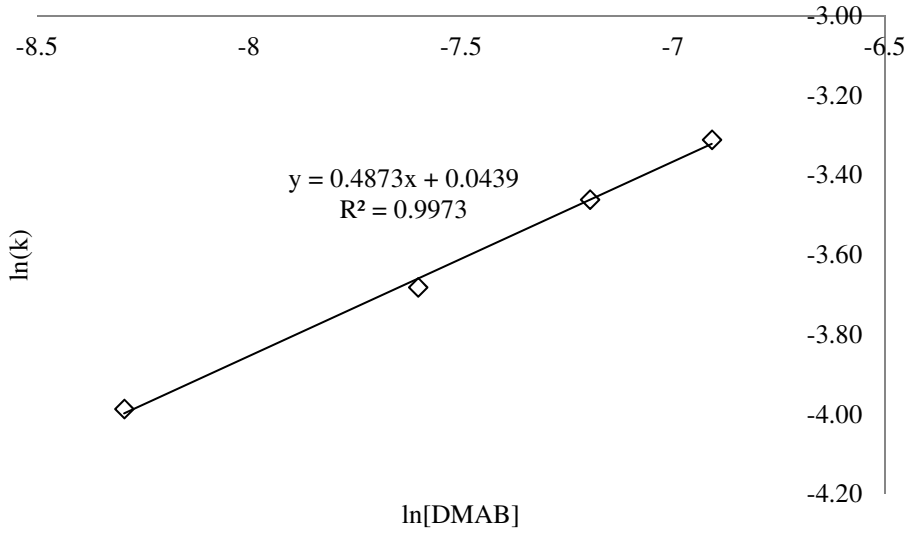

Figure 4.21: A plot of ln(k) against ln[DMAB] from initial rates data for reactions between 2.5 x10^{-5} mol **V-Ca** and 0.25, 0.5, 0.75 and 1.0 mmol DMAB at 50 °C to establish the partial order with respect to [DMAB].

Figures 4.20 and 4.21 produce partial rate orders of 0.59 $\pm$ 0.07 (2 d.p.) for [**V-Ca**] and 0.49 $\pm$ 0.02 (2 d.p.) for [DMAB]. The data plotted in Figure 4.20 has an R^2 value of 0.9693, reduced by the data point from the reaction of 10 mol % **V-Ca** with DMAB deviating from the line of best fit. If this data point is discarded the partial order for [**V-Ca**] becomes 0.50 $\pm$ 0.01 with an R^2 value of 0.9984 and an overall reaction order of 1 for this initial protonolysis process, suggesting that the rate determining step involves the dissociation of a dimeric species.

Reactions between 5 mol % **V-Ca** and 0.5 mmol of the deuterated dimethylamine borane species **LXXXII** and **XCIII** were carried out at 50 °C and compared to the analogous reaction with DMAB. These deuteration experiments were once again carried out in isolation, similar to the reactions with **LXV** described in Chapter 3, Section 3.3.1, and the method reported by Manners.[7] The consumption of dimethylamine borane was monitored by the initial rates method and the results from these experiments are shown in Figure 4.22.

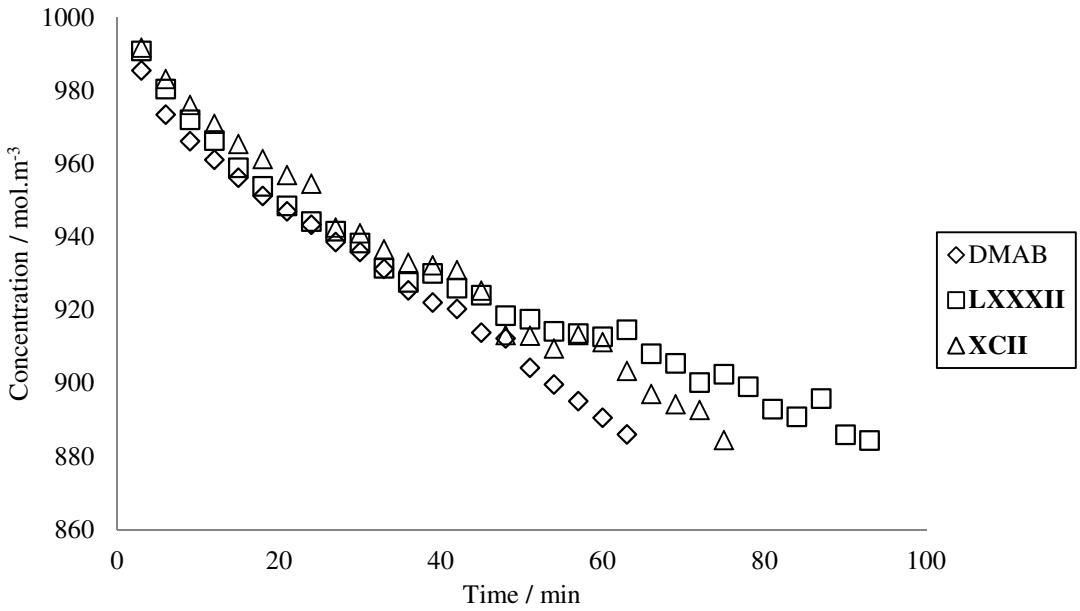

Figure 4.22: A zero order kinetic data plot of reactions between 5 mol % **V-Ca** and 0.5 mmol DMAB (diamonds), **LXXXII** (squares) and **XCIII** (triangles) at 50 °C.

Figure 4.22 shows that there is little difference between the consumption of amine borane for the reactions between 5 mol % **V-Ca** and 0.5 mmol DMAB, **LXXXII** and **XCIII** at 50 °C for the initial 40 minutes, after which a difference in consumption can be observed. The data for DMAB (diamonds) describe a linear dependence but the data for **LXXVII** (squares) and **XCIII** (triangles) in Figure 4.22 do not fit straight lines, resulting in a lack of suitable data from which to calculate kinetic isotope effect values.

4.2.1 Kinetic Analysis of the Dehydrocoupling of the Primary Amine Borane *Tert*-Butylamine Borane

So far this thesis has described investigations of the kinetics of amine borane dehydrocoupling which have focused on reactions of the commercially available secondary amine borane DMAB with widely reported and well-characterised reaction products, in order to simplify as far as possible the reaction under investigation. In Chapter 3, Section 3.2.6, however, stoichiometric reactions with the primary amine borane TBAB were described, indicating that the reactivity of this substrate with alkaline earth reagents exhibited similarities to the proposed mechanism in Chapter 3, Figure 3.45, whilst other products identified from

stoichiometric and catalytic reactions could only have been formed by alternative mechanistic pathways. Qualitative assessment of reactions utilising TBAB suggested that this primary amine borane displayed greater reactivity with alkaline earth reagents than the secondary amine boranes DMAB and PB.

In an attempt to quantify the difference in reactivity of TBAB and DMAB, reactions of 0.5 mmol amine borane and 5 mol % **V-Ca** were carried out at 50 °C. The method of initial rates was again employed and the decrease in amine borane concentration was monitored by ^{11}B NMR spectroscopy. The results of these reactions are shown in Figure 4.23.

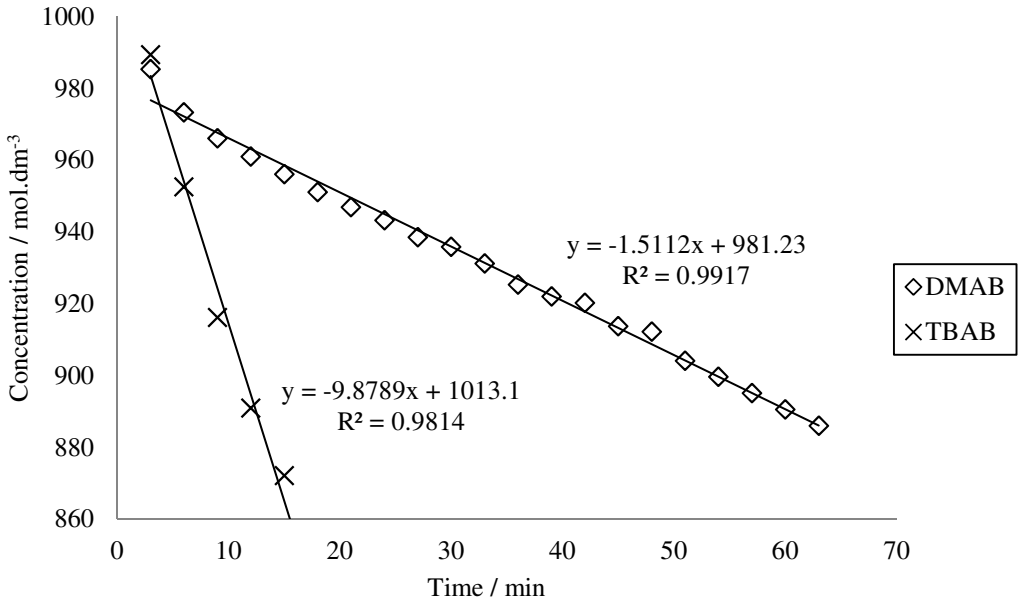

Figure 4.23: A zero order initial rates kinetic data plot for reactions between 5 mol % **V-Ca** and 0.5 mmol DMAB (diamonds) and TBAB (squares) at 50 °C.

The data plotted in Figure 4.23 show that the rate of consumption of TBAB was over 6 times as fast as the consumption of DMAB, providing quantitative evidence that this primary amine borane is more reactive than the secondary amine borane DMAB with catalytic quantities of **V-Ca**. Although analogous reactions were not carried out with **VI** and the magnesium species **XV** and **V-Mg**, the reactivity of the primary amine borane TBAB is expected to also be superior to that of the secondary amine borane DMAB for each of these precatalysts. Whilst it is beyond the scope of this thesis, an interesting study would be to compare the reactivity of a wide range of

amine borane substrates, observing the dependence of steric and electronic effects on reaction rate.

4.3 Kinetic Analysis of Catalytic Dehydrocoupling of DMAB by Magnesium Precatalysts **XV** and **V-Mg**

Section 4.2 has described a kinetic investigation of the dehydrocoupling of amine boranes by calcium precatalysts **VI** and **V-Ca**, with results displaying complicated concentration profile plots for products and intermediate species and highlighting ligand protonation as a fundamental issue in these reactions. This section describes a kinetic investigation of the dehydrocoupling of DMAB with magnesium precatalysts **XV** and **V-Mg**, and a comparison of the behaviour and rate of these reactions to those described in Section 4.2.

An NMR-scale reaction between 0.05 mmol DMAB and 5 mol % of the alkyl magnesium precatalyst **XV** was carried out at 70 °C. The results displayed in Figure 4.24 show that, unlike the silylamido calcium β-diketiminate species **VI**, the reaction between **XV** and DMAB proceeded smoothly to completion. The major product of this reaction was **XXXVI** whilst a small proportion (ca. 1.5 %) of **XLVII** was also formed.

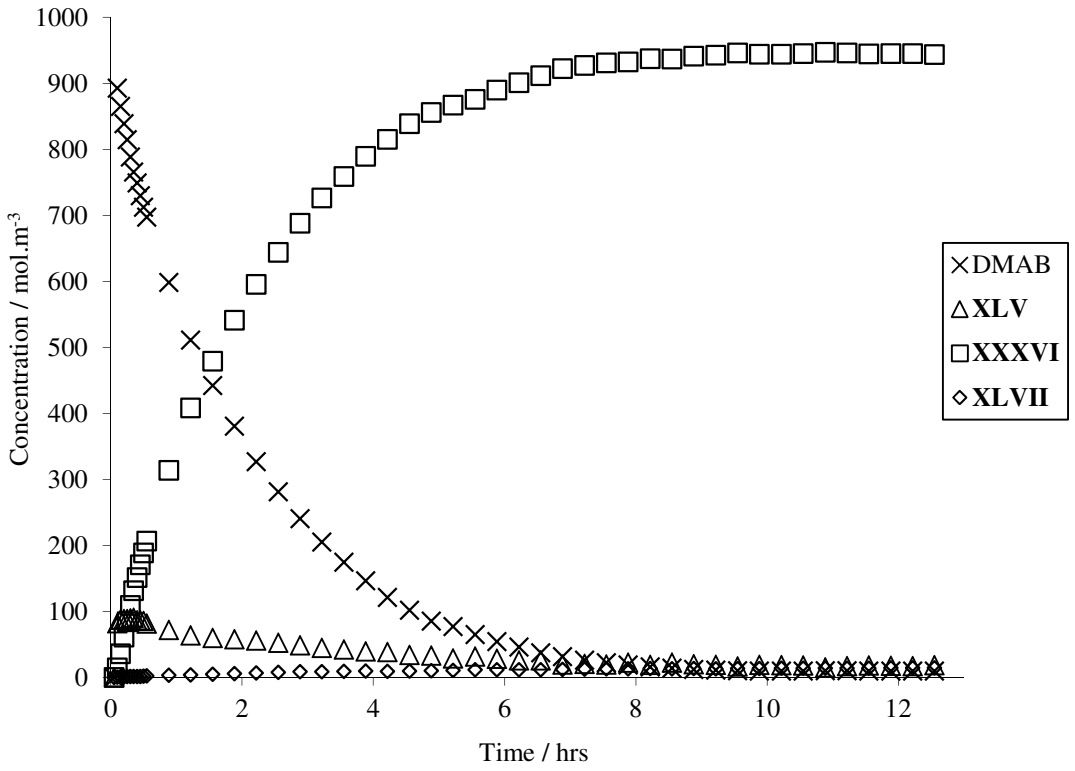

Figure 4.24: A zero order kinetic data plot for the reaction between 0.5 mmol DMAB and 5 mol % **XV** at 70 °C.

Although the formation of **XXXVI** could not be modelled by either 0, 1st nor 2nd order kinetics the decrease in concentration of DMAB for the first 8 hours of the reaction displayed well behaved 1st order kinetics as shown by Figure 4.25.

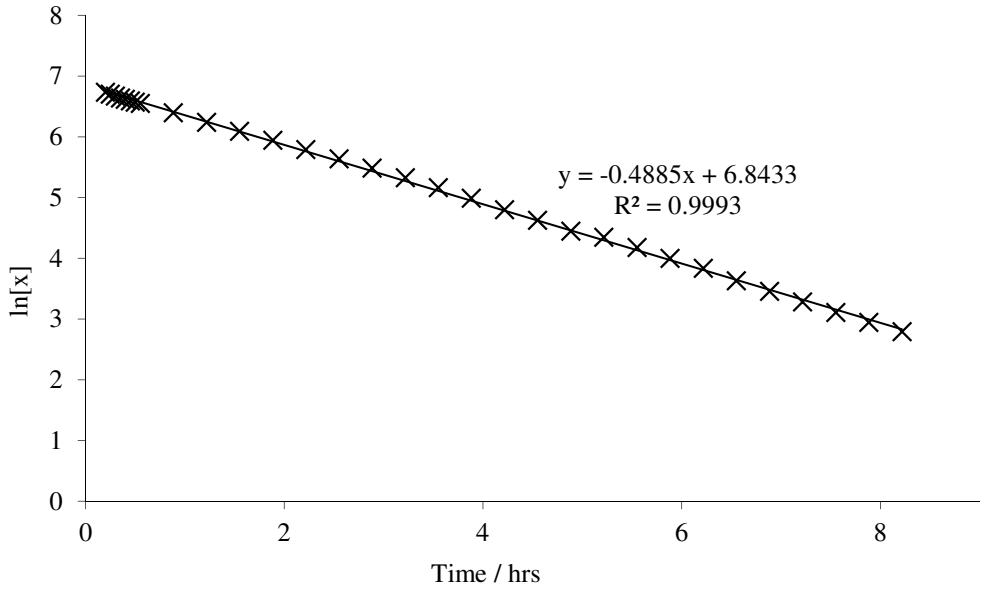

Figure 4.25: A first order kinetic data plot for the decrease in concentration of DMAB for the reaction between 0.5 mmol DMAB and 5 mol % **XV** at 70 °C.

In contrast to the behaviour of **VI**, **XV** was relatively stable towards β-diketiminate protonation during dehydrocoupling of DMAB and displayed instantaneous and irreversible protonolysis of the *n*-butyl ligand to form species containing the $[NMe_2BH_2NMe_2BH_3]^-$ anion. The rapidity of this reaction precluded any valid comparison to the Group 3 or calcium-based catalyses. Reactions between 0.05 mmol DMAB and 5 mol % **XV** were carried out at temperatures between 40 °C and 60 °C, with the change in concentration of DMAB monitored using integration from ^{11}B NMR spectroscopy. The Eyring and Arrhenius plots resulting from these initial rate data reactions are shown in Figures 4.26 and 4.27 respectively.

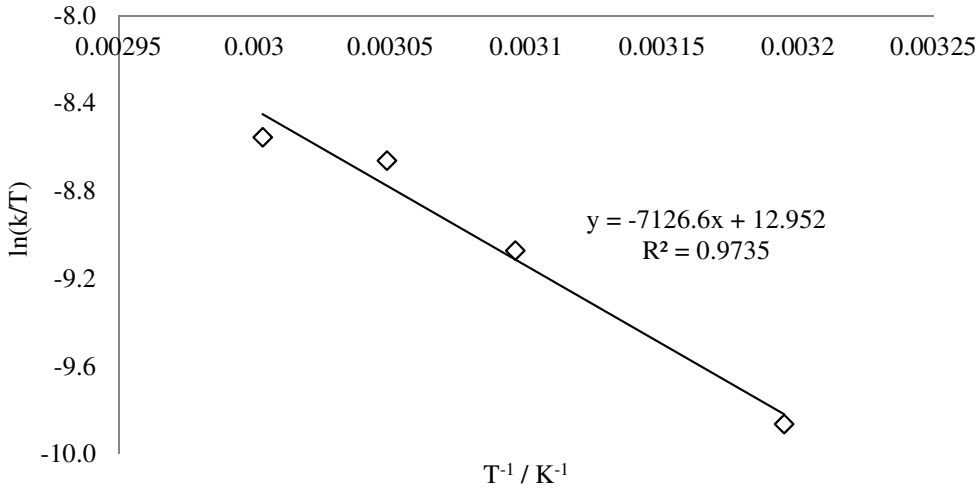

Figure 4.26: Eyring plot for variable temperature reactions between 0.5 mmol DMAB and 5 mol % **XV**.

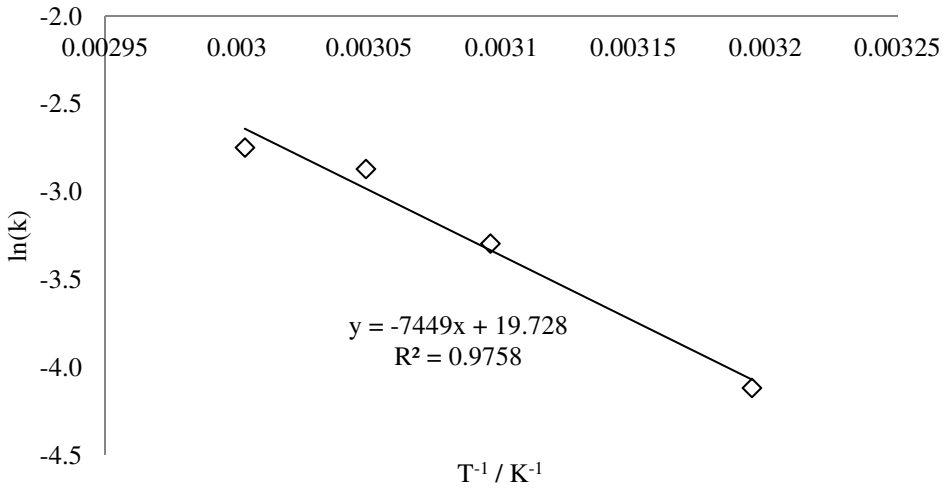

Figure 4.27: Arrhenius plot for variable temperature reactions between 0.5 mmol DMAB and 5 mol % **XV**.

The data plotted in Figures 4.26 and 4.27 were used to calculate the values of E_a, $\Delta H^{\ddagger}$ and $\Delta S^{\ddagger}$ in Table 4.2. As previously stated, however, the values in Table 4.2 are not comparable to other data due to a variety of factors.

	E_a / kJmol^{-1}	$\Delta H^{\ddagger}$ / kJmol^{-1}	$\Delta S^{\ddagger}$ / JK^{-1}mol^{-1}	$\Delta G_{298}^{\ddagger}$ / kJmol^{-1}
XV	61.9 $\pm$ 1.8	59.3 $\pm$ 1.0	–89.9 $\pm$ 3.4	86.0 $\pm$ 2.0

Table 4.2: Table of kinetic data from Eyring and Arrhenius plots for variable temperature reactions between DMAB and 5 mol % **XV** (data utilising a *pseudo*-initial rates method).

Following the demonstration of stability of the β-diketiminato alkyl precatalyst **XV** towards ligand protonation, the analogous reaction between 0.5 mmol DMAB and 5 mol % of the homoleptic silylamide **V-Mg** was carried out at 70 °C. The zero order kinetic data plot for this reaction is shown in Figure 4.28.

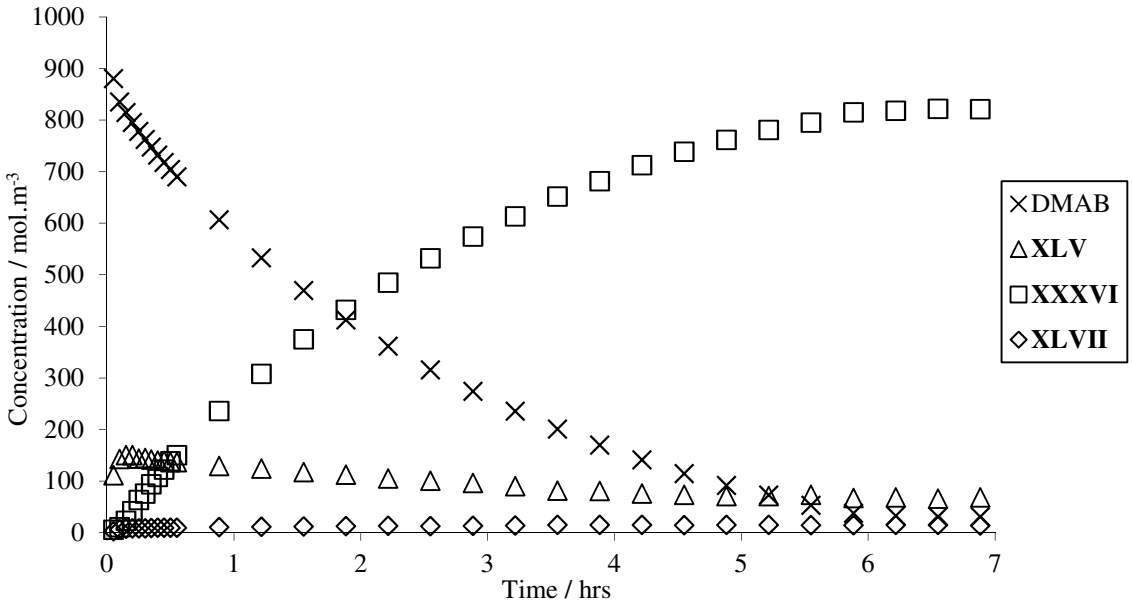

Figure 4.28: A zero order kinetic data plot for the reaction between 0.5 mmol DMAB and 5 mol % **V-Mg** at 70 °C.

The data plotted in Figure 4.28 show that this reaction also proceeded smoothly to completion, in contrast to reactions between DMAB and either of the calcium silylamides **VI** or **V-Ca**, with conversion to **XXXVI** as the major product and ca. 1.4 % **XLVII**. Similar to the reaction with **XV**, rapid initiation occurs despite the change from alkyl to amide precatalyst, consistent with the variable transamidation reactivity of the alkaline earth silylamides (Mg-Sr) reported by Hill.[6, 8] Once again

the change in concentration of boron-containing species could not be modelled by either 0, 1st, or 2nd order kinetics, however, the consumption of DMAB could be modelled by 1st order kinetics and is shown in Figure 4.29.

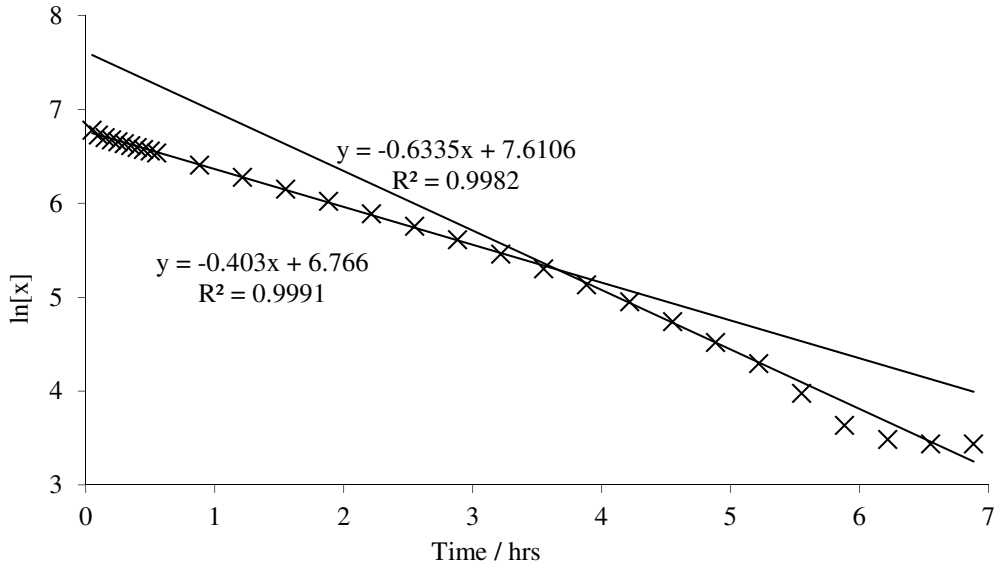

Figure 4.29: A first order kinetic data plot for the decrease in concentration of DMAB for the reaction between 0.5 mmol DMAB and 5 mol % **V-Mg** at 70 °C.

The first order plot in Figure 4.29 appears to show that after ca. 3.5 hours of the reaction there is a transition to a period of increased reaction rate, also characterised by 1st order kinetics, before the rate of reaction again declines. After 3.5 hours of the reaction, however, the reaction has reached ca. 80 % completion and might reasonably be expected to show some variation in reaction rate.

The magnesium precatalysts **XV** and **V-Mg** do not, therefore, undergo deactivation during dehydrocoupling reactions with DMAB under these conditions. Whether these species undergo ligand protonation or some facile exchange whilst remaining active, however, is unclear.

4.4 Comparison of Reactivity of Group 1 Precatalysts **LIX** for Catalytic Dehydrocoupling of Amine Boranes

Chapter 3, Section 3.2.2, described catalytic dehydrocoupling experiments between DMAB and the Group 1 precatalysts **LIX-Li**, **LIX-Na** and **LIX-K** which suggested

a reactivity trend in the order Li > Na > K based upon qualitative data. To establish the veracity of this empirically deduced trend in reactivity, the initial rates method was applied to reactions between 0.5 mmol DMAB and 5 mol % catalyst at 50 °C. The consumption of DMAB was monitored by ^{11}B NMR spectroscopy. The results of these experiments are shown in Figure 4.30.

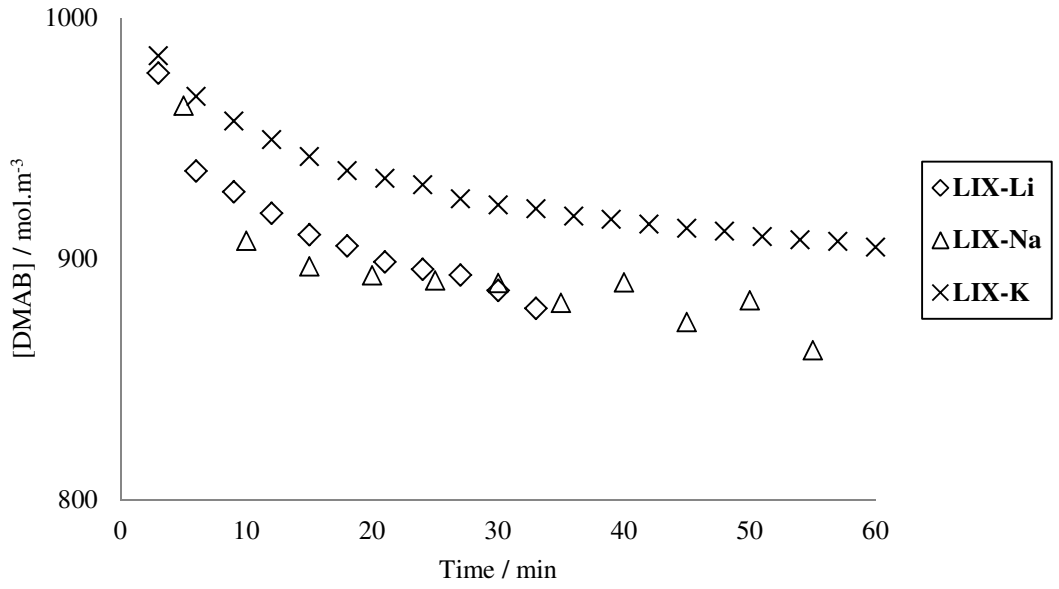

Figure 4.30: A zero order initial rates kinetic data plot for reactions between 0.5 mmol DMAB and 5 mol % **LIX-Li** (diamonds), **LIX-Na** (triangles) and **LIX-K** (crosses) at 50 °C.

The results in Figure 4.30 show that dehydrocoupling by **LIX-Li** and **LIX-Na** proceeded at very similar rates, whilst the reaction between **LIX-K** and DMAB proceeded at a slower rate. These initial rates of reaction suggest a trend in reactivity of Li ≈ Na > K, supporting the notion of a dependence upon the identity of the metal centre on dehydrocoupling reactivity of these species. Qualitative evidence described in Chapter 3, Section 3.2.5 suggested that **LIX-Li** was a superior precatalyst to the sodium and potassium analogues and suggested that the rate of these reactions slowed markedly after some initial period. Based upon evidence of reactions between DMAB and the calcium species **VI** and **V-Ca** in Section 4.2, the observation of a reduction in dehydrocoupling activity of these species was tentatively rationalised as resulting from formation of barely hydrocarbon-soluble Group 1 hydride species. A full kinetic study beyond the scope of this thesis would

be required to completely characterise these reactions and verify the proposed process of catalyst deactivation.

4.5 The Trend in Reactivity of Group 1, 2 and 3 Precatalysts for Catalytic Dehydrocoupling of Amine Boranes

Sections 4.1 and 4.4 compared the reactivity of Group 3, Group 2 and Group 1 species respectively in dehydrocoupling reactions with 0.5 mmol DMAB and 5 mol % precatalyst at 50 °C. Initial rates experiments established trends in reactivity of Sc > Y for **XL** and **XLI**, Mg > Ca, and Li ≈ Na > K for **LIX-Li**, **LIX-Na** and **LIX-K**. Figure 4.31 shows this data compiled on the same axes to illustrate an overall trend in reactivity for these d^0 precatalysts.

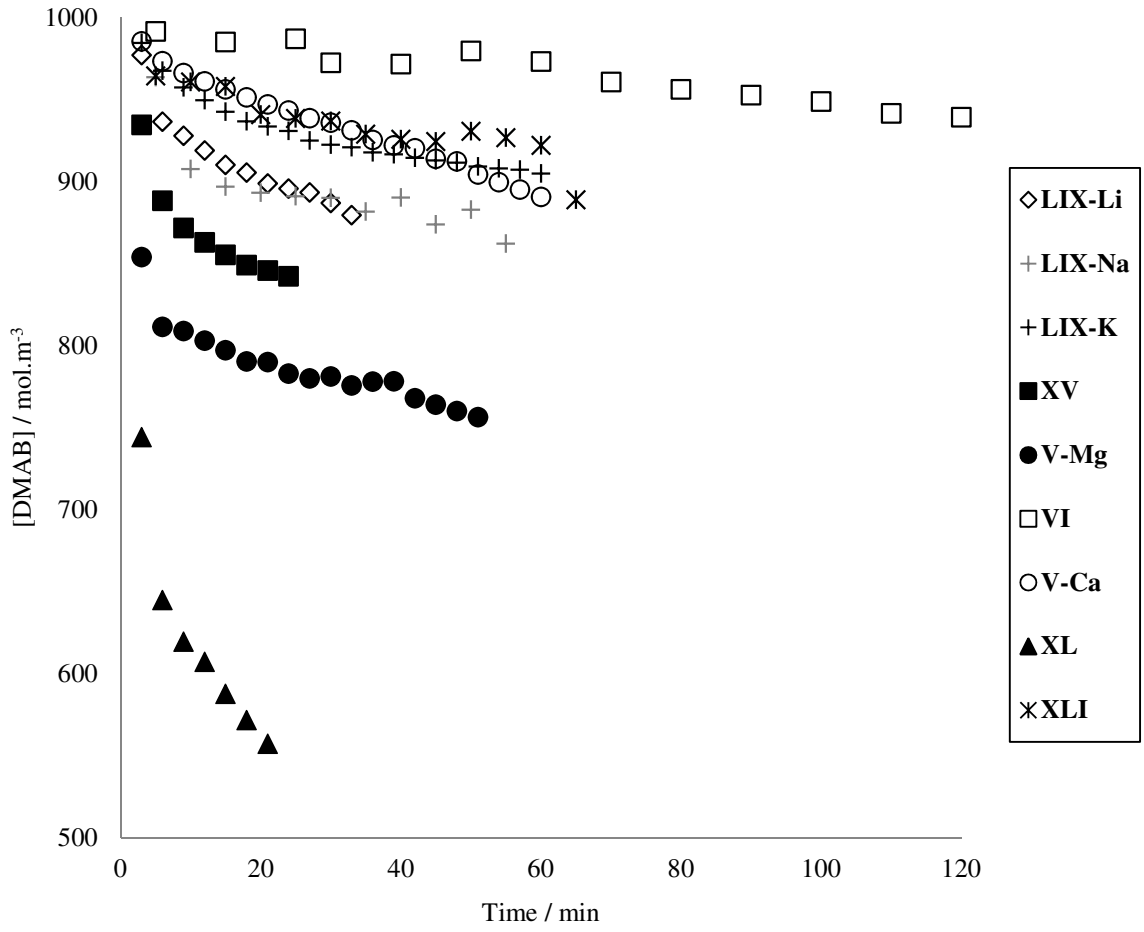

Figure 4.31: A zero order initial rates kinetic data plot for reactions between 0.5 mmol DMAB and 5 mol % **LIX-Li** (diamonds), **LIX-Na** (grey pluses), **LIX-K** (black pluses), **XV** (black squares), **V-Mg** (black circles), **VI** (white squares), **V-Ca** (white circles), **XL** (black triangles) and **XLI** (stars) at 50 °C. The time axis has been adjusted to enable comparison of faster reactions; full data for the reaction of **V-Ca** is not shown.

Figure 4.31 shows that the most active precatalyst is **XL**, rapidly forming a scandium-coordinated $[NMe_2BH_2NMe_2BH_3]^-$ species, followed by the two magnesium species **V-Mg** and **XV** respectively whilst the least active precatalyst is **VI**. As described in Section 4.4 the dehydrocoupling activity of **LIX-Li** is similar to that of **LIX-Na**, whilst Figure 4.31 shows that **LIX-K**, **V-Ca** and **XLI** all provide similar reaction rates. This produces a reactivity trend of Sc > Mg > Li ≈ Na > K ≈ Ca ≈ Y, reflecting a general relationship between decreasing reactivity and increasing ionic radius of the metal centre as Groups 1, 2 and 3 are descended. This

comparison does not consider the difference in the changing charge density of the ions of Groups 1-3 which is hypothesised to be a key factor in dehydrocoupling reactivity of these species. The number of amidoborane units that each metal centre may accommodate and the solubility of these species will also be influential in these reactions.

In all of the reactions described in this chapter, other than that of β-diketiminate magnesium ^{n}Bu **XV**, initiation of the precatalyst results in formation of an amine. Hill reported transamination equilibria of alkaline earth complexes,[9] suggesting that for the establishment of similar equilibria involving the silylamine **XCIV** formed in the initial protonolysis and amine borane species cannot be discounted. Although these equilibria cannot be quantified in such a complex system, Hill's reports on the effects of similar reactivity on hydroamination catalysis suggest that they are likely to be highly influencial in the overall efficacy of amine borane dehydrocoupling catalysis.[6, 8, 10-14] For reactions with **XV** the alkane formed in the initial protonolysis is expected to have negligible involvement in the catalysis, however, transamination equilibria between amine borane fragments could potentially influence the catalytic activity.

4.6 Chapter 4 Conclusion

The mechanism of dehydrocoupling of amine boranes by d^0 species has, throughout this chapter, been shown to be a complex process giving rise to kinetic data that does not conform to any simple rate dependence for boron-containing species other than DMAB. Kinetic data derived from catalytic dehydrocoupling reactions may not always be rationalised. For example, more reactive dehydrocoupling species do not always yield rate determining reaction barriers which reflect the global kinetics of the catalysis, raising questions as to what process this data was characterising. These reactions may be somewhat entropically controlled, with activity defined by more or less ordered transition states, reminiscent of Group 2 catalysed intermolecular hydroamination.[6]

An investigation seeking to evaluate the dependence of the dehydrocoupling reactivity on catalyst identity for species of Groups 1, 2 and 3 proved to be overly ambitious and highlighted the pitfalls inherent in attempting to overgeneralise comparisons between even chemically similar species. The instability to ligand protonation of the calcium reagents **VI** and **V-Ca** required the method of initial rates in order to obtain quantitative data from these reactions. For these reagents the initial 10 % consumption of amine borane is a period of ligand protonation, impeding formation of metallated $[NMe_2BH_2NMe_2BH_3]^-$ species and prohibiting a meaningful kinetic investigation. In contrast the magnesium reagents **XV** and **V-Mg** and the scandium reagent **XLI** rapidly form a metallated $[NMe_2BH_2NMe_2BH_3]^-$ species upon initiation. In the absence of superior methodology the initial rates data did reveal, however, a dependence upon the identity of the metal centre of the dehydrocoupling activity of reagents of Groups 1-3. The gross trend in reactivity was found to follow the order Sc > Mg > Li ≈ Na > K ≈ Ca ≈ Y, and identified a decrease in reactivity with increasing ionic radius and decreasing cation charge density as each group is descended, i.e. Li ≈ Na > K, Mg > Ca and Sc > Y. The reactivity trend did not reflect, however, an absolute correlation between ionic radius and reactivity and was partially rationalised by the futility in comparing the metals of Groups 1-3.

4.7 Experimental Procedures for Chapter 4

All reactions were carried out using glovebox techniques under an inert argon atmosphere. NMR experiments were conducted in Youngs tap NMR tubes prepared and sealed in a glovebox. NMR spectra were collected on a Bruker AV300 spectrometer operating at 75.5 MHz (^{13}C), 96.3 MHz (^{11}B). Solvents (toluene, THF, hexane) were dried by a commercially available solvent purification system (Innovative Technologies) under nitrogen before storage in ampoules over molecular sieves. C_6D_6, d_8-toluene and d_8-THF were purchased from Goss Scientific Instruments Ltd., dried over molten potassium before distillation under nitrogen and storage over molecular sieves. $Me_2NH.BH_3$, $^tBuNH_2.BH_3$ and Group 1 [M{N(SiMe$_3$)$_2$}] **LIX** reagents were purchased from Sigma-Aldrich Ltd. and used without further purification. β-diketiminate **VI** and **XV**,[15-17] bis(amide) [M{N(SiMe$_3$)$_2$}$_2$]$_2$ **V**,[18] and Group 3 tris(amide) **XL** and **XLI** reagents were all synthesised by literature procedures.[19, 20]

General Experimental Procedure

All kinetic experiments were carried out on an NMR-scale in Youngs tap NMR tubes. Compounds were weighed out and added to 0.5 ml d_8-toluene inside a glovebox under an inert argon atmosphere, before being sealed inside a Youngs tap NMR tube. On removal from the glovebox the sample was frozen in liquid nitrogen and thawed before insertion into the NMR spectrometer. Reactions were monitored by ^{11}B NMR spectroscopy, with concentration of boron-containing reaction species determined using integration across all observed species. Boron-containing species were identified using values of chemical shift obtained from literature reports of known compounds and species described elsewhere in this thesis. Reactions requiring elevated temperatures were heated inside the NMR spectrometer and equilibrated for ca. 10 minutes prior to use. The internal temperature of the NMR spectrometer deviated from the temperature at which it was set by a relationship characterised using methanol chemical shifts.[21] The resulting calibration curve was utilised to set the NMR spectrometer to a temperature at which the desired internal temperature for heating of the NMR tube was achieved. Reactions requiring prolonged heating times (> ca. 13 hours) were heated in thermostatically controlled

oil baths and monitored periodically by ^{11}B NMR spectroscopy. Kinetic experiments were conducted until 3 half-lives had passed, unless the reaction prohibited this (e.g. in the case of deactivation of catalyst). The method of initial rates was utilised to characterise reactions exhibiting more complex behaviour and the initial 10 % of the reaction was monitored. For reactions in which the initial 10 % of reaction was too rapid to characterise, however, the 10 % of reaction subsequent to the conversion at the first ^{11}B NMR spectrum was monitored. The method of initial rates is invalid in these situations as commented upon in the text.

Equations Used for Calculations:

$r = k\,[\text{Amine borane}]^{\alpha}\,[\text{Catalyst}]^{\beta}$

(a) Zero-order kinetics:

$r = k = -d[\text{Amine borane}]/dt$

(**Eqn 1**) $[\text{Amine borane}]_t = -kt + [\text{Amine borane}]_0$

(b) First-order kinetics:

$r = k[\text{Amine borane}] = -d[\text{Amine borane}]/dt$

(**Eqn 2**) $\ln[\text{Amine borane}]_t = -kt + \ln[\text{Amine borane}]_0$

(c) Pseudo first-order kinetics:

(**Eqn 3**) When [Y] is in excess, $r = k\,[X]^{\alpha}\,[Y]^{\beta} = k'[X]^{\alpha}$

(c) Second-order kinetics:

$r = -d[\text{Amine borane}]/dt = 2k[\text{Amine borane}]^2$

(**Eqn 4**) $(1/[\text{Amine borane}]_t) = (1/[\text{Amine borane}]_0) + kt$

Eyring Equation

$k = (k_B T/h).\exp(-\Delta G^{\ddagger}/RT) = (k_B T/h).\exp(-\Delta H^{\ddagger}/RT).\exp(\Delta S^{\ddagger}/R)$

(**Eqn 5**) $\ln(k/T) = (-\Delta H^{\ddagger}/R).(1/T) + \ln(k_B/h) + (\Delta S^{\ddagger}/R)$

Where:

k = Reaction rate constant

T = Temperature (K)

k_B = Boltzmann constant = 1.380649×10^{-23} JK^{-1}

R = Universal gas constant = 8.314462 $JK^{-1}mol^{-1}$

h = Planck's constant = 6.626070×10^{-34} Js

$\Delta H^{\ddagger}$ = Enthalpy of activation

$\Delta S^{\ddagger}$ = Entropy of activation

$\Delta G^{\ddagger}$ = Gibbs free energy

A plot of $\ln(k/T)$ vs $(1/T)$ should be a straight line with a gradient of $(-\Delta H^{\ddagger}/R)$ and y-axis intercept of $[\ln(k_B/h) + (\Delta S^{\ddagger}/R)]$ from which $\Delta H^{\ddagger}$ and $\Delta S^{\ddagger}$ can be calculated.

<u>Arrhenius Equation</u>

$k = A.\exp(-E_a/RT)$

(**Eqn 6**) $\ln(k) = (-E_a/R).(1/T) + \ln(A)$

Where:

k = Reaction rate constant

T = Temperature (K)

R = Universal gas constant = 8.314462 $JK^{-1}mol^{-1}$

E_a = Activation energy $Jmol^{-1}$

A = Pre-exponential constant

A plot of ln(k) vs (1/T) should be a straight line with a gradient of ($-E_a/R$) and y-axis intercept of ln(A) from which E_a can be calculated.

Determination of Partial Rate Order

$r = k\,[\text{Amine borane}]^{\alpha}\,[\text{Catalyst}]^{\beta}$

In a series of reactions for which [Catalyst] is constant:

(**Eqn 7**) $\ln(r) = \alpha[\text{Amine borane}] + \text{Constant}$

A graph of ln(r) vs [Amine borane] should give a straight line with a gradient of α.

In a series of reactions for which [Amine borane] is constant:

(**Eqn 8**) $\ln(r) = \beta[\text{Catalyst}] + \text{Constant}$

A graph of ln(r) vs [Catalyst] should give a straight line with a gradient of β.

Calculation of errors

Errors were calculated by the least squares method.

Kinetic Isotope Effect (KIE):

(**Eqn 9**) $KIE = k_H/k_D$

Where:

k_H = Reaction rate constant for protio substrate

k_D = Reaction rate constant for deuterated substrate

4.7.1 Kinetic Characterisation of Catalytic Dehydrocoupling of [$Me_2HN.BH_3$] by Group 3 Species

4.7.1.1 Variable Temperature Catalytic Dehydrocoupling of [$Me_2HN.BH_3$] by [$Sc\{N(SiHMe_2)_2\}_3(THF)_2$] **XL**

D_8-toluene (0.5 ml) was added to a solid mixture of $Me_2NH.BH_3$ (29.4 mg, 0.5 mmol) and 5 mol % [$Sc\{N(SiHMe_2)_2\}_3(THF)_2$] **XL** (14.6 mg, 0.025 mmol), and the solution sealed in a Youngs tap NMR tube before the reaction at (i) 308 K, (ii) 313 K, (iii) 318 K, (iv) 323 K and (v) 328 K, was monitored by ^{11}B NMR spectroscopy using a Bruker AV400 spectrometer. The results of these reactions is shown in Figure 4.32, a first-order kinetic data plot for the consumption of $Me_2NH.BH_3$. This data was using to plot Eyring and Arrhenius plots shown in Figures 4.2 and 4.3 respectively. Values of E_a, $\Delta H^{\ddagger}$, $\Delta S^{\ddagger}$ and $\Delta G^{\ddagger}_{298}$ were calculated using equations **Eqn 5** and **Eqn 6**.

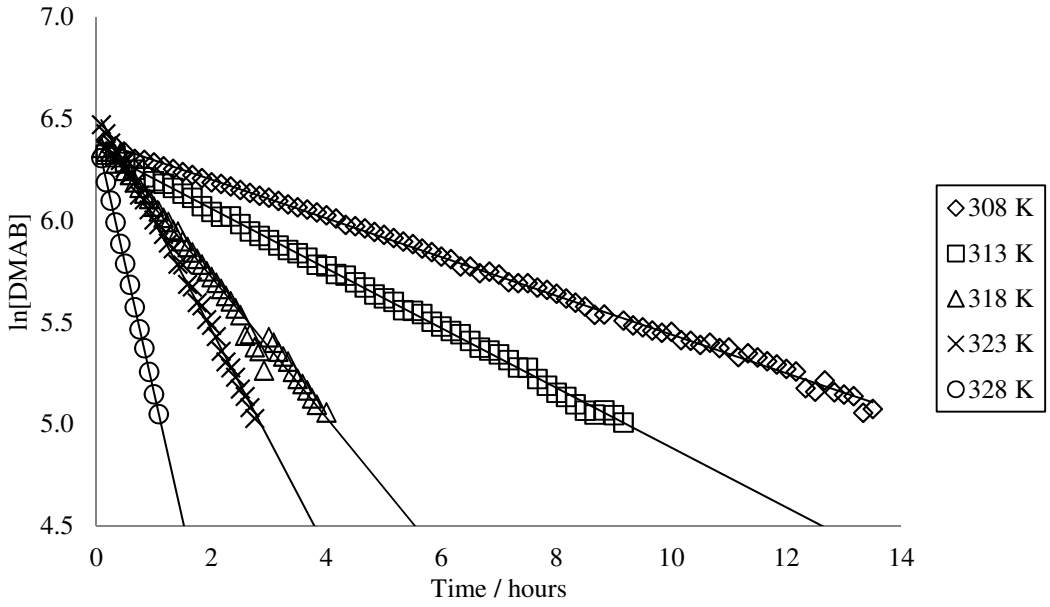

Figure 4.32: First-order kinetic data plot for variable temperature catalytic dehydrocoupling of [$Me_2HN.BH_3$] by 5 mol % [$Sc\{N(SiHMe_2)_2\}_3(THF)_2$] **XL** at 308 K (diamonds), 313 K (squares), 318 K (triangles), 323 K (crosses) and 328 K (circles).

Temperature / K	Equation for line of best fit	R^2
308	y = -0.0951x + 6.3919	0.9978
313	y = -0.1467x + 6.3513	0.9988
318	y = -0.3451x + 6.4124	0.9913
323	y = -0.5377x + 6.5385	0.9977
328	y = -1.254x + 6.4094	0.9998

Table 4.3: Data derived from Figure 4.34 for variable temperature catalytic dehydrocoupling of $[Me_2HN.BH_3]$ by 5 mol % $[Sc\{N(SiHMe_2)_2\}_3(THF)_2]$ **XL**.

4.7.1.2 Variable Temperature Catalytic Dehydrocoupling of $[Me_2HN.BH_3]$ by $[Y\{N(SiMe_3)_2\}_3]$ **XLI**

D_8-toluene (0.5 ml) was added to a solid mixture of $Me_2NH.BH_3$ (29.4 mg, 0.5 mmol) and 5 mol % $[Y\{N(SiMe_3)_2\}_3]$ **XLI** (14.3 mg, 0.025 mmol), and the solution sealed in a Youngs tap NMR tube before the reaction at (i) 328 K, (ii) 333 K, (iii) 338 K, (iv) 343 K and (v) 348 K, was monitored by ^{11}B NMR spectroscopy using a Bruker AV400 spectrometer. The results of these reactions is shown in Figure 4.33, a first-order kinetic data plot for the consumption of $Me_2NH.BH_3$. This data was used to plot Eyring and Arrhenius plots, shown in Figures 4.2 and 4.3 respectively. Values of E_a, $\Delta H^{\ddagger}$, $\Delta S^{\ddagger}$ and $\Delta G^{\ddagger}_{298}$ were calculated using equations **Eqn 5** and **Eqn 6**.

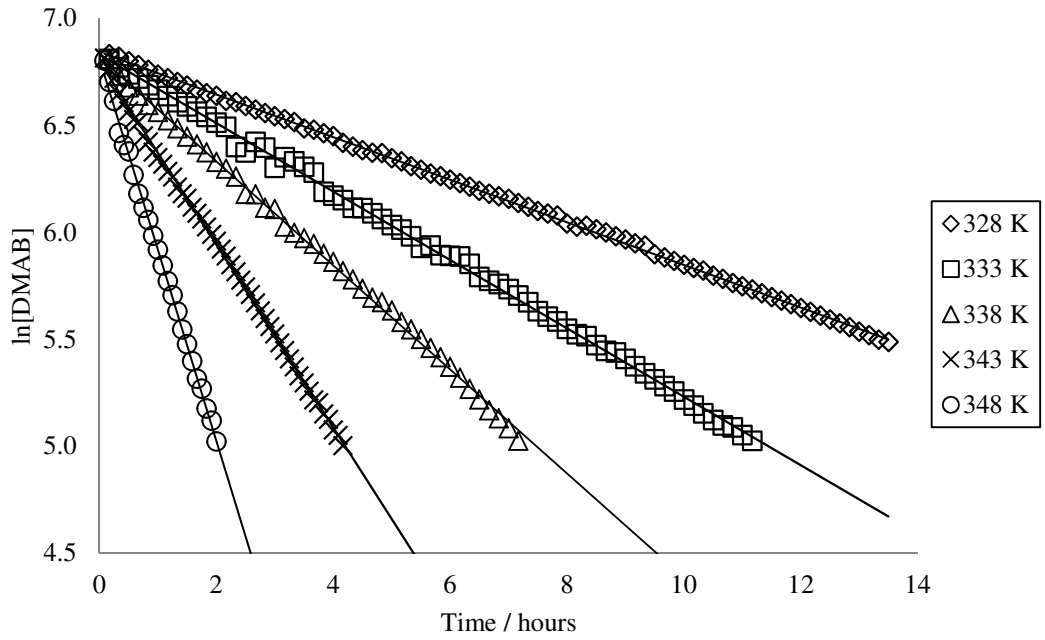

Figure 4.33: First-order kinetic data plot for variable temperature catalytic dehydrocoupling of $[Me_2HN.BH_3]$ by 5 mol % $[Y\{N(SiMe_3)_2\}_3]$ **XLI** at 308 K (diamonds), 313 K (squares), 318 K (triangles), 323 K (crosses) and 328 K (circles).

Temperature / K	Equation for line of best fit	R^2
328	y = -0.0995x + 6.843	0.9995
333	y = -0.1599x + 6.8304	0.9985
338	y = -0.2431x + 6.8181	0.9985
343	y = -0.4277x + 6.7993	0.999
348	y = -0.8934x + 6.8128	0.9978

Table 4.4: Data derived from Figure 4.35 for variable temperature catalytic dehydrocoupling of $[Me_2HN.BH_3]$ by 5 mol % $[Y\{N(SiMe_3)_2\}_3]$ **XLI**.

4.7.1.3 Catalytic Dehydrocoupling of $[Me_2HN.BH_3]$ by $[Sc\{N(SiHMe_2)_2\}_3(THF)_2]$ **XL** and $[Y\{N(SiMe_3)_2\}_3]$ **XLI** at 323 K Using The Method of Initial Rates

D_8-toluene (0.5 ml) was added to a solid mixture of $Me_2NH.BH_3$ (29.4 mg, 0.5 mmol) and 5 mol % $[Sc\{N(SiHMe_2)_2\}_3(THF)_2]$ **XL** (14.6 mg, 0.025 mmol) or $[Y\{N(SiMe_3)_2\}_3]$ **XLI** (14.3 mg, 0.025 mmol) and the solution sealed in a Youngs tap NMR tube before the reaction at 323 K was monitored by ^{11}B NMR

spectroscopy using a Bruker AV500 spectrometer in a *pseudo*-initial rates method, in which the 10% of reaction following the first ^{11}B NMR spectrum was followed. The results of these reactions are shown in Figure 4.4, a zero-order kinetic data plot for the consumption of $Me_2NH.BH_3$.

4.7.1.4 Determination of Rate Law for the Reaction Between [$Me_2HN.BH_3$] and [$Y\{N(SiMe_3)_2\}_3$] **XLI** at 323 K Using The Method of Initial Rates

D_8-toluene (0.5 ml) was added to solid mixtures of $Me_2NH.BH_3$ and catalytic quantities of [$Y\{N(SiMe_3)_2\}_3$] **XLI**, as detailed in Table 3.10, and the solution sealed in a Youngs tap NMR tube before the reaction at 323 K was monitored by ^{11}B NMR spectroscopy using a Bruker AV500 spectrometer in a pseudo-initial rates method, in which the 10 % of reaction following the first ^{11}B NMR spectrum was followed. Experiments were conducted at a fixed concentration of $Me_2NH.BH_3$ whilst varying the concentration of [$Y\{N(SiMe_3)_2\}_3$] **XLI**, to obtain a partial order of reaction w.r.t. [$Y\{N(SiMe_3)_2\}_3$] **XLI**, in addition to experiments at a fixed concentration of [$Y\{N(SiMe_3)_2\}_3$] **XLI** whilst varying the concentration of $Me_2NH.BH_3$, to obtain a partial order of reaction w.r.t. $Me_2NH.BH_3$. The results of these experiments are shown in Figure 4.34. Determination of the partial orders w.r.t. concentration of [$Y\{N(SiMe_3)_2\}_3$] **XLI** and [$Me_2NH.BH_3$] was by using **Eqn 7** and **Eqn 8** and logarithm plots are shown in Figures 4.5 and 4.6 respectively.

	[$Y\{N(SiMe_3)_2\}_3$] **XLI**	[$Me_2NH.BH_3$]
1	14.2 mg, 0.025 mmol	29.4 mg, 0.5 mmol
2	7.1 mg, 0.0125 mmol	29.4 mg, 0.5 mmol
3	21.4 mg, 0.0375 mmol	29.4 mg, 0.5 mmol
4	28.5 mg, 0.05 mmol	29.4 mg, 0.5 mmol
5	14.2 mg, 0.025 mmol	14.7 mg, 0.25 mmol
6	14.2 mg, 0.025 mmol	58.8 mg, 1.0 mmol
7	14.2 mg, 0.025 mmol	44.1 mg, 0.75 mmol

Table 4.5: Initial rates experiments at 323 K between various concentrations of [$Y\{N(SiMe_3)_2\}_3$] **XLI** and [$Me_2NH.BH_3$] to determine partial orders of reaction for these species.

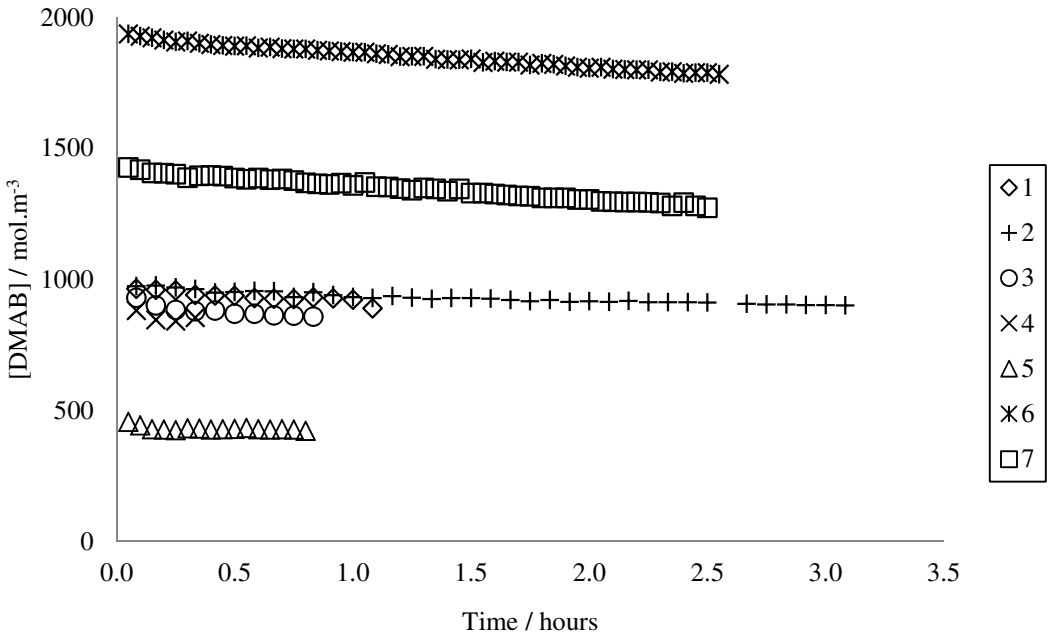

Figure 4.34: Initial rates kinetic data plot for reactions between $Me_2HN.BH_3$ and $[Y\{N(SiMe_3)_2\}_3]$ **XLI** at 323 K, according to the reactions in Table 4.5, to determine partial orders of reaction for these species.

Experiment	Equation for line of best fit	R^2
1	y = -0.924x + 966.59	0.8245
2	y = -0.5696x + 972.95	0.9032
3	y = -1.3004x + 914.78	0.8083
4	y = -1.7216x + 876.95	0.3876
5	y = -0.3349x + 438.34	0.3406
6	y = -0.988x + 1925.3	0.9806
7	y = -0.9609x + 1418.2	0.9753

Table 4.6: Data derived from Figure 4.34 for catalytic dehydrocoupling reactions between $[Me_2HN.BH_3]$ and $[Y\{N(SiMe_3)_2\}_3]$ **XLI**, to determine partial orders of reaction for these species.

4.7.2 Kinetic Characterisation of Catalytic Dehydrocoupling of [$Me_2HN.BH_3$] by Calcium Precatalysts [β-diketiminato.Ca{$N(SiMe_3)_2$}] **VI** and [Ca{{$N(SiMe_3)_2$}] **V-Ca**

4.7.2.1 Variable Temperature Catalytic Dehydrocoupling of [$Me_2HN.BH_3$] by [β-diketiminato.Ca{$N(SiMe_3)_2$}] **VI**

D_8-toluene (0.5 ml) was added to a solid mixture of $Me_2NH.BH_3$ (29.4 mg, 0.5 mmol) and 5 mol % [β-diketiminato.Ca{$N(SiMe_3)_2$}] **VI** (14.7 mg, 0.025 mmol), and the solution sealed in a Youngs tap NMR tube before the reaction at (i) 343 K, (ii) 353 K, and (iii) 363 K was monitored by ^{11}B NMR spectroscopy using a Bruker AV500 spectrometer. After reaction times of between 2 and 12 hours the samples were removed from the NMR spectrometer and heated by thermostatically controlled oil baths. The reactions were monitored periodically by ^{11}B NMR spectroscopy using a Bruker AV300 spectrometer. The results of these reactions are shown by zero-order kinetic data plots in Figures 4.7 and 4.8 for the reaction at 343 K, Figures 4.9 shows the initial period of consumption of $Me_2NH.BH_3$ for reactions at 343 K, 353 K and 363 K, whilst Figures 4.10 and 4.11 show zero-order kinetic data plots for the consumption of $Me_2NH.BH_3$ and formation of (Me_2N-BH_2) **XXXVI** respectively in these reactions. An Arrhenius plot for the consumption of $Me_2NH.BH_3$ is shown in Figure 4.35 and a value for E_a was calculated using **Eqn 6**.

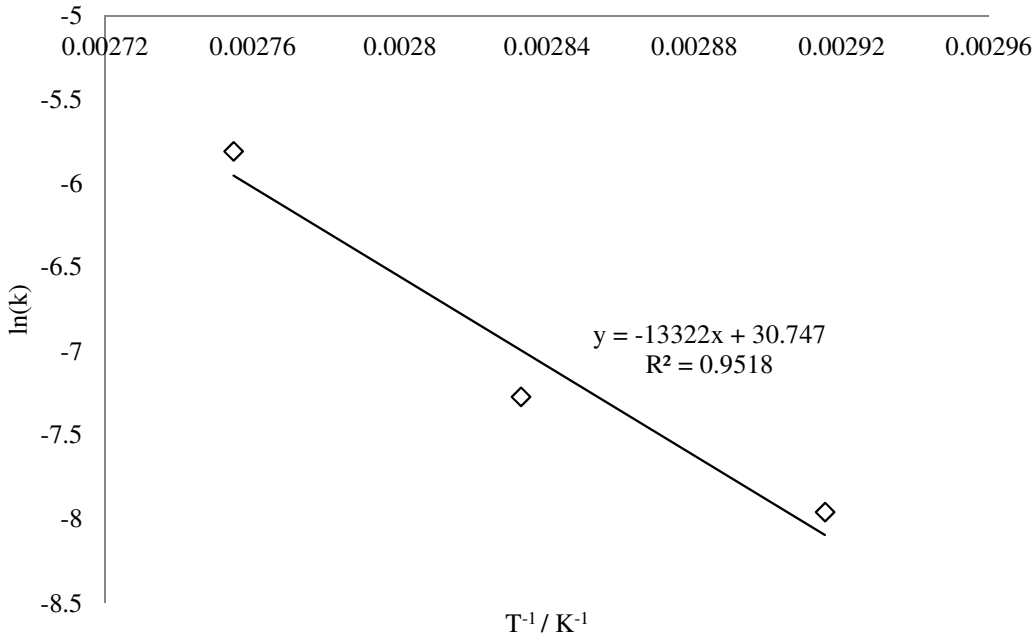

Figure 4.35: Arrhenius plot for the reaction between DMAB and 5 mol % **VI** at 70 °C, 80 °C and 90 °C.

4.7.2.2 Catalytic Dehydrocoupling of [$Me_2HN.BH_3$] by [β-diketiminato.Ca{$N(SiMe_3)_2$}] **VI** in THF

D_8-THF (0.5 ml) was added to a solid mixture of $Me_2NH.BH_3$ (29.4 mg, 0.5 mmol) and 5 mol % [β-diketiminato.Ca{$N(SiMe_3)_2$}] **VI** (14.7 mg, 0.025 mmol), and the solution sealed in a Youngs tap NMR tube before the NMR tube was heated at 353 K by a thermostatically controlled oil bath. The reaction was monitored periodically by ^{11}B NMR spectroscopy using a Bruker AV300 spectrometer. The results of this reaction are shown by a zero-order kinetic data plots in Figures 4.12.

4.7.2.3 Catalytic Dehydrocoupling of [$Me_2HN.BH_3$] by 10 mol % [β-diketiminato.Ca{$N(SiMe_3)_2$}] **VI**

(i) 5 mol %, followed by 5 mol % [β-diketiminato.Ca{$N(SiMe_3)_2$}] **VI**

D_8-toluene (0.5 ml) was added to a solid mixture of $Me_2NH.BH_3$ (29.4 mg, 0.5 mmol) and 5 mol % [β-diketiminato.Ca{$N(SiMe_3)_2$}] **VI** (14.7 mg, 0.025 mmol), and the solution sealed in a Youngs tap NMR tube before the reaction at 343 K was monitored by ^{11}B NMR spectroscopy using a Bruker AV500 spectrometer. After a

reaction time of 1 hour the samples was removed from the NMR spectrometer and taken back into a glove box. Another 5 mol % [β-diketiminato.Ca{$N(SiMe_3)_2$}] **VI** (14.7 mg, 0.025 mmol) was added to the NMR tube before being sealed and the reaction at 343 K was monitored by ^{11}B NMR spectroscopy using a Bruker AV500 spectrometer.

(ii) 10 mol % [β-diketiminato.Ca{$N(SiMe_3)_2$}] **VI**

D_8-toluene (0.5 ml) was added to a solid mixture of $Me_2NH.BH_3$ (29.4 mg, 0.5 mmol) and 10 mol % [β-diketiminato.Ca{$N(SiMe_3)_2$}] **VI** (29.4 mg, 0.05 mmol), and the solution sealed in a Youngs tap NMR tube before the reaction at 343 K was monitored by ^{11}B NMR spectroscopy using a Bruker AV500 spectrometer. The results of these experiments are shown by the zero-order kinetic data plot in Figure 4.13.

4.7.2.4 Variable Temperature Catalytic Dehydrocoupling of [$Me_2HN.BH_3$] by [β-diketiminato.Ca{$N(SiMe_3)_2$}] **VI** Using the Method of Initial Rates

D_8-toluene (0.5 ml) was added to a solid mixture of $Me_2NH.BH_3$ (29.4 mg, 0.5 mmol) and 5 mol % [β-diketiminato.Ca{$N(SiMe_3)_2$}] **VI** (14.7 mg, 0.025 mmol), and the solution sealed in a Youngs tap NMR tube before the reaction at (i) 318 K, (ii) 323 K, (iii) 333 K and (iv) 338 K, was monitored by ^{11}B NMR spectroscopy using a Bruker AV500 spectrometer in a pseudo-initial rates method, in which the 10% of reaction following the first ^{11}B NMR spectrum was monitored. The results of these reactions are shown in Figure 4.36, a zero-order kinetic data plot for the consumption of $Me_2NH.BH_3$, with the best-fit lines shown in Table 4.7. This data was used to plot Eyring and Arrhenius plots, shown in Figures 4.14 and 4.15 respectively. Values of E_a, $\Delta H^{\ddagger}$, $\Delta S^{\ddagger}$ and $\Delta G^{\ddagger}_{298}$ were calculated using equations **Eqn 5** and **Eqn 6**.

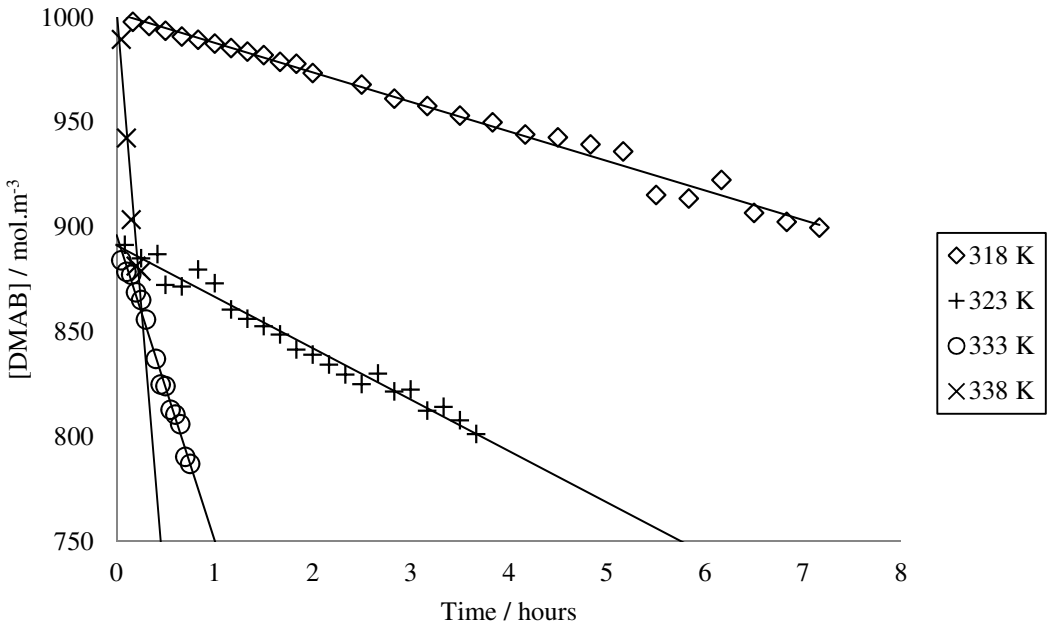

Figure 4.36: Initial rates kinetic data plot for reactions between $Me_2HN.BH_3$ and 5 mol % [β-diketiminato.Ca{$N(SiMe_3)_2$}] **VI** at 318 K (diamonds), 323 K (pluses), 333 K (circles) and 338 K (crosses).

Reaction Temperature / K	Equation for line of best fit	R^2
318	y = -0.235x + 1002	0.9877
323	y = -0.4087x + 891.16	0.9767
333	y = -2.4296x + 896.12	0.9888
338	y = -9.4141x + 1003.8	0.9071

Table 4.7: Data derived from Figure 4.36 for variable temperature catalytic dehydrocoupling reactions between [$Me_2HN.BH_3$] and 5 mol % [β-diketiminato.Ca{$N(SiMe_3)_2$}] **VI**.

4.7.2.5 Catalytic Dehydrocoupling of [$Me_2HN.BH_3$] by 5 mol % [Ca{$N(SiMe_3)_2$}$_2$] **V-Ca** at 343 K

D_8-toluene (0.5 ml) was added to a solid mixture of $Me_2NH.BH_3$ (29.4 mg, 0.5 mmol) and 5 mol % [Ca{$N(SiMe_3)_2$}$_2$] **V-Ca** (9.0 mg, 0.025 mmol) and the solution sealed in a Youngs tap NMR tube before the reaction at 343 K was monitored by ^{11}B NMR spectroscopy using a Bruker AV500 spectrometer. After two hours reaction

time the sample was removed from the NMR spectrometer and heated by a thermostatically controlled oil bath at 343 K. The reaction was monitored periodically by ^{11}B NMR spectroscopy using a Bruker AV300 spectrometer. The results of this reaction is shown by a zero-order kinetic data plot for the consumption of $Me_2NH.BH_3$ in Figures 4.16.

4.7.2.6 Variable Temperature Catalytic Dehydrocoupling of [$Me_2HN.BH_3$] by 5 mol % [$Ca\{N(SiMe_3)_2\}_2$] **V-Ca** Using the Method of Initial Rates

D_8-toluene (0.5 ml) was added to a solid mixture of $Me_2NH.BH_3$ (29.4 mg, 0.5 mmol) and 5 mol % [$Ca\{N(SiMe_3)_2\}_2$] **V-Ca** (9.0 mg, 0.025 mmol), and the solution sealed in a Youngs tap NMR tube before the reactions at (i) 318 K, (ii) 323 K, (iii) 328, (iv) 333 K and (v) 338 K, were monitored by ^{11}B NMR spectroscopy using a Bruker AV500 spectrometer in an initial rates method, in which the 10% of reaction following the first ^{11}B NMR spectrum was monitored. The results of these reactions are shown in Figure 4.37, a zero-order kinetic data plot for the consumption of $Me_2NH.BH_3$, with the best-fit lines shown in Table 4.8. This data was used to plot Eyring and Arrhenius plots, shown in Figures 4.18 and 4.19 respectively. Values of E_a, $\Delta H^{\ddagger}$, $\Delta S^{\ddagger}$ and $\Delta G^{\ddagger}_{298}$ were calculated using equations **Eqn 5** and **Eqn 6**.

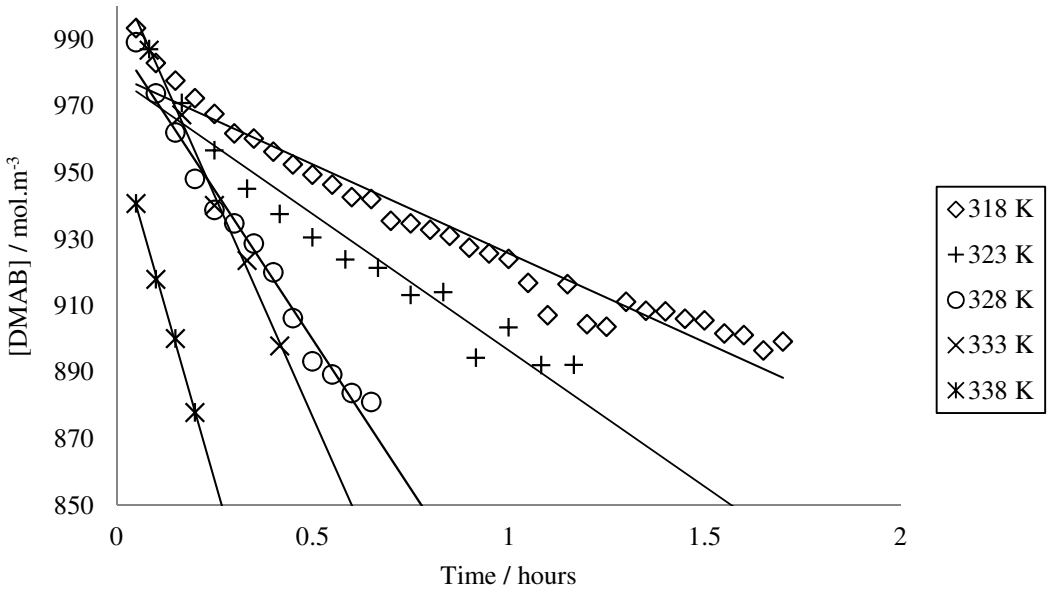

Figure 4.37: Initial rates kinetic data plot for reactions between $Me_2HN.BH_3$ and 5 mol % $[Ca\{N(SiMe_3)_2\}_2]$ **V-Ca** at 318 K (diamonds), 323 K (pluses), 328 K (circles), 333 K (crosses) and 338 K (stars).

Reaction Temperature / K	Equation for line of best fit	R^2
318	y = -0.891x + 979.25	0.947
323	y = -1.3659x + 978.56	0.9372
328	y = -2.9933x + 989.73	0.9815
333	y = -4.433x + 1009.6	0.9957
338	y = -6.878x + 960.73	0.9979

Table 4.8: Data derived from Figure 4.37 for variable temperature catalytic dehydrocoupling reactions between $[Me_2HN.BH_3]$ and 5 mol % $[Ca\{N(SiMe_3)_2\}_2]$ **V-Ca**.

4.7.2.7 Determination of Rate Law for the Reaction Between $[Me_2HN.BH_3]$ and $[Ca\{N(SiMe_3)_2\}_2]$ **V-Ca** at 323 K Using The Method of Initial Rates

D_8-toluene (0.5 ml) was added to solid mixtures of $Me_2NH.BH_3$ and catalytic quantities of $[Ca\{N(SiMe_3)_2\}_2]$ **V-Ca**, as detailed in Table 4.9, and the solution sealed in a Youngs tap NMR tube before the reaction at 323 K was monitored by ^{11}B

NMR spectroscopy using a Bruker AV500 spectrometer by the method of initial rates, in which the 10% of reaction following the first ^{11}B NMR spectrum was followed. Experiments were conducted at a fixed concentration of $Me_2NH.BH_3$ whilst varying the concentration of $[Ca\{N(SiMe_3)_2\}_2]$ **V-Ca**, to obtain a partial order of reaction w.r.t. $[Ca\{N(SiMe_3)_2\}_2]$ **V-Ca**, in addition to experiments at a fixed concentration of $[Ca\{N(SiMe_3)_2\}_2]$ **V-Ca** whilst varying the concentration of $Me_2NH.BH_3$, to obtain a partial order of reaction w.r.t. $Me_2NH.BH_3$. The results of these experiments are shown in Figure 4.38. Determination of the partial orders w.r.t. concentration of $[Ca\{N(SiMe_3)_2\}_2]$ **V-Ca** and $[Me_2NH.BH_3]$ was by using equations **Eqn 7** and **Eqn 8** and logarithm plots are shown in Figures 4.20 and 4.21 respectively.

	$[Ca\{N(SiMe_3)_2\}_2]$ **V-Ca**	$[Me_2NH.BH_3]$
1	4.5 mg, 0.0125 mmol	29.4 mg, 0.5 mmol
2	13.5 mg, 0.0375 mmol	29.4 mg, 0.5 mmol
3	18.0 mg, 0.05 mmol	29.4 mg, 0.5 mmol
4	9.0 mg, 0.025 mmol	14.7 mg, 0.5 mmol
5	9.0 mg, 0.025 mmol	44.1 mg, 0.75 mmol
6	9.0 mg, 0.025 mmol	58.8 mg, 1.0 mmol
7	9.0 mg, 0.025 mmol	29.4 mg, 0.5 mmol

Table 4.9: Initial rates experiments at 323 K between various concentrations of $[Ca\{N(SiMe_3)_2\}_2]$ **V-Ca** and $[Me_2NH.BH_3]$ to determine partial orders of reaction with respect to these species.

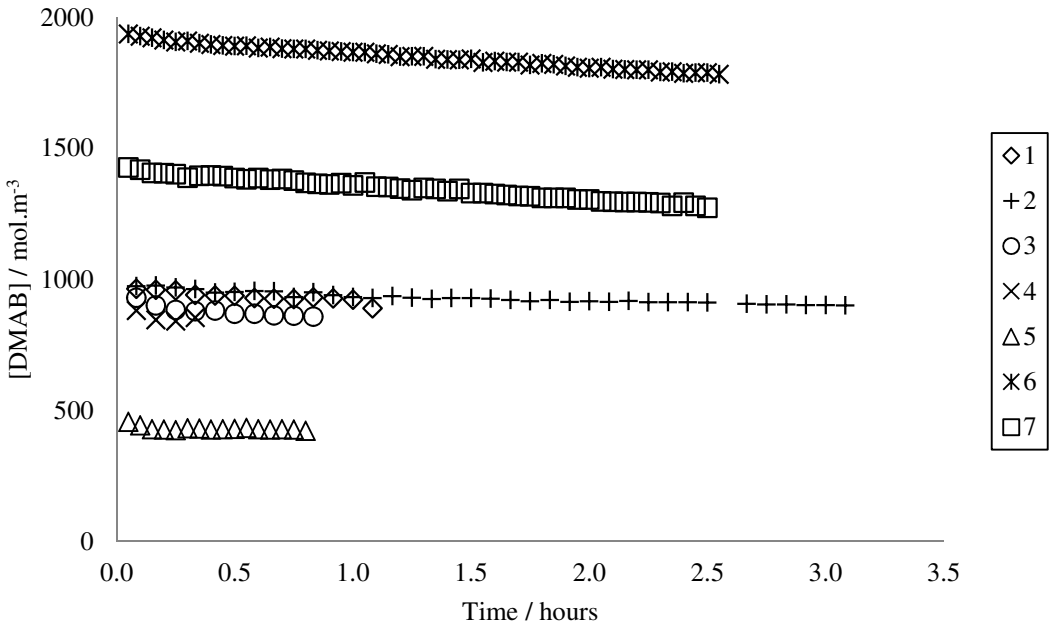

Figure 4.38: Initial rates kinetic data plot for reactions between $Me_2HN.BH_3$ and $[Ca\{N(SiMe_3)_2\}_2]$ **V-Ca** at 323 K, according to the reactions in Table 4.9, to determine partial orders of reaction for these species.

Experiment	Equation for line of best fit	R^2
1	y = -1.0473x + 972.68	0.9404
2	y = -1.8149x + 983.42	0.9373
3	y = -2.4993x + 977.26	0.9505
4	y = -1.1134x + 485.69	0.9613
5	y = -1.8828x + 1476	0.951
6	y = -2.187x + 1969.3	0.9397
7	y = -1.5112x + 981.23	0.9917

Table 4.10: Data derived from Figure 4.38 for catalytic dehydrocoupling reactions between $[Me_2HN.BH_3]$ and $[Ca\{N(SiMe_3)_2\}_2]$ **V-Ca**, to determine partial orders of reaction with respect to these species.

4.7.2.8 Catalytic Dehydrocoupling of (i) [$Me_2HN.BH_3$], (ii) [$Me_2HN.BD_3$] and (iii) [$Me_2DN.BH_3$] by 5 mol % [$Ca\{N(SiMe_3)_2\}_2$] **V-Ca** to Determine Values of Kinetic Isotope Effect at 323 K Using the Method of Initial Rates

D_8-toluene (0.5 ml) was added to 5 mol % [$Ca\{N(SiMe_3)_2\}_2$] **V-Ca** (9.0 mg, 0.025 mmol) and (i) $Me_2HN.BH_3$ (29.4 mg, 0.5 mmol), (ii) $Me_2HN.BD_3$ (31.0 mg, 0.5 mmol) and (iii) $Me_2DN.BH_3$ (30.0 mg, 0.5 mmol), and the solution sealed in a Youngs tap NMR tube before the reaction at 323 K was monitored by ^{11}B NMR spectroscopy using a Bruker AV500 spectrometer by the method of initial rates, in which the 10 % of reaction following the first ^{11}B NMR spectrum was followed. The results of these reactions are shown in Figure 4.22, a zero-order kinetic data plot for the consumption of amine borane.

4.7.2.9 Catalytic Dehydrocoupling of (i) [$Me_2HN.BH_3$] and (ii) [$^tBuH_2N.BH_3$] by 5 mol % [$Ca\{N(SiMe_3)_2\}_2$] **V-Ca** at 323 K Using the Method of Initial Rates

D_8-toluene (0.5 ml) was added to 5 mol % [$Ca\{N(SiMe_3)_2\}_2$] **V-Ca** (9.0 mg, 0.025 mmol) and (i) $Me_2HN.BH_3$ (29.4 mg, 0.5 mmol) and (ii) $^tBuH_2N.BH_3$ (43.5 mg, 0.5 mmol), and the solution sealed in a Youngs tap NMR tube before the reaction at 323 K was monitored by ^{11}B NMR spectroscopy using a Bruker AV500 spectrometer by the method of initial rates, in which the 10% of reaction following the first ^{11}B NMR spectrum was followed. The results of these reactions are shown in Figure 4.23, a zero-order kinetic data plot for the consumption of amine borane.

4.7.3 Kinetic Characterisation of Catalytic Dehydrocoupling of [$Me_2HN.BH_3$] by Magnesium Precatalysts [β-diketiminato.Mg^{n}Bu] **XV** and [$Mg\{N(SiMe_3)_2\}$] **V-Mg**

4.7.3.1 Catalytic Dehydrocoupling of (i) [$Me_2HN.BH_3$] and (ii) [$^tBuH_2N.BH_3$] by 5 mol % [β-diketiminato.Mg^{n}Bu] **XV** at 343 K

D_8-toluene (0.5 ml) was added to $Me_2HN.BH_3$ (29.4 mg, 0.5 mmol) and 5 mol % [β-diketiminato.Mg^{n}Bu] **XV** (12.5 mg, 0.025 mmol) and the solution sealed in a Youngs tap NMR tube before the reaction at 343 K was monitored by ^{11}B NMR spectroscopy using a Bruker AV500 spectrometer. The results of this reaction are shown in Figure 4.24 and 4.25, a zero-order kinetic data plot for the variation in

concentration of all boron-containing species and a first-order kinetic data plot for the consumption of amine borane respectively.

4.7.3.2 Variable Temperature Catalytic Dehydrocoupling of [$Me_2HN.BH_3$] by [β-diketiminato.Mg^{n}Bu] **XV** Using the Method of Initial Rates

D_8-toluene (0.5 ml) was added to a solid mixture of $Me_2NH.BH_3$ (29.4 mg, 0.5 mmol) and 5 mol % [β-diketiminato.Mg^{n}Bu] **XV** (12.5 mg, 0.025 mmol), and the solution sealed in a Youngs tap NMR tube before the reactions at (i) 313 K, (ii) 323 K, (iii) 328 and (iv) 333 K, were monitored by ^{11}B NMR spectroscopy using a Bruker AV500 spectrometer in a *pseudo*-initial rates method, in which the 10% of reaction following the first ^{11}B NMR spectrum was monitored. The results of these reactions are shown in Figure 4.39, a zero-order kinetic data plot for the consumption of $Me_2NH.BH_3$, with the best-fit lines shown in Table 4.11. This data was used to plot Eyring and Arrhenius plots, shown in Figures 4.26 and 4.27 respectively. Values of E_a, $\Delta H^{\ddagger}$, $\Delta S^{\ddagger}$ and $\Delta G^{\ddagger}_{298}$ were calculated using equations **Eqn 5** and **Eqn 6**.

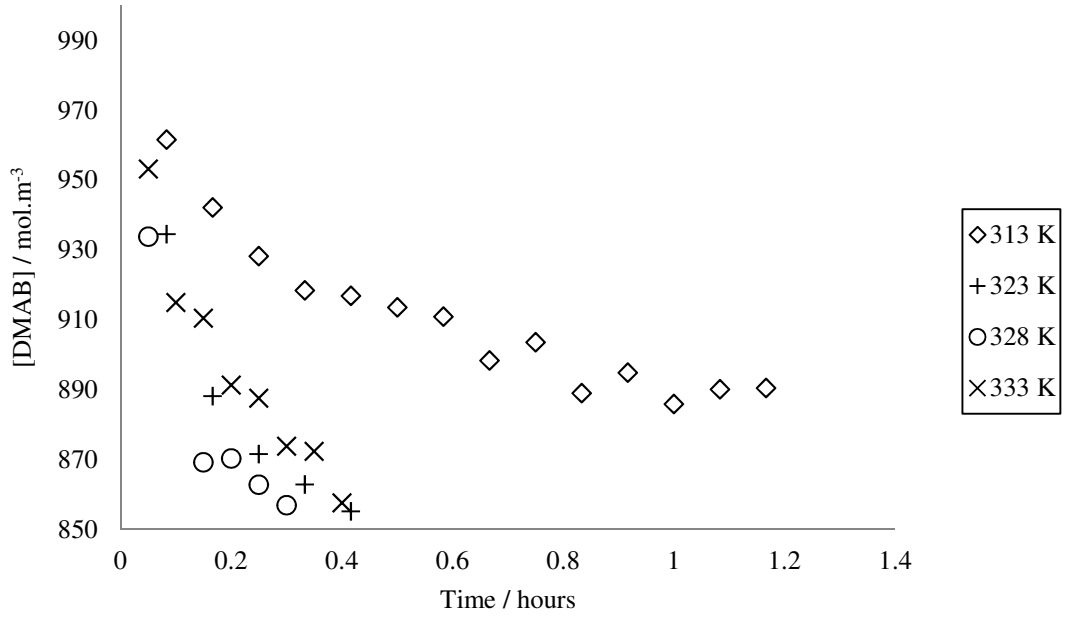

Figure 4.39: Initial rates kinetic data plot for reactions between $Me_2HN.BH_3$ and 5 mol % [β-diketiminato.Mg^{n}Bu] **XV** at 313 K (diamonds), 323 K (pluses), 328 K (circles) and 333 K (crosses).

Reaction Temperature / K	Equation for line of best fit	R^2
313	y = -0.9776x + 946.96	0.8544
323	y = -2.2246x + 918.71	0.7920
328	y = -3.404x + 920.02	0.8108
333	y = -3.8432x + 947.42	0.9340

Table 4.11: Data derived from Figure 4.39 for variable temperature catalytic dehydrocoupling reactions between [$Me_2HN.BH_3$] and 5 mol % [β-diketiminato.Mg^{n}Bu] **XV**.

4.7.4 Kinetic Characterisation of Catalytic Dehydrocoupling of [$Me_2HN.BH_3$] by 5 mol % (i) [Li{$N(SiMe_3)_2$}] **LIX-Li**, (ii) [Na{$N(SiMe_3)_2$}] **LIX-Na** and (iii) [K{$N(SiMe_3)_2$}] **LIX-K** at 323 K Using the Method of Initial Rates

D_8-toluene (0.5 ml) was added to $Me_2HN.BH_3$ (29.4 mg, 0.5 mmol) and 5 mol % (i) [Li{$N(SiMe_3)_2$}] **LIX-Li** (4.2 mg, 0.025 mmol), (ii) [Na{$N(SiMe_3)_2$}] **LIX-Na** (4.5 mg, 0.025 mmol) and (iii) [K{$N(SiMe_3)_2$}] **LIX-K** (5.0 mg, 0.025 mmol), and the solutions sealed in a Youngs tap NMR tube before the reactions at 323 K were monitored by ^{11}B NMR spectroscopy using a Bruker AV500 spectrometer by the method of initial rates, in which the 10% of reaction following the first ^{11}B NMR spectrum was followed. The results of these reactions are shown in Figure 4.30, a zero-order kinetic data plot for the consumption of amine borane.

4.8 References for Chapter 4

1. L. J. Sewell, G. C. Lloyd-Jones and A. S. Weller, *J. Am. Chem. Soc.*, 2012, **134**, 3598-3610.
2. T. J. Clark, C. A. Russell and I. Manners, *J. Am. Chem. Soc.*, 2006, **128**, 9582-9583.
3. C. A. Jaska and I. Manners, *J. Am. Chem. Soc.*, 2004, **126**, 9776-9785.
4. E. V. Anslyn and D. A. Dougherty, *Mod. Phys. Org. Chem.*, University Science Books, 2006.
5. M. S. Hill, G. Kociok-Köhn and T. P. Robinson, *Chem. Commun. (Camb)*, 2010, **46**, 7587-7589.
6. C. Brinkmann, A. G. M. Barrett, M. S. Hill and P. A. Procopiou, *J. Am. Chem. Soc.*, 2012, **134**, 2193-2207.
7. M. E. Sloan, A. Staubitz, T. J. Clark, C. A. Russell, G. C. Lloyd-Jones and I. Manners, *J. Am. Chem. Soc.*, 2010, **132**, 3831-3841.
8. A. G. Avent, M. R. Crimmin, M. S. Hill and P. B. Hitchcock, *Dalton Trans.*, 2005, 278-284.
9. A. G. M. Barrett, M. R. Crimmin, M. S. Hill, G. Kociok-Koehn, J. R. Lachs and P. A. Procopiou, *Dalton Trans.*, 2008, 1292-1294.
10. C. Brinkmann, A. G. M. Barrett, M. S. Hill, P. A. Procopiou and S. Reidt, *Organometallics*, 2012, **31**, 7287-7297.
11. M. Arrowsmith, M. R. Crimmin, A. G. M. Barrett, M. S. Hill, G. Kociok-Koehn and P. A. Procopiou, *Organometallics*, 2011, **30**, 1493-1506.
12. A. G. M. Barrett, I. J. Casely, M. R. Crimmin, M. S. Hill, J. R. Lachs, M. F. Mahon and P. A. Procopiou, *Inorg. Chem.*, 2009, **48**, 4445-4453.
13. A. G. M. Barrett, C. Brinkmann, M. R. Crimmin, M. S. Hill, P. Hunt and P. A. Procopiou, *J. Am. Chem. Soc.*, 2009, **131**, 12906-12907.
14. M. R. Crimmin, M. Arrowsmith, A. G. M. Barrett, I. J. Casely, M. S. Hill and P. A. Procopiou, *J. Am. Chem. Soc.*, 2009, **131**, 9670-9685.
15. M. H. Chisholm, J. C. Gallucci and K. Phomphrai, *Inorg. Chem.*, 2004, **43**, 6717-6725.
16. M. H. Chisholm and K. Phomphrai, *Inorg. Chim. Acta*, 2003, **350**, 121-125.

17. A. P. Dove, V. C. Gibson, P. Hormnirun, E. L. Marshall, J. A. Segal, A. J. P. White and D. J. Williams, *Dalton Trans.*, 2003, 3088-3097.
18. M. Westerhausen, *Inorg. Chem.*, 1991, **30**, 96-101.
19. R. Anwander, O. Runte, J. Eppinger, G. Gerstberger, E. Herdtweck and M. Spiegler, *J. Chem. Soc.*, 1998, 847-858.
20. D. C. Bradley, J. S. Ghotra and F. A. Hart, *J. Chem. Soc.*, 1973, 1021-1027.
21. A. L. Vangeet, *Anal. Chem.*, 1968, **40**, 2227-2229.

5 Alkaline Earth Mediated Reactions of Amine Boranes With Amines

This chapter describes catalytic dehydrocoupling reactions of amine boranes in reaction mixtures containing an amine, mediated by $[M\{N(SiMe_3)_2\}_2]$ **V** where M = Mg, Ca. The reactivity of the secondary amine boranes, dimethylamine borane (DMAB) and pyrrolidine borane (PB), and the primary amine borane, *tert*-butylamine borane (TBAB), are investigated in combination with primary and secondary amines. These reactions probe the proposed insertion reactivity in the presence of protic reagents.

The initial work on the dehydrocoupling of secondary amine boranes published by Hill and the work described in Chapters 2 and 3 of this thesis indicated that the polarised and unsaturated $[H_2B{=}NR_2]$ species can undergo insertion reactions into available M-E bonds. In Chapter 3 it was shown, however, that β-hydride elimination of the amidoborane species required the presence of an additional protic reagent to take place, an equivalent of amine borane in this case, suggestive of a proton-assisted and possibly concerted mechanism. In a catalytic regime, at equilibrium only small amounts of the amine borane will be deprotonated, undergoing a proposed proton-assisted β-hydride elimination to form the corresponding unsaturated $[H_2B{=}NR_2]$ species. In Chapter 3 it was shown that $[H_2B{=}NR_2]$ could insert into the M-N bond of a $[LM(NR_2BH_3)]$ species, producing a symmetrical $[HB(NR_2)_2]$ **XLVII** species following subsequent proton-assisted β-hydride elimination. In the presence of a better nucleophile than the $R_2HN.BH_3$ molecule itself, however, other protic reagents such as amines present suitably polarised bonds for insertion reactivity. In this regime the protic amine reagent promotes β-hydride elimination of the $[LM(NR_2BH_3)]$ species, with the generated $[H_2B{=}NR_2]$ fragment inserting into the M-N bond of the deprotonated reagent, producing a $[LM(NR_2BH_2NR'_2)]$ intermediate species with formation of a new B-N bond. This is shown by Step (**i**) in Figure 5.1 and represented by transition states **A** and **B**. A further β-hydride elimination, Step (**ii**) in Figure 5.1, produces the product, a diamineborane in the reaction with an amine. Similar to Step (**i**) and the catalytic cycle represented in Figure 3.45, this final β-hydride elimination, Step (**ii**), is once again proton-assisted. This regime would represent a novel route to unsymmetrical

diamineboranes [$(R_2N)BH(NR'_2)$] where the R_2N and R'_2N components of the molecule arise from the amine and amine borane reaction partners. Literature searches for diamineboranes reveals only symmetrical species such as [$HB(NMe_2)_2$] **XLVII**, thus, formation of any [$(R_2N)BH(NR'_2)$] species would result in novel structures. Successful formation of such species would also provide further evidence in support of the proposed mechanism of amine borane dehydrocoupling via an insertion step.

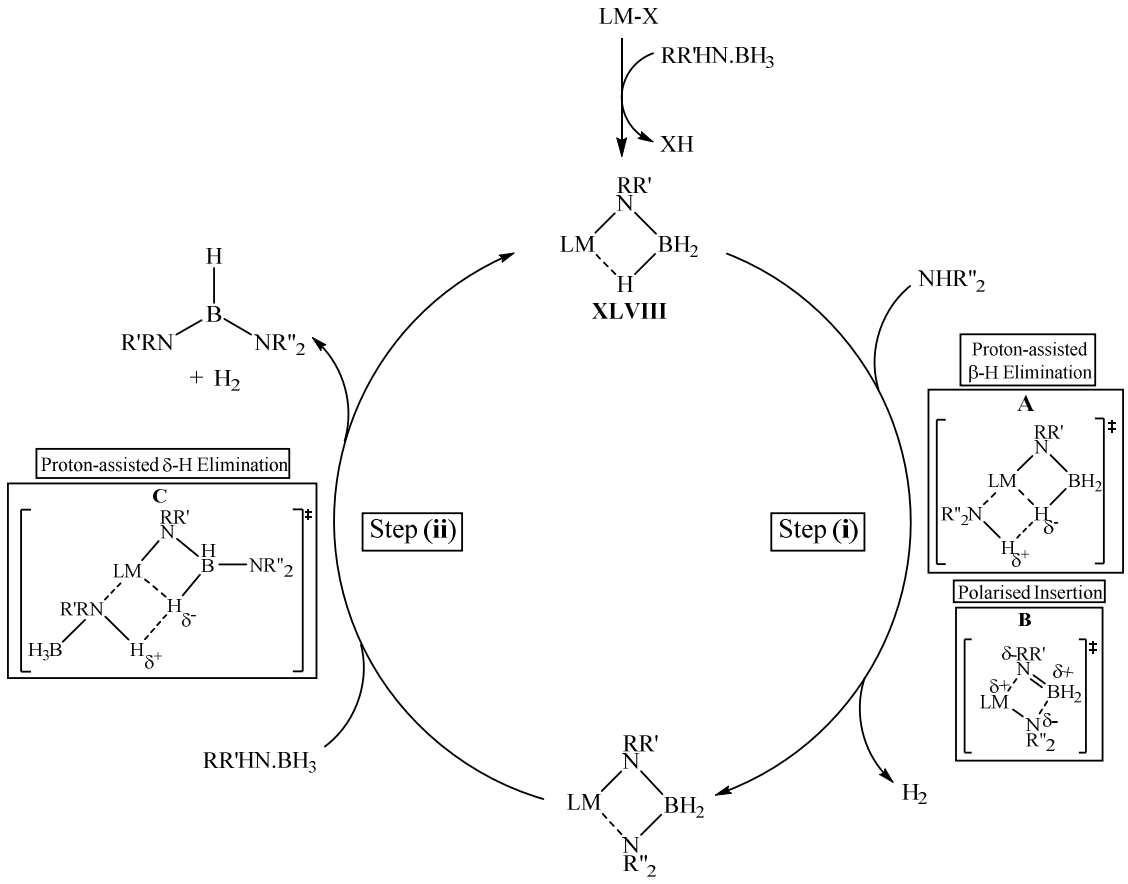

Figure 5.1: Proposed reaction scheme for the formation of new B-N bonds via dehydrocoupling reactions of amine boranes with protic amines.

5.1 Catalytic Insertion Reactions with Amines

Catalytic NMR scale reactions were carried out between 5 mol % **V-Ca**, the secondary amine boranes, DMAB and PB, and the primary amine borane, TBAB, in the presence of a stoichiometric quantity of amine. The amines used were pyrrolidine, di-*iso*-propylamine, diphenylamine (secondary amines) and *tert*-

butylamine (primary amine). The dehydrocoupling reactions of PB with pyrrolidine and TBAB with *tert*-butylamine were not carried out due to the identical amine substrate being present, which would result in the symmetrical [HB(NRR')$_2$] products. Reactions were heated in thermostatically controlled oil baths and monitored by ^{1}H and ^{11}B NMR spectroscopy. Uncatalysed reactions between amine borane and amine were carried out to assess the effect of metal species on these reactions, yielding low or zero conversion to products after extended heating times.

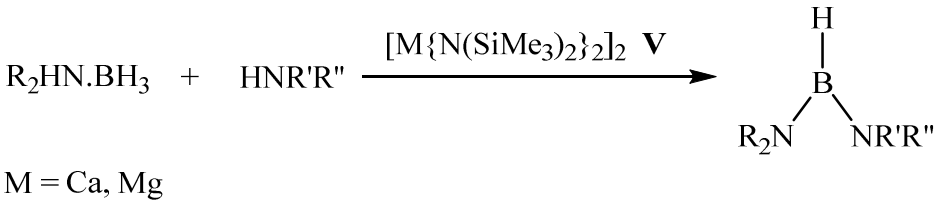

Figure 5.2: Reaction scheme for a catalytic reaction between amine borane and amine to produce a diamineborane [HB(NR$_2$)(NR'R")] product.

Each reaction, as shown in Figure 5.2, gave rise to a distinctive doublet resonance in the ^{11}B NMR spectrum relating to the formation of the novel unsymmetrical diamineborane product, the exact shift of which was dependent upon the nitrogen-bound alkyl groups. Example ^{11}B NMR spectra are shown in Figures 5.3 and 5.4.

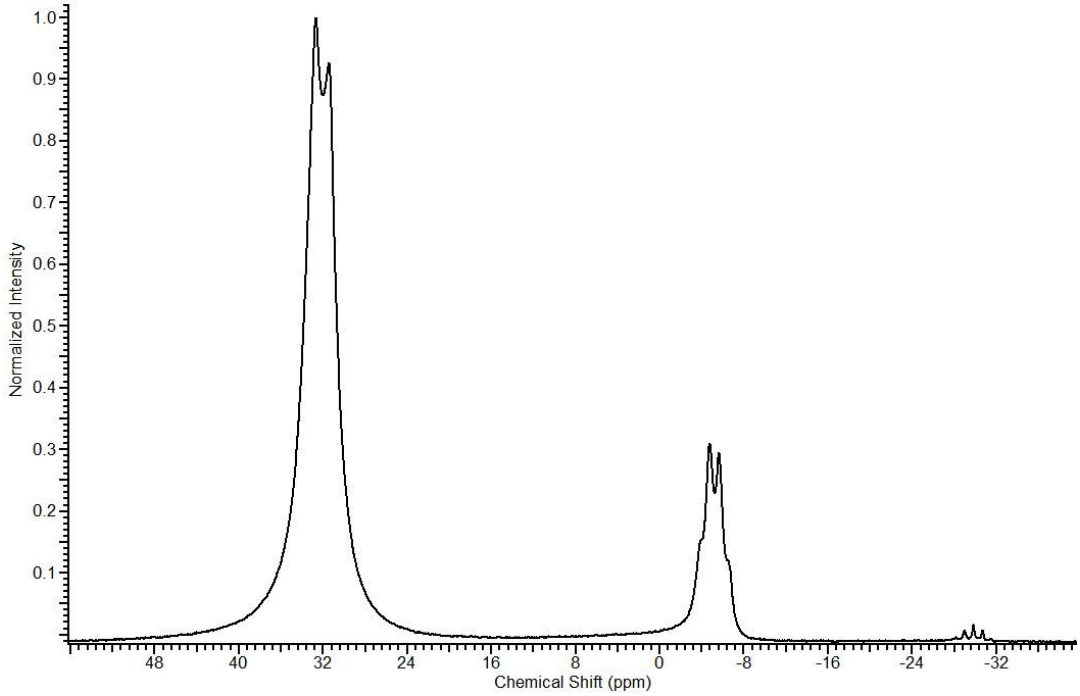

Figure 5.3: ^{11}B NMR spectrum for the reaction between DMAB, diphenylamine and 5 mol % **V-Ca** after heating at 90 °C for ca. 101 hours. (C_6D_6, 298 K, 96.3 MHz)

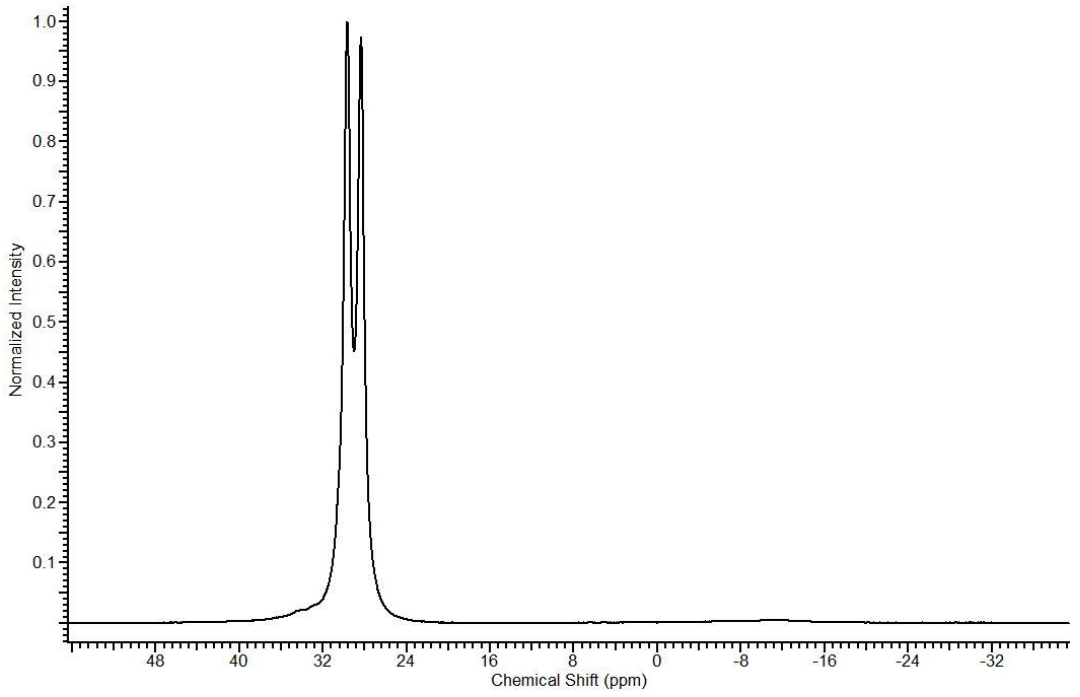

Figure 5.4: ^{11}B NMR spectrum for the reaction between TBAB, pyrrolidine and 5 mol % **V-Ca** after heating at 70 °C for ca. 24 hours. (C_6D_6, 298 K, 96.3 MHz)

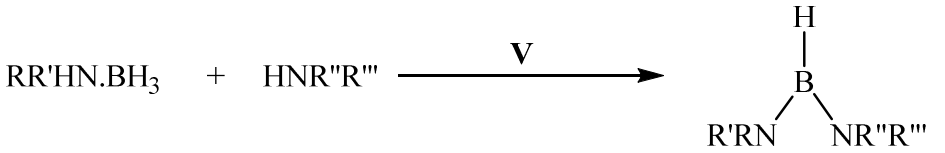

52: R = R' = Me, R" = R'" = $(CH_2)_2$
53: R = R' = Me, R" = H, R'" = $C(CH_3)_3$
54: R = R' = Me, R" = R'" = $CH(CH_3)_2$
55: R = R' = Me, R" = R'" = C_6H_5
56: R = R' = $(CH_2)_2$, R" = H, R'" = $C(CH_3)_3$
57: R = R' = $(CH_2)_2$, R" = R'" = $CH(CH_3)_2$
58: R = R' = $(CH_2)_2$, R" = R'" = C_6H_5
59: R = H, R' = $C(CH_3)_3$, R" = R'" = $CH(CH_3)_2$
60: R = H, R' = $C(CH_3)_3$, R" = R'" = C_6H_5

Figure 5.5: Reaction of amine borane, amine and catalyst to produce a diamineborane product.

The catalytic dehydrocoupling reaction of DMAB and pyrrolidine (**V-Ca**; ca. 24 hours at 70 °C, **V-Mg**; ca. 24 hours 70 °C) produced both the symmetrical $HB(NMe_2)_2$ **XLVII** product and the unsymmetrical product $[\{Me_2N\}BH\{NC_4H_8\}]$ **52** in a similar ratio for both calcium (1:1.2) and magnesium (1:1) catalysts. When *tert*-butylamine was employed, however, (**V-Ca**; ca. 48 hours at 70 °C, **V-Mg**; ca. 92 hours at room temperature) the calcium-catalysed reaction produced the unsymmetrical compound $[[\{Me_2N\}BH\{NH(^tBu)\}]$ **53** as the major product, alongside a small proportion (ca. 8 %) of **XLVII**, whilst the magnesium-catalysed reaction produced only compound **53**. The reactions with di-*iso*-propylamine and diphenylamine produced only the unsymmetrical products, $[[\{Me_2N\}BH\{N(^iPr)_2\}]$ **54** and $[[\{Me_2N\}BH\{NPh_2\}]$ **55** respectively. In contrast to this behaviour, the dehydrocoupling of PB and TBAB with any of the amines produced only the unsymmetrical products.

It is unclear why the reactions involving DMAB should produce both the symmetrical and unsymmetrical products in this way, whilst the other amine boranes did not. The variation in reactivity observed could suggest that the steric demands of the amine substrates have an influence in the reactions with DMAB, with bulkier groups promoting the production of the unsymmetrical product. In addition, amine boranes with bulkier substituents (compared to a methyl in the case of DMAB) appear to produce only the unsymmetrical product. It is unclear whether the identity

of the metal centre could influence the tendency for formation of the symmetrical product.

Reactions between the secondary amine boranes and the more sterically hindered amines, di-*iso*-propylamine and diphenylamine, required longer heating and higher temperatures (90 °C compared to 70 °C) to induce reaction. In contrast, reactions involving TBAB or *tert*-butylamine required either shorter heating times or lower temperatures to achieve high conversion to the diamineborane product. This was rationalised as a consequence of the difference in steric demands and electronic character of the particular amine borane and amine in question. The dehydrocoupling reactions of TBAB described in Chapter 3, Section 3.2.6 and the kinetic analysis described in Chapter 4, Section 4.2, suggested that this primary amine borane reacted faster than the secondary amine boranes DMAB and PB. It is not unreasonable therefore for reactions between amines and TBAB to show similarly enhanced reactivity compared to the analogous reactions with secondary amine boranes. A full kinetic and/or a computational study on these reactions would be required, however, to validate this qualitative data and assess the effect on reaction rate of the different amine substituents present for both reactants.

The results were consistent with the proposed reaction scheme shown in Figure 5.1, for both the secondary amine boranes (DMAB and PB) and the primary amineborane, TBAB, which were used in these experiments. The dehydrocoupling of the primary amine borane TBAB was described in Chapter 3, Section 3.2.6, the products of which highlighted that the dehydrocoupling mechanism was more complicated and involves additional reaction pathways compared to the mechanism for secondary amine boranes. The two reactions to produce compound **56**, PB with *tert*-butylamine and TBAB with pyrrolidine, suggested that the reaction between TBAB and pyrrolidine was the more favourable route to **56**, requiring a lower heating temperature.

All reactions proceeded faster when catalysed by an alkaline earth species compared to the uncatalysed reactions, apart from the **V-Ca** catalysed reaction between TBAB and diphenylamine, which appeared to proceed at a very similar rate irrespective of the presence of **V-Ca**. The reaction was repeated using an identical catalyst loading

of **V-Mg** as the catalyst, achieving 100 % conversion to compound **60** (by integration of ^{11}B NMR spectrum) after 24 hours at room temperature, showing that the reaction is indeed promoted by catalysis and proceeds faster when the appropriate metal centre is present. The results of the catalysed and uncatalysed reactions also demonstrate that the reactivity in the presence of a catalyst does indeed proceed by a defined catalytic pathway, similar to that suggested in Figure 5.1, and is not simply an interaction of fragments produced by thermolysis.

As a comparison, reactions between DMAB and amines were carried out using **V-Mg**, with an identical 5 mol % catalyst loading to reactions with **V-Ca**. In every case the reactions proceeded faster and required less or no heating compared to the calcium catalysed reactions. This observation that magnesium catalysed reactions are more facile than those with calcium is consistent with the previously observed trend in reactivity of Mg > Ca for Group 2 amine borane dehydrocoupling reported by Hill and the kinetic analysis described in Chapter 4.[1] Further reactions between DMAB, pyrrolidine and 5 mol % **V-Ca**, **V-Mg** and β-diketiminato calcium [N(SiMe$_3$)$_2$] **VI** at 60 °C were carried out to validate this qualitative data. The concentration of boron-containing species other than the consumption of DMAB could not be followed by either 0, 1st or 2nd order kinetic data plots. A second order kinetic data plot for the consumption of DMAB is shown in Figure 5.6.

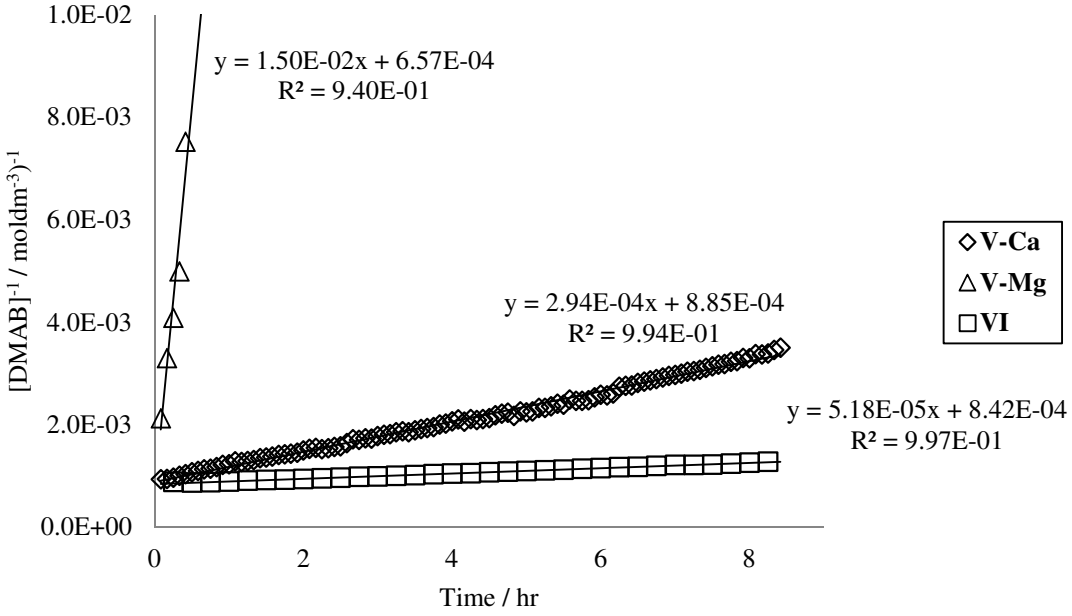

Figure 5.6: A second order kinetic data plot for the consumption of DMAB in the reactions between DMAB, pyrrolidine and 5 mol % **V-Ca** (diamonds), **V-Mg** (triangles) and β-diketiminato calcium [$N(SiMe_3)_2$] **VI** (squares) at 60 °C.

The data plotted in Figure 5.6 demonstrates that **V-Mg** is a more active catalyst than **V-Ca** for the reaction between DMAB and pyrrolidine at 60 °C, in agreement with qualitative observations. The reaction with **V-Mg** has a second-order rate constant which is ca. 51 times the magnitude of that for the reaction with **V-Ca**. This is rationalised as a consequence of the smaller, more highly polarising Mg^{2+} centre. The reaction with **VI** is by far the slowest shown in Figure 5.6, with a second-order rate constant ca. 6 times smaller than for the analogous reaction with **V-Ca**. Although other reactions were not carried out, a similar reactivity trend is expected for the other combinations of amine borane and amine reagents. Inspection of the ^1H NMR spectra for reactions with the calcium reagents, **V-Ca** and **VI**, reveals partial ligand protonation and formation of calcium hydride species, whilst reactions with **V-Mg** appeared unaffected, similar to that observed for the amine borane dehydrocoupling reactions described in Chapter 4. This deactivation via ligand protonation, in part, explains the superior reactivity of **V-Mg** for these reactions and could also explain why the reaction between TBAB and the more acidic amine diphenylamine proceeded no faster than an uncatalysed reaction when in the presence of **V-Ca**. The diamineborane products proved to be stable in solution, but

quite unstable upon attempted isolation by sublimation or slow evaporation in an inert atmosphere, undergoing decomposition. In addition, some of the products were expected to be liquids/oils increasing the difficulty of characterisation. Products synthesised using DMAB proved the most difficult to characterise due to the formation of volatile decomposition fragments under vacuum in addition to small fragments in GCMS analysis.

Each of the diamineborane products **52** - **60** was characterised by ^{1}H NMR and ^{11}B NMR spectroscopy and GCMS analysis, enabling the structures of compounds **52** to **60** to be assigned as shown in Table 5.1.

Amine	Amine Borane		
	DMAB	PB	TBAB
$(C_4H_8)NH$	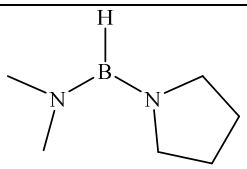 **52**		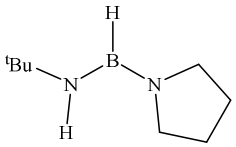 **56**
$^tBuNH_2$	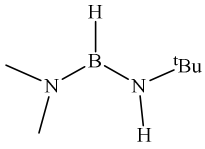 **53**	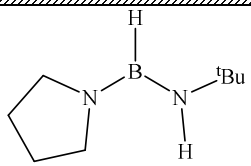 **56**	
$^iPr_2NH$	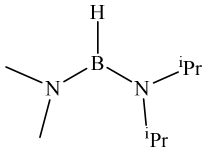 **54**	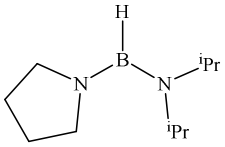 **57**	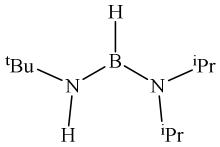 **59**
Ph_2NH	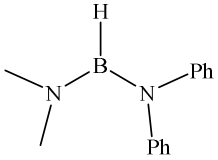 **55**	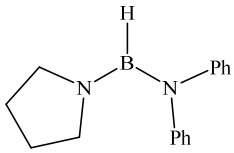 **58**	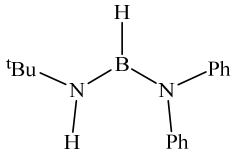 **60**

Table 5.1: Unsymmetrical diamineboranes, compounds **52** to **60**, synthesised by catalytic dehydrocoupling of amine boranes and amines by alkaline earth species.

Only compound **60**, the unsymmetrical diamineborane product of the reaction between TBAB and diphenylamine, was successfully isolated in a pure form as crystals suitable for X-ray diffraction analysis from concentrated toluene, shown in Figure 5.7. Accurate CHN analysis was also obtained for this compound.

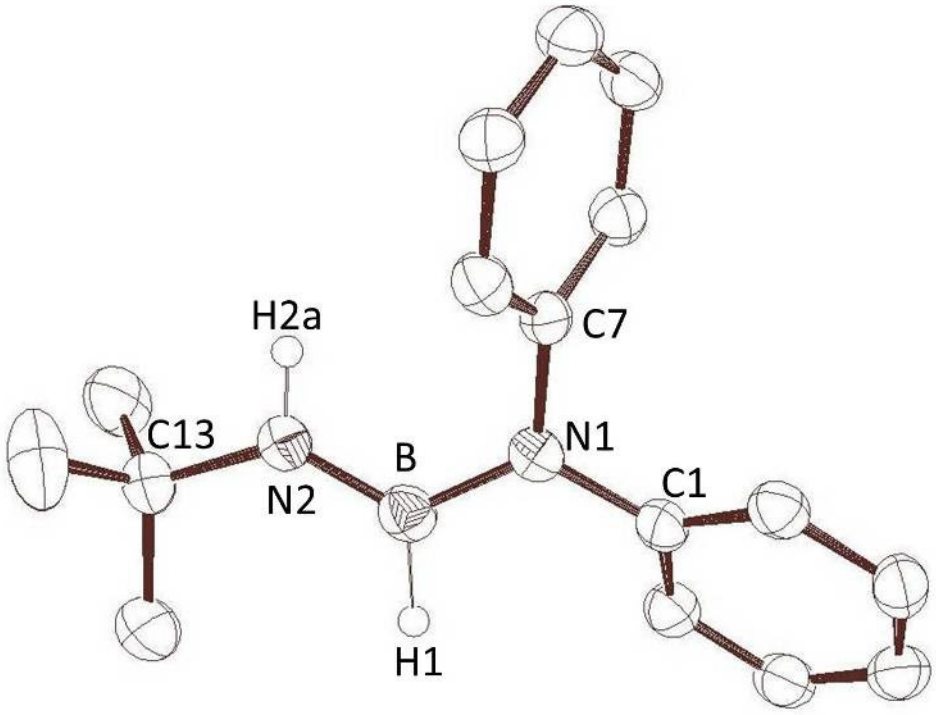

Figure 5.7: ORTEP representation of the solid-state structure of compound **60**. Thermal ellipsoids set at 50 % probability. Hydrogen atoms other than those bonded to boron and nitrogen removed for clarity. Selected bond lengths (Å) and angles (°); B-N1 1.388(4), B-N2 1.434(4), N1-C1 1.432(4), N1-C7 1.441(4), N1-B-N2 122.7(3), C1-N1-C7 116.4(2).

The trigonal boron centre of compound **60** forms a plane comprising of the C13-N2-B-N1-C1/C7 atoms, to which the plane of the C1 phenyl ring is rotated 62.8° and the plane of the C7 phenyl ring is rotated 35.8°. The dihedral angle of the the C13-N2-H2a/N2-B-H1 planes is essentially 180°, indicating the presence of pi-bonding between B and N2. The only previous reported example of a diamineborane to have been characterised by X-ray diffraction analysis is [HB{NH(Dipp)}$_2$] **LI**.[2] Other than this the most relevant data relates to the bora-amidinate dianion **XCVI** shown in Figure 5.8.

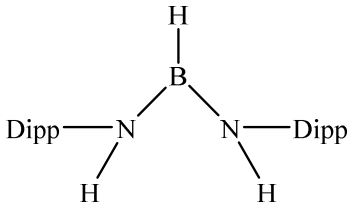

LI

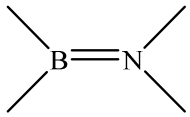

XCV

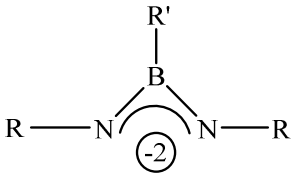

XCVI

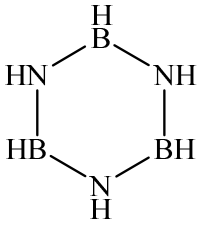

XCVII

Figure 5.8: Example B-N bond lengths; $[HB\{NH(Dipp)\}_2]$ **LI**,[2] $Me_2B{=}NMe_2$ **XCV**,[3] bora-amidinate ligand **XCVI**,[4-6] borazine **XCVII**.[7]

By comparison to the bond lengths of the structures in Figure 5.8, the B-N1 bond length of **60 [**1.434(4) Å] is longer than the B-N2 bond length **[**1.388(4) Å] and the B-N bonds of $[HB\{NH(Dipp)\}_2]$ **LI** [1.415(2) Å],[2] but identical to the doubly-deprotonated bora-amidinate ligand **XCVI** (1.42-1.48 Å) and borazine **XCVII** [1.436(2) Å].[4-7] The B-N2 bond length of compound **61 [**1.388(4) Å] is shorter than the B-N bond of $[HB\{NH(Dipp)\}_2]$ **LI** [1.415(2) Å] but identical to the B=N bond of $Me_2B{=}NMe_2$ **XCV** (1.40 Å).[2, 3] The shorter B-N2 bond is rationalised as resulting from increased π-bonding from the *tert*-butylamine nitrogen. The N1-B-N2 bond angle [122.72(3)°] is identical to that of borazine [122.9(1)°], but more obtuse than for $[HB\{NH(Dipp)\}_2]$ **LI** [121.9(1)°].[2, 7] The rotation of the C1 and C7 phenyl rings (62.8° and 35.8° respectively) to the C13-N2-B-N1-C1/C7 plane could be explained by the competing steric demands of the phenyl rings around the nitrogen atom.

5.2 Stoichiometric Reactions Between Calcium Amidoborane and Amine

In an attempt to isolate the proposed metal-centred insertion product, $LCaNR_2BH_2NR'_2$, stoichiometric reactions between the isolated calcium amidoborane species **LXV** and amines were carried out.

A stoichiometric NMR-scale reaction between β-diketiminato calcium [NMe_2BH_3] **LXV** and pyrrolidine was carried out at 70 °C and monitored by ^{11}B NMR spectroscopy, attempting to form the calcium [$NMe_2BH_2N(C_4H_8)$] intermediate **61** suggested by the proposed mechanism in Figure 5.1 and shown in Figure 5.9.

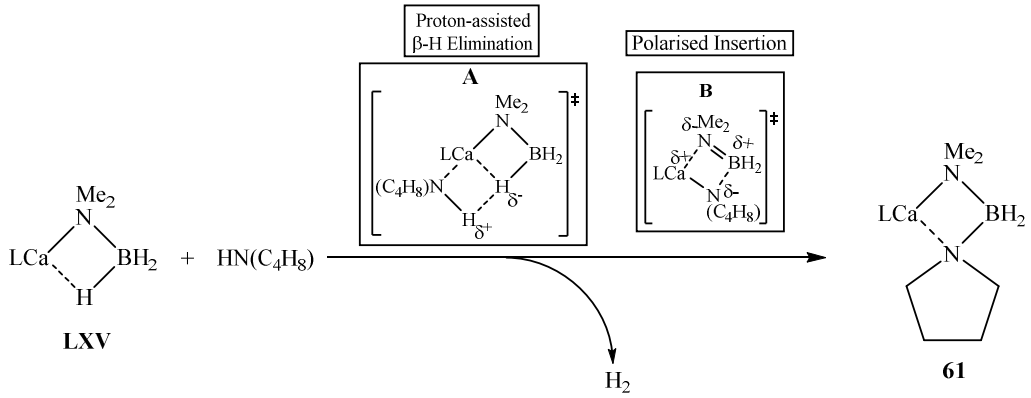

Figure 5.9: Stoichiometric reaction between **LXV** and pyrrolidine at 70 °C to form the β-diketiminato calcium [$NMe_2BH_2N(C_4H_8)$] intermediate **61**.

After heating this reaction for ca. 108 hours at 70 °C the ^{11}B NMR spectrum comprised a triplet resonance at δ = 1.45 ppm, $^1J_{BH}$ = 87 Hz attributed to compound **61**, and a doublet resonance attributed to the formation of [$HB(NMe_2)(NC_4H_8)$] **52** resulting from decomposition of **61**. This is shown in Figure 5.10.

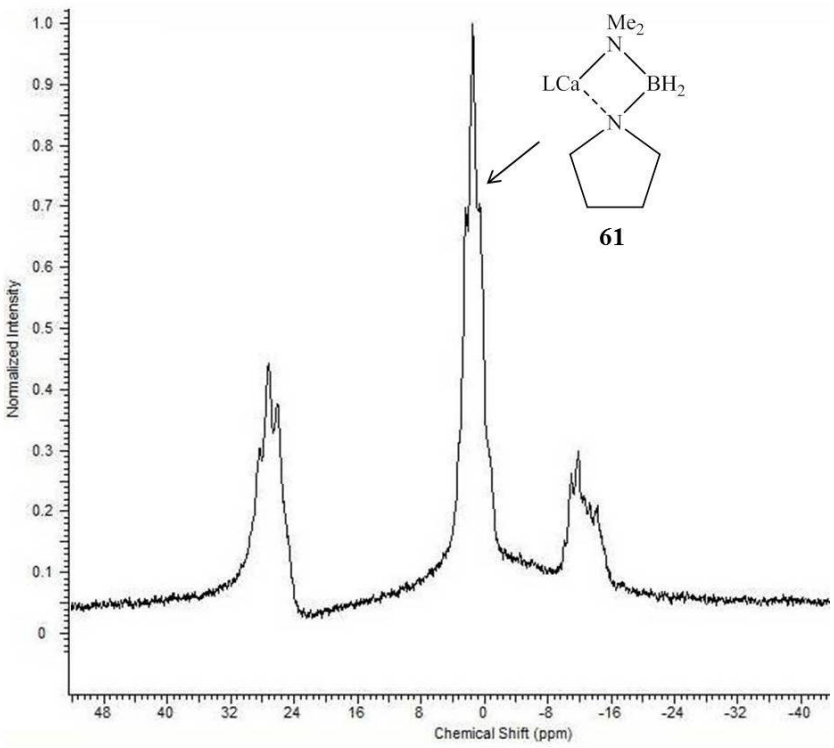

Figure 5.10: ^{11}B NMR spectrum, showing the formation of compound **61**, an intermediate β-diketiminato calcium [$NMe_2BH_2N(C_4H_8)$] species. (d_8-tol, 298 K, 96.3 MHz)

Compound **61** could not, however, be isolated from the reaction mixture, frustrating efforts to confirm its chemical structure and assist in mechanistic determination for these reactions.

In a similar manner equimolar quantities of **LXV** and *tert*-butylamine were heated at 50 °C and monitored by ^{11}B NMR spectroscopy in an attempt to form the β-diketiminato calcium [$NMe_2BH_2NH^tBu$] intermediate, compound **62**. ^{11}B NMR spectra for this reaction, however, showed only unreacted **LXV** and formation of [$HB(NMe_2N)(NH^tBu)$] **53**, exhibiting no sign of a species analogous to **62**. This result is rationalised as a consequence of the reactivity of the intermediate species **62**, which is unstable to β-hydride elimination and formation of **53**. This reaction once again illustrates the enhanced activity of these reactions with a primary amine compared to those with secondary amines.

5.3 Conclusion for Chapter 5

This chapter has described alkaline earth catalysed dehydrocoupling reactions between amine boranes and amines to form novel diamineborane compounds. These reactions are consistent with the proposed mechanism in Figure 5.1, however, once again the kinetic reactions illustrated in Figure 5.6 and the lack of fit to simple kinetic plots other than for the consumption of DMAB, demonstrated that these reactions have an intrinsic complexity. Qualitative data and the preliminary kinetic experiments confirm a dependency upon the identity of the metal centre for these reactions, with a reactivity trend of Mg > Ca reminiscent of the Group 2 amine borane dehydrocoupling reactivity described in Chapters 3 and 4, and reports by Hill.[1]

The issue of ligand protonation and catalyst deactivation observed for amine borane dehydrocoupling reactions between DMAB and the calcium reagents **VI** and **V-Ca** in Chapter 4, Section 4.2, was also observed during reactions between these reagents and amines. The dehydrocoupling reactions described in Chapter 4, Section 4.6, questioned the innocence of protonated ligand in dehydrocoupling reaction mixtures. This section demonstrates that the amines resulting from ligand protonation reactions are unlikely to be innocent in dehydrocoupling reactions and may influence not only the kinetics of the reaction but may also be incorporated into reaction products, increasing the complexity of these systems. Chapter 3, Section 3.2.4, described reactions of the cyclic borazane $[Me_2N\text{-}BH_2]_2$ **XXXVI** with metallated amidoborane and pyrrolidide, showing that **XXXVI** reacted rapidly in stoichiometric proportions to form products of the form $[HB(NR_2)(NR'_2)]$. Although only very minor concentrations of **XXXVI** are seen in these reactions, a competitive reaction to form this species must be considered. In such a regime, the observed lack of larger quantities of **XXXVI** could be rationalised as a consequence of the reactivity of **XXXVI**, reacting with amidoborane $[LMNR_2BH_2]$ or amide species $[LMNR'_2]$ which are present in relatively high proportions. As discussed in Chapter 3, Section 3.4, the dihydrogen evolved in these closed system reactions may not be innocent, creating additional reaction pathways or reversible reactions within the mechanism. The observed reactivity can, however, be described as consistent with the proposed

mechanism in Figure 5.1, irrespective of additional side reactions which may occur in the real systems. It remains to be seen whether this regime can be successfully extended to other elements with formation of new B-E bonds, via a reaction scheme such as that depicted in Figure 5.11.

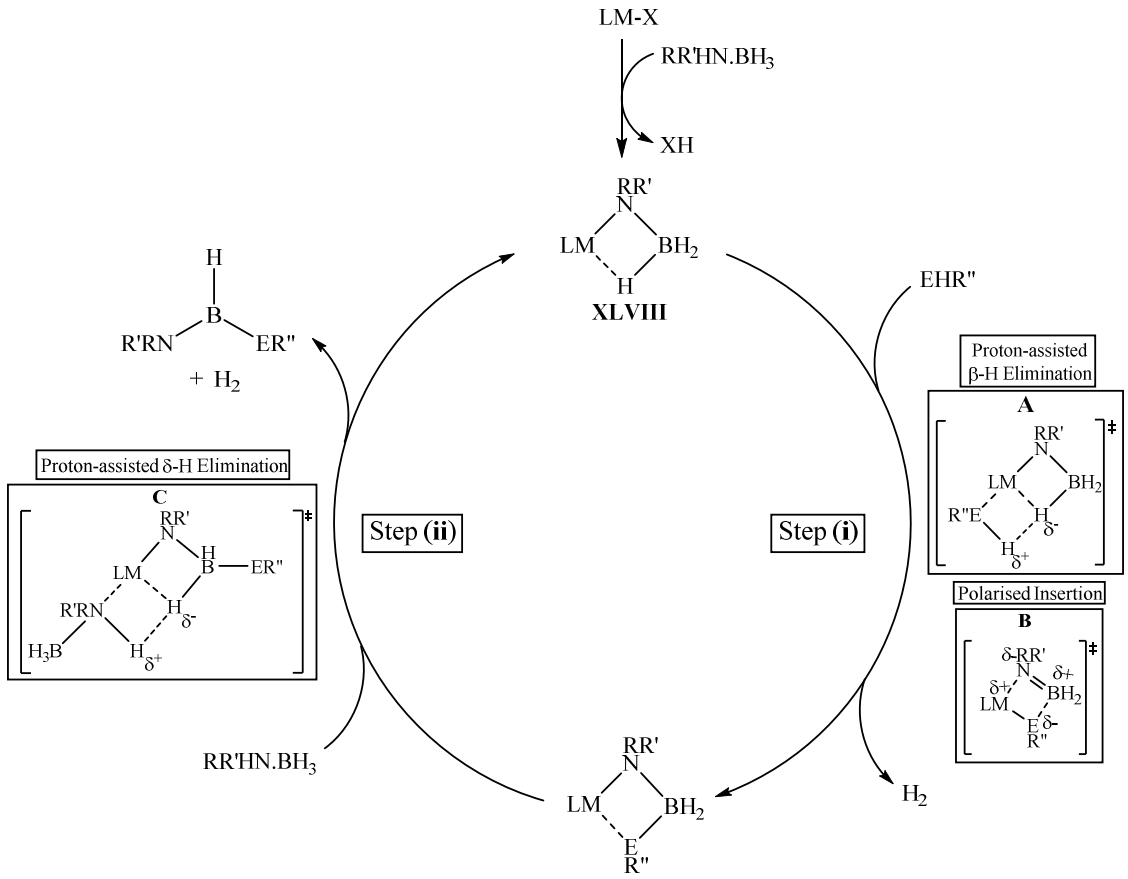

Figure 5.11: Proposed reaction scheme for the formation of new B-E bonds via dehydrocoupling reactions of amine boranes with protic E-R" reagents.

5.4 Experimental Procedures for Chapter 5

All reactions were carried out using standard glovebox techniques under an inert argon atmosphere. NMR experiments were conducted in Youngs tap NMR tubes prepared and sealed in a glovebox. NMR spectra were collected on a Bruker AV300 spectrometer operating at 75.5 MHz (^{13}C), 96.3 MHz (^{11}B). Kinetic experiments were recorded on a Bruker AV400 spectrometer. Solvents (toluene, THF, hexane) were dried by a commercially available solvent purification system (Innovative Technologies) under nitrogen before storage in ampoules over molecular sieves. C_6D_6 and d_8-toluene were purchased from Goss Scientific Instruments Ltd., dried over molten potassium before distillation under nitrogen and storage over molecular sieves. $Me_2NH.BH_3$ and $^tBuNH_2.BH_3$, were purchased from Sigma-Aldrich Ltd. and used without further purification. The alkaline earth reagents, calcium β-diketiminate **VI**, $[M\{N(SiMe_3)_2\}_2]_2$ **V**, were all synthesised by literature procedures.[8-10] CHN microanalysis was conducted by Mr. Stephen Boyer of London Metropolitan University.

Typical Procedure for NMR-Scale Reactions

C_6D_6, d_8-toluene or d_8-THF (ca. 0.5 ml) was added to a solid mixture of reactants in a glovebox and the solution sealed in a Youngs tap NMR tube. The reactions were monitored by ^1H and ^{11}B NMR spectroscopy. Reactions requiring elevated temperatures were heated using a thermostatically controlled oil bath. Formation of **XLVII** was confirmed via comparison to literature NMR data.[11]

5.4.1 Experimental Procedures for Catalytic Amine Insertion Reactions

5.4.1.1 Catalytic NMR-Scale Reaction of $Me_2NH.BH_3$ and C_4H_8NH to Synthesise $[\{Me_2N\}BH\{NMe_2\}]$ **XLVII** and $[\{Me_2N\}BH\{NC_4H_8\}]$ **52**

(i) Using $[Ca\{N(SiMe_3)_2\}_2]$ **V-Ca**

C_6D_6 (ca. 0.5 ml) was added to a solid mixture of $Me_2NH.BH_3$ (59 mg, 1 mmol), one molar equivalent of C_4H_8NH (71 mg, 1 mmol) and **V-Ca** (18 mg, 5 mol %) and the

solution sealed in a Youngs tap NMR tube before heating to 70 °C for 24 hours. Approx. conversion using ^{11}B NMR: 44 % **XLVII**, 54 % **52**.

(ii) Using [Mg{N(SiMe$_3$)$_2$}$_2$] **V-Mg**

C_6D_6 (ca. 0.5 ml) was added to a solid mixture of $Me_2NH.BH_3$ (59 mg, 1 mmol), one molar equivalent of C_4H_8NH (71 mg, 1 mmol) and **V-Mg** (17 mg, 5 mol %) and the solution sealed in a Youngs tap NMR tube before heating to 70 °C for 24 hours. Approx. conversion using ^{11}B NMR: 40 % **XLVII**, 40 % **52**.

(iii) Data

XLVII and **52** proved unstable to concentration under vacuum or by evaporation in a glovebox. The complete molecular ions of **XLVII** and **52** were not observed in GCMS results. ^{1}H NMR (C_6D_6, 298 K) δ = ca. 1.48 (m, (N(CH$_2$)$_2$(C*H*$_2$)$_2$)), ca. 1.52 (m, (N(CH$_2$)$_2$(C*H*$_2$)$_2$)), 2.54 (s, N-C*H*$_3$), 2.57 (s, N-C*H*$_3$), 2.62 (s, N-C*H*$_3$), 2.70 (s, N-C*H*$_3$), 3.04 (t, (N(C*H*$_2$)$_2$(CH$_2$)$_2$), J_{HH} = 6.78 Hz), 3.08 (t, (N(C*H*$_2$)$_2$(CH$_2$)$_2$), J_{HH} = 6.78 Hz), 3.20 (t, (N(C*H*$_2$)$_2$(CH$_2$)$_2$), J_{HH} = 6.60 Hz), 3.28 (t, (N(C*H*$_2$)$_2$(CH$_2$)$_2$), J_{HH} = 6.60 Hz). ^{13}C{^{1}H} NMR (C_6D_6, 298 K) δ = 26.6 (N(CH$_2$)$_2$(*C*H$_2$)$_2$), 26.9 (N(CH$_2$)$_2$(*C*H$_2$)$_2$), 39.9 (N-*C*H$_3$), 40.0 (N-*C*H$_3$), 40.2 (N-*C*H$_3$), 41.3 (N-*C*H$_3$), 48.2 (N(*C*H$_2$)$_2$(CH$_2$)$_2$), 50.0 (br, N(*C*H$_2$)$_2$(CH$_2$)$_2$). ^{11}B NMR (C_6D_6, 298 K) δ = 29.9 (d, **52** *B*H, $^1J_{BH}$ = 100 Hz).

5.4.1.2 Catalytic NMR-Scale Reaction of $Me_2NH.BH_3$ and $(CH_3)_3CNH_2$ to Synthesise [{Me$_2$N}BH{NMe$_2$}] **XLVII** and [{Me$_2$N}BH{NH^{t}Bu}] **53**

(i) Using [Ca{N(SiMe$_3$)$_2$}$_2$] **V-Ca**

C_6D_6 (ca. 0.5 ml) was added to a solid mixture of $Me_2NH.BH_3$ (59 mg, 1 mmol), one molar equivalent of $(CH_3)_3CNH_2$ (73 mg, 1 mmol) and **V-Ca** (18 mg, 5 mol %) and the solution sealed in a Youngs tap NMR tube before heating to 70 °C for 48 hours. Approx. conversion using ^{11}B NMR: 8 % **XLVII**, 75 % **53**.

(ii) Using [Mg{N(SiMe$_3$)$_2$}$_2$] **V-Mg**

C_6D_6 (ca. 0.5 ml) was added to a solid mixture of $Me_2NH.BH_3$ (59 mg, 1 mmol), one molar equivalent of $(CH_3)_3CNH_2$ (73 mg, 1 mmol) and **V-Mg** (17 mg, 5 mol %) and the solution sealed in a Youngs tap NMR tube before allowing to react at room temperature for 92 hours. Approx. conversion using ^{11}B NMR: 0 % **XLVII**, 79 % **53**.

(iii) Data

XLVII and **53** proved unstable to concentration under vacuum or by evaporation in a glovebox. The complete molecular ions of **XLVII** and **53** were not observed in GCMS results. However, an ion with *m/z* of 113.0 corresponding to **53** with the loss of CH_3 was observed. ^{1}H NMR (C_6D_6, 298 K) δ = 1.16 (s, C(C*H*$_3$)$_3$), 2.48 (broad s, N-C*H*$_3$), 2.53 (s, N-C*H*$_3$), 2.62 (s, N-C*H*$_3$). ^{13}C{^{1}H} NMR (C_6D_6, 298 K) δ = 33.9 (C(*C*H$_3$)$_3$), 39.9 (N-*C*H$_3$), 41.3 (N-*C*H$_3$), 48.8 (*C*(CH$_3$)$_3$). ^{11}B NMR (C_6D_6, 298 K) δ = 30.2 (d, **53** *B*H, $^1J_{BH}$ = 128 Hz).

5.4.1.3 Catalytic NMR-Scale Reaction of $Me_2NH.BH_3$ and $^iPr_2NH$ to Synthesise [{Me$_2$N}BH{N^{i}Pr$_2$}] **54**

(i) Using [Ca{N(SiMe$_3$)$_2$}$_2$] **V-Ca**

D_8-toluene (ca. 0.5 ml) was added to a solid mixture of $Me_2NH.BH_3$ (29 mg, 0.5 mmol), one molar equivalent of $^iPr_2NH$ (51 mg, 0.5 mmol) and **V-Ca** (9 mg, 5 mol %) and the solution sealed in a Youngs tap NMR tube before heating to 90 °C for ca. 101 hours. Approx. conversion using ^{11}B NMR: 67 %.

(ii) Using [Mg{N(SiMe$_3$)$_2$}$_2$] **V-Mg**

C_6D_6 (ca. 0.5 ml) was added to a solid mixture of $Me_2NH.BH_3$ (29 mg, 0.5 mmol), one molar equivalent of $^iPr_2NH$ (51 mg, 0.5 mmol) and **V-Mg** (9 mg, 5 mol %) and the solution sealed in a Youngs tap NMR tube before heating to 60 °C for ca. 44 hours. Approx. conversion using ^{11}B NMR: 69 %.

(iii) Data

Compound **54** proved unstable to concentration under vacuum or by evaporation in a glovebox. The complete molecular ion of **54** was not observed in GCMS results, owever, an ion with *m/z* of 139.0 corresponding to **54** with the loss of 2H and CH_3 was observed. ^{1}H NMR (d_8-tol, 298 K) δ = 0.92 (d, ^{i}Pr C*H*$_3$, J_{HH} = 6.0 Hz), 1.11 (d, ^{i}Pr C*H*$_3$, J_{HH} = 6.8 Hz), 2.67 (s, N-C*H*$_3$), 2.74 (spt, ^{i}Pr C*H*, J_{HH} = 6.0 Hz), 3.42 (spt, ^{i}Pr C*H*, J_{HH} = 6.8 Hz). ^{13}C{^{1}H} NMR (d_8-tol, 298 K) δ = 23.9 (^{i}Pr *C*H$_3$), 25.3 (^{i}Pr *C*H$_3$), 42.4 (N-*C*H$_3$), 45.7 (^{i}Pr *C*H), 46.0 (^{i}Pr *C*H). ^{11}B NMR (d_8-tol, 298 K) δ = 29.7 (d, *B*H, $^1J_{BH}$ = 119 Hz).

5.4.1.4 Catalytic NMR-Scale Reaction of $Me_2NH.BH_3$ and Ph_2NH to Synthesise [{Me_2N}BH{NPh_2}] **55**

(i) Using [Ca{N(SiMe$_3$)$_2$}$_2$] **V-Ca**

D_8-toluene (ca. 0.5 ml) was added to a solid mixture of $Me_2NH.BH_3$ (29 mg, 0.5 mmol), one molar equivalent of Ph_2NH (84 mg, 0.5 mmol) and **V-Ca** (9 mg, 5 mol %) and the solution sealed in a Youngs tap NMR tube before heating to 90 °C for ca. 101 hours. Approx conversion using ^{11}B NMR: 83 %.

(ii) Using [Mg{N(SiMe$_3$)$_2$}$_2$] **V-Mg**

C_6D_6 (ca. 0.5 ml) was added to a solid mixture of $Me_2NH.BH_3$ (29 mg, 0.5 mmol), one molar equivalent of Ph_2NH (84 mg, 0.5 mmol) and **V-Mg** (9 mg, 5 mol %) and the solution sealed in a Youngs tap NMR tube before heating to 50 °C for ca. 26 hours. Approx conversion using ^{11}B NMR: 95 %.

(iii) Data

Compound **55** proved unstable to concentration under vacuum or by evaporation in a glovebox. The complete molecular ion was not observed in GCMS results, however, an ion with *m/z* of 207.0 corresponding to **55** with the loss of 2H and CH_3 was observed. ^{1}H NMR (d_8-tol, 298 K) δ = 1.95 (s, N-C*H*$_3$), 2.61 (s, N-C*H*$_3$), 6.67-7.01 (Ar). ^{13}C{^{1}H} NMR (d_8-tol, 298 K) δ = 38.8 (N-*C*H$_3$), 44.0 (N-*C*H$_3$), 118.5 (Ar),

121.5 (Ar), 123.7 (Ar). 126.0 (Ar), 129.3 (Ar), 129.8 (Ar), 144.0 (Ar), 149.9 (Ar). ^{11}B NMR (d_8-tol, 298 K) δ = 32.1 (d, *B*H, $^1J_{BH}$ = 122 Hz).

5.4.1.5 Catalytic NMR-Scale Reaction of $C_4H_8NH.BH_3$ and $(CH_3)_3CNH_2$ to Synthesise [{C_4H_8N}BH{NH^{t}Bu}] **56**

D_8-toluene (ca. 0.5 ml) was added to a solid mixture of $C_4H_8NH.BH_3$ (85 mg, 1 mmol), one molar equivalent of $(CH_3)_3CNH_2$ (73 mg, 1 mmol) and **V-Ca** (18 mg, 5 mol %) and the solution sealed in a Youngs tap NMR tube before heating to 90 °C for ca. 44 hours. Approx. conversion using ^{11}B NMR: 87 %. **57** proved unstable to concentration under vacuum or by evaporation in a glovebox. GCMS results did not identify the ion of the complete molecular fragment of **56**, however, an ion with *m/z* of 152.0 was identified, corresponding to **56** with the loss of 2H. ^{1}H NMR (d_8-tol, 298 K) δ = 1.18 (s, C(C*H*$_3$)$_3$), 1.54 (s br., (N(CH$_2$)$_2$(C*H*$_2$)$_2$)), 2.61 (s broad, 1H, (N(C*H*$_2$)$_2$(CH$_2$)$_2$)), 2.80 (s broad, 1H, (N(C*H*$_2$)$_2$(CH$_2$)$_2$)), ca. 3.14 (s broad, 1H, (N(C*H*$_2$)$_2$(CH$_2$)$_2$)), 3.25 (t, (N(C*H*$_2$)$_2$(CH$_2$)$_2$), J_{HH} = 6.6 Hz). ^{13}C{^{1}H} NMR (d_8-tol, 298 K) δ = 26.9 (br., (N(CH$_2$)$_2$(*C*H$_2$)$_2$)), 33.9 (C(*C*H$_3$)$_3$), 44.8 (br. N(CH$_2$)$_2$(C*H*$_2$)$_2$)), 48.9 (*C*(CH$_3$)$_3$), 50.9 (br. (N(*C*H$_2$)$_2$(CH$_2$)$_2$)). ^{11}B NMR (d_8-tol, 298 K) δ = 28.9 (d, *B*H, $^1J_{BH}$ = 126 Hz).

5.4.1.6 Catalytic NMR-Scale Reaction of $C_4H_8NH.BH_3$ and ^{i}Pr$_2$NH to Synthesise [{C_4H_8N}BH{N^{i}Pr$_2$}] **57**

D_8-toluene (ca. 0.5 ml) was added to a solid mixture of $C_4H_8NH.BH_3$ (43 mg, 0.5 mmol), one molar equivalent of ^{i}Pr$_2$NH (51 mg, 0.5 mmol) and **V-Ca** (9 mg, 5 mol %) and the solution sealed in a Youngs tap NMR tube before heating to 90 °C for ca. 96 hours. Approx conversion using ^{11}B NMR: 79 %. **57** proved unstable to concentration under vacuum or by evaporation in a glovebox. GCMS results identified an ion with *m/z* of 182.1, corresponding to **57**. ^{1}H NMR (d_8-tol, 298 K) δ = 0.93 (d, ^{i}Pr C*H*$_3$, J_{HH} = 6.4 Hz), 1.14 (d, ^{i}Pr C*H*$_3$, J_{HH} = 6.8 Hz), ca. 1.53 (quint., (N(CH$_2$)$_2$(C*H*$_2$)$_2$), J_{HH} = 6.6 Hz), ca. 1.54 (quint., (N(CH$_2$)$_2$(C*H*$_2$)$_2$), J_{HH} = 6.6 Hz), 2.76 (spt, ^{i}Pr C*H*, J_{HH} = 6.0 Hz), 3.22 (t, (N(C*H*$_2$)$_2$(CH$_2$)$_2$), J_{HH} = 6.8 Hz), 3.26 (t, (N(C*H*$_2$)$_2$(CH$_2$)$_2$), J_{HH} = 6.8 Hz), 3.53 (spt, ^{i}Pr C*H*, J_{HH} = 6.3 Hz). ^{13}C{^{1}H} NMR (d_8-tol, 298 K) δ = 24.0 (^{i}Pr *C*H$_3$), 25.5 (^{i}Pr *C*H$_3$), 25.6 (N(CH$_2$)$_2$(*C*H$_2$)$_2$), 27.1

($N(CH_2)_2(CH_2)_2$), 45.8 (^{i}Pr *C*H), 45.9 (^{i}Pr *C*H), 50.9 (br, $N(CH_2)_2(CH_2)_2$). ^{11}B NMR (d_8-tol, 298 K) δ = 29.8 (d, *B*H, $^1J_{BH}$ = 123.1 Hz).

5.4.1.7 Catalytic NMR-Scale Reaction of $C_4H_8NH.BH_3$ and Ph_2NH to Synthesise [{C_4H_8N}BH{NPh_2}] **58**

D_8-toluene (ca. 0.5 ml) was added to a solid mixture of $C_4H_8NH.BH_3$ (43 mg, 0.5 mmol), one molar equivalent of Ph_2NH (84 mg, 0.5 mmol) and **V-Ca** (9 mg, 5 mol %) and the solution sealed in a Youngs tap NMR tube before heating to 90 °C for ca. 96 hours. Approx conversion using ^{11}B NMR: 97 %. The product proved unstable to concentration under vacuum or by evaporation in a glovebox. GCMS results did not identify the complete molecule, but did show pyrrolidine and NPh_2 fragments, consistent with **58**. ^{1}H NMR (d_8-tol, 298 K) δ = 1.28 (quint., $N(CH_2)_2(CH_2)_2$), J_{HH} = 6.4 Hz), 1.41 (quint., $N(CH_2)_2(CH_2)_2$), J_{HH} = 6.8 Hz), 2.40 (t, $N(CH_2)_2(CH_2)_2$), J_{HH} = 6.8 Hz), 3.31 (t, $N(CH_2)_2(CH_2)_2$), J_{HH} = 6.0 Hz), 6.76 (d, Ar, J_{HH} = 6.8 Hz), 6.81 (d, Ar, J_{HH} = 7.5 Hz), 6.88 (t, Ar, J_{HH} = 6.8 Hz), 7.02 (t, Ar, J_{HH} = 7.5 Hz), 7.07 (t, Ar, J_{HH} = 7.2 Hz). ^{13}C{^{1}H} NMR (d_8-tol, 298 K) δ = 26.1 ($N(CH_2)_2(CH_2)_2$), 26.8 ($N(CH_2)_2(CH_2)_2$), 47.7 ($N(CH_2)_2(CH_2)_2$), 52.5 ($N(CH_2)_2(CH_2)_2$), 118.5 (Ar), 121.5 (Ar), 123.8 (Ar), 126.3 (Ar), 129.4 (Ar), 144.0 (Ar), 150.0 (Ar). ^{11}B NMR (d_8-tol, 298 K) δ = 30.5 (br. s, *B*H).

5.4.1.8 Catalytic NMR-Scale Reaction of ^{t}BuNH$_2$.BH$_3$ and C_4H_8NH to Synthesise [{^{t}BuHN}BH{NC_4H_8}] **56**

C_6D_6 (ca. 0.5 ml) was added to a solid mixture of ^{t}BuNH$_2$.BH$_3$ (87 mg, 1 mmol), one molar equivalent of C_4H_8NH (71 mg, 1 mmol) and **V-Ca** (18 mg, 5 mol %) and the solution sealed in a Youngs tap NMR tube before heating to 70 °C for ca. 24 hours. Approx. conversion using ^{11}B NMR: 100 %. **56** proved unstable to concentration under vacuum or by evaporation in a glovebox. GCMS results identified ion with *m/z* of 154.2 corresponding to the complete molecule. ^{1}H NMR (C_6D_6, 298 K) δ = 1.20 (s, 9H, $C(CH_3)_3$), 1.51 (s broad, 4H, ($N(CH_2)_2(CH_2)_2$)), 2.65 (s broad, 1H, ($N(CH_2)_2(CH_2)_2$)), 2.80 (s broad, 1H, ($N(CH_2)_2(CH_2)_2$)), ca. 3.09 (s broad, 1H, ($N(CH_2)_2(CH_2)_2$)), 3.27 (t, 1H, ($N(CH_2)_2(CH_2)_2$), J_{HH} = 6.8 Hz). ^{13}C{^{1}H} NMR (C_6D_6, 298 K) δ = 26.9 (br., $N(CH_2)_2(CH_2)_2$)), 33.9 ($C(CH_3)_3$), 44.8 (br.

$N(CH_2)_2(CH_2)_2$)), 48.9 ($C(CH_3)_3$), 51.1 (br., $N(CH_2)_2(CH_2)_2$)). ^{11}B NMR (C_6D_6, 298 K) δ = 29.0 (d, *B*H, $^1J_{BH}$ = 127 Hz).

5.4.1.9 Catalytic NMR-Scale Reaction of $^tBuNH_2.BH_3$ and $^iPr_2NH$ to Synthesise [{^{t}BuHN}BH{N^{i}Pr$_2$}] **59**

C_6D_6 (ca. 0.5 ml) was added to a solid mixture of $^tBuNH_2.BH_3$ (43 mg, 0.5 mmol), one molar equivalent of $^iPr_2NH$ (51 mg, 0.5 mmol) and **V-Ca** (9 mg, 5 mol %) and the solution sealed in a Youngs tap NMR tube before heating to 70 °C for ca. 96 hours. **59** proved unstable to concentration under vacuum. Approx. conversion using ^{11}B NMR: 81 %. The complete molecular ion of **59** was not observed in GCMS results, however, ions with *m/z* of 167.1 (**59** with the loss of CH_3 and 2H), 140.9 (**59** with the loss of 2(CH_3) and 2H) and 128.0 (**59** with the loss of iPr), corresponding to fragments of **59** were identified. ^1H NMR (C_6D_6, 298 K) δ = 0.95 (d, ^{i}Pr C*H*$_3$, J_{HH} = 6.4 Hz), 1.09 (d, ^{i}Pr C*H*$_3$, J_{HH} = 6.8 Hz), 1.20 (s, C(C*H*$_3$)$_3$), 2.78 (spt, ^{i}Pr C*H*, J_{HH} = 6.4 Hz), 3.20 (spt, ^{i}Pr C*H*, J_{HH} = 6.7 Hz). $^{13}C\{^1H\}$ NMR (C_6D_6, 298 K) δ = 24.1 (^{i}Pr *C*H$_3$), 24.7 (^{i}Pr *C*H$_3$), 33.9 C(*C*H$_3$)$_3$, 45.7 (s, ^{i}Pr *C*H), 46.1 (s, ^{i}Pr C*H*), 49.1 (s, *C*(CH$_3$)$_3$). ^{11}B NMR (C_6D_6, 298 K) δ = 29.2 (d, *B*H, $^1J_{BH}$ = 124 Hz).

5.4.1.10 Catalytic NMR-Scale Reaction of $^tBuNH_2.BH_3$ and Ph_2NH to Synthesise [{^{t}BuHN}BH{NPh$_2$}] **60**

(i) Using [Ca{N(SiMe$_3$)$_2$}$_2$] **V-Ca**

C_6D_6 (ca. 0.5 ml) was added to a solid mixture of $^tBuNH_2.BH_3$ (43 mg, 0.5 mmol), one molar equivalent of Ph_2NH (84 mg, 0.5 mmol) and **V-Ca** (9 mg, 5 mol %) and the solution sealed in a Youngs tap NMR tube before heating to 70 °C for ca. 72 hours. Approx conversion using ^{11}B NMR: 100 %.

(ii) Using [Mg{N(SiMe$_3$)$_2$}$_2$] **V-Mg**

C_6D_6 (ca. 0.5 ml) was added to a solid mixture of $^tBuNH_2.BH_3$ (87 mg, 1 mmol), one molar equivalent of Ph_2NH (169 mg, 1 mmol) and **V-Mg** (17 mg, 5 mol %) and the solution sealed in a Youngs tap NMR tube before allowing the contents to react at room temperature for ca. 24 hours. Approx conversion using ^{11}B NMR: 100 %.

(iii) Data

GCMS results identified an ion with *m/z* of 207.1, corresponding to **60** with the loss of 3(CH_3). ^{1}H NMR (C_6D_6, 298 K) δ = 0.97 (s, 9H, C(C*H*$_3$)$_3$), 3.19 (d, 1H, N*H*, J_{HH} = 9.0 Hz), 6.70 (d, Ar, J_{HH} = 7.2 Hz), 6.72 (d, Ar, J_{HH} = 6.8 Hz), 6.82 (t, Ar, J_{HH} = 6.4 Hz), 6.99 (t, Ar, J_{HH} = 6.9 Hz), 7.01 (t, Ar, J_{HH} = 8.3 Hz). ^{13}C{^{1}H} NMR (C_6D_6, 298 K) δ = 33.7 (C(*C*H$_3$)$_3$), 49.4 (*C*(CH$_3$)$_3$), 118.5 (Ar), 121.5 (Ar), 124.1 (Ar), 125.90(Ar), 129.8 (Ar), 129.9 (Ar), 143.9 (Ar), 149.1 (Ar). ^{11}B NMR (C_6D_6, 298 K) δ = 29.8 (br. s, *B*H).

5.4.2 Preparative-Scale Synthesis of [{^{t}BuHN}BH{NPh$_2$}] **60**

Toluene (ca. 10ml) was added to a solid mixture of ^{t}BuNH$_2$.BH$_3$ (173 mg, 2 mmol), one molar equivalent of Ph$_2$NH (338 mg, 2 mmol) and **V-Ca** (36 mg, 5 mol %) and the solution sealed in a Youngs tap ampoule before heating to 80 °C for ca. 96 hours. A single crystal suitable for X-ray diffraction analysis was isolated from concentrated toluene. **60** was isolated as a white powder after complete removal of solvent. Accurate CHN analysis was obtained. Anal. Calc. for $C_{16}H_{21}BN_2$: C, 76.21; H, 8.39; N, 11.11 %. Found: C, 76.08; H, 8.29; N, 11.02 %.

Molecular Formula	$C_{16}H_{21}BN_2$
Formula Weight / g.mol^{-1}	252.16
Crystal System, Space Group	Orthorhombic, P 2_1 2_1 2_1
a, b, c / Å	5.9250(4), 10.9299(7), 22.9280(19)
α, β, γ / °	90, 90, 90
V / Å^3	1484.81(19)
Z	4
μ / mm^{-1}	0.065
ρ / g.cm^{-3}	1.128
θ range / °	4.13 - 25.10
Collected / Unique Reflections / R_{int}	4759 / 2551 / 0.0698
R_1, wR_2 [I > 2σ(I)]	R_1 = 0.0581, wR_2 = 0.1124
R_1, wR_2 (All data)	R_1 = 0.0939, wR_2 = 0.1261

5.4.3 Experimental Procedures for Uncatalysed Amine Insertion Reactions

5.4.3.1 Uncatalysed NMR-Scale Reaction of $Me_2NH.BH_3$ and C_4H_8NH to Synthesise [{Me_2N}BH{NMe_2}] **XLVII** and [{Me_2N}BH{NC_4H_8}] **52**

C_6D_6 (ca. 0.5 ml) was added to a solid mixture of $Me_2NH.BH_3$ (59 mg, 1 mmol) and one molar equivalent of C_4H_8NH (71 mg, 1 mmol) and the solution sealed in a Youngs tap NMR tube before heating to 70 °C for 207 hours. Approx. conversions using ^{11}B NMR: 12 % **XLVII**, 15 % **52**. ^{1}H NMR (C_6D_6, 298 K) δ = ca. 1.48 (m, ($N(CH_2)_2(CH_2)_2$)), ca. 1.52 (m, ($N(CH_2)_2(CH_2)_2$)), ca. 2.54 (s, N-CH_3), 2.56 (s, N-CH_3), ca. 2.65 (s, N-CH_3), ca. 3.14 (t, ($N(CH_2)_2(CH_2)_2$), J_{HH} = 6.40 Hz), ca. 3.15 (t, ($N(CH_2)_2(CH_2)_2$), J_{HH} = 6.40 Hz). ^{11}B NMR (C_6D_6, 298 K) δ = 29.8 (d, *B*H, $^1J_{BH}$ = 113 Hz).

5.4.3.2 Uncatalysed NMR-Scale Reaction of $Me_2NH.BH_3$ and $(CH_3)_3CNH_2$ to Synthesise [{Me_2N}BH{NMe_2}] **XLVII** and [{Me_2N}BH{NH^tBu}] **53**

C_6D_6 (ca. 0.5 ml) was added to a solid mixture of $Me_2NH.BH_3$ (59 mg, 1 mmol) and one molar equivalent of $(CH_3)_3CNH_2$ (73 mg, 1 mmol) and the solution sealed in a Youngs tap NMR tube before heating to 70 °C for 207 hours. Approx. conversion using ^{11}B NMR: 0 % **XLVII**, 3 % **53**. ^{1}H NMR (C_6D_6, 298 K) δ = 1.16 (s, $C(CH_3)_3$), 2.46 (broad s, N-CH_3), 2.57 (s, N-CH_3). ^{11}B NMR (C_6D_6, 298 K) δ = 30.3 (d, *B*H, $^1J_{BH}$ = 130 Hz).

5.4.3.3 Uncatalysed NMR-Scale Reaction of $Me_2NH.BH_3$ and $^iPr_2NH$ to Synthesise [{Me_2N}BH{NMe_2}] **XLVII** and [{Me_2N}BH{N^iPr_2}] **54**

C_6D_6 (ca. 0.5 ml) was added to a solid mixture of $Me_2NH.BH_3$ (29 mg, 0.5 mmol) and one molar equivalent of $^iPr_2NH$ (51 mg, 0.5 mmol) and the solution sealed in a Youngs tap NMR tube before heating to 70 °C for ca. 119 hours and 80 °C for ca. 115 hours. Approx. conversion using ^{11}B NMR: 7 % **XLVII**, 0 % **54**. ^{1}H NMR (C_6D_6, 298 K) δ = 2.60 (s, N-CH_3).

5.4.3.4 Uncatalysed NMR-Scale Reaction of $Me_2NH.BH_3$ and Ph_2NH to Synthesise [{Me_2N}BH{NPh_2}] **55**

C_6D_6 (ca. 0.5 ml) was added to a solid mixture of $Me_2NH.BH_3$ (29 mg, 0.5 mmol) and one molar equivalent of Ph_2NH (84 mg, 0.5 mmol) and the solution sealed in a Youngs tap NMR tube before heating to 70 °C for ca. 119 hours and 80 °C for ca. 115 hours. Approx conversion using ^{11}B NMR: 34 %. ^{1}H NMR (C_6D_6, 298 K) δ = 1.91 (s, N-CH_3), 2.77 (s, N-CH_3), 6.95-7.06 (Ar). ^{11}B NMR (C_6D_6, 298 K) δ = 32.1 (d, *B*H, $^1J_{BH}$ = 109 Hz).

5.4.3.5 Uncatalysed NMR-Scale Reaction of $C_4H_8NH.BH_3$ and $(CH_3)_3CNH_2$ to Synthesise [{C_4H_8N}BH{NH^tBu}] **56**

D_8-toluene (ca. 0.5 ml) was added to a solid mixture of $C_4H_8NH.BH_3$ (85 mg, 1 mmol and one molar equivalent of $(CH_3)_3CNH_2$ (73 mg, 1 mmol) and the solution sealed in a Youngs tap NMR tube before heating to 90 °C for ca. 144 hours. Approx. conversion using ^{11}B NMR: 64 %. ^{1}H NMR (d_8-tol, 298 K) δ = 1.18 (s, C(CH_3)$_3$), 1.53 (s br., (N(CH$_2$)$_2$(CH_2)$_2$)), 2.63 (s broad, (N(CH_2)$_2$(CH$_2$)$_2$)), 2.81 (s broad, (N(CH_2)$_2$(CH$_2$)$_2$)), ca. 3.14 (s broad, (N(CH_2)$_2$(CH$_2$)$_2$)), 3.22 (t, (N(CH_2)$_2$(CH$_2$)$_2$), J_{HH} = 6.4 Hz). ^{11}B NMR (d_8-tol, 298 K) δ = 28.9 (d, *B*H, $^1J_{BH}$ = 126 Hz).

5.4.3.6 Uncatalysed NMR-Scale Reaction of $C_4H_8NH.BH_3$ and $^iPr_2NH$ to Synthesise [{C_4H_8N}BH{NC_4H_8}] **57**

D_8-toluene (ca. 0.5 ml) was added to a solid mixture of $C_4H_8NH.BH_3$ (43 mg, 0.5 mmol) and one molar equivalent of $^iPr_2NH$ (51 mg, 0.5 mmol) and the solution sealed in a Youngs tap NMR tube before heating to 80 °C for ca. 120 hours. Approx conversion using ^{11}B NMR: 12 %. ^{1}H NMR (d_8-tol, 298 K) δ = 0.95 (d, ^{i}Pr CH_3, J_{HH} = 5.8 Hz), 1.14 (d, ^{i}Pr CH_3, J_{HH} = 7.3 Hz), ca. 1.51 (s br., (N(CH$_2$)$_2$(CH_2)$_2$)), ca. 1.55 (s br., (N(CH$_2$)$_2$(CH_2)$_2$)), 2.77 (s br., ^{i}Pr C*H*), ca. 3.22 (s br., (N(CH_2)$_2$(CH$_2$)$_2$)), 3.27 (s br., (N(CH_2)$_2$(CH$_2$)$_2$)), 3.55 (s br., ^{i}Pr C*H*). ^{11}B NMR (d_8-tol, 298 K) δ = 29.6 (d, *B*H, $^1J_{BH}$ = 128 Hz).

5.4.3.7 Uncatalysed NMR-Scale Reaction of $C_4H_8NH.BH_3$ and Ph_2NH to Synthesise [{C_4H_8N}BH{NPh_2}] **58**

D_8-toluene (ca. 0.5 ml) was added to a solid mixture of $C_4H_8NH.BH_3$ (43 mg, 0.5 mmol) and one molar equivalent of Ph_2NH (84 mg, 0.5 mmol) and the solution sealed in a Youngs tap NMR tube before heating to 80 °C for ca. 120 hours. Approx. conversion using ^{11}B NMR: 31 %. ^{1}H NMR (d_8-tol, 298 K) δ = ca. 1.29 (m, ($N(CH_2)_2(CH_2)_2$)), ca. 1.39 (m, ($N(CH_2)_2(CH_2)_2$)), ca. 2.39 (m, ($N(CH_2)_2(CH_2)_2$)), 3.31 (t, ($N(CH_2)_2(CH_2)_2$), J_{HH} = 6.8 Hz), 6.76 – 7.11 (Ar). ^{11}B NMR (d_8-tol, 298 K) δ = 30.7 (br. s, *B*H).

5.4.3.8 Uncatalysed NMR-Scale Reaction of ^{t}BuNH$_2$.BH$_3$ and C_4H_8NH to Synthesise [{^{t}BuHN}BH{NC_4H_8}] **56**

C_6D_6 (ca. 0.5 ml) was added to a solid mixture of ^{t}BuNH$_2$.BH$_3$ (87 mg, 1 mmol) and one molar equivalent of C_4H_8NH (71 mg, 1 mmol) and the solution sealed in a Youngs tap NMR tube before heating to 70 °C for ca. 142 hours. Approx. conversion using ^{11}B NMR: 19 %. ^{1}H NMR (C_6D_6, 298 K) δ = 1.17 (s, $C(CH_3)_3$), ca. 1.49 (m, ($N(CH_2)_2(CH_2)_2$)), ca. 2.51 (m, ($N(CH_2)_2(CH_2)_2$)), ca. 2.85 (m, ($N(CH_2)_2(CH_2)_2$)), ca. 2.89 (m, ($N(CH_2)_2(CH_2)_2$)). ^{11}B NMR (C_6D_6, 298 K) δ = 28.9 (d, *B*H, $^1J_{BH}$ = 126 Hz).

5.4.3.9 Uncatalysed NMR-Scale Reaction of ^{t}BuNH$_2$.BH$_3$ and ^{i}Pr$_2$NH to Synthesise [{^{t}BuHN}BH{N^{i}Pr$_2$}] **59**

D_8-toluene (ca. 0.5 ml) was added to a solid mixture of ^{t}BuNH$_2$.BH$_3$ (43 mg, 0.5 mmol) and one molar equivalent of ^{i}Pr$_2$NH (51 mg, 0.5 mmol) and the solution sealed in a Youngs tap NMR tube before heating to 80 °C for ca. 157 hours. Approx. conversion using ^{11}B NMR: 58 %. ^{1}H NMR (d_8-tol, 298 K) δ = 0.94 (d, ^{i}Pr C*H*$_3$, J_{HH} = 6.0 Hz), 1.07 (d, ^{i}Pr C*H*$_3$, J_{HH} = 6.8 Hz), 1.18 (s, $C(CH_3)_3$), 2.77 (spt, ^{i}Pr C*H*, J_{HH} = 6.8 Hz), 3.18 (spt, ^{i}Pr C*H*, J_{HH} = 6.8 Hz). ^{11}B NMR (d_8-tol, 298 K) δ = 29.0 (d, *B*H, $^1J_{BH}$ = 125 Hz).

5.4.3.10 Uncatalysed NMR-Scale Reaction of $^{t}BuNH_2.BH_3$ and Ph_2NH to Synthesise [{^{t}BuHN}BH{NPh_2}] **60**

D_8-toluene (ca. 0.5 ml) was added to a solid mixture of $^{t}BuNH_2.BH_3$ (43 mg, 0.5 mmol) and one molar equivalent of Ph_2NH (84 mg, 0.5 mmol) and the solution sealed in a Youngs tap NMR tube before heating to 80 °C for ca. 67 hours. Approx conversion using ^{11}B NMR: 96 %. ^{1}H NMR (d_8-tol, 298 K) δ = 0.97 (s, C(C*H*$_3$)$_3$), 3.19 (d, 1H, N*H*, J_{HH} = 9.4 Hz), 6.73 -7.06 (Ar). ^{11}B NMR (d_8-tol, 298 K) δ = 30.5 (br. s, *B*H).

5.4.4 Kinetic Dehydrocoupling of $Me_2HN.BH$ and Pyrrolidine by d^0 Species

Kinetic experiments were carried out on an NMR-scale in Youngs tap NMR tubes. Compounds were weighed out and added to 0.5 ml d_8-toluene inside a glovebox under an inert argon atmosphere, before being sealed inside a Youngs tap NMR tube. On removal from the glovebox the sample was frozen in liquid nitrogen and thawed before insertion into the NMR spectrometer. Reactions were monitored by ^{11}B NMR spectroscopy on a Bruker AV400 spectrometer, with concentration of boron-containing reaction species determined using integration across all boron-containing species. Boron-containing species were identified using values of chemical shift obtained from literature reports of known compounds and species described in this thesis. Reactions requiring elevated temperatures were heated inside the NMR spectrometer, equilibrated for ca. 10 minutes prior to use. The internal temperature of the NMR spectrometer deviated from the temperature at which it was set by a relationship characterised using methanol chemical shifts.[12] The resulting calibration curve was utilised to set the NMR spectrometer to a temperature at which the desired internal temperature for heating of the NMR tube was achieved. Kinetic experiments were conducted until 3 half-lives had passed, unless the reaction prohibited this (e.g. in the case of deactivation of catalyst).

Equations Used:

Second-order kinetics:

$r = -d[\text{Amine borane}]/dt = 2k[\text{Amine borane}]^2$

(**Eqn 4**) $(1/[\text{Amine borane}]_t) = (1/[\text{Amine borane}]_0) + kt$

Kinetic Dehydrocoupling of $Me_2HN.BH$ and Pyrrolidine by **V-Mg**, **V-Ca** and β-diketiminato Calcium [$N(SiMe_3)_2$] **VI**

D_8-tol (0.5 ml) was added to a solid mixture of $Me_2NH.BH_3$ (59 mg, 1 mmol), one molar equivalent of C_4H_8NH (71 mg, 1 mmol) and 5 mol % (i) **V-Mg** (17.2 mg), (ii) **V-Ca** (18 mg) and (iii) **VI** (29.4 mg) and the solution sealed in a Youngs tap NMR tube before heating to 60 °C and monitored by ^{11}B NMR spectroscopy. The second order kinetic data plots for these reactions are shown in Figure 5.6.

5.4.5 Stoichiometric Reactions Between β-diketiminato Calcium dimethylamidoborane **LXV** and Amines

5.4.5.1 Stoichiometric Reaction Between β-diketiminato Calcium dimethylamidoborane **LXV** and Pyrrolidine, to Synthesise **61**

C_6D_6 (ca. 0.5 ml) was added to a solid mixture of **LXV** (102.8 mg, 0.175 mmol) and one molar equivalent of C_4H_8NH (12.4 mg, 0.175 mmol) and the solution sealed in a Youngs tap NMR tube before heating at 70 °C for ca. 108 hours, monitored by ^{11}B NMR spectroscopy. Approx. conversion by ^{11}B NMR: 48.1 % **61**, 30.1 % **52** and **XLVII**. ^1H NMR (C_6D_6, 298 K) δ = 1.24 (d, 6H, $CH(CH_3)_2$, J_{HH} = 6.8 Hz), 1.30 (d, 6H, $CH(CH_3)_2$, J_{HH} = 6.8 Hz), 1.38 (m, 4H, (CH_2)), 1.55 (s, 3H, $N(CH_3)$), 1.69 (s, 3H, $N(CH_3)$), 1.83 (s, 6H, $C(CH_3)$), 2.98-3.14 (m, 4H, $CH(CH_3)_2$), 3.27 (m, 4H, (CH_2)), 4.81 (s, 1H, CH), 7.12-7.23 (Ar). ^{11}B NMR (d_8-tol, 298 K) δ = 1.45 (t, BH_2, $^1J_{BH}$ = 87 Hz).

5.4.5.1 Stoichiometric Reaction Between β-diketiminato Calcium dimethylamidoborane **LXV** and *Tert*-butylamine, to Synthesise **62**

C_6D_6 (ca. 0.5 ml) was added to a solid mixture of **LXV** (20 mg, 0.034 mmol) and one molar equivalent of $^tBuNH_2$ (2.5 mg, 0.034 mmol) and the solution sealed in a Youngs tap NMR tube before heating at 50 °C for ca. 24 hours, monitored by ^{11}B NMR spectroscopy. Approx. conversion by ^{11}B NMR: 45.6 % **53**.

5.5 References for Chapter 5

1. D. J. Liptrot, M. S. Hill, M. F. Mahon and D. J. MacDougall, *Chem.- Eur. J.*, 2010, **16**, 8508-8515.
2. J. Spielmann, M. Bolte and S. Harder, *Chem. Commun.*, 2009, 6934-6936.
3. P. Paetzold, *Pure Appl. Chem.*, 1991, **63**, 345-350.
4. H. Fussstetter and H. Noth, *Chem. Ber.*, 1979, **112**, 3672-3681.
5. A. Heine, D. Fest, D. Stalke, C. D. Habben, A. Meller and G. M. Sheldrick, *J. Chem. Soc.-Chem. Commun.*, 1990, 742-743.
6. J. Konu, M. S. Balakrishna, T. Chivers and T. W. Swaddle, *Inorg. Chem.*, 2007, **46**, 2627-2636.
7. R. Boese, A. H. Maulitz and P. Stellberg, *Chem. Ber.*, 1994, **127**, 1887-1889.
8. M. H. Chisholm, J. C. Gallucci and K. Phomphrai, *Inorg. Chem.*, 2004, **43**, 6717-6725.
9. M. H. Chisholm and K. Phomphrai, *Inorg. Chim. Acta*, 2003, **350**, 121-125.
10. M. Westerhausen, *Inorg. Chem.*, 1991, **30**, 96-101.
11. A. J. M. Miller and J. E. Bercaw, *Chem. Commun.*, 2010, **46**, 1709-1711.
12. A. L. Vangeet, *Anal. Chem.*, 1968, **40**, 2227-2229.

6 Conclusions

A disparity exists between the wide range of metallic species reported for the dehydrocoupling of amine boranes and limited selection of publications regarding precise mechanistic detail relating to these processes. The central aim of this thesis was investigating the dehydrocoupling of secondary amine boranes by alkaline earth precatalysts, accumulating evidence in validation or contradiction of the mechanism proposed by Hill (shown in Chapter 1, Figure 1.30 and reshown here as Figure 6.1).[1, 2]

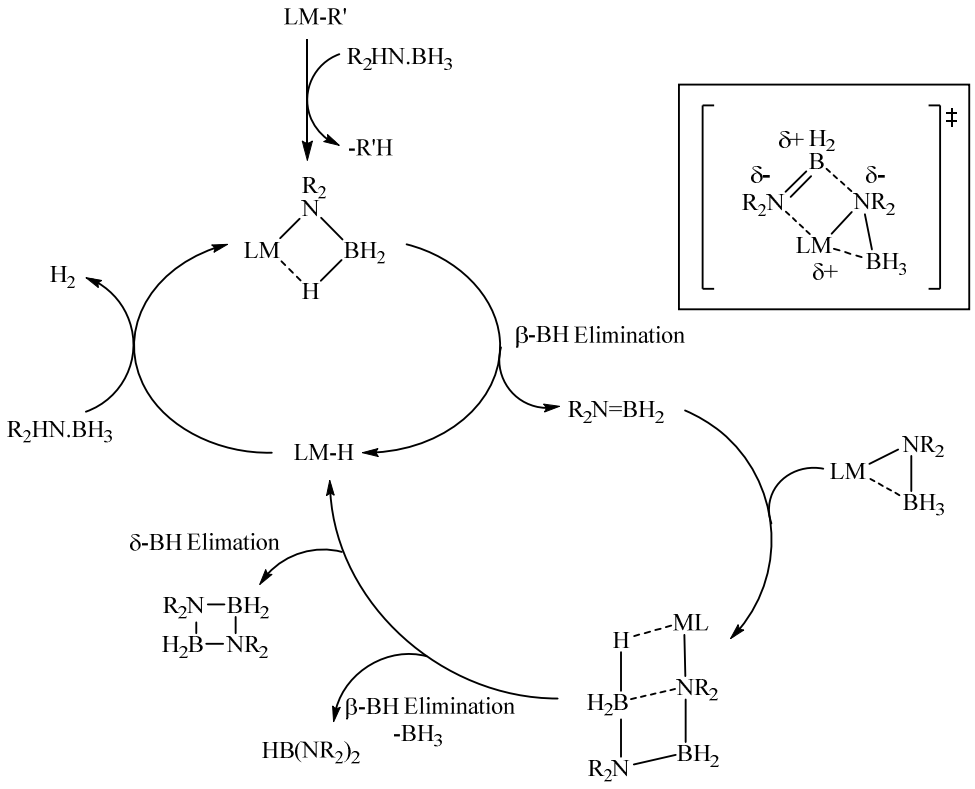

Figure 6.1: Mechanism of dehydrocoupling of amine boranes by alkaline earth silylamides proposed by Hill,[1, 2] where M = Mg, Ca, Sr, Ba.

The stoichiometric reactions between secondary amine boranes and Group 2 dialkyl species (**IIMg**, **IICa** and **IISr**) described in Chapter 2 supported the validity of polarised insertion of the unsaturated [$R_2N{=}BH_2$] **XXXVII** species into a M-C bond as a viable pathway for B-E bond formation, whilst the reactions between amines and amine boranes described in Chapter 5 provided further evidence in support of

the proposed mechanism of polarised insertion of **XXXVII** into available M-N bonds. In both instances novel boron-containing products and intermediates were identified in support of the proposed reaction mechanisms.

Attempts to investigate isolated processes within the proposed mechanism, by virtue of monitoring the concentration of boron-containing products in reactions between amine borane and isolated intermediates, highlighted complex behaviour of those species which could not be rationalised. These reactions did, however, identify the high thermal stability of β-diketiminate alkaline earth amidoborane compounds **LXV** and **XLVI**, whilst displaying high reactivity in the presence of a protic source, through a proton-assisted hydride elimination in what is potentially a concerted process. This suggestion is supported by the absence, or very low concentrations, of **XXXVII** observed in ^{11}B NMR spectra of alkaline earth amine borane dehydrocoupling reactions. A controlled reaction between **LXV** and DMAB led to isolation of β-diketiminato calcium [$NMe_2BH_2NMe_2BH_3$] **36**, the existence of which had only previously been inferred by low concentrations of this species in ^{11}B NMR spectra of reaction mixtures. Reactions attempting to identify from which reagent each N-B unit of β-diketiminato calcium [$NR_2BH_2NR_2BH_3$] compound originated proved fruitless. In addition, [Me_2N-$BH_2]_2$ **XXXVI** was identified as an intermediate in the ultimate formation of [$HB(NMe_2)_2$] **XLVII**, highlighting an additional mechanistic pathway. These observations did not refute the proposed mechanism in Figure 6.1, but required additional details to be added leading to the refined model proposed in Figure 6.2. The dehydrocoupling of the primary amine borane *tert*-butylamine borane by alkaline earth reagents highlighted the increased complexity of reactions with additional protic residues, necessitating the inclusion of additional mechanistic pathways in addition to those depicted in Figure 6.2 to result in the range of products identified. A separate study would be required to adequately characterise the additional mechanistic pathways which operate in reactions with primary amine boranes.

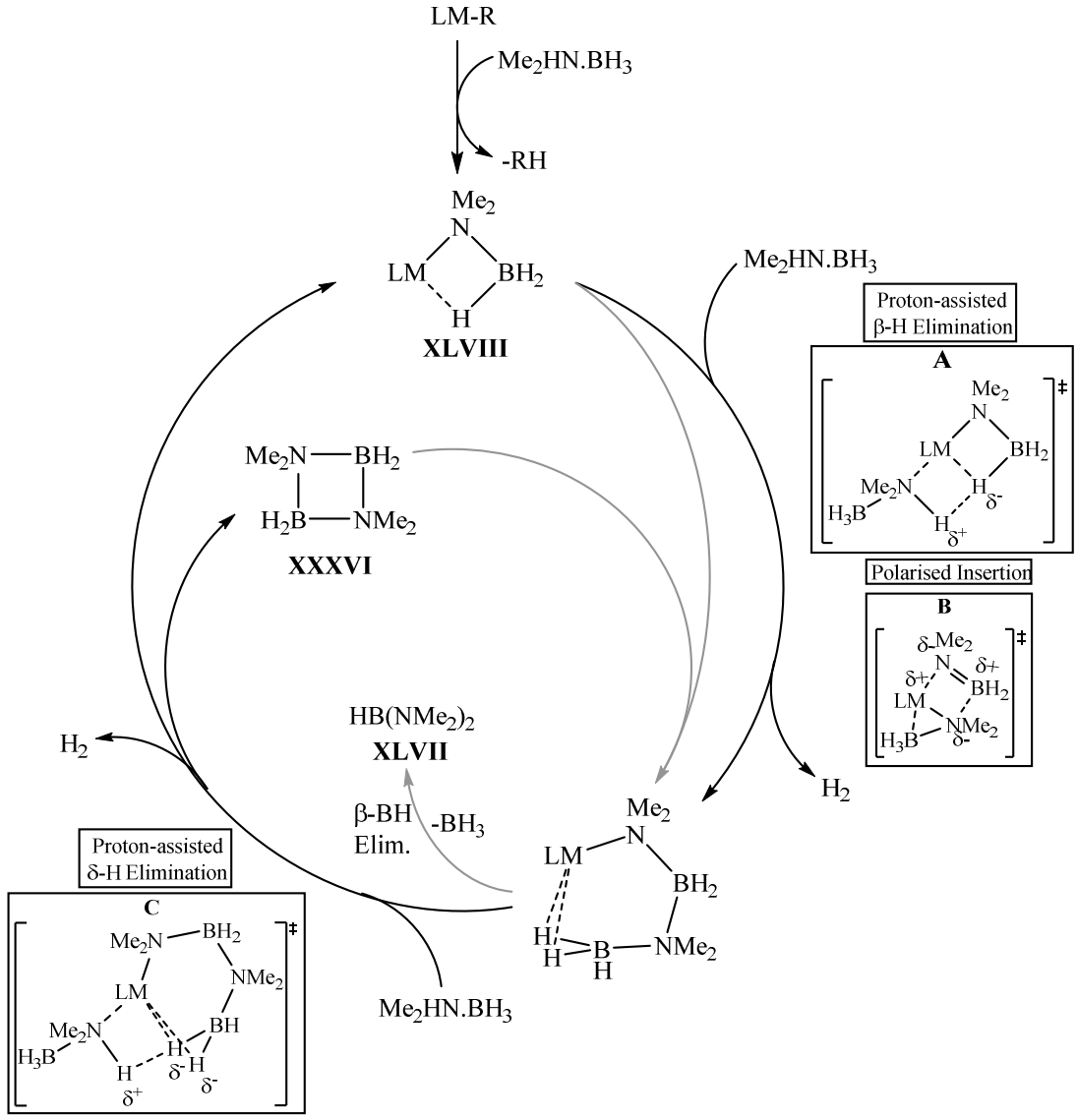

Figure 6.2: Proposed mechanism of amine borane dehydrocoupling by alkaline earth elements (M = Mg, Ca, Sr, Ba), with modifications based upon observations from the work described in this thesis.

The reactions described in this thesis were limited to closed systems. It is not clear whether the activation of dihydrogen gas evolved during these reactions imparts a significant effect on the mechanism of these reactions. In addition to this the effect of complex transamination equilibria involving protonated ligand and amine borane fragments, whilst uncharacterisable in such a complex system, is likely to be significant. A further consideration is that the formation of $[HB(NMe_2)_2]$ **XLVII** necessitates the formation of one equivalent of BH_3, the fate of which was not

resolved in this thesis. These points suggest that further mechanistic validation should focus on;

- A comparison between open, or periodically degassed, and closed dehydrocoupling reaction systems to assess the impact of evolved dihydrogen gas.
- Stable Group 2 alkyl precatalysts featuring alkyl ligands, such as **VII**, which undergo an irreversible protonation, reducing the impact of potential transamination reactions on the efficacy of dehydrocoupling.
- A headspace gas analysis study to assess whether diborane is produced during these reactions, accounting for the formation of BH_3 in conversion of amine borane to species such as **XLVII**.

The kinetic analysis described in Chapters 3 and 4 highlighted the complexity of these reactions with only the concentration of dimethylamine borane conforming to simple kinetics. The choice of precatalyst proved decisive to the outcome of the kinetic study, with deactivation of calcium species **V-Ca** and **VI** resulting from ligand protonation. A more stable catalyst system than the bis(trimethylsilyl) and β-diketiminate ligands used in this study is required to assist in providing comparable data between metal centres. The results did suggest, however, that these reactions may be somewhat entropically controlled, reminiscent of Group 2 intermolecular hydroamination reported by Hill.[3] The comparison of dehydrocoupling reactivity of reagents from Groups 1, 2 and 3 proved to be overly ambitious, but highlighted the pitfalls in generalisations made regarding even chemically similar species. Despite this, a dependence upon the identity of the metal centre of the dehydrocoupling activity of reagents of Groups 1-3 was found. The gross trend in reactivity followed the order Sc > Mg > Li ≈ Na > K ≈ Ca ≈ Y, and identified a decrease in reactivity with increasing ionic radius and decreasing cation charge density as each group is descended, i.e. Li ≈ Na > K, Mg > Ca and Sc > Y, but did not extend to an absolute correlation.

A range of novel alkaline earth and boron-containing compounds have been identified in this thesis, including the homoleptic Group 2 anilido-imine complexes. In addition, the dehydrocoupling of the primary amine borane *tert*-butylamine

borane by alkaline earth reagents was described, characterising the previously unreported cycloborazane of a primary amine borane, [^{t}BuHN-BH_2]$_2$ **47**, and identified as an intermediate in the formation of the corresponding borazane [^{t}BuN-BH]$_3$ **49**. The first known study of the amine borane dehydrocoupling activity of Group 1 bis(trimethylsilyl)amides **LIX** was also described and, whilst of inferior activity to transition metal reagents, were shown to possess synthetic use in formation of amidoborane species.

Throughout this thesis the mechanism of secondary amine borane dehydrocoupling by d^0 reagents has been shown to be complex, suggesting that although generalisation can be made, a generic mechanism which fully describes dehydrocoupling of secondary-, primary- and ammonia borane will be too much of an oversimplification. In addition, the reactions described in this thesis have once again exhibited the divergent behaviour of a series of alkaline earth reagents, reminiscent of the previously reported reactivity of these species,[1, 2, 4-16] underlining the rich and diverse chemistry displayed by the elements of Group 2.

6.1 References for Chapter 6

1. M. S. Hill, M. Hodgson, D. J. Liptrot and M. F. Mahon, *Dalton Trans.*, 2011, **40**, 7783-7790.
2. D. J. Liptrot, M. S. Hill, M. F. Mahon and D. J. MacDougall, *Chem.- Eur. J.*, 2010, **16**, 8508-8515.
3. C. Brinkmann, A. G. M. Barrett, M. S. Hill and P. A. Procopiou, *J. Am. Chem. Soc.*, 2012, **134**, 2193-2207.
4. M. S. Hill, D. J. Liptrot, D. J. MacDougall, M. F. Mahon and T. P. Robinson, *Chem. Sci.*, 2013, **4**, 4212-4222.
5. B. Liu, T. Roisnel, J.-F. Carpentier and Y. Sarazin, *Angew. Chem.-Int. Ed.*, 2012, **51**, 4943-4946.
6. C. Brinkmann, A. G. M. Barrett, M. S. Hill, P. A. Procopiou and S. Reidt, *Organometallics*, 2012, **31**, 7287-7297.
7. M. Arrowsmith, M. S. Hill and G. Kociok-Koehn, *Organometallics*, 2010, **29**, 4203-4206.
8. A. G. M. Barrett, M. R. Crimmin, M. S. Hill and P. A. Procopiou, *Proc. R. Soc. A*, 2010, **466**, 927-963.
9. A. G. M. Barrett, I. J. Casely, M. R. Crimmin, M. S. Hill, J. R. Lachs, M. F. Mahon and P. A. Procopiou, *Inorg. Chem.*, 2009, **48**, 4445-4453.
10. A. G. M. Barrett, C. Brinkmann, M. R. Crimmin, M. S. Hill, P. Hunt and P. A. Procopiou, *J.Am. Chem. Soc.*, 2009, **131**, 12906-12907.
11. M. R. Crimmin, M. Arrowsmith, A. G. M. Barrett, I. J. Casely, M. S. Hill and P. A. Procopiou, *J. Am. Chem. Soc.*, 2009, **131**, 9670-9685.
12. M. R. Crimmin, A. G. M. Barrett, M. S. Hill, D. J. MacDougall, M. F. Mahon and P. A. Procopiou, *Chem.- Eur. J.*, 2008, **14**, 11292-11295.
13. M. R. Crimmin, A. G. M. Barrett, M. S. Hill, P. B. Hitchcock and P. A. Procopiou, *Organometallics*, 2008, **27**, 497-499.
14. J. R. Lachs, A. G. M. Barrett, M. R. Crimmin, G. Kociok-Koehn, M. S. Hill, M. F. Mahon and P. A. Procopiou, *Eur. J. Inorg. Chem.*, 2008, 4173-4179.
15. M. R. Crimmin, A. G. M. Barrett, M. S. Hill and P. A. Procopiou, *Org. Lett.*, 2007, **9**, 331-333.

16. A. G. Avent, M. R. Crimmin, M. S. Hill and P. B. Hitchcock, *Dalton Trans.*, 2005, 278-284.